Burgert Blom

Reactivity of Ylenes at Late Transition Metal Centers

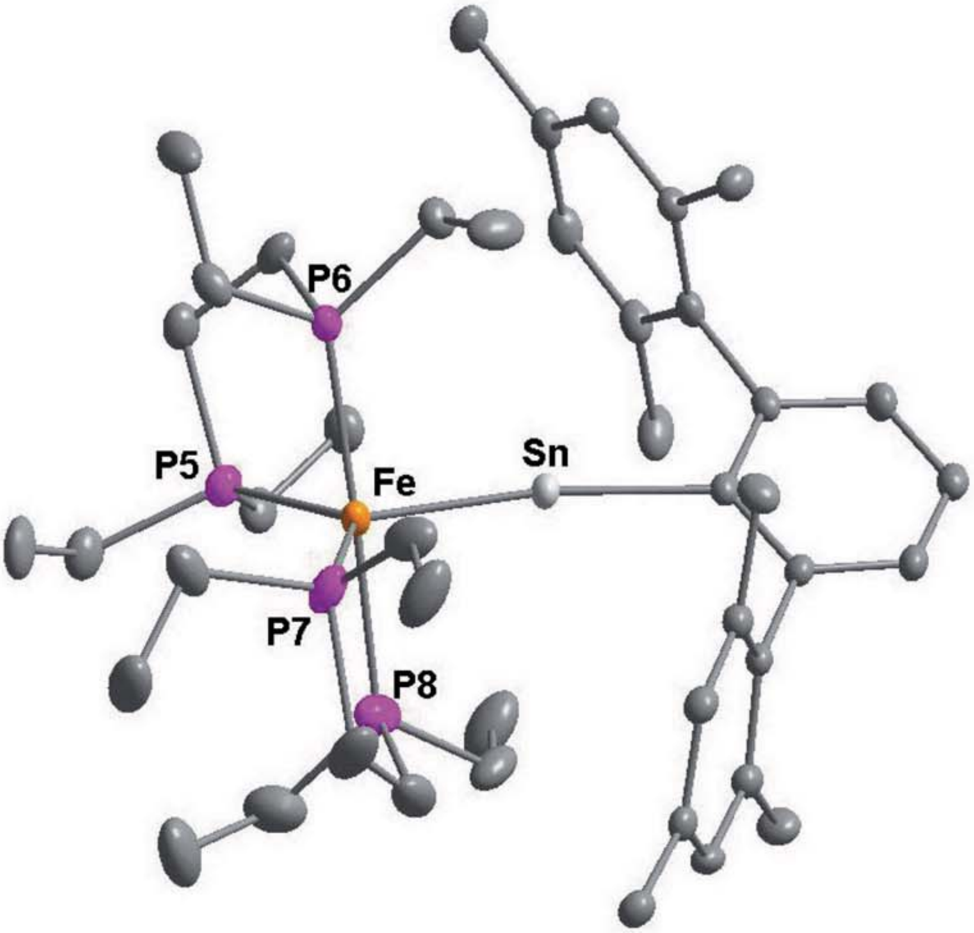

Cuvillier Verlag Göttingen

Dieses Werk ist copyrightgeschützt und darf in keiner Form vervielfältigt werden noch an Dritte weitergegeben werden.
Es gilt nur für den persönlichen Gebrauch.

Reactivity of Ylenes at Late Transition Metal Centers

DISSERTATION

Submitted in fulfilment of the degree
doctor rerum naturalium
(Dr. rer. nat)

of the
Faculty of Mathematics and Natural Sciences

of the

Rheinische Friedrich-Wilhelms-University of Bonn

By
MSc. Burgert Blom
born 14.10.1980 in Pretoria, South Africa

Bonn, April 2011

Dieses Werk ist copyrightgeschützt und darf in keiner Form vervielfältigt werden noch an Dritte weitergegeben werden.
Es gilt nur für den persönlichen Gebrauch.

Bibliografische Information der Deutschen Nationalbibliothek
Die Deutsche Nationalbibliothek verzeichnet diese Publikation in der
Deutschen Nationalbibliografie; detaillierte bibliografische Daten
sind im Internet über http://dnb.d-nb.de abrufbar.
1. Aufl. - Göttingen : Cuvillier, 2011
Zugl.: Bonn, Univ., Diss., 2011

978-3-86955-907-0

Prepared with the consent of Faculty of Mathematics and Natural Sciences of the Rheinische Friedrich-Wilhelms-University of Bonn.

1st Examiner: Prof. Dr. A. C. Filippou

2nd Examiner: Prof. Dr. E. Niecke

3rd Examiner: Prof. Dr. A. Gansäuer

4th Examiner: Prof. Dr. K. Maier

External Examiner: Prof. Dr. K. Lammertsma

Date of dissertation defense: 14.10.2011

© CUVILLIER VERLAG, Göttingen 2011
Nonnenstieg 8, 37075 Göttingen
Telefon: 0551-54724-0
Telefax: 0551-54724-21
www.cuvillier.de

Alle Rechte vorbehalten. Ohne ausdrückliche Genehmigung des Verlages ist es nicht gestattet, das Buch oder Teile daraus auf fotomechanischem Weg (Fotokopie, Mikrokopie) zu vervielfältigen.
1. Auflage, 2011
Gedruckt auf säurefreiem Papier

978-3-86955-907-0

Dieses Werk ist copyrightgeschützt und darf in keiner Form vervielfältigt werden noch an Dritte weitergegeben werden.
Es gilt nur für den persönlichen Gebrauch.

Somewhere, something incredible is waiting to be known.

Carl Sagan (1934 – 1996)

In memory of Prof John R Moss

Dieses Werk ist copyrightgeschützt und darf in keiner Form vervielfältigt werden noch an Dritte weitergegeben werden.
Es gilt nur für den persönlichen Gebrauch.

Dieses Werk ist copyrightgeschützt und darf in keiner Form vervielfältigt werden noch an Dritte weitergegeben werden.
Es gilt nur für den persönlichen Gebrauch.

Acknowledgements

First and foremost, I would like to express my gratitude to Prof. Dr. A. C. Filippou for giving me the opportunity to promote in his research group. I thank him for his guidance, direction and most of all patience, during the last three years. It has been an exciting journey for me scientifically. I am sure this is not the end of our collaboration.

So many other people enabled this work to come to fruition:

- Dr. Gregor Schnakenburg – for solving most of the X-ray structures included in this dissertation. His willingness always to try is something I will be indebted to. I also have to thank him for useful discussions concerning the modelling of my germylidyne complexes. I would also like to thank Dr. Sebastian Schwieger for solving some structures included in this dissertation.
- Bernhard Beile – who worked under my supervision during my tenure in Bonn. Many of his results are included here, and without him the results I obtained would have taken far longer – thank you.
- Lars Zimmer – for useful discussions concerning the modelling of my Fe complexes, as well as running all the UV-Vis spectra – thank you.
- The countless students I had the privilege of working with – their hard work and results form, to a large extent, the backbone of some of my work: I. Gadazcek, B. Wesizla, F. Wechter, M. Peintinger, S. Daova, S. Claus, C. Landvogt.
- Dr. M. van Gastel for running EPR spectra (and the interpretation) thereof of the Fe(I) complexes.
- Dr. P. Portius and Dr. H. Cui for collaborative work on the insertion chemistry and useful discussions.
- Kim Heymann for help with some ^{31}P NMR spectral simulations.
- Dr. E. Bill at MPI Mulheim for collecting all the Mößbauer spectra included here.
- The NMR department: C. Schmidt, K. Prochnicki and H. Spitz deserve a big thank you – especially for their patience!
- The elemental analysis department: Dr. S. Rings and her colleagues.
- Dr. P. Liu who made some of the starting materials as part of an introductory practical under my supervision on joining the group – the results of which are also included here.
- Dr. N. Weidemann – who has become a good friend and ally.

Dieses Werk ist copyrightgeschützt und darf in keiner Form vervielfältigt werden noch an Dritte weitergegeben werden.
Es gilt nur für den persönlichen Gebrauch.

- Henning Arp – who made the first two years here an absolute joy – I look forward to working together again in the future!
- A thanks to Prof. Dr. A. C. Filippou for carefully proof reading my first draft, and his suggestions.
- A thanks to those who also had a look at my first draft (or sections thereof) with some comments: Henning Arp, Bram Pluijmaekers, Dr. Nils Weidemann, Dr. Gregor Schnakenburg and Prof. Dr. Christoph Marschner.
- To all the other members of the research group – every single one of them – thank you for an awesome four years.
- My friends and family: here in Germany and in South Africa – There are too many to list by name – but they all know who they are. Thank you also to everyone in the “Bonn Players” my theatre group for providing me with the creative distraction and outlet I needed to stay balanced.

Dieses Werk ist copyrightgeschützt und darf in keiner Form vervielfältigt werden noch an Dritte weitergegeben werden.
Es gilt nur für den persönlichen Gebrauch.

INDEX

Dieses Werk ist copyrightgeschützt und darf in keiner Form vervielfältigt werden noch an Dritte weitergegeben werden.
Es gilt nur für den persönlichen Gebrauch.

Dieses Werk ist copyrightgeschützt und darf in keiner Form vervielfältigt werden noch an Dritte weitergegeben werden.
Es gilt nur für den persönlichen Gebrauch.

Dieses Werk ist copyrightgeschützt und darf in keiner Form vervielfältigt werden noch an Dritte weitergegeben werden.
Es gilt nur für den persönlichen Gebrauch.

Dieses Werk ist copyrightgeschützt und darf in keiner Form vervielfältigt werden noch an Dritte weitergegeben werden.
Es gilt nur für den persönlichen Gebrauch.

Index of compounds discussed in this dissertation

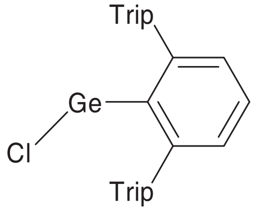

1-Ge

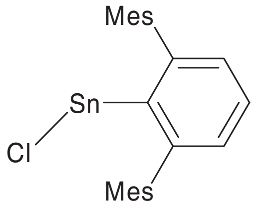

1-Sn

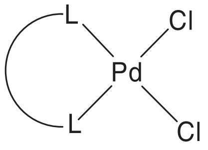

L-L = cod: **1-Pd**

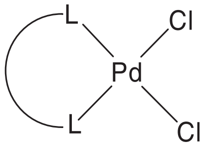

L-L = dppe: **2-Pd**

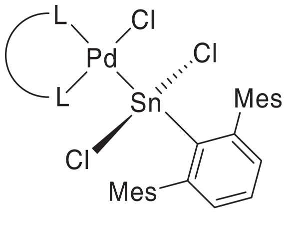

L-L = cod: **3-Pd**

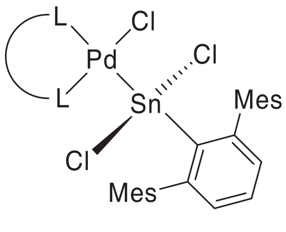

L-L = dppe: **4-Pd**

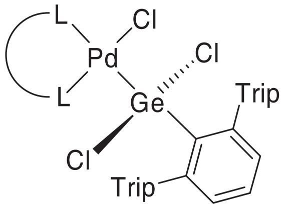

L-L = cod: **5-Pd**

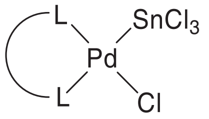

L-L = cod: **6-Pd**

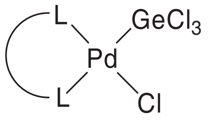

L-L = cod: **7-Pd**

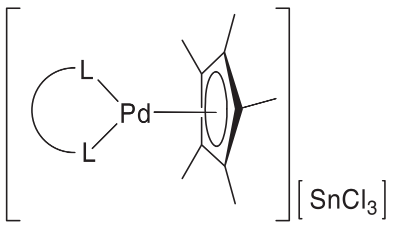

8-Pd

$[RhCl(\eta^2\text{-}C_2H_4)_2]_2$

1-Rh

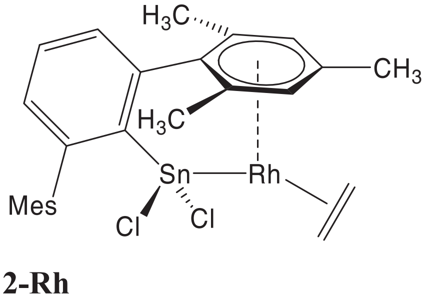

2-Rh

Dieses Werk ist copyrightgeschützt und darf in keiner Form vervielfältigt werden noch an Dritte weitergegeben werden.
Es gilt nur für den persönlichen Gebrauch.

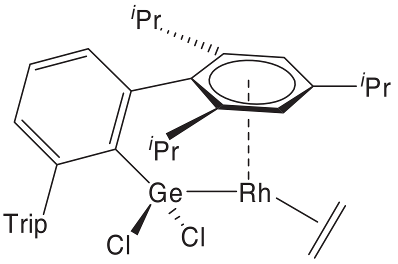

3-Rh

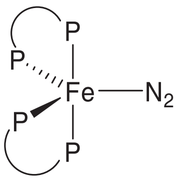

P-P = depe: **1-Fe**

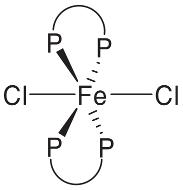

P-P = depe: **2-Fe**

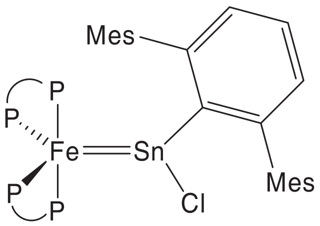

P-P = depe: **3-Fe**

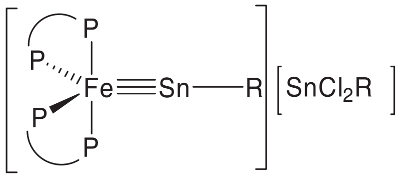

P-P = depe, R = 2,6-Mes_2-C_6H_3

4-Fe

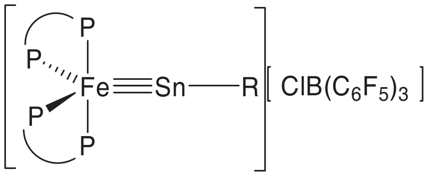

P-P = depe, R = 2,6-Mes_2-C_6H_3

5-Fe

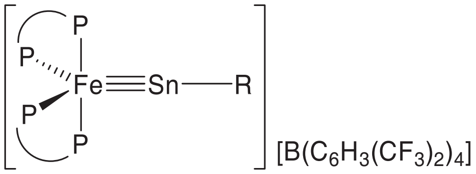

P-P = depe, R = 2,6-Mes_2-C_6H_3

6-Fe

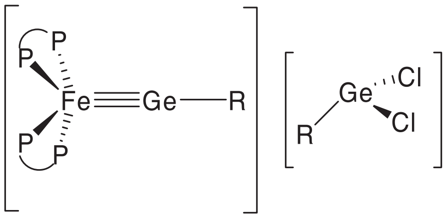

P-P = depe, R = 2,6-$Trip_2$-C_6H_3

8-Fe

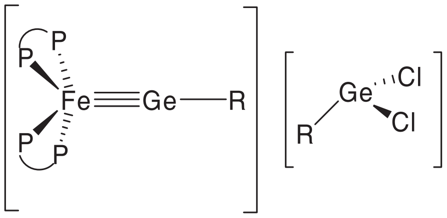

P-P = depe, R = 2,6-Mes_2-C_6H_3

9-Fe

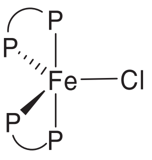

P-P = depe: **10-Fe**

Dieses Werk ist copyrightgeschützt und darf in keiner Form vervielfältigt werden noch an Dritte weitergegeben werden.
Es gilt nur für den persönlichen Gebrauch.

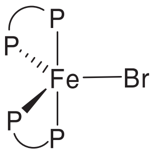

P-P = depe: **11-Fe**

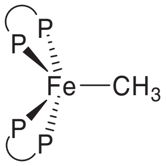

P-P = depe: **12-Fe**

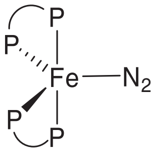

P-P = dmpe: **13-Fe**

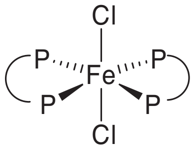

P-P = dmpe: **14-Fe**

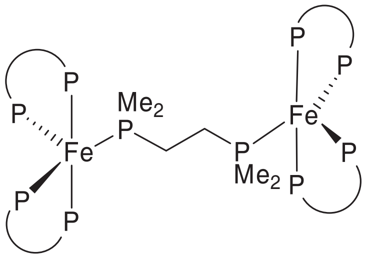

P-P = dmpe: **15-Fe**

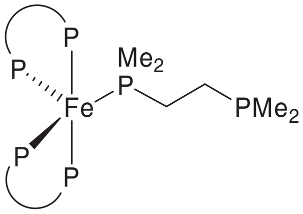

P-P = dmpe: **15-Fe-m**

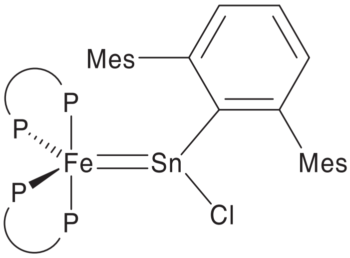

P-P = dmpe: **16-Fe**

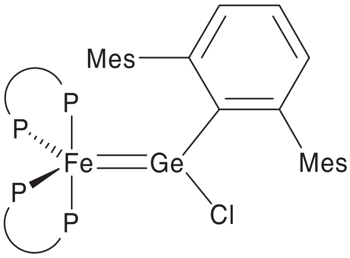

P-P = dmpe: **16-Fe-2**

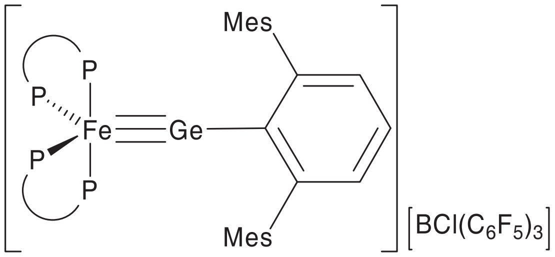

P-P = dmpe**: 16-Fe-3**

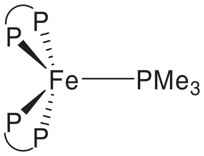

P-P = dmpe: **17-Fe**

[FeH{η^2-CH_2PMe_2}$(PMe_3)_3$]

18-Fe

[$FeCl_2(PMe_3)_2$]

19-Fe

Dieses Werk ist copyrightgeschützt und darf in keiner Form vervielfältigt werden noch an Dritte weitergegeben werden.
Es gilt nur für den persönlichen Gebrauch.

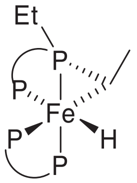

P-P = depe: **22-Fe**

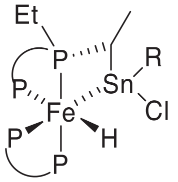

P-P = depe: **23-Fe**

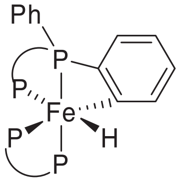

P-P = dppe: **24-Fe**

[FeCl(dppe)$_2$]

25-Fe

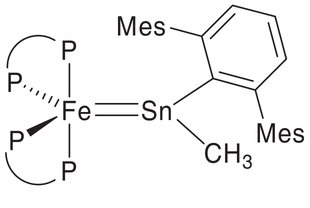

P-P = depe: **26-Fe**

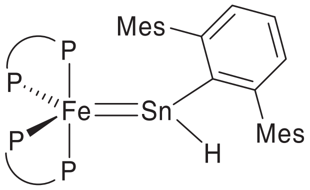

P-P = depe: **27-Fe**

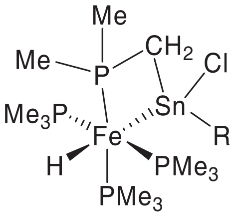

R = 2,6-Mes$_2$-C$_6$H$_3$: **20-Fe**

(one stereoisomer shown)

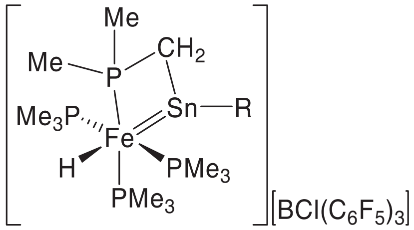

R = 2,6-Mes$_2$-C$_6$H$_3$: **21-Fe**

(one stereoisomer shown)

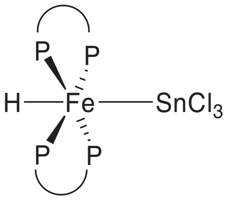

P-P = depe: **28-Fe**

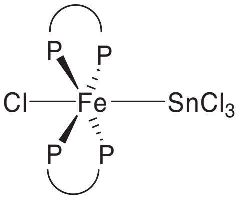

P-P = depe: **29-Fe**

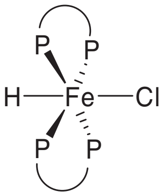

P-P = depe: **30-Fe**

Dieses Werk ist copyrightgeschützt und darf in keiner Form vervielfältigt werden noch an Dritte weitergegeben werden.
Es gilt nur für den persönlichen Gebrauch.

[$RuCl_2(depe)_2$]

3-Ru

trans-[$RuHCl(depe)_2$]

4-Ru

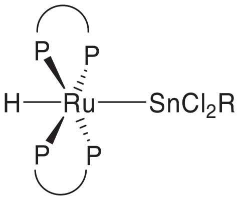

P-P = depe, R = 2,6-Mes_2-C_6H_3

5-Ru

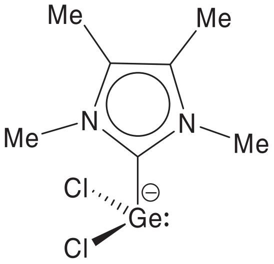

5-Ge

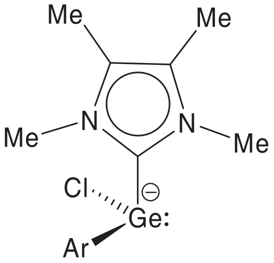

6-Ge

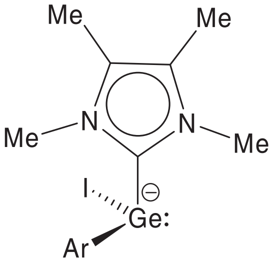

7-Ge

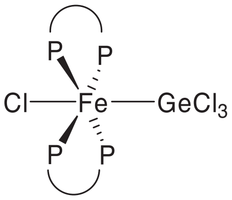

P-P = depe: **31-Fe**

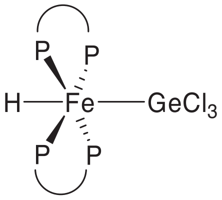

P-P = depe: **32-Fe**

[$RuH_2(depe)_2$]

1-Ru

[$RuCl_2(DMSO)_4$]

2-Ru

[Ge(2,6-Mes_2-C_6H_3)Cl(PMe_3)]

8-Ge

Dieses Werk ist copyrightgeschützt und darf in keiner Form vervielfältigt werden noch an Dritte weitergegeben werden.
Es gilt nur für den persönlichen Gebrauch.

Dieses Werk ist copyrightgeschützt und darf in keiner Form vervielfältigt werden noch an Dritte weitergegeben werden.
Es gilt nur für den persönlichen Gebrauch.

1. Introduction

1.1 Heavy group 14 element analogues of alkenes

Multiple bonding in compounds containing carbon and the lighter element atoms can readily be explained by simple models such as valence bond theory and hybridisation[1] and is a common ingredient in most introductory undergraduate textbooks. Early attempts at preparing compounds containing Si=Si bonds by Kipping[2] were dashed when he realised he had actually isolated oligomeric Si cyclic compounds as opposed to unsaturated Si compounds.[3,4] He later concluded that multiple bonds to silicon were simply not possible.[5] A similar picture emerged for As and P,[6] and these persistent failures to isolate multiply bonded compounds containing heavier main group element atoms lead to the formulation of the so-called "double bond rule" by Pitzer[7] and Mulliken.[8] This rule stated that elements with a principal quantum number greater than 2 cannot form multiple bonds, a conclusion which was accepted as fact as late as 1980.[9] By 1975 a few exceptions to this rule were known involving (p–p)π bonding between C and the elements P, As, Sb, Bi, Si and Ge,[10] but it was only conclusively overturned in 1981[11] by the report of the first stable silene by Brook and co-workers[12,13] and that of the first stable disilene by West and co-workers.[14] This, together with a report the same year by Yoshifuji of the first stable diphosphene,[15] initiated substantial academic interest in this field. By the end of the 1980s, germenes[16,17,18] and stannenes [19] had also made an appearance in the literature.

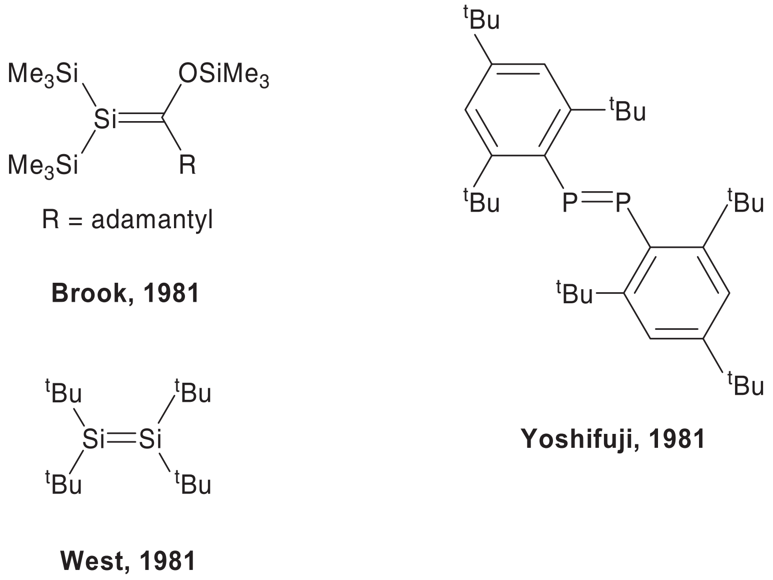

Brook, 1981

West, 1981

Yoshifuji, 1981

Figure 1.1: The first report of a silene, disilene and diphosphene in 1981: the "double bond rule" was disproved.

Dieses Werk ist copyrightgeschützt und darf in keiner Form vervielfältigt werden noch an Dritte weitergegeben werden.
Es gilt nur für den persönlichen Gebrauch.

Symmetrical heavy alkene analogues, those being homodinuclear [20] were also reported for Ge by Masamune and Hanzawa,[21,22] by Lappert and co-workers for Sn;[23] and by Grützmacher and Klinkhammer for Pb, completing the series of symmetrical alkene analogues (Figure 1.2).[24]

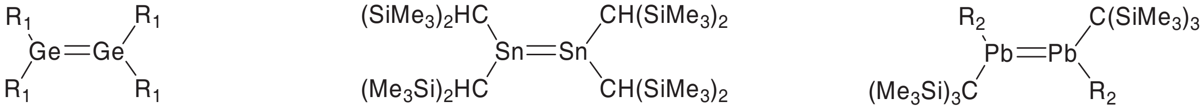

Masamune and Hanzawa, 1982   **Lappert, 1976**   **Grützmacher, 1998**

Figure 1.2: The first symmetrical heavy alkene analogues (congeners) for Ge, Sn and Pb. (R_1 = 2,6-diethylphenyl; R_2 = 2,4,6-trimethylphenyl).

Subsequently a large array of other heavy symmetrical alkene congeners have appeared in the literature.[25] In many experimental solid state structural studies on these compounds, a *trans*-bending geometry is observed for the substituents bound to the tetrel atom, in contrast to that of ethene. In the case of disilene compounds this ranges from $\delta = 0°$ to 18°; for digermenes from $\delta = 0°$ to 47.3°; for distannenes from $\delta = 21.1°$ to 64.4° and for lead from $\delta = 34.2°$ to 71° (Figure 1.3). The degree of *trans* bending within each group (Si, Ge, Sn and Pb) is governed by the electronegativity and π-donor ability of the ligands,[26,27,28] but this is difficult to separate from the steric influences. The trend, nevertheless, on average points to an increase in this *trans*-bending angle on descending from Si to Pb, with corresponding increased pyramidalisation of the tetrel atom. This phenomenon is due to the increasing energy difference between s and p electrons on descending group 14 resulting in the decreased participation of the s electrons in bonding, decreased hybridisation with p orbitals, and increased lone pair character on the tetrel atoms.[29] The bonding picture in these heavy alkene analogues can be explained by two sets of donor acceptor interactions $n_\sigma \rightarrow p_\pi$, between two carbene-like monomers taking into account the fact that the higher homologues of carbenes possess a singlet, rather than triplet ground state (Figure 1.3).[30,31,32]

Dieses Werk ist copyrightgeschützt und darf in keiner Form vervielfältigt werden noch an Dritte weitergegeben werden.
Es gilt nur für den persönlichen Gebrauch.

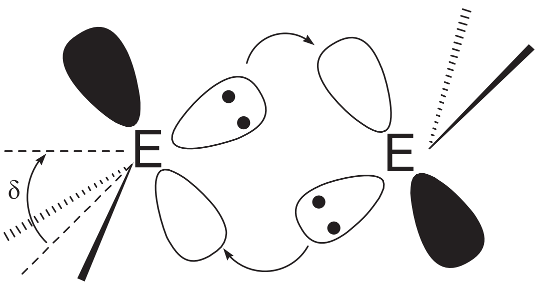

Figure 1.3: Bonding model explaining the *trans* bent geometry (defined by δ) of substituents of heavy alkene analogues (E = Si – Pb).

This bonding interaction becomes weaker in the case of Ge, Sn and Pb and often results in dissociation of the dimers in solution, to give monomeric singlet carbene analogues,[33] referred to as ylenes further on in the discussion. This is typically not the case for Si, where this is not usually observed, probably due to the fact that Si adopts a more classical σ and π bonding picture, as with ethene, on the basis of solid state ^{29}Si NMR data, according to one investigation.[34]

Monomeric ylenes for Ge, Sn and Pb in the solid state are well known, but their existence in the solid state is largely dependent on the nature of the substituents. For example, $(Me_3Si)_3CGeCH(SiMe_3)_2$ reported by Jutzi and co-workers is reported to be a monomer in the solid state,[35] in contrast to the closely related $Ge\{CH(SiMe_3)_2\}_2$, reported by Lappert and co-workers to be dimeric in the solid state.[36] Similarly, the stannylene $[Sn\{CH(SiMe_3)_2\}_2]_2$ is dimeric in the solid state, but the closely related cyclic version reported by Kira and co-workers is monomeric.[37] Monomeric silylenes are far less accessible, and more reactive than their Ge, Sn or Pb counterparts. For example, the silylene $Si\{N(SiMe_3)_2\}_2$ reported by West and co-workers was found to be thermally labile undergoing rapid decomposition above 0 °C in solution.[38] This is in contrast to the Ge, Sn and Pb analogues found by Lappert and co-workers, 30 years earlier, which are thermally stable.[39]

Monomeric homoleptic stannylenes bearing purely σ-bonded aromatic substituents were reported by Zuckerman and co-workers[40] and Edelmann and co-workers.[41] These were stabilised sterically but more importantly, through fluorine tin contacts from peripheral CF_3 groups, which prevented dimerisation, or oligomerisation of the monomers. The analogous monomeric plumbylene,[42] and germylene have also been reported.[43] Homoleptic monomeric ylenes (Ge, Sn and Pb) stabilised exclusively on steric grounds have been

Dieses Werk ist copyrightgeschützt und darf in keiner Form vervielfältigt werden noch an Dritte weitergegeben werden.
Es gilt nur für den persönlichen Gebrauch.

reported by Power and co-workers. These make use of kinetically stabilising, sterically very demanding *m*-terphenyl substituents:[44] C_6H_3-2,6-R_2 (R: Mes = 2,4,6-Me_3-C_6H_2,[45] Dipp = 2,6-$^iPr_2$-C_6H_2[46]).

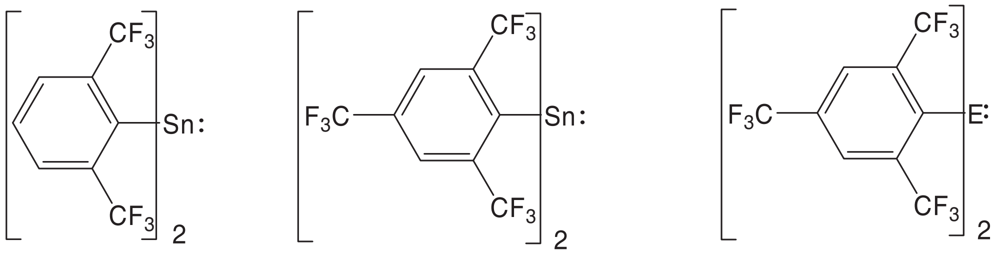

Zuckerman, 1981

Edelmann, 1991

E = Ge, **Kampf, 1997**

E = Pb, **Edelmann, 1991**

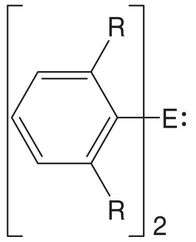

E = Ge, Sn, Pb; R = Mes

Power 1997

E = Ge, Sn, Pb; R = Dipp

Power 2006

Figure 1.4: Monomeric ylenes using steric protection and CF_3 groups, enabling stabilisation through intramolecular F-Sn contacts.

Jutzi and Leue reported the first monomeric heteroleptic germylene, containing a σ-bonded aromatic substituent and a halogen: GeClMes* (Mes* = 2,4,6-$^tBu_3$-C_6H_2).[47] Power and co-workers followed by reporting [SnCl(2,6-Mes_2-C_6H_3)]$_2$ and [GeCl(2,6-Mes_2-C_6H_3)]$_2$ (Mes = 2,4,6-Me_3-C_6H_2),[45a] prepared by metathetical exchange using [Li(2,6-Mes_2-C_6H_3)]$_2$.[48] This was followed by the lead analogue, [PbBr(2,6-$Trip_2$-C_6H_3)]$_2$ (Trip = 2,4,6-$^iPr_3$-C_6H_2),[49] prepared in an analogous way. The propensity of these ylenes to dimerise typically via halogen bridging is strongly dependant on the nature of the halogen, and *m*-terphenyl substituent, but generally are assumed to form monomers in solution.

Dieses Werk ist copyrightgeschützt und darf in keiner Form vervielfältigt werden noch an Dritte weitergegeben werden.
Es gilt nur für den persönlichen Gebrauch.

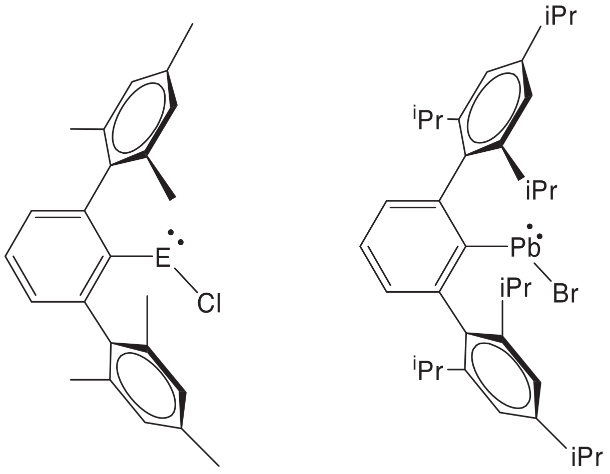

E = Ge, Sn

Power, 1997

Power, 2000

Figure 1.5: Heteroleptic sterically encumbered *m*-terphenyl ylenes by Power (The monomeric forms are depicted here, which are their assumed form in solution).

1.2 Heavy group 14 element analogues of alkynes

Up until 1999, the isolation of heavy alkyne congeners was still an open question, owing in part to the fact that each tetrel would only bear one substituent, resulting in increased steric requirements to stabilise the emerging compound. The previous facile entry to sterically very demanding ylenes by Power, however, enabled the isolation of a diplumbylene: 2,6-$Trip_2$-H_3C_6Pb—PbC_6H_3-2,6-$Trip_2$ (Trip = 2,4,6-$^iPr_3$-C_6H_2), in 2000, obtained serendipitously during an attempt at preparing PbH(2,6-$Trip_2$-C_6H_3) from PbBr(2,6-$Trip_2$-C_6H_3) by action of HAl^iBu_2.[50] The molecular structure of this compound, revealed a heavily *trans*-bent configuration, in contrast to that of a linear arrangement of atoms as seen with ethyne [51] (Pb-Pb-C 94.26(4)°), pointing to localised lone pairs on each lead centre. In addition, the Pb—Pb bond length of 3.1881(1) Å was significantly longer than that of typical diplumbanes such as Ph_3Pb—$PbPh_3$ at 2.844(4) Å.[52] These two facts illustrated a complete lack of hybridisation in the lead atoms, and almost exclusive use of p orbitals in σ-bonding.[53] This was followed 2002 by the report of the first digermyne: 2,6-$Dipp_2$-H_3C_6Ge—GeC_6H_3-2,6-$Dipp_2$ (Dipp = 2,6-$^iPr_2$-C_6H_3).[54] In this case, the Ge—Ge bond length of 2.2850(6) Å was found to be considerably shorter than normal Ge—Ge single bonds (2.44 Å)[55] and indicative of multiple bonding character.[56] A *trans* bent configuration was also observed for this compound (Ge-Ge-C 128.67(8)°), albeit not to the same extent as that of the Pb compound. The distannyne was reported in the same year[57] and featured a Sn—Sn bond length of

Dieses Werk ist copyrightgeschützt und darf in keiner Form vervielfältigt werden noch an Dritte weitergegeben werden.
Es gilt nur für den persönlichen Gebrauch.

2.6675(4) Å, shorter compared to Sn—Sn single bonds,[58] and again indicative, of multiple bond character. The Sn-Sn-C angle in this case was found to be 125.24(7)°, which was also later found to depend on the nature of the terphenyl substituent.[59] The series of heavy alkyne congeners was completed in 2004 for Si, in a report by Sekiguchi and co-workers, presenting the first disilyne.[60] The Si–Si bond length was observed to be 2.0622(9) Å, considerably shorter (13.5 %) than that of typical Si–Si single bonds, and 3.8 % shorter than that of typical Si=Si double bonds.[61] The authors, and subsequent investigations assert the bond order to be three, [62] but others have suggested, on the basis of calculations, the bond order to be two, rather than three.[63,64] This case in point draws attention to the contentious issue surrounding the assignment of bond order in these higher homologues. A further example of this includes the first example of a gallyne by Robinson, claimed to be a Ga≡Ga triple bond.[65] This was subsequently disputed by Cotton as rather being a "double bond with a significant role for noncovalent interactions" on the basis of density functional theory.[66]

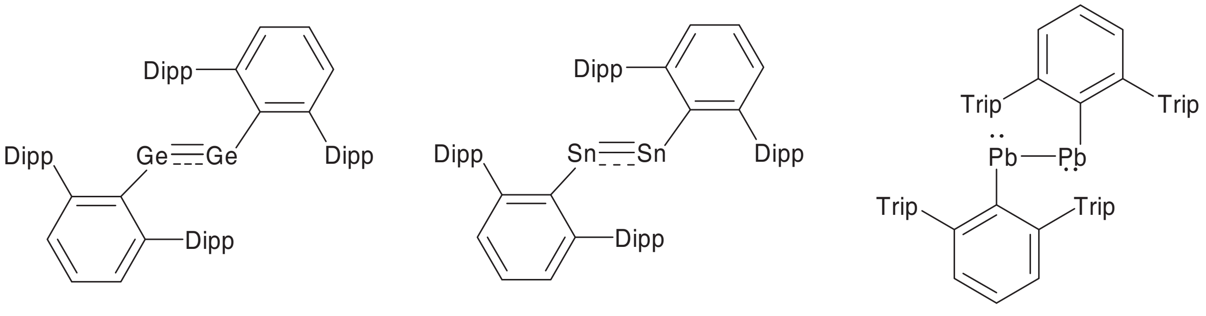

Power, 2002 **Power, 2002** **Power, 2000**

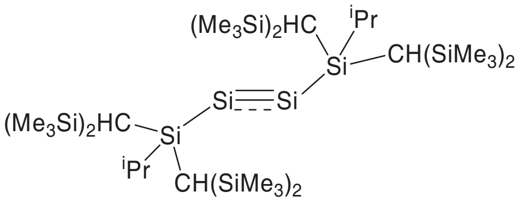

Sekiguchi, 2004

Figure 1.6: The first isolated examples of group 14 alkyne analogues.

The *trans* bending observed in the higher homologues can be attributed to the increased energy requirements to access the quartet state, rather than the doublet state in the M–R moiety. If twice this energy exceeds the energy gained from the two emerging π bonds, a bent geometry is observed, if not, as is the case with ethyne, a linear geometry results. This approximation does not take into consideration the steric or σ-bonding effects, but does qualitatively explain the differences.[29]

Dieses Werk ist copyrightgeschützt und darf in keiner Form vervielfältigt werden noch an Dritte weitergegeben werden.
Es gilt nur für den persönlichen Gebrauch.

	H—C≡C—H	H—Si≡Si—H	H—Ge≡Ge—H
$2\Delta E_{D,Q}$ (kcal·mol^{-1})	28.9	76.0	82.4
$E_{2\pi}$ (kcal·mol^{-1})	120–130	46–62	44–50
	$2\Delta E_{D,Q} < E_{2\pi}$	$2\Delta E_{D,Q} > E_{2\pi}$	$2\Delta E_{D,Q} > E_{2\pi}$
Geometry	linear	*trans*-bent	*trans*-bent

Table 1.1: Summary of π-bond energies, and $\Delta E_{D,Q}$ energies accounting for *trans*-bending in the higher alkyne analogues (from ref 29)

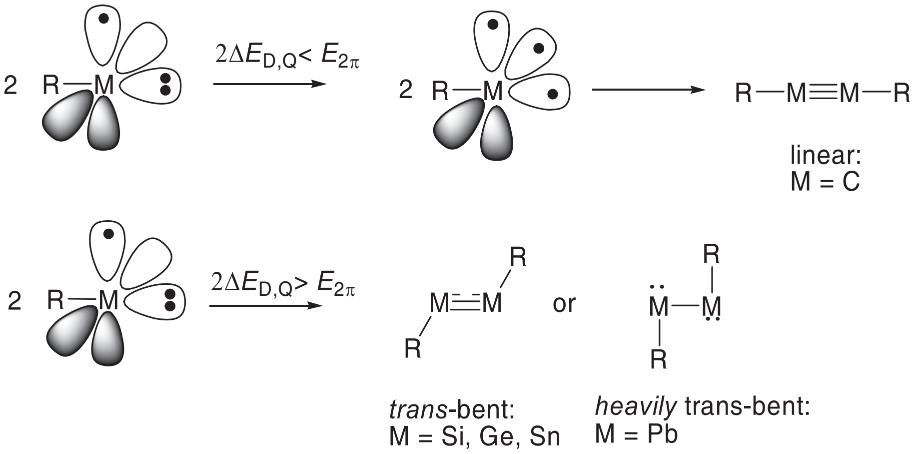

Figure 1.7: *trans*-bending effect in heavier alkyne homologues (adapted from ref 29)

The results obtained so far for the heavy group 14 alkynes point to an ever decreasing bond order on descending from Si to Pb, exemplified by bond lengths and the decreasing E-E-C angle. A continuum of bond orders can tentatively be imagined for these compounds: ethyne being on the one end, with a bond order of 3, and lead on the other with a bond order of 1. Si, Ge and Sn fall in-between these two extremes, with that of Si > 2, Ge ≥ 2, Sn ≈ 2.

Several reactivity studies, further probing the nature of the multiple bond in the case of Ge and Sn have also been carried out, for example activation of dihydrogen[67,68] at ambient conditions, activation of ethene,[69] reactivity towards N_2O,[70] and reactivity towards other unsaturated molecules.[71] The nature of the reduction products of Ge and Sn alkyne analogues have also been investigated, typically resulting in singly reduced radical species of the type M[R–E–E–R], (M = Na or K, E = Ge or Sn, R = bulky terphenyl substituent), or the doubly reduced counterparts.[72]

Dieses Werk ist copyrightgeschützt und darf in keiner Form vervielfältigt werden noch an Dritte weitergegeben werden.
Es gilt nur für den persönlichen Gebrauch.

Asymmetric alkyne analogues are very uncommon. Couret and co-workers have reported a germaacetylene generated *via* photolysis of a diazomethylgermylene,[73] and Kira and co-workers that of a stannaacetylene, generated also *via* a similar photolytic pathway.[74] In both studies the asymmetric acetylene was not formally isolated and to date none have been structurally characterised.[75]

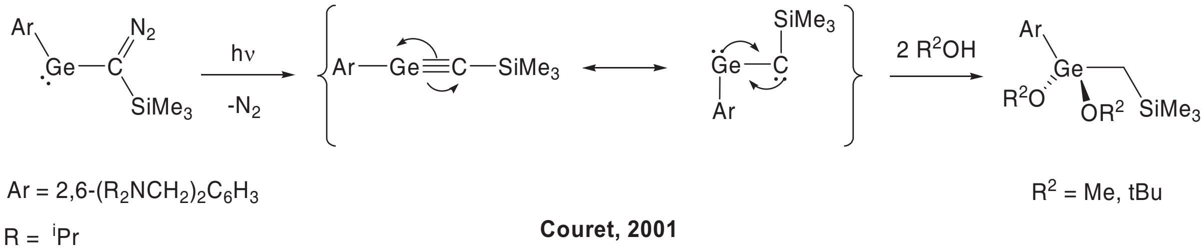

Scheme 1.1: Chemical evidence for the formation of a germyne, by Couret and co-workers.

1.3 Heavy group 14 element analogues of alkylidene (carbene) complexes*

Having introduced the developments in multiple bonding of the heavy homologues of carbon from a main group chemistry perspective, we now turn our attention to the analogous transition metal chemistry.

Fischer and Maasböl announced the discovery of the first alkylidene complexes, $[(CO)_5W{=}C(Me)(OMe)]$ and $[(CO)_5W{=}C(Ph)(OMe)]$ in 1964,[76] shown later by X-ray crystallographic investigation to bear a planar carbon atom bound to the metal centre,[77] as did the Cr analogues.[78] This important discovery heralded the era of carbon to metal multiple bonding, and ten years later, Schrock reported an example of an alkylidene complex of Ta: $[Ta\{CH_2{}^tBu\}_3\{{=}CH^tBu\}]$.[79] The Schrock compound differed from those of Fischer in the respect that the carbene carbon atom bears a hydrogen atom[80] and was not bonded to any stabilising heteroatomic substituent. This lead to the formulation of two distinct classes of carbene complexes those of Fischer type, and those of Schrock type (Table 1.2).

---

[*] See as examples: (a) J. W. Herdon, *Coord. Chem. Rev.* **2009**, 86; (b) R. R. Schrock, *Chem. Rev.* 2009, *109*, 3211; (c) W. Zhang, J. S. Moore, *Adv. Synth. Cat.* **2007**, *349*, 93; (d) R. R. Schrock, C. Czekelius, *Adv. Synth. Cat.* **2007**, *349*, 55 and references therein; (e) A. Mortreux, O. Coutelier, *J. Mol. Cat. A* **2006**, *254*, 96; (f) R. R. Schrock, *J. Chem. Soc. Chem. Commun.* **2005**, *22*, 2773 and references therein; (g) A. Mayr, H. Hoffmeister, *Adv. Organomet. Chem.* **1991**, *32*, 227 and references therein

Dieses Werk ist copyrightgeschützt und darf in keiner Form vervielfältigt werden noch an Dritte weitergegeben werden.
Es gilt nur für den persönlichen Gebrauch.

Fischer Type	Schrock Type
Low oxidation state metals	High oxidation state metals
Middle to late transition metals	Early transition metals
π–acceptor ligand	π–donor ligand
Bond described as a σ-donation π-acceptor interaction with the metal	Bond described as a covalent σ and π interaction with metal
Carbene centre electrophillic	Carbene centre nucleophillic
Heteroatom substituents on carbene carbon atom	Alkyl or H substituents on carbene carbon atom

Table 1.2: Comparison of Schrock and Fischer carbene complexes.

By use of the Dewar-Chatt-Duncanson model,[81,82] the differences between Fischer and Schrock type systems can be seen (Figure 1.8).

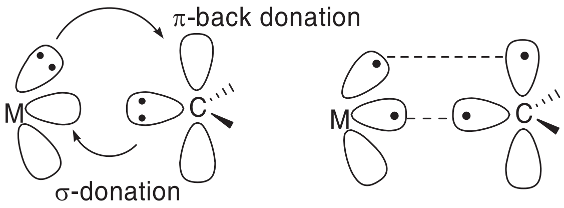

Figure 1.8: Fischer (left) vs Schrock (right) carbene complexes, according to the Dewar-Chatt-Duncanson model, originally developed to explain bonding in alkene complexes.

The logical extension of double bonding between metals and the heavy tetrel atoms was first reported 1976 when Jutzi and co-workers reported the first germylidene complex $[(CO)_5Cr\{Ge(SR_2)_2\}]$,[83] and Lappert and co-workers that of $[(CO)_5Cr\{Ge(CH(SiMe_3)_2)_2\}]$.[84] Lappert also reported the first series of analogous stannylidene complexes. It was only in 1985, however that the first plumbylidene complex was structurally characterised $[(\eta^5\text{-}C_5H_5)(CO)_2Mn{=}Pb{=}Mn(CO)_2(\eta^5\text{-}C_5H_5)]$.[85] Tilley and co-workers then reported the isolation of the first silylidene complex some 10 years later, $[(PCy_3)_2HPt{=}Si(SEt)_2][BPh_4]$.[86] Today, a plethora of ylidene complexes exist,[87] and typically involve low oxidation state metals, and hence can for the most part be considered as Fischer type carbene complexes.[33]

Dieses Werk ist copyrightgeschützt und darf in keiner Form vervielfältigt werden noch an Dritte weitergegeben werden.
Es gilt nur für den persönlichen Gebrauch.

These compounds can be categorised into five distinct classes:

(a) Homoleptic ylidene complexes of the type [$L_nM=ER_2$] (L_n = ligand sphere around metal, E = Ge, Sn or Pb).

(b) Heteroleptic ylidene complexes of the type [$L_nM=ER_1R_2$] (L_n = ligand sphere around metal, E = Ge, Sn or Pb, $R_1 \neq R_2$). An example of this is [$(CO)_5W=Ge(Cl)(\eta^2\text{-}C_5Me_5)$][88]

(c) Neutral, typically N or O, Lewis base stabilised ylidene complexes of the type [$L_nM=E(R_1)_x(\text{donor})_{3-x}$], ($L_n$ = ligand sphere around metal, R_1= substituent(s)) which are ubiquitous,[33] (although only two examples of structurally investigated complexes of the type [$L_nM=EX_2(\text{donor})$] (L_n = ligand sphere around metal, X = halogen) exist, which can also be classified in this category.[89]

(d) Stabilisation of the tetrel atom with bidentate ligands e.g. β-diketiminato ligands, resulting in 3 coordinate tetrel atoms, which can, for example be coordinated to W, resulting in heteroleptic germylidene and stannylidene complexes.[90]

(e) “Naked” tetrel atoms bound between two metal centres. Structurally characterised examples for Ge also exist, [91,92] none for Sn, and the one for lead already mentioned.

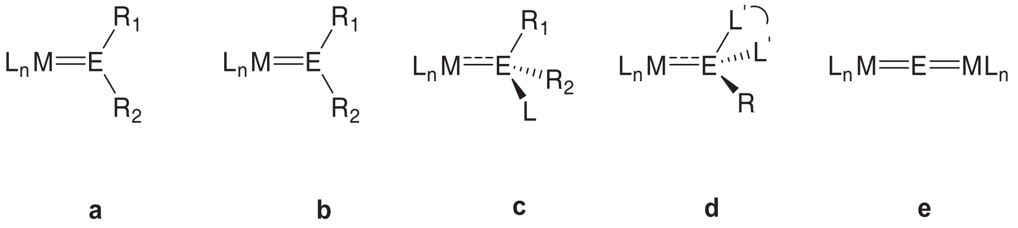

L_n = ligand sphere on metal, E = tetrel atom (Si-Pb)

a: R_1 = R_2

b: R_1 = R_2

c: R_1 = R_2 or R_1 = R_2, L = donor ligand

d: R = organic substituent or halogen, L' ⌒ L' = bidentate ligand

Figure 1.9: Categorisation of ylidene complexes of Si–Pb

Dieses Werk ist copyrightgeschützt und darf in keiner Form vervielfältigt werden noch an Dritte weitergegeben werden.
Es gilt nur für den persönlichen Gebrauch.

1.4 Heavy group 14 element analogues of alkylidyne (carbyne) complexes

1.4.1 Fischer and Schrock type carbyne complexes

In attempting to prepare halo-carbene complexes of the type [$(CO)_5M=C(R)(X)$] (M = Cr, Mo, W), R = CH_3 or C_6H_5, X = Cl, Br, I), by reaction of [$(CO)_5M=C(R)(OMe)$] with BX_3, Fischer and co-workers fortuitously uncovered the formation of the first carbyne complexes (Scheme 1.2). This resulted from halogen transfer to the metal, with concomitant CO elimination and OMe abstraction by the borane, as opposed to what was expected.[93] In 1978, Schrock reported the first carbyne complex of a metal in a high oxidation state.[94] As with carbene complexes, carbyne complexes can also be classed as Fischer type, or Schrock type (Figure 1.10).

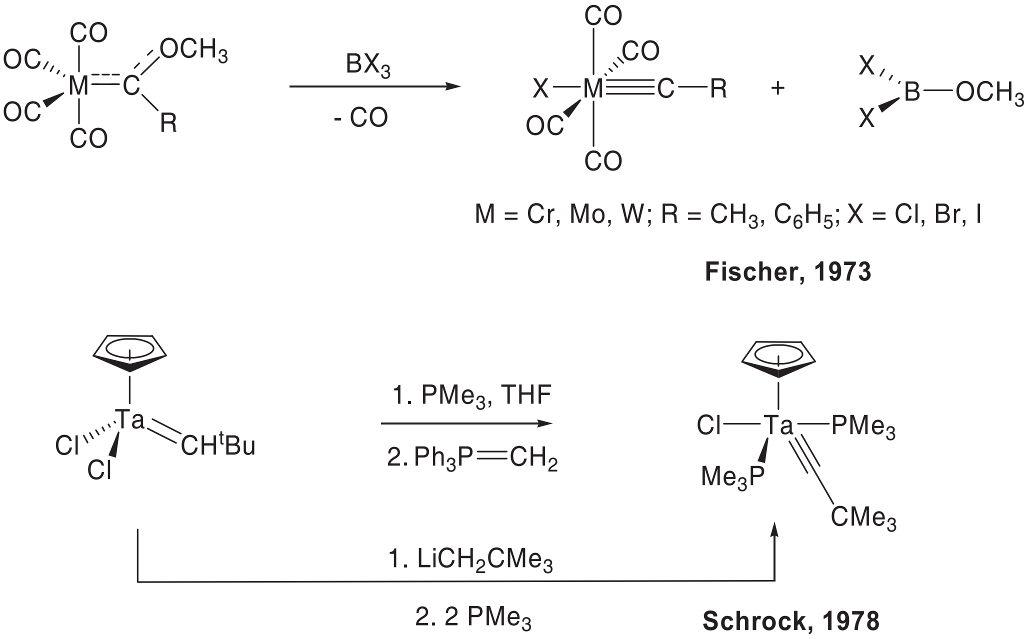

Scheme 1.2: Synthetic routes to the first Fischer type carbyne (above) and Schrock type carbyne (below) complexes.

Dieses Werk ist copyrightgeschützt und darf in keiner Form vervielfältigt werden noch an Dritte weitergegeben werden.
Es gilt nur für den persönlichen Gebrauch.

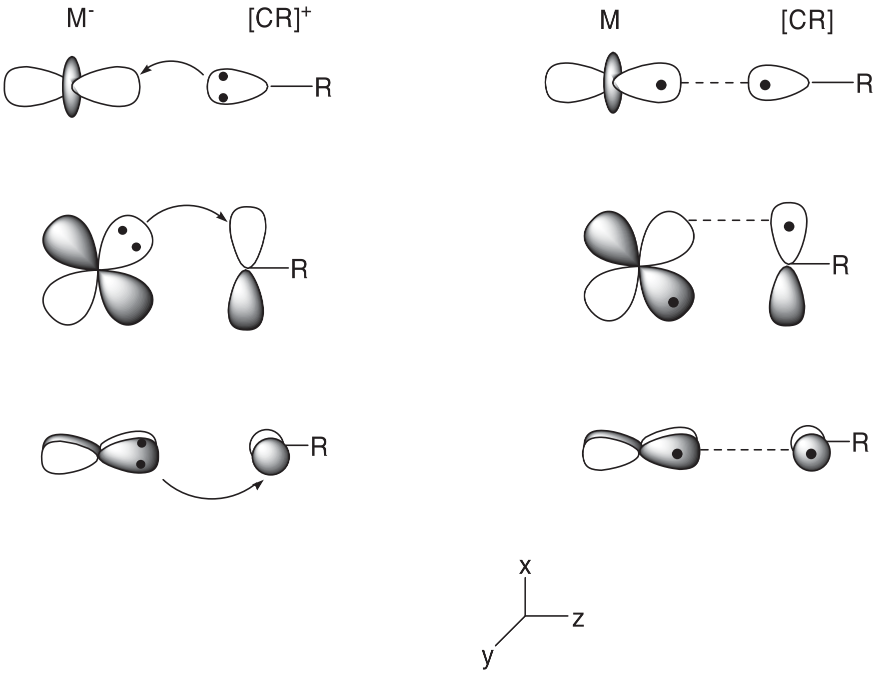

Figure 1.10: Comparison of Fischer type carbyne complexes (left) and Schrock type carbyne complexes (right) according to the Dewar-Chatt-Duncanson model.

1.4.2 Heavy group 14 analogues of Fischer type alkylidyne complexes

Nearly 20 years after the report of the first carbyne complex, Tilley and co-workers reported a base stabilised silylidyne complex. Despite the fact that it was base stabilised and not two coordinate, this was an important first step in the direction towards heavy group 14 carbyne analogues.

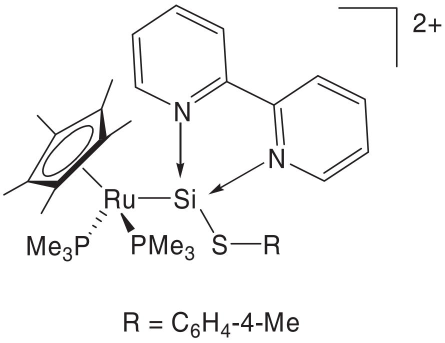

Tilley, 1992

Figure 1.11: Base stabilised silylidyne complex, by Tilley.

In 1997 Simons and Power reported the first heavy group 14 element analogue of a carbyne complex: [(η^5-C_5H_5)(CO)$_2$Mo≡Ge(2,6-Mes$_2$-C_6H_3)], generated *via* a metathetical route from Na[Mo(η^5-C_5H_5)(CO)$_3$] with GeCl(2,6-Mes$_2$-C_6H_3) at 50 °C.[95] The Mo-Ge-C1 bond angle

Dieses Werk ist copyrightgeschützt und darf in keiner Form vervielfältigt werden noch an Dritte weitergegeben werden.
Es gilt nur für den persönlichen Gebrauch.

of 172.2(2) ° along with a short Mo—Ge bond length of 2.271(1) Å supported the fact that the Mo-Ge bond was a triple bond. It was later found that analogous reactions with Cr and W resulted in metallogermylenes, which could only be converted to germylidyne complexes under harsh (refluxing in toluene, or UV light) conditions.[96] This difference in reactivity was attributed to the increased reactivity of Mo carbonyls, compared to those of Cr and W.

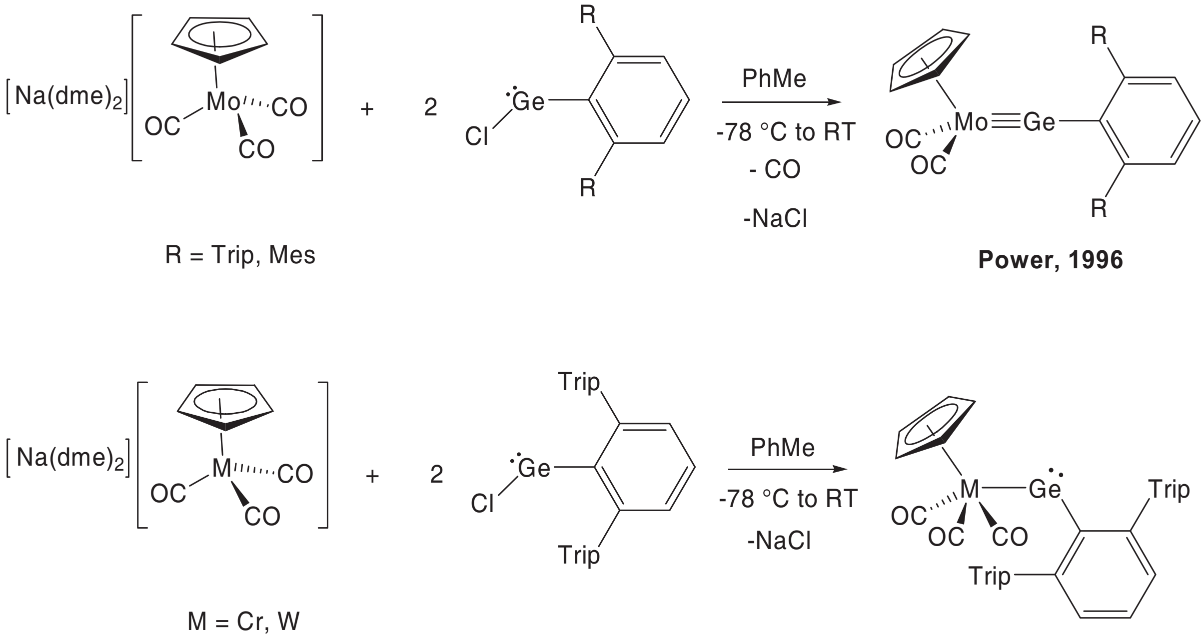

Scheme 1.3: Synthesis of first germylidyne complex and comparative metallogermylenes by Power.

The next step in the development of this chemistry was taken in 2000, when Filippou and co-workers reported the synthesis of a germylidyne complex of the type $[X(dppe)_2W{\equiv}Ge{-}Cp^*]$, ($X$ = Cl, Br, $Cp^* = C_5Me_5$).[97] This complex was prepared using a clean *bis*-dinitrogen elimination strategy, as opposed to the salt metathesis approach of Power. Starting from *trans*-$[W(dppe)_2(N_2)_2]$, which was reacted with germylenes $[GeCp^*X]$ in refluxing toluene, the germylidyne complexes could be isolated. This key breakthrough enabled rapid development in this field and in 2003 employing a similar strategy, the first stannylidyne complex, $[Cl(PMe_3)_4W{\equiv}Sn(2,6\text{-}Mes_2\text{-}C_6H_3)]$, starting from *cis*-$[W(PMe_3)_4(N_2)_2]$ reacted with the stannylene, $[SnCl(2,6\text{-}Mes_2\text{-}C_6H_3)]$ was isolated.[98] A cationic stannylidyne complex was also later reported, starting from $[Cl(dppe)_2W{\equiv}Sn(2,6\text{-}Mes_2\text{-}C_6H_3)]$ and performing Cl abstraction at the metal centre with $TlPF_6$, resulting in $[(dppe)_2W{\equiv}Sn(2,6\text{-}Mes_2\text{-}C_6H_3)][PF_6]$, the cation was found to be square pyramidal is the solid state.[99] The dinitrogen elimination strategy also facilitated the isolation of the first plumbylidyne complex, $[Br(PMe_3)_4Mo{\equiv}Pb(2,6\text{-}Trip_2\text{-}C_6H_3)]$, by reaction of the plumbylene $[PbBr(2,6\text{-}Trip_2\text{-}C_6H_3)]$ with *cis*-$[Mo(PMe_3)_4(N_2)_2]$,[100] and in an analogous way, $[X(PMe_3)_4W{\equiv}Pb(2,6\text{-}Trip_2\text{-}C_6H_3)]$,

Dieses Werk ist copyrightgeschützt und darf in keiner Form vervielfältigt werden noch an Dritte weitergegeben werden.
Es gilt nur für den persönlichen Gebrauch.

(X = Br, I) could also be prepared.[101] The mechanistic details of the successive dinitrogen elimination at the metal centres was also the subject of a subsequent rigorous computational investigation.[102]

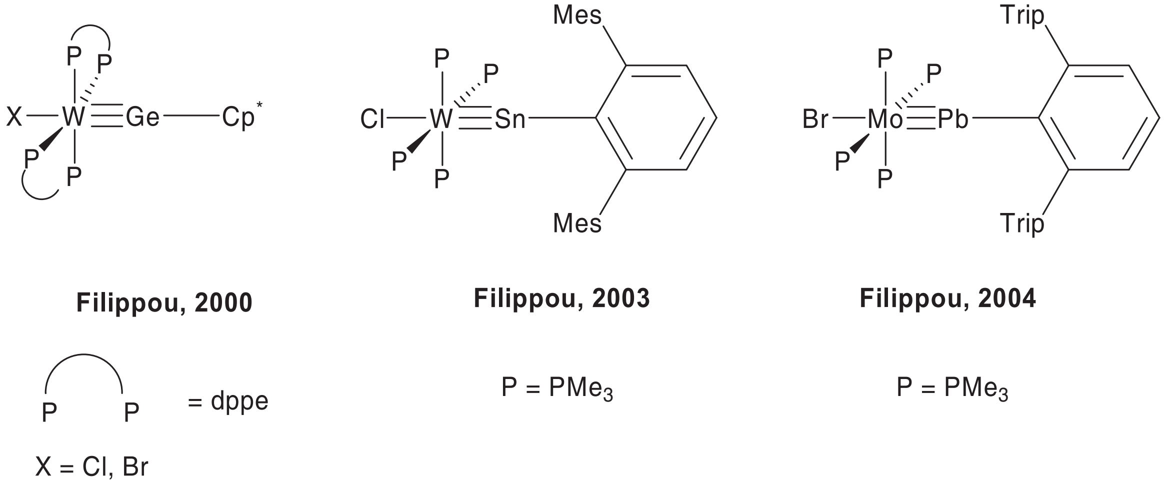

Filippou, 2000

P P = dppe

X = Cl, Br

Filippou, 2003

P = PMe_3

Filippou, 2004

P = PMe_3

Figure 1.12: First examples of isolated germylidyne, stannylidyne, and plumbylidyne, by Filippou and co-workers, utilising the bis-dinitrogen elimination strategy.

In the case of Si, Tilley and Mork reported a Mo complex with "considerable silylidyne character" [103] but owing to the fact a H atom could bridge the Mo and Si centres, the bonding situation is different from that of a silyidyne complex.

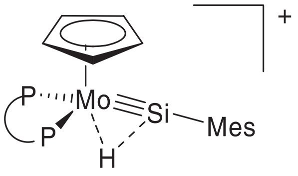

Tilley, 2003

P P = dmpe

Figure 1.13: Compound with "considerable silylidyne character" by Tilley.

The first example of a complex featuring a formal triple bond to Si was only very recently achieved in the Filippou group. The silylidyne complex $[Cp(CO)_2Mo{\equiv}Si(2,6\text{-}Trip_2\text{-}C_6H_3)]$ (Figure 1.14) was prepared from the precursor $[Cp(CO)_2Mo{\equiv}Si(2,6\text{-}Trip_2\text{-}C_6H_3)(IMe_2Me_2)]$ (IMe_2Me_2 = N-heterocyclic carbene) by carbene abstraction using $B(C_6H_4\text{-}4\text{-}CH_3)_3$.[104] This finding completed the array of triply bonded complexes to the heavy homologues of carbon.

Dieses Werk ist copyrightgeschützt und darf in keiner Form vervielfältigt werden noch an Dritte weitergegeben werden.
Es gilt nur für den persönlichen Gebrauch.

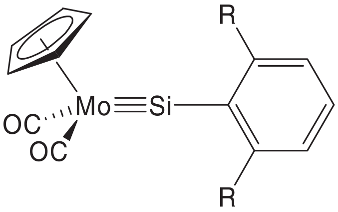

Filippou, 2010

R = Trip

Figure 1.14: First silylidyne complex: All heavy tetrel atoms (Si – Pb) are now known to possess the possibility of forming triple bonds to transition metals.

Dieses Werk ist copyrightgeschützt und darf in keiner Form vervielfältigt werden noch an Dritte weitergegeben werden.
Es gilt nur für den persönlichen Gebrauch.

1.5 Goals and Objectives

As pointed out in the introduction, complexes featuring triple bonds between the tetrel atoms (Si–Pb) has been achieved, but can still be considered very rare. Moreover, in all the existing examples the transition metal element atom is always exclusively restricted to group 6: Cr, Mo or W, and there are *no* examples of complexes outside group 6 featuring triple bonding to the heavier tetrel atoms (Si–Pb) to date.

This comprises the principle objective of this work:

- to prepare complexes with transition metal element atoms outside group 6, featuring triple bonding to the heavier tetrel element atoms.

In addition, the complexes so far reported featuring triple bonds to the heavier tetrel element atoms, for the most part, bear the kinetically stabilising and sterically demanding *m*-terphenyl substituents on the tetrel atom (2,6-Mes_2-C_6H_3 or 2,6-$Trip_2$-C_6H_3). Hence another objective of this work was to

- Explore the general reactivity of the ylenes of the type [EClR], E = Ge, R = 2,6-$Trip_2$-C_6H_3 (**1-Ge**) or 2,6-Mes_2-C_6H_3 (**2-Ge**); E = Sn, R = 2,6-Mes_2-C_6H_3 (**1-Sn**) towards late transition metal element complexes, systematically.

To this end, complexes of d^8 electron configuration in the group 8, 9 and 10 were selected and their reactivities towards ylenes of Ge and Sn investigated.

Dieses Werk ist copyrightgeschützt und darf in keiner Form vervielfältigt werden noch an Dritte weitergegeben werden.
Es gilt nur für den persönlichen Gebrauch.

2. Results and Discussion

2.1 Reactivity of EClR[†] (E = Ge, R = 2,6-Trip$_2$-C$_6$H$_3$; E = Sn, R = 2,6-Mes$_2$-C$_6$H$_3$) towards group 10 metal complexes

Our ultimate goal was the preparation of complexes featuring multiple, in particular triple bonds between Pd and Ge or Sn; but in addition, we were also interested in the general reactivities of the germylene **1-Ge** and stannylene **1-Sn**: E = Ge, R = 2,6-Trip$_2$-C$_6$H$_3$ (**1-Ge**); E = Sn, R = 2,6-Mes$_2$-C$_6$H$_3$ (**1-Sn**) towards Pd(II) complexes of the type [Pd(L-L)Cl$_2$], where L-L = cod (1,5-cyclooctadiene) **1-Pd** or dppe (1,2-bis(biphenylphosphino)ethane) **2-Pd**. Principally, two plausible reaction pathways can be envisaged for the reaction of these square planar Pd(II) complexes with ylenes (Scheme 2.1.1):

(a) coordination of the ylene to the Pd centre resulting from displacement of one of the chelate arms: this is unlikely, given the fact that the ligand is chelating (cod or dppe).
(b) insertion of the tetrel atom into the Pd–Cl bond: this is more likely, as there is precedence in the literature for such reactions to occur (see below).

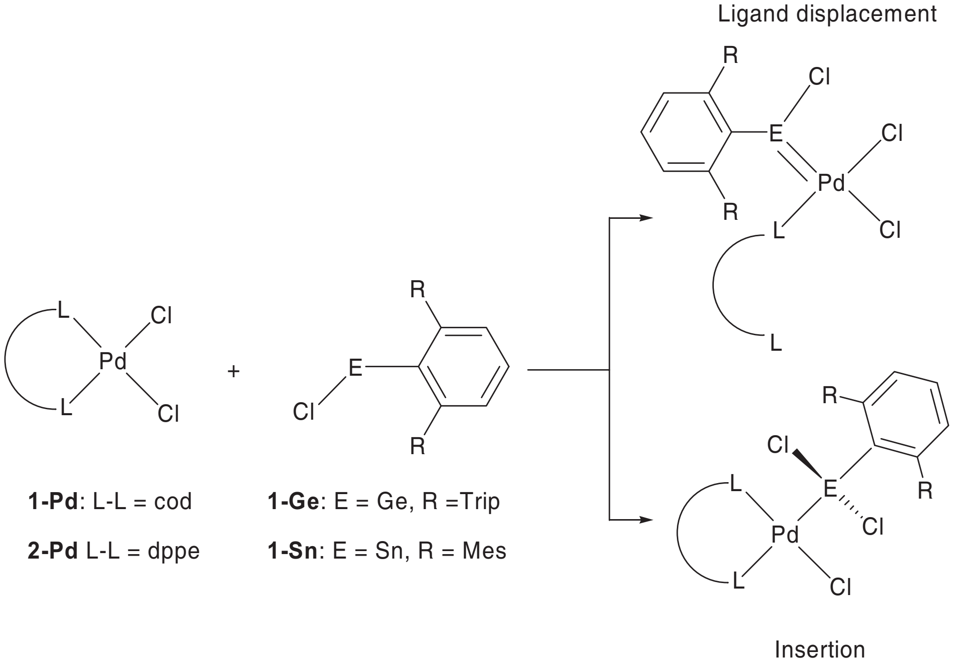

Scheme 2.1.1: Plausible reaction pathways of ylenes with square planar Pd(II) complexes. The insertion pathway is more likely, but competitive displacement of the ligand would yield precursors that could principally be used to access complexes with Pd≡E bonds (E = Ge,Sn).

[†] In the entire dissertation, for the sake of simplicity, the ylenes will be represented as monomeric entities, despite the fact that they can exist as dimers in the solid state (see introduction)

Dieses Werk ist copyrightgeschützt und darf in keiner Form vervielfältigt werden noch an Dritte weitergegeben werden.
Es gilt nur für den persönlichen Gebrauch.

2.1.1 Insertion of EClR (E = Ge, R = 2,6-Trip$_2$-C$_6$H$_3$; E = Sn, R = 2,6-Mes$_2$-C$_6$H$_3$) into Pd–Cl bonds of square planar Pd(II) complexes

Insertion reactions of $SnCl_2$ into group 10 metal halogen bonds has been known since the late 1960s, when van den Akker and Jellinek described a nickel stannyl complex.[105] Following this finding, Mason and Whimp obtained the first structurally characterised transition metal stannyl complex, $[Pd(SnCl_3)(PPh_3)(\eta^3\text{-allyl})]$.[106] Subsequently, a large array of such complexes have been synthesized[107] and structurally characterised[108] and are now ubiquitous in organometallic chemistry. Complexes containing stannyl ligands of the type $SnRX_2$ (R = aryl substituent, X = halogen), are far less common and in fact are unprecedented for palladium, and only a limited number of examples have been reported for platinum,[109] where tin usually bears a phenyl group. Furthermore, only one example was reported of a structurally characterised complex bearing a EX_2Ar ligand (M = Pd or Pt, E = Sn, Ge, X = halogen) in 2001 by Janzen *et al*. In this instance oxidative addition reactions of tin compounds over a square planar platinum centre occurred resulting in the formation of octahedral complexes of the type $[Pt(CH_3)_2Cl(SnPh_nCl_{3-n})(bpy)]$. Consequently, insertion of the stannylene **1-Sn** into Pd–Cl bonds, of complexes of the type $[PdCl_2(L\text{-}L)]$ could provide facile entry to hitherto unprecedented Pd complexes featuring stannyl ligands of this type.

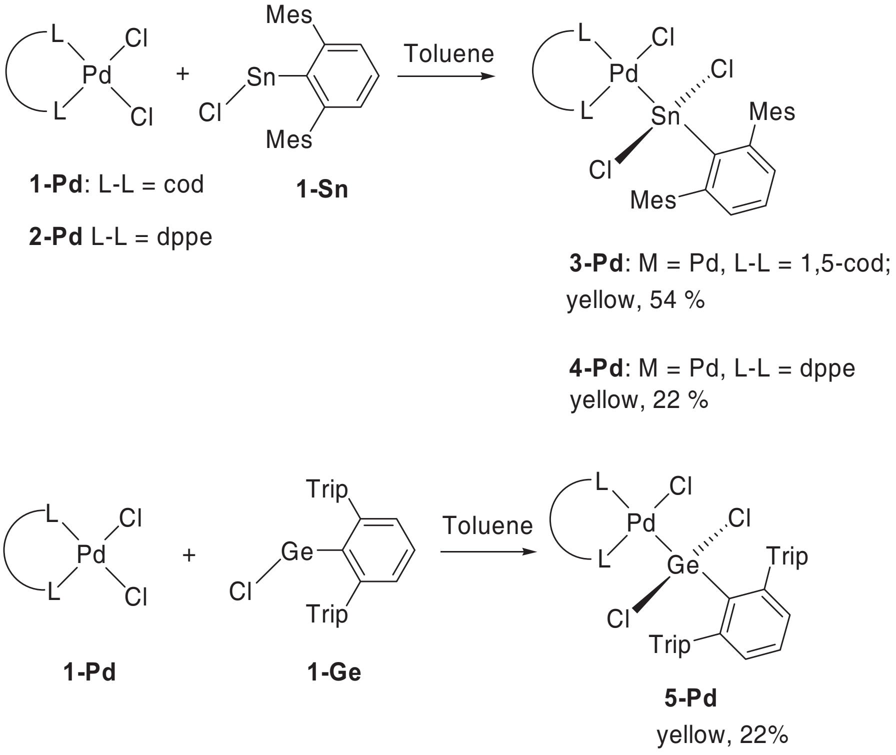

Scheme 2.1.2: Summary of reactions carried with square-planar Pd(II) precursors, and their reaction products with yields and colours.

Dieses Werk ist copyrightgeschützt und darf in keiner Form vervielfältigt werden noch an Dritte weitergegeben werden.
Es gilt nur für den persönlichen Gebrauch.

The insertion reactions (Scheme 2.1.2) were usually carried out by adding toluene to a 1:1 equimolar mixture of the metal dichloride and **1-Sn** at −78 °C. Concentrating the reaction solution and cooling prompted crystallisation, after which the products could be isolated by filtration as yellow solids in low to moderate yields. Complex **3-Pd** is well soluble in toluene, while complex **4-Pd** was only sparingly soluble in toluene, but soluble in CH_2Cl_2 and THF. Slow evaporation of a toluene solution of **3-Pd** in the glove-box yielded suitable crystals for X-ray diffraction analysis.

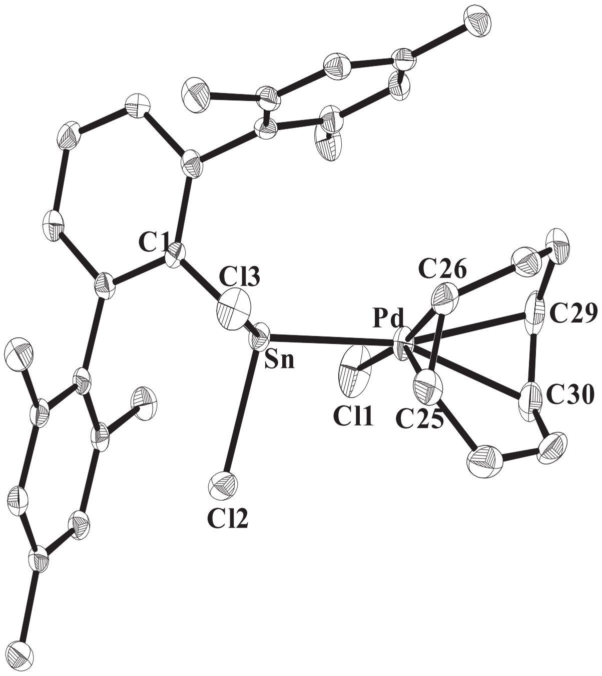

Figure 2.1.1: DIAMOND plot of the molecular structure of **3-Pd** in the solid state. H atoms are omitted for clarity, and the thermal ellipsoids are set at the 50 % probability level. Selected bond lengths [Å]: Pd–Sn 2.5214(2), Sn–C1 2.160(2), Sn–Cl2 2.3505(6), Sn–Cl3 2.4047(6), Pd–Cl1 2.3104(7), Pd–C25 2.177(2), Pd–C26 2.200(2), Pd–C29 2.369(2), Pd–C30 2.386(2). Selected bond angles [°] C1-Sn-Pd 128.74(6), Cl3-Sn-Cl2 93.84(2), C1-Sn-Cl2 113.70(6), Cl2-Sn-Pd 103.78(2), Cl3-Sn-Pd 109.12(2).

Complex **3-Pd** is the first example of a Pd complex bearing a stannyl ligand of the type SnX_2Ar, (Ar = an aromatic substituent, X = halogen). The Sn atom in **3-Pd** is four coordinate, and can be described as distorted tetrahedral: most of the angles around the Sn atom deviate from the ideal tetrahedral bond angles of 109.4° a consequence of the decreased s,p hybridisation in the Sn atom. The most interesting structural feature **3-Pd** is that the bond lengths between the Pd centre and the pairs of ligating carbon atoms of the cod ligand are slightly longer *trans* to the tin atom compared with *trans* to the Cl atom. This observation

Dieses Werk ist copyrightgeschützt und darf in keiner Form vervielfältigt werden noch an Dritte weitergegeben werden.
Es gilt nur für den persönlichen Gebrauch.

demonstrates that the stannyl ligand is exerting a larger *trans* influence than the Cl ligand, in accordance with what is observed in the case of $SnCl_3$ ligands.[110]

Complex **5-Pd**[111] was obtained in analogy from reaction of **1-Ge** with **1-Pd** in toluene. Crystals suitable for X-ray diffraction analysis where obtained by slow cooling of a hexane solution (Figure 2.1.2).

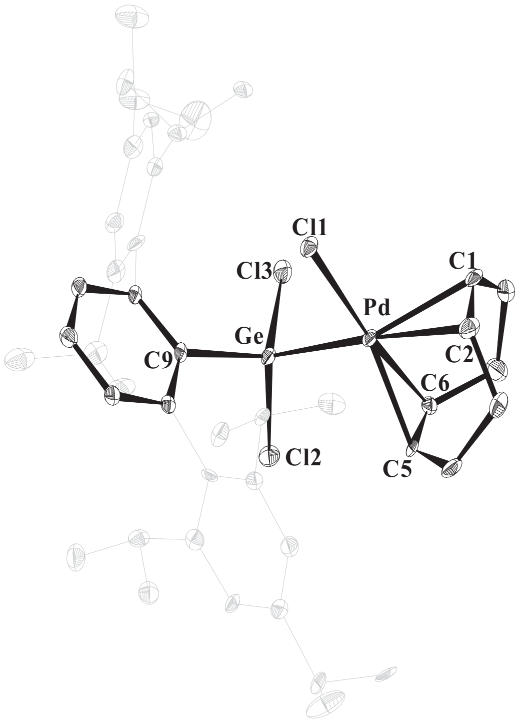

Figure 2.1.2: DIAMOND plot of the molecular structure of **5-Pd**, hydrogen atoms and the co-crystallised solvent molecules are omitted for clarity. Trip substituents are greyed out for clarity. Thermal ellipsoids are set at the 30% probability level. Selected bond lengths [Å]: Pd–Ge 2.371(2), Pd–C1 2.38(1), Pd–C2 2.39(1), Pd–C5 2.178(10), Pd–C6 2.23(1), Ge–C9 1.998(11), Pd–Cl 2.300(3), Ge–Cl3 2.175(3). Selected bond angles [°] C9-Ge-Cl(3) 114.3(3), C9-Ge-Cl(2) 107.6(3), Cl(3)-Ge-Cl(2) 98.3(1), C9-Ge-Pd 123.5(3), Cl(3)-Ge-Pd 97.35(10), Cl(2)-Ge-Pd 112.7(1).

Structurally characterised Pd complexes bearing a germyl ligand are remarkably rare, and in fact no examples exist to date where the germyl ligand possesses a halogen atom, making **5-Pd** the first in this class. In analogy with **3-Pd**, the Pd-C(cod) bonds *trans* to the Ge atom are longer than those *trans* to Cl in **5-Pd**. The Cl3-Ge-Cl2 bonding angle (98.3(1)°) is slightly larger than the corresponding angle in **3-Pd**, whereas the C9-Ge-Pd bonding angle in **5-Pd** (ca. 124)° is slightly smaller than the corresponding angle in **3-Pd**. The aryl group is considerably more bulky than the analogous mesityl ligand and the rings are again tilted

Dieses Werk ist copyrightgeschützt und darf in keiner Form vervielfältigt werden noch an Dritte weitergegeben werden.
Es gilt nur für den persönlichen Gebrauch.

nearly orthogonal to the central phenyl ring bound to the Ge atom. The C5-Pd-Ge bonding angle (ca. 98°) is slightly less than the corresponding angle in complex **3-Pd**. This implies that the cod ligand is tilted inwards slightly, more so than in **3-Pd**.

The ^{1}H NMR spectrum of complex **5-Pd** in toluene-d_8 solution at r.t. shows coalescent bands due to the restricted rotation of the *m*-terphenyl substituent. Also, non-coordinated COD is present in an approximate 1 : 13 ratio (non-coordinated / coordinated). These observations are suggestive that COD only loosely binds to the complex with the $C_6H_3Trip_2$ substituent exerting substantial steric pressure, consistent with an increased trans influence of the germal ligand.. At 223 K, a 2 : 2 : 4 : 2 : 2 pattern for the methyl groups and three septets in a 1 : 1 : 1 ratio for the methyne protons of the ^{i}Pr groups is observed, suggesting that the low temperature limit has been reached, with rotational locking of the *m*-terphenyl substituent.

Bright yellow crystals of **4-Pd**, suitable for X-ray diffraction analysis, were obtained by slow cooling to 6°C of a saturated solution in benzene-d_6 (Figure 2.1.3). This solvation results in a hexameric arrangement of metal complexes around seven included benzene molecules, which form channels through the crystal lattice.

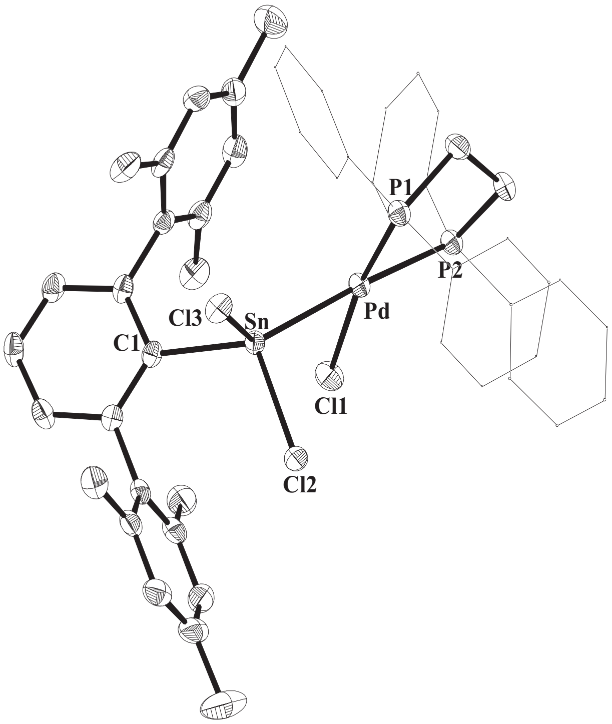

Figure 2.1.3: DIAMOND plot of the solid state molecular structure of **4-Pd·** 13/6 C_6D_6. H atoms and the co-crystallised benzene-d_6 molecules are omitted and dppe phenyl rings represented by lines, for clarity. Thermal ellipsoids are set at the 50 % probability level. Selected bond lengths [Å]: Pd–Sn 2.5769(3), Sn–C1 2.174(2), Pd–P1 2.2430(6), Pd–P2 2.3178, Sn–C1 2.174(2). Selected bond angles [°] C1-Sn-Cl(2) 113.70(6), C1-Sn-Cl(3) 102.04(6), Cl(2)-Sn-Cl(3) 93.84(2), C1-Sn-Pd 128.74(6), Cl(2)-Sn-Pd 103.78(2), Cl(3)-Sn-Pd 109.19(2).

Dieses Werk ist copyrightgeschützt und darf in keiner Form vervielfältigt werden noch an Dritte weitergegeben werden.
Es gilt nur für den persönlichen Gebrauch.

As before, the complex **4-Pd** exhibits metal to ligand bond length elongation, *trans* to the Sn atom as in all the other complexes discussed so far. The Sn atom, as with complex **3-Pd** exhibits a distorted tetrahedral geometry. The Cl-Sn-Cl bonding angle is also approximately 90° in **4-Pd**, as seen with **3-Pd** and the C1-Sn-Pd bonding angle is 128.74(6)° in **4-Pd**, identical to that observed in **3-Pd**. The distance between the Sn atom and the *ipso* carbon atom of the organic moiety in **4-Pd** is of similar length to that of **3-Pd**.

The ^{119}Sn{^{1}H} NMR spectrum of complex **4-Pd** reveals a resonance signal with a doublet of doublets multiplicity at δ = –57.1 ppm. This pattern results from *trans*oid and *cis*oid $^{2}J(^{119}\mathrm{Sn},\mathrm{P})$ couplings to each of the in equivalent phosphorus atoms of the dppe ligand of 3812 (*trans*) and 145 Hz (*cis*), respectively. The ^{31}P{^{1}H} NMR spectra of **4-Pd** mirror the results from the ^{119}Sn{^{1}H} NMR spectra and show two doublet resonance signals, the multiplicity of which can be explained in terms of $^{2}J(\mathrm{P},\mathrm{P})$ coupling, between the in equivalent phosphorus atoms of the dppe ligand ($^{2}J(\mathrm{P},\mathrm{P})$ = 26.7 Hz). Both ^{117}Sn and ^{119}Sn satellite signals are well resolved, readily identifiable and assignable for both doublet resonance signals (Figure 2.1.4) owing to their differing characteristic gyromagnetic ratios. The $^{2}J(\mathrm{P},\mathrm{Sn})$ *trans* coupling constants (to ^{119}Sn = 3813 Hz, to ^{117}Sn = 3643 Hz) are substantially larger in magnitude than those of the related complex *cis*-[Pd(dppe)Cl(SnClMe$_2$)] reported to exhibit a *trans* coupling constant to ^{119}Sn of 2445.1 Hz.[112] Furthermore the complexes [PdH(SnR$_3$)(R$'_2$PCH$_2$CH$_2$PR$'_2$)], R = Me, ^{n}Bu; R$'$= ^{i}Pr, ^{t}Bu, are shown to exhibit $^{2}J(\mathrm{P},^{119}\mathrm{Sn})$ *trans* coupling constants ranging in magnitude from 1571 – 1789 Hz,[113] while the complex *cis*-[PdCl(SnCl$_3$)(PPh$_3$)$_2$] is shown to exhibit a markedly higher *trans* $^{2}J(\mathrm{P},^{119}\mathrm{Sn})$ coupling constant of 4833 Hz.[114] This trend points on average to a dependence in the magnitude of this *trans* coupling constant on the number of Cl atoms on the stannyl ligand, and given the fact that complex **4-Pd** possesses two Cl atoms bonded to the Sn centre, its *trans* $^{2}J(\mathrm{P},^{119}\mathrm{Sn})$ coupling constant would be expected to fall between that of *cis*-[Pd(dppe)Cl(SnClMe$_2$)] and *cis*-[PdCl(SnCl$_3$)(PPh$_3$)$_2$], which is indeed the case.

Dieses Werk ist copyrightgeschützt und darf in keiner Form vervielfältigt werden noch an Dritte weitergegeben werden.
Es gilt nur für den persönlichen Gebrauch.

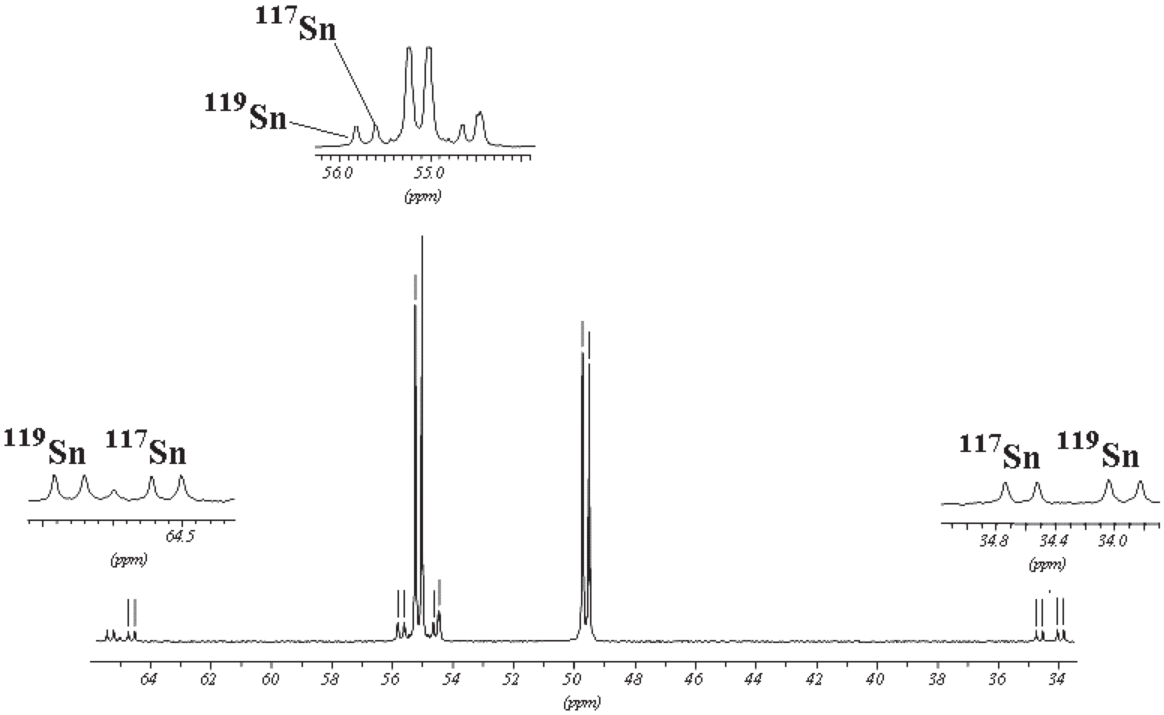

Figure 2.1.4: $^{31}P\{^1H\}$ NMR spectrum of complex **4-Pd** in CD_2Cl_2 at 303 K. The doublet multiplicity for each inequivalent P atom is visible, along with ^{117}Sn and ^{119}Sn satellite signals.

2.1.2 Insertion of ECl_2 (E = Ge, E = Sn) into Pd–Cl bonds of square planar Pd(II) complexes

For the sake of comparison, reactions of the complex **1-Pd** with $SnCl_2$ or $GeCl_2$(1,4-dioxane) were also carried out. The reaction of $SnCl_2$ with **1-Pd** in CH_2Cl_2 solution yielded the trichlorostannyl complex [PdCl($SnCl_3$)(cod)], **6-Pd**, in good yields. This compound has already been reported,[115] but was prepared *via* reaction of $SnCl_2$ with the complex [$PdCl_2(MeCN)_2$] and was not structurally characterised.

The analogous insertion of $GeCl_2$ into the Pd–Cl bond was also investigated by reacting $GeCl_2$·(1,4-dioxane) with **1-Pd** in the same solvent to yield the complex [PdCl($GeCl_3$)(cod)], **7-Pd** in good yield. Pd complexes bearing $GeCl_3$ as ligand are surprisingly rare,[116] making complex **7-Pd** another rare example in this class. As with **3-Pd** and **5-Pd**, 2 sets of olefinic proton resonance signals are observed as before due to a loss of symmetry resulting from the insertion: these signals are broad in the case of **6-Pd**, whereas in **7-Pd** they are sharp. The chemical shift of these olefinic resonance signals are virtually identical in **6-Pd** and **7-Pd**,

Dieses Werk ist copyrightgeschützt und darf in keiner Form vervielfältigt werden noch an Dritte weitergegeben werden.
Es gilt nur für den persönlichen Gebrauch.

suggesting no major shielding change in going from Sn to Ge**.** Bright yellow crystals suitable for X-ray crystallographic analyses for both **6-Pd** and **7-Pd** were obtained from CH_2Cl_2 solutions of the compounds with cooling to –30 °C. The X-ray diffraction analyses reveal the compounds to be isostructural in the solid state (Figure 2.1.5).

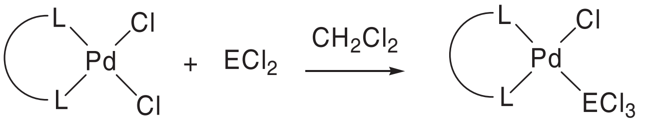

1-Pd

6-Pd: E = Sn, L-L = 1,5-cod

7-Pd: E = Ge, L-L = 1,5-cod

Scheme 2.1.3: Reaction of the precursor complex, **1-Pd** with ECl_2 (E = Sn, Ge‡) also yield selectively the insertion products, as with the analogous reactions with **1-Sn** or **1-Ge**.

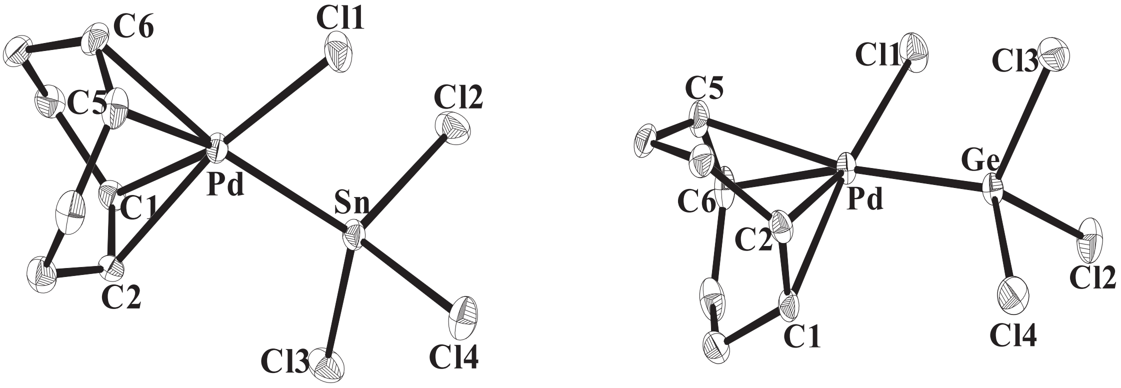

Figure 2.1.5: Solid state molecular structure of the iso-structural complexes **6-Pd** (left), and **7-Pd** (right) thermal ellipsoids are set at the 50% probability level and H atoms are omitted for clarity. Selected bond lengths [Å]: **6-Pd:** Pd–Cl1 2.3013(6), Pd–Sn 2.5158 (2), Pd–C1 2.194(2), Pd–C2 2.214(2), Pd–C6 2.352 (2), Pd–C5 2.302(2) Å and **7-Pd:** Pd–C11 2.290(8), Pd–Ge 2.355(4), Pd–C1 2.219(3), Pd–C2 2.201(3), Pd–C5 2.357(3), Pd–C6 2.315(2). Selected bond angles [°] **6-Pd:** Cl(2)-Sn-Cl(3) 98.32(2), Cl(2)-Sn-Cl(4) 99.51(2), Cl(4)-Sn-Cl(3) 101.43(2), Cl(2)-Sn-Pd 117.18(2), Cl(4)-Sn-Pd 118.60(2), Cl(3)-Sn-Pd 118.16(2); **7-Pd:** Cl(3)-Ge-Cl(2) 103.09(3), Cl(3)-Ge-Cl(4) 101.27(3), Cl(2)-Ge-Cl(4) 101.61(3), Cl(3)-Ge-Pd 115.03(3), Cl(2)-Ge-Pd 116.55(2), Cl(4)-Ge-Pd 117.00(2).

The coordination sphere around the tin atom in complex **6-Pd** deviates slightly from an ideal tetrahedron, with the Cl2-Sn-Pd bonding angle at 117.2°; Cl3-Sn-Pd = 118.2° and Cl4-Sn-Pd

---

[‡] For germanium, $GeCl_2$(1,4-dioxane) was used.

Dieses Werk ist copyrightgeschützt und darf in keiner Form vervielfältigt werden noch an Dritte weitergegeben werden.
Es gilt nur für den persönlichen Gebrauch.

= 118.6°. The distances between the Pd and C atoms of the cod ligand *trans* to the stannyl ligand is slightly longer than those *trans* to the chlorine atom, in analogy with all the above mentioned complexes (Figure 2.1.5). The structure of compound **6-Pd** compared with that of the related **3-Pd** shows little deviation in the Pd–Sn bond length: Pd–Sn = 2.5214(2) Å for **3-Pd**, compared to Pd–Sn = 2.5158(2) Å for **6-Pd**. This comparison indicates that by changing the ligands on the tin atom (from two chlorine atoms and an organic residue (**3-Pd**) to three chlorine atoms (**6-Pd**) does not significantly affect the Pd–Sn bond length.

No structurally characterised Pd complexes bearing a $GeCl_3$ ligand exist making complex **7-Pd** the first example. The Pd–Ge bond length of 2.355(4) Å is *ca.* 16 pm smaller in magnitude than that of the corresponding Pd–Sn bond length in complex **6-Pd**, in close approximation with the decreased covalent radius of Ge 1.20(4) Å vs Sn 1.39(3) Å.

The $^{119}Sn\{^{1}H\}$ NMR shift of **6-Pd** at $\delta = -311$ ppm is shifted 100 ppm up-field compared to **3-Pd** (although the NMR of **6-Pd** was recorded in CD_2Cl_2, whereas **3-Pd** was recorded in C_6D_6).

Far infrared (FIR) studies were also conducted on selected insertion products in polyethylene pellets. In complex **6-Pd**, a stretching vibration appears at 334 cm^{-1}, with shoulders at 355 and 303 cm^{-1} respectively. In **3-Pd** a similar band at 339 $cm^{-1}$is visible, with one side shoulder at 328 cm^{-1}. The close proximity of these two stretching vibrations (334 and 339 cm^{-1}) suggests that they correspond to that of ν(Sn–Cl). In complex **7-Pd**, a stretching vibration, almost identical to that observed in **6-Pd**, but shifted to higher wave numbers is visible at 375 cm^{-1} bearing shoulder peaks at 390 and 345 cm^{-1}. These results are in agreement with those of Crociani *et al.* who reported IR data for a series of Pd trichlorogermyl and trichlorostannyl complexes in 1970.[116] In addition, the shift to higher wave numbers in complex **7-Pd** compared to **3-Pd** and **6-Pd** is also in accordance with what is expected as Ge–Cl bonds are stronger than Sn–Cl (Figure 2.1.6).[117]

Dieses Werk ist copyrightgeschützt und darf in keiner Form vervielfältigt werden noch an Dritte weitergegeben werden.
Es gilt nur für den persönlichen Gebrauch.

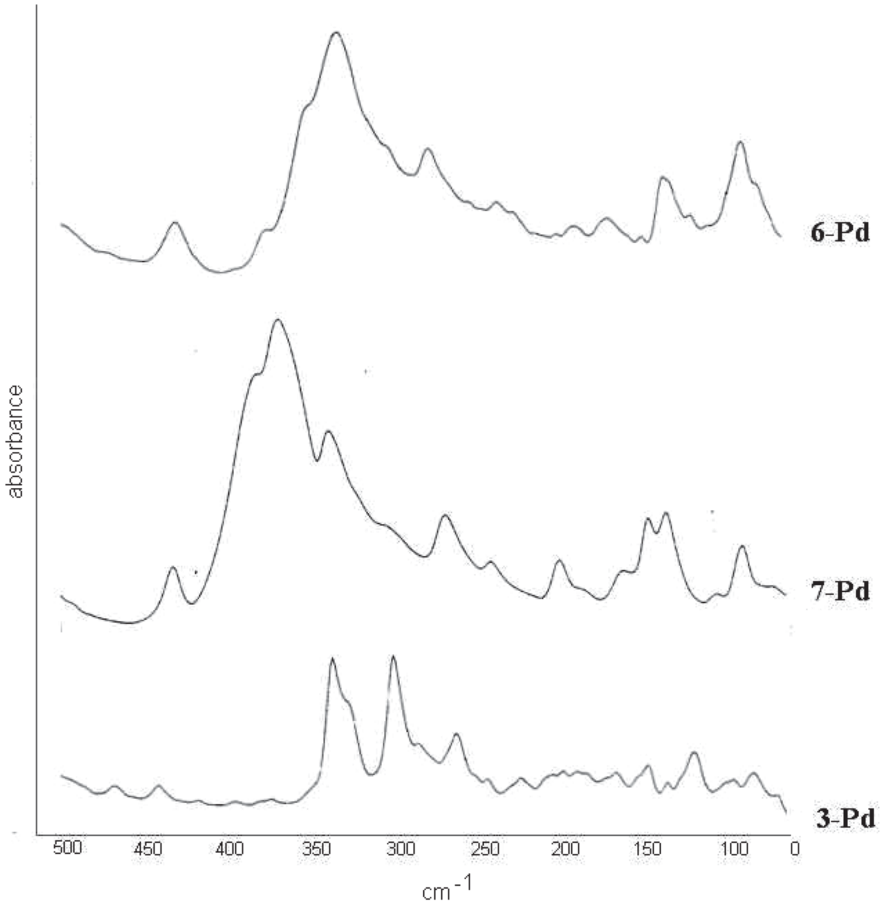

Figure 2.1.6: Stacked FIR spectra of complex **3-Pd**, **6-Pd** and **7-Pd** in the range (500cm^{-1} – 0 cm^{-1}) (Absorbance units omitted).

Table 2.1.1 shows a summary of ^{119}Sn{^{1}H} NMR shifts of all complexes reported here.

Complex, solvent	δ ^{119}Sn/ ppm
3-Pd, C_6D_6	–211.5
4-Pd, CD_2Cl_2	– 57.1
6-Pd, CD_2Cl_2	–310.9

Table 2.1.1: Summary of ^{119}Sn{^{1}H} NMR shifts of the insertion complexes **3-Pd**, **4-Pd** and **6-Pd** referenced to $SnMe_4$.

Table 2.1.2 shows a summary of bond lengths, highlighting the *trans* influence of the group 14 ligand on the Pd-L bond distance, based on the solid state molecular structures. In all cases the Pd-L bond *trans* to the group 14 ligand is longest.

Dieses Werk ist copyrightgeschützt und darf in keiner Form vervielfältigt werden noch an Dritte weitergegeben werden.
Es gilt nur für den persönlichen Gebrauch.

Complex E = Sn or Ge	D(M-L$_{\text{trans-E}}$) / Å	D(M-L$_{\text{trans-Cl}}$) / Å
3-Pd[a]	2.378	2.189
5-Pd[a]	2.39	2.21
4-Pd	2.317(8)	2.174(2)
6-Pd[a]	2.327	2.204
7-Pd[a]	2.336	2.208

Table 2.1.2: Summary of selected bond lengths (in Å) between metal and coordinated bidentate ligand. [a]Values reported are the average of the bond distances between the Pd centre and the coordinated C atoms of the cod ligand. (standard deviations of these averages omitted).

2.1.3 Reactivity of [SnCl(η^5-C_5Me_5)] 2-Sn with 1-Pd: Cp* transfer to Pd

In order to further study the generality of this ylene insertion chemistry, we were also interested in the reactivity of the stannylene, [SnCl(η^5-C_5Me_5)][118] **2-Sn** with the complex **1-Pd**. Insertion does *not* occur in this instance as with the stannylene **1-Sn**, under similar reaction conditions, and instead formation of the red-brown, dichloromethane soluble, ionic compound [Pd(η^5-C_5Me_5)(cod)][$SnCl_3$] **8-Pd** is observed. In this case **2-Sn** acts as a "Cp* transfer reagent" to the Pd centre, resulting in the cation [Pd(η^5-C_5Me_5)(cod)] with concomitant formation of the $SnCl_3$ anion by chloride abstraction at the Pd centre. This difference in reactivity between **1-Sn** and **2-Sn** is likely a result of changing the purely σ-bonded *m*-terphenyl substituent in **1-Sn**, to a π–bonded η^5 coordinated Cp* ring in **2-Sn**, which can readily form an η coordination to the Pd(II) centre, whilst the *m*-terphenyl substituent in **1-Sn** cannot. Gusev *et al*.[119] has reported a similar ionic complex, obtained by reaction of [$PdCl_2$(η^4-C_5Me_5H)] with $AgBF_4$ in the presence of free 1,5-cyclooctadiene, resulting in the ionic complex [Pd(η^5-C_5Me_5)(cod)][BF_4].

Dieses Werk ist copyrightgeschützt und darf in keiner Form vervielfältigt werden noch an Dritte weitergegeben werden.
Es gilt nur für den persönlichen Gebrauch.

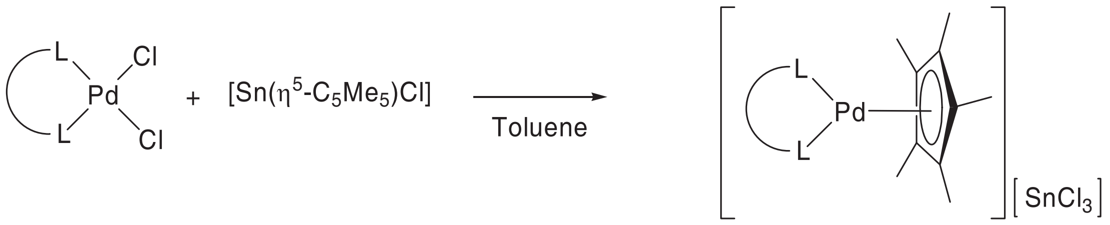

1-Pd **2-Sn** **8-Pd**: L-L = 1,5-cod

Scheme 2.1.4: Cp* transfer reaction from the stannylene **2-Sn** to the square planar Pd(II) complex **1-Pd** with concomitant chloride abstraction resulting in the ionic complex **8-Pd**.

Despite recrystallisation and thorough washing with toluene, it was not possible to obtain **8-Pd** in pure form, and a persistent impurity which could not be removed (ca 10 %). Despite this, the constitution of **8-Pd** was confirmed on the basis of Maldi-tof MS, where a peak at m/z = 349.1 was observed with the expected isotope distribution pattern for the cation [Pd(η^5-C_5Me_5)(cod)]. Additionally, ^{1}H NMR spectroscopy in CD_2Cl_2 further confirmed the identity of **8-Pd** with resonance signals[§] at δ = 1.92 ppm (s) (corresponding to the equivalent CH_3 groups of the coordinated Cp* ring); δ = 2.56 – 2.70 ppm (m) (corresponding to the CH_2 groups of the coordinated cod ligand) and δ = 4.88 – 4.99 ppm (m) (corresponding to the C*H*=C*H* groups of the coordinated cod ligand). These values are comparable to those of [Pd(η^5-C_5Me_5)(cod)][BF_4].[119]

The existence of $SnCl_3^-$ as the counter anion was confirmed by ^{119}Sn{^{1}H} NMR spectroscopy (Figure 2.1.7). The chemical shift of the resonance signal (δ = -50.6 ppm) is typical of $SnCl_3^-$ which is also solvent dependent: Objartel *et al.* reported a chemical shift of δ = -67.5 ppm[120] which is also close to that of [M($SnCl_3$)(CN^{t}Bu)$_3$(PMe_3)$_3$] (M = Mo, W) reported by Fernandez-Trujillo *et al.* [121]

[§] Excluding the impurity signals, which occur at δ = 1.99 (s), 2.07 (s), 2.34 (s) in a ratio 4:1:1 relative to the Cp* signal integrating to 15 for the equivalent methyl groups.

Dieses Werk ist copyrightgeschützt und darf in keiner Form vervielfältigt werden noch an Dritte weitergegeben werden.
Es gilt nur für den persönlichen Gebrauch.

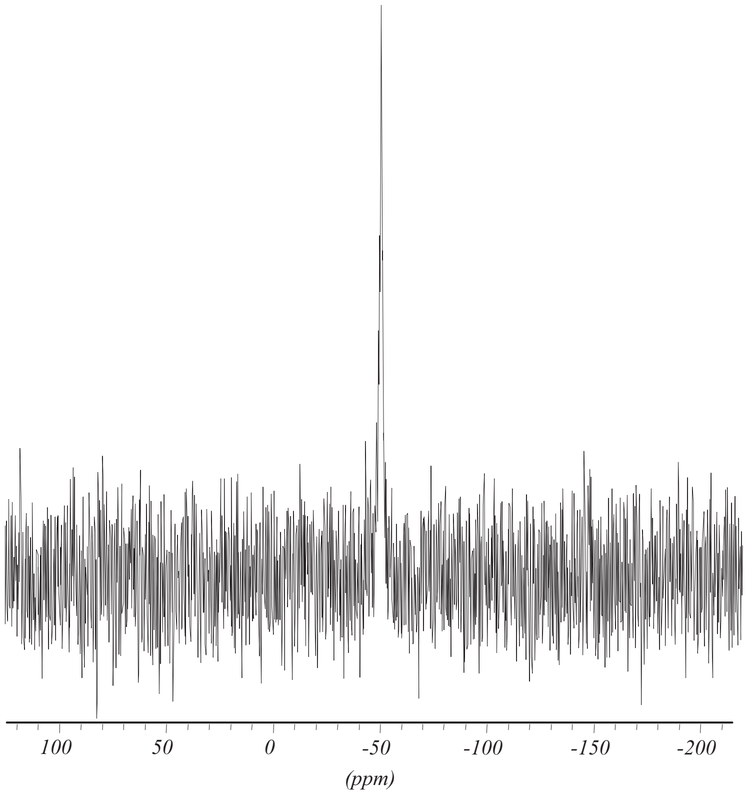

Figure **2.1.7:** ^{119}Sn{^{1}H} NMR spectrum of **8-Pd** in CD_2Cl_2.

Attempts at growing crystals, suitable for X-ray diffraction analysis of **8-Pd** were not successful, however, reaction of **8-Pd** with $TlPF_6$ in CD_2Cl_2 at room temperature resulted in the derivative [Pd(η^5-C_5Me_5)(cod)][X] **8-Pd-b**, where the identity of X could not unambiguously be established. The ^{1}H NMR spectrum of the emerging ionic complex **8-Pd-b** was identical to that of **8-Pd**, although the unidentifiable impurity signals were not visible (Figure 2.1.8).

Dieses Werk ist copyrightgeschützt und darf in keiner Form vervielfältigt werden noch an Dritte weitergegeben werden.
Es gilt nur für den persönlichen Gebrauch.

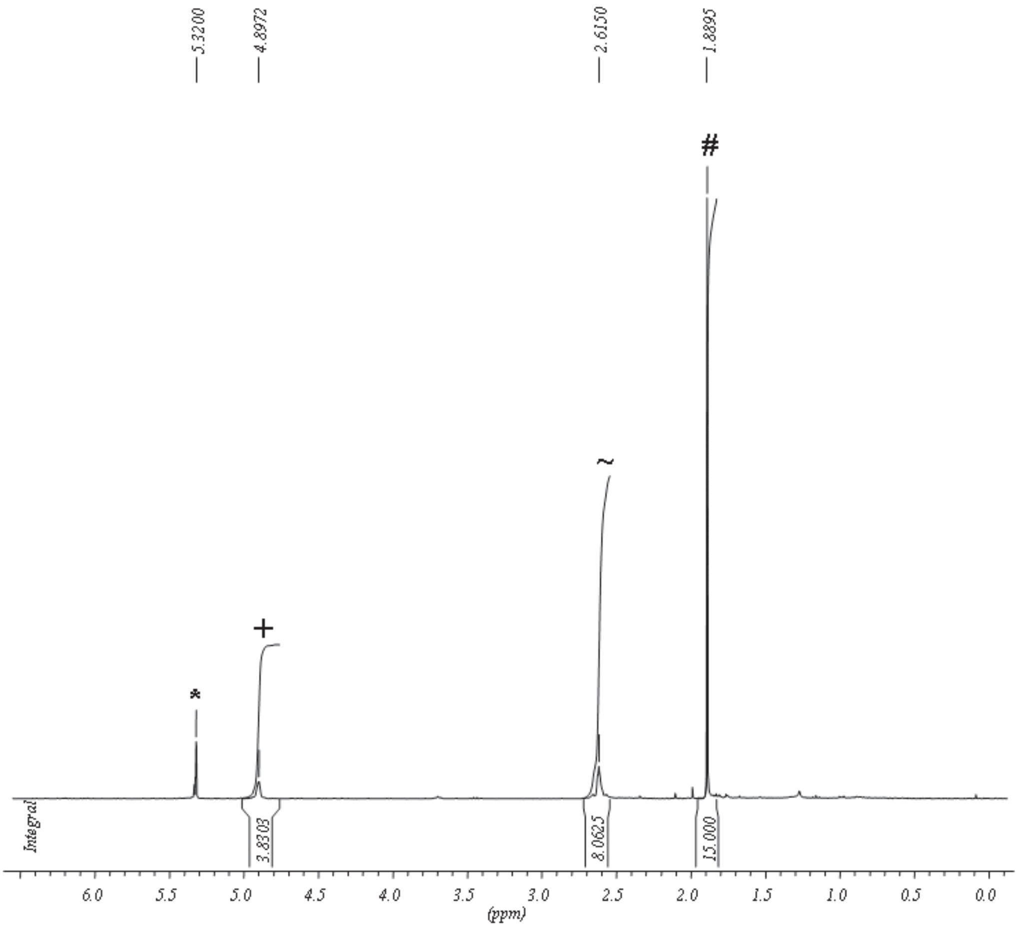

Figure 2.1.8: ^{1}H NMR spectrum of **8-Pd-b** in CD_2Cl_2 at 303 K. # = $C_5(CH_3)_5$, ~ = 4 × CH_2, + = 2 × $CH_2{=}CH_2$, * = residual solvent peak.

Crystals of **8-Pd-b** suitable for X-ray diffraction analysis were grown from CH_2Cl_2, and indeed confirmed the structure of the cation (Figure 2.1.9). The anion on the other hand could not unambiguously be solved, and on the basis of electron density could be either one of two cyclic counter anions: I or II shown in Figure 2.1.9. The discussion following is limited to the solved structure with I as counter anion, although there are no substantial differences in the metric parameters of the cation, in comparing the two structure solutions.

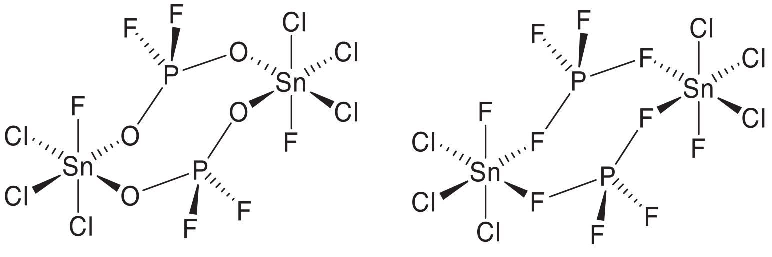

I

II

Figure 2.1.9: Two possible counter anions for the **8-Pd-b** on the basis of X-ray diffraction analysis.

Dieses Werk ist copyrightgeschützt und darf in keiner Form vervielfältigt werden noch an Dritte weitergegeben werden.
Es gilt nur für den persönlichen Gebrauch.

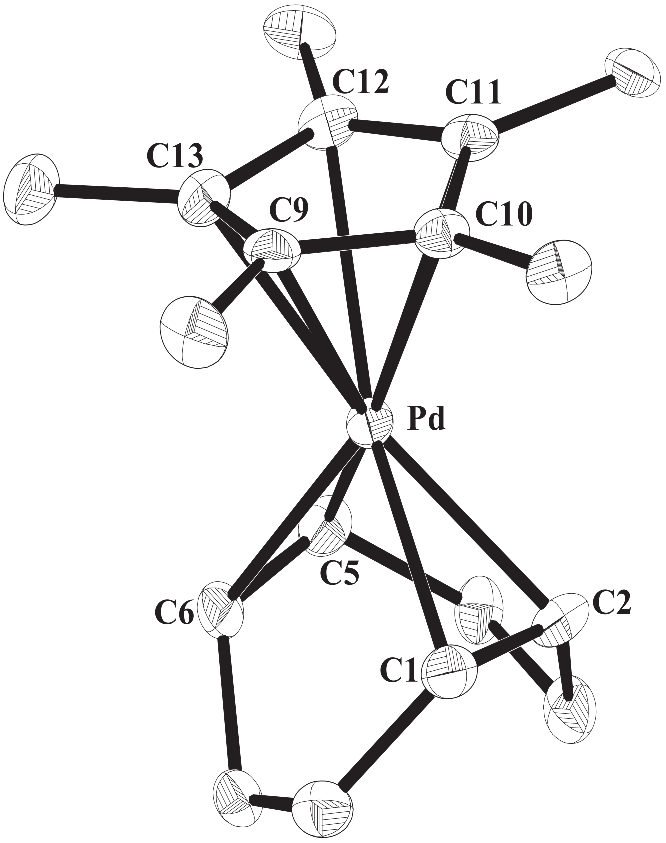

Figure 2.1.10: DIAMOND plot of the cation in **8-Pd-b·CH_2Cl_2**. Included CH_2Cl_2 molecules and H atoms omitted for clarity. Thermal ellipsoids set at 30 % probability. Selected bond lengths [Å]: Pd–C1 2.175(10), Pd–C2 2.188(10), Pd–C5 2.176(9), Pd–C6 2.208(9), Pd–C9 2.294(10), Pd–C10 2.196(9), Pd–C11 2.315(10), Pd–C12 2.303(9), Pd–C13 2.256(10), C9–C10 1.46(2), C10–C11 1.48(2), C11–C12 1.38(2), C12–C13 1.48(2), C13–C9 1.38(2), C1–C2 1.39(2), C5–C6 1.39(2).

Although transition metal complexes mutually bearing cyclopentadienyl ligands, along with two coordinated alkene ligands are ubiquitous in organometallic chemistry, the cation in **8-Pd-b** is the first structurally characterised example for Pd. Furthermore, structural reports of Pd complexes bearing Cp^* ligands are relatively rare, and **8-Pd-b** is only the fourth example.[122] The bond lengths between the Pd atom and the C atoms of the Cp^* nucleus vary in the range 2.196(9) – 2.315(10) Å, slightly perturbing the planarity of the ring, and indicative of asymmetric coordination of the Cp^* ring to the Pd centre. This is further evidenced by the fact that the C–C bond lengths in the ring are not identical, and there are two short bond lengths (1.38(2) Å), and three longer ones (1.46(2) – 1.48(2) Å), which also point to more double bond character in the C9–C13 and C11–C12 bonds respectively. This implies, at least in the solid state, the Cp^* ring cannot be considered strictly to be in η^5 coordination mode to Pd, but rather of lower hapticity. The bond lengths of the

Dieses Werk ist copyrightgeschützt und darf in keiner Form vervielfältigt werden noch an Dritte weitergegeben werden.
Es gilt nur für den persönlichen Gebrauch.

coordinating alkene carbon atoms C1–C2 and C5–C6 are identical at 1.39(2) Å and comparable to the analogous C–C bond lengths in **1-Pd**, previously determined by Benchekroun and Herpin at 1.384 and 1.385 Å respectively.[123] The alkene bond lengths are elongated with respect to the typical C=C bond length (1.34 Å), as an expected consequence of coordination.

Dieses Werk ist copyrightgeschützt und darf in keiner Form vervielfältigt werden noch an Dritte weitergegeben werden.
Es gilt nur für den persönlichen Gebrauch.

2.2 Reactivity of $[ECl R]_2$ (E = Ge, R = 2,6-Trip$_2$-C$_6$H$_3$; E = Sn, R = 2,6-Mes$_2$-C$_6$H$_3$) towards a d^8 configured group 9 complex: $[Rh(\eta^2\text{-}C_2H_4)_2Cl]_2$: tetrel insertion into the Rh–Cl bond and C_2H_4 elimination

Having explored the reactivity of the stannylene **1-Sn** and the germylene **1-Ge** towards square planar Pd(II) complexes which yielded interesting, but stable insertion products, as opposed to the ultimate target which was metal-tetrel multiply (particularly triply) bonded complexes, we decided next to turn our attention to the reactivity of **1-Sn** and **1-Ge** towards a Rh complex bearing ligand(s) capable of elimination, such as C_2H_4, and that are non-chelating as in the case of the Pd(II) complexes.

In this context, we focused on the easily accessible Rh dimer complex, $[RhCl(\eta^2\text{-}C_2H_4)_2]_2$ **1-Rh**, where C_2H_4 elimination at the Rh centre in **1-Rh** is reported to occur readily for phosphanes, acetonitrile, pyridine, and 1,5-cyclooctadiene.[124] With this in mind, we envisaged that analogous reactions of **1-Rh** with **1-Sn** and **1-Ge** could by C_2H_4 elimination result in halo-ylidene complexes after which suitable Cl abstraction reactions, could result in ylidyne complexes of Rh. The envisaged halo-ylidene complexes could additionally be stabilised by arene-coordination of the peripheral aromatic substituents to Rh, to satisfy its electronic requirements (scheme 2.2.1).

Dieses Werk ist copyrightgeschützt und darf in keiner Form vervielfältigt werden noch an Dritte weitergegeben werden.
Es gilt nur für den persönlichen Gebrauch.

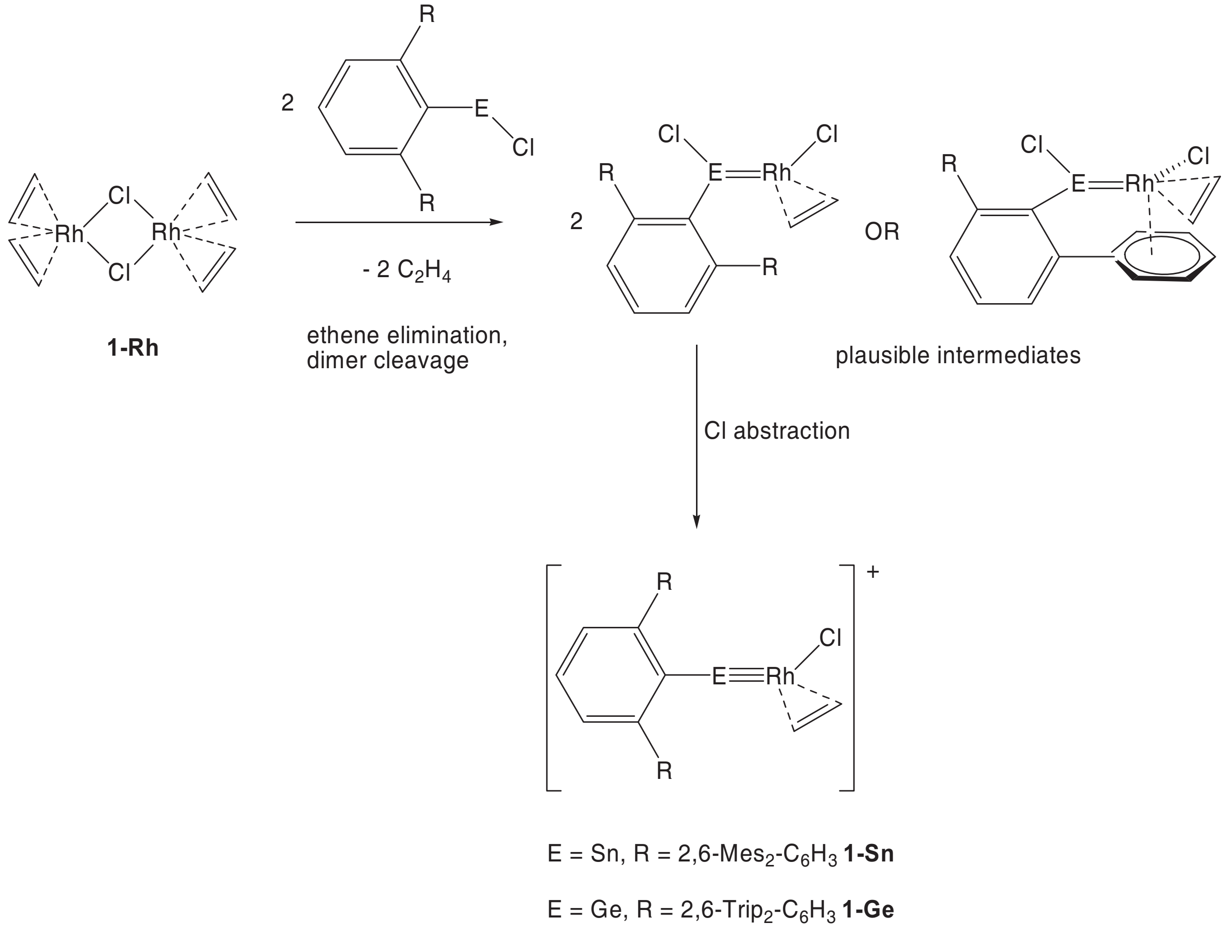

Scheme 2.2.1: Our envisaged strategy to access germylidyne and stannylidyne complexes of rhodium.

Reaction of **1-Rh** with 2 molar equivalents **1-Sn** or **1-Ge** under similar reaction conditions (stirring in toluene at room temperature) did not result in the formation of the desired halo-ylidene complex highlighted in Scheme 2.2.1. Instead, neutral stannyl and germyl η-arene stabilised complexes of Rh(I) resulted from *insertion* of the ylene into the Rh–Cl bond with dimer cleavage, *along with* concomitant elimination of 1 eq. ethene at each Rh centre. The ethene elimination is the result of one of the peripheral substituents on the *m*-terphenyl ligand (Mes in **1-Sn** or Trip in **1-Ge**) coordinating to the Rh centre in an η fashion, consequently resulting in $[\{SnCl_2(2\text{-}Mes\text{-}C_6H_3)(\eta^6\text{-}Mes)\}Rh(C_2H_4)]$ (**2-Rh**) and the closely related Ge analogue $[\{GeCl_2(2\text{-}Trip\text{-}C_6H_3)(\eta^6\text{-}Trip)\}Rh(C_2H_4)]$ (**3-Rh**) respectively (Scheme 2.2.2).

Dieses Werk ist copyrightgeschützt und darf in keiner Form vervielfältigt werden noch an Dritte weitergegeben werden.
Es gilt nur für den persönlichen Gebrauch.

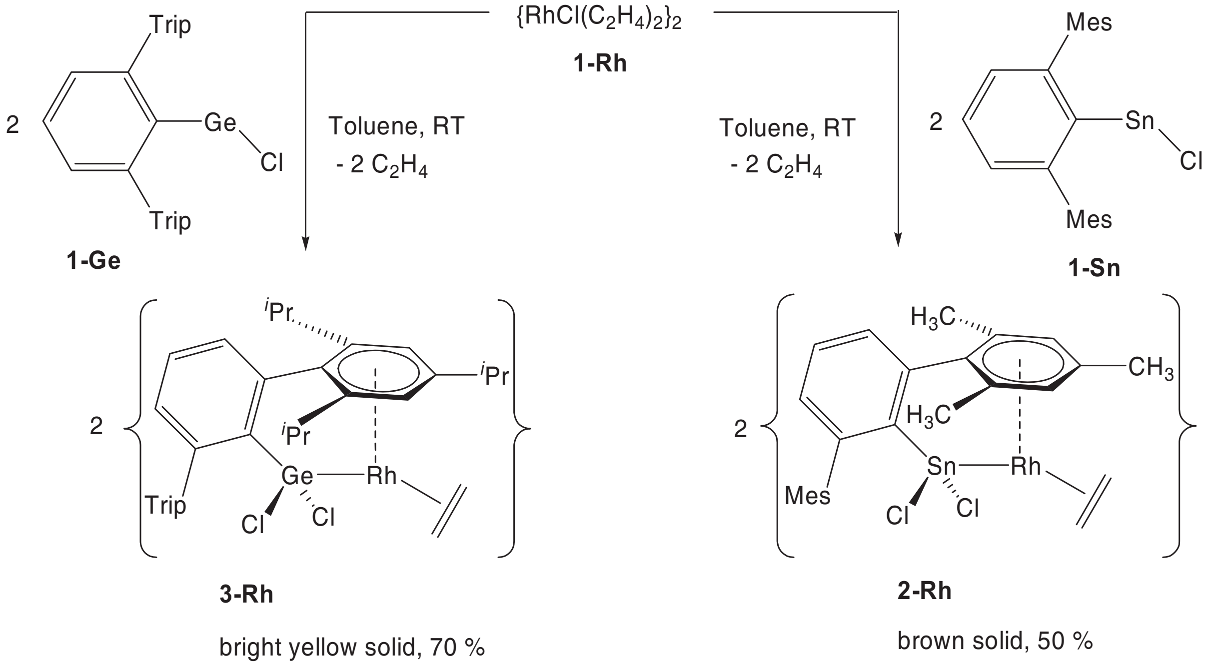

Scheme 2.2.2: Formation of the neutral η–arene complexes **2-Rh** and **3-Rh**, from **1-Rh**.

Although arene complexes of rhodium[125] are common in organometallic chemistry, they are for the most part typically cationic.[126] In contrast, rhodium arene complexes containing stannyl ligands are remarkable rare[127] and those bearing germyl ligands, have not been reported to date. This makes compound **2-Rh** another rare example in this class, and **3-Rh** the first example of an arene rhodium complex bearing a germyl ligand. Complexes containing Rh-Ge bonds are in themselves extremely rare[128] and to date only six solid state X-ray structure determinations have been carried out nearly all of which are Ge-Rh cluster complexes.[129]

Compound **2-Rh** is a brown, only moderately air-sensitive solid while **3-Rh** is bright yellow, and also only moderately air sensitive and can be handled for short periods in air. Both compounds are soluble in toluene, and **3-Rh** is partially soluble in pentane, due to the increased lipophilicity induced by the presence of the ^{i}Pr substituents. Reaction of the dimer, $[RhCl(\eta^2\text{-}C_2H_4)_2]_2$ with only 1 molar equivalent stannylene or germylene yields the same products in both cases, but in lower yields. The synthesis of **2-Rh** results in a significant amount of a toluene insoluble olive-green side product, which appears to be air stable, and only poorly soluble in dichloromethane and chloroform.[130] The identity of this product could not be established, but it is conceivably a product resulting from a competitive redox reaction between Sn and Rh. This is conceivable, since attempts at preparing analogous Pb

Dieses Werk ist copyrightgeschützt und darf in keiner Form vervielfältigt werden noch an Dritte weitergegeben werden.
Es gilt nur für den persönlichen Gebrauch.

analogues were unsuccessful: reaction of the plumbylene [PbBr(2,6-Trip$_2$-C$_6$H$_3$)], **1-Pb** with **1-Rh** in a 2: 1 ratio only yielded black, toluene insoluble material, an indication that on descending from the germylene to the plumbylene, redox chemistry seems to play a more dominant role in the reactivity towards **1-Rh**.

For both complexes **2-Rh** and **3-Rh** crystals suitable for X-ray diffraction were grown and the molecular structures determined in the solid state (**2-Rh:** from a concentrated C$_6$D$_6$ solution with slow evaporation at room temperature in the glove-box, and **3-Rh:** from a concentrated toluene solution at – 30 °C).

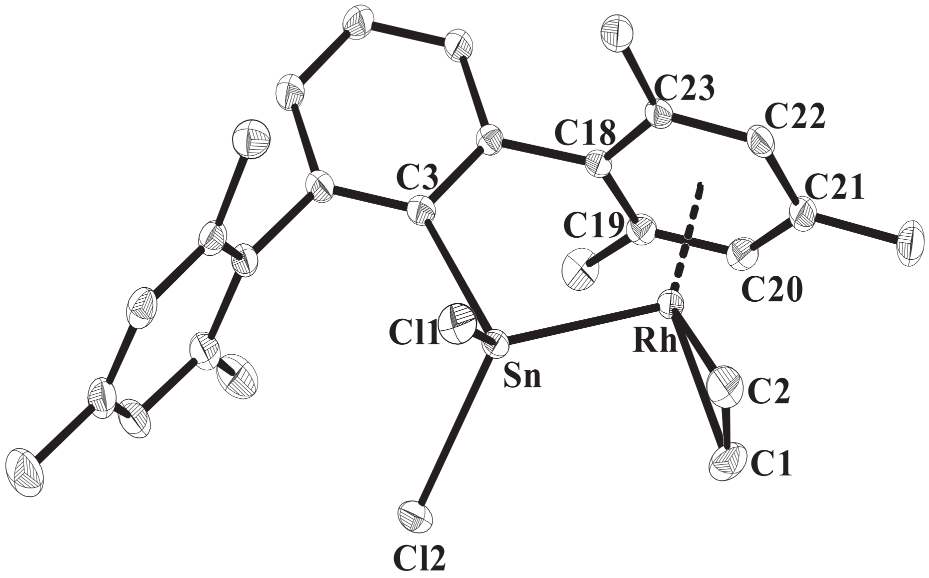

Figure 2.2.1: DIAMOND plot of the molecular structure of compound **2-Rh** in the solid state determined by X-ray diffraction analysis (thermal ellipsoids are set at the 50 % probability level and H atoms omitted for clarity).

Dieses Werk ist copyrightgeschützt und darf in keiner Form vervielfältigt werden noch an Dritte weitergegeben werden.
Es gilt nur für den persönlichen Gebrauch.

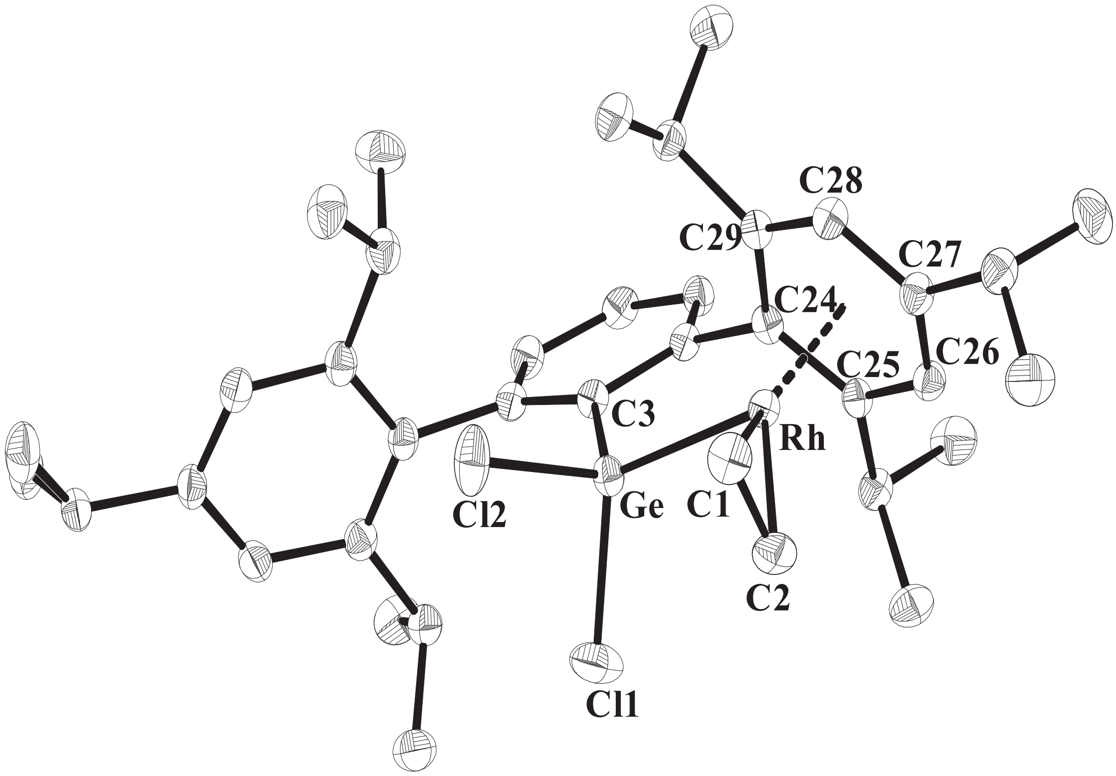

Figure 2.2.2: DIAMOND plot of the molecular structure of compound **3-Rh·C_7H_8** in the solid state determined by X-ray diffraction analysis (thermal ellipsoids are set at the 50 % probability level and H atoms and included toluene are omitted for clarity).

(a) Bond lengths (Å)			
2-Rh		**3-Rh**	
Rh–Sn	2.4920(2)	Rh–Ge	2.326(2)
Sn–Cl(1)	2.3818(5)	Ge–Cl(1)	2.203(1)
Sn–Cl(2)	2.3738(5)	Ge–Cl(2)	2.196 (2)
Rh–C(18)	2.208 (2)	Rh–C(24)	2.171(2)
Rh–C(19)	2.318(2)	Rh–C(25)	2.265(2)
Rh–C(20)	2.336(2)	Rh–C(26)	2.347(3)
Rh–C(21)	2.317(2)	Rh–C(27)	2.387(3)
Rh–C(22)	2.300(2)	Rh–C(28)	2.346(2)
Rh–C(23)	2.284(2)	Rh–C(29)	2.286(2)
(b) Bond angles (°)			
Rh–Sn–C(3)	100.92(5)	Rh–Ge–C(3)	105.52(7)
Cl(1)–Sn–Rh	115.02(2)	Cl(1)–Ge–Rh	117.80(4)
Cl(2)–Sn–Rh	124.17(1)	Cl(2)–Ge–Rh	117.67(5)
Sn–Rh–C(18)	80.62(5)	Ge–Rh–C(24)	80.78(7)

Table 2.2.1: Selected bond lengths and bond angles in the complexes **2-Rh** and **3-Rh**.

Dieses Werk ist copyrightgeschützt und darf in keiner Form vervielfältigt werden noch an Dritte weitergegeben werden.
Es gilt nur für den persönlichen Gebrauch.

A comparison of the Rh–E (E = Sn (**2-Rh**), Ge (**3-Rh**)) bond lengths reveal a shorter bond in compound **3-Rh**, in accordance with the decreased covalent radius of the main group element. In compound **2-Rh** the Rh–Sn bond length is 2.4920(2) Å, shorter than those reported in the literature which range from 2.554(1) Å to 2.5833(5) Å for known η^6 arene Rh complexes bearing stannyl ligands. In compound **3-Rh** the Rh–Ge bond length of 2.326(2) Å is the shortest so far reported being markedly shorter that of the compound reported by Dysard and Tilley at 2.488(2) Å,[128] to the examples by Veith *et al.* at 2.3366(9) Å[129] and the cluster compounds of Adams *et al*.[129] This observation might be attributed to the fact that in both cases the inserted ylene acts as a chelating ligand, which might account for this bond length contraction.

The distance from Rh to the centre of gravity of the coordinated ring is comparable in compounds **2-Rh** and **3-Rh** at 1.8023(8) Å and 1.811(2) Å respectively, indicating no dramatic influence on changing from a germyl to a stannyl ligand on degree of coordination. Moreover in compound **2-Rh** the bond lengths between Rh and the carbon atoms constituting the coordinated aromatic ring vary between 2.208(2) and 2.336(2) Å, and in **3-Rh** these bond lengths vary between 2.171(2) and 2.387(3) Å. These variable bond lengths result in a boat configuration, with slight deviations in the planarity of the coordinated rings, a typical phenomenon of η^6– arene coordinations.[127] In both cases, the C^1 atom of the coordinating ring is bound more strongly to the Rh centre, due to ligand strain of the chelating stannyl or germyl ligand.[131] The main group element atom in both **2-Rh** and **3-Rh** is four coordinate, and can be considered to be in oxidation state +II. The Rh-Ge-C(3) bond angle in **3-Rh** is slightly larger in comparison to the analogous bonding angle Rh-Sn-C(3) in **2-Rh**.

^{1}H NMR spectroscopy at room temperature in C_6D_6 for both **2-Rh** and **3-Rh** support the findings of the solid state structure. In both cases, several sets of resonances, corresponding to the in equivalent alkyl substituents (CH_3 in **2-Rh**; ^{i}Pr in **3-Rh**) on the aromatic rings of the *m*-terphenyl substituent are observed. In both compounds **2-Rh** and **3-Rh** a vertical pseudo-mirror plane passes through the C^1 and C^4 carbon atoms of the coordinated rings, which renders the *o*-substituents of the coordinated and non-coordinated ring chemically equivalent. In compound **2-Rh** four sets of methyl resonances are observed, in a ratio 3:6 (non-coordinated ring) : 3:6 (coordinated ring), corresponding to the *p*-CH_3 : *o*-CH_3 groups of each mesityl ring respectively. The same is observed in **3-Rh**, where more signals are observed due to the diastereotopic nature of the *o*-positioned ^{i}Pr groups on the aromatic rings resulting

Dieses Werk ist copyrightgeschützt und darf in keiner Form vervielfältigt werden noch an Dritte weitergegeben werden.
Es gilt nur für den persönlichen Gebrauch.

in 6 sets of doublets in a 6:6:6:6:6:6 ratio. In compound **3-Rh** four additional characteristic sets of resonance signals, corresponding to the methine protons of the ^{i}Pr substituents are also clearly observed, in a 1:2 (non-coordinated ring) : 1:2 (coordinated ring) ratio, corresponding to the *p*-^{i}Pr : *o*-^{i}Pr methine hydrogen atoms (Figure 2.2.3). Another common feature observed in both **2-Rh** and **3-Rh** is a doublet resonance signal corresponding to the coordinated C_2H_4 ligand. The multiplicity arises from coupling to Rh, resulting in a ^2J(H,Rh) = 2.4 Hz in both cases, suggesting no difference in the influence exerted by the germyl or stannyl group on the ethylene ligand. Only 1 resonance signal is observed for the C_2H_4 ligand in both compounds, which is indicative of a rapid rotation of the ligand on NMR time scale at room temperature, as a statically coordinated ligand would give rise to 2 sets of resonance signals, due to in equivalent hydrogen atoms on the ligand. Furthermore, a high field shifted resonance signal corresponding to the *m*-H atoms of the coordinated ring system is observed in both **2-Rh**: 5.50 ppm and **3-Rh**: 6.25 ppm, an expected consequence of the coordination of the ring to the Rh centre.[132] The difference (0.75 ppm) in the position of this resonance signal between the two compounds is a direct result of going from CH_3 (**2-Rh**) to ^{i}Pr (**3-Rh**) substituents, which induce a low field shift in the latter case owing to the increased +I effect of the substituents.

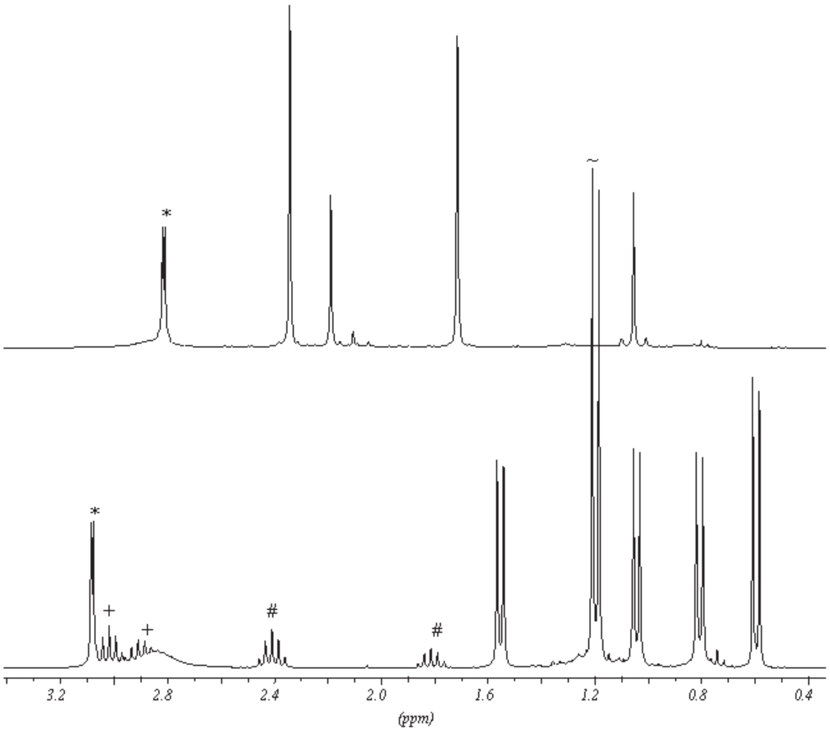

Figure 2.2.3: ^{1}H NMR spectra of compound **2-Rh** (top) and **3-Rh** (bottom) in C_6D_6 at 298 K between 0.4 and 3.4 ppm. * = C_2H_4; $^+$ = methine protons free trip; $^\#$ = methine protons coordinated trip; $^\sim$ = 2 overlapping doublet signals clarified by 2-D correlation spectroscopy.

Dieses Werk ist copyrightgeschützt und darf in keiner Form vervielfältigt werden noch an Dritte weitergegeben werden.
Es gilt nur für den persönlichen Gebrauch.

The $^{13}C\{^1H\}$ NMR spectra in C_6D_6 of compounds **2-Rh** and **3-Rh** at 298 K also both reveal a typical low field shift position of the resonance signal associated with carbon atom bound to the main group element. In compound **2-Rh** this is observed at 166.1 ppm, and in **3-Rh** at 160.1 ppm, and in both cases this signal is split into a doublet, resulting from ^2J coupling to Rh. Other characteristic resonance signals common to both compounds are the four doublet signals associated with the carbon atoms of the rings bound to the Rh centre, resulting from ^1J coupling to Rh. The values of the coupling constants vary slightly, supporting the results of the solid state structure determination that the bonding interaction between each member of the coordinated ring and the Rh centre is not entirely equivalent. These signals are also generally shifted to higher fields in comparison to the analogous ring carbon atoms in the non-coordinated substituent, as would normally be expected.

$^{119}Sn\{^1H\}$ NMR spectroscopy of complex **2-Rh** in C_6D_6 at 298 K reveals a doublet signal, which results from a ^1J (^{119}Sn –^{103}Rh) = 1095 Hz which is in good agreement with complexes of the type $[Rh(Sn\{N(R_2)\}_3)(PPh_3)(\eta^6\text{-arene})]$ reported by Killian.[127] The chemical shift of the resonance signal (δ = 54.3 ppm) is within the expected region of transition metal stannyl complexes,[133] although it is considerably low field shifted in comparison to the complexes of Killian, owing to the presence of amino ligands at tin in their case.[127]

The reactivity of compound **3-Rh** was also briefly investigated. Firstly, in an attempt to induce thermal elimination of the remaining ethene ligand and migration of one of the Cl ligands on the Ge centre to Rh, an NMR scale experiment was conducted by heating a sample of **3-Rh** in a sealed NMR tube at 60 °C, and following any reaction by *in situ* ^1H NMR spectroscopy over several hours. No reaction is observed under these reaction conditions, and even when a sample is refluxed in toluene after a period of 15 minutes, no observable changes in the ^1H NMR spectrum are detected. Secondly, Reaction of **3-Rh** with $B(C_6F_5)_3$ did not yield the predicted product, $[Rh\{GeCl(2\text{-Trip-6-}\eta^6\text{-Trip-}C_6H_3)\}(\eta^2\text{-}C_2H_4)][BCl(C_6F_5)_3]$, which would have resulted from Cl abstraction by the Lewis acidic borane at the Ge centre. Again, even upon reflux in toluene, no visible signs of any reaction were observed. These two facts illustrate the robust stability of these complexes, and highlight their apparently inert nature.

Although the target of Rh≡E E = Ge, Sn was not achieved, an unexpected novel route enabling facile entry to neutral stannyl and germyl complexes of Rh(I) was uncovered. This

Dieses Werk ist copyrightgeschützt und darf in keiner Form vervielfältigt werden noch an Dritte weitergegeben werden.
Es gilt nur für den persönlichen Gebrauch.

resulted in the first example of an η-Arene Rh compound containing a germyl ligand, and a rare example of a stannyl analogue, following insertion of the ylenes into the Rh-Cl bond, with concomitant C_2H_4 elimination. The success of these reactions lie in the nature of the stannylene and germylene employed, in that they have aromatic substituents which can readily coordinate to Rh, rendering the germyl and stannyl ligands chelating and generating stable 18 VE Rh(I) complexes.

Dieses Werk ist copyrightgeschützt und darf in keiner Form vervielfältigt werden noch an Dritte weitergegeben werden.
Es gilt nur für den persönlichen Gebrauch.

2.3 Reactivity of the germylenes, stannylenes and plumbylenes [EXR] (E = Ge, Sn, R = 2,6-Mes_2-C_6H_3 or 2,6-$Trip_2$-C_6H_3, X = Cl; E = Pb, R = 2,6-$Trip_2$-C_6H_3, X = Br) towards d^8 iron complexes

Thus far, the reactivity of stannylene **1-Sn** and germylene **1-Ge** towards palladium complexes and a representative rhodium complex has been discussed. In the case of palladium insertion occurred, and in the case of Rh, a combination of insertion and ligand elimination took place. As was earlier pointed out, our ultimate goal was the extension of transition metal (outside group 6) to Sn and Ge triple bonding. To achieve this goal, we returned to the original strategy of N_2 elimination at the metal centre in a low oxidation state, supported by electron rich phosphanes, which as was shown in the introduction, enabled easy access to an array of group 6 tetrelylidyne complexes (see introduction and references).

2.3.1 Reactions of [Fe(depe)$_2$(N_2)] with [EClR] (E = Ge and Sn, R = 2,6-Mes_2-C_6H_3 or 2,6-$Trip_2$-C_6H_3, X = Cl)

A number of low oxidation state iron complexes exist, which bear N_2 ligands. Some examples of these complexes include that of Chirik and co-workers [$Fe(N_2)_2$(^{iPr}PDI)] ^{iPr}PDI = ((2,6-$CHMe_2$)$_2C_6H_3N$=CMe)$_2C_5H_3N$;[134] Trigonally coordinated Fe N_2 anionic complexes by Peters' group;[135] $Na_2[Fe(EDTA)(N_2)].2H_2O$ by Lopez-Alcala *et al*;[136] or the complex $[FeH(N_2)(N(CH_2CH_2PPh_2)_3][BPh_4]$ by George *et al*.[137] These complexes constitute plausible starting materials to access ylidyne complexes on reaction with ylenes of Ge, Sn or Pb, but reactive neutral Fe(0) complexes, bearing N_2 ligands, with innocent, non redox active ligands[138] would be a more prudent choice to minimize the chances of emerging redox-chemistry.

In this view, the monodinitrogen complex, [Fe(depe)$_2$(N_2)][139,140] **1-Fe**, readily accessible by reduction of *trans*-[$FeCl_2$(depe)$_2$][141] **2-Fe** with sodium naphthalene under N_2, represented a feasible precursor for the preparation of Fe ylidyne complexes. Complex **2-Fe**, which can be prepared by simple complexation of two equivalents free depe to anhydrous $FeCl_2$,[142] exhibits a temperature dependant spin equilibrium, evidenced by the progressive sharpening of the resonance signal in the $^{31}P\{^1H\}$ NMR spectrum on descent in temperature (Figure 2.3.1). These spectra also suggest a preference for the *trans* isomer of **2-Fe**, as the presence

Dieses Werk ist copyrightgeschützt und darf in keiner Form vervielfältigt werden noch an Dritte weitergegeben werden.
Es gilt nur für den persönlichen Gebrauch.

of the *cis* isomeric form would result in two sets of triplet resonance signals resulting from ^2J P,P coupling.

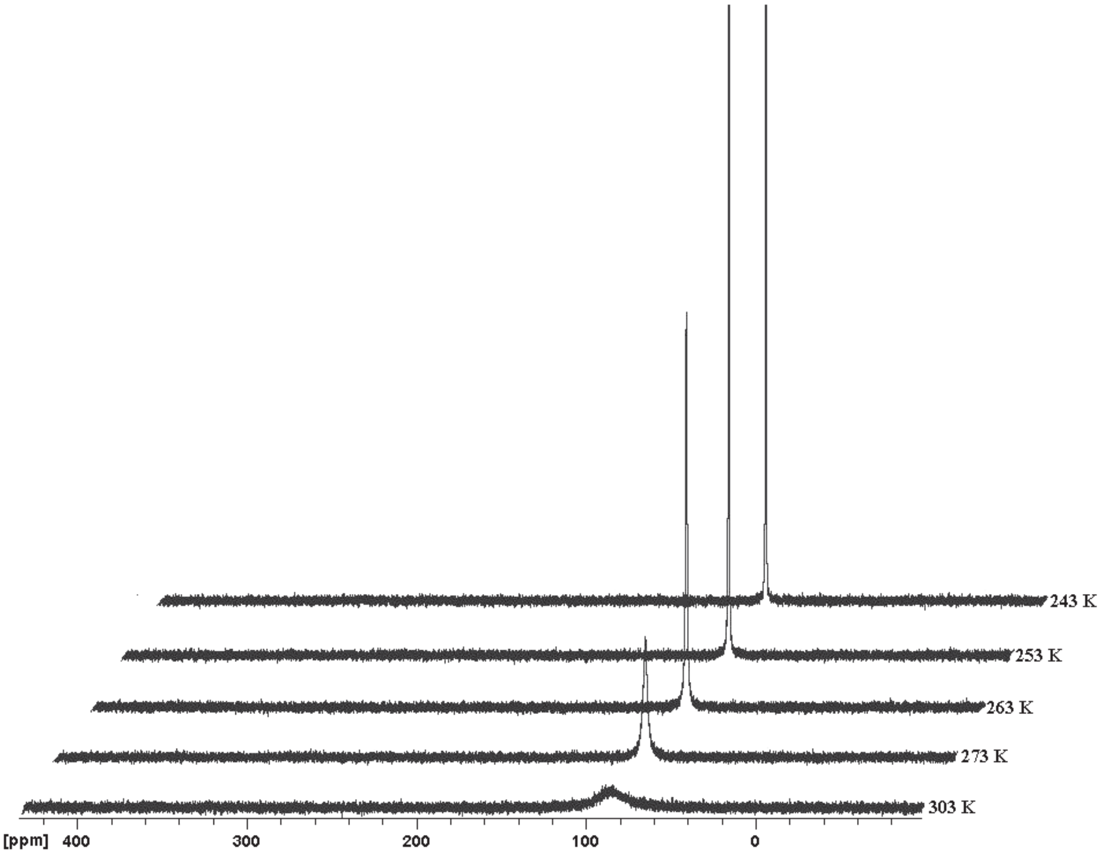

Figure 2.3.1: Stacked variable temperature $^{31}P\{^1H\}$ NMR spectra in toluene-d_8 of **2-Fe**. Temperature dependant high spin – low spin equilibrium evidenced by sharpening of the resonance signal on descent in temperature consistent with the t_{2g}^6 ground-state configuration.

The mono-dinitrogen complex **1-Fe** is formally an d^8 configured Fe(0) complex which is trigonal bipyramidal in the solid state, with the end-on coordinated N_2 ligand occupying one of the planar coordination sites.[139,140] The solution $^{31}P\{^1H\}$ NMR spectrum reveals a sharp singlet resonance signal, which cannot be frozen out at low temperatures, as a result of rapid Berry pseudo-rotation,[143] rendering all phosphorus atoms equivalent. In our case, **1-Fe** was accessed by reduction of **2-Fe** with 2.3 eq. Na sand, in THF resulting in higher yields of **1-Fe** than those reported in the literature (Scheme 2.3.1).

Dieses Werk ist copyrightgeschützt und darf in keiner Form vervielfältigt werden noch an Dritte weitergegeben werden.
Es gilt nur für den persönlichen Gebrauch.

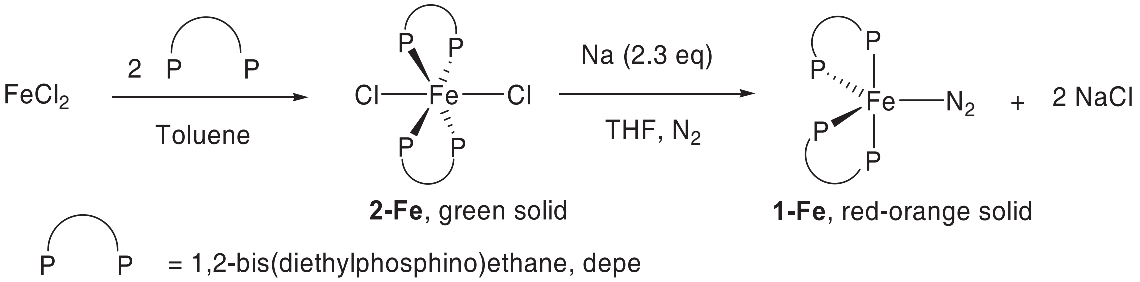

Scheme 2.3.1: Synthesis of the dinitrogen complex, **1-Fe**, starting from FeCl$_2$.

The envisaged synthetic strategy henceforth thus involved elimination of dinitrogen at iron by reaction with 1 molar equivalent of ylene [EXR], (E = Ge, X = Cl; Sn, X = Cl or Pb, X = Br) resulting in an intermediate halo-ylidene complex, and then to perform halide abstraction at the tetrel atom to form a complex featuring a triple bond between iron and the tetrel atom (Scheme 2.3.2).

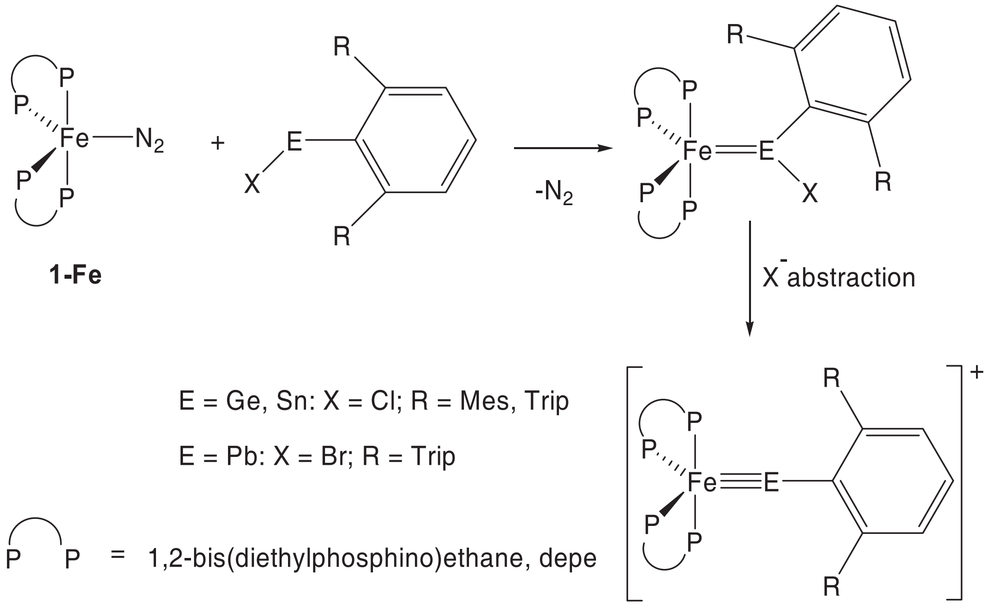

Scheme 2.3.2: Synthetic strategy to access iron ylidyne complexes of heavy tetrel atoms.

2.3.1.1 Double bonding between Fe and Sn: The first example of an iron halostannylidene complex and the first structurally characterised transition metal haloylidene complex.

The implementation of the first step of this synthetic strategy indeed resulted in the isolation of an iron chlorostannylidene complex. Reaction of **1-Fe** with 1 molar equivalent SnCl(2,6-Mes$_2$-C$_6$H$_3$) **1-Sn** in pentane results in the selective formation of the complex

Dieses Werk ist copyrightgeschützt und darf in keiner Form vervielfältigt werden noch an Dritte weitergegeben werden.
Es gilt nur für den persönlichen Gebrauch.

$[(depe)_2Fe{=}SnCl(2,6\text{-}Mes_2\text{-}C_6H_3)]$ **3-Fe**, with concomitant dinitrogen elimination. Complex **3-Fe** represents the first example of an iron halostannylidene complex.

The pathway of this reaction is probably associative, since according to one study, reaction of **1-Fe** with ligands such as CO, C_2H_4, H_2 showed large variations in the half life reaction values, in accordance with associative kinetics.[144]

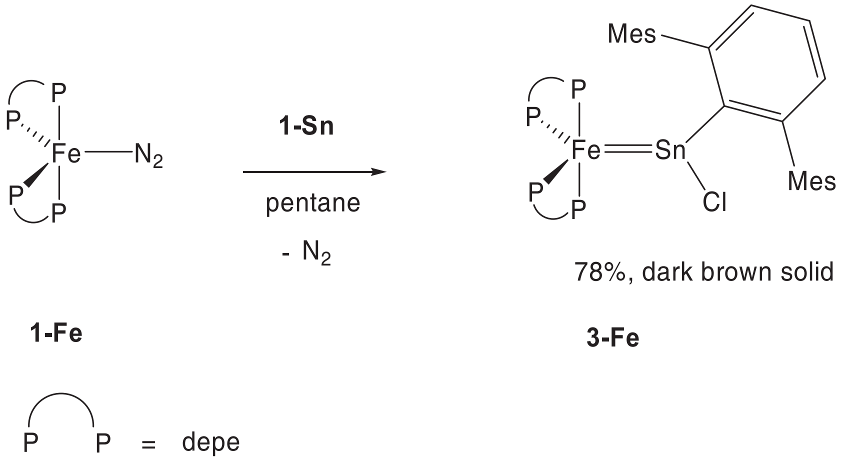

Scheme 2.3.3: Synthesis of chlorostannylidene complex **3-Fe** *via* dinitrogen elimination at Fe.

Compound **3-Fe** was isolated in 78% yield as a dark brown, air-sensitive solid and is highly soluble in diethyl ether, pentane and benzene. Dark brown solutions of **3-Fe** turn colourless on contact with air, owing to its reactive nature – the iron centre is susceptible to oxidation, and the Sn–Cl bond to hydrolysis. It however exhibits high thermal stability with a decomposition temperature of 148 – 152 °C .

The *m*-terphenyl substituent in **3-Fe** is rotationally locked in solution as evidenced by ^1H NMR spectroscopy at room temperature in C_6D_6, in which three sets of methyl resonance signals each integrating to 6 protons for the methyl groups of the mesityl rings are observed. Free rotation of the *m*-terphenyl substituent, would result in a 1:2 ratio of the methyl resonance signals (*para*-methyl : *ortho*-methyl), which is not observed. Moreover, the ^1H NMR spectrum shows two sets of broad resonance signals for the CH_3 groups of the depe ligands, each integrating to 12 protons, indicative of their diastereotopic nature. The $^1H\{^{31}P\}$ NMR spectrum of **3-Fe** in C_6D_6 at room temperature reveales two "pseudo-triplet" resonance signals for both CH_3 groups, which are in fact two sets of doublet of doublets arising from $^3J(H,H)$ coupling to two distinct diastereotopic CH^XH^Yatoms on the adjacent CH_2 groups.

Dieses Werk ist copyrightgeschützt und darf in keiner Form vervielfältigt werden noch an Dritte weitergegeben werden.
Es gilt nur für den persönlichen Gebrauch.

A sharp singlet resonance signal in the $^{31}P\{^{1}H\}$ NMR spectrum in C_6D_6 at $\delta = 76.8$ ppm, flanked by tin satellites, suggests Berry pseudo rotation of the depe ligands, at room temperature, resulting in equivalence of the four phosphorus atoms on NMR time scale in solution. This is reflected in the $^{119}Sn\{^{1}H\}$ NMR spectrum in C_6D_6, where a quintet signal at $\delta = 471.5$ ppm ($^{2}J(^{119}Sn,P) = 100$ Hz) evidences coupling to four chemically equivalent phosphorus atoms. The most characteristic signal in the $^{13}C\{^{1}H\}$ NMR spectrum of **3-Fe** is that of the low field shifted tin bonded carbon atom at $\delta = 175.1$ ppm.

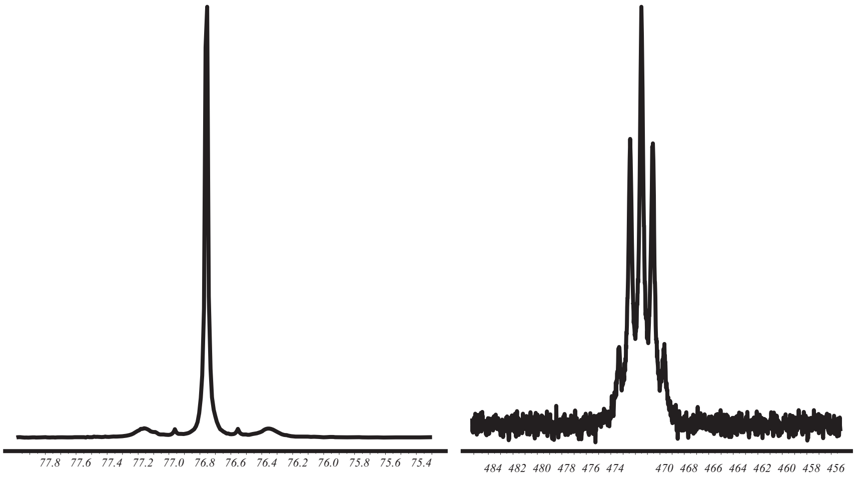

Figure 2.3.2: $^{31}P\{^{1}H\}$ NMR spectrum of **3-Fe** in C_6D_6 (left), $^{119}Sn\{^{1}H\}$ in C_6D_6 (right) at room temperature. In the case of the $^{31}P\{^{1}H\}$ NMR spectrum, broad satellite signals are visible, which represent both ^{117}Sn and ^{119}Sn nuclei.

Single crystals of complex **3-Fe**, suitable for X-ray diffraction analysis, were grown from diethyl ether by slow evaporation of the solvent at –30 °C in the glove-box (Figure 2.3.3).

Dieses Werk ist copyrightgeschützt und darf in keiner Form vervielfältigt werden noch an Dritte weitergegeben werden.
Es gilt nur für den persönlichen Gebrauch.

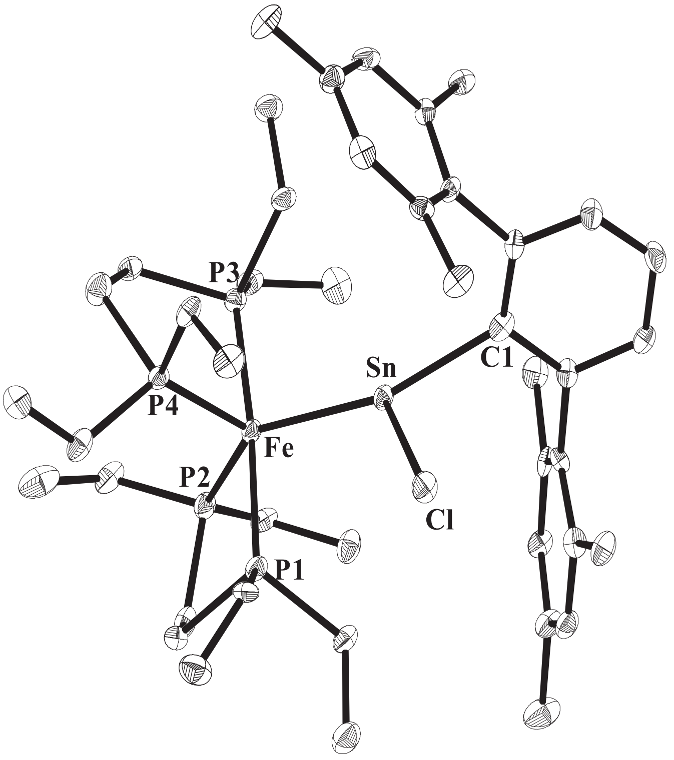

Figure 2.3.3: DIAMOND plot of the molecular structure of complex **3-Fe** in the solid state. Thermal ellipsoids are set at the 30% probability level, H atoms are omitted for clarity. Selected bond lengths [Å]: Fe–P1 2.235(3), Fe–P2 2.216(3), Fe–P3 2.228(3), Fe–P4 2.195(3), Fe–Sn 2.409(1), Sn–C1 2.530(2), Sn–C(l) 2.25(1). Selected bond angles [°]: P1-Fe-P3 173.6(1), P4-Fe-P2 114.0(1), P4-Fe-Sn 112.43(8), Fe-Sn-Cl 114.04(7), Fe-Sn-C(1) 158.5(2), C(1)-Sn-Cl 87.3(2).

No examples of structurally characterised halostannylidene complexes exist, and **3-Fe** is indeed the first example in this class. Furthermore, with the exception of the complex $[(dmpe)Mo(\eta^5\text{–}C_5Me_5)H{=}SiCl(Mes)]$[**] by Tilley and co-workers, no structurally characterised complexes exist bearing a three coordinate tetrel atom (Si–Pb) with a halogen as substituent thus making complex **3-Fe** even more remarkable. The iron centre in **3-Fe** adopts a near perfect trigonal bipyramidal geometry, characterised by a τ value close to unity ($\tau = 0.99$).[145] This is not an altogether unusual geometry for five co-ordinate Fe^0 complexes, with the starting material $[Fe(depe)_2(N_2)]$ and $[Fe(depe)_2(CO)]$ for example, also exhibiting trigonal bipyramidal geometries about the Fe centre. The Fe–Sn bond length of 2.409(1) Å is notably shorter than that of iron stannyl complexes (2.542 Å)[146] and slightly shorter than that of the only other existing structurally characterised iron stannylidene complex: $[(CO)_4Fe{=}SnR_2]$, (R = bulky aromatic group, alkyl) (2.488(1) Å).[147] This bond length contraction can be attributed to the presence of electron rich phosphane ligands on the iron

---

[**] The possibility of the H atom forming a bridge between the Mo and Si centre strictly speaking exempts this complex as belonging to the class under discussion.

Dieses Werk ist copyrightgeschützt und darf in keiner Form vervielfältigt werden noch an Dritte weitergegeben werden.
Es gilt nur für den persönlichen Gebrauch.

centre in **3-Fe** compared to π electron withdrawing CO ligands in [(CO)$_4$Fe=SnR$_2$], resulting in weaker π back-bonding to the tin atom in the latter case, and a consequent elongation of the Fe–Sn bond.[147]

The C(1)-Sn-Cl bond angle of 87.3(2)° together with that of the Fe-Sn-C(1) angle 158.5(2)° and Fe-Sn-Cl 114.04(7)° bond angle reveal a planar coordination geometry around Sn, as the arithmetic sum of these angles approximates 360°. These bond angles also point towards decreased sp^2 hybridisation at the Sn centre, evidenced by deviations from ideal trigonal planar geometry (120° bond angles). This is expected for Sn, and additionally supported by calculations on the related model complex [Fe(PH$_3$)$_4$=Sn(C$_6$H$_5$)Cl], which indicate the σ-donation from tin to iron to originate from an s orbital with low p-character, while the π–back bonding interaction from iron to tin is into a virtually pure p orbital ($d_{xy} \rightarrow p_y$). Furthermore, calculations also point to a singlet ground state, with trigonal bipyramidal geometry at iron, in accordance with these experimental findings, with the corresponding triplet state geometry optimised minima being substantially higher in energy (42, 43 or 90 kJ·mol^{-1}).[148]

2.3.1.2: Triple bonding between Fe and Sn: The first examples of transition metal complexes outside group 6 bearing triple bonds to tin.

Following the successful isolation of complex **3-Fe**, various strategies were employed to effect chloride abstraction at the Sn centre, which indeed resulted in complexes featuring a triple bond between Sn and Fe. These complexes constitute the first examples of transition metal complexes outside group 6 featuring triple bonds to tin and hence constitute a significant development in this field.

The synthetic strategies employed to perform the chloride abstraction from **3-Fe** were:

a) abstraction by another equivalent **1-Sn**
b) abstraction through the borane B(C$_6$F$_5$)$_3$
c) by salt metathesis, using Na[B{C$_6$H$_3$-3,5-(CF$_3$)$_2$}$_4$]

Dieses Werk ist copyrightgeschützt und darf in keiner Form vervielfältigt werden noch an Dritte weitergegeben werden.
Es gilt nur für den persönlichen Gebrauch.

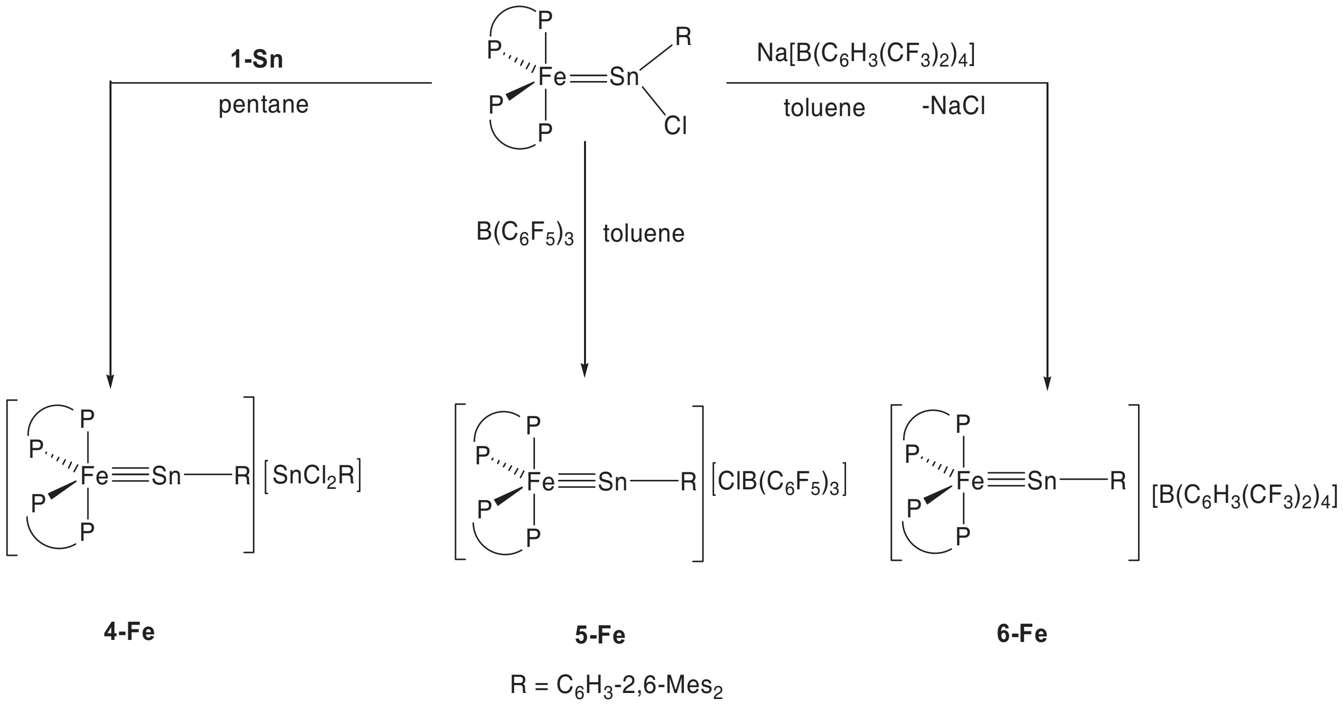

Scheme 2.3.4: Strategies employed to access stannylidyne complexes **4-Fe**, **5-Fe** and **6-Fe**

Approach (a)

The first approach took advantage of the inherent Lewis acidity of the stannylene **1-Sn**, and reaction of **3-Fe** with an additional equivalent of **1-Sn** resulted in the formation of the pentane insoluble brown ionic complex: [(depe)$_2$Fe≡Sn–2,6-Mes$_2$-C$_6$H$_3$][Sn(2,6-Mes$_2$-C$_6$H$_3$)Cl$_2$] **4-Fe**. This product could also be isolated in a one pot synthesis starting from **1-Fe**, directly reacted with 2 molar equivalents of **1-Sn**. The ionic complex **4-Fe** is soluble in THF and benzene and dissolves to give red-brown solutions, which rapidly decolourise on contact with air. Complex **4-Fe** exhibits exceptionally high thermal stability with a decomposition temperature of 229 – 232 °C.

Dark brown-orange single crystals of compound **4-Fe** were grown by adding pentane slowly to a saturated toluene solution of **4-Fe** and slow cooling to 7 °C. The cation in the ionic complex **4-Fe** represents the first example of a triple bond between tin and a transition metal element atom outside group 6. Additionally, it can be considered the first example of a structurally characterised complex featuring a triple bond between Fe and **any** main group element atom with principal quantum number $n \geq 3$ making it exceptional.[149,150]

Two crystallographically independent molecules, with different geometries about the iron centre, are present in the asymmetric unit: they exhibit distorted trigonal bipyramidal geometry ($\tau = 0.83$), and a slightly distorted square pyramidal geometry ($\tau = 0.12$) about the

Dieses Werk ist copyrightgeschützt und darf in keiner Form vervielfältigt werden noch an Dritte weitergegeben werden.
Es gilt nur für den persönlichen Gebrauch.

Fe centre. This observation provides compelling experimental evidence for the close proximity of the two geometry configurations on the potential energy hyper surface, a result reflected by calculations (BP86/Basis – Basis: H,C – G-31G(d,p); P, Cl, Fe – G-311G(2d); Sn – TZVPP, ECP(46)) where only a 9 $kJ \cdot mol^{-1}$ difference in energy is found for the singlet state model cation: $[(PH_3)_4Fe{\equiv}Sn(C_6H_5)]^+$ where the square pyramidal geometry is higher in energy.

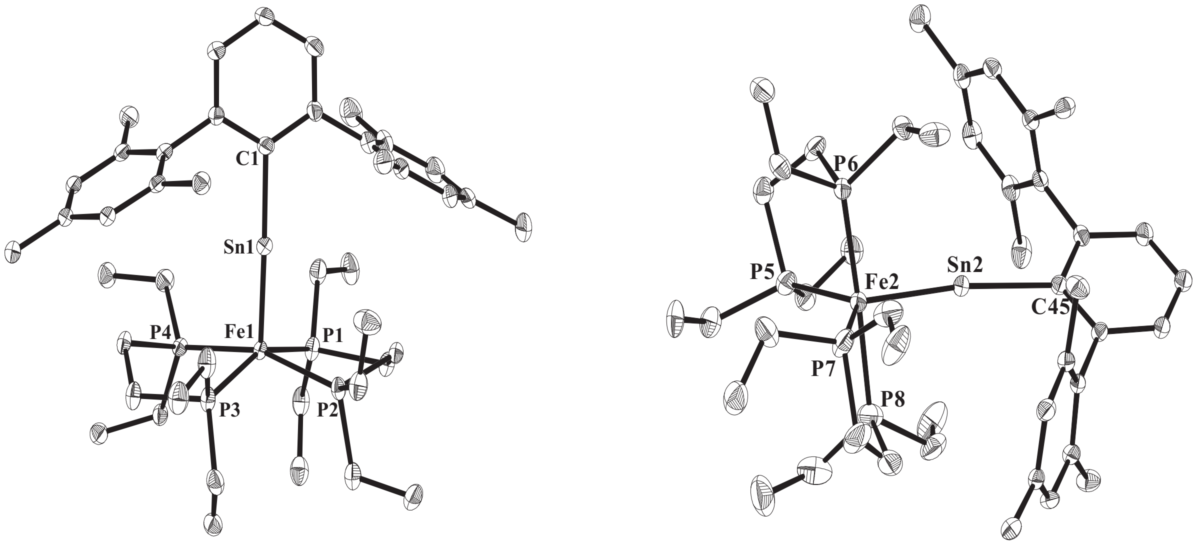

Figure 2.3.4: DIAMOND plot of the molecular structure of the cation(s) in **4-Fe** in the solid state (both independent molecules in the asymmetric unit). Thermal ellipsoids are set at the 30% probability level, H atoms are omitted for clarity. Selected bond lengths [Å]: Fe1–Sn1 2.327(1), Fe2–Sn2 2.3193(9), Sn1–C1 2.177(6), Sn2–C45 2.174(5), Fe1–P1 2.245(2), Fe1–P2 2.246(2), Fe1–P3 2.232(2), Fe1–P4 2.252(2), Fe2–P5 2.267(2), Fe2–P6 2.258(2), Fe2–P7 2.195(2), Fe2–P8 2.287(3). Selected bond angles [°]: P3-Fe1-Sn1 106.72 (6), P1-Fe1-Sn1 101.14(6), P2-Fe1-Sn1 101.58(6), P4-Fe1-Sn1 98.79(5), P3-Fe1-P2 91.74(7), P3-Fe1-P4 82.85(6), Fe1-Sn1-C1 173.3(2), Fe2-Sn2-C45 172.7(2), P6-Fe2-P8 176.42(8), P7-Fe2-P5 126.76(8), P7-Fe2-Sn2 111.76(7), P4-Fe1-P2 159.62(8), P1-Fe1-P3 152.14(8).

The two crystallographically independent molecules in the asymmetric unit reveal a nearly linear Fe–Sn–C_{ipso} bond angle of 173.3(2)° and 172.7(2)° respectively. This, together with a short Fe–Sn bond length of 2.327(1) and 2.3193(9) Å are suggestive of the presence of a triple bond. These Fe–Sn bond lengths are significantly shorter than that observed in **3-Fe** and are the shortest tin to transition metal bond lengths so far to be reported, with W–Sn triple bonds ranging from 2.4641(7) – 2.504(1) Å. The two coordinate Sn centre occupies the apical position in the independent molecule of square pyramidal geometry, whereas in the trigonal

Dieses Werk ist copyrightgeschützt und darf in keiner Form vervielfältigt werden noch an Dritte weitergegeben werden.
Es gilt nur für den persönlichen Gebrauch.

bipyramidal isomer it is located in one of the equatorial positions, as in the parent complex, **3-Fe**.

Calculations on the model cation $[(PH_3)_4Fe{\equiv}Sn(C_6H_5)]^+$ have pointed to near absence in hybridisation of the tin atom in the cation, and the bonding interaction can essentially can be viewed as a σ-donation from a 5s orbital from tin to iron, with two successive π-back donations originating from the iron centre into unhybridised p orbitals at tin, respectively. The presence of a formal triple bond between Fe and Sn was additionally validated by calculations: the Atoms In Molecules (AIM) theory was used to analyse the electron density of the trigonal bipyramidal cation in **4-Fe**. The Laplacian ($\nabla^2\rho(r_c) = 3.81$ eÅ^5) and the Hessian ($H(r_c) = -0.19$ Hartee·Å^3) at the bond critical point of the Fe–Sn bond prove that this bond complies with a closed-shell donor acceptor interaction. The very small elipticity $\varepsilon = 0.014$ shows the almost perfect radial shape of the electron density at the bond critical point as it is expected for a triple bond. The latter can also be seen at the distribution of localized electron density using the electron localization function (Figure 2.3.5). The toroidal shape of the localized electron density in the trigonal bipyramidal geometry in the cation of **4-Fe** is typical for acetylenes and indeed indicate the presence of a triple bond.[151]

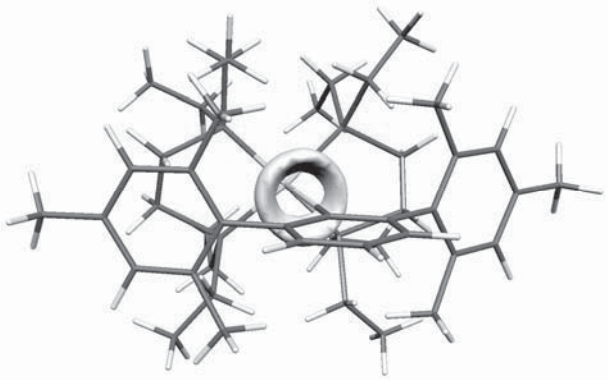

Figure 2.3.5:. Localized electron density between iron and tin in **2-TBP** (isosurface value = 0.85:BP86/Basis: H,C – G-31G(d,p); P, Cl, Fe – G-311G(2d); Sn – TZVPP, ECP(46)).

The anion in **4-Fe,** $[Sn(R)Cl_2]^-$ is notably the first example of a structurally characterised organo-stannate anion (Figure 2.3.6). The tin centre is pyramidalised: reflected by the sum of the bond angles around tin (287.7°) additionally indicative of the presence of a lone pair. The widening of the C89–Sn3–Cl2 bond angle by more than 10° compared to the C89–Sn3–Cl1 angle can be attributed to the close proximity of the Cl2 atom to the mesityl ring (3.332(1) Å distance from Cl2 atom to the centre of gravity of (C_g) one peripheral mesityl ring), resulting in a repulsive interaction.

Dieses Werk ist copyrightgeschützt und darf in keiner Form vervielfältigt werden noch an Dritte weitergegeben werden.
Es gilt nur für den persönlichen Gebrauch.

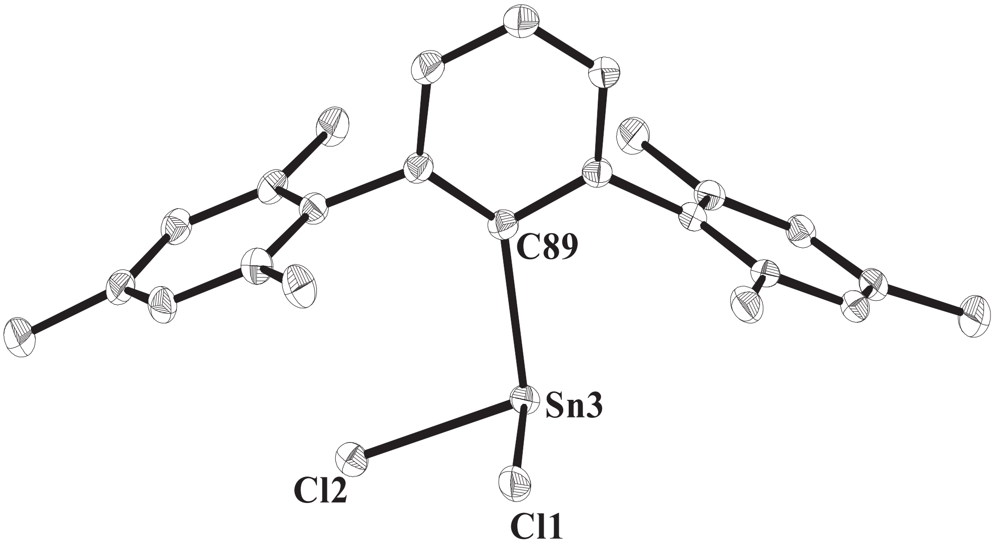

Figure 2.3.6: DIAMOND plot of the molecular structure of the anion in **4-Fe** in the solid state. Thermal ellipsoids are set at the 30% probability level, H atoms are omitted for clarity. Selected bond lengths [Å]: Sn3–C89 2.243(6), Sn3–Cl1 2.498(1), Sn3–Cl2 2.489(1). Selected bond angles [°]: C89-Sn3-Cl2 103.3(2), C89-Sn3-Cl1 90.9(1), Cl2-Sn3-Cl1 93.5(1).

The $^{31}P\{^{1}H\}$ NMR spectrum of **4-Fe** at room temperature in C_6D_6 reveals a sharp singlet resonance signal a $\delta = 77.0$ ppm, suggesting rapid exchange on the NMR time scale in solution between the two geometries observed in the solid state, *via* Berry pseudo rotation. A broad resonance signal is detected in the $^{13}C\{^{1}H\}$ NMR spectrum for both tin bonded carbon atoms in **4-Fe** at $\delta = 173.1$ ppm, in C_6D_6 at room temperature, which could not be resolved. There is some evidence that **4-Fe** undergoes reverse formation to **3-Fe** in THF: $^{31}P\{^{1}H\}$ NMR spectrum of **4-Fe** in THF shows the identical resonance signal as in **3-Fe**, which appears stable in THF, along with the same $^{2}J(P,^{117/119}Sn)$ coupling constant (100 Hz). Additionally, the UV/Vis spectrum of **4-Fe** in THF shows an identical absorption band in nearly the same position as in **3-Fe** (see section on UV/Vis studies later).

Approach (b)

Chloride abstraction from **3-Fe** induced by reaction with the borane, $B(C_6F_5)_3$ afforded the ionic stannylidyne complex **5-Fe**. Complex **5-Fe** could not be isolated in pure form. The ^{1}H NMR spectra of **5-Fe** revealed the formation of several products and the identity of which could not be established. Despite this, as with **4-Fe** a singlet in the $^{31}P\{^{1}H\}$ spectrum was also observed at room temperature, in the same position as with ionic complex **4-Fe**. Additionally, a broad resonance signal at $\delta = -7.4$ ppm was observed in the $^{11}B\{^{1}H\}$-NMR

Dieses Werk ist copyrightgeschützt und darf in keiner Form vervielfältigt werden noch an Dritte weitergegeben werden.
Es gilt nur für den persönlichen Gebrauch.

spectrum. An X-ray crystallographic investigation confirmed the structure of **5-Fe**, despite the average quality of the crystallographic data set, and also evidenced the Cl abstraction at Sn. As is the case with complex **4-Fe**, both trigonal bipyramidal, and square pyramidal geometries of the complex cation are observed in the solid state in the asymmetric unit, indicating that this is a factor which in independent on the nature of the anion. The Fe–Sn bond lengths in each independent cation are 2.312(3) and 2.314(3) Å respectively (mean = 2.314(4) Å), and comparable to that of complex **4-Fe**, as expected. The anion features a tetrahedral geometry with a propeller configuration of the C_6F_5 rings. The mean B–Cl bond length is 1.89(2) Å, comparable to that found in $[CPh_3][ClB(C_6F_5)_3]$, at 1.928(2) Å,[152] or $[Pd(dppe)_2][ClB(C_6F_5)_3]$ 1.925(4) Å.[153]

Approach (c)

The third and final synthetic strategy to obtain stannylidyne complexes of iron involved metathetical exchange of **3-Fe** with $Na[B\{C_6H_3\text{-}3,5\text{-}(CF_3)_2\}]$ **2-B** and indeed resulted in the ionic stannylidyne complex **6-Fe**, subject to rigorous spectroscopic investigations. This complex, contrary to the related complex **4-Fe**, features the counter anion $[B\{C_6H_3\text{-}3,5\text{-}(CF_3)_2\}_4]$, which significantly simplified the NMR spectroscopic analyses. As expected, ^1H NMR spectroscopy in THF-d_8 reveals a 6 : 12 ratio for the *para* : *ortho* methyl groups of the peripheral mesityl substituents, in contrast to **4-Fe**, which features two sets of signals for the cation and anion respectively (Figure 2.3.7).

Dieses Werk ist copyrightgeschützt und darf in keiner Form vervielfältigt werden noch an Dritte weitergegeben werden.
Es gilt nur für den persönlichen Gebrauch.

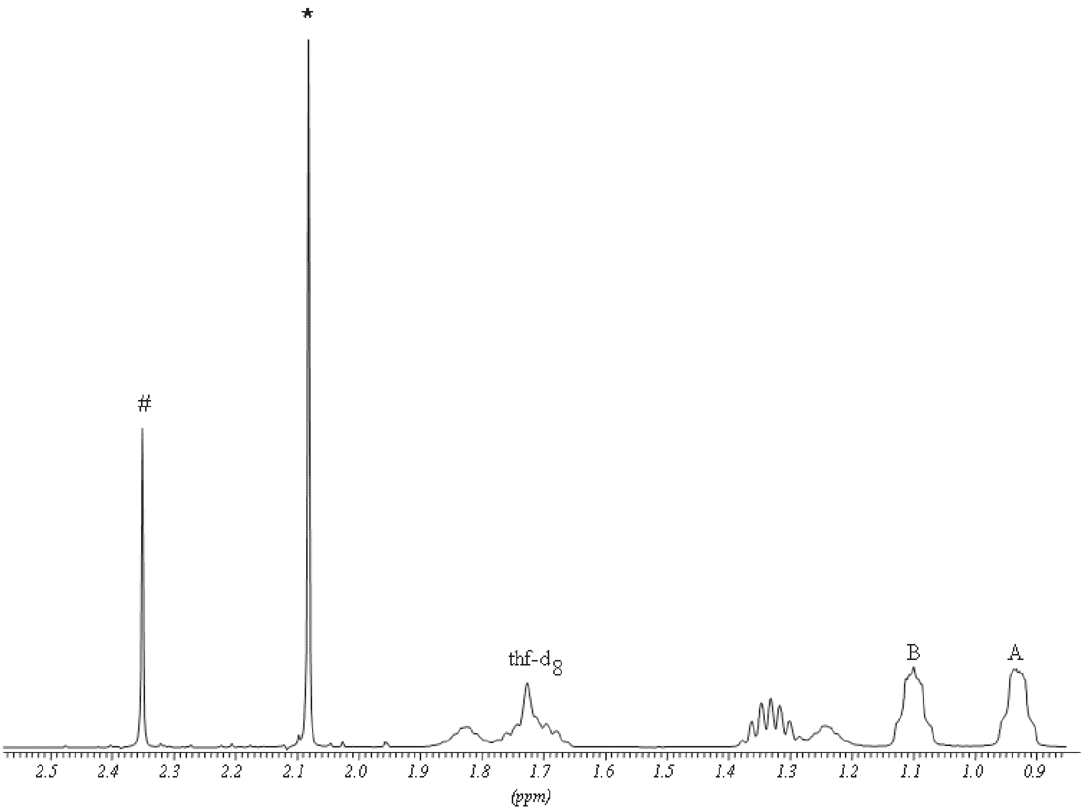

Figure 2.3.7: ^{1}H NMR spectrum of **6-Fe** in THF-d_8 at room temperature, in the chemical shift range δ= 0.9 – 2.5 ppm. # = *p*-CH_3, * = *o*-CH_3 on the peripheral mesityl rings. Note the two sets of resonance signals A and B, corresponding to diastereotopic CH_3 groups on the depe ligand (highest field shifted), along with the diastereotopic CH_2 groups of the depe ligand system.

A sharp resonance signal is also observed in the $^{31}P\{^1H\}$ NMR spectrum at δ= 77.5 ppm in THF-d_8, as with **4-Fe** and **5-Fe** and a singlet resonance signal in $^{11}B\{^1H\}$ NMR appears at δ = –6.47 ppm, a typical expected chemical shift of borates.[154] In contrast to **4-Fe** which only exhibited a very broad resonance signal in $^{119}Sn\{^1H\}$ NMR at δ= 209 ppm in C_6D_6, **6-Fe** features a better defined resonance signal at δ= 983 ppm. This dramatic higher field shifted resonance signal in **4-Fe** suggests an interaction between the captions and anions in solution, resulting in a broad resonance signal which is the average of that of the cation (≈ 983 ppm) and the anion, $[SnCl_2(2,6\text{-}Mes_2\text{-}C_6H_3)]^-$, which would be expected to have a significantly higher field chemical shift.[155]

In summary, three halogen abstraction strategies were successfully implemented with complex **3-Fe** to form the first examples of iron stannylidyne complexes.

Dieses Werk ist copyrightgeschützt und darf in keiner Form vervielfältigt werden noch an Dritte weitergegeben werden.
Es gilt nur für den persönlichen Gebrauch.

2.3.1.3: Triple bonding between Fe and Ge: The first transition metal complexes outside group 6 bearing a triple bond to germanium.

Attempts to obtain the complex $[(\mathrm{depe})_2\mathrm{Fe{=}GeCl}(2,6\text{-}\mathrm{Trip}_2\text{-}\mathrm{C}_6\mathrm{H}_3)]$ **7-Fe** following an analogous strategy to obtain **3-Fe** were unsuccessful. Instead, reaction of **1-Fe** with one equivalent of **1-Ge** resulted directly in low yields (27 %) of the ionic germylidyne complex $[(\mathrm{depe})_2\mathrm{Fe{\equiv}Ge}(2,6\text{-}\mathrm{Trip}_2\text{-}\mathrm{C}_6\mathrm{H}_3)][\mathrm{GeCl}_2(2,6\text{-}\mathrm{Trip}_2\text{-}\mathrm{C}_6\mathrm{H}_3)]$ **8-Fe**. This result suggests, on first inspection, that the steric strain associated with the peripheral Trip substituents, precludes the formation of a stable isolable chloro-germylidene complex, and the reaction proceeds directly to the germylidyne complex. It can, however, also be a result of the reduced covalent radius of Ge, in comparison to Sn (19 pm) which prevented the formation of this complex due to the resulting increased steric congestion of the *m*-terphenyl substituent and depe ligands, as attempts at preparing the Mes analogue of **7-Fe** $[(\mathrm{depe})_2\mathrm{Fe{=}GeCl}(2,6\text{-}\mathrm{Mes}_2\text{-}\mathrm{C}_6\mathrm{H}_3)]$ were also unsuccessful.

Repeating the reaction of the dinitrogen complex **1-Fe** with 2 molar equivalents of **1-Ge**, **1-** afforded moderate yields (60 %) of the ionic germylidyne complex, **8-Fe.** These results are summarised in Scheme 2.3.5

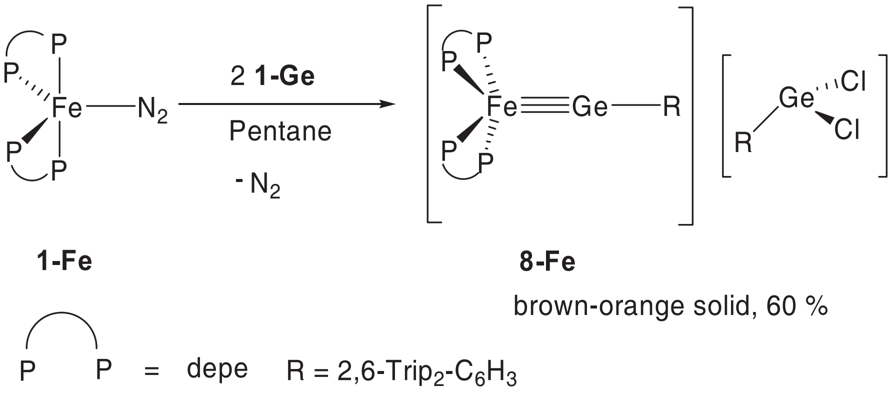

Scheme 2.3.5. Formation of the ionic germylidyne complex **8-Fe** from **1-Fe** and **1-Ge**.

The brown-orange germylidyne complex **8-Fe** is pentane insoluble, and immediately precipitates out of pentane as the reaction proceeds, in analogy to the formation of **4-Fe.** It is highly air sensitive and decolourises in the solid state and in solution on contact with air within seconds. The compound is soluble in benzene and THF and dissolves to form dark red solutions and has remarkable thermal stability with a decomposition temperature of 148 - 151 °C. Single crystals of the ionic complex **8-Fe**, suitable for X-ray diffraction analysis were

Dieses Werk ist copyrightgeschützt und darf in keiner Form vervielfältigt werden noch an Dritte weitergegeben werden.
Es gilt nur für den persönlichen Gebrauch.

grown from a saturated benzene solution by pentane diffusion at ambient temperature in the glove box, over a period of two days, as dark red blocks. The structure of the cation is shown in Figure 2.3.8.

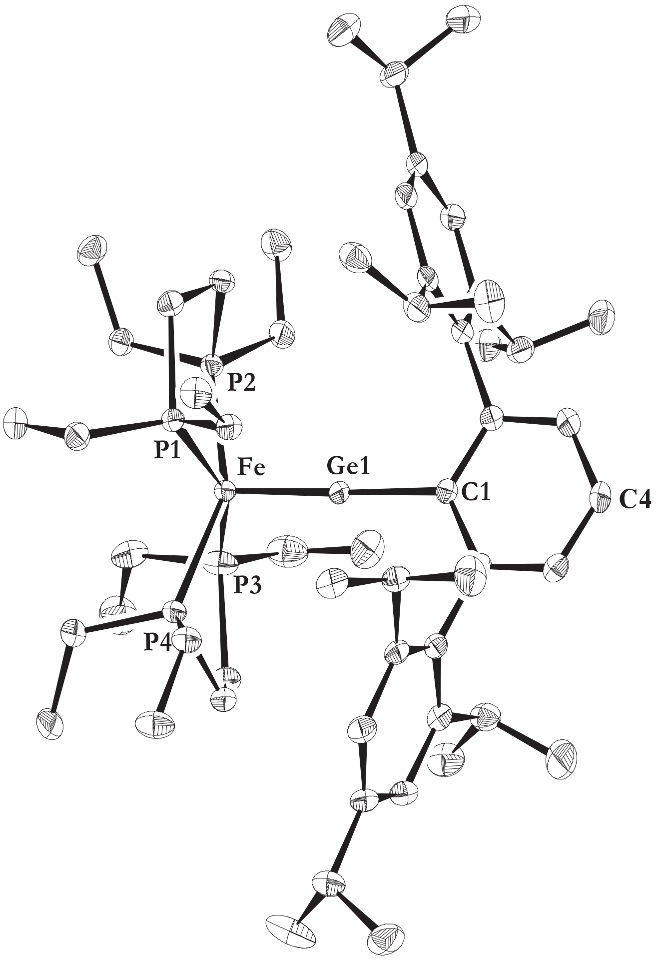

Figure 2.3.8: DIAMOND plot of the molecular structure of the cation in **8-Fe·C_6D_6** in the solid state. Thermal ellipsoids are set at the 30% probability level and H atoms and included benzene-d_6 are omitted for clarity. Selected bond lengths [Å]: Ge–C1 1.994(2), Fe–Ge 2.1198(4), Fe–P1 2.2386(7), Fe–P2 2.2358(6), Fe–P3 2.2364, Fe–P4 2.2371(6). Selected bond angles [°]: Fe-Ge-C1 178.36(7), Ge-Fe-P4 106.88(2), Ge-Fe-P3 105.35(3), Ge-Fe-P2 103.83(2), Ge-Fe-P1 101.84(2), P1-Fe-P4 89.75(2), P1-Fe-P3 152.76(3), P1-Fe-P2 82.53(2), P2-Fe-P3 92.42(2), P2-Fe-P4 149.26(3), P3-Fe-P4 80.99(3).

The square pyramidal isomer is exclusively present in the asymmetric unit, in contrast to that of **4-Fe** and **5-Fe** – an effect likely due to the increased steric bulk of the *m*-terphenyl substituent. The iron centre in the cation of **8-Fe** adopts an almost ideal perfect square pyramidal geometry ($\tau = 0.06$) with the nearly linearly two coordinated germanium atom occupying the apical position. A view along the C4-C1-Ge1-Fe axis reveals a near collinear arrangement of the central phenyl ring of the *m*-terphenyl substituent with the P2-Fe-P4 axes.

Dieses Werk ist copyrightgeschützt und darf in keiner Form vervielfältigt werden noch an Dritte weitergegeben werden.
Es gilt nur für den persönlichen Gebrauch.

The Fe–Ge bond length of 2.1198(4) Å is the shortest so far reported for an Fe-Ge bond. Moreover, it represents the shortest germanium to transition metal bond length so far reported, comparable only in magnitude to the example by Power of a Cr–Ge bond length of 2.1666(4) Å. A near linear Fe-Ge1-C1 bond angle of 178.36(7)° together with the very short bond length is suggestive of a triple bond between Fe and Ge, a conclusion supported by the results of our quantum chemical calculations, in analogy to the tin system.[156]

The anion in **8-Fe** is the first example of a structurally characterised example of the type $[Ge(R)X_2]^-$(R = Alkyl or Aryl group; X = halogen), and shows a distorted trigonal pyramidal geometry about the Ge centre, and deviation in the magnitude of bonding angles when compared to $[GeCl_3]^-$ [157]: The Cl1-Ge2-C57 bond angle is nearly 10° larger than the remaining Cl-Ge2-C57 bond angles in the anion, which can be explained by the repulsion between the Trip substituent and the Cl1 atom, which is located in close proximity to the plane of one of the peripheral phenyl substituents, in analogy to the anion of **4-Fe**. The Ge–Cl bond lengths (2.3288(6) Å and 2.3455(7) Å) do not deviate from those in $[GeCl_3]^-$ (2.3017(6) – 2.3158(6) Å) significantly (Figure 2.3.9)

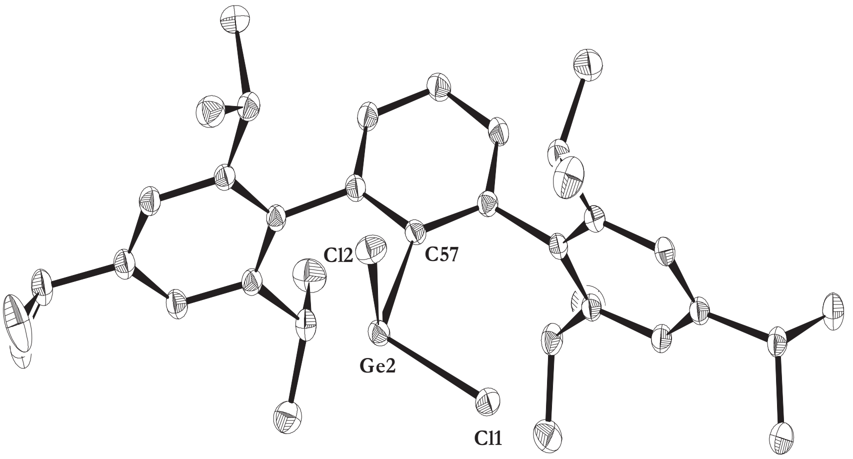

Figure 2.3.9: DIAMOND plot of the molecular structure of the anion in **8-Fe·C_6D_6** in the solid state. Thermal ellipsoids are set at the 30% probability level and H atoms and included benzene-d_6 are omitted for clarity. Selected bond lengths [Å]: Ge2-Cl1 2.3288(6), Ge2-Cl2 2.3455(7). Selected bond angles [°]: C57-Ge2-Cl1 103.93(6), C57-Ge2-Cl2 92.35(7), Cl1-Ge2-Cl2 95.28(2).

The Ge analogue of complex **4-Fe** was also prepared, using two molar equivalents of the sterically less crowded germylene, GeCl(2,6-Mes_2-C_6H_3), **2-Ge**. This resulted in moderate yields (50 %) of the terracotta-brown ionic germylidyne complex **9-Fe**. Crystals suitable for

Dieses Werk ist copyrightgeschützt und darf in keiner Form vervielfältigt werden noch an Dritte weitergegeben werden.
Es gilt nur für den persönlichen Gebrauch.

X-ray crystallographic analyses were grown by slow evaporation from a C_6D_6 solution in the glove box.

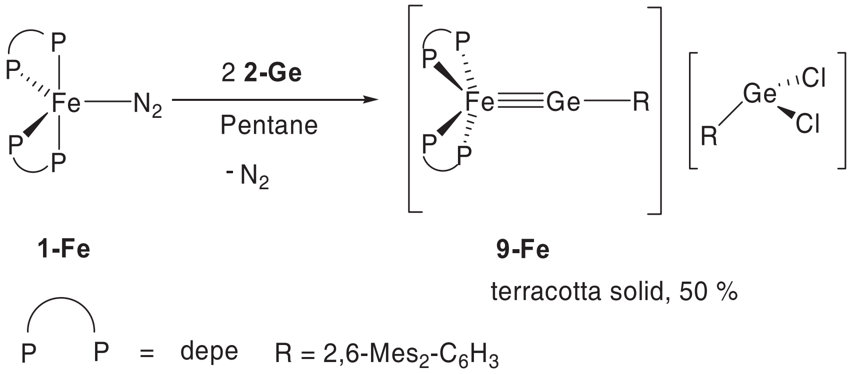

Scheme 2.3.5b. Formation of the ionic germylidyne complex **9-Fe** from **1-Fe** and **2-Ge**.

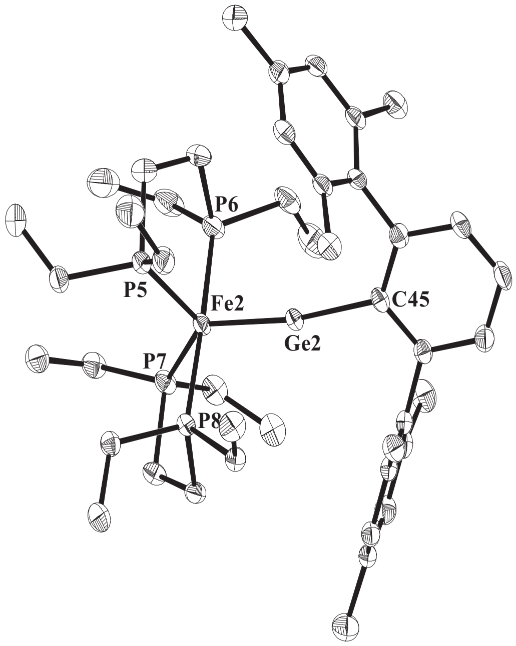

Figure 2.3.10: DIAMOND plot of the molecular structure of the cation of trigonal bipyramidal geometry in **9-Fe** in the solid state. Thermal ellipsoids are set at the 30% probability level, H atoms are omitted for clarity. Selected bond lengths [Å]: Fe2–Ge2 2.1342(4), Ge2–C45 1.993(2), Fe2–P5 2.2430(8), Fe2–P6 2.2365(8), Fe2–P7 2.2675(7), Fe2–P8 2.2602(8). Selected bond angles [°]: Fe2-Ge2-C45 171.29(8), P6-Fe2-Ge2 89.18(2), P8-Fe2-Ge2 93.81(2), P6-Fe2-P8 176.37(3), P5-Fe2-P8 95.65(3), P5-Fe2-P7 121.76(3), P6-Fe2-P5 85.03(3).

Dieses Werk ist copyrightgeschützt und darf in keiner Form vervielfältigt werden noch an Dritte weitergegeben werden.
Es gilt nur für den persönlichen Gebrauch.

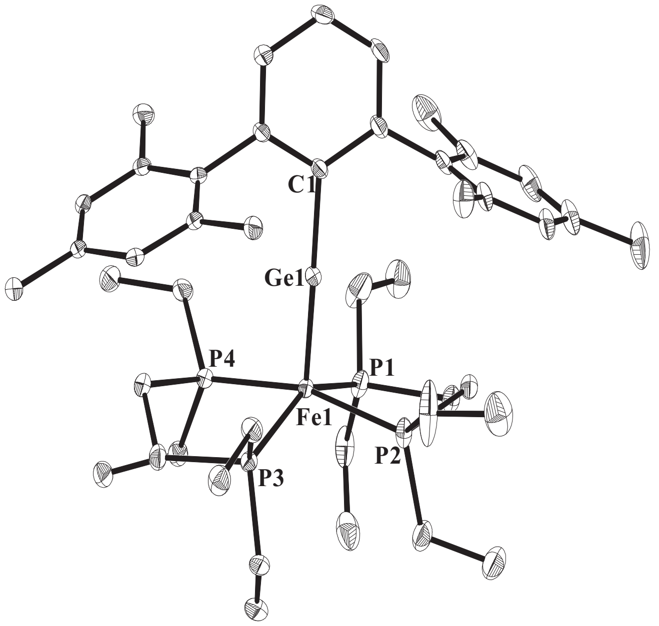

Figure 2.3.11: DIAMOND plot of the molecular structure of the cation of slightly distorted square pyramidal geometry in **9-Fe** in the solid state. Thermal ellipsoids are set at the 30% probability level, H atoms are omitted for clarity. Selected bond lengths [Å]: Fe1–Ge1 2.1221(5), Ge1–C1 1.980(3), Fe1–P1 2.2550(8), Fe1–P2 2.2393(7), Fe1–P3 2.2511(8), Fe1–P4 2.2495(7). Selected bond angles [°]: Fe1-Ge1-C1 175.57(8), P1-Fe1-P4 92.94(3), P1-Fe1-P3 145.73(3), P2-Fe1-P4 163.12(3).

In contrast to the complex **8-Fe** bearing a sterically more demanding *m*-terphenyl subsitutent, where only the square pyramidal stereoisomer was found in the solid state, in the case of **9-Fe**, as with the related tin analogues **4-Fe** and **5-Fe** both square pyramidal ($\tau = 0.23$) and trigonal bipyramidal ($\tau = 0.91$) stereoisomers co-exist in the asymmetric unit in the solid state. This is evidence that the relative energies of the two isomeric forms is largely driven by the steric bulk of the *m*-terphenyl substituent: in the case of the Trip substituted terphenyl, only a square pyramidal stereoisomer is found in the solid state structure, while lowering the steric demand to Mes, both in the case of Sn (**4-Fe**, or **5-Fe**) and Ge (**9-Fe**), result in both geometries in the solid state structures, indicative of their energies being close together on the energy hyper surface. In the case of **9-Fe** the average Fe–Ge bond length, over both independent molecules, of 2.1282(6) Å compares well with that of the bulkier Ge analogue complex **8-Fe** at 2.1198(11) Å. It is however, shorter than the average of the Fe–Sn bond length in the tin analogue, **4-Fe** which was found to be 2.3232(9) Å, in close approximation of the decreased covalent radius of Ge: 1.22 Å vs. Sn 1.40 Å.[158] The bond angles associated with the square pyramidal isomer of **9-Fe** reflect distortion from an ideal square pyramidal geometry: the P2-Fe2-P4 bond angle 163.12(3)° is markedly larger than the P1-Fe1-P3 at 145.73(3)° and can better be described as a square pyramidal geometry distorted in the

Dieses Werk ist copyrightgeschützt und darf in keiner Form vervielfältigt werden noch an Dritte weitergegeben werden.
Es gilt nur für den persönlichen Gebrauch.

direction of a trigonal bipyramidal geometry, additionally reflected by the calculated τ parameter.

The ^{1}H NMR spectrum in C_6D_6 reveals the expected resonance signals, corresponding to two sets of terphenyl substituents, in the cation and anion respectively (Figure 2.3.12).

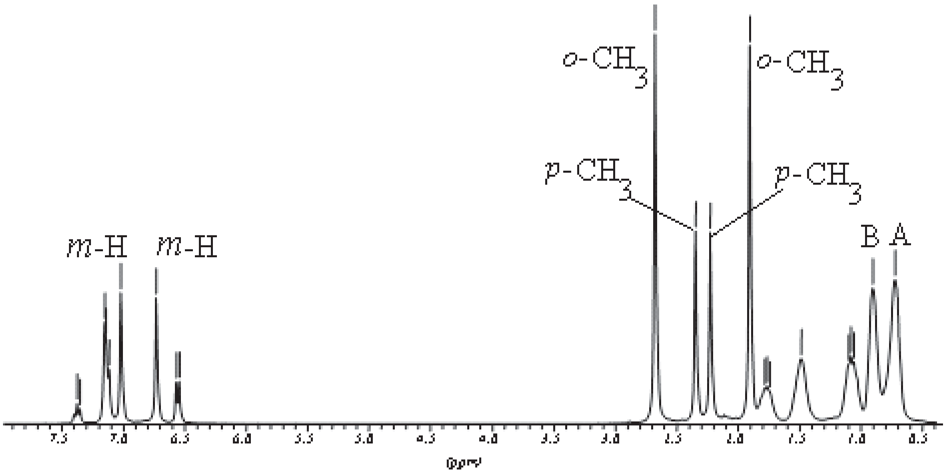

Figure 2.3.12: ^{1}H NMR spectrum of complex **9-Fe** in C_6D_6 at room temperature. Diastereotopic CH_3 groups of the depe ligands are depicted A and B. The CH_3 groups of the mesityl substituents are clearly visible for both the cation and the anion.

In the $^{31}P\{^{1}H\}$ NMR spectrum in C_6D_6 at room temperature a sharp singlet resonance signal at δ = 78.4 ppm appears, again as before suggestive of the equivalence of the four phosphorus atoms and free rotation of the terphenyl substituent about the $Ge–C_{ipso}$ bond at ambient temperature. It is interesting to note that this chemical shift is comparable to the stannylidyne complexes, discussed previously. The $^{13}C\{^{1}H\}$ NMR spectrum in C_6D_6 at ambient temperature revealed two signals for the C_{ipso} atoms in the cation and anion at δ = 163.4 ppm and 163.7 ppm, respectively.

Comparative variable temperature $^{31}P\{^{1}H\}$ NMR spectroscopy of the ionic germylidyne complexes **8-Fe** and **9-Fe** were also carried out (Figure 2.3.13). Notable differences are clearly observable on first inspection: in the case of **8-Fe**, on descent from 298 K, where a sharp singlet resonance signal is visible, progressive broadening of the signal occurs, and clean separation into two broad signals at 193 K, in a 1:1 ratio is observed. In contrast, in **9-Fe**, the resonance signal initially broadens on descent in temperature, but then sharpens again, and does not split into two separate resonance signals as with **8-Fe**.

Dieses Werk ist copyrightgeschützt und darf in keiner Form vervielfältigt werden noch an Dritte weitergegeben werden.
Es gilt nur für den persönlichen Gebrauch.

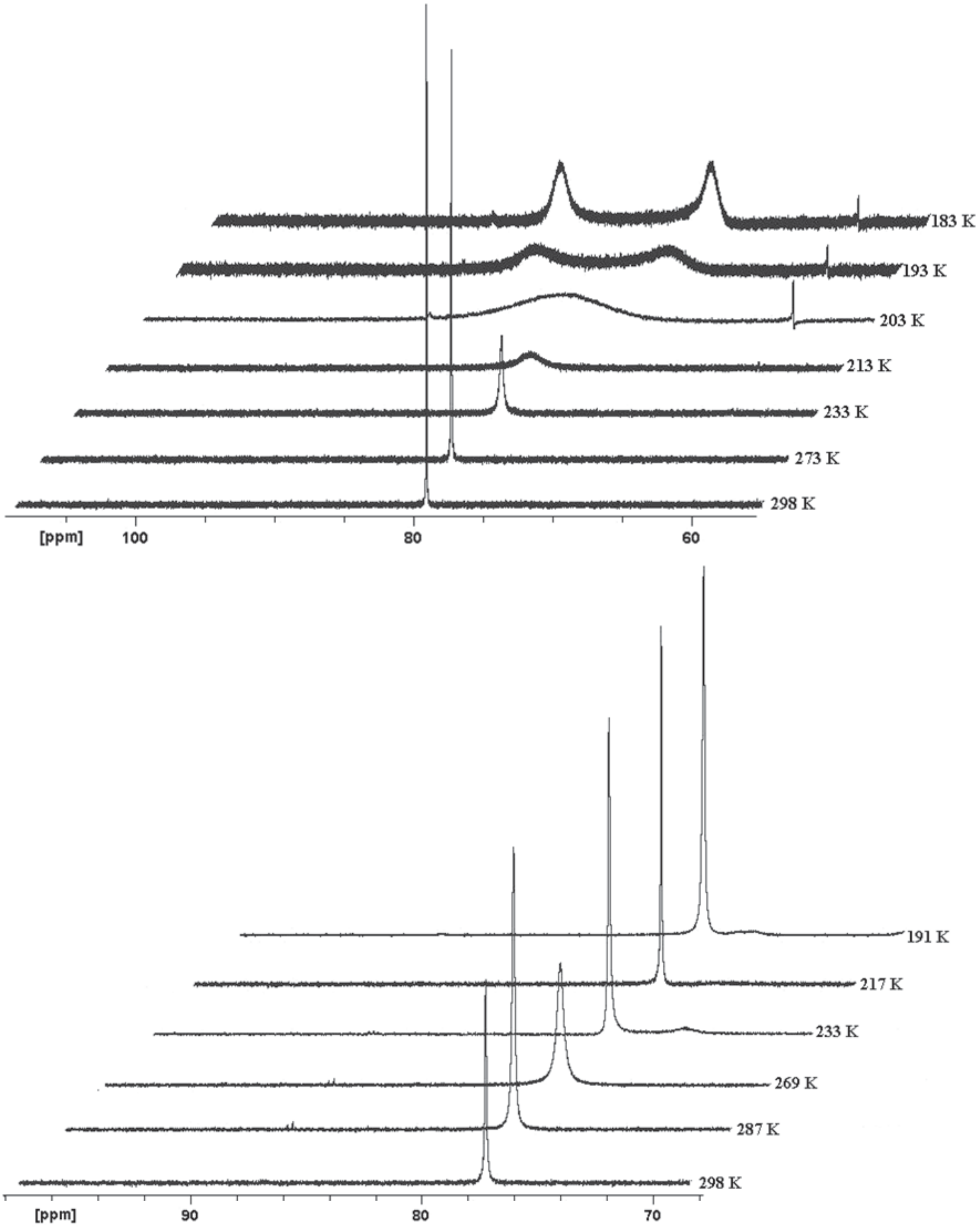

Figure 2.3.13: Stacked variable temperature (VT) $^{31}P\{^{1}H\}$ NMR spectra of **8-Fe** (top) and **9-Fe** (bottom) in THF-d_8. (The aberration in the baseline seen at lower temperatures for **9-Fe** is a slight impurity).

These differences are obviously linked to the change in steric bulk associated with the *m*-terphenyl substituent in **8-Fe** and **9-Fe**, which already on the basis of X-ray analysis was shown to have an effect. However, interpretation of these NMR results are somewhat complicated by the fact that two competing dynamic processes are likely, in both compounds:

Dieses Werk ist copyrightgeschützt und darf in keiner Form vervielfältigt werden noch an Dritte weitergegeben werden.
Es gilt nur für den persönlichen Gebrauch.

(a) The Berry pseudo-rotation of the phosphane ligands, and
(b)The free rotation of the *m*-terphenyl substituent attached to Ge.

Matters are further complicated by the presence of only one stereoisomer in the solid state of **8-Fe** (square pyramidal) and both square pyramidal and trigonal bipyramidal geometries in **9-Fe** according to X-ray diffraction analysis. It is tempting to assume that in the case of **8-Fe** only the static square pyramidal isomer exists in solution, as is observed in the solid state, but Berry pseudo rotation of the phosphane ligands in solution cannot be ruled out, and is likely. In the case of **9-Fe**, given the presence of both stereoisomers in the solid state, it is very likely that pseudo rotation of the phosphane ligands is in occurrence. In order to explain the phenomenon, we are forced to consider three distinct scenarios which could account for the VT NMR observations in **8-Fe**:

(a) Locked rotation of *m*-terphenyl substituent *and* simultaneous “frozen out” Berry pseudo rotation of depe ligands. (i.e. both dynamic processes frozen out)
(b) “Frozen out” rotation of *m*-terphenyl substituent but continued Berry pseudo rotation of depe ligands.
(c) Free *m*-terphenyl rotation but “frozen out” Berry pseudo rotation of ligands.

In scenario (a) both dynamic processes are frozen out. In this case, for **8-Fe**, assuming the static structure in solution resulting from both processes being frozen out is the same as that of the X-ray structure, 2 signals in a 1:1 ratio would indeed be expected in the $^{31}P\{^1H\}$ NMR spectrum below the coalescence temperature, owing to C_2 symmetry at the Fe centre (See Fig 2.3.14). This scenario is hence a likely candidate to explain the observations.

Dieses Werk ist copyrightgeschützt und darf in keiner Form vervielfältigt werden noch an Dritte weitergegeben werden.
Es gilt nur für den persönlichen Gebrauch.

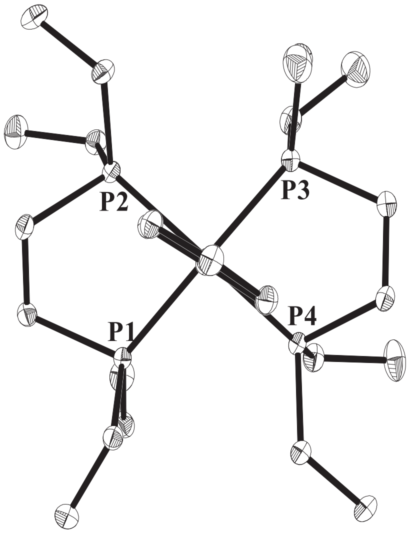

Figure 2.3.14: DIAMOND plot of the cation in complex **8-Fe** (H atoms, and Trip substituents in 2 and 6 position of the central phenyl ring omitted for clarity). Thermal ellipsoids set at 30 % probability. View down the C4-C1-Ge-Fe axis. The collinear arrangement of the central phenyl ring with the P2-Fe-P4 bond axis results in a pseudo-C_2 symmetric cation, which would yield 2 resonance signals in the $^{31}P\{^1H\}$ NMR spectrum, as is observed.

In scenario (b), we consider the *m*-terphenyl substituent to be rotationally locked, but the phosphane ligands to continue rapid interconversion. Regardless of the relative locked orientation of the *m*-terphenyl substituent, only one resonance signal would result – this scenario can therefore immediately be ruled out.

In scenario (c), we consider free rotation of the *m*-terphenyl, while the phosphane pseudo-rotation is frozen out. This would result in 1 singlet resonance signal for **8-Fe**, since it would be rendered C_{2v} symmetric if the Fe centre is square pyramidal which enables us to rule this scenario out. However, two signals would indeed be observed if the geometry at Fe was trigonal bipyramidal in solution, with free rotation of the *m*-terphenyl substituent, in a 1:1 ratio, which is observed. With both isomers simultaneously present, 3 signals would result which can be ruled out. The latter two suggestions are unlikely, in this scenario, again due to the fact that the square pyramidal geometry seems to be favoured on descent in temperature.

From the above discussion, it is clear that scenario (a) accounts for the observations, i.e. both dynamic processes are frozen out. The energy barrier associated with the dynamic process in **8-Fe** can estimated from the coalescence temperature, T_c which from the spectra lies between

Dieses Werk ist copyrightgeschützt und darf in keiner Form vervielfältigt werden noch an Dritte weitergegeben werden.
Es gilt nur für den persönlichen Gebrauch.

193 K and 203 K. If we assume it to be 198 K, the mid-point between these two temperatures, and by application of the equation (1)

$\Delta G^{\#} = RT_c(22.96 + \ln(T_c/\Delta\nu)$ [159] (1)

where R: ideal gas constant, $\Delta\nu$: the frequency difference between the maxima of the two signals at T_l, the low temperature limit

the energy barrier can be calculated at 33.8 kJ·mol^{-1}. Calculations[160] have shown the barrier of rotation of the *m*-terphenyl ligand around the Ge–C_{ipso} bond in the square pyramidal geometry of the cation in **8-Fe** to be *ca.* 58 kJ·mol^{-1}, which can be regarded as an upper bound for this rotational process since relaxed potential energy surface scans yield much higher energy barriers than normal transition state searches. The close agreement of the experimental and theoretical values therefore further support the interpretation of the experimental spectra. Furthermore, an AIM analysis[161] has shown repulsive interactions to exist between the sterically demanding *m*-terphenyl ligand of **8-Fe** and the depe ligand, which further suggest the interpretation of the spectra is correct. (Figure 2.3.15).

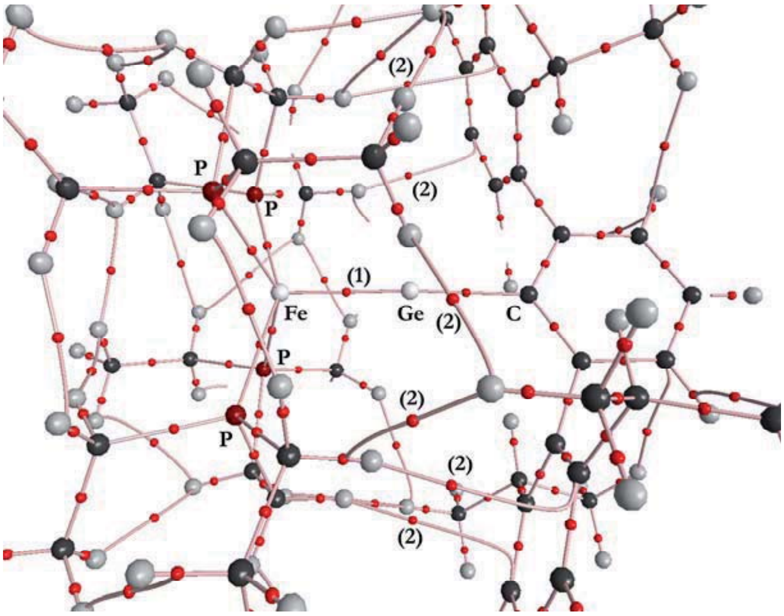

Figure 2.3.15:. Cutaway of the molecular graph of **8-Fe**. (1) depicts the bond path (incarnadine line) between Fe and Ge with the corresponding bond critical point (bcp, red ball). (2) shows some of many repulsive interactions between the depe ligands and the terphenyl substituents which might explain why the rotation around the Ge–C axis is hindered.

Dieses Werk ist copyrightgeschützt und darf in keiner Form vervielfältigt werden noch an Dritte weitergegeben werden.
Es gilt nur für den persönlichen Gebrauch.

In summary, the comparative variable temperature NMR results highlight the effect of changing the steric properties of the *m*-terphenyl substituent on Ge. The increase in the steric bulk of the *m*-terphenyl substituent in **8-Fe** results in both Berry pseudo rotation and ring rotation being frozen out, while in **9-Fe**, bearing less steric bulk on the m-terphenyl, no such process is observed.

Dieses Werk ist copyrightgeschützt und darf in keiner Form vervielfältigt werden noch an Dritte weitergegeben werden.
Es gilt nur für den persönlichen Gebrauch.

2.3.2 Reactivity of [Fe(depe)$_2$(N$_2$)] towards [PbXR] (X = Br, R = 2,6-Trip$_2$-C$_6$H$_3$; X = Cl, R = C(tms)$_3$): Formation of Fe(I) complexes

Extension of the dinitrogen elimination strategy at Fe, to reactions with plumbylenes did not result in the formation of plumbylidene or plumbylidyne complexes. Instead redox chemistry was observed, and Fe(I) complexes of the type [Fe(depe)$_2$X] X = Br, Cl resulted.

In particular reaction of **1-Fe** with [PbCl(C(tms)$_3$)] **2-Pb** resulted in the formation of the Fe(I) complex: [FeCl(depe)$_2$], **10-Fe**, which was identified by X-ray crystallographic analysis, and ^{1}H NMR spectral comparison to an authentic sample (see later). Owing to the small scale of the experiment, the identification of the resulting lead product was precluded. However, the similar reaction of **1-Fe** with [PbBr(2,6-Trip$_2$-C$_6$H$_3$)], **1-Pb** resulted in the formation of a mixture of [FeBr(depe)] **11-Fe**, the identity of which was shown by X-ray diffraction analysis[††] and the diplumbylene, [Pb(2,6-Trip$_2$-C$_6$H$_3$)]$_2$ verified by ^{1}H and ^{13}C{^{1}H} NMR spectra.[‡‡] Separation of these two products from each other was attempted by fractional crystallisation experiments, but was unsuccessful.

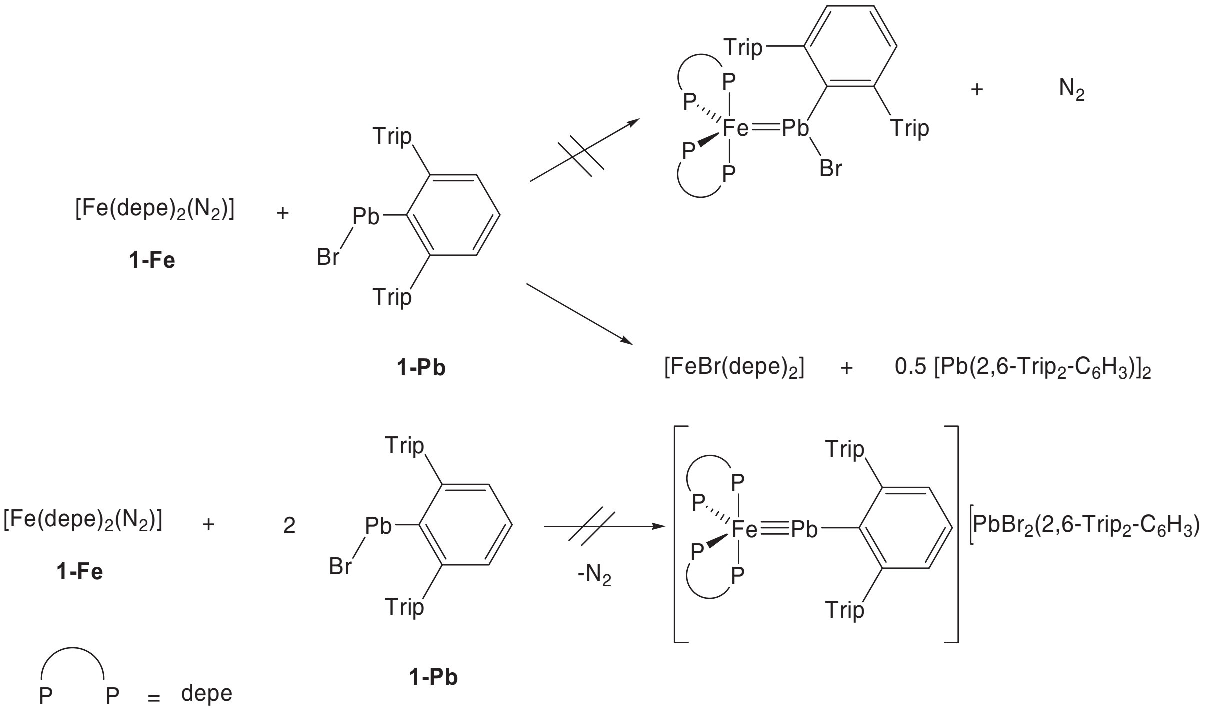

Scheme 2.3.6: Reaction of the complex **1-Fe** with the plumbylene **1-Pb** results in redox chemistry.

[††] The structure is omitted from this dissertation owing to its poor quality. The structural motif was however determined as trigonal bipyramidal, the bromide ligand occupying one of the equitorial coordination sites in the trigonal bipyramid.

[‡‡] The formation of other products cannot be precluded. These were however the two products resulting from the reaction that could be positively identified.

Dieses Werk ist copyrightgeschützt und darf in keiner Form vervielfältigt werden noch an Dritte weitergegeben werden.
Es gilt nur für den persönlichen Gebrauch.

The reactivity of the related plumbylenes towards **1-Fe**, are in contrast to that of the corresponding germylene (**1-Ge** or **2-Ge**) or stannylenes (**1-Sn**). This is most likely a consequence of decreased π-bond strength of Pb compared to Ge or Sn, which precludes stable multiple bond formation to Fe. Nevertheless, the observation of the Fe(I) complexes, prompted a brief excursion into this area, owing to the fact that Fe(I) complexes are very rare.

2.3.2.1 Excursion into Fe(I) chemistry: Facile synthesis and isolation of the first Fe(I) alkyl complex

Exploring the chemistry of Fe(I) complexes has been hampered by their inaccessibility owing to their propensity to disproportionate to Fe(0) and Fe(II) complexes. Examples reported so far include the recent $[Fe(3,5\text{-}^{i}Pr_2\text{-}2,6\text{-}Trip_2\text{-}C_6H_3)(\eta^6\text{-}C_6H_6)]$ compound reported by Power;[162] heteroleptic mononuclear Fe(I) carbonyl compounds, for example $[FeBr(CO)_2\{P(OMe)_3\}_2]$; [163] the Fe(I) alkynyl complexes of Bianchini;[164] and only a few other examples, such as the Fe^{I} arenes of Astruc and co-workers.[165] They have also been implicated in the homologization of olefins[166] and in the reductive cleavage of CO_2 at ambient temperatures[167] and have been proposed to be crucial in certain biological processes, which has motivated their study.[168] Fe(I) alkyl compounds have been observed transiently[169] and species of the type $[FeR(CO)_4]$ (R = acyl, H or alkyl) have been reported to be readily undergoing dimerisation, to be thermally very unstable and have not been isolated to date.[170] Square planar bis(imino)pyridyl Fe mono chloride and methyl complexes have been reported,[171] but subsequently shown to be high spin Fe(II) complexes, due to the non-innocence of the supporting ligand.[172] A comproportionation approach, similar to that used previously by Kandler *et al*. to prepare Fe(I) iodides and bromides, was used to access the precursor Fe(I) chloride complex: $[FeCl(depe)_2]$ **10-Fe** the first example in this class. This was achieved by reacting **1-Fe** with $[FeCl_2(depe)_2]$ in a 1:1 molar ratio in toluene with heating to 60 °C to afford high yields of the **12-Fe** as an air sensitive dark green-orange dichroic compound. Compound **10-Fe** could then be further reacted with MeLi in pentane at room temperature to afford **12-Fe** as a very air sensitive, bright orange solid. This reaction sequence is depicted in Scheme 2.3.7.

Dieses Werk ist copyrightgeschützt und darf in keiner Form vervielfältigt werden noch an Dritte weitergegeben werden.
Es gilt nur für den persönlichen Gebrauch.

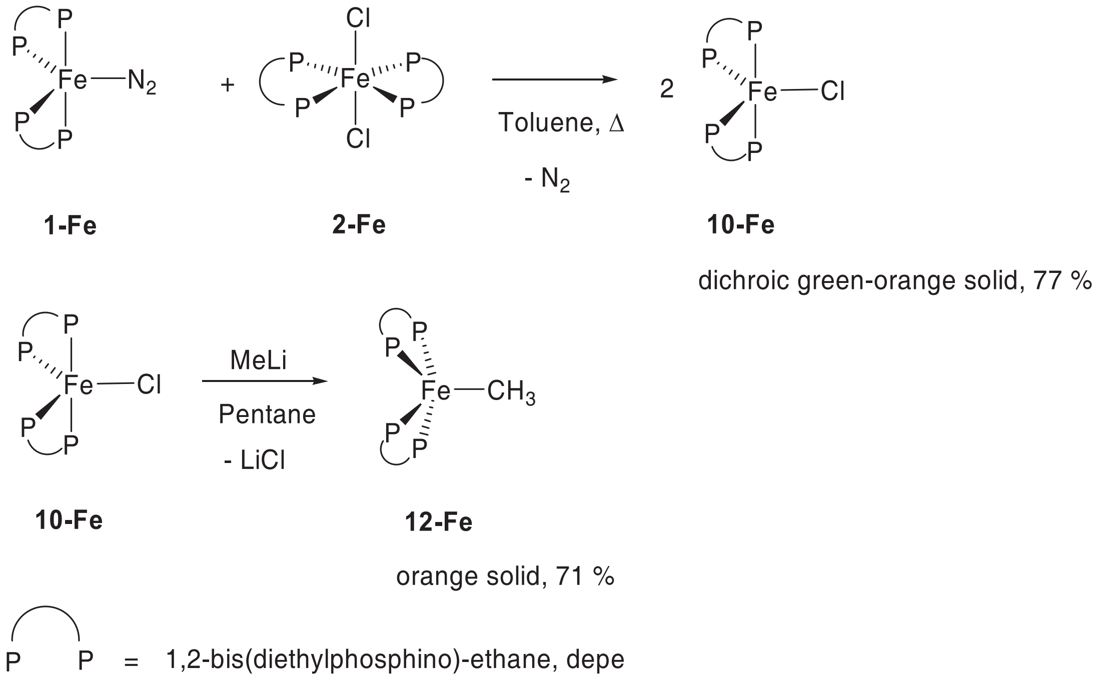

Figure 2.3.7: Synthesis of the Fe(I) chloride complex **10-Fe**, by comproportionation and its reaction with MeLi resulting in the first Fe(I) alkyl complex, **12-Fe**.

Both compounds **10-Fe** and **12-Fe** are remarkably thermally stable, and very soluble in pentane, benzene, cyclohexane and THF.

Crystals suitable for X-ray diffraction analysis for **10-Fe** were obtained by cooling a concentrated pentane solution to –30 °C to obtain green-orange dichroic crystals. Despite the extremely high lipophilicity of **12-Fe**, we managed to grow crystals suitable for X-ray diffraction analysis from Et_2O at –60 °C. Figure 2.3.16 and 2.3.17 show the molecular structures of compounds **10-Fe** and **12-Fe** in the solid state respectively.

Dieses Werk ist copyrightgeschützt und darf in keiner Form vervielfältigt werden noch an Dritte weitergegeben werden.
Es gilt nur für den persönlichen Gebrauch.

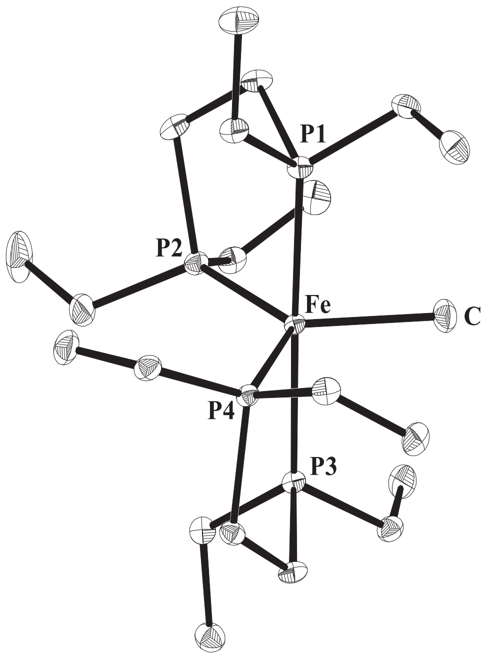

Figure 2.3.16: DIAMOND plot of the molecular structure of compound **10-Fe** in the solid state. Thermal ellipsoids are set at the 30% probability level, H atoms are omitted for clarity. Selected bond lengths [Å]: Fe–Cl 2.3145(6) Fe–P1 2.2306(6) Fe–P2 2.2154(6) Fe–P3 2.2542(6) Fe–P4 2.2231(7). Selected bond angles [°] P1-Fe-Cl 89.02(2) P4-Fe-P2 118.34(3) P3-Fe-P1 178.28(3) P2-Fe-Cl 122.49(3).

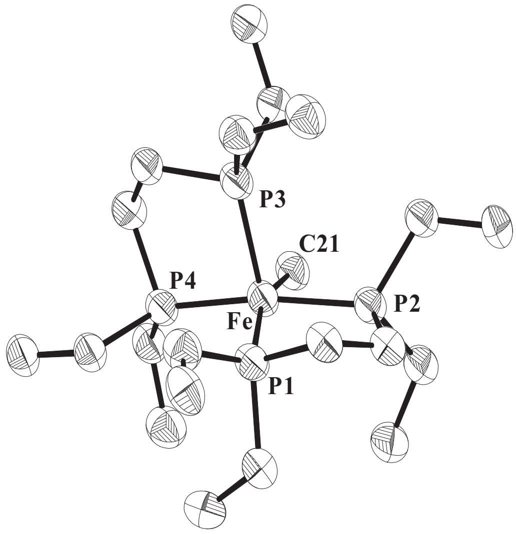

Figure 2.3.17: DIAMOND plot of the molecular structure of **12-Fe** in the solid state. Thermal ellipsoids are set at the 30% probability level, H atoms are omitted for clarity. Selected bond lengths [Å]: Fe–C21 2.070(5), Fe–P1 2.182(2), Fe–P2 2.192(2), Fe–P3 2.223(2), Fe–P4 2.210(2). Selected bond angles [°]: P4-Fe-P2 165.92(6), P4-Fe-P1 101.55(6), P4-Fe-P3 87.27(6), P2-Fe-P3 103.67(6), P1-Fe-P3 103.20(6), C21-Fe-P3 97.8(2), C21-Fe-P4 84.7(2), C21-Fe-P1 160.0(2).

Dieses Werk ist copyrightgeschützt und darf in keiner Form vervielfältigt werden noch an Dritte weitergegeben werden.
Es gilt nur für den persönlichen Gebrauch.

Compound **10-Fe** is the first structurally characterised Fe(I) chloride complex. It exhibits an ideal trigonal bipyramidal geometry about the Fe centre ($\tau = 1$), with little or no deviation(s) in the expected angles of 120° formed by the atoms in the trigonal plane, and 180° along the z axis. d^7 Configured systems that exhibit trigonal bipyramidal geometry are expected to show major Jahn-Teller distortions, resulting in symmetry lowering.[164] This is not the case for **10-Fe**, in contrast to the example Bianchini *et al*, where dramatic deviations from ideal trigonal bipyramidal geometry of an Fe(I) alkynyl complex were assumed to be linked to the Jahn-Teller effect.[164] The Fe–Cl bond length (2.3145(6) Å) is in the expected range from extrapolation of X-ray bonding parameters available for similar trigonal bipyramidal Fe(I)-I (2.610(1) Å) and Fe(I)-Br (2.423(2) Å) complexes.[163a] Compound **12-Fe** features a slightly distorted square pyramidal geometry ($\tau = 0.1$) , in contrast to that of **10-Fe**, with the methyl group occupying one of the basal positions and the phosphane ligands orientated in a spiro cyclic arrangement with Fe at the centre. The Fe-C21 bond length of 2.070(5) Å is slightly longer than that reported by Bianchini *et al*. (1.92(1) Å). This can be explained by the different hybridisation of the metal bonded carbon atom in **12-Fe** (sp^3); alkynyl complex (sp).

In compound **10-Fe** a broad signal at $\delta = -1.17$ ppm, $\Delta\nu_{½} = 314.57$ Hz is observed in the ^{1}H NMR spectrum in C_6D_6 at room temperature, while in **12-Fe** a resonance signal at $\delta = -1.49$, $\Delta\nu_{½} = 447.5$ Hz is observed, the increased line width probably resulting from the proximity of the CH_3 group paramagnetic d^7 iron centre (Figure 2.3.18 and 2.3.19). Additional NMR experiments where conducted for **10-Fe** in the chemical shift range $\delta = -200$ to + 200 ppm, and no additional resonance signals where located. Furthermore, Low temperature NMR experiments, also in the range $\delta = -200$ to + 200 ppm revealed no additional signals.

In both complexes resonance signals corresponding to $[FeCl_2(depe)_2]$ in the ^{1}H NMR spectrum of **10-Fe** and a mixture of *cis* and *trans* $[Fe(CH_3)_2(depe)_2]$ in the case of **12-Fe** are observable in the diamagnetic spectral window of the ^{1}H NMR spectrum.. These signals correspond to only trace amounts of the diamagnetic impurities, whose differing relaxation times compared to the paramagnetic components exaggerate their actual relative amount (see ref 173).[173]

Dieses Werk ist copyrightgeschützt und darf in keiner Form vervielfältigt werden noch an Dritte weitergegeben werden.
Es gilt nur für den persönlichen Gebrauch.

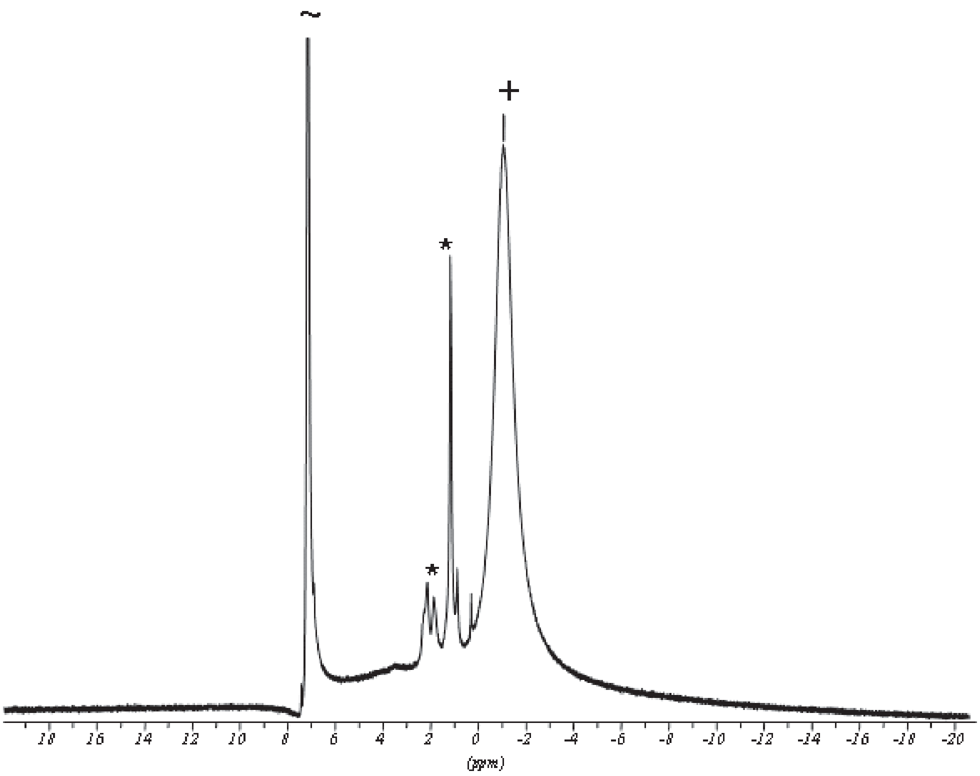

Figure 2.3.18: ^{1}H NMR spectrum of compound **10-Fe** in C_6D_6 at room temperature in the range δ = -20 to +20 ppm. ~ = solvent signal, * = diamagnetic impurities corresponding to $[FeCl_2(depe)_2]$, + = broad signal of **10-Fe** at δ = –1.17 ppm.

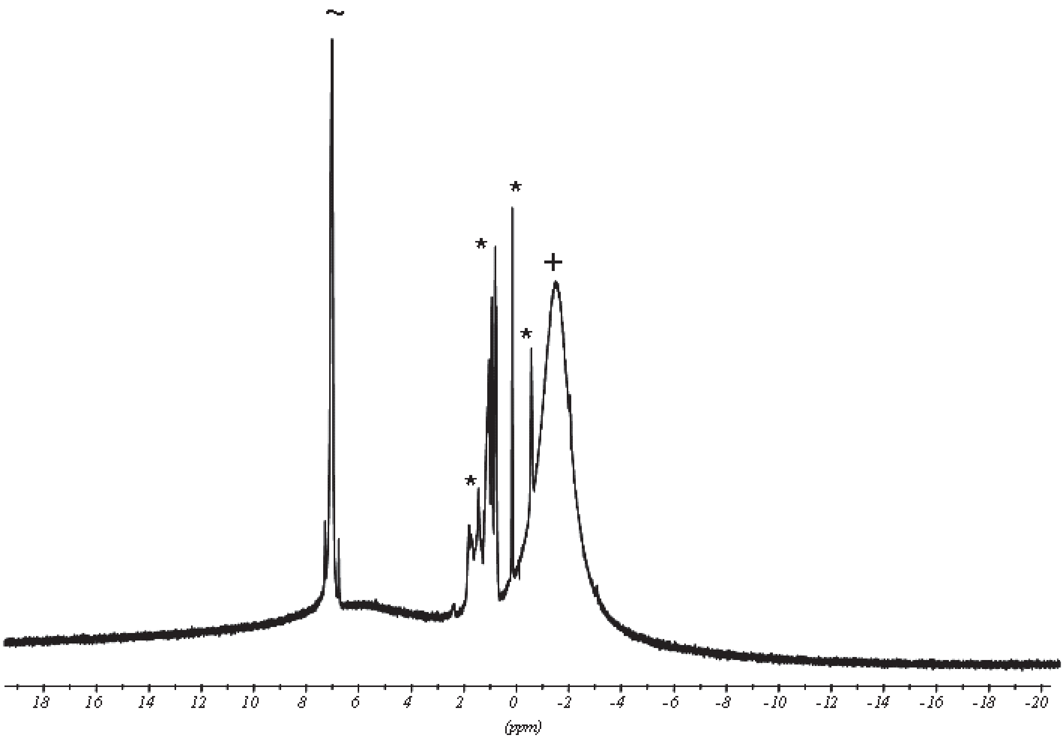

Figure 2.3.19: ^{1}H NMR spectrum of compound **2** in C_6D_6 at room temperature in the range δ = -20 to +20 ppm. ~ = solvent signal, * = diamagnetic impurities corresponding to *cis* and *trans* $[Fe(CH_3)_2(depe)_2]$, + = broad signal of **12-Fe** at δ = –1.49 ppm

Dieses Werk ist copyrightgeschützt und darf in keiner Form vervielfältigt werden noch an Dritte weitergegeben werden.
Es gilt nur für den persönlichen Gebrauch.

Compound **10-Fe** displays a structure less, isotropic EPR signal at $g_e = 2.0023$ at 30 K. The EPR spectrum is compatible with a d^7, S = ½ ground state of Fe. This state comprises a dynamic equilibrium of the degenerate d^1_{xy} and $d^1_{x}2\text{-}_{y}2$ states, in accordance with the observed trigonal bipyramidal ligand field. Compound **12-Fe** is characterized by *g* values of 2.14, 2.09 and 2.01 and displays ^{31}P (I = ½) hyperfine structure. The *g* values as well as the hyperfine structure are compatible with a non-degenerate d^7, $d^1{}_z{}^2$ ground state, expected for a square pyramid. The ^{31}P hyperfine structure at $g_x = 2.14$ shows a hyperfine structure with 1:2:2:2:1 intensity ratio, indicating the presence of two equivalent ^{31}P atoms and one ^{31}P with approximately twice the hyperfine coupling. The hyperfine structure at $g_z = 2.01$ display a composite pattern with 1:2:3:3:2:1 intensity ratio (Figure 2.3.20).

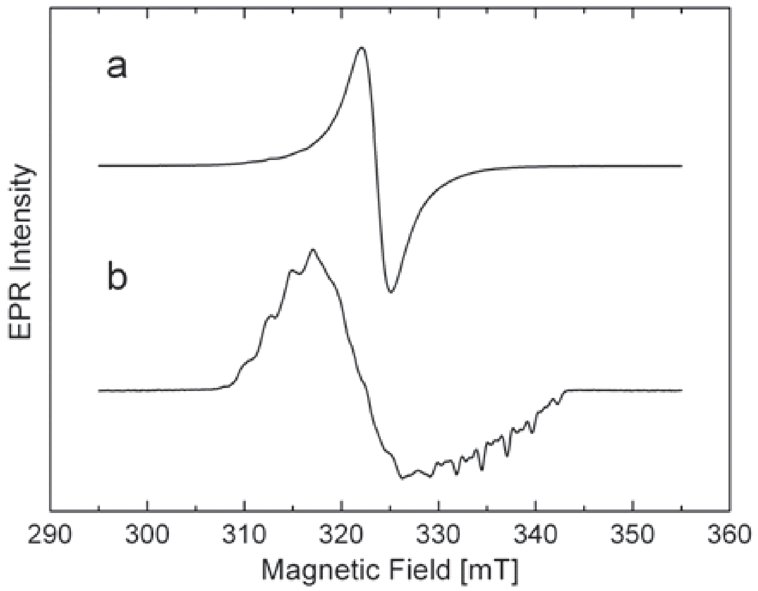

Figure 2.3.20: cw EPR spectra (T = 30 K) of compound **10-Fe** (a) and **12-Fe** (b). Experimental settings: $\nu_{mw} = 9.432$ GHz, $P_{mw} = 63$ µW, modulation amplitude 0.5 mT. For b: Coupling constants: $a_x(^{31}P) = 2.3$ mT = 64 MHz; $a_y(^{31}P) = 1.5$ mT = 43 MHz; $a_z(^{31}P) = 2.56$ mT = 72 MHz.

Dieses Werk ist copyrightgeschützt und darf in keiner Form vervielfältigt werden noch an Dritte weitergegeben werden.
Es gilt nur für den persönlichen Gebrauch.

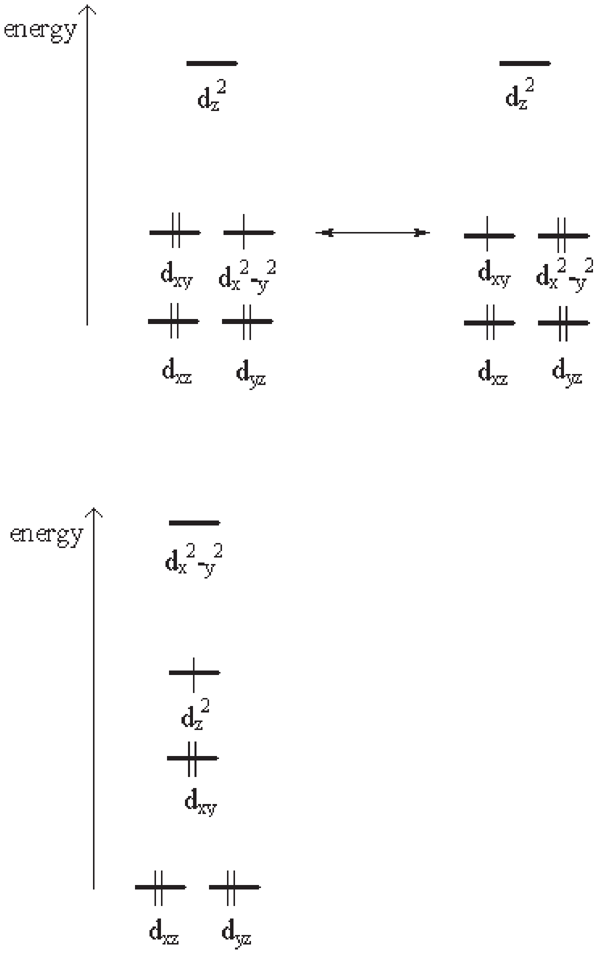

Figure 2.3.21: d^7 electron occupancy of a trigonal bipyramidal complex **10-Fe** (top) compared to a square pyramidal methyl complex **12-Fe** (bottom). The structure less EPR spectrum of complex **10-Fe**, along with the observed *g* value of a free electron, suggests dynamic behaviour of the electron between the approximately degenerate d_{xy} and $d_{x^2-y^2}$ orbitals. In complex **12-Fe** the electron is localised in the d_{z^2} orbital, which explains the hyperfine pattern observed.

Dieses Werk ist copyrightgeschützt und darf in keiner Form vervielfältigt werden noch an Dritte weitergegeben werden.
Es gilt nur für den persönlichen Gebrauch.

2.3.3 Complexes featuring double and triple bonding between Fe and Ge or Sn atoms: Facile access by phosphane elimination

In order to study the effect of reducing the steric bulk of the ligand on the Fe centre on multiple bonding to the tetrel atoms, a suitable precursor containing dmpe: 1,2-bis(dimethylphosphino)ethane as a supporting ligand at Fe was sought. Although the complex, [Fe(dmpe)$_2$(N$_2$)] **13-Fe** has been reported, it has not been formally isolated due to its apparent high reactivity.[174,175] Indeed, our attempts at preparing the complex in an analogous way to that of complex **1-Fe**, i.e. by reduction of the diamagnetic precursor complex, [Fe(dmpe)$_2$Cl$_2$] **14-Fe**, with Na sand under an atmosphere of N$_2$ in THF resulted, instead, in the very slow formation of the binuclear complex, [{Fe(dmpe)$_2$}$_2$(μ-dmpe)] **15-Fe**[176] as the major product with only trace amounts of the desired [Fe(dmpe)$_2$(N$_2$)] complex detectible by ^{31}P{^{1}H} NMR spectroscopy. Typically in these reduction reactions, free dmpe is liberated by decomposition during the course of the reaction, and the availability thereof can account for the formation of **15-Fe**.

Following this observation, the next obvious experiment was to perform the reduction of **14-Fe** with 2.3 eq. Na sand, in the *presence* of an additional 1 eq. free dmpe so as to prepare **15-Fe** selectively. This was also carried out in THF by stirring at room temperature, under argon and followed by *in situ* ^{31}P{^{1}H} NMR spectroscopy. The reduction is very slow, and takes *ca.* 94 h to converge, to **15-Fe** and proceeds *via* the formation of the related monomeric complex [Fe(dmpe)$_3$] **15-Fe-m**. Initially (after 2 h) only **15-Fe-m** is detectible as a result of the slow reduction rate and the presence of free dmpe in the system. As the dmpe is progressively consumed, however, a relative increase of the dimer **15-Fe** is observed, with concomitant consumption of **15-Fe-m** (Figure 2.3.23).

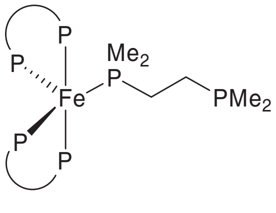

15-Fe-m

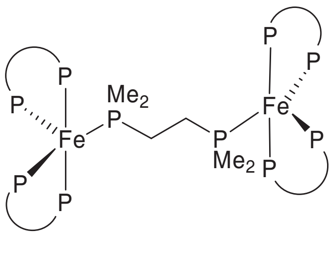

15-Fe

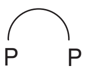

= 1,2-bis(dimethylphosphino)-ethane, dmpe

Figure 2.3.22: The monomeric complex **15-Fe-m** is an intermediate in the reduction of **14-Fe** with Na in THF resulting in **15-Fe**.

Dieses Werk ist copyrightgeschützt und darf in keiner Form vervielfältigt werden noch an Dritte weitergegeben werden.
Es gilt nur für den persönlichen Gebrauch.

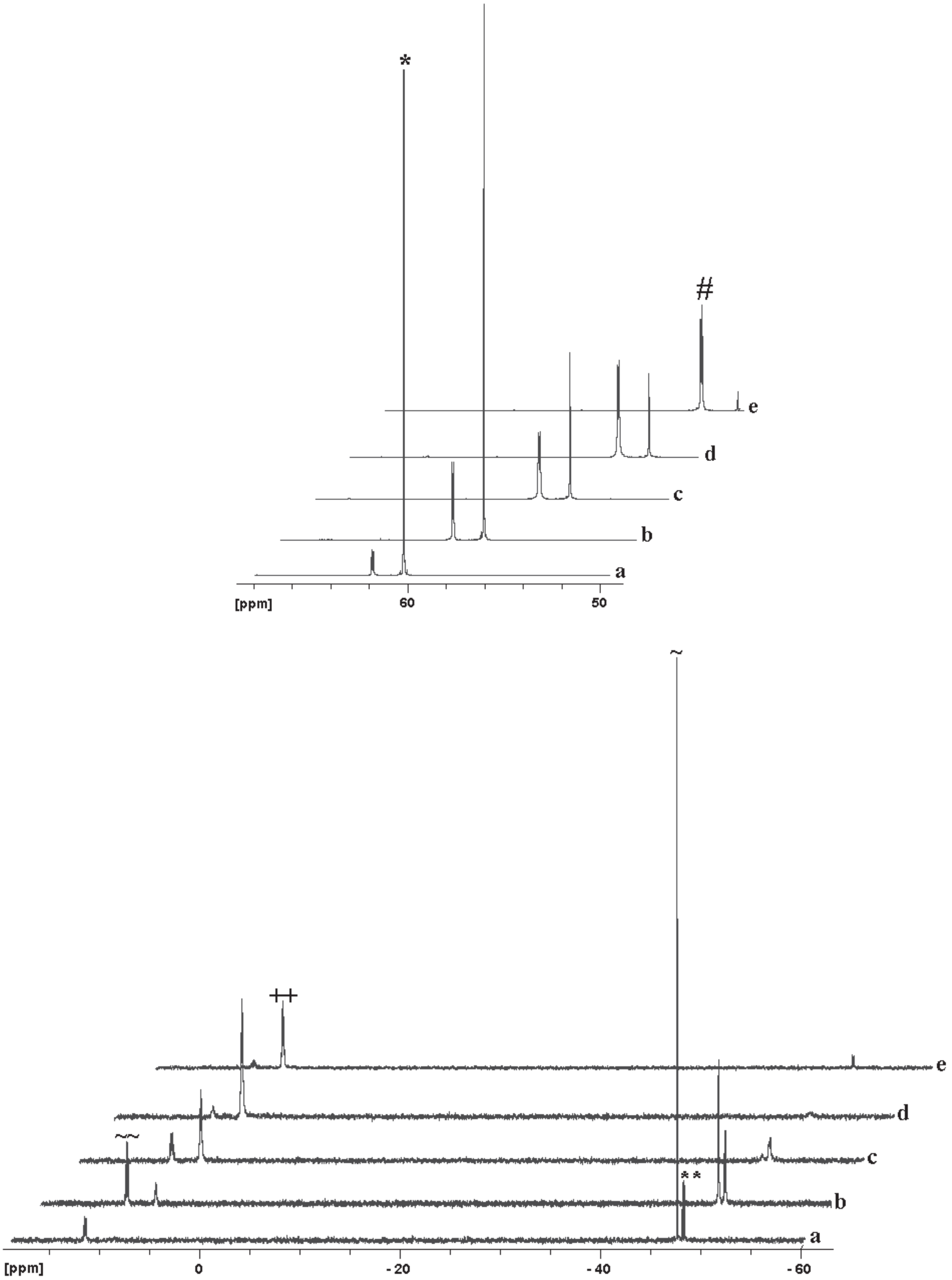

Figure 2.3.23: stacked *in situ* $^{31}P\{^{1}H\}$ NMR spectra of the reduction of **14-Fe** with 2.3 eq. Na sand in THF in the ranges $\delta = 50 - 68$ ppm (top) and $\delta = -60 - 20$ ppm (bottom). a = 2 h, b = 21 h, c = 46 h, d = 70 h, e = 94 h (after work up). * = **14-Fe**; # = two overlapping doublet signals resulting from dmpe in **15-Fe** and **15-Fe-m**; ~ = free dmpe; ** = pendant uncoordinated P atom in **15-Fe-m**; ~~ = η^1-dmpe P atom in **15-Fe-m**; ++ = η^1-dmpe P atoms in **15-Fe.**

Dieses Werk ist copyrightgeschützt und darf in keiner Form vervielfältigt werden noch an Dritte weitergegeben werden.
Es gilt nur für den persönlichen Gebrauch.

Owing to the high electron density at Fe in **15-Fe**, and since phosphane elimination reactions have been used before to access Mo germylidyne complexes,[177] **15-Fe** represented an ideal alternative precursor for the purposes of our chemistry, and so we abandoned further synthetic attempts at isolating the dinitrogen complex **13-Fe**.

Complex **15-Fe** has escaped characterisation by X-ray crystallographic analysis before, and so such an investigation was carried out. Despite the medium quality of the crystals and the resulting structure, various salient features are noted: the bridging phosphane ligand exists in a zigzag configuration, resulting in the two iron containing moieties being *trans* to each relative to the P···P linkage in close analogy to $[\{FeD(dmpe)_2\}(\mu\text{-}dmpe)][BPh_4]_2$, reported by Hughes *et al*.[178] Both Fe centres (Fe2 and Fe1) exhibit distorted square pyramidal geometries, with the phosphorus atom of the bridging phosphane occupying the apical site of the coordination sphere. The metric parameters are omitted for this molecular structure, owing to its medium quality.

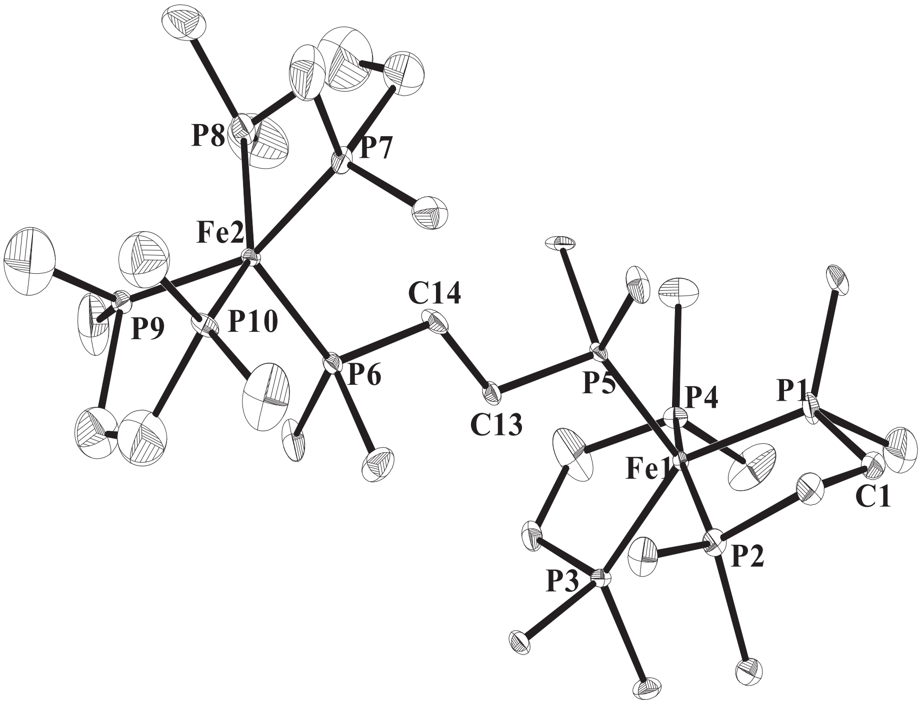

Figure 2.3.24: DIAMOND plot of the molecular structure of the **15-Fe** in the solid state. Thermal ellipsoids are set at the 30% probability level, H atoms are omitted for clarity. Atoms P10, P9, P8 and C1 exhibited side occupancies which have been omitted for clarity.

Complex **15-Fe** was shown in one NMR scale experiment, carried out in C_6D_6, indeed to rapidly react with **1-Sn** to form the brown stannylidene complex, $[(dmpe)_2Fe{=}SnCl(2,6\text{-}$

Dieses Werk ist copyrightgeschützt und darf in keiner Form vervielfältigt werden noch an Dritte weitergegeben werden.
Es gilt nur für den persönlichen Gebrauch.

Mes_2-C_6H_3)], **16-Fe** as the major product *via* phosphane elimination; along with [Fe(dmpe)$_2$Cl$_2$], resulting from redox chemistry as a minor product.

Following this result, reduction of **14-Fe** using excess KC_8 as reducing agent, in the presence of excess PMe_3, as opposed to free dmpe, was carried out to target the related reactive mononuclear complex, [Fe(dmpe)$_2$(PMe$_3$)] **17-Fe**, which we reasoned should show similar reactivity towards **1-Sn** as with **15-Fe**. The rationale behind targeting **17-Fe** as an alternative starting material to **15-Fe** was the availability and cost of PMe_3 compared to dmpe; and the fact that PMe_3 upon elimination resulting from the reaction with **1-Sn**, could easily be removed owing to its volatility, thereby possibly simplifying workup steps.

Indeed, the reduction of **14-Fe** with excess KC_8 in THF is very selective on the basis of *in situ* $^{31}P\{^1H\}$ NMR spectroscopy, which readily shows progressive and clean conversion to **17-Fe** (Figure 2.3.25).

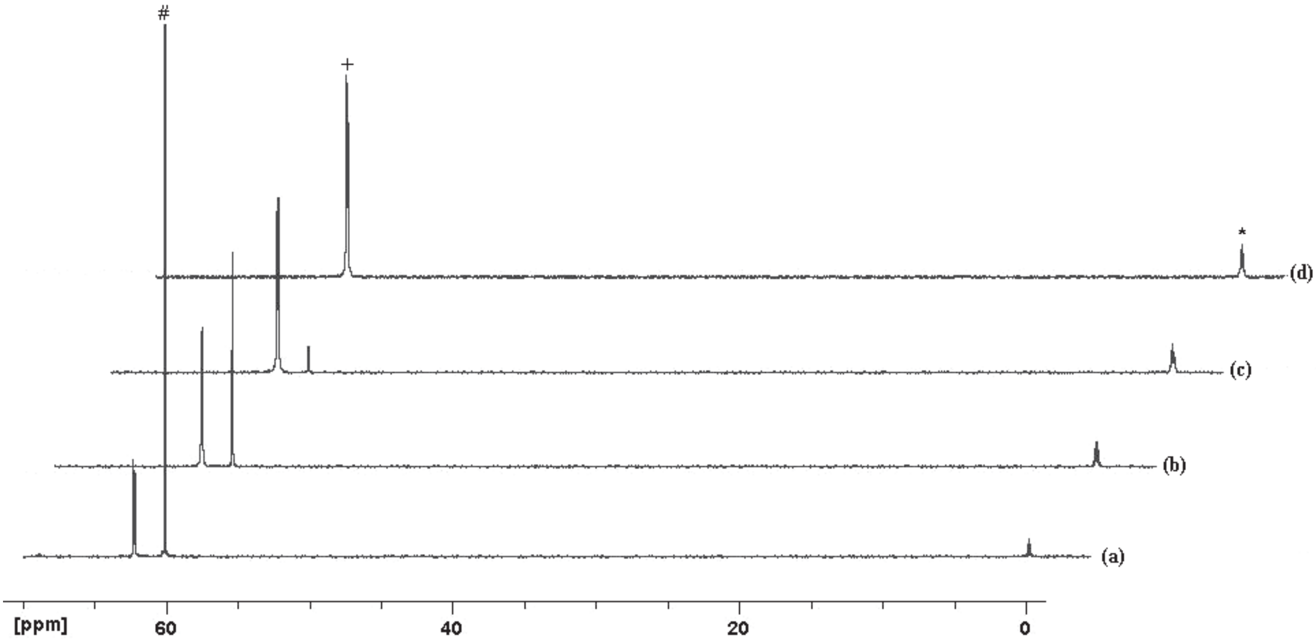

Figure 2.3.25: Stacked *in situ* $^{31}P\{^1H\}$ NMR spectra of the reduction of **14-Fe** with KC_8 in the presence of excess PMe_3, resulting in the clean and progressive formation of the complex **17-Fe**. * = quintet signal resulting from PMe_3; + = doublet signal resulting from dmpe ligands, # = **14-Fe**, progressively consumed. (a) After 3 h reaction time at 0 °C, (b) After a total of 4.5 h reaction time at 0 °C, and additionally 0.5 h at room temperature, (c) Additional stirring at RT for a further 2.5 h, (d) Additional stirring at RT for a further 1 h.

Dieses Werk ist copyrightgeschützt und darf in keiner Form vervielfältigt werden noch an Dritte weitergegeben werden.
Es gilt nur für den persönlichen Gebrauch.

Work-up by pentane extraction results in high isolable yields of the very air sensitive orange complex, **17-Fe** as is depicted in Scheme 2.3.8.

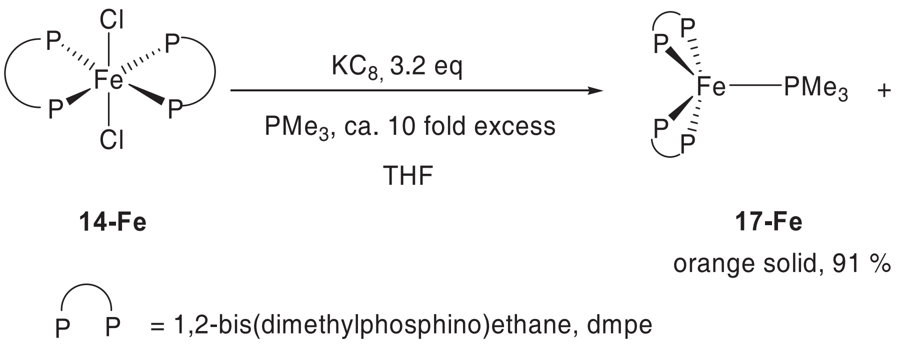

Scheme 2.3.8: Synthesis of complex **16-Fe** from **14-Fe** by reduction.

The $^{31}P\{^1H\}$ NMR spectrum of **17-Fe** in C_6D_6 shows two resonance signals in a ratio 1:4, corresponding to the PMe_3 ligand and dmpe ligands respectively. The 4 phosphorus atoms of both dmpe ligands are rendered equivalent by dynamic processes at room temperature, resulting in a doublet signal (at $\delta = 62.1$ ppm) through a $^2J(P,P)$ coupling to the PMe_3 ligand which appears as a quintet signal at $\delta = 0$ ppm. (Figure 2.3.26).

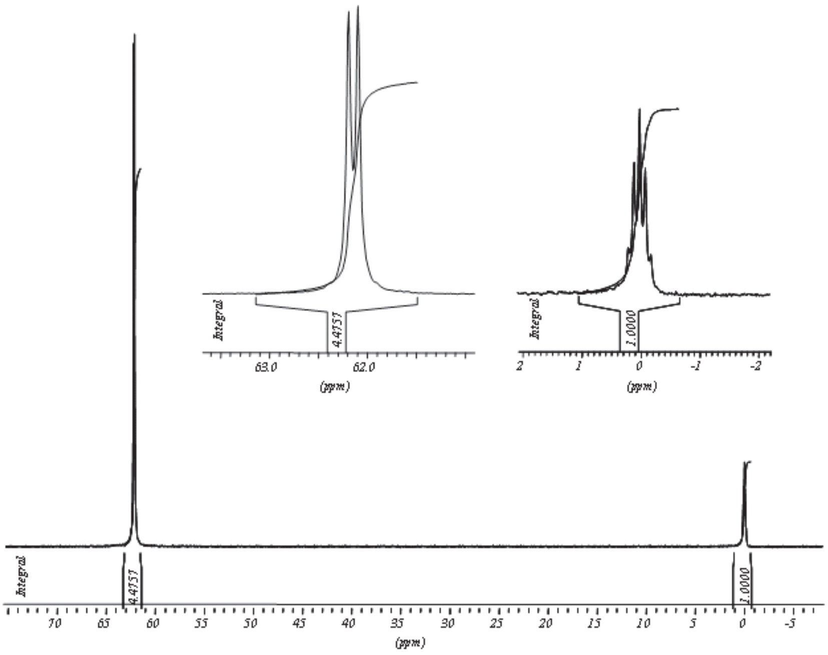

Figure 2.3.26: $^{31}P\{^1H\}$ NMR spectrum of **17-Fe** in C_6D_6 at room temperature. A clear doublet resonance signal corresponding to the dmpe phosphorus atoms, equivalent resulting from Berry pseudo rotation, and a double corresponding to the PMe_3 ligand are visible.

Dieses Werk ist copyrightgeschützt und darf in keiner Form vervielfältigt werden noch an Dritte weitergegeben werden.
Es gilt nur für den persönlichen Gebrauch.

Crystals, suitable for X-ray crystallographic analysis of **17-Fe** were also obtained by slow evaporation at room temperature of a concentrated C_6D_6 solution of the complex. Mononuclear Fe(0) pentacoordinate polyphosphane complexes are relatively rare and only a few solid state structural investigations have been carried out in this direction. An example of this is the study by Elschenbroich *et al.* in which a pentakis(η^1-phosphinine)Fe complex is reported to be distorted trigonal bipyramidal.[179] The complex [Fe{$(PF_2)_2NCH_3$}$_4$], by King *et al*. containing three monodentate and one bidentate $(PF_2)_2NCH_3$ ligand is also found to possess a distorted trigonal bipyramidal geometry in the solid state, with the P_{ax}-Fe-P_{eq} angle reported to be 69° due to the small bite angle of the bidentate ligand.[180] In contrast, Wong *et al.* has reported [Fe(dmpm)$_2$(η^1-dmpm)], where dmpm = bis(dimethylphosphino)methane, as square pyramidal in the solid state, with the apical site occupied by the pendant phosphane ligand.[181] In close analogy to this example, the geometry at the Fe centre in **17-Fe** can be viewed as distorted square pyramidal (τ = 0.21), the distortion in the direction of trigonal bipyramidal geometry, with the PMe_3 ligand occupying the apical coordination site. The Fe–P bond lengths are all comparable in the case of complex **17-Fe**, which is in close agreement with the example by Wong.

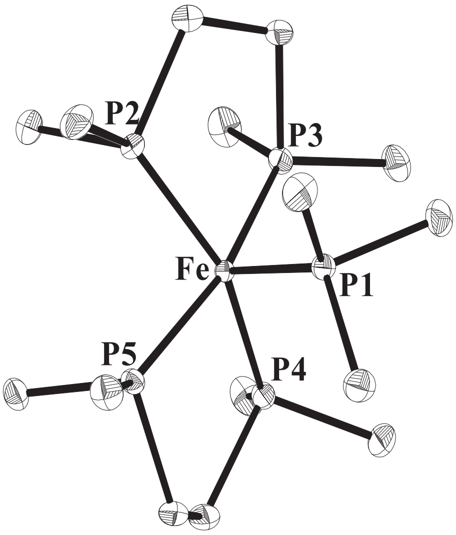

Figure 2.3.27: DIAMOND plot of the molecular structure of the complex **17-Fe** in the solid state. Thermal ellipsoids are set at the 50% probability level, H atoms are omitted for clarity. Selected bond lengths [Å]: Fe–P1 2.1582(7), Fe–P2 2.1629(7), Fe–P3 2.1620(8), Fe–P4 2.1580(7), Fe–P5 2.1618(7). Selected bond angles [°]: P4-Fe-P1 106.16(3), P4-Fe-P5 84.40(3), P1-Fe-P5 99.13(3), P4-Fe-P3 91.10(3), P1-Fe-P3 100.75(3), P5-Fe-P3 160.10(3), P4-Fe-P2 147.26(3), P1-Fe-P2 106.55(3), P5-Fe-P2 92.05(3), P3-Fe-P2 81.29(3).

Dieses Werk ist copyrightgeschützt und darf in keiner Form vervielfältigt werden noch an Dritte weitergegeben werden.
Es gilt nur für den persönlichen Gebrauch.

Reaction of **17-Fe** with **1-Sn** yields an immediate colour change to brown in Et_2O (as with **15-Fe**), and results in the formation of [$(dmpe)_2Fe{=}SnCl(2,6\text{-}Mes_2\text{-}C_6H_3)$], **16-Fe** (Scheme xx), with concomitant PMe_3 elimination (also visible in the *in situ* $^{31}P\{^1H\}$ NMR spectrum of the reaction mixture before work up) (Scheme 2.3.9).

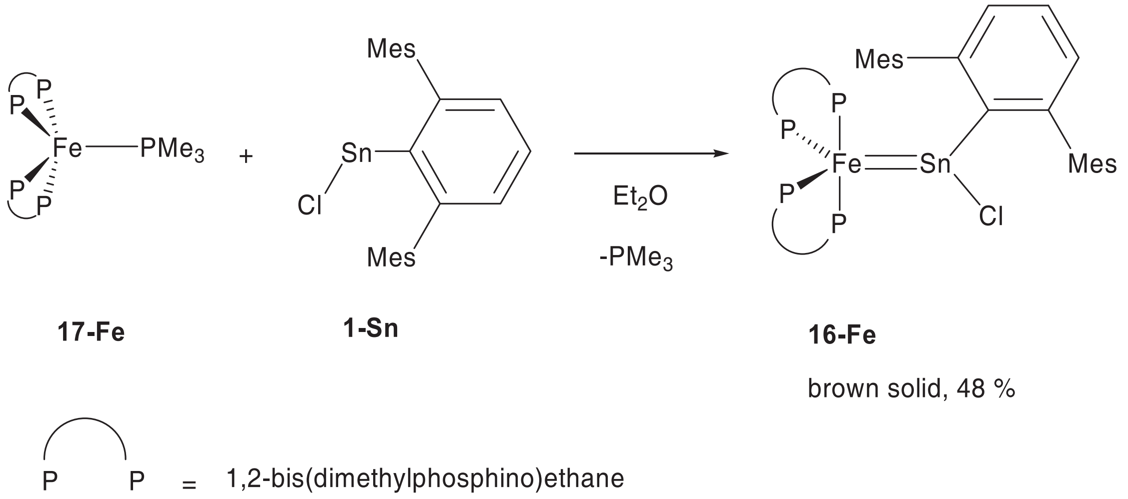

17-Fe **1-Sn** **16-Fe**

brown solid, 48 %

1,2-bis(dimethylphosphino)ethane

Scheme 2.3.9: Synthesis of complex **16-Fe** by reaction with **1-Sn** with **17-Fe**.

Comparison of the NMR spectral features of **16-Fe** with the more sterically demanding analogue, **3-Fe**, yields some obvious differences: in complex **16-Fe**, the $^{31}P\{^1H\}$ resonance signal appears as a singlet signal with tin satellites at $\delta =$ 60.2 ppm, considerably up field from that of **3-Fe**. The coordination induced chemical shift difference of P, relative to the free ligand according to ^{31}P NMR spectroscopy, however, in **3-Fe** is 96 ppm compared to that of **16-Fe** at 108 ppm, a negligible difference between the two compounds which does not warrant further discussion.[182] The $^2J(P,^{119}Sn)$ coupling constant in complex **16-Fe** is, however, considerably lower (*ca.* 50 Hz) in comparison to complex **3-Fe** at 100 Hz, and the $^{119}Sn\{^1H\}$ resonance signal in C_6D_6 of complex **16-Fe** appears at $\delta =$ 527.2 ppm, compared with that of $\delta =$ 471.5 ppm of complex **3-Fe** (both are quintet signals). These differences are commented on later on in the discussion.

The molecular structure of **16-Fe** in the solid state was also determined by X-ray crystallographic analysis and is presented in Figure 2.3.28.

Dieses Werk ist copyrightgeschützt und darf in keiner Form vervielfältigt werden noch an Dritte weitergegeben werden.
Es gilt nur für den persönlichen Gebrauch.

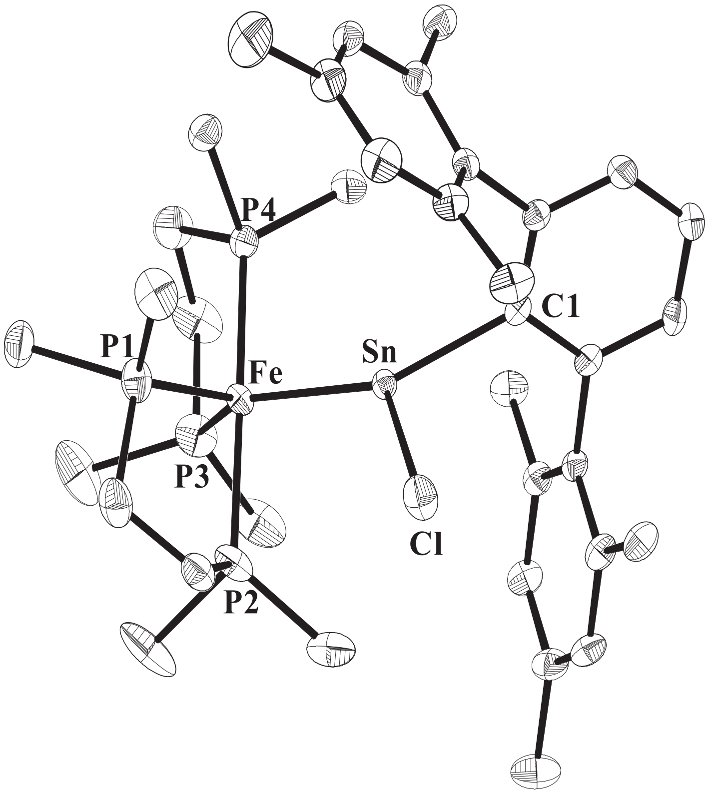

Figure 2.3.28: DIAMOND plot of the molecular structure of complex **16-Fe** in the solid state. Thermal ellipsoids are set at the 50% probability level. H atoms are omitted for clarity. Selected bond lengths [Å]: Fe–Sn 2.3776(5), Sn–Cl 2.5005(9), Sn–C(1) 2.208(3), Fe–P1 2.1680(10), Fe–P2 2.2089(19), Fe–P3 2.1746(10), Fe–P4 2.1912(10). Selected bond angles [°]: Fe-Sn-Cl 118.51(2), Fe-Sn-C(1) 149.79(8), C(1)-Sn-Cl 91.70(8), P1-Fe-P3 117.86(4), P1-Fe-P4 98.71(4), P3-Fe-P4 83.84(4), P1-Fe-P2 84.02(4), P3-Fe-P2 91.55(4), P4-Fe-P2 175.34(4), P1-Fe-Sn 109.02(3), P3-Fe-Sn 133.02(4), P4-Fe-Sn 92.46(3), P2-Fe-Sn 90.20(3).

The Fe–Sn bond lengths of complex **3-Fe** (2.409(1) Å) and **16-Fe** (2.3776(5) Å) are comparable, suggesting no dramatic changes in the π-back bonding to Sn on changing from depe to dmpe as supporting ligand at the Fe centre. The geometry at the Fe centre of **16-Fe** is trigonal bipyramidal ($\tau = 0.96$) , as in the case of **3-Fe**, but in contrast to its precursor, **17-Fe**. The stannylene ligand, as with **3-Fe** is in an upright configuration to accommodate optimal π-back bonding from the Fe centre. Comparison of the metric parameters of **16-Fe** to **3-Fe** yields some interesting differences; the most striking of which is the Fe-Sn-C(1) bond angle of 149.79(8)° compared to the analogous angle in **3-Fe** at 158.5(2)° (Figure 2.3.29). This observation can be linked to the decreased steric bulk of the dmpe ligand in complex **16-Fe**, compared to depe in **3-Fe**, which enables the stannylene moiety to tilt closer towards the iron centre. The Cl-Sn-C(1) bond angle in complex **16-Fe** is 5° larger than the corresponding bond angle in complex **3-Fe**, and the Fe-Sn-Cl bond angle in **16-Fe** is 118.51(2)° compared

Dieses Werk ist copyrightgeschützt und darf in keiner Form vervielfältigt werden noch an Dritte weitergegeben werden.
Es gilt nur für den persönlichen Gebrauch.

to that of 114.04(7)° in **3-Fe**. These angular changes evidence the three coordinate Sn centre in **16-Fe** to approach a Y-shaped planar coordination (trigonal planar), compared to a more T-shaped planar coordination in **3-**Fe and could account for the ^{2}J(P,^{119}Sn) coupling constant variation between the two complexes (see discussion later). Hence decrease of steric bulk on the Fe centre by exchanging depe for dmpe ligands, does have an effect on the geometry of the Sn centre.

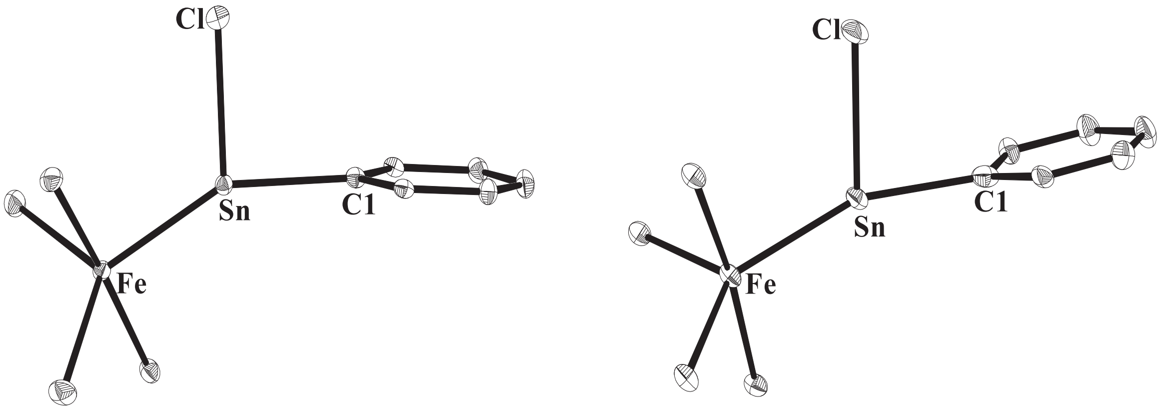

Figure 2.3.29: DIAMOND plot of complex **16-Fe** (left) and **3-Fe** (right) (H atoms, Mes groups, omitted, only P atoms represented at Fe centre for clarity). A decrease in the linearity of the Fe-Sn-C(1) bond axis in the former complex can be explained by the decreased steric bulk of the ligand at the Fe centre, enabling the stannylene moiety to tilt towards the Fe centre, with an accompanying change to Y-shaped geometry.

Attempts at preparing the ionic stannylidyne complex [(dmpe)$_2$Fe≡Sn(2,6-Mes$_2$-C$_6$H$_3$)][SnCl$_2$(2,6-Mes$_2$-C$_6$H$_3$)] by reacting **16-Fe** with an additional equivalent of **1-Sn** in analogy to the synthesis of the depe stannylidyne complex analogue **4-Fe** were unsuccessful. Stirring a 1:1 mixture of **16-Fe** with **1-Sn** in Et$_2$O at room temperature, followed by the addition of another equivalent **1-Sn** resulted in the formation of [FeCl$_2$(dmpe)$_2$] with unreacted **16-Fe** present in the reaction mixture based on ^{1}H and ^{31}P{^{1}H} NMR spectroscopy. This result suggests a different reactivity of **16-Fe** to **3-Fe** towards **1-Sn**, and suggests a decreased propensity of chloride abstraction from Sn in **16-Fe**.

Reaction of the precursor complex **17-Fe** with the germylene **2-Ge**, indeed enabled the isolation of the Ge analogue of **16-Fe,** denoted **16-Fe-2**, which represents the first halo-germylidene complex of iron [Fe(dmpe)$_2$=GeCl(2,6-Mes$_2$-C$_6$H$_3$)]. As pointed out in section

Dieses Werk ist copyrightgeschützt und darf in keiner Form vervielfältigt werden noch an Dritte weitergegeben werden.
Es gilt nur für den persönlichen Gebrauch.

2.3.1.3, earlier attempts at isolating the iron chlorogermylidene complex, [Fe(depe)$_2$=GeCl(2,6-Trip$_2$-C$_6$H$_3$)], failed and it was ascribed to the steric pressure associated with the depe ligands and **1-Ge** containing peripheral Trip substituents. This reaction instead resulted in the direct formation of the germylidyne complex [Fe(depe)$_2$≡Ge(2,6-Trip$_2$-C$_6$H$_3$)][GeCl$_2$(2,6-Trip$_2$)] in low yields (27 %). By lowering the steric bulk on the Fe centre from depe to dmpe *and* decreasing the steric bulk on the germylene from Trip to Mes, isolation of the chloro-germylidene is possible; demonstrating the argument of sterics *was* responsible for the inability to isolate the bulkier chloro-germylidene earlier. Crystals, suitable for X-ray diffraction analysis of **16-Fe-2** were obtained from pentane at –30 °C. The solid state structure reveals distortion of the dmpe bridges, which on closer inspection can be accounted for by a combination of two co-existing isomeric forms (Figure 2.3.30), although the remainder of the structure is unaffected by this disorder.

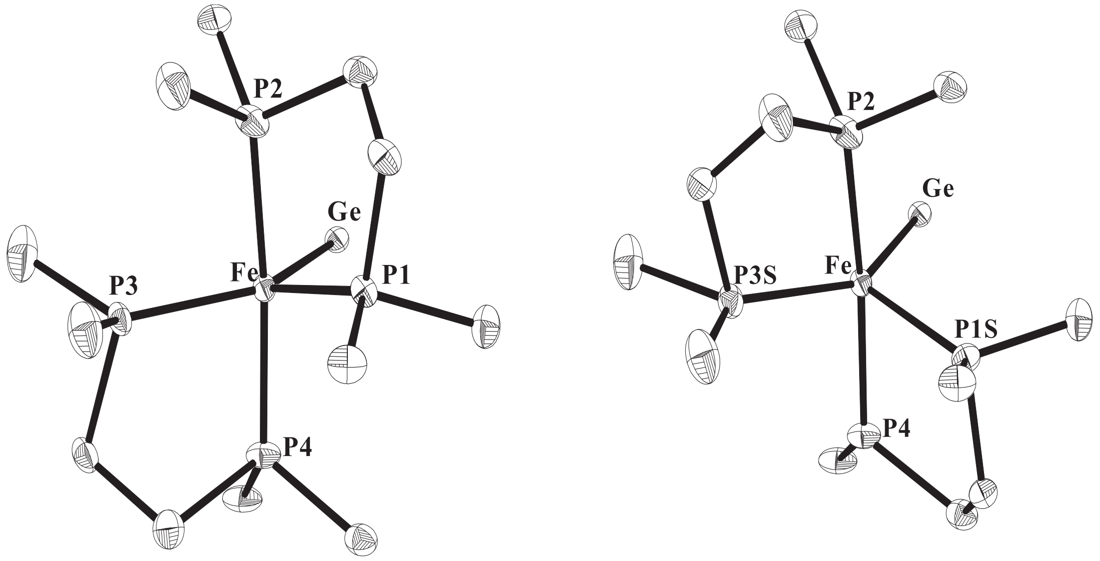

Figure 2.3.30: Two stereoisomeric (diastereomeric) forms of complex **16-Fe-2**. The isomer shown on the left accounts for 78 % occupancy, while that on the right, 22 %.

Figure 2.3.31 shows the solid state structure of the major stereoisomer in the solid state as determined by X-ray diffraction analysis, upon which the following discussion is based.

Dieses Werk ist copyrightgeschützt und darf in keiner Form vervielfältigt werden noch an Dritte weitergegeben werden.
Es gilt nur für den persönlichen Gebrauch.

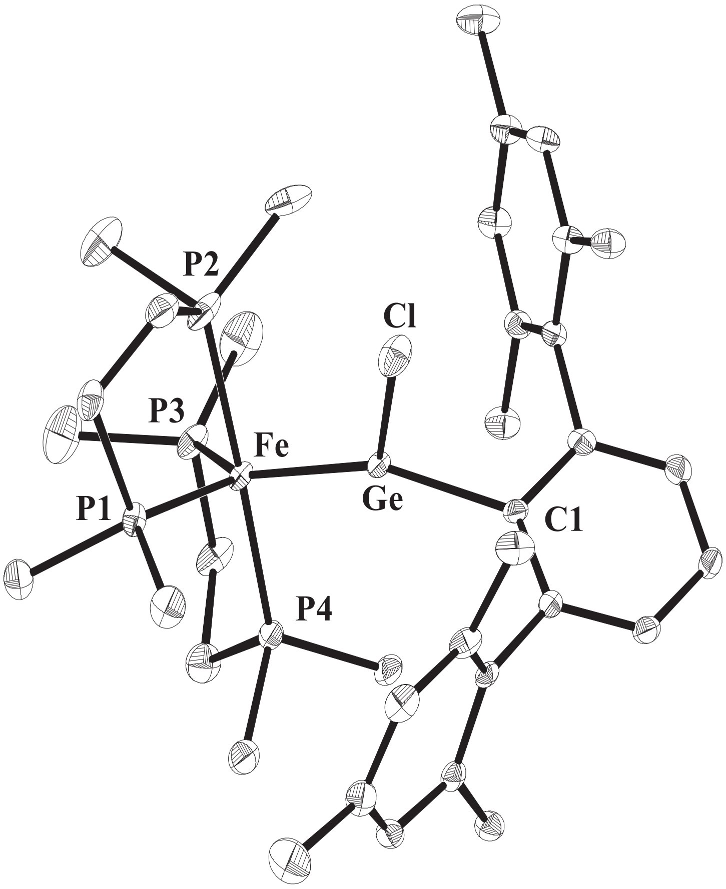

Figure 2.3.31: DIAMOND plot of complex **16-Fe-2** in the solid state. Thermal ellipsoids are set at 30 % probability. H atoms omitted for clarity. Selected bond lengths [Å]: Fe–Ge 2.2011(7), Ge–Cl 2.322(1), Fe–P1 2.167(2), Fe–P2 2.202(1), Fe–P3 2.178(3), Fe–P4 2.185(1). Selected bond angles [°]: Fe-Ge-C(1) 148.5(1), Fe-Ge-Cl 119.89(4), C1-Ge-C(1) 91.6(1), P2-Fe-P4 174.67(5), P3-Fe-P1 117.50(10), P2-Fe-Ge 90.46(4).

Complex **16-Fe-2** exhibits a trigonal bipyramidal geometry ($\tau = 0.95$) about the iron centre, as with the Sn analogue, **16-Fe**. The Fe–Ge bond length of 2.2011(7) Å is 18 pm shorter than that of the Fe–Sn bond length observed in **16-Fe,** in accordance with the decreased covalent radius of Ge vs Sn. The Ge centre is planar, as with **16-Fe**, and only small angular changes are observed in comparing the bond angles around the Ge centre is **16-Fe-2** to **16-Fe** (Figure 2.3.32).

Dieses Werk ist copyrightgeschützt und darf in keiner Form vervielfältigt werden noch an Dritte weitergegeben werden.
Es gilt nur für den persönlichen Gebrauch.

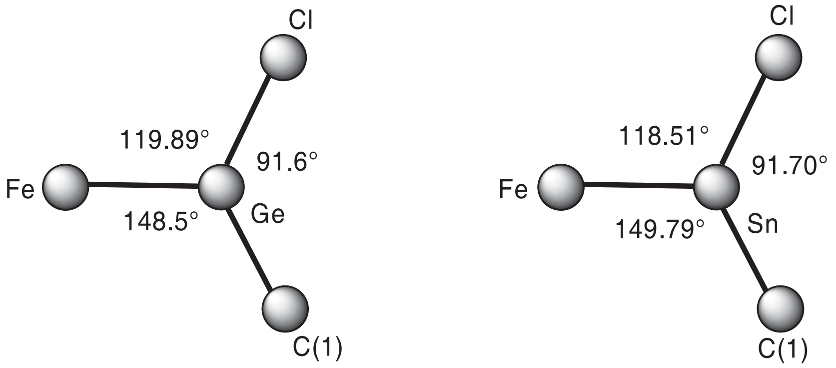

Figure 2.3.32: Comparison of **16-Fe-2** (left) and **16-Fe** (right) showing comparable angular parameters around the tetrel atom (standard deviations omitted).

Chloride abstraction from **16-Fe-2** with $B(C_6F_5)_3$ in toluene did result in the selective formation of the germylidyne complex $[Fe(dmpe)_2{\equiv}Ge(2,6\text{-}Mes_2\text{-}C_6H_3)][BCl(C_6F_5)_3]$ (**16-Fe-3**), with small amounts of the $[FeCl_2(dmpe)_2]$ as an impurity in high yields (Scheme 2.3.10)

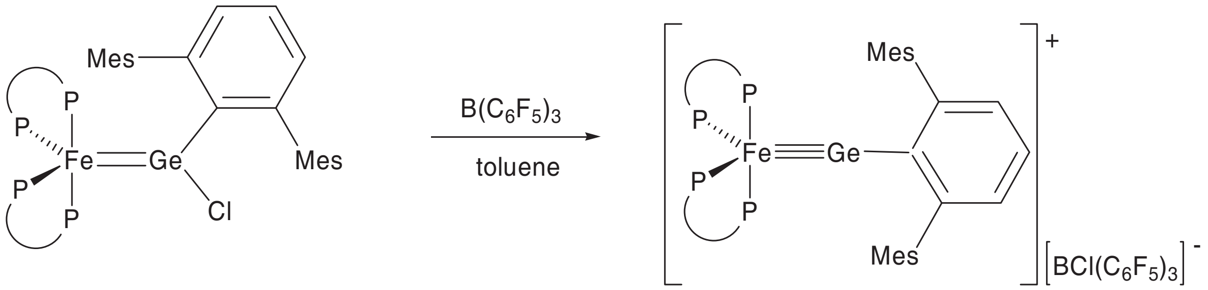

16-Fe-2

16-Fe-3

Golden yellow solid, 82 %

Scheme 2.3.10: Synthesis of the germylidyne complex **16-Fe-3** from the germylidene complex **16-Fe-2**.

The ^1H NMR spectrum of **16-Fe-3** in THF-d_8 shows two sets of singlet resonance signals for the diastereotopic CH_3 groups of the two dmpe ligands, and two sets of diastereotopic CH_2 groups (each integrating to 4 protons) for the bridging protons of the dmpe ligands. A 6:12 ratio is observed for the resonance signals of the mesityl groups (para:ortho) along with a doublet (2 protons), singlet (4 protons) and triplet (1 proton) in the aromatic region, consistent with the structure of **16-Fe-3**. (Figure 2.3.33).

Dieses Werk ist copyrightgeschützt und darf in keiner Form vervielfältigt werden noch an Dritte weitergegeben werden.
Es gilt nur für den persönlichen Gebrauch.

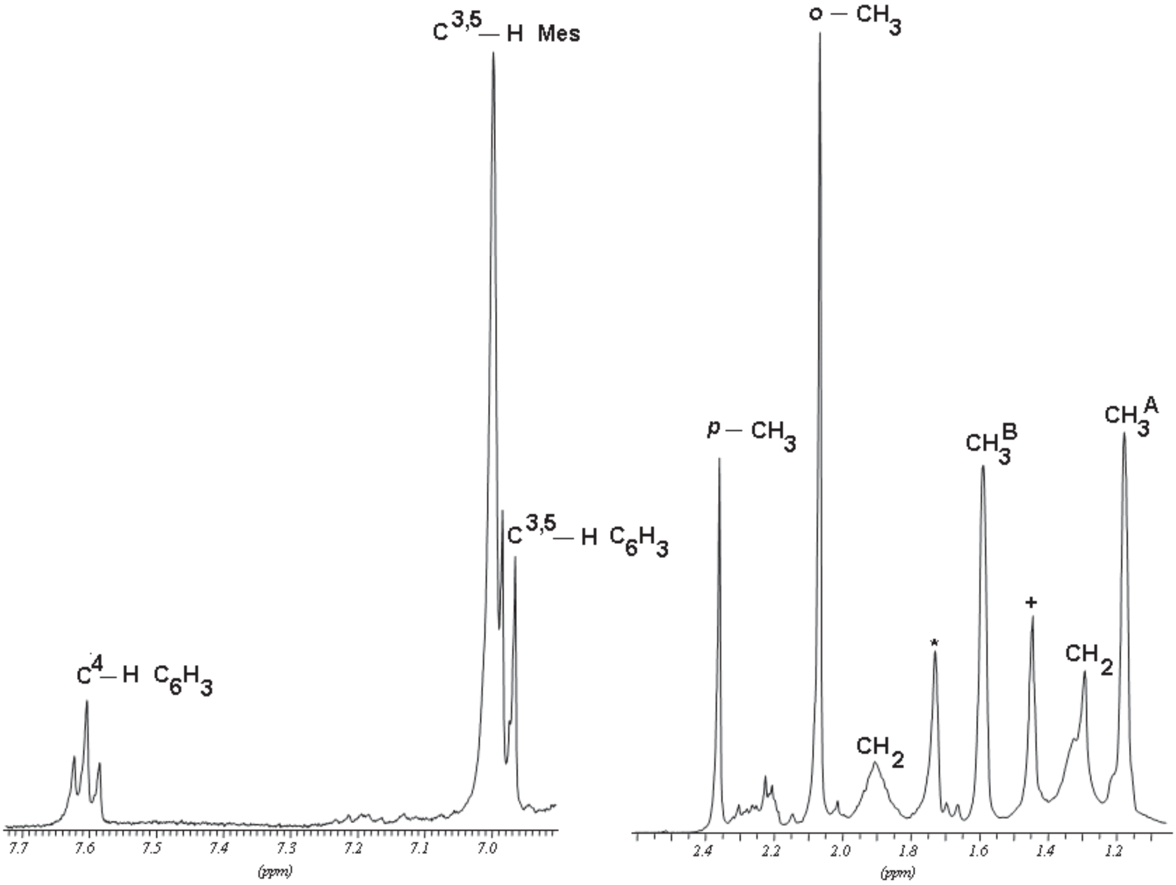

Figure 2.3.33: ^{1}H NMR spectrum of germylidyne complex **16-Fe-3** depicted in the aromatic region (left) and aliphatic region (right). * = THF solvent residue signal, + = impurity = [FeCl$_2$(dmpe)$_2$].

As with all the other complexes discussed in this section, a sharp resonance signal in the ^{31}P{^{1}H} NMR spectrum is observed at δ = 62.5 ppm in THF-d$_8$, resulting from Berry pseudo rotation. The ^{11}B{^{1}H} NMR spectrum shows a broad resonance signal at δ = -7.5 ppm in THF-d$_8$ for the counter-anion, which is identical to the shift measured for the complex [(depe)$_2$Fe≡Sn(2,6-Mes$_2$-C$_6$H$_3$)][BCl(C$_6$F$_5$)$_3$] **5-Fe** discussed earlier, clearly indicating its presence. The characteristic ipso carbon atom, bonded to germanium resonates at δ = 162.2 ppm in THF-d$_8$ in the ^{13}C{^{1}H} NMR spectrum.

Unfortunately attempts at obtaining suitable crystals of **16-Fe-3** for X-ray crystallographic analysis where not successful.

Dieses Werk ist copyrightgeschützt und darf in keiner Form vervielfältigt werden noch an Dritte weitergegeben werden.
Es gilt nur für den persönlichen Gebrauch.

2.3.4: Reactivity of C,H activated iron complexes towards 1-Sn: insertion, reverse CH activation, and redox chemistry.

Having extensively investigated the reactivity of ylenes of Ge, Sn towards iron complexes bearing ligands capable of elimination (N_2 or PMe_3) we next turned our attention to explore the reactivity of the stannylene **1-Sn** towards iron precursors bearing ligands involved in CH activation. Precedence exists for the reactivity of such complexes with **1-Ge** and **1-Pb** in the case of W, resulting in germylidyne and plumbylidyne complexes. In the case of the reactive seven coordinate CH activated complex, $[WH(PMe_3)_4\{\eta^2\text{-}CH_2PMe_2\}]$ it was shown that reaction with **1-Ge** results in the formation of the insertion product $[W(H)Cl(PMe_3)_3\{=Ge(2,6\text{-}Trip_2\text{-}C_6H_3)(CH_2PMe_2)\}]$ below –20 °C, with PMe_3 elimination, which could be converted to the germylidyne complex *trans*-$[WCl(PMe_3)_4{\equiv}Ge(2,6\text{-}Trip_2\text{-}C_6H_3)]$ by heating in toluene at 50 °C. The latter step involves a reversal of the previously CH activated group. Similarly, the reaction of $[WH(PMe_3)_4\{\eta^2\text{-}CH_2PMe_2\}]$ with **1-Pb**, readily results in the complex *trans*-$[Br(PMe_3)_4W{\equiv}Pb(2,6\text{-}Trip_2\text{-}C_6H_3)]$ with PMe_3 elimination, even at –78 °C, again with CH activation reversal.[183] We therefore envisaged a similar reactivity would result from similar Fe complexes bearing phosphane ligands engaged in CH activation, and particularly focussed on the reactivities of these complexes with **1-Sn**, with the view extending the approach to access ylidyne complexes of W, to Fe.

2.3.4.1 Insertion of 1-Sn into $[FeH\{\eta^2\text{-}CH_2PMe_2\}(PMe_3)_3]$ 18-Fe

We first targeted targeted the complex $[FeH\{\eta^2\text{-}CH_2PMe_2\}(PMe_3)_3]$[184,185] **18-Fe** as a suitable starting material, which is closely related to $[WH(PMe_3)_4\{\eta^2\text{-}CH_2PMe_2\}]$, although the latter is seven coordinate. Complex **18-Fe** can readily be prepared from $[FeCl_2(PMe_3)_2]$ **19-Fe** by reduction over Na/Hg in THF in the presence of PMe_3. Owing to the reported thermolability and sensitivity of the complex, it was prepared *in situ* and reacted immediately with and equivalent of **1-Sn** at low temperatures with progressive warming to room temperature. This procedure enabled, after work-up, the isolation of an orange solid **20-Fe** in moderate yields (Scheme 2.3.11) as a mixture of 3 stereoisomers as evidenced by ^1H NMR in the hydride region, where 3 distinctive hydride resonance signals are observed. In this case, selective *insertion* of **1-Sn** into the Fe–CH_2 linkage occurs.

The $^1H\{^{31}P\}$ NMR spectrum in the hydride region clearly shows tin satellites, generated through $^2J(H,{}^{117/119}Sn)$ couplings (Figure 2.3.34). There is no evidence, whatsoever, that any

Dieses Werk ist copyrightgeschützt und darf in keiner Form vervielfältigt werden noch an Dritte weitergegeben werden.
Es gilt nur für den persönlichen Gebrauch.

of the signals in the hydride region are un-reacted starting material, since all signals in the $^{1}H\{^{31}P\}$ NMR spectrum are flanked with Sn satellites. Although the starting material for this complex was not characterised, and only generated *in situ*, this reaction was carried out on multiple occasions, with comparable results.

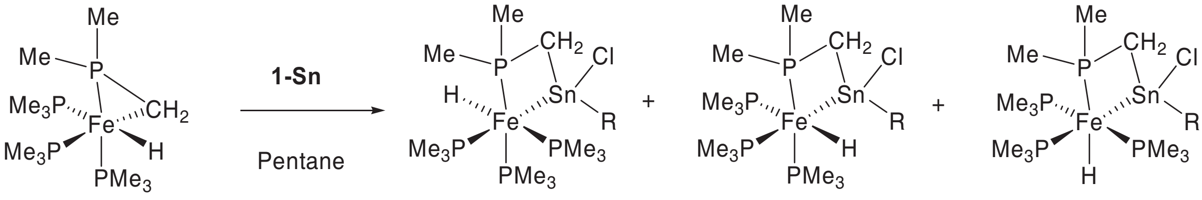

18-Fe

20-Fe

Orange solid, 64 %

R = 2,6-Mes$_2$-C$_6$H$_3$

Scheme 2.3.11: Reaction of **18-Fe** with **1-Sn** results in insertion and the formation of three detectable stereoisomers.

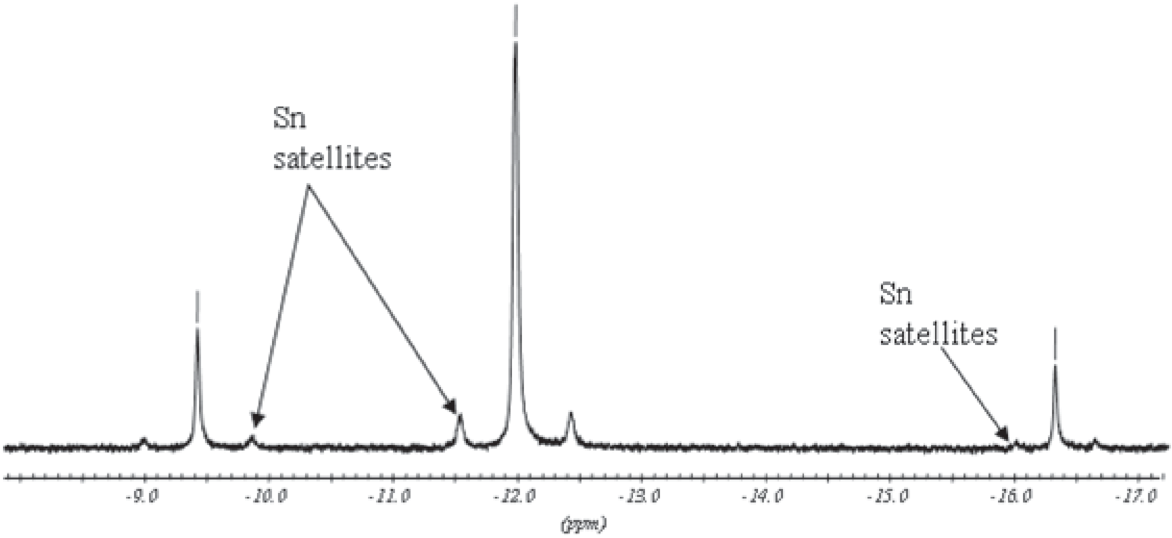

Figure 2.3.34: $^{1}H\{^{31}P\}$ NMR spectrum of **20-Fe** in C_6D_6 in the Fe-H region of **20-Fe**. 3 signals, corresponding to three different stereoisomers are clearly visible, along with Sn satellites. The signals at $\delta = -9.43$ and -11.99 ppm both have $^{2}J(H,^{117/119}Sn) = 260$ Hz, while the signal at $\delta = -16.33$ ppm has $^{2}J(H,^{117/119}Sn) = 191$ Hz.

According to the $^{1}H\{^{31}P\}$NMR spectrum, the ratio of the three isomers is 73:10:17 (Figure 2.3.34). The two low field shifted hydride resonance signals both exhibit coupling constants of $^{2}J(H,^{117/119}Sn) = 260$ Hz, while the high field shifted signal has a $^{2}J(H,^{117/119}Sn) = 191$ Hz. It is likely that these three stereoisomers are cis-configured hydride complexes (with respect to

Dieses Werk ist copyrightgeschützt und darf in keiner Form vervielfältigt werden noch an Dritte weitergegeben werden.
Es gilt nur für den persönlichen Gebrauch.

the stannyl ligand), as the coupling constants are comparable. A trans arranged hydride ligand should result in a significantly higher $^{2}J(\mathrm{H},^{117/119}\mathrm{Sn})$ coupling constant.

A full spectroscopic assignment of the different isomers was not possible due to the signal broadness, despite an attempt at 2D H,H COSY and HMBC experiments. Furthermore, the $^{31}P\{^{1}H\}$ NMR spectrum revealed an intractable array of signals which could not be deconvoluted and assigned to the respective stereoisomers. The $^{119}Sn\{^{1}H\}$ Spectrum of **20-Fe,** in C_6D_6 reveals two detectible but broad signals at $\delta = -34$ and $\delta = -84$ ppm respectively. Complex **20-Fe** was also the subject of a ^{57}Fe Mößbauer spectroscopic investigation, yielding one quadrupole doublet signal. This study additionally proves the assertion that **20-Fe** is indeed a mixture of stereoisomers on an octahedral Fe centre, following the Bancroft point charge model. This is further commented on in section **2.3.6.2**.

Crystals, suitable for x-ray analysis of **20-Fe** were grown from toluene with slow evaporation at room temperature in the glove-box, and is shown in Figure 2.3.34, where one of the three *cis* isomers crystallised (Figure 2.3.35).

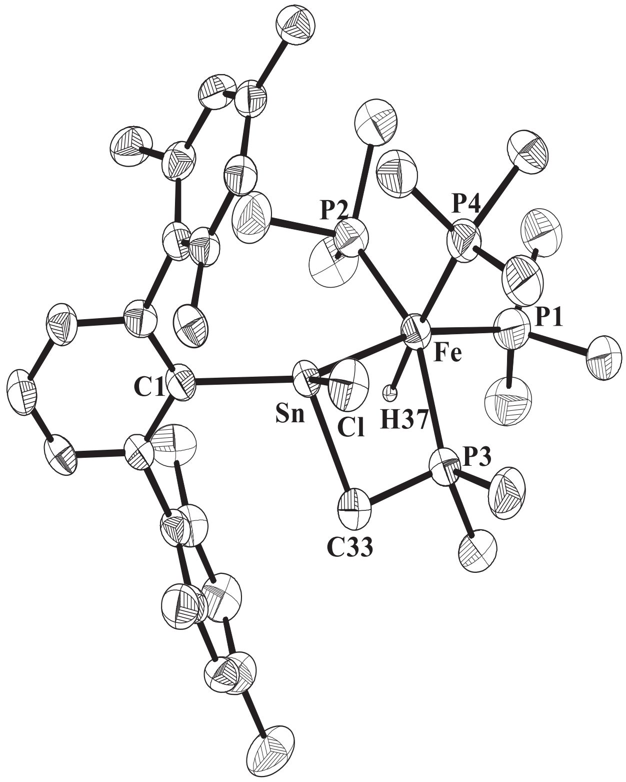

Figure 2.3.35: DIAMOND plot of the molecular structure of one of the stereoisomers of compound **20-Fe** in the solid state. Thermal ellipsoids are set at the 50% probability level. H atoms are omitted for clarity, with exception the hydride, H37. Selected bond lengths [Å]: Fe–Sn 2.6084(9), Fe–P1 2.176(2), Fe–P2 2.190(2), Fe–P3 2.257(2), Fe–P4 2.229(2), Fe–H 1.38(6), Sn–C(1) 2.237(5), Sn-Cl

Dieses Werk ist copyrightgeschützt und darf in keiner Form vervielfältigt werden noch an Dritte weitergegeben werden.
Es gilt nur für den persönlichen Gebrauch.

2.447(2). Selected bond angles [°] P1-Fe-P2 93.38(8), P1-Fe-P4 96.95(8), P2-Fe-P4 97.97(7), P1-Fe-P3 92.07(7), P2-Fe-P3 153.54(7), P4-Fe-P3 107.03(7), P1-Fe-Sn 164.91(6), P2-Fe-Sn 96.91(5), P3-Fe-Sn 73.88(5), P4-Fe-Sn 92.53(6), C(1)-Sn-Fe 145.2(2), C(1)-Sn-C33 112.1(2).

To date no solid state structural investigation of a compound bearing an Fe-P-C-Sn metallcyclic subunit has been reported, and indeed this is the first.[186] The molecular structure of **20-Fe** in the solid state reveals a distorted octahedral environment around the Fe centre, induced in part by the presence of the strained 4-membered metallacycle containing Fe-Sn-C-P atoms. The Sn-Fe-P3 bond angle of 73.88(5)° highlights this deviation from ideal octahedral geometry, in addition to the P2-Fe-P3 bond angle of 153.54(7)°. The Sn centre is 4 coordinate, and has a distorted tetrahedral geometry: The Fe-Sn-C(1) bond angle is 145.20(15)° which can be attributed to the steric repulsion between the bulky mesityl groups and the PMe_3 ligands bound to the Fe centre, which results in an increase in the C1-Sn-Fe bond angle. There is no apparent interaction between the hydride H atom bound to iron and the Sn centre, a result consistent with what is observed in the IR spectrum, where typical Fe-*H* terminal vibrations are observed at 1930 and 1867 cm^{-1}.

This result highlights the different reactivity of complex **18-Fe** towards **1-Sn** compared with that of $[WH(PMe_3)_4\{\eta^2\text{-}CH_2PMe_2\}]$, which although was not reacted with **1-Sn** did in both cases of reaction with **1-Pb** and **1-Ge** yield ylidyne complexes, so it can be anticipated that the same reactivity pattern will occur with **1-Sn**. In the case of **18-Fe**, a simple insertion of the tetrel atom into the C–Fe bond occurs, without Cl transfer to the Fe centre, while in the reactions with $[WH(PMe_3)_4\{\eta^2\text{-}CH_2PMe_2\}]$ PMe_3 elimination occurs, and halogen transfer from the tetrel atom to the metal centre takes place. This difference in reactivity can be attributed to the fact that $[WH(PMe_3)_4\{\eta^2\text{-}CH_2PMe_2\}]$ is a seven coordinate complex, which eliminates PMe_3, thereby inducing halogen transfer from the tetrel atom to the W centre, due to the resulting electron deficiency at W. This is not the case with the Fe system.

Chlorine abstraction from the Sn centre in complex **20-Fe** was possible by reaction with the Lewis acidic $B(C_6F_5)_3$ in toluene, which resulted in the isolation of a blue-purple solid **21-Fe**: $[FeH(PMe_3)_3\{{=}Sn(2,6\text{-}Mes_2\text{-}C_6H_3)\}][BCl(C_6F_5)_3]$. Crystals, suitable for X-ray diffraction analysis were obtained, but yielded a highly disordered structure, where the hydride could not be located. The pseudo mirror symmetrical asymmetric unit exhibited a 50:50 % splitting, whereby considering Sn, C28S is a methylene group, while C25 a methyl group,

Dieses Werk ist copyrightgeschützt und darf in keiner Form vervielfältigt werden noch an Dritte weitergegeben werden.
Es gilt nur für den persönlichen Gebrauch.

while considering SnS, C25 is a methylene group and C28S a methyl group. Despite the disorder, the structure solution does prove the abstraction of the Cl atom at Sn was successful, additionally validated by the existence of the anion, $BCl(C_6F_5)_3$. Compound **21-Fe** was poorly soluble in most solvents, except THF, in which it is unstable – shown by a progressive colour change from blue-purple to orange, possibly indicative of the reverse formation of the starting material **20-Fe**.

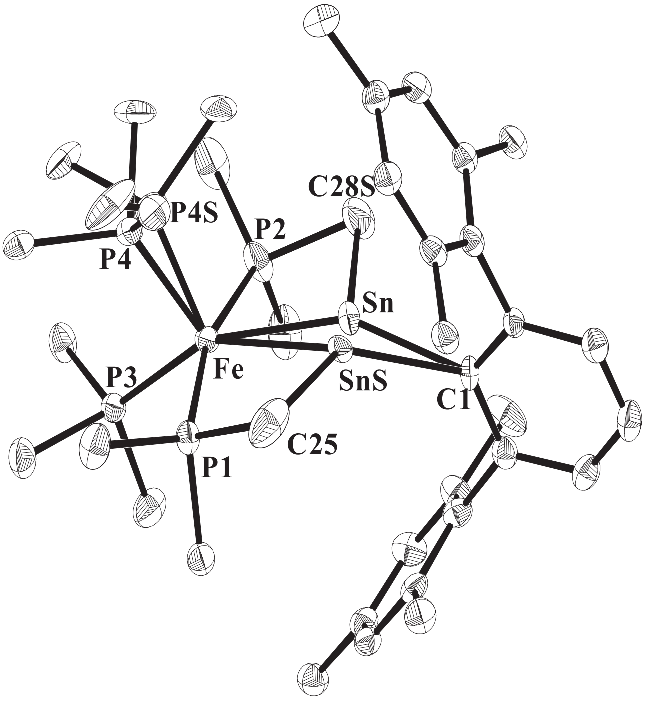

Figure 2.3.36: DIAMOND plot of the molecular structure of the cation of compound **21-Fe** in the solid state. Thermal ellipsoids are set at 50 % probability. All metric parameters are omitted owing to disorder in the structure.

2.3.4.2 Reactivity of 1-Sn towards [FeH(η^3-$MeCHPEtC_2H_4PEt_2$)(depe)]

We next moved to a sterically more encumbered CH activated complex, based on depe, to probe the effect of increasing the steric bulk of the ligand sphere at the Fe centre, on the reactivity towards **1-Sn**. To this end, reduction of **2-Fe** with Na sand under an argon atmosphere resulted the C,H activation and [FeH(η^3-$MeCHPEtC_2H_4PEt_2$)(depe)] **22-Fe**. Complex **22-Fe** has previously been prepared by Baker and Field by reaction of *trans*-[FeHCl(depe)$_2$] with Me_2Mg at low temperature, followed by reductive elimination of CH_4 above 240 K.[187] Complex **22-Fe** is thought to exist in equilibrium with the 16 VE complex [Fe(depe)$_2$] in solution and so this also represented a possible starting material to access stannylidene complexes of Fe, since this reactive species could principally be "trapped" by **1-**

Dieses Werk ist copyrightgeschützt und darf in keiner Form vervielfältigt werden noch an Dritte weitergegeben werden.
Es gilt nur für den persönlichen Gebrauch.

Sn resulting in the stannylidene complex, **3-Fe**. In much the same way reaction of [Fe(depe)$_2$] with ethylene is said to form *cis*-[FeH(depe)$_2$(C$_2$H$_3$)] which is in equilibrium with the *trans* isomer, and at 25 °C converts to the trigonal bipyramidal complex, [Fe(depe)$_2$(C$_2$H$_4$)].[188]

^{31}P{^{1}H} NMR spectroscopy of **22-Fe** in C$_6$D$_6$ shows the formation of cis / trans [FeDPh(depe)$_2$], as a result of C,D activation of the deuterated benzene, resulting in several signals in the ^{31}P{^{1}H} NMR (see Figure 2.3.37a), which are absent in THF-*d*$_8$ (Figure 2.3.37b). Complex **22-Fe** itself is an ABCD system, where 4 multiplet signals would be expected, and is indeed the case, as is the case for *cis*–FeDPh(depe)$_2$. The *trans*–FeDPh(depe)$_2$ complex only has one singlet resonance signal, which is also visible from the ^{31}P{^{1}H} spectrum.

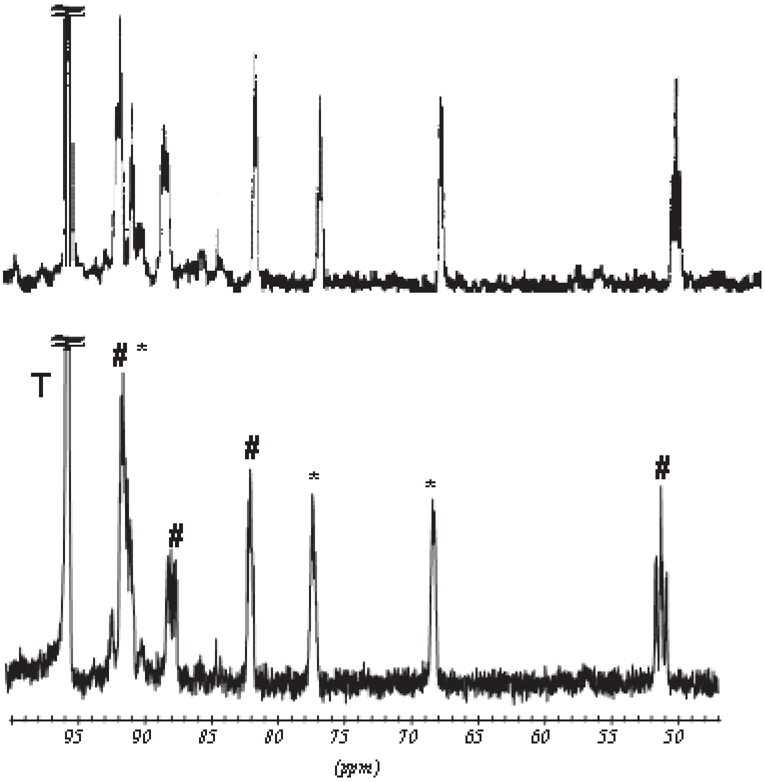

Figure 2.3.37a: Comparison of ^{31}P{^{1}H} NMR spectrum of **22-Fe** in C$_6$D$_6$ from ref [187] (above) and this work (below). # = **22-Fe** * = *cis*–Fe(D)Ph(depe)$_2$, T = *trans*–Fe(D)Ph(depe)$_2$. Chemical shift range $\delta = 45 – 100$ ppm.

Dieses Werk ist copyrightgeschützt und darf in keiner Form vervielfältigt werden noch an Dritte weitergegeben werden.
Es gilt nur für den persönlichen Gebrauch.

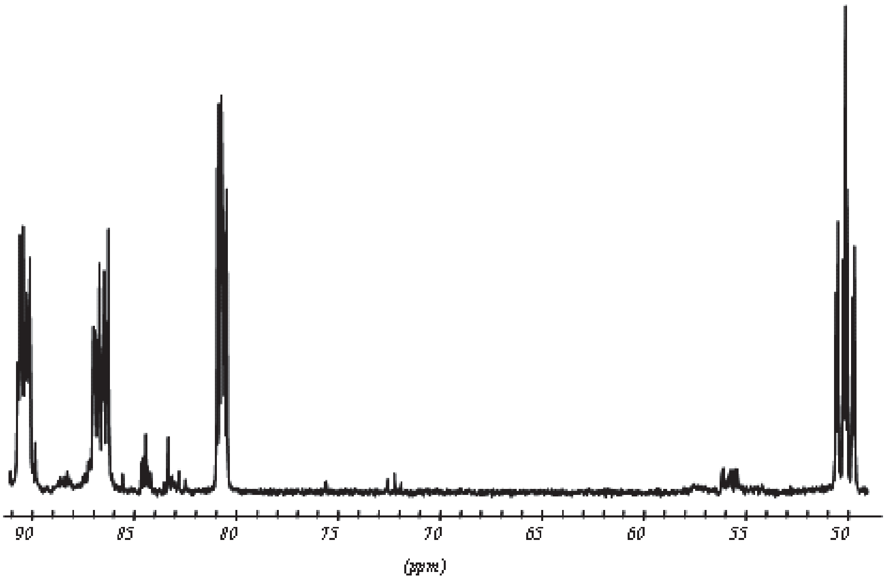

Figure 2.3.37b: $^{31}P\{^1H\}$ NMR spectrum of **22-Fe** in THF-d_8 in the range $\delta = 48 - 92$ ppm. Four sets of multiplet resonance signals are visible, corresponding to four inequivalent P atoms.

Subsequent reaction of **22-Fe** with **1-Sn** is not selective and yields at least two identifiable products on the basis of NMR spectroscopy: **3-Fe**, and what was identified from NMR as having the identity: [FeH(depe)($Et_2PCH_2CH_2PEtCH_2CH\{Sn(Cl)(C_6H_3\text{-}Mes_2)\}$], **23-Fe**, the insertion product, in analogy to **20-Fe**. The ratio based on *in situ* $^{31}P\{^1H\}$ was 40:60 (**3-Fe:23-Fe**), whereby the proportion of **3-Fe** could be increased by recrystallisation to 63:37, from pentane, but even repeated fractional crystallisation did not enable the separation of the products. Figure 2.3.38 shows the $^{31}P\{^1H\}$ NMR spectrum of the recrystallised mixture.

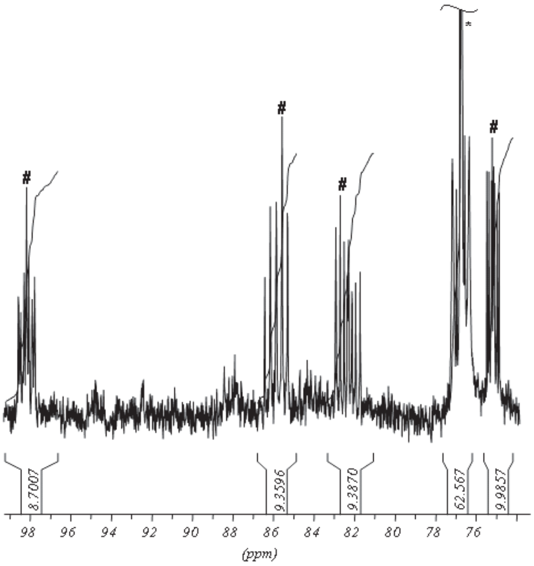

Figure 2.3.38: $^{31}P\{^1H\}$ NMR spectrum in C_6D_6 of reaction product after the recrystallisation from pentane. # = **23-Fe**, * = **3-Fe** resulting in a ratio of 63 : 37 (**3-Fe** :**2 3Fe**).

Dieses Werk ist copyrightgeschützt und darf in keiner Form vervielfältigt werden noch an Dritte weitergegeben werden.
Es gilt nur für den persönlichen Gebrauch.

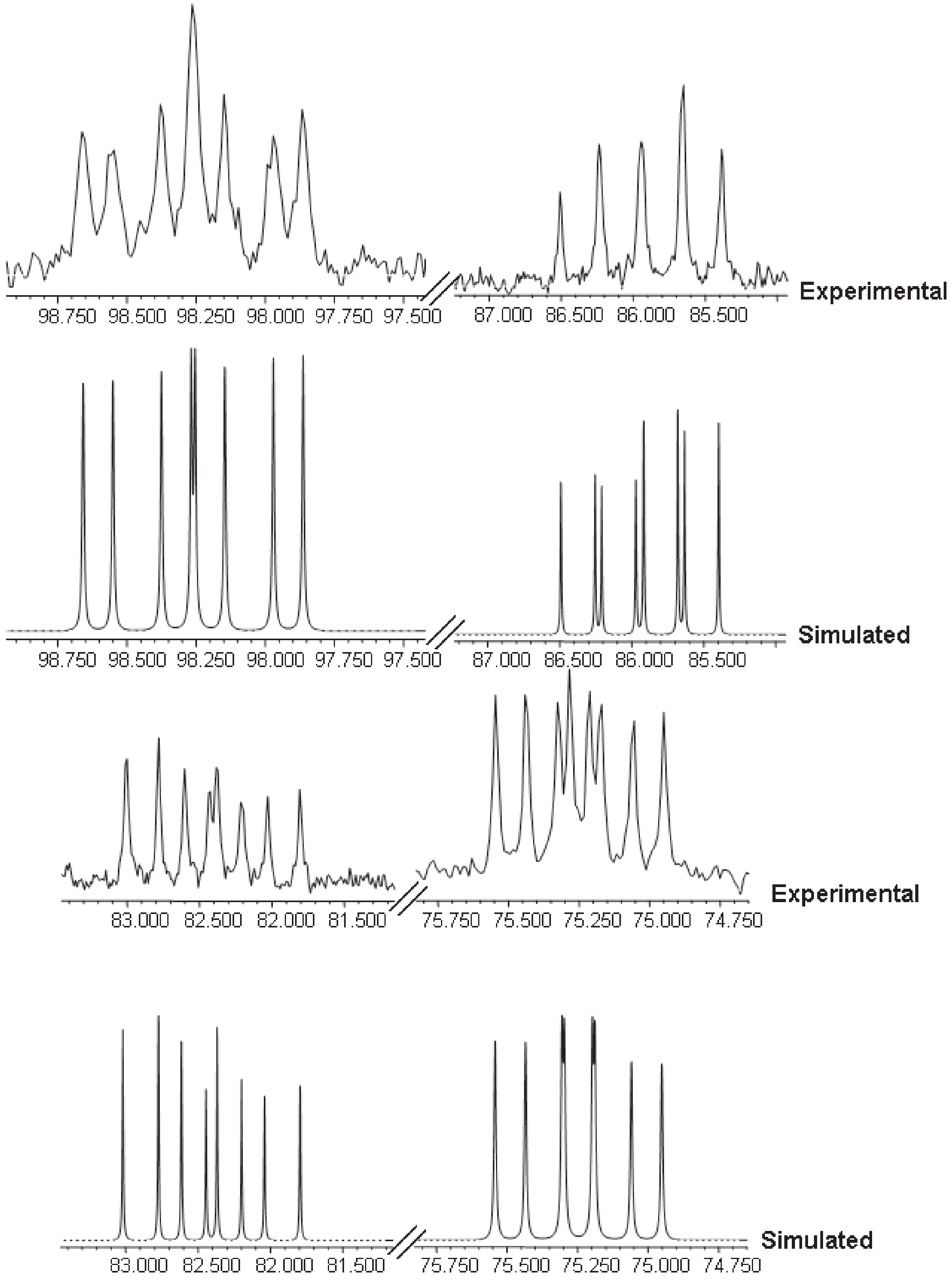

Figure 2.3.38b: Simulated and experimental $^{31}P\{^{1}H\}$ NMR spectrum of = **23-Fe** in C_6D_6.

Further evidence for the formation of **23-Fe** in the reaction mixture is the presence of Fe-*H* resonances in the ^{1}H NMR spectrum in C_6D_6, of which two are clearly visible at $\delta = -11.22$

Dieses Werk ist copyrightgeschützt und darf in keiner Form vervielfältigt werden noch an Dritte weitergegeben werden.
Es gilt nur für den persönlichen Gebrauch.

and -13.25, both multiplets, due to coupling to phosphorus nuclei. This is indicative of two stereoisomers of **23-Fe** being present in the mixture in analogy to **20-Fe**. Additionally, ^{119}Sn NMR in C_6D_6 also has two clear resonance signals, at δ = 470.8 (quint) and 22.7 (br) ppm corresponding to **3-Fe** and **23-Fe** respectively, the latter resonance signal a combination of the two stereoisomers of **23-Fe**. Moreover, the ratio of these two signals in the ^{119}Sn{^{1}H} NMR are identical to those in the ^{31}P{^{1}H} NMR spectrum i.e. 63:17 (**3-Fe**:**23-Fe**). (Figure 2.3.38b)

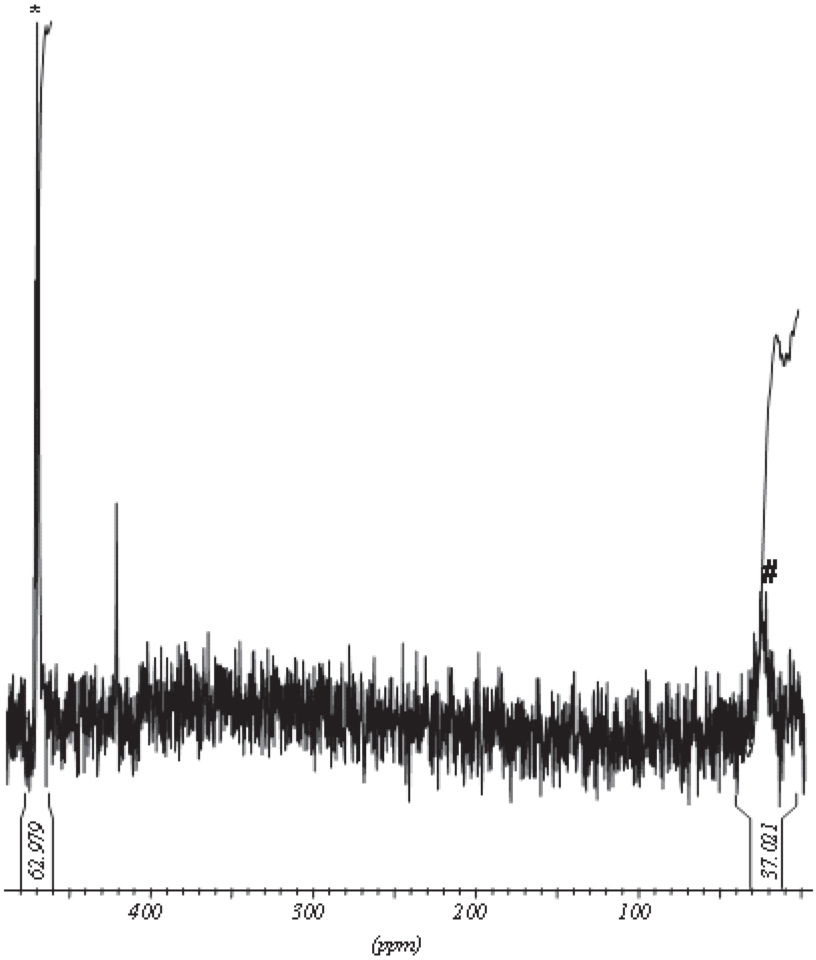

Figure 2.3.38b: ^{119}Sn{^{1}H} NMR spectrum in C_6D_6 the recrystallisation from pentane. # = **23-Fe**, * = **3-Fe**, the ratio of which is identical to the ^{31}P{^{1}H} NMR spectrum (Figure 2.3.38a).

These results point to a different reactivity of **22-Fe** to **18-Fe**, where selective insertion of the stannylene was shown to occur. In the reactivity of **22-Fe** towards **1-Sn**, two competing reaction pathways are likely to account for the observations:

Dieses Werk ist copyrightgeschützt und darf in keiner Form vervielfältigt werden noch an Dritte weitergegeben werden.
Es gilt nur für den persönlichen Gebrauch.

A CH activation reversal (intramolecular reductive elimination) is required as a first step, resulting in the reactive 16VE complex, [Fe(depe)$_2$], which is subsequently trapped by **1-Sn** to access **3-Fe**. Alternatively, a direct insertion of **1-Sn** can occur to result in **23-Fe** (Scheme 2.3.12).

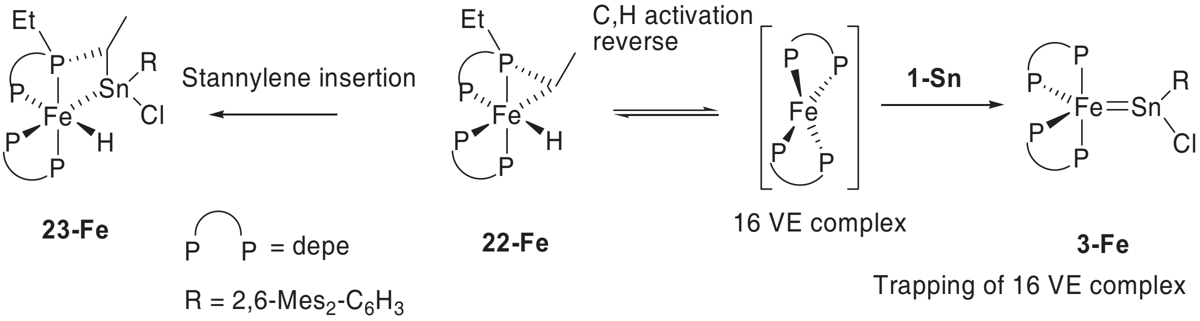

Scheme 2.3.12: Reactivity of **1-Sn** with **22-Fe** is not selective; two competing pathways result in two products, **23-Fe** which is a mixture of stereoisomers on the basis on NMR spectroscopy.

2.3.4.3 Reactivity of 1-Sn towards [FeH(dppe)[η^3-Ph$_2$PCH$_2$CH$_2$PPhC$_6$H$_4$}] 24-Fe

The precursor complex, [FeCl$_2$(dppe)], **25-Fe** was synthesised according to the procedure by Sacco and co-workers.[189] According to their report, the complex [FeCl$_2$(dppe)$_2$] was isolated, but in our case **25-Fe** was isolatd as the product, as evidenced by elemental analysis in addition to un-reacted free dppe (1. eq). A slightly different work-up procedure was employed in our case (see experimental section), where a careful filtration resulted in the isolation of **25-Fe**. Sacco and co-workers employed complete precipitation from the reaction mixture, and potentially, despite a fitting elemental analysis in their report, actually isolated a mixture of **25-Fe** and free dppe since no other indicative data was supplied. Compound **25-Fe** was reduced with [Mg(anthracene)(thf)$_x$] in the presence of free dppe in THF yielding the orthometallation product, [FeH(dppe)[η^3-Ph$_2$PCH$_2$CH$_2$PPhC$_6$H$_4$}], **24-Fe** after work-up. Complex **24-Fe** was first reported by Hata *et al*. accessed by the reduction of [Fe(acac)$_3$] in the presence of dppe, followed by UV radiation resulting in **24-Fe**.[190]

The ^{31}P{^{1}H} NMR spectrum showed several multiplet resonance signals, typical of an ABCD system as would be expected for an orthometallation product, and is shown in Figure 2.3.39. The spectrum is in close agreement with that of Ittel *et al*, who also reported a

Dieses Werk ist copyrightgeschützt und darf in keiner Form vervielfältigt werden noch an Dritte weitergegeben werden.
Es gilt nur für den persönlichen Gebrauch.

simulated spectrum of **24-Fe**.[191] The assignment of the high field shifted resonance signal (Figure 2.3.39) can be made by a 2-dimensional (^{1}H, P) COSY NMR experiment, where a high intensity cross peak to the hydride is located with the multiplet signal at $\delta = 25.0$ ppm in the ^{31}P{^{1}H} NMR spectrum, suggesting its identity is that of the phosphorus atom in the four membered ring, located *trans* to the hydride. This finding supports the supposition of Ittel *et al*. who attribute the high field shift of this phosphorus atom to its inclusion in a four membered ring.[191] Furthermore, the ^{1}H{^{31}P} NMR spectrum in C_6D_6 of **24-Fe** shows the characteristic Fe–*H* resonance signal at $\delta = -14.31$ which appears as a singlet. In the normal ^{1}H NMR spectrum, this signal appears as a multiplet in the ^{1}H NMR spectrum due to ^2J(H,P) coupling, and is identical to that of Hata *et al*.

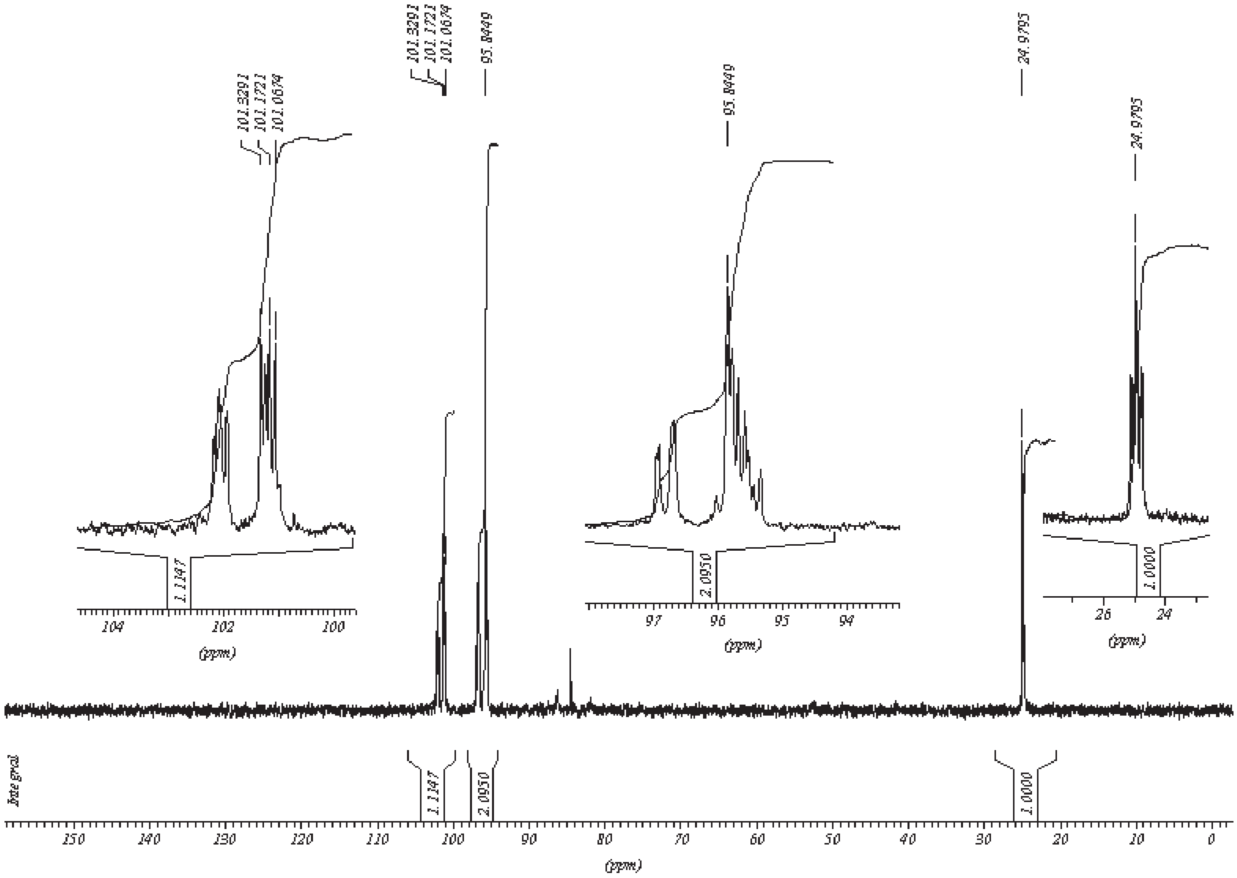

Figure 2.3.39: ^{31}P{^{1}H} NMR spectrum of **24-Fe** [FeH(dppe)[η^3-$Ph_2PCH_2CH_2PPhC_6H_4$}]in C_6D_6, typical of an ABCD system.

Dieses Werk ist copyrightgeschützt und darf in keiner Form vervielfältigt werden noch an Dritte weitergegeben werden.
Es gilt nur für den persönlichen Gebrauch.

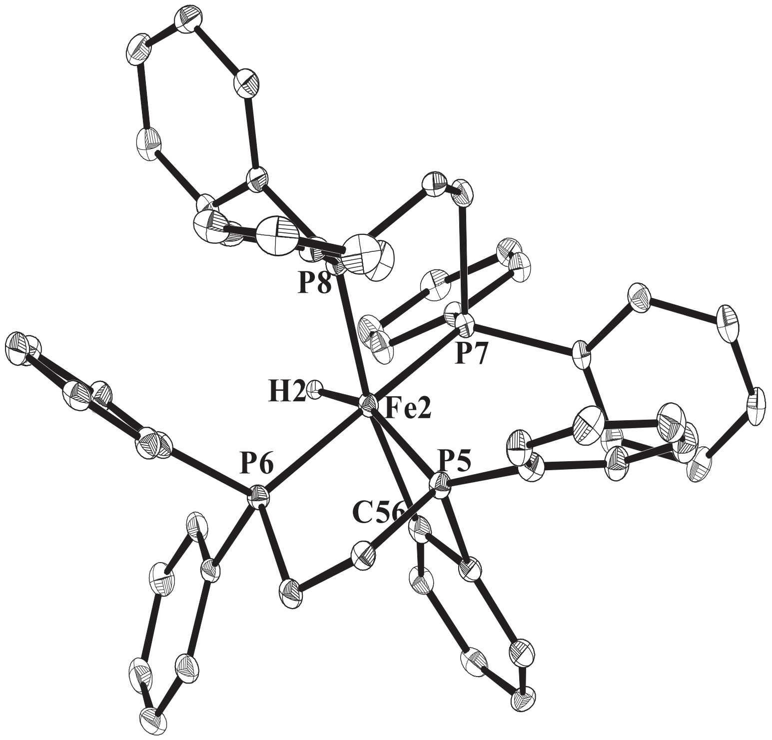

Figure 2.3.40: DIAMOND plot of **24-Fe** in the solid state. Thermal ellipsoids are represented at the 50 % probability level. All H atoms, with exception the hydride (H2) are omitted for clarity. The corresponding metric parameter of the second crystallographically independent molecule is included in parenthesis afterwards. Selected bond lengths [Å] Fe2–H2 1.40(3) [1.42(3)], Fe2–P5 2.220(1) [2.233(1)], Fe2–P8 2.189(1) [2.186(1)], Fe2–P7 2.183(1) [2.188(1)], Fe2–P6 2.174(1) [2.166(1)], Fe2–C56 2.021(4) [2.023(4)]. Selected bond angles [°]: H2-Fe2-P5 159(2) [160(2)], P8-Fe2-C56 169.3(1) [169.4(1)].

In our case for **24-Fe**, crystallisation from Et_2O at 7 °C for several weeks resulted in crystals suitable for X-ray crystallographic analysis. Despite numerous further reports of **24-Fe** in the literature[193] the complex has not been structurally characterised to date, and so we carried out such an investigation.

Solid state structural investigations of complexes similar to **24-Fe** are rather rare. Moreover no previous examples of complexes featuring a metallacyclobutane ring system with Fe¨P¨C¨C atoms as members, along with exclusively phosphane ligands as the remaining supporting ligands at the Fe centre exist. Complexes containing the Fe¨P¨C¨C metallacyclic moiety with other supporting ligands have however been reported, but are also limited.[194] Two crystallographically independent molecules were found to be present in the asymmetric unit, co-crystallised with 2.5 Et_2O molecules. One of the independent molecules is presented in figure 2.3.40. Compound **24-Fe** is six coordinate, with one of the coordination sites

Dieses Werk ist copyrightgeschützt und darf in keiner Form vervielfältigt werden noch an Dritte weitergegeben werden.
Es gilt nur für den persönlichen Gebrauch.

occupied by a hydride ligand, and exhibits dramatic distortions from ideal octahedral geometry: for example the P6-Fe2-P7 bond angle is distorted by nearly 20 ° from linearity, and the P8-Fe2-C56 bond axis also shows a similar deviation. These are attributable to immense steric strain induced by the sterically demanding dppe ligands on the iron centre, in addition to the ring strain induced by the four membered metallacyclic ring.

Subsequent reaction of **1-Sn** with the incumbent orthometallation product **24-Fe** in toluene was carried out at elevated temperatures. The reaction was followed by *in situ* $^{31}P\{^1H\}$ NMR spectroscopy, which revealed progressive consumption of **24-Fe**, by the multiplet signals disappearing, and formation of a new product, as a singlet. Upon work up, however, [FeCl(dppe)$_2$], **25-Fe** was obtained – Possibly as a decomposition product from the *in situ* generated stannylidene complex, resulting from the immense steric strain originating from the dppe ligand sphere on the Fe centre. Compound **25-Fe** was studied by X-ray crystallography, after suitable crystals were obtained from slow evaporation in the glove-box from C_6D_6. The molecular structure of **25-Fe** is shown in Figure 2.3.41 below.

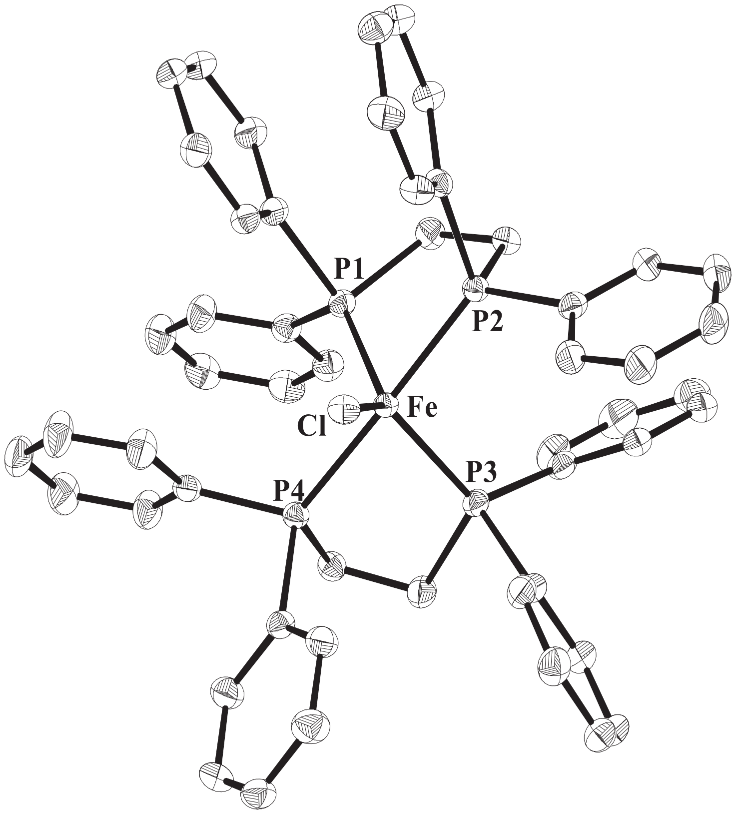

Figure 2.3.41: DIAMOND plot of the molecular structure of compound **25-Fe.C$_6$D$_6$** in the solid state. Thermal ellipsoids are set at the 50% probability level, H atoms are omitted for clarity. Selected bond lengths [Å]: Fe–Cl 2.3293(5), Fe–P1 2.2285(5), Fe–P2 2.2436(5), Fe–P3 2.2212(5), Fe–P4 2.2285(5). Selected bond angles [°] P1-Fe-P3 109.85(2), P3-Fe-P4 83.14(2), P4-Fe-P1 93.95(2), P3-Fe-P2

Dieses Werk ist copyrightgeschützt und darf in keiner Form vervielfältigt werden noch an Dritte weitergegeben werden.
Es gilt nur für den persönlichen Gebrauch.

95.94(2), P4-Fe-P2 173.84(2), P1-Fe-P2 80.61(2), P3-Fe-Cl 124.63(2), P4-Fe-Cl 92.29(2), P1-Fe-Cl 125.52(2), P2-Fe-Cl 93.23(2).

This is only the second example of a Fe(I) chloride, the first being that of **25-Fe**, mentioned earlier in this dissertation. The Fe–Cl bond length in **25-Fe** is comparable to that of **10-Fe**, although it is slightly elongated. The coordination sphere around the Fe centre is that of trigonal bipyramidal, as is the case with **10-Fe**, with the Cl ligand occupying one of the equatorial coordination sites. This therefore seems to be the generally preferred coordination arrangement in Fe(I) complexes of the type FeL_4Cl, where L_4 are phosphane ligands.

In summary the reactivity of **1-Sn** towards Fe complexes bearing C,H activated ligands at the Fe centre seems largely to depend on the steric, and electronic nature of the ligand: in the case of $[FeH\{\eta^2\text{-}CH_2PMe_2\}(PMe_3)_3]$, the insertion product, **20-Fe** is selectively formed as a mixture of stereoisomers, in contrast to the reactivity with the related seven coordinate W analogue, where Cl migration from the tetrel atom to the W centre was observed. Changing to the more sterically encumbered depe ligand sphere results in a mixture of the insertion product and the stannylidene complex **3-Fe** on the basis of NMR spectroscopy, upon reaction with **1-Sn**. Reaction of **1-Sn** with the even more sterically encumbered ortho-metallation compound, containing dppe as supporting ligands at Fe (**24-Fe**) results in consumption of the starting material evidenced by *in situ* NMR spectroscopy, but upon work-up results in the Fe(I) complex, **25-Fe**.

2.3.5: Some reactions of iron stannylidenes

2.3.5.1 Reactivity of the iron stannylidene complex 3-Fe

The presence of a Cl atom on the Sn centre in the stannylidene complex, **3-Fe** already readily enabled isolation of the stannylidyne complexes **4-Fe, 5-Fe** and **6-Fe** by facile chloride abstraction using a suitable base or metathetical exchange reactions. We subsequently decided to explore the reactivity of complex **3-Fe** owing to the synthetic “handle” provided by the Cl atom. Several reactions were carried out in this context, which are summarised in Scheme 2.3.13.

Dieses Werk ist copyrightgeschützt und darf in keiner Form vervielfältigt werden noch an Dritte weitergegeben werden.
Es gilt nur für den persönlichen Gebrauch.

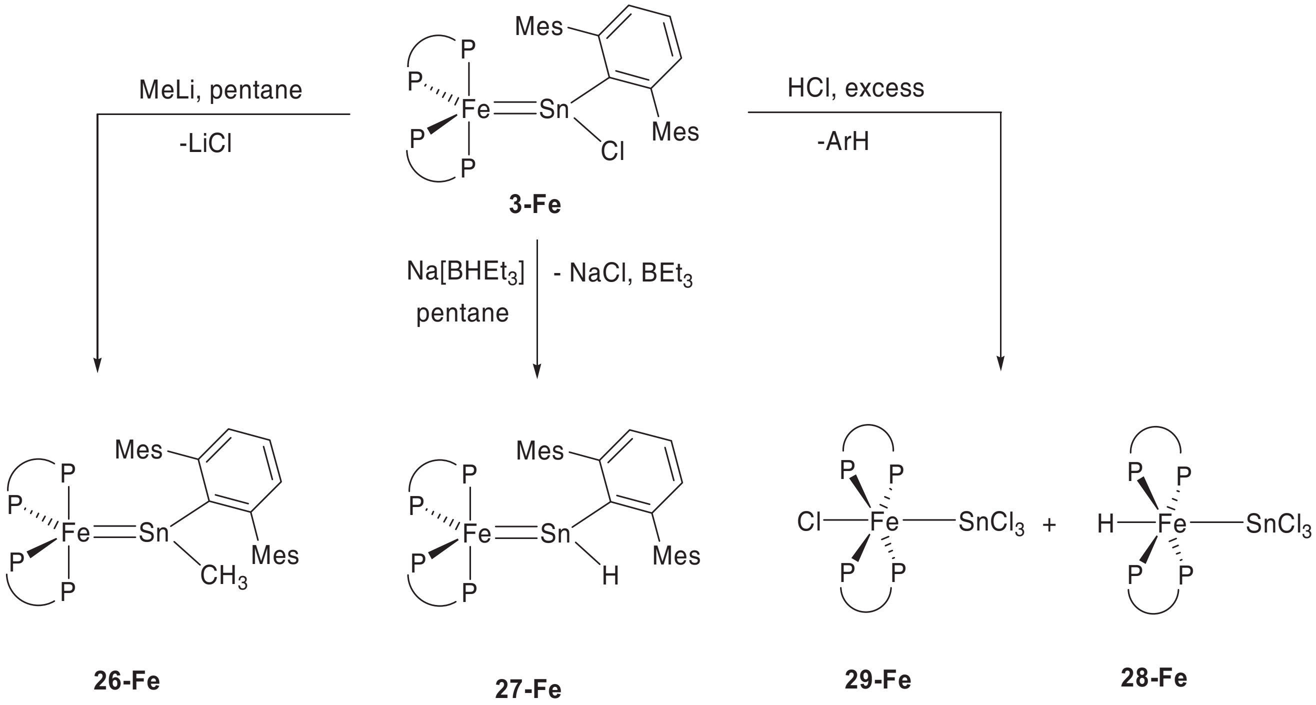

depe = 1,2-bis(diethylphosphino)ethane

Scheme 2.3.13: Summary of some reactions of the stannylidene complex, **3-Fe**.

(a) Reaction of 3-Fe with MeLi

Reaction of complex **3-Fe** with MeLi, targeting [(depe)$_2$Fe=Sn(Me)C$_6$H$_3$-Mes$_2$], **26-Fe** was first investigated. This reaction was carried out in pentane at room temperature and followed by *in situ* ^{31}P{^{1}H} NMR spectroscopy. A reaction is observed, but is only clear from the difference in the coupling constants of ^2J(P, $^{117/119}$Sn) between **3-Fe** and **26-Fe**. No dramatic shift in the singlet in the ^{31}P{^{1}H} NMR spectrum is observed (See figure 2.3.42). This appears to be a clean and selective reaction. This difference in the coupling constants is attributed to the replacement of an electron withdrawing group (Cl) on the Sn centre with an electron donating group (Me), which influences the magnitude of the coupling to between these two nuclei, as is discussed later.

Dieses Werk ist copyrightgeschützt und darf in keiner Form vervielfältigt werden noch an Dritte weitergegeben werden.
Es gilt nur für den persönlichen Gebrauch.

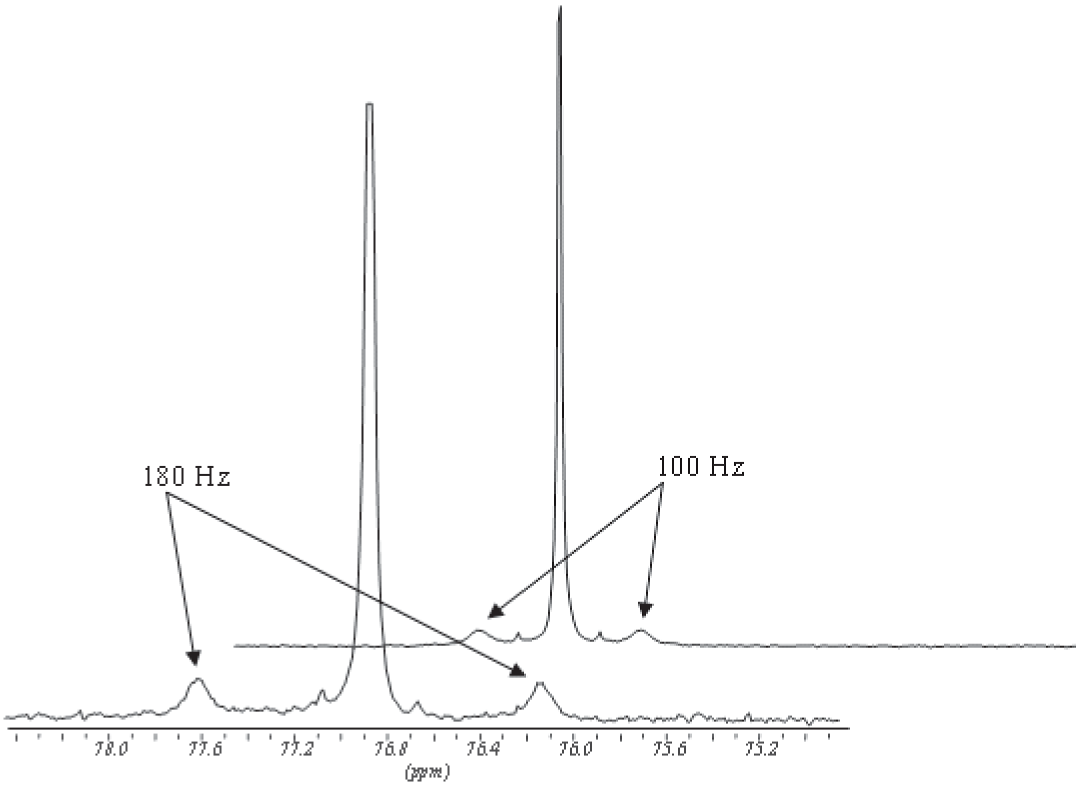

Figure 2.3.42: Comparison of the $^{31}P\{^{1}H\}$ NMR spectra (stacked) in C_6D_6 of **3-Fe** (back) and **26-Fe** (front). The difference of chemical shift of the singlet resonance is negligible, but there is an increase in the coupling constant $^{2}J(P, ^{117/119}Sn)$ to 180 Hz.

The Sn-CH_3 group can readily be identified in the ^{1}H spectrum by the HMBC spectrum, where a cross peak to the Sn-C resonance signal is observed. Compound **26-Fe** is highly lipophillic, and hence purification by recrystallisation was problematic, despite several attempts, and hence was not isolated in analytically pure form although it was possible to make a full assignment in ^{1}H and ^{13}C NMR spectroscopy in C_6D_6. Crystals, suitable for X-ray crystallographic analysis were obtained by storage of **26-Fe** in pentane at –30 °C for several weeks, and further confirmed the identity of the complex.

Dieses Werk ist copyrightgeschützt und darf in keiner Form vervielfältigt werden noch an Dritte weitergegeben werden.
Es gilt nur für den persönlichen Gebrauch.

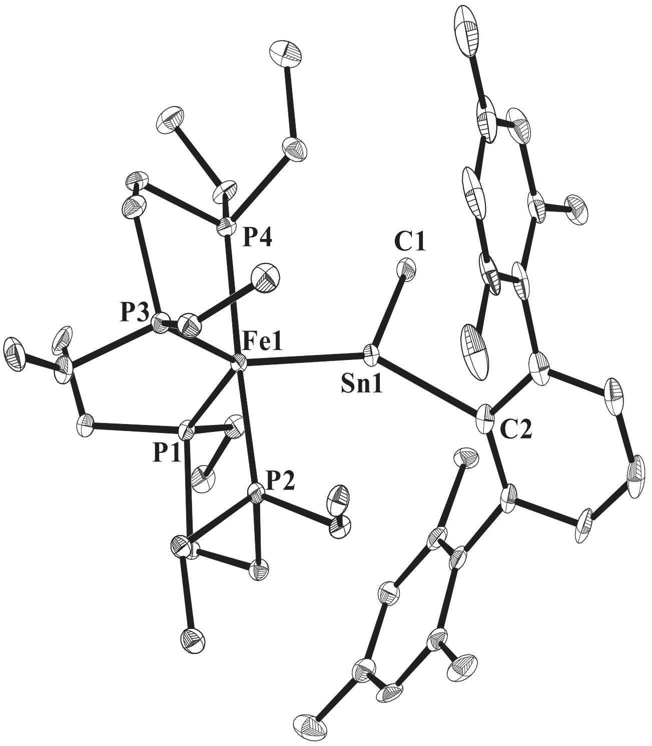

Figure 2.3.43: DIAMOND plot of the molecular structure of complex **26-Fe** in the solid state (one of the independent molecules represented, along with its metric parameters. The corresponding metric parameters of the other two independent molecules included in parenthesis afterwards[§§]). Thermal ellipsoids are set at the 30% probability level, H atoms are omitted for clarity. Selected bond lengths [Å]: Fe1–Sn1 2.439(1) [2.452(1), 2.457(1)], Sn1–C1 2.228(8) [2.219(8), 2.225(8)], Sn1–C2 2.249(8) [2.246(7), 2.259(7)]. Selected bond angles [°]: Fe1-Sn1-C2 144.5(2) [147.0(2), 147.4(2)], Fe1-Sn1-C1 120.4(2) [122.4(2), 118.7(2)], C1-Sn1-C2 94.1(3) [90.3(3), 92.7(3)].

Complex **26-Fe**, as with the parent complex **3-Fe**, exhibits trigonal bipyramidal geometry in the solid state, with a planar three coordinate Sn centre, evidenced by the sum of the bonding angles, in analogy to **3-Fe** and the related complex **16-Fe**. The average of the Fe–Sn bond lengths (2.449(2) Å) is slightly elongated in comparison to the parent complex, **3-Fe** (2.409(1) Å). A noticeable difference between the parent complex, **3-Fe** and **26-Fe** is the Fe-Sn-C_{ipso} bond angle (average = 146.3(3)°) compared with 158.5(2)° in **3-Fe**.

[§§] Actually, four independent molecules were found in the asymmetric unit, one of which was highly disordered, and its metric parameters are omitted here.

Dieses Werk ist copyrightgeschützt und darf in keiner Form vervielfältigt werden noch an Dritte weitergegeben werden.
Es gilt nur für den persönlichen Gebrauch.

(b) Reaction of 3-Fe with Na[BHEt$_3$]: Access to the first example of a hydridostannylidene complex of iron

Exchange of the Cl atom at the Sn centre of **3-Fe** was effected using Na[BHEt$_3$]. On reaction with one equivalent, unreacted starting material was re-isolated in ca. 50 % yield, so two molar equivalents Na[BHEt$_3$] was used in the reaction. This resulted in the isolation of [(depe)$_2$Fe=SnH(2,6-Mes$_2$-C$_6$H$_3$)] **27-Fe**, as a brown solid which is the first example of a three coordinate tin centre bound to Fe bearing H as a substituent. It is worth mentioning that Tilley and co-workers have reported a similar silylidene Os complex of the type [(η^5-C$_5$Me$_5$)H(^{i}Pr$_3$P)Os=SiH(Trip)][195] and its tin analogue,[196] both obtained by reactions with the precursor [(η^5-C$_5$Me$_5$)Os(^{i}Pr$_3$P)CH$_2$Ph] with H$_3$E(Trip), E = Si and Sn respectively.

^{1}H NMR spectroscopy of **27-Fe** in C$_6$D$_6$ reveals a 1:2 ratio of the resonance signals corresponding to the *para:ortho* methyl groups on the mesityl rings, in contrast to **3-Fe**. This indeed suggests reducing the steric bulk of the third substituent on tin (in this case from Cl to H) facilitates free rotation of the *m*-terphenyl substituent in solution at ambient temperatures, rendering all *ortho* positioned methyl groups equivalent. The possibility that these signals are accidentally isochronous can be ruled out on the basis of the ^{1}H NMR spectrum in the aromatic region, where one singlet resonance signal corresponding to the *m*-H on the mesityl rings is located. Additionally in the ^{13}C{^{1}H} NMR spectrum only two resonance signals, corresponding to the *ortho* : *para* methyl groups of the mesityl rings are observed. These observations are in accordance with the reports of Tilley and co-workers, where close inspection of their spectroscopic data for the related complex [(η^5-C$_5$Me$_5$)H(^{i}Pr$_3$P)Os=SnH(Trip)] reveal only two sets of methine signals in a 2:1 ratio, corresponding to *o*-^{i}Pr : *p*-^{i}Pr, also suggesting free rotation of the aryl substituent, and equivalence of the *o*-positioned ^{i}Pr group, and also supported by only one signal corresponding to *o*-*C*HMe$_2$ in the ^{13}C{^{1}H} NMR spectrum, in analogy to **27-Fe**. In the case of the Si analogue, 3 sets of methine signals are observed in the ^{1}H NMR spectrum, evidencing locked rotation of the Trip substituent in [(η^5-C$_5$Me$_5$)H(^{i}Pr$_3$P)Os=SiH(Trip)]. This results seems to suggest that the main group element plays a significant role in the barrier of rotation associated with the aryl substituent, rather than the steric bulk of thereof.

The most characteristic resonance signal in the ^{1}H NMR spectrum is that of the Sn-*H* located at δ= 14.50 ppm, as a quintet signal flanked with broad Sn satellites *via* a ^1J coupling to

Dieses Werk ist copyrightgeschützt und darf in keiner Form vervielfältigt werden noch an Dritte weitergegeben werden.
Es gilt nur für den persönlichen Gebrauch.

$^{117/119}$Sn. The quintet multiplicity originates from coupling to four equivalent phorphorus atoms from the depe ligands, as before rendered equivalent by Berry pseudo rotation on NMR timescale. It is noteworthy to compare this chemical shift to that of Sn-*H* [(η^5-C_5Me_5)H(^{i}Pr$_3$P)Os=SnH(Trip)][196] which occurs at δ = 19.3 ppm in benzene-d_6. The considerable downfield shift (*ca* 5 ppm) is a consequence of changing the metal from Fe to Os.[197] The chemical shift is, however, comparable to that of the recently reported β-diketiminato supported Sn(II) hydride found at δ= 13.96 ppm.[198]

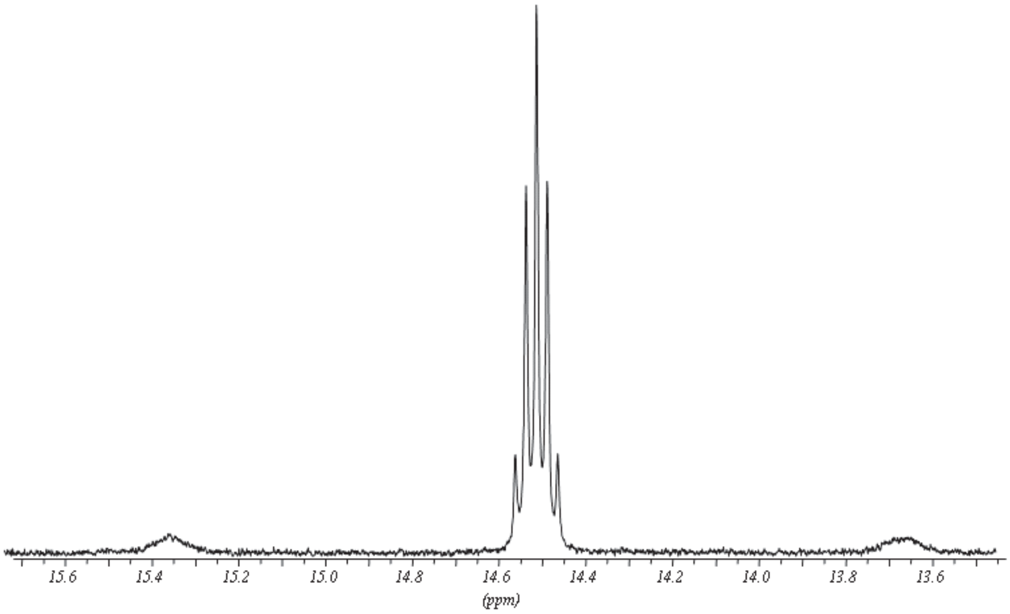

Figure 2.3.44: Expansion of the ^{1}H NMR spectrum of **27-Fe** in C_6D_6 in the region containing the Sn-*H* resonance signal. A quintet multiplicity, flanked with $^{119/117}$Sn satellites is clearly visible.

At this point it makes sense to present comparative summary of ^{31}P{^{1}H} and ^{119}Sn{^{1}H} NMR spectra of the related stannylidene complexes, **3-Fe**, **16-Fe**, **26-Fe**, **27-Fe**, and the stannylidyne complex, **6-Fe** (Table 2.3.1).

Complex	^{31}P{^{1}H} NMR shift, C_6D_6	^{119}Sn{^{1}H} NMR shift, C_6D_6
stannylidene complexes (in C_6D_6)		
3-Fe	76.8 ^2J(P,$^{117/119}$Sn) = 100 Hz	471.5 ^2J(^{119}Sn,P) = 100 Hz
16-Fe	60.2 ^2J(P,$^{117/119}$Sn)= 49.6 Hz	527.2 ^2J(^{119}Sn,P) = 51.1 Hz
26-Fe	76.9 ^2J(P,$^{117/119}$Sn) = 179 Hz	Could not be located
27-Fe	79.4 ^2J(P,$^{117/119}$Sn) = 206 Hz	578.7 ^2J(^{119}Sn,P) = 213 Hz
Stannylidyne complex		
6-Fe (in THF-d_8)	77.5 (no tin satellites)	983 (broad)

Table 2.3.1: Summary of ^{31}P{^{1}H} and ^{119}Sn{^{1}H} chemical shifts, at room temperature.

Dieses Werk ist copyrightgeschützt und darf in keiner Form vervielfältigt werden noch an Dritte weitergegeben werden.
Es gilt nur für den persönlichen Gebrauch.

The $^{31}P\{^1H\}$ chemical shifts of the complexes based on depe as supporting ligand at the Fe centre are relatively unaffected by the changing substituent on the tin atom, or by changing from a stannylidene complex (**3-Fe**, **26-Fe** or **27-Fe**) to a stannylidyne complex (**6-Fe**). The parameter most affected is the value of the $^2J(P,^{117/119}Sn)$ coupling constant. Increasing the electro negativity of the substituent on the tin atom leads to a decrease in the value of this coupling constant (Cl < CH_3 < H). This cannot be rationalised by the classical application of Bent's rule to main group elements,[199] whereby electronegative substituents result in high p-character directed orbitals, and electropositive substituents in turn result in higher s-character directed orbitals. Application of this rule should therefore result in the Sn→Fe donation for **3-Fe** having the highest s-character owing to the presence of an electronegative substituent, and consequently, a larger coupling constant.[200] The rule is probably not applicable in our case since the tin atom is essentially unhybridised, and transition metal complexes, particularly, are known to be exceptions to Bent's rule in any event. The trend is the reverse, which suggests that it is driven exclusively by electro negativity of the substituents. In fact, a plot of the electro negativity (χ) to the observed $^2J(P,^{117/119}Sn)$ coupling constants of the complexes based on depe reveal a negative linear relation, suggesting the greater the electro negativity of the substituent, the lower will be the expected value of the coupling constant. (Figure 2.3.45).

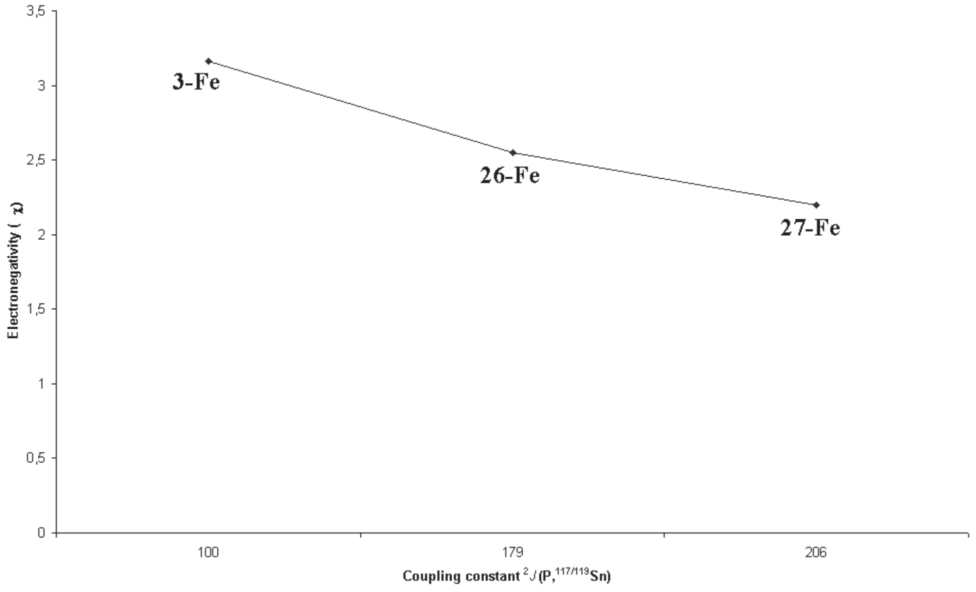

Figure 2.3.45: Plot of Electronegativity (χ) of substituent on Sn to coupling constant for the depe based complexes: **3-Fe**, **26-Fe** and **27-Fe**. (linear regression: $R^2 = 0.9761$).

Dieses Werk ist copyrightgeschützt und darf in keiner Form vervielfältigt werden noch an Dritte weitergegeben werden.
Es gilt nur für den persönlichen Gebrauch.

(c) Reaction of 3-Fe with HCl

The reaction of complex **3-Fe** with an excess of HCl was also explored. Reaction of **3-Fe** with excess (5 equivalents) HCl, in an ethereal solution, yields a mixture of two green-blue identifiable products: *trans*-[FeH($SnCl_3$)(depe)$_2$], **28-Fe** and *trans*-[FeCl($SnCl_3$)(depe)$_2$], **29-Fe** (ratio 1:2 based on $^{31}P\{^1H\}$ integration) along with observable 2,6-Mes$_2$-C_6H_4 (ArH), in the corresponding ^1H NMR spectrum, in C_6D_6. Separation of **28-Fe** and **29-Fe** by fractional crystallisation was not successful, but the identity of these two products was independently confirmed by selective synthesis of each (see below). Figure 2.3.46 shows the $^{31}P\{^1H\}$ NMR spectrum in C_6D_6 of the mixture resulting from this reaction.

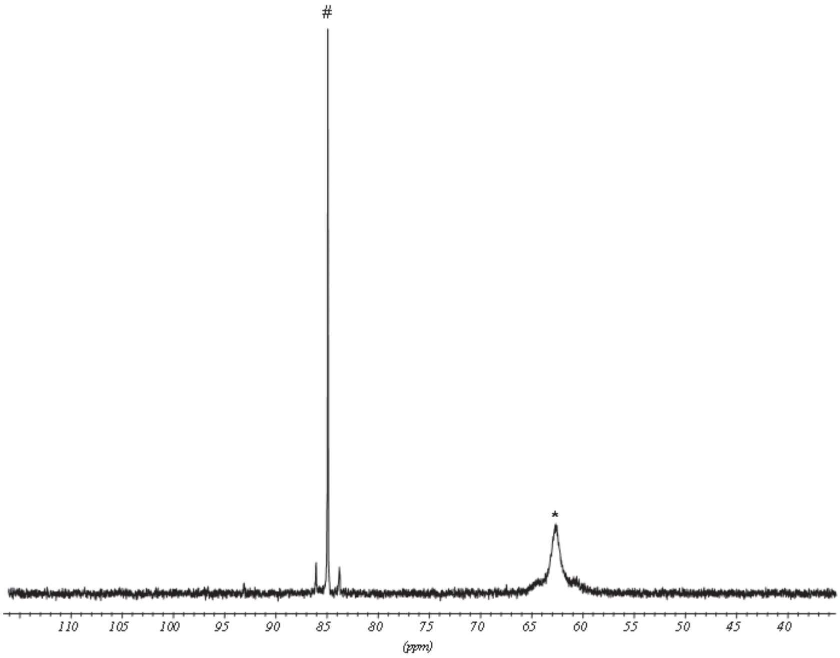

Figure 2.3.46: $^{31}P\{^1H\}$ NMR spectrum of product resulting from reaction of **3-Fe** with HCl (excess). $^{\#}$ = **28-Fe** * = **29-Fe**.

In addition, X-ray crystallographic analysis of the product mixture revealed three crystallographically independent molecules in the asymmetric unit, of which two molecules were solved (based on electron density) as having H : Cl double occupancies: 18.6 % Cl, 81.4 % H and 58.4 % Cl, 41.6 % H, respectively. The third was solved as having 100 % Cl *trans* to the $SnCl_3$ ligand. Consequently, both spectroscopic and X-ray crystallographic analyses point to a mixture of **28-Fe** and **29-Fe** resulting from this reaction. Figure 2.3.47 shows the solid state structure of the mixture of **29-Fe** and **29-Fe**, determined by X-ray crystallographic analysis. A discussion of their metric parameters are omitted, since both **28-Fe** and **29-Fe** where individually structurally characterised and are discussed later.

Dieses Werk ist copyrightgeschützt und darf in keiner Form vervielfältigt werden noch an Dritte weitergegeben werden.
Es gilt nur für den persönlichen Gebrauch.

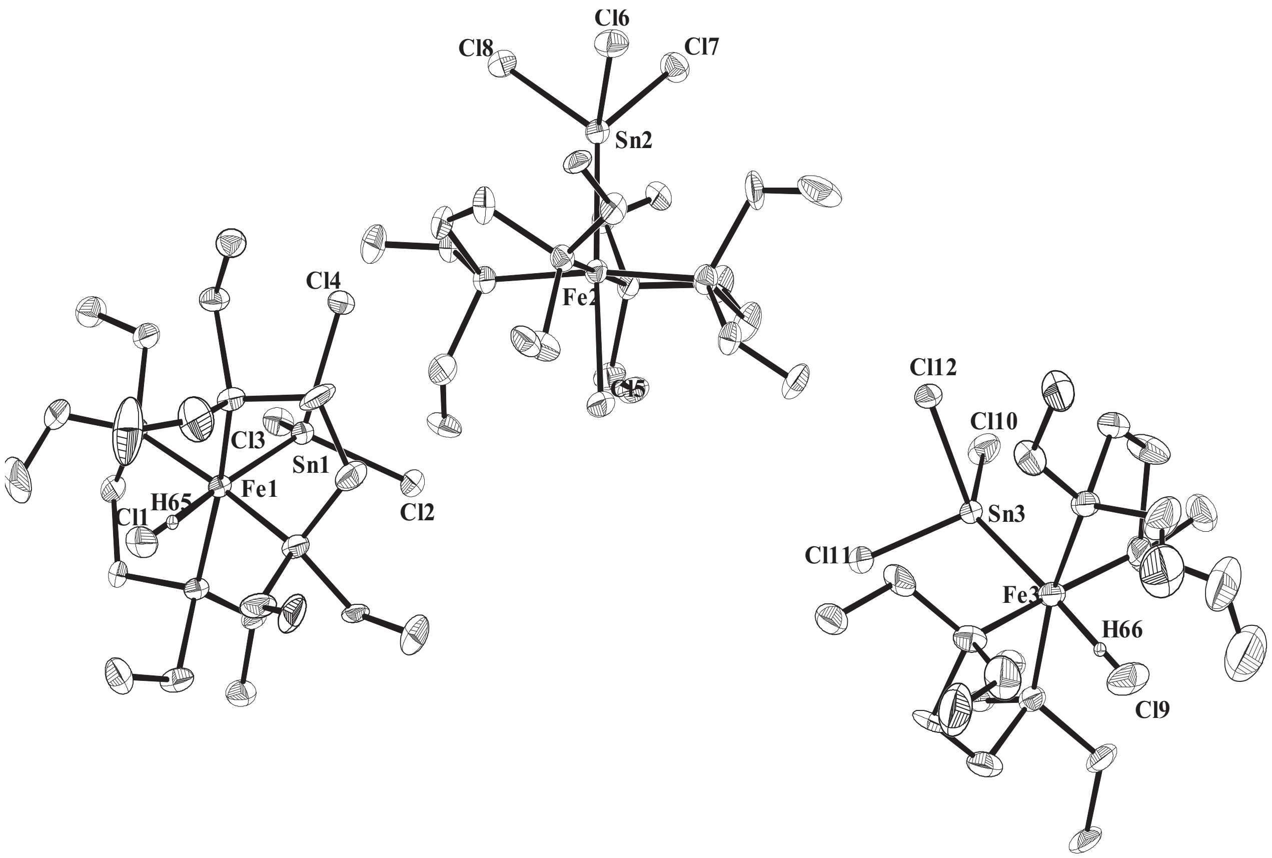

Figure 2.3.47: DIAMOND Plot of the product of the reaction of **3-Fe** with excess HCl, resulting in a mixture of **28-Fe** and **29-Fe**. H atoms are omitted for clarity. Thermal ellipsoids are set at 30 % probability. Three independent molecules are located in the asymmetric unit, two of which have H, Cl split occupancies: (H65, Cl1) and (H66, Cl9). The metric parameters are omitted.

Complex **29-Fe**[201] was selectively synthesised by insertion of $SnCl_2$ into the Fe–Cl bond of the precursor, **2-Fe**, by stirring a 1:1 mixture of the two compounds in CH_2Cl_2, resulting in the isolation of the turquoise solid, **29-Fe**. Although it has been reported before, no NMR spectroscopy has been reported, to our knowledge. The $^{31}P\{^1H\}$ NMR spectrum of **29-Fe** corresponds to that of the high field shifted resonance signal observed in the reaction mixture (Figure 2.3.45) with a broad signal flanked with Sn satellites at $\delta = 63$ ppm. The broad line shape of the resonance signal on first inspection, suggests it to be paramagnetic at room temperature but this is surprising given the strong field characteristics of $SnCl_3^-$ as a ligand: higher even then that of CO.[202] It is plausible that the broadness associated with the $^{31}P\{^1H\}$ resonance signal can be accounted for by reverse formation of $SnCl_2$ and **2-Fe**, in solution from **29-Fe**. This explanation has some precedence, for example $[Pt(SnBr_3)_5]^{3-}$ is reported in acetone solution to undergo loss of $SnBr_2$ resulting in $[PtBr_2(SnBr_3)_2]^{2-}$ or $[PtBr_3(SnBr_3)]^{3-}$, although in this report the $SnCl_3^-$ analogues are reported to be stable in solution.[203] In

Dieses Werk ist copyrightgeschützt und darf in keiner Form vervielfältigt werden noch an Dritte weitergegeben werden.
Es gilt nur für den persönlichen Gebrauch.

addition, complexes of the type [Fe($SnCl_3$)(CO)(diars)$_2$]BPh_4, diars = *o*-phenylenebis(dimethylarsine) have been postulated to eliminate $SnCl_2$, further lending support to the above mentioned hypothesis.[204] Low temperature $^{31}P\{^1H\}$ NMR spectroscopy in Toluene-d_8, at 213 K, reveal two sets of resonance signals, corresponding to **29-Fe** and **2-Fe**, respectively which provide further evidence for the above mentioned reverse reaction in solution. Crystals, suitable for X-ray crystallographic analysis were grown on several occasions, but did not result in a good quality data set, although the structural motif was in agreement with the proposed structure.

The complex, **28-Fe** was also selectively synthesised. Early attempts at conversion of **29-Fe** to **28-Fe** by reaction with Na[$BHEt_3$] with attempted Cl, H exchange at Fe did not result in clean conversion to **28-Fe**. Instead, ^1H NMR spectroscopy of the reaction mixture showed two distinct products: *trans*-[FeH($SnCl_2H$)(depe)$_2$] (minor) and **28-Fe** (major). Consequently, *trans*-[FeHCl(depe)$_2$], **30-Fe** was used instead as a suitable starting material, with a view of performing an insertion reaction of $SnCl_2$ into the Fe–Cl bond. Early reports of **30-Fe**[205,206] employed reduction reactions using $LiAlH_4$, followed by ethanol quenching. Baker *et al.* subsequently reported that by this methodology, impure products were obtained,[207] and so we decided to prepare **30-Fe** by careful reaction of **2-Fe** with Na[$BHEt_3$] by employing a Cl, H exchange reaction at Fe. In our hands this worked well in THF, and enabled moderate yields of **30-Fe** in pure form, on the basis on multinuclear NMR spectroscopy and elemental analysis.

Complex **30-Fe** was reacted with $SnCl_2$ and by insertion into the Fe–Cl bond, complex **28-Fe** could be isolated in moderate yields. (Scheme 2.3.14)

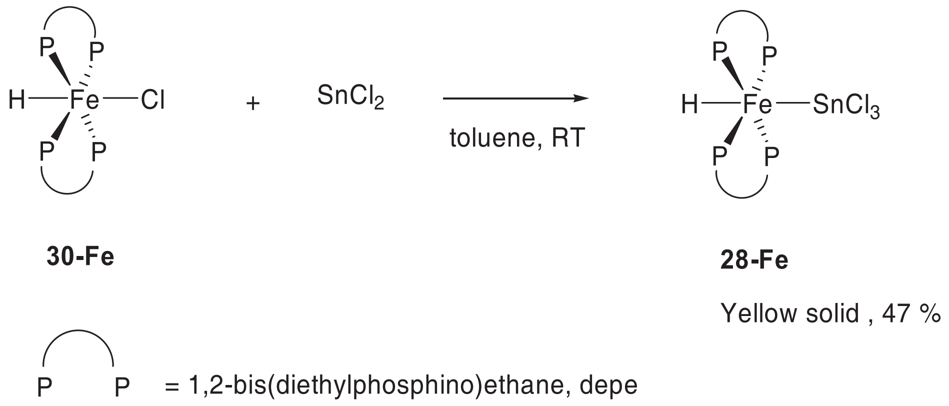

Scheme 2.3.14: Selective synthesis of complex **28-Fe** by insertion of $SnCl_2$ into the Fe-Cl bond of **30-Fe,** prepared by a new route.

Dieses Werk ist copyrightgeschützt und darf in keiner Form vervielfältigt werden noch an Dritte weitergegeben werden.
Es gilt nur für den persönlichen Gebrauch.

In contrast to **29-Fe**, **28-Fe** yields sharp, well defined resonance signals in the ^{1}H and $^{31}P\{^{1}H\}$ NMR spectra. Based on the previous assumption that the broadness associated with the resonance signals in **29-Fe** are associated with the loss of $SnCl_2$, having a hydride ligand as opposed to a Cl situated *trans* to the $SnCl_3$ ligand appears to hinder this reverse process. $^{31}P\{^{1}H\}$ NMR spectroscopy of complex **28-Fe** in THF-d_8 showed a doublet resonance signal at $\delta = 85.2$ (d, $^{2}J(P, {}^{117/119}Sn) = 274.6$ Hz). The origin of the doublet multiplicity comes from coupling to the Fe-*H*. Although proton decoupled, given the remote chemical shift of the hydride in ^{1}H NMR spectroscopy ($\delta = -19.58$ ppm (quint)), P,H coupling is still observable with conventional decoupling using the standard routine measurement parameters. Of interest is the rather large chemical shift differences associated with the hydride resonance signals in the ^{1}H NMR spectrum: in complex **30-Fe** it is observed at $\delta = -31.91$ ppm (in C_6D_6), in comparison to that of **28-Fe** significantly downfield shifted to $\delta = -19.58$ ppm, on account on changing from Cl to $SnCl_3$ as ligand *trans* to the hydride. Both these signals appear as quintets, and in the case of complex **28-Fe**, additional Sn satellite signals are observable. The *trans* configured H ligand (relative to $SnCl_3$) in **28-Fe** was additionally confirmed by X-Ray diffraction analysis (Figure 2.3.48). This is the first structurally characterised iron complex featuring mutually a trihalostannyl and a hydride ligand.

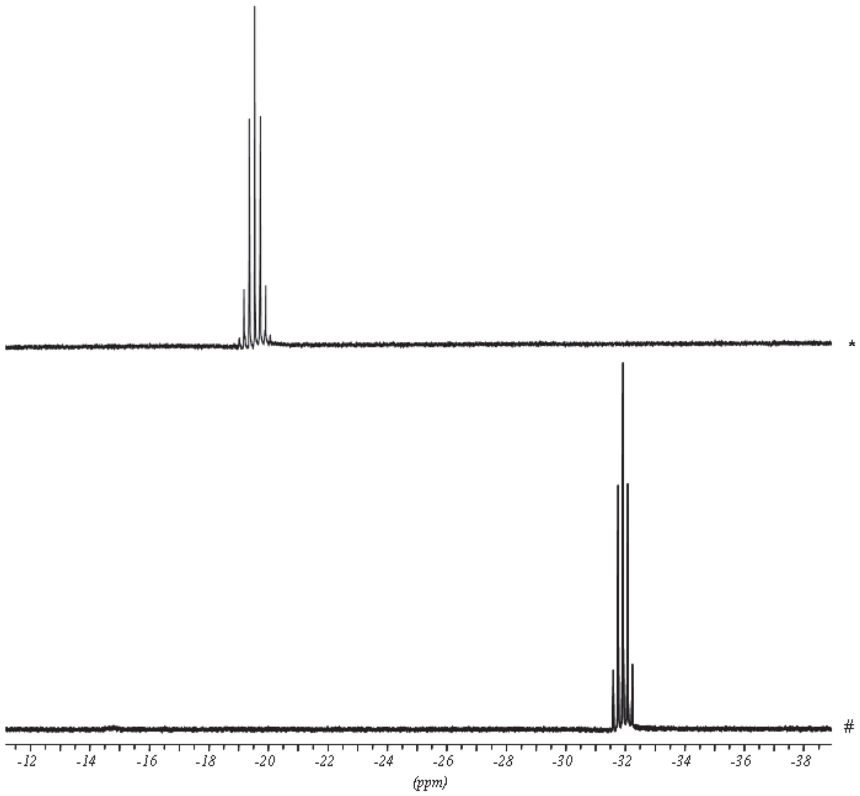

Dieses Werk ist copyrightgeschützt und darf in keiner Form vervielfältigt werden noch an Dritte weitergegeben werden.
Es gilt nur für den persönlichen Gebrauch.

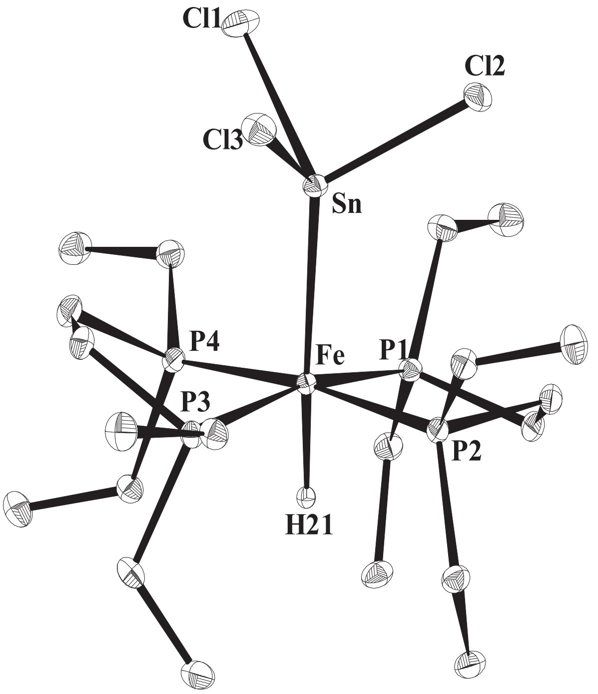

Figure 2.3.48: Comparison of ^{1}H NMR spectra at room temperature of **28-Fe**(*) (in THF-d_8) and **30-Fe** ($^\#$) (in C_6D_6) in the hydride region (previous page) and DIAMOND plot of the molecular structure of complex **28-Fe** in the solid state (below). (H atoms omitted for clarity, with exception H21). Thermal ellipsoids are set at the 30% probability level). Selected bond lengths [Å]: Fe-Sn 2.4641(4), Fe-H21 1.44(3). Selected bond angles [°] Sn-Fe-H21 176.3(12), Sn-Fe-P1 97.54(2), Sn-Fe-P2 91.72(2), Sn-Fe-P3 95.48(2), Sn-Fe-P4 95.57.

For the sake of comparison, the easily accessible germanium analogues of complex **28-Fe** and **29-Fe** were also prepared in a similar fashion, i.e. by simple insertion reactions of the accessible source of $GeCl_2$: $GeCl_2$·(1,4-dioxane). This is summarised in Scheme 2.3.15 below.

Dieses Werk ist copyrightgeschützt und darf in keiner Form vervielfältigt werden noch an Dritte weitergegeben werden.
Es gilt nur für den persönlichen Gebrauch.

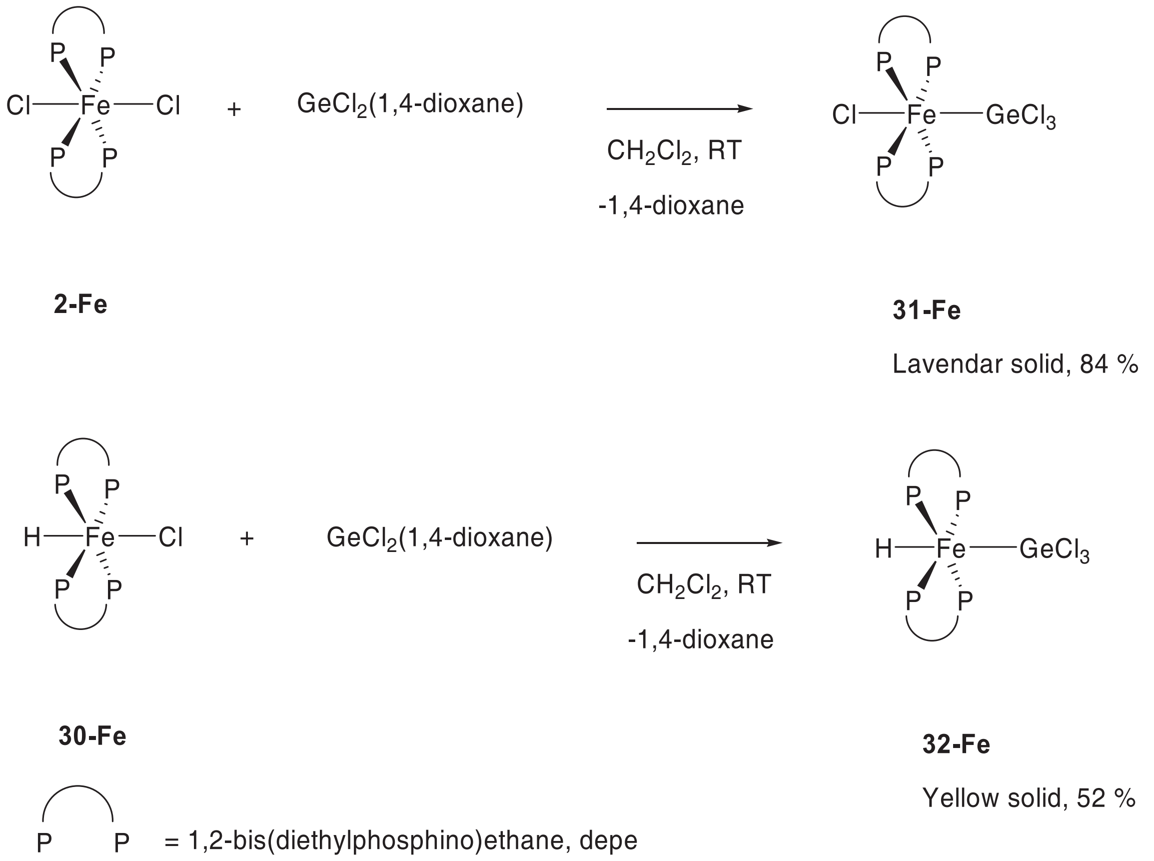

Scheme 2.3.15: Synthesis of the Ge analogues of **31-Fe** and **32-Fe** by analogous insertion of $GeCl_2$ into Fe–Cl bonds of the precursors **2-Fe** and **30-Fe** respectively.

Complex **31-Fe** in contrast to the tin analogue, **29-Fe** features a sharp resonance signal in the $^{31}P\{^1H\}$ NMR spectrum ($\delta = 65.1$ ppm, C_6D_6), indicative a *trans* configuration of the $GeCl_3$ and Cl ligands. Furthermore, the resonance signals in the ^1H NMR spectrum are also well resolved and sharp, in contrast to that of complex **29-Fe**. This observation lends further support to the earlier proposed dissociation of the $SnCl_3$ ligand of **29-Fe** into $SnCl_2$ and **2-Fe**, since $GeCl_3$ would certainly be expected to be a weaker field ligand than $SnCl_3$, and so if **31-Fe** is diamagnetic at room temperature on the basis of signal sharpness in NMR, the broadness seen in the spectra of the tin analogue at room temperature must be linked to a chemical process, such as was proposed earlier. It also suggests no similar dissociation of $GeCl_3$ into $GeCl_2$ and **2-Fe** occurs in solution in the case of **31-Fe**, which is a reasonable assumption, since $GeCl_2$ typically can only exist in the presence of a donor ligand, such as 1,4-dioxane, which would preclude such a process in the case of **31-Fe**.[208]

Crystals, suitable for X-ray crystallographic analysis of **31-Fe** were obtained by slow cooling of a concentrated solution of **31-Fe** in toluene to – 30 °C. The solid state structure of

Dieses Werk ist copyrightgeschützt und darf in keiner Form vervielfältigt werden noch an Dritte weitergegeben werden.
Es gilt nur für den persönlichen Gebrauch.

complex **31-Fe** represents the only to date of a trichlorogermyl iron complex. Solid state structural investigations of transition metal complexes bearing a trichlorogermyl ligand t*rans* to a halogen, as is the case with **31-Fe**, are also very rare. In fact, only one other example exists of a complex bearing a $GeCl_3$ ligand, *trans* to a halogen, where it happens to be anionic: $[ClAu(GeCl_3)]^-$.[209] Typically $GeCl_3$ as a ligand bound to a transition metal exists in a *cis* configuration relative to the halogen on the transition metal, or in a non-*trans* orientation.[210] Some examples also exist where $GeCl_3$ is *cis* to a bridging halogen,[211] or where a bridging Cl exists between the transition metal centre and the $GeCl_3$ moiety.[212] That makes complex **31-Fe** surprisingly rare. Four crystallographically independent molecules were located in the asymmetric unit, in the solid state. Figure 2.3.49 shows one of the independent molecules in the asymmetric unit with its associated metric parameters, and Figure 2.3.50 the other independent molecules.

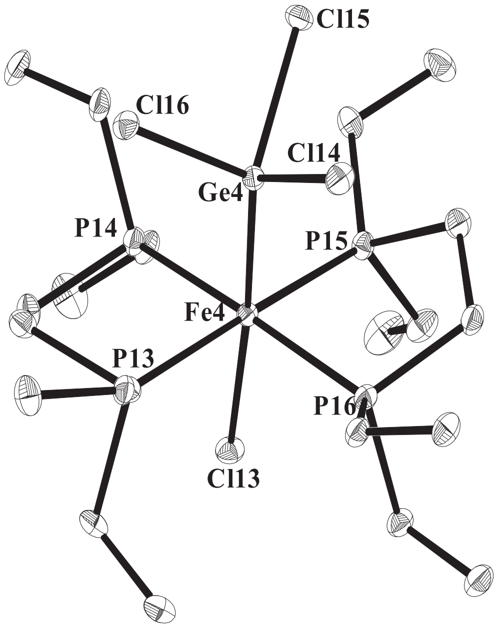

Figure 2.3.49: DIAMOND plot of the molecular structure of complex **31-Fe** in the solid state (one of the independent molecules represented, along with its metric parameters. Thermal ellipsoids are set at the 30% probability level, H atoms are omitted for clarity. Selected bond lengths [Å]: Fe4–Cl13 2.351(2), Fe4–Ge4 2.302(1). Selected bond angles [°]: Ge4-Fe4-Cl13 175.67(7), P14-Fe4-P15 95.22(6), P13-Fe4-P14 84.55(7), P15-Fe4-P16 81.76(7), P13-Fe4-P16 98.27(6), P14-Fe4-P16 173.46(7), P13-Fe4-P15 177.98(7), Cl16-Ge4-Cl14 94.81(6), Cl16-Ge4-Cl15 95.26(6), Cl14-Ge4-Cl15 92.85(6).

Dieses Werk ist copyrightgeschützt und darf in keiner Form vervielfältigt werden noch an Dritte weitergegeben werden.
Es gilt nur für den persönlichen Gebrauch.

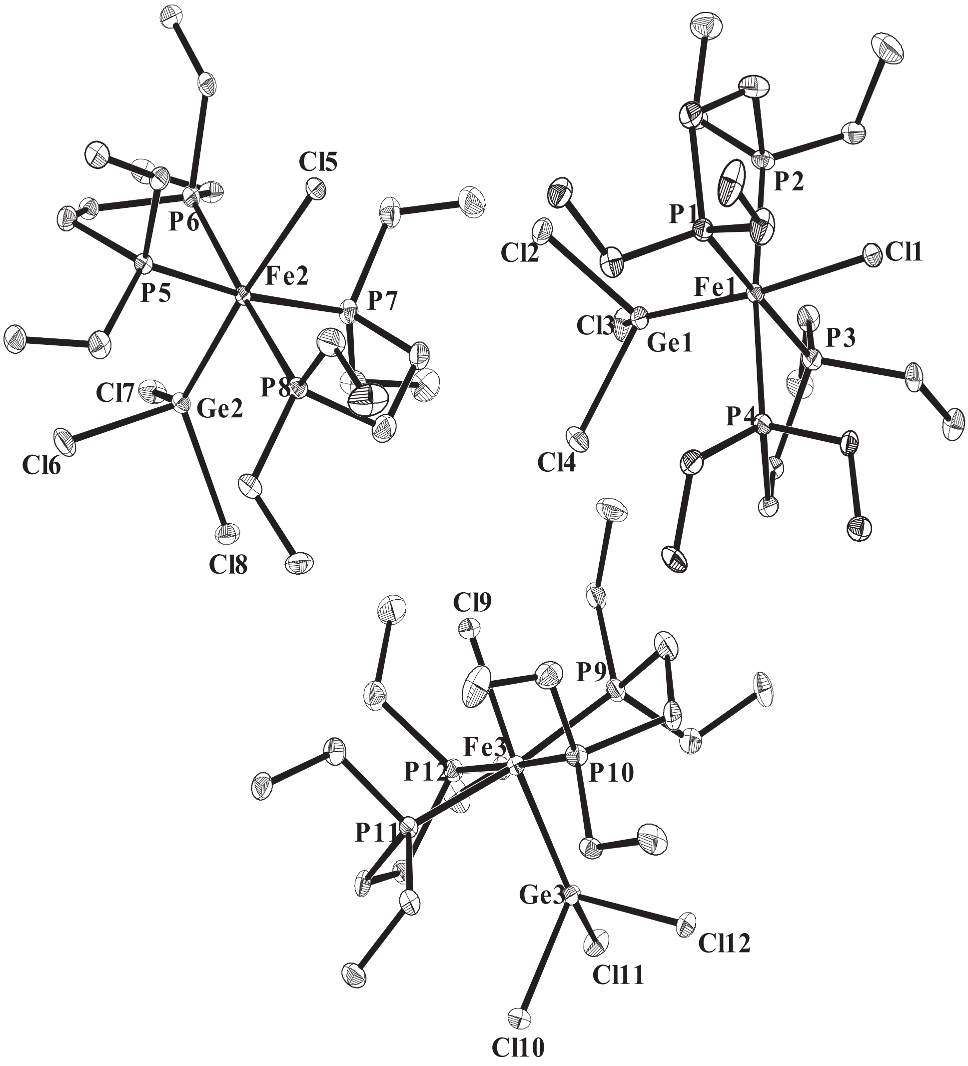

Figure 2.3.50: DIAMOND plot of the molecular structure of complex **31-Fe** in the solid state (the other three independent molecules in the asymmetric unit represented) Thermal ellipsoids are set at the 30% probability level, H atoms are omitted for clarity, associated metric parameters listed in Table 2.3.2 below.

Dieses Werk ist copyrightgeschützt und darf in keiner Form vervielfältigt werden noch an Dritte weitergegeben werden.
Es gilt nur für den persönlichen Gebrauch.

Molecule 1		**Molecule 2**		**Molecule 3**	
Selected bond lengths					
Fe1–Cl1	2.356(2)	Fe2–Cl5	2.358(2)	Fe3–Cl9	2.351(2)
Fe1–Ge1	2.298(1)	Fe2–Ge2	2.302(1)	Fe3–Ge3	2.306(1)
Selected bond angles					
Ge1-Fe1-Cl1	174.83(6)	Ge2-Fe2-Cl5	175.16(5)	Ge3-Fe3-Cl9	175.57(6)
P1-Fe1-P4	95.17(6)	P5-Fe2-P8	95.81(6)	P10-Fe3-P11	97.90(6)
P2-Fe2-P3	95.62(6)	P6-Fe2-P7	95.16(6)	P9-Fe3-P10	84.66(7)
P1-Fe1-P2	86.11(6)	P5-Fe2-P6	82.75(6)	P9-Fe3-P11	173.48(7)
P4-Fe1-P3	82.76(6)	P7-Fe2-P8	85.87(6)	P11-Fe3-P12	81.53(7)
P1-Fe1-P3	176.58(7)	P5-Fe2-P7	173.18(7)	P12-Fe3-P10	177.63(7)
P2-Fe1-P4	172.81(7)	P6-Fe2-P8	176.17(7)	P9-Fe3-P12	95.67(7)
Cl2-Ge1-Cl3	94.83(7)	Cl6-Ge2-Cl7	93.49(7)	Cl12-Ge3-Cl10	95.44(6)
Cl2-Ge1-Cl4	96.09(7)	Cl6-Ge2-Cl8	96.14(7)	Cl10-Ge3-Cl11	93.33(6)
Cl4-Ge1-Cl3	94.22(7)	Cl7-Ge2-Cl8	95.35(6)	Cl11-Ge3-Cl12	93.93(6)

Table 2.3.2: Metric parameters of the remaining 3 independent molecules in the asymmetric unit in the solid state of **31-Fe** (omitted from Figure 2.3.48).

The Fe–Ge bond length (2.298(1) – 2.306(1) Å)[***] is somewhat shorter than the shortest Fe–Ge bond length hitherto reported in the literature (with the exception of our iron germylidyne complexes) (2.338(2) Å [213] for [Cp*Fe(CO)$_2$(GeMe$_2$Cl)]. This is directly a result of having three electronegative Cl atoms on the Ge centre, a trend apparently also observed with transition metal silyl-complexes.[214] It is also interesting to note the pronounced elongation of the Fe–Ge bond length in complex **31-Fe** compared to the germylidyne complexes, **8-Fe** and **9-Fe** (2.1198(4) – 2.1342(4) Å).

Complex **31-Fe** exhibits nearly ideal octahedral geometry at the iron centre. The GeCl$_3$ ligand is trans to the Cl ligand, and forms a nearly linear bond angle: Ge-Fe-Cl (174.83(6) – 175.67(7)°). The two depe ligands occupy the remaining four equatorial coordination sites where the phosphorus atoms are coplanar, evidenced by the summation of the four P-Fe-P bond angles around Fe adding up to *ca*. 360° for each independent molecule. Two sets of P-Fe-P bond angles are slightly smaller in magnitude (81.53(7) – 86.11(6)°) compared to the other two (95.16(6) – 98.27(6)°), resulting from the bite angle of the depe chelating ligand.

[***] In the discussion a range will be indicated for a given metric parameter over all four independent molecules.

Dieses Werk ist copyrightgeschützt und darf in keiner Form vervielfältigt werden noch an Dritte weitergegeben werden.
Es gilt nur für den persönlichen Gebrauch.

The observation of one well resolved singlet resonance in the $^{31}P\{^1H\}$ NMR spectrum is suggestive of free rotation of the $GeCl_3$ ligand in solution, and the existence of two vertical mirror planes, rendering all phosphorus atoms equivalent.

The hydride complex, **32-Fe** was prepared in analogy to its tin analogue, **28-Fe**. The most characteristic resonance signal in the ^1H NMR spectrum in THF-d_8, is that of the Fe-H $\delta = -18.79$ ppm which has, as with **28-Fe** a quintet multiplicity, owing to the ^2J coupling to four equivalent P atoms. The chemical shift of this resonance signal is slightly downfield shifted on changing from Sn to Ge, both of which are dramatically downfield shifted from the precursor, **30-Fe**. Crystals, suitable for X-ray diffraction analysis of **32-Fe** were grown from a concentrated THF solution at –30 °C. Two crystallographically independent molecules were located in the asymmetric unit, one of those is represented in Figure 2.3.51. There are only minor metric and angular deviations between the two independent molecules in the asymmetric unit, and does not warrant further discussion (Figure 2.3.51).

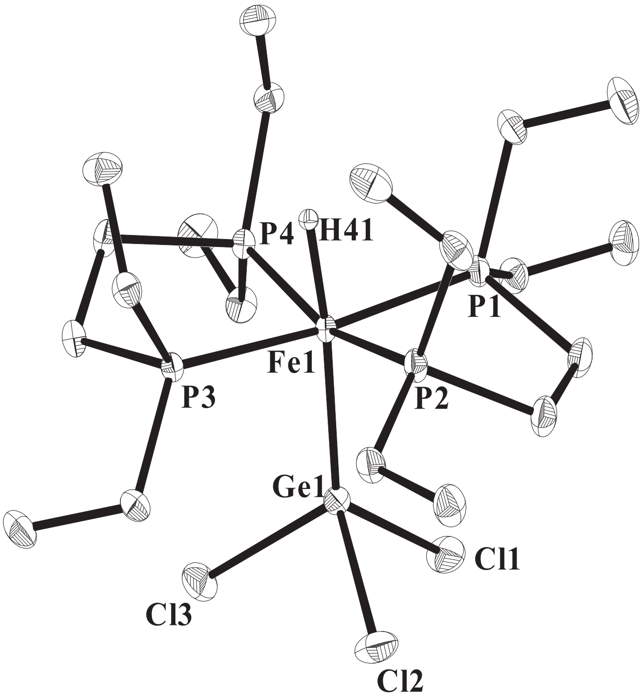

Figure 2.3.51: DIAMOND plot of one of the crystallographically independent molecules of **32-Fe** in the solid state (The corresponding metric parameter of the other independent molecule represented in parenthesis afterwards). Thermal ellipsoids are set at 50 % probability. H atoms omitted for clarity (with the exception of the hydride hydrogen atom H41) Selected bond lengths [Å]: Fe1–Ge1 2.2934(3) [2.2956(3)], Fe1–H41 1.47(3) [1.44(2)]. Selected bond angles [°]: H41-Fe1-Ge1 174.7(10) [177.4(9)].

Dieses Werk ist copyrightgeschützt und darf in keiner Form vervielfältigt werden noch an Dritte weitergegeben werden.
Es gilt nur für den persönlichen Gebrauch.

Complex **32-Fe** is the first example of a structurally characterised hydrido germyl iron complex, and the first hydrido trihalogermyl complex of any transition metal element to date, making it surprisingly rare. The molecular structure reveals a *trans* situated hydride ligand, relative to the germyl ligand, in accordance with the spectroscopic findings. The local geometry at the Fe centre can best be described as distorted octahedral, with the four phosphorus atoms positioned in a non-planar arrangement. This is shown by an inspection of the H-Fe-P angles in both independent molecules being < 90° (range: 78(1)° – 88.9(10)°, average = 84.6°). This observation is in contrast to the *trans* Cl complex, **31-Fe**, where the average of the Cl-Fe-P angles over all four crystallographically independent molecules is slightly larger in magnitude (87.77°, range: 82.00°(6) – 91.76(6)°), the latter approaching, on average, a more regular octahedral geometry. The smaller magnitude of these bond angles in complex **32-Fe** is hence likely due to the fact that the hydride ligand imparts less steric pressure compared to Cl, thereby allowing the phosphorus atoms to tilt out of plane to a greater extent, and thereby relieving the steric pressure between the germyl and depe ligand system. The average of the Fe–Ge bond length over both independent molecules is 2.2945(4) Å, which is comparable that found in **31-Fe** (2.298(1) – 2.306(1) Å). This result suggests that the bond lengths are rather unaffected on changing from a Cl to a H atom, *trans* to the germyl ligand.

To further probe the effect of changing from $SnCl_3$ to $GeCl_3$ as ligand, IR spectroscopy on pure samples of **28-Fe** and **32-Fe** was also employed, particularly to locate the Fe–H stretching vibrations (Figure 2.3.52).

Dieses Werk ist copyrightgeschützt und darf in keiner Form vervielfältigt werden noch an Dritte weitergegeben werden.
Es gilt nur für den persönlichen Gebrauch.

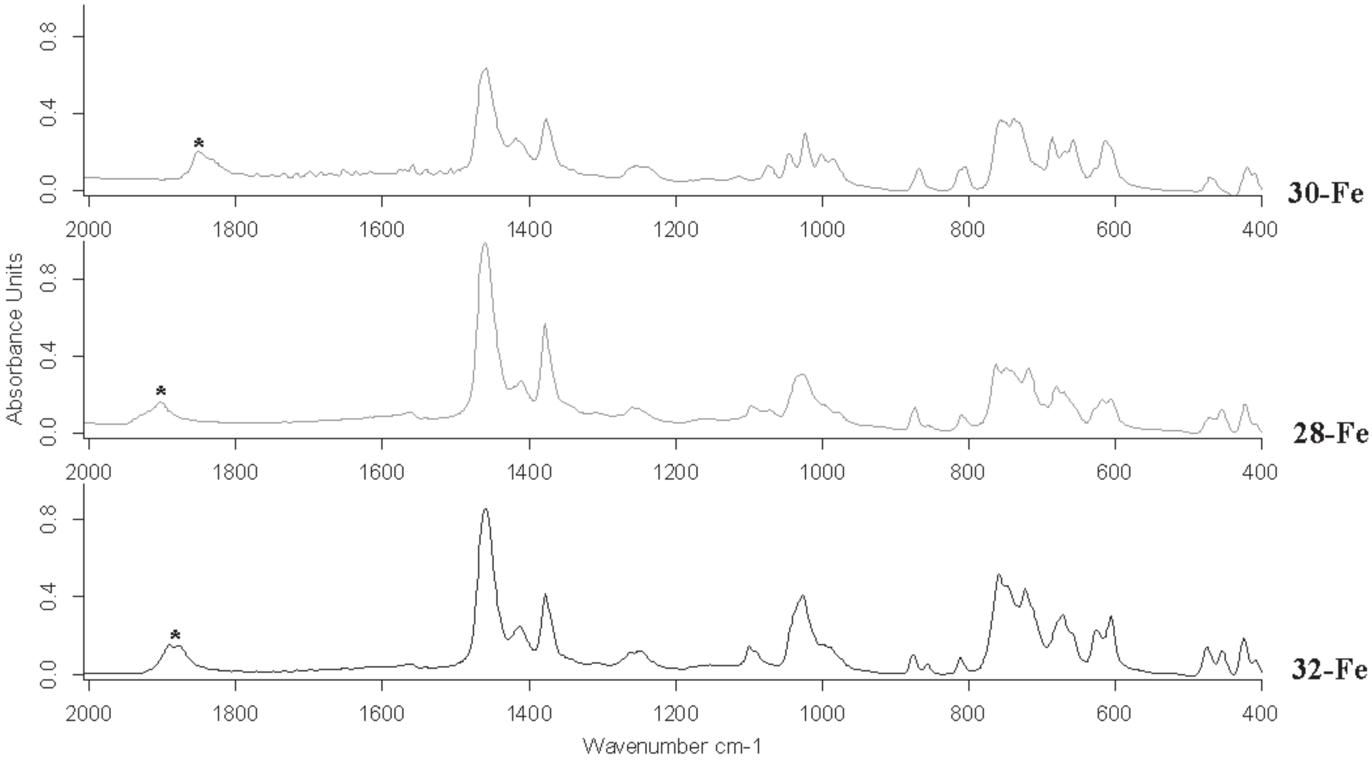

Figure 2.3.52: Comparative IR (2000 – 400 cm^{-1}) spectra in nujol of **30-Fe**, **28-Fe** and **32-Fe**. * = Fe-H stretching vibration.

In all cases (the precursor **30-Fe**[†††] and **28-Fe** and **32-Fe**) the Fe-H stretching vibration appears broad with a side shoulder (**30-Fe** and **28-Fe**), and in the case of **32-Fe** is split into a doublet (ν = 1890 and 1878 cm^{-1}). This phenomenon is likely due to a solid state or Fermi resonance effect,[215] as only a single stretching vibration is expected in all cases. The Fe-H stretching vibration in **32-Fe** is shifted to lower wave numbers (ca 20 cm^{-1}) compared to the tin analogue **28-Fe**, indicative of the fact that the $GeCl_3$ ligand exerts a greater *trans* influence compared to $SnCl_3$ on the *trans*-hydride ligand, resulting in a weaker Fe-H bond strength. These results are in agreement with what has been reported in the literature: $SnCl_3$ is known to induce a very low *trans* influence,[216] and for a series of iridium complexes, on the basis of IR spectroscopy, it was shown that $SnMe_3$ exhibits a much lower *trans* influence in comparison to $GeMe_3$, in analogy to our observations.[217] Furthermore, it has also been shown for Pt complexes, that $SnMe_3$ exhibits a similar *trans* influence as $SnCl_3$, but considerably less than $GeMe_3$.[218] It is also interesting to recall the similar trend that was observed in the case of the Pd insertion complexes (section 2.1) where the germyl ligands were found to exert a stronger *trans* influence compared to the stannyl ligands.

[†††] Chatt and Hayter have reported the Fe-H stretching vibration at 1849 cm^{-1} in Nujol, almost identical to our spectrum where it is located at 1851 cm^{-1}.

Dieses Werk ist copyrightgeschützt und darf in keiner Form vervielfältigt werden noch an Dritte weitergegeben werden.
Es gilt nur für den persönlichen Gebrauch.

2.3.6 ^{57}Fe Mößbauer spectroscopic investigations

Since the first reports of the Mößbauer effect in the late 1950s,[219] Mößbauer spectroscopy has developed into an indispensable modern spectroscopic technique in the characterisation of solids containing Mößbauer active nuclei.[220] The basis of the technique rests on nuclear transitions, in much the same way as nuclear magnetic resonance. These can involve the emission or absorption of γ-rays, the energy of which is reduced by the recoil of the emission or absorption on the basis of momentum conservation. The energy associated with the recoiling nucleus, following absorption or emission (eq 3) is:

$$E_R = \frac{E_\gamma^2}{2mc^2} \qquad (3)$$

Where, E_γ^2 is the energy of the emitted, or absorbed γ-ray, m is mass of the emitting or absorbing body, and c the velocity of light. It follows that in a gas resonance is difficult or impossible to achieve owing to the fact that m is rather small since the emission or absorptions occurs with individual particles, and the recoil energy, E_R of an absorption or emission event is very large. In solids on the other hand, m can be considered to be the mass of the entire lattice, and consequently according to the Lamb-Mößbauer factor,[221] a certain proportion of emissions are essentially recoil free. This enables resonance at an absorbing nucleus. The actual energy is ultimately dependant on the electronic environment at the absorbing nucleus, and by varying the velocity of the source, and by use of the Doppler effect, this chemical environment can be probed. A variety of element isotopes are able to exhibit in the Mößbauer effect and among these ^{57}Fe is probably the most common.

A Mößbauer spectrum yields three measurable parameters which can be used to elucidate the environment around the nucleus:

(a) *The electric quadroupole splitting parameter (ΔE_Q, mm·s^{-1}):* This is the result of the interaction of the electric quadrupole moment of the Fe nucleus and an electric field gradient (EFG). An Fe nucleus in the ground state exhibits spherical charge distribution, and hence possesses no quadrupole moment. On excitation, however, it takes on an ellipsoidal shape, which does possess an electric quadrupole moment, and consequently two possible orientations in an electric field gradient result in two different possible energy transitions. Generally, the probabilities associated with these transitions are equal, given random orientation of the measured sample. The resulting splitting that is observed is proportional to

Dieses Werk ist copyrightgeschützt und darf in keiner Form vervielfältigt werden noch an Dritte weitergegeben werden.
Es gilt nur für den persönlichen Gebrauch.

the magnitude of the EFG at the nucleus. The EFG is in turn a reflection of the asymmetry associated with electrons in the atom itself, and secondly, by neighbouring ions. This parameter therefore yields information regarding the geometry around the Fe atom in the solid state.

(b) *The isomer shift value (δ, mm·s^{-1}):* this is a reflection of the s-electron density near to the nucleus of the absorbing atom, and yields information relating to the oxidation state of Fe. The isomer shift is temperature-dependent, since it contains a contribution from the thermal motion of the individual absorbing atoms, according to (eq. 4):

$$\delta = \delta_{T=0} - \frac{< v^2 >}{2c} \qquad (4)$$

where δ is isomer shift as a function of temperature, T is temperature, $<v^2>$ is the mean squared velocity of atoms due to lattice vibrations, and c is the velocity of light. The second term in eq. 4 is the so-called second order Doppler shift.

(c) *The Zeeman or magnetic hyperfine splitting (H):* is a consequence of the interaction between the magnetic dipole moment, and the magnetic field at the nucleus. Six possible transitions result, which are in turn proportional to the magnetic field at the nucleus. For our purposes, evaluation of parameters (a) and (b) need only be considered.

2.3.6.1 ^{57}Fe Mößbauer spectra of some of our investigated Fe(0) complexes

According to the Bancroft point-charge model,[222,223,224,225] the observed isomer shift is an arithmetic sum of partial isomer shifts (p.i.s) of the ligands at iron (eq. 5):

$$\delta_{obs} = \sum p.i.s \qquad (5)$$

The p.i.s values in turn reflect the ($\sigma + \pi$) donation from the individual ligand to the iron centre, with more positive values suggesting less overall donation to the metal centre.[226] An increase in σ-donation from a ligand, results in an increase in the effective s-electron density, and a consequent decrease in the δ value. Similarly, a good π-accepting ligand, through deshielding, effectively increases the s-electron density, and hence also results in a decrease in δ. The point charge model works well for six coordinate octahedral systems, but in the case of five coordinate systems, due to loss of octahedral symmetry cannot be employed.

Dieses Werk ist copyrightgeschützt und darf in keiner Form vervielfältigt werden noch an Dritte weitergegeben werden.
Es gilt nur für den persönlichen Gebrauch.

Separating σ and π effects, and their respective effects on the isomer shift are not straight forward: Collins and Pettit reported a dominance in σ-effects on the isomer shift values for complexes [$Fe(CO)_4L$], where L occupies an equatorial site in a TBP geometry,[227] while axially substituted TBP complexes depend on synergistic σ *and* π interactions.[228] The situation is further complicated by the fact that a series of five coordinate complexes of the type [$M'Fe(CO)_4$], where M' = main group metal, don't fall into either of these two categories,[229] and consequently interpretation of Mößbauer spectra associated with 5 coordinate Fe complexes is a challenge.

The complexes **1-Fe**, **3-Fe**, **4-Fe, 6-Fe**, **8-Fe, 9-Fe**, **16-Fe** were the subject of a comparative ^{57}Fe Mößbauer spectroscopic investigation at 80 K. A starting point in this investigation was the determination of the Mößbauer spectrum of the parent N_2 complex, **1-Fe**, previously unreported in the literature (Figure 2.3.53) It exhibits an δ value of 0.24 $mm{\cdot}s^{-1}$ and a ΔE_Q value of 2.14 $mm{\cdot}s^{-1}$. The δ value of **1-Fe**, (and all the other complexes measured) is within the expected range for Fe(0) complexes, but somewhat higher than that observed for complexes of the type [$Fe(CO)_4L$] L = any arbitrary ligand.[227] Phosphane ligands are generally better σ-donors than CO ligands and so an effective increase in the s-electron density at Fe would be anticipated, which should result in a *decreased* δ value. The reverse is however observed and can be explained by the fact that phosphanes are weaker π-acceptors than CO, and so the increased π-accepting ability of CO results in an increase in the s-electron density at Fe through deshielding, and a consequent lower δ value, compared to depe ligands. The π-accepting ability in this instance offsets the σ-donation effect.

It is interesting to compare the parameters of **1-Fe** to the stannylidene complex, **3-Fe**, which exhibits a slightly higher δ value (0.31 $mm{\cdot}s^{-1}$), and a lower ΔE_Q value (1.00 $mm{\cdot}s^{-1}$). A direct comparison between these two complexes can be made, since they are both neutral, and trigonal bipyramidal in the solid state on the basis of X-ray diffraction analyses with the only difference being the ligand occupying one of the positions in the equatorial plane. According to Sosinsky *et al.*,[230] both δ and ΔE_Q parameters depend strongly on σ-donation for trigonal bipyramidal complexes of the type [$Fe(CO)_4L$] L = variable equatorial ligand, and generally an inverse relationship should exist between ΔE_Q and δ in these cases. On this basis, the data suggests that the N_2 ligand (in **1-Fe**), is a *stronger* σ-donor than the stannylene ligand (in **3-Fe**). This can be explained by the fact that the Sn atom in **3-Fe** is essentially

Dieses Werk ist copyrightgeschützt und darf in keiner Form vervielfältigt werden noch an Dritte weitergegeben werden.
Es gilt nur für den persönlichen Gebrauch.

unhybridised (see earlier discussion) and hence the σ-donation to Fe originates from a pure s orbital, with limited directionality towards the Fe centre. In N_2, the donating electron pair originates from an sp hybrid orbital, and given the higher p-character, possibly facilitates better directionality in the bond, and makes it a better σ-donor. This is purely suggestive, since it will be shown later, differences in isomer shifts can even occur in complexes featuring identical cations, with different anions, and hence drawing conclusions from small differences in isomer shifts should be guarded against.

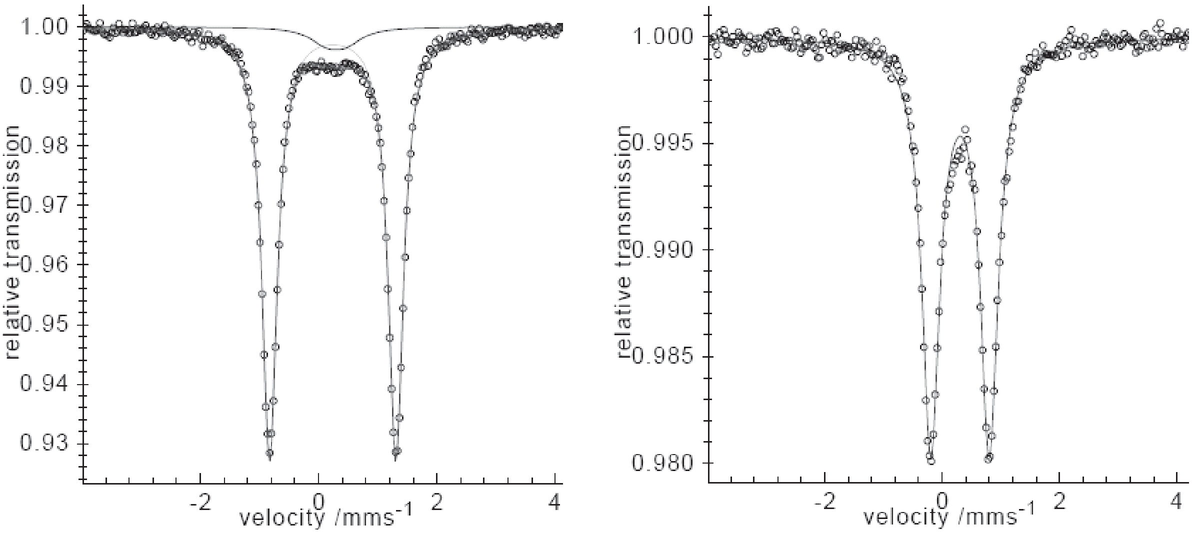

Figure 2.3.53: ^{57}Fe Mößbauer spectrum of the parent dinitrogen complex, **1-Fe** at 80 K (left), and the stannylidene complex, **3-Fe** at 80 K (right). The black circles are the data, and the lines the simulated spectra.

In the case of the stannylidyne complexes **4-Fe** and **6-Fe** two sets of quadrupole doublet signals are visible, each doublet corresponding to an isomeric form (TBP and SQPY) of the cation previously observed in the solid state by X-ray analysis in **4-Fe**. This result can hence be viewed as additional spectroscopic evidence for the coexistence of both stereoisomers in the solid state**.** Although **6-Fe** was not the subject of an X-ray structure determination, given the fact that the complex **5-Fe** also exhibits two isomeric forms in the asymmetric unit, it is reasonable to assume the same would be the case for **6-Fe**, since this clearly depends on the cation (which are identical in all three compounds), and not on the counter anion. The relative ratio of each isomer (TBP : SQPY) in each compound is also different, a result likely attributable to thermodynamics: **4-Fe** is synthesised in pentane and precipitates out of solution as a solid, potentially resulting in a higher proportion of the kinetically stable isomer (blue) contrasted to **6-Fe** which was prepared by stirring overnight, resulting in a higher proportion of the thermodynamically stable isomer (green) (Figure 2.3.54). The change in

Dieses Werk ist copyrightgeschützt und darf in keiner Form vervielfältigt werden noch an Dritte weitergegeben werden.
Es gilt nur für den persönlichen Gebrauch.

reaction conditions and reaction time can account for the different distribution ratio of each isomer in **4-Fe** and **5-Fe**. Nevertheless, the fact that in *both* ^{57}Fe Mößbauer spectra, two doublet signals are visible is convincing evidence of both stereoisomers being observed. (this is further discussed in section 2.3.6.1.2).

The δ value for both doublets in each spectrum is the same (in **4-Fe**) and only differs by 0.01 mm.s^{-1} (in **6-Fe**), but curiously both the δ and ΔE_Q values differ from each other in **4-Fe** and **6-Fe**. This is surprising, since the cations are identical, and only the anion is different, but similar observations have been reported before: the radical anions $[Na(thf)_x][Fe(CO)_4(SnMe_2)]$ and $[Na(4\text{-}MeC_5H_4NO)_{1.4}][Fe(CO)_4(SnMe_2)]$ were shown to exhibit a difference of 0.11 mm·s^{-1} in the observed δ value.[230] This difference was subsequently attributed to a second order Doppler shift effect, and could also be responsible for the discreprency in the parameters of **4-Fe** and **6-Fe**. It is henceforth important not to over interpret differences in the isomer shift parameter.

In contrast, the germylidyne complex, **8-Fe** features only one doublet signal in the ^{57}Fe Mößbauer spectrum at 80 K. This result is consistent, again, with the solid state X-ray structure determination, where only SQPY geometry is observed. It follows, from this that, the doublet signals in both **4-Fe** and **6-Fe** of lower ΔE_Q probably correspond to the SQPY isomeric form present in the solid state.

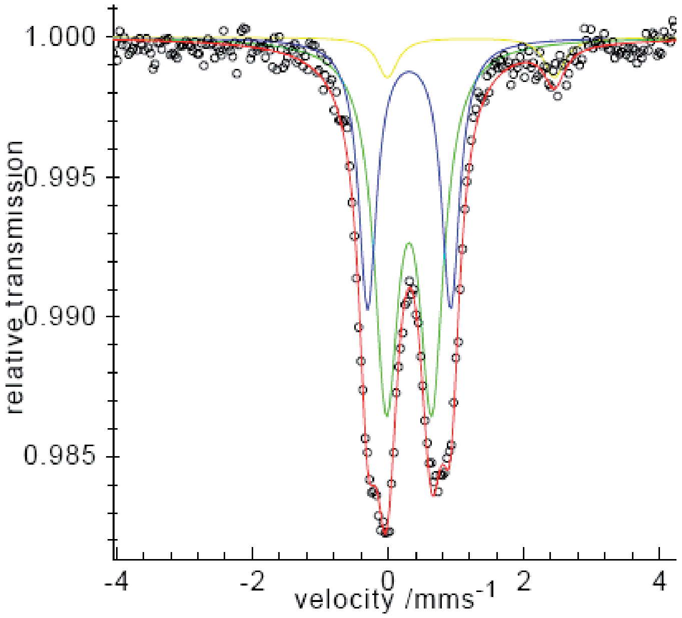

4-Fe

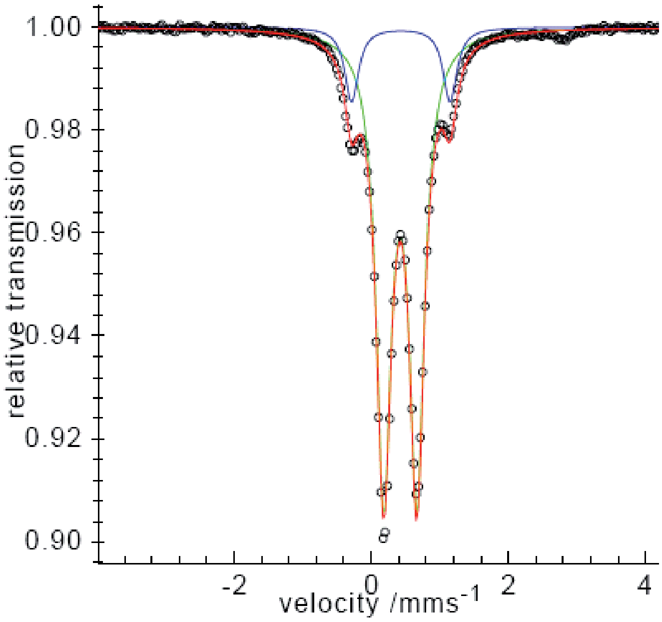

6-Fe

Dieses Werk ist copyrightgeschützt und darf in keiner Form vervielfältigt werden noch an Dritte weitergegeben werden.
Es gilt nur für den persönlichen Gebrauch.

Figure 2.3.54: ^{57}Fe Mößbauer spectra of the ionic stannylidyne complexes **4-Fe** (left) and **6-Fe** (right) at 80 K. The black circles are the data, and the lines the simulated spectra. **4-Fe** (blue line 34.57 %): $\delta = 0.31$ $\Delta E_Q = 1.22$; (green line 59.60 %): $\delta = 0.31$ $\Delta E_Q = 0.67$. **6-Fe** (blue line 12.94 %): $\delta = 0.43$ $\Delta E_Q = 1.44$ (green line 87.06 %): $\delta = 0.42$ $\Delta E_Q = 0.48$ mm·s^{-1}

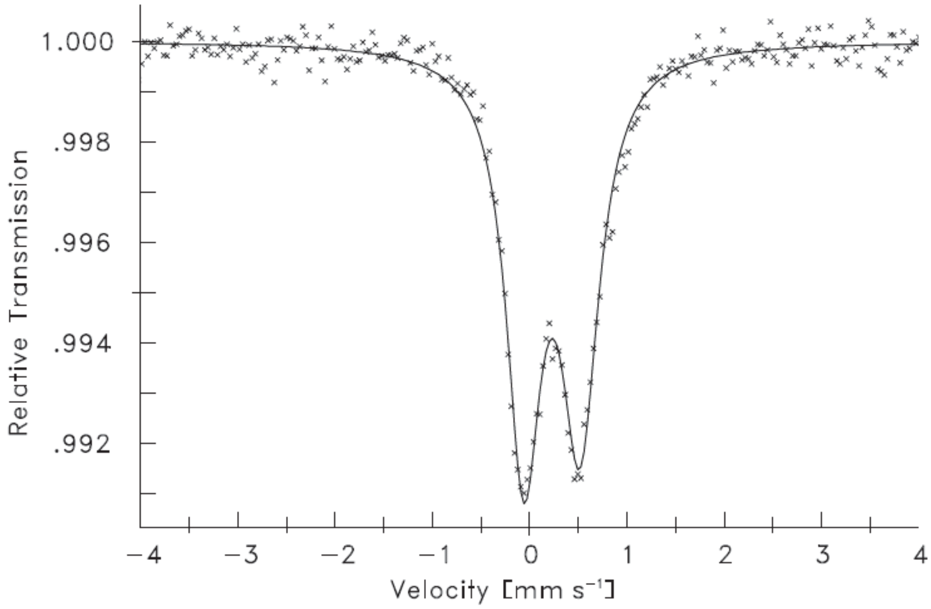

Figure 2.3.55: ^{57}Fe Mößbauer spectra of the ionic germylidyne complex **8-Fe** at 80 K. The black crosses are the data, and the line the simulated spectrum. Only one doublet signal is observed, consistent with only one stereoisomer being present in the solid state, as shown by X-ray diffraction analysis.

Complex	δ mm·s^{-1}	ΔE_Q mm·s^{-1}
1-Fe	0.24	2.14
3-Fe	0.31	1.00
4-Fe	0.31	1.22
	0.31	0.67
6-Fe	0.43	1.44
	0.42	0.48
8-Fe	0.23	0.58
16-Fe	0.23	1.15

Table 2.3.3: Measured ^{57}Fe Mößbauer parameters for the Fe(0) complexes **1-Fe**, **3-Fe**, **4-Fe**, **6-Fe, 8-Fe** and **16-Fe** at 80 K, measured relative to Fe.

Dieses Werk ist copyrightgeschützt und darf in keiner Form vervielfältigt werden noch an Dritte weitergegeben werden.
Es gilt nur für den persönlichen Gebrauch.

2.3.6.1.2: Theory versus Experiment

The assignment of each stereoisomer was additionally confirmed by calculations.[‡‡‡] These firstly revealed a linear relationship between the measured ΔE_Q value to the τ value, reflecting the degree of distortion from square pyramidal ($\tau = 0$) to trigonal bipyramidal ($\tau = 1$) geometries (Figure 2.3.56). These findings corroborate the assignment made earlier in the Mößbauer spectra containing two doublet signals – the one of lower ΔE_Q must correspond to a stereoisomer of square pyramidal geometry, and the doublet of larger ΔE_Q is the trigonal bipyramidal isomer.

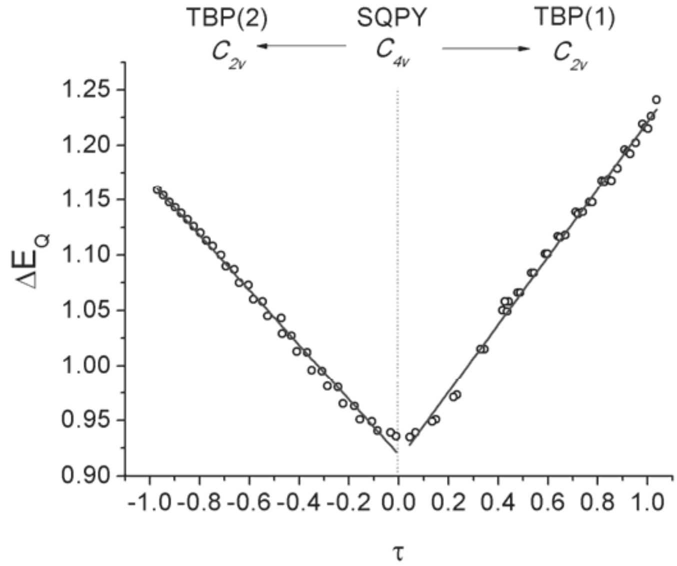

Figure 2.3.56: Linear response of TPSS/TZVP calculated qudrupole splitings along the $C_{2v} \rightarrow C_{4v} \rightarrow C_{2v}$ pathway[‡‡‡]

Moreover, detailed DFT calculated ^{57}Fe Mößbauer spectra for the complexes **3-Fe**, **8-Fe**, **9-Fe** and **4-Fe** / **6-Fe** are in good agreement with the experimental results, and the proposed assignment of the doublet signals. (Table 2.3.4a and b). These results point again to the isomer of square pyramidal geometry exhibiting a lower ΔE_Q value, compared with the trigonal bipyramidal geometry, lending further support to our interpretation of the experimental results.

[‡‡‡] Performed by L. Zimmer (Mößbauer simulations reproduced with permission – Table 2.3.4) and Dr. D. Manganas (Figure 2.3.56).

Dieses Werk ist copyrightgeschützt und darf in keiner Form vervielfältigt werden noch an Dritte weitergegeben werden.
Es gilt nur für den persönlichen Gebrauch.

				ΔE_Q	
	[(depe)$_2$Fe=Sn(Ar^{Mes})Cl]	ρ_{Fe} (a.u.$^{-3}$)	δ (mms^{-1})	mms^{-1}	MHz
	tbp, xray, exp		0,31	1,00	
TPSS	tbp, xray, calc	11821,442761	0,34	1,00	11,65

Table 2.3.4a: Comparison of experimental and calculated ^{57}Fe Mößbauer parameters for **3-Fe.** (Ar^{Mes} = 2,6-Mes$_2$-C$_6$H$_3$). Meta-GGA-Functional:TPSS. Basis Sets:Fe - CP(PPP); Sn, P, Cl – TZVPP; C, H – SVP. Calculations carried out using *Orca* 2.7.0

				ΔE_Q	
	[(depe)$_2$Fe≡GeAr^{Mes}]$^+$	ρ_{Fe} (a.u.$^{-3}$)	δ (mms^{-1})	mms^{-1}	MHz
	tbp, xray, exp		0,25	1,11	
TPSS	tbp, xray, calc	11821,583868	0,28	-1,15	-13,32
				ΔE_Q	
	[(depe)$_2$Fe≡GeAr^{Trip}]$^+$	ρ_{Fe} (a.u.$^{-3}$)	δ (mms^{-1})	mms^{-1}	MHz
	sqpy, xray, exp		0,23	0,58	
TPSS	sqpy, xray, calc	11821,676875	0,24	-0,82	-9,50
				ΔE_Q	
	[(depe)$_2$Fe≡SnAr^{Mes}]$^+$	ρ_{Fe} (a.u.$^{-3}$)	δ (mms^{-1})	mms^{-1}	MHz
	tbp, xray, exp		0.31/0.43	1.22/1.44	
TPSS	tbp, xray, calc	11821,527933	0,30	1,25	14,54
	sqpy, xray, exp		0.31/0.42	0.67/0.48	
TPSS	sqpy, xray, calc	11821,526334	0,30	0,89	10,36

Table 2.3.4b: Comparison of experimental and calculated ^{57}Fe Mößbauer parameters for **9-Fe.** (Ar^{Mes} = 2,6-Mes$_2$-C$_6$H$_3$) (top), **8-Fe** (middle) and **4-Fe/6-Fe** (bottom) Meta-GGA-Functional:TPSS. Basis Sets:Fe - CP(PPP); Sn, Ge,P, Cl – TZVPP; C, H – SVP. Calculations carried out using *Orca* 2.7.0.

The use of ^{57}Fe Mößbauer spectroscopy, to distinguish these two isomeric forms for Fe(0) complexes (TBP and SQPY) and their relative ratios in a sample where both happen to be present is, to our knowledge, unprecedented. These findings highlight a possible future application where such stereochemical discrimination could be of value, for example in material science, or catalysis.

Dieses Werk ist copyrightgeschützt und darf in keiner Form vervielfältigt werden noch an Dritte weitergegeben werden.
Es gilt nur für den persönlichen Gebrauch.

2.3.6.1.3 Dependence on reaction conditions of the relative ratio of trigonal bipyramidal and square pyramidal isomers detectible by ^{57}Fe Mößbauer spectroscopy

The question of the different ratios of stereoisomers was next addressed. In the case of complex **9-Fe** several different batches of the ionic germylidyne complex where submitted for Mößbauer measurements, with each sample having an identical set of NMR data (^{1}H and ^{31}P{^{1}H}). A parent sample of the complex was prepared by precipitation of **9-Fe** from pentane upon reaction of [Fe(depe)$_2$(N$_2$)] with two molar equivalents of **2-Ge**. A sample of this product was submitted for Mößbauer spectroscopy, revealing only one doublet signal. The precipitated product was then stirred in benzene at room temperature, the benzene removed *in vacuo* and the resulting solid washed with pentane, and the solid dried *in vacuo*. This solid was then also submitted for Mößbauer spectroscopy. This spectrum revealed two doublet resonance signals stereoisomers (δ = 0.39 mm·s^{-1}ΔE_Q = 1.40 mm·s^{-1}: 62 %; δ = 0.30 mm·s^{-1} ΔE_Q = 0.97 mm·s^{-1}: 38 %) – indicating the presence of *both* stereoisomers. A third experiment was also carried out. The parent sample was dissolved in THF, and crystallised there from at -30 °C. The resulting crystals where isolated, dried *in vacuo* and crushed into a solid powder and also submitted for Mößbauer analysis. In this instance, also both stereoisomers (δ = 0.37 mm·s^{-1} ΔE_Q = 1.47 mm·s^{-1}: 22 %; δ = 0.25 mm·s^{-1} ΔE_Q = 1.06 mm·s^{-1}: 78 %); where present, albeit it in a different ratio to the second batch. Finally, in a separate experiment complex **9-Fe** was synthesised in toluene (i.e. reaction of [Fe(depe)$_2$(N$_2$)] with two molar equivalents of **2-Ge**), the solvent removed *in vacuo*, and the remaining solid washed with pentane, and subsequently dried *in vacuo*. A sample of this batch was also submitted for Mößbauer spectroscopy, also revealing two doublet resonance signals: (δ = 0.40 mm·s^{-1}, ΔE_Q = 1.40 mm·s^{-1}: 55 %; δ = 0.30 mm·s^{-1} ΔE_Q = 1.00 mm·s^{-1}: 45 %). It is interesting to note the similarity of this last data set mentioned to that of the batch of sample stirred over benzene, as would be expected. (Figure 2.3.57).

These experiments categorically show how thermodynamics and solvation effects play a role in the distribution of these stereoisomers.

These experiments again highlight the powerful spectroscopic utility of ^{57}Fe Mößbauer spectroscopy as a window into the co-existance and relative ratio of trigonal bipyramidal and square pyramidal stereoisomers for Fe systems was highlighted for the first time.

Dieses Werk ist copyrightgeschützt und darf in keiner Form vervielfältigt werden noch an Dritte weitergegeben werden.
Es gilt nur für den persönlichen Gebrauch.

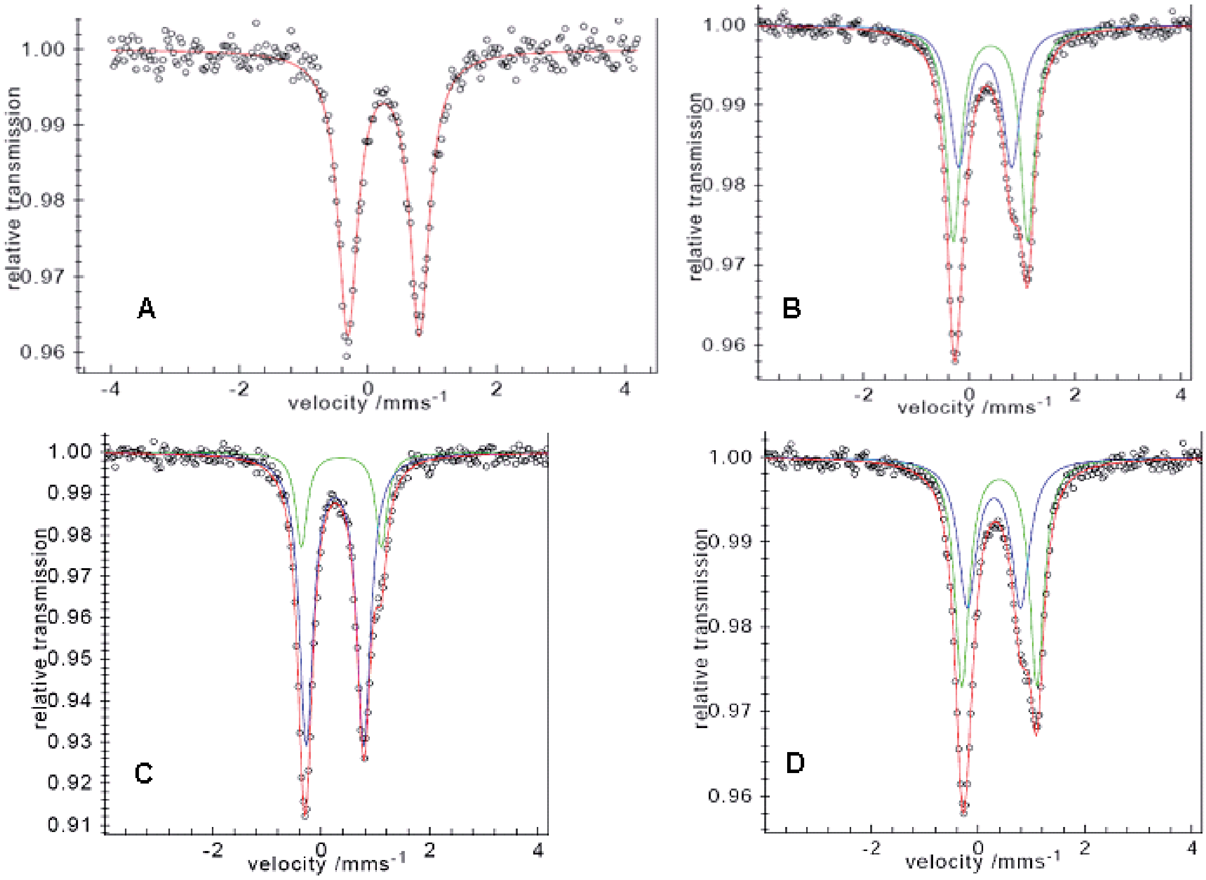

Figure 2.3.57: Comparison of the ^{57}Fe Mößbauer spectra at 80 K of germylidyne complex **9-Fe** after exposure to different conditions. (A = parent complex (precipitated from pentane), B = parent complex stirred in benzene, C = parent complex dissolved in THF, then crystallised, D = **9-Fe** synthesised in toluene (note the similarities in B and D). Lines are the simulated, black circles the experimental data.

A plot of all the available ΔE_Q values obtained from our Mößbauer spectra vs τ determined from X-ray crystallographic analysis of the complexes **3-Fe**, **4-Fe**, **8-Fe**, **9-Fe** and **16-Fe** are presented in Figure 2.3.58. (that is for all stannylidene, stannylidyne, and germylidyne complexes for which we have Mößbauer spectroscopic data and a solid state structure determination by X-ray diffraction). In **4-Fe**, and **9-Fe** both trigonal bipyramidal and square pyramidal isomers where present in the asymmetric unit, and is correlated to the appropriate doublet signal in the ^{57}Fe Mößbauer spectrum.

The general trend is in agreement with those predicted by calculation (see Figure 2.3.56), that is a proportional relationship between ΔE_Q to τ.

Dieses Werk ist copyrightgeschützt und darf in keiner Form vervielfältigt werden noch an Dritte weitergegeben werden.
Es gilt nur für den persönlichen Gebrauch.

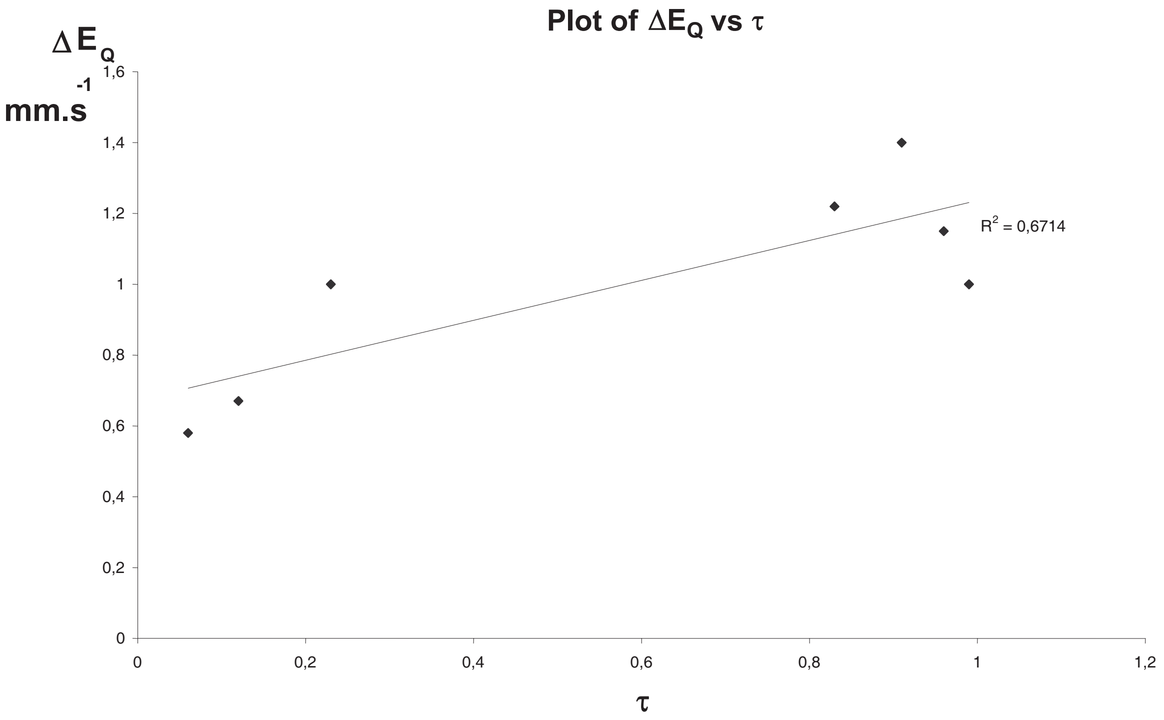

Figure 2.3.58: Plot of ΔE_Q values to τ of **3-Fe**, **4-Fe**, **8-Fe**, **9-Fe*** and **16-Fe** according to the experimental findings. * The data set chosen was that of the ^{57}Fe Mößbauer spectrum obtained from the batch of sample synthesed in toluene, containing both stereoisomers according to the ^{57}Fe Mößbauer spectrum).

2.3.6.2 Mößbauer spectra of Fe(I) complexes

Mößbauer spectroscopy of the Fe(I) complexes (**10-Fe** and **12-Fe**) was also carried out (Figure 2.3.59, Table 2.3.5). Principally, we used Mößbauer spectroscopy in this instance to additionally ensure the purity of the products and confirm they were free of any disproportionation Fe(II) side products, which was indeed the case.

Dieses Werk ist copyrightgeschützt und darf in keiner Form vervielfältigt werden noch an Dritte weitergegeben werden.
Es gilt nur für den persönlichen Gebrauch.

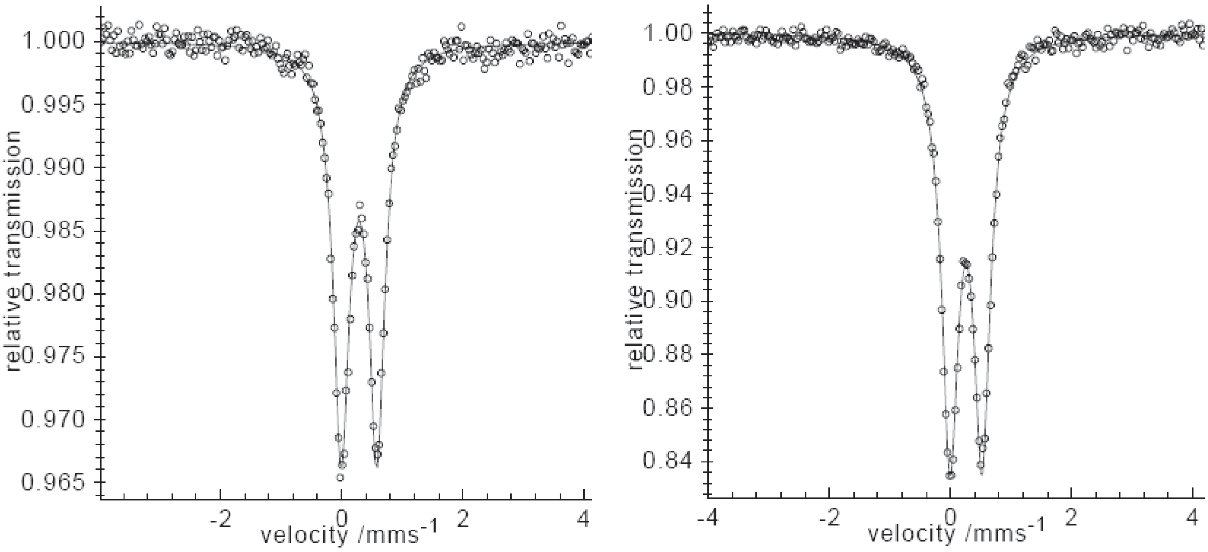

Figure 2.3.59: Mößbauer spectra of the Fe(I) complexes **10-Fe** (left) and **12-Fe** (right) at 80 K relative to Fe. The black circles are the data, and the lines the simulated spectra.

Complex	δ mm·s^{-1}	ΔE_Q mm·s^{-1}
10-Fe	0.29	0.59
12-Fe	0.26	0.53

Table 2.3.5: Summary of Mößbauer parameters for the Fe(I) complexes **10-Fe** and **12-Fe** at 80 K relative to Fe.

Both compounds exhibit quadrupole doublets and their isomer shift and quadrupole splitting values were found to be comparable at 80 K (Table 2.3.4).These values are expected for Fe(I) S = ½, and so are additional confirmation of the proposed oxidation state.[231] The Mößbauer spectra have rather similar δ values to the parent complex **1-Fe,** (oxidation state 0) however, and suggests comparable s-electron densities at the Fe centre in both cases. This can be attributed to a degree of π-back bonding from the Fe centre to the N_2 ligand in [Fe(depe)$_2$(N$_2$)], which would also result in decreased spherical electron density symmetry at Fe, and a higher ΔE_Q, as is observed. The comparability of both δ and ΔE_Q values in **12-Fe** suggest similar electronic density at Fe, compared to **10-Fe** and similar spherical symmetry despite the change to square pyramidal geometry.

Dieses Werk ist copyrightgeschützt und darf in keiner Form vervielfältigt werden noch an Dritte weitergegeben werden.
Es gilt nur für den persönlichen Gebrauch.

2.3.6.3 Mößbauer spectrum of 20-Fe

The product **20-Fe** shown to be a mixture of stereoisomers on the basis on ^{1}H NMR spectroscopy was also the subject of a Mößbauer study at 80 K (Figure 2.3.60), to establish its purity and confirm its oxidation state.

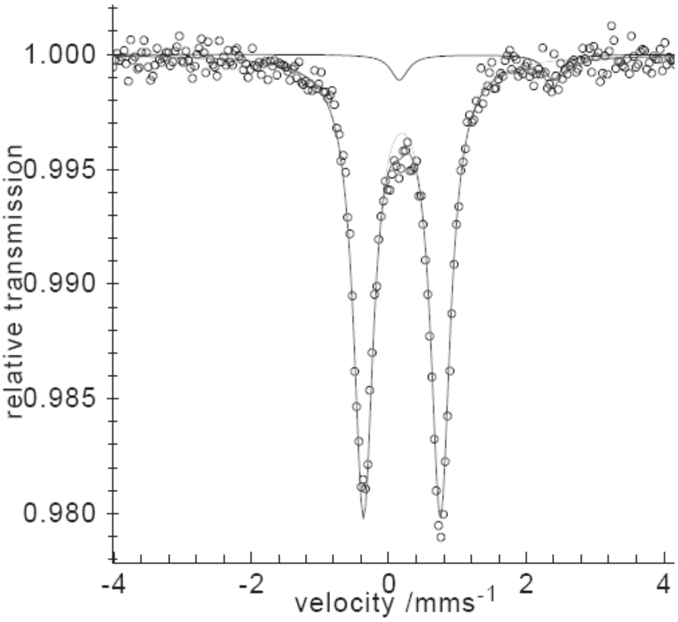

Figure 2.3.60: Mößbauer spectrum of the Fe(II) complex **20-Fe** at 80 K relative to Fe. The black circles are the data, and the line the simulated spectrum. $\delta = 0.19$ mm·s^{-1} $\Delta E_Q = 1.12$ mm·s^{-1}. The main doublet corresponds to the complex (95.21 %), and a second smaller doublet signal to an impurity (4.79 %) $\delta = 1.27$ mm·s^{-1} $\Delta E_Q = 2.23$ mm·s^{-1}.

Only one quadrupole doublet signal corresponding to **20-Fe** is visible in the Mößbauer spectrum, despite the presence of three stereoisomers on the basis on NMR spectroscopy. This can be rationalised by application of the point charge model which can be applied in the case of complex **20-Fe** although it is a distorted octahedron. Since the ligands are identical, application of (eq. 5) should result in the same observed isomer shift for all three strereoisomers, which is indeed the case. The δ value is considerably lower than those of typical low spin iron(II) complexes which range from $\delta = 0.3 - 0.45$ mm·s^{-1}, but the ΔE_Q value is in range for these complexes, which usually occur < 1.5 mm·s^{-1}.[232] The intermediate-spin complex $[FeH(depe)_2]^+$ has a more comparable isomer shift value to **20-Fe** ($\delta = 0.23$ mm·s^{-1}) but a noticeably higher ΔE_Q value at 1.53 mm·s^{-1}.[233] Complex **20-Fe** is therefore most likely low-spin d^6 Fe(II), and the reduced isomer-shift value is likely a result of the lower partial isomer shift associated with the main-group ligand.

Dieses Werk ist copyrightgeschützt und darf in keiner Form vervielfältigt werden noch an Dritte weitergegeben werden.
Es gilt nur für den persönlichen Gebrauch.

2.3.7 UV/Vis Studies

A representative from each new class of Fe complex prepared: the stannylidene complex **3-Fe**, the stannylidyne complex **6-Fe** and the germylidyne complex **8-Fe** was also the subject of a UV/Vis investigation Figure (2.3.61–64).

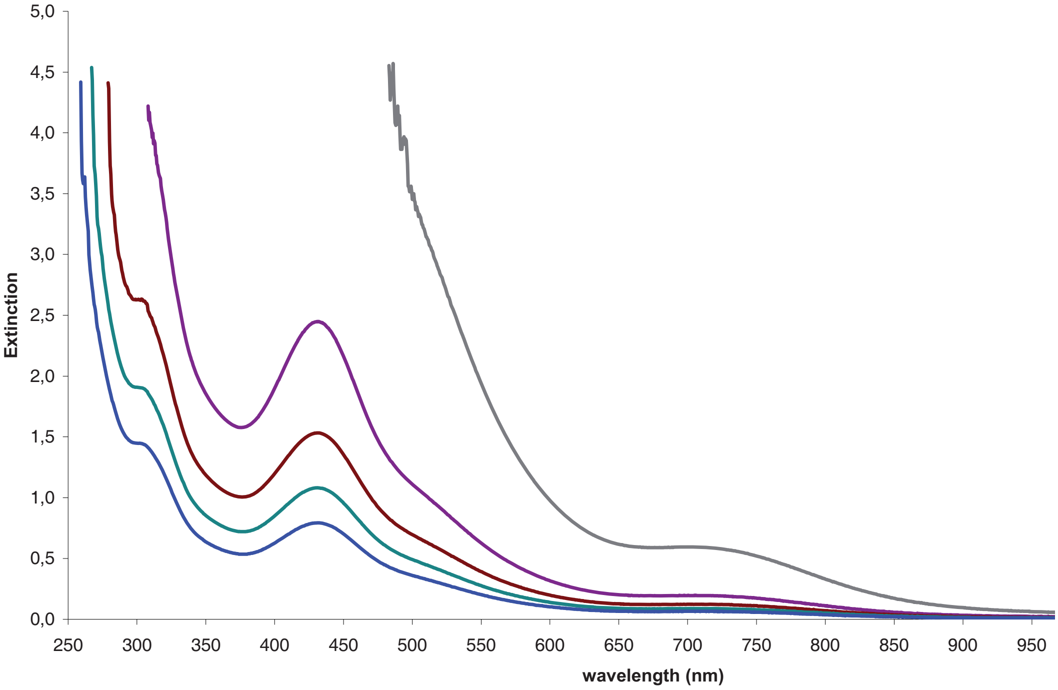

Figure 2.3.61: Variable concentration UV/Vis spectra of **3-Fe** in THF: 1.58 × 10^{-3} mol·l^{-1} (grey); 5.7 × 10^{-4} mol·l^{-1} (magenta); 3.8 × 10^{-4} mol·l^{-1} (red); 2.8 × 10^{-4} mol·l^{-1} (turquoise); 2.2 × 10^{-4} mol·l^{-1} (blue).

Dieses Werk ist copyrightgeschützt und darf in keiner Form vervielfältigt werden noch an Dritte weitergegeben werden.
Es gilt nur für den persönlichen Gebrauch.

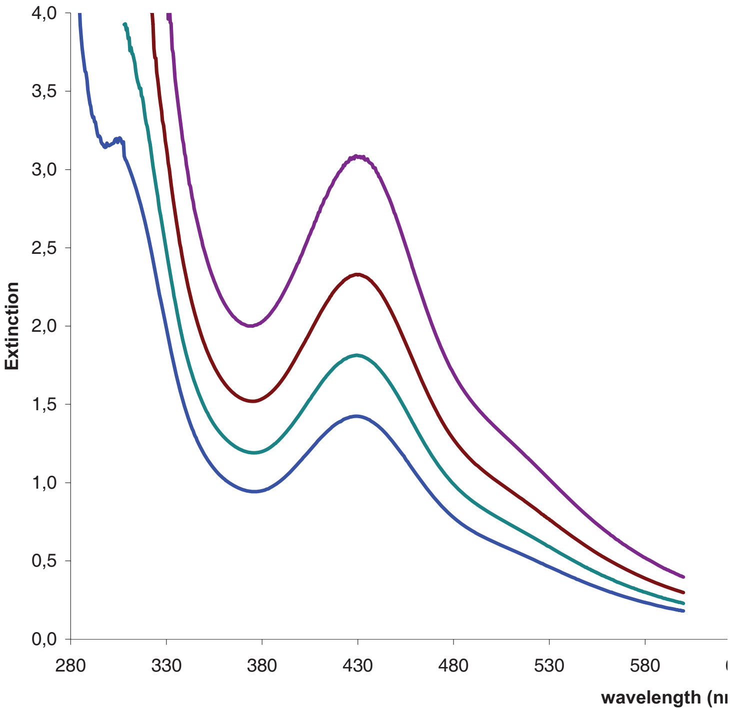

Figure 2.3.62: Variable concentration UV/Vis spectra of **4-Fe** in THF: 4.8 × 10^{-4} mol·l^{-1} (magenta); 3.9 × 10^{-4} mol·l^{-1}(red); 3.2 × 10^{-4} mol·l^{-1}(turquoise); 2.6 × 10^{-4} mol·l^{-1} (blue).

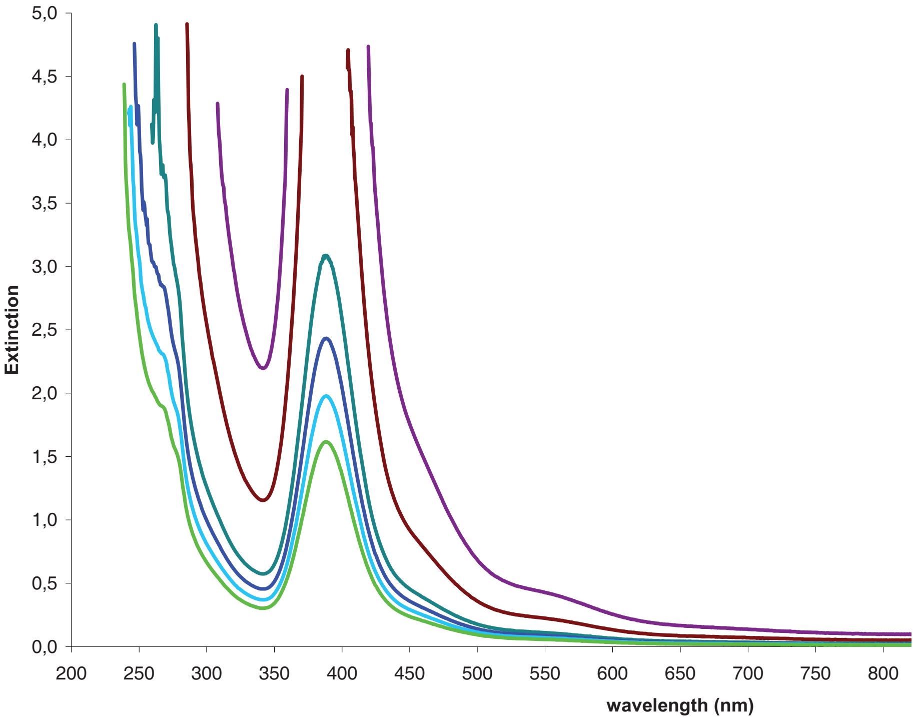

Figure 2.3.63: Variable concentration UV/Vis spectra of **6-Fe** in THF: 5.3 × 10^{-4} mol·l^{-1} (magenta); 2.8 × 10^{-4} mol·l^{-1} (red); 1.4 × 10^{-4} mol·l^{-1} (turquoise); 1.1 × 10^{-4} mol·l^{-1} (dark blue); 9 × 10^{-5} mol·l^{-1} (light blue); 8 × 10^{-5} mol·l^{-1} (green).

Dieses Werk ist copyrightgeschützt und darf in keiner Form vervielfältigt werden noch an Dritte weitergegeben werden.
Es gilt nur für den persönlichen Gebrauch.

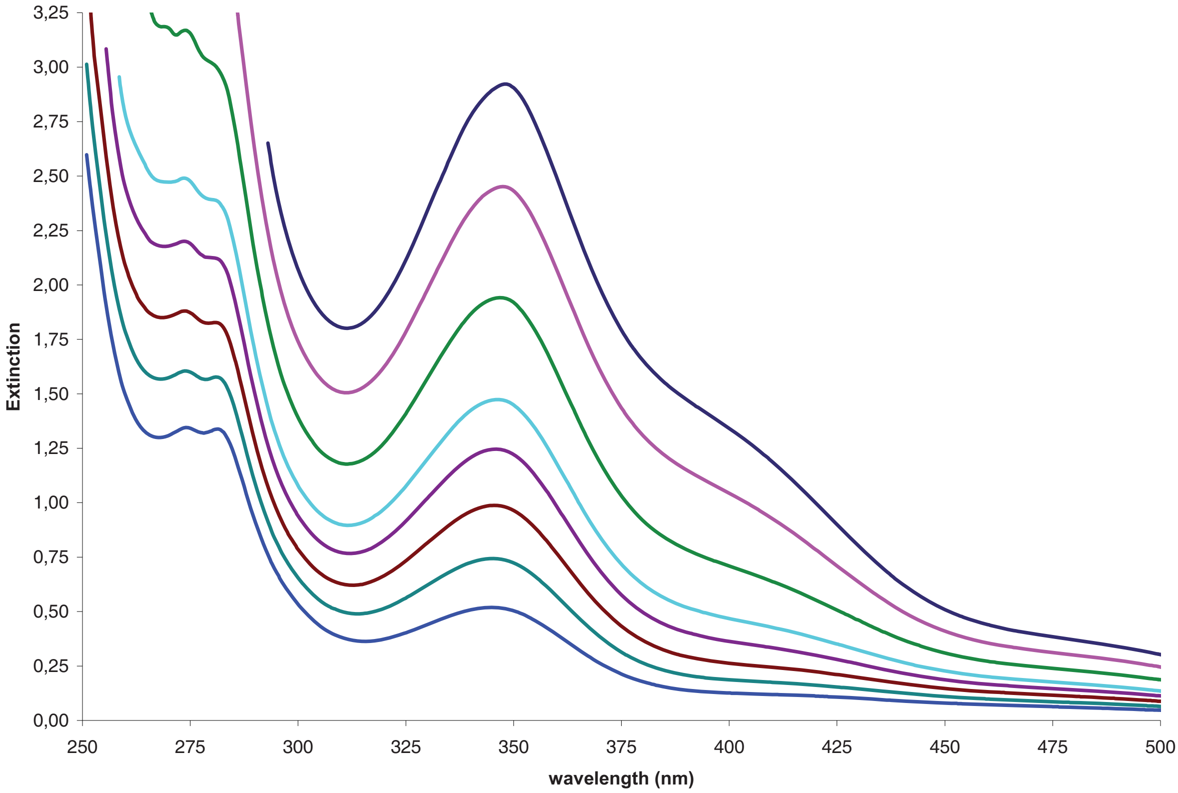

Figure 2.3.64: Variable concentration UV/Vis spectra of **8-Fe** in THF: 3.3 × 10^{-4} mol·l^{-1} (purple); 2.9 × 10^{-4} mol·l^{-1} (pink); 2.6 × 10^{-4} mol·l^{-1} (green); 2.1 × 10^{-4} mol·l^{-1} (light blue); 1.9 × 10^{-4} mol·l^{-1} (magenta); 1.7 × 10^{-4} mol·l^{-1} (red); 1.5 × 10^{-4} mol·l^{-1} (turquoise); 1.3 × 10^{-4} mol·l^{-1} (blue).

All spectra exhibit an intensive absorption band and low intensity shoulder absorptions at slightly higher wave lengths to this main absorption. The intense absorptions are attributable to $\pi \rightarrow \pi^*$ transitions and although these molecular orbitals are somewhat delocalised between the metal and tetrel atoms they can be regarded as MLCT bands, since generally, the π^* molecular orbitals are situated closer to the tetrel atom.[234] The spectra of **3-Fe** and **4-Fe** are very similar with the absorption band occurring at nearly the same wavelength. This is suggestive that in THF **4-Fe** undergoes reverse formation back to **3-Fe**, which was additionally validated by solution NMR spectroscopy. A comparison of the main absorption wavelengths with their associated extinction coefficients is presented in table 2.3.6.

Dieses Werk ist copyrightgeschützt und darf in keiner Form vervielfältigt werden noch an Dritte weitergegeben werden.
Es gilt nur für den persönlichen Gebrauch.

Complex	**λ (nm)**	**ε ($l \cdot mol^{-1} \cdot cm^{-1}$)**
3-Fe	431	4142.1
4-Fe	429	6055.7
6-Fe	388.5	21640.1
8-Fe	346	11909.6[§§§]

Table 2.3.6: Comparison of the main absorption band and the associated extinction coefficient in the UV/Vis spectra of **3-Fe**, **6-Fe** and **8-Fe**.

The extinction coefficient of the stannylidyne complex **6-Fe** and the germylidyne complex, **8-Fe** is markedly larger in magnitude than that of the stannylidene complex **3-Fe**. This is can be explained by the presence of two sets of $\pi \rightarrow \pi^*$ transitions in the ylidyne complexes, compared to only one in **3-Fe**. Furthermore, the transitions in the ylidyne complexes appear to be degenerate, since there appears only one absorption band, and the shoulder absorption bands are too weak in intensity to be attributable to a $\pi \rightarrow \pi^*$ transition. Furthermore, given the fact that Berry pseudo rotation was evidenced to occur in all complexes bearing depe at ambient temperature on the basis on NMR spectroscopy, it follows that the spectra obtained in all cases may reflect the fluxional picture, and distinction of stereoisomers which would be expected to exhibit different $\pi \rightarrow \pi^*$ transitions can be precluded.

Complex **3-Fe** exhibits the lowest $\pi \rightarrow \pi^*$ transition energy of the three complexes, which is what would be expected on the basis of a reduced bond order compared to the ylidyne complexes, and increased separation between the Fe and Sn centres. The stannylidyne complex **6-Fe** in turn exhibits a lower $\pi \rightarrow \pi^*$ transition energy compared to the germylidyne complex **8-Fe** which is a reflection of the decreased π-bond strength between Fe and Sn in **6-Fe** compared to Fe and Ge in **8-Fe**, as expected.

[§§§] A plot of absorbance to concentration at this absorbance band was linear, but anomalously did not pass through the origin. The value quouted here is that resulting from the best fitted line through the data points ($R^2 = 0.99933$). Allowing the regression line to pass through the origin resulted in a poor fit ($\varepsilon = 7459.34\ l \cdot mol^{-1} \cdot cm^{-1}$,$R^2 = 0.84698$).

Dieses Werk ist copyrightgeschützt und darf in keiner Form vervielfältigt werden noch an Dritte weitergegeben werden.
Es gilt nur für den persönlichen Gebrauch.

2.4 An brief excursion into ruthenium chemistry: attempted photochemical access to ruthenium germylidyne and stannylidyne complexes

Our original intention was to extend the chemistry based on the [Fe(depe)$_2$(N$_2$)] **1-Fe**, and its reactivity towards **1-Sn** and **1-Ge**, to ruthenium so as to prepare the ruthenium stannylidyne and germylidyne complexes. The Ru analogue of **1-Fe**, however, does not exist, and so we decided to use another approach to access ylidyne complexes of Ru. Cronin *et al.* has reported that photolysis of a *cis/trans* mixture of [RuH$_2$(depe)$_2$][235] **1-Ru** in a CO saturated heptane solution resulted in the complex [Ru(depe)$_2$CO], and similarly photolysis of **1-Ru** under an atmosphere of ethene yielded the complexes *cis*-[RuH(depe)$_2$(C$_2$H$_3$)] and [Ru(depe)$_2$(C$_2$H$_4$)], in both cases with loss of H$_2$.[236] This investigation also revealed that cis/trans-[RuH$_2$(depe)$_2$] itself was stable under photolytic conditions as steady-state photolysis thereof in C$_6$D$_6$ yielded no observable changes in either the ^{1}H or ^{31}P{^{1}H} NMR spectra over a period of 14 h (λ > 285 nm). Given this fact, we reasoned that similar photolytic reactions could result principally in the formation of ylidyne complexes of Ru, since both **1-Sn** and **1-Ge**, as with CO, are σ-donors and π-acceptors. Our strategy therefore was to attempt photolytic reactions of **1-Ru** in the presence of 2 equivalents **1-Sn** or **1-Ge**, in the hope of the first equivalent forming the intermediate halo-Ru ylidene complexes, and the second equivalent, as before with the Fe chemistry, act as a Lewis acid and abstract the Cl atom to afford the ylidyne complexes.

2.4.1 Synthesis of the precursor complex 1-Ru

Starting from [RuCl$_2$(DMSO)$_4$][237] **2-Ru**, reaction with 2 eq. depe in acetone under reflux results in [RuCl$_2$(depe)$_2$][238] **3-Ru** as a mixture of *trans* and *cis* isomers: **3-Ru-trans** and **3-Ru-cis**, in a ratio 2 : 1. On one occasion it was possible, by fractional crystallisation, to isolate exclusively **3-Ru-trans**. These findings are in contrast to the report by Winter *et al.* who reported selective conversion under these reaction conditions to **3-Ru-cis**.[****] The mixture can be reduced with Na/Hg amalgam under an atmosphere of H$_2$ slowly to the **1-Ru**, also as a mixture of *cis* and *trans* isomers: **1-Ru-cis** and **1-Ru-trans.** In our hands, this reduction proceeded very slowly, but resulted in a ratio of **1-Ru-cis: 1-Ru-trans** (2.6 : 1),

---

[****] Also see D. Geiß, Diplomarbeit, University of Bonn, 2010. Analagous results where obtained independently and are reported in this thesis.

Dieses Werk ist copyrightgeschützt und darf in keiner Form vervielfältigt werden noch an Dritte weitergegeben werden.
Es gilt nur für den persönlichen Gebrauch.

similar to that of Cronin *et al.* which report a 3 : 1 ratio. Further on in this discussion, **1-Ru** will refer to this mixture.

2.4.2 Photolytic reactions of 1-Ru with 1-Ge and 1-Sn

Under photolytic conditions in NMR scale experiments, typically C_6D_6 solutions of the above obtained *cis/trans* mixture of **1-Ru** were added together with 2 equivalents **1-Sn** or **1-Ge** in quartz NMR tubes, and irradiated with UV light ($\lambda > 254$ nm). In both cases colour changes from the initially yellow solutions to red (in the case of **1-Ge**) and a turbid red-brown (in the case of **1-Sn**) were observed shortly after onset of the irradiation experiments.

In the case of the reaction of **1-Ru** with 2 molar equivalents **1-Ge**, *in situ* $^{31}P\{^1H\}$ NMR spectroscopy revealed complete consumption of **1-Ru** after 1.5 h. The reaction is relatively selective and yields a singlet resonance signal at $\delta = 64.8$ ppm (85 %) along with several other intractable resonance signals in the baseline of the spectrum (15 %), that could not positively be identified.

The ^1H NMR spectrum also recorded after 1.5 h is mostly intractable, however, in the hydride region three new detectible hydride resonance signals are visible all of which show quintet multiplicity, the largest of which (75 % based on integration) occurs at $\delta = -21.26$. This resonance signal corresponds closely to that of the chemical shift of the hydride in the complex *trans*-[RuHCl(depe)$_2$] **4-Ru** reported at $\delta = -21.8$ ppm in $CDCl_3$[239] suggesting that under these reaction conditions, **4-Ru** appears to be the major product. The identity of **4-Ru** was further validated by the use of X-ray diffraction analysis. Complex **4-Ru** has not been the subject of an X-ray diffraction investigation, and since we managed to obtain suitable crystals thereof, we carried out such an investigation. Two crystallographically independent molecules were located in the asymmetric unit. One of these molecules is presented in Figure 2.4.1. The metric and angular parameters of both independent molecules are very similar (see values in parenthesis in Figure 2.4.1).

Dieses Werk ist copyrightgeschützt und darf in keiner Form vervielfältigt werden noch an Dritte weitergegeben werden.
Es gilt nur für den persönlichen Gebrauch.

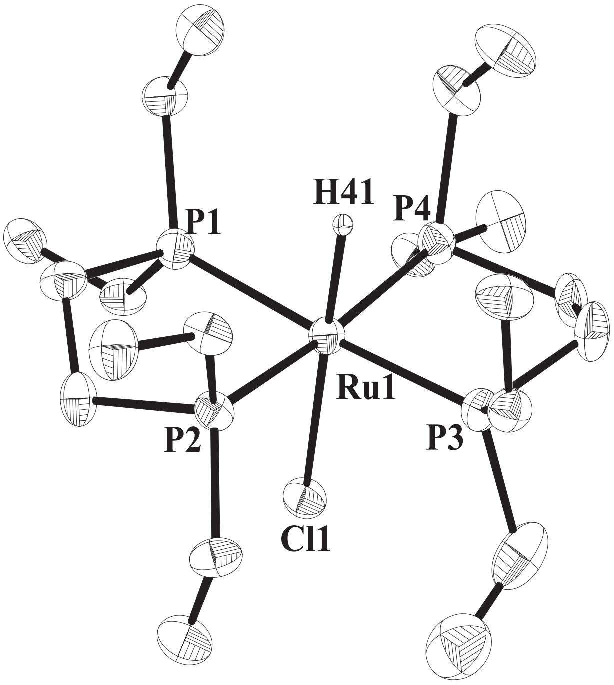

Figure 2.4.1: DIAMOND plot of the molecular structure of one of the crystallographic independent molecules in the asymmetric unit of **4-Ru** in the solid state. Thermal ellipsoids are set at 50 % probability. H atoms omitted for clarity. The corresponding metric parameters of the other independent molecule is included in parenthesis. Selected bond lengths [Å]: Ru1–H41 1.700(2) [1.700(2)], Ru1–Cl1 2.566(2) [2.559(2)]. Selected bond angles [°]: H41-Ru1-Cl1 177.89(10) [179.3(1)].

Complex **4-Fe** is octahedral in the solid state, with typical and expected metric parameters and discussion thereof is omitted for the sake of brevity. The investigation does however additionally prove it to be the major product resulting from the photolysis reaction discussed above.

The reaction of **1-Ru** with 2 molar equivalents **1-Sn** under analogous photolytic conditions as in the case of **1-Ge**, also resulted in complete consumption of **1-Ru** at the time the first *in situ* $^{31}P\{^{1}H\}$ spectrum was recorded (1 h). Two new products were detectible: $\delta = 62.4$ ppm and $\delta = 64.5$ ppm in a 56:44 ratio, based on integration in the $^{31}P\{^{1}H\}$ spectrum. The latter signal is flanked with $^{119/117}$Sn satellites $^{2}J(P, {}^{119/117}Sn) = 161.5$ Hz and was likely identified as the tin insertion product, $[(depe)_2RuH\{SnCl_2(2,6\text{-}Mes_2\text{-}C_6H_3)\}]$ **5-Ru.**[240] As in the case of reaction with **1-Ge**, a largely intractable ^{1}H NMR spectrum resulted, which could not be assigned.

Additionally, a light green precipitate also results from this reaction which could not subsequently be identified owing to its poor solubility properties. It was separated from the

Dieses Werk ist copyrightgeschützt und darf in keiner Form vervielfältigt werden noch an Dritte weitergegeben werden.
Es gilt nur für den persönlichen Gebrauch.

reddish supernatant solution, containing the mixture of the two products, and colourless crystals suitable for X-ray analysis of **5-Ru** were obtained there from by cooling the C_6D_6 supernatant solution, layered with Et_2O to 6 °C. The molecular structure of **5-Ru** is depicted in Figure 2.4.2.

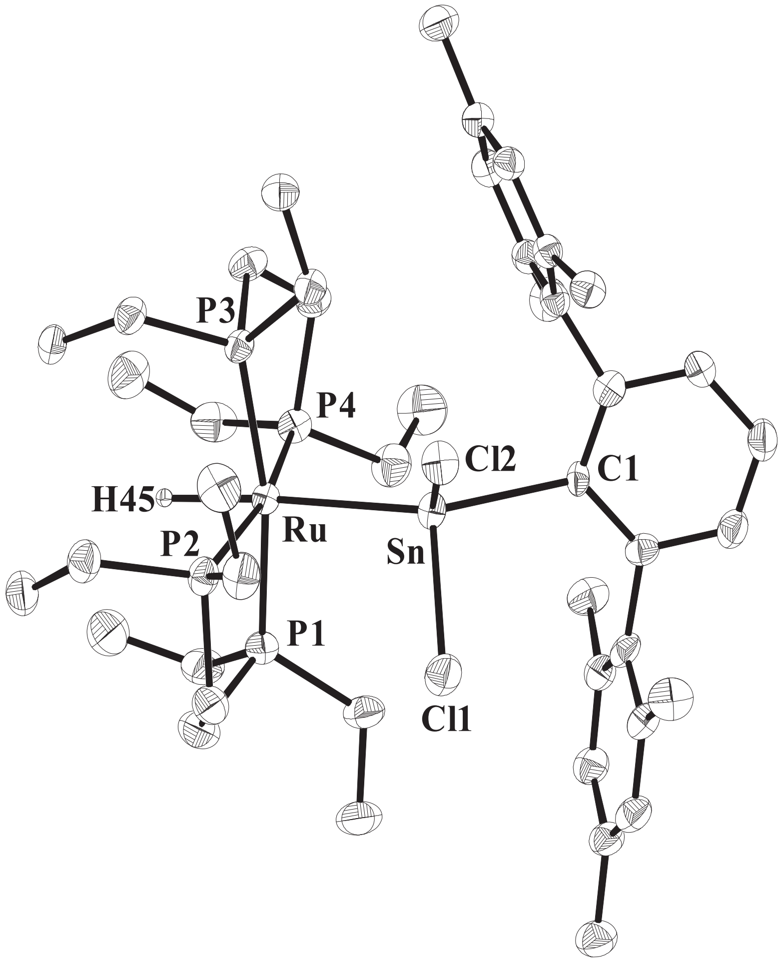

Figure 2.4.2: DIAMOND plot of the molecular structure of **5-Ru** in the solid state. Thermal ellipsoids are set at 50 % probability. H atoms omitted for clarity (with exception the hydride atom). Selected bond lengths [Å]: Ru–H45 1.63(2), Ru–Sn 2.7397(4), Ru–P1 2.336(1), Ru–P2 2.357(1), Ru–P3 2.338(1), Ru–P4 2.311(1), Sn–Cl1 2.491(2), Sn–Cl2 2.428(1), Sn–C1 2.282(4). Selected bond angles [°]: Cl1-Sn-Ru 104.40(4), Cl2-Sn-Ru 113.01(3), C1-Sn-Ru 148.0(1), Cl2-Sn-Cl1 86.56(4), C1-Sn-Cl1 98.9(1), C1-Sn-Cl2 89.7(1), H45-Ru-Sn 176(2), P1-Ru-Sn 96.95(3), P2-Ru-Sn 92.63(3), P3-Ru-Sn 95.52(3), P4-Ru-Sn 100.41(3), P1-Ru-P4 93.15(4), P3-Ru-P4 83.80(4), P1-Ru-P3 167.51(5), P4-Ru-P2 166.85(4), P1-Ru-P2 83.50(4), P3-Ru-P2 96.74(4).

Ruthenium complexes mutually bearing a hydride and stannyl ligand are rare and in fact structural studies so far reported are for the most part binuclear[241] or cluster in nature.[242] Only one other structurally characterised example of a mononuclear Ru complex exists where the stannyl ligand happens to be arranged in a *cis* configuration to the hydride: *cis*-

Dieses Werk ist copyrightgeschützt und darf in keiner Form vervielfältigt werden noch an Dritte weitergegeben werden.
Es gilt nur für den persönlichen Gebrauch.

$[RuH(SnPh_3)(CO)_4]$.[243] Complex **5-Ru** is hence the first example of a structurally characterised mononuclear Ru complex bearing a *trans* arrangement of the stannyl and hydride ligands. The geometry around the Ru centre in **5-Ru** can best be described as a slightly distorted octahedron, evidenced particularly by the P_x-Ru-Sn, x = 1 – 4, bond angles ranging in magnitude from 92.63(3) – 100.41(3)°. The increase from the ideal 90 ° angle in all cases can be attributed to the presence of the hydride occupying the sixth coordination site at the Ru centre, offering very little steric pressure, enabling the P_x-Ru-Sn bond angles to distort from 90° thereby relieving the steric repulsion that exists between the bulky *m*-terphenyl substituent on the Sn centre and the depe ligand system. The Ru–Sn bond length in **5-Ru** (2.7397(4) Å) is also comparable, albeit it 3 pm longer than the corresponding parameter in *cis*-$[RuH(SnPh_3)(CO)_5]$ at 2.7108(3) Å, suggesting a change in the ligand sphere at the Sn centre has little or no effect on the bonding interaction between the Sn and Ru centres.

The photolytically induced elimination of H_2 at Ru followed by attachment of **1-Sn** or **1-Ge** to the Ru centre did not occur despite several attempts and so this direction of investigation was not pursued any further. Given the fact that these experiments where carried out on NMR scale, isolation and full characterisation of products for further spectroscopic investigations where impossible.

The mechanisms resulting in the formation of **4-Ru** and **5-Ru** from **1-Ru** are not understood, however, Cl transfer from the ylene seems to be the first step in the reaction, evidenced by the formation and isolation of **4-Ru**, followed by ylene insertion into the resulting Ru–Cl bond, resulting in **5-Ru**. In the case of **1-Ge** there was no evidence of this subsequent insertion taking place, possibly due to the increased steric demand associated with the *m*-terphenyl substituent in **1-Ge**.

Dieses Werk ist copyrightgeschützt und darf in keiner Form vervielfältigt werden noch an Dritte weitergegeben werden.
Es gilt nur für den persönlichen Gebrauch.

2.5 An excursion into low valent germanium chemistry: synthesis and characterisation of base stabilised germylenes of the type GeRCl(L), where R = aryl, L = Lewis base.

N-Heterocyclic carbenes (NHCs) have recently been shown to stabilise Si(II) halides, resulting in compounds of the type SiX_2(NHC), where X = Cl or Br.[244] These findings prompted the development of the first aryl Si(II) halides of the type SiRCl(NHC)[245] R = aryl substituent, which were even more recently used successfully in the synthesis of the first formal siliylidyne complex.[104] SiRCl(NHC), R = 2,6-Mes_2-C_6H_3 or 2,6-$Trip_2$-C_6H_3; NHC = IMe_2Me_2 (IMe_2Me_2 = 1,2,3,4-tetramethylimidazol-2-ylidene) was prepared by reaction of the silane $SiRCl_2H$ with two molar equivalents of the NHC: IMe_2Me_2 resulting in a separable mixture of SiRCl(IMe_2Me_2) and $IMe_2Me_2H^+Cl^-$.[246] The success in using SiRCl(NHC) as a Si(II) aryl transfer reagent, prompted us to explore the analogous chemistry with Ge, i.e. the preparation of the Ge(II) compounds of the type GeRX(L), where R = aryl, X = Cl, I; L = Lewis base, with a view of enabling comparison between the Si(II) compounds and their Ge(II) analogues.

Previously, in our group, reaction of the germylene **1-Ge** with PMe_3 or IMe_2Me_2 afforded the base stabilised germylenes, GeCl(2,6-$Trip_2$-C_6H_3)L; (L = PMe_3 or IMe_2Me_2)[247] In this approach the Lewis base is attached to the electron deficient Ge(II) centre *after* the *m*-terphenyl has been attached in a previous synthetic step. We were interested in exploring the possibility of performing these synthetic steps in the reverse order, i.e. to first attach the Lewis base to the Ge(II) centre, and *then* attach the *m*-terphenyl substituent by a suitable salt metathetical route. Baines and co-workers has reported on the preparation of NHC stabilised Ge(II) compounds, where one of the approaches used was starting from $GeCl_2$(NHC), and performing a double metathesis reaction using Mes_2Mg as a transfer reagent, resulting in $Ge(Mes)_2$(NHC).[248] In an earlier approach, access to $Ge(Mes)_2$(NHC) was obtained by reaction of tetramesityldigermene with 2 molar equivalents of the NHC: $I^iPr_2Me_2$ resulting in $Ge(Mes)_2(I^iPr_2Me_2)$.[249] The work of Baines and co-workers demonstrated that it is indeed possible to perform the attachment by metathetical means of the aryl substituent *after* the Lewis base, in their case an NHC, has been attached to the Ge centre.

Dieses Werk ist copyrightgeschützt und darf in keiner Form vervielfältigt werden noch an Dritte weitergegeben werden.
Es gilt nur für den persönlichen Gebrauch.

2.5.1 Synthesis and characterisation of GeRX(L), where R = aryl, X = Cl, I; L = Lewis base.

We were additionally interested in varying the Lewis base at Ge, from an NHC to a phosphane and so in a synthetic approach similar to that of Baines and co-workers, $GeCl_2L$, where L = PMe_3 or IMe_2Me_2 was first prepared by reaction of $GeCl_2$(1,4-dioxane) with IMe_2Me_2 or PMe_3 to afford $GeCl_2(IMe_2Me_2)$ **5-Ge** or $GeCl_2(PMe_3)$ **4-Ge** respectively, in good yields. Subsequent salt metathesis reactions were performed on **4-Ge** and **5-Ge** with the aryl transfer reagent, **1-Li**, resulting in GeCl(2,6-Mes_2-C_6H_3)(IMe_2Me_2) **6-Ge** or GeCl(2,6-Mes_2-C_6H_3)(PMe_3) **8-Ge** respectively, also in good yields. Additionally, a halogen exchange reaction of **6-Ge** was performed resulting in GeI(2,6-Mes_2-C_6H_3)L, **7-Ge** upon halogen exchange with LiI in Et_2O. A summary of these reactions is presented in scheme 2.5.1 below.

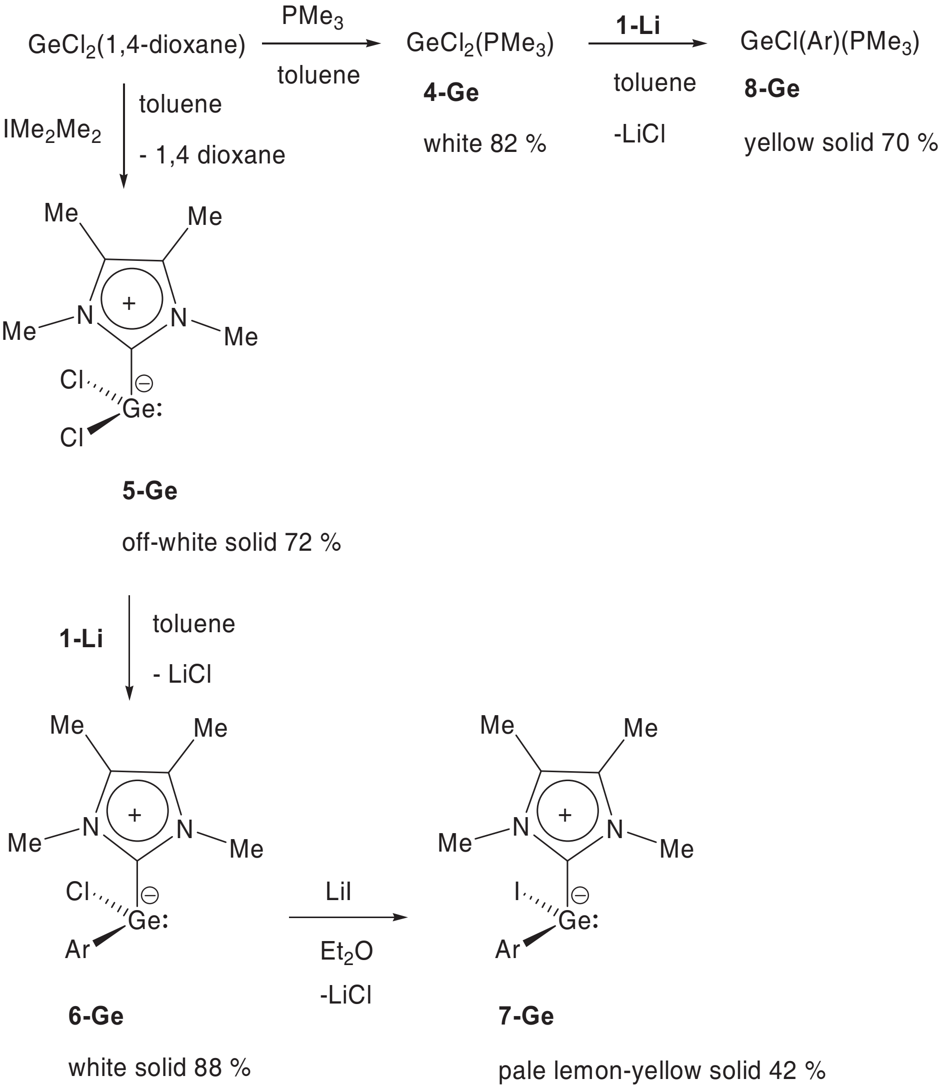

Scheme 2.5.1: Summary of reactions leading to base stabilised Ge(II) compounds. (Ar = 2,6-Mes_2-C_6H_3).

Dieses Werk ist copyrightgeschützt und darf in keiner Form vervielfältigt werden noch an Dritte weitergegeben werden.
Es gilt nur für den persönlichen Gebrauch.

All compounds were fully characterised by the routine spectroscopic methodologies. Compounds **6-Ge** and **7-Ge** possess a stereogenic Ge centre, which renders the *ortho* and *meta* positions on the mesityl rings chemically inequivalent. This is evidenced by a 6 : 6 : 6 ratio of the CH_3 resonance signals in the ^{1}H NMR spectrum in C_6D_6 at ambient temperature, corresponding to the two inequivalent sets of *ortho* positioned CH_3 groups, and the equivalent *para* positioned CH_3 groups on the *m*-terphenyl substituent. This is also the case in the ^{13}C{^{1}H} NMR spectrum, where three sets of singlet resonance signals are observed, corresponding to the C atoms of the CH_3 groups. In contrast, compound **8-Ge** features a 6 : 12 ratio (*para*:*ortho*) in the ^{1}H NMR spectrum in C_6D_6 at room temperature in this region, despite the presence of a stereogenic Ge centre in the static molecule. This phenomenon can be rationalised by a dynamic coordination / decoordination of the PMe_3 ligand at Ge in solution, which results in the loss of the stereogenic nature of the Ge centre, and the observed arrangement of resonance signals. This conclusion is further evidenced by variable temperature ^{1}H NMR spectroscopy in toluene-d_8, where on cooling, progressive broadening of one of these signals is observed, and ultimate separation into two individual resonance signals, resulting in a similar pattern as with **6-Ge** and **7-Ge** (Figure 2.5.2). This suggests that on cooling, the coordinated PMe_3 form becomes favoured, and the stereogenic nature of the Ge centre results in the same 6 : 6 : 6 ratio as was observed with **6-Ge** and **7-Ge**. Furthermore this result also suggests the PMe_3 ligand to be more weakly bound to the Ge centre, compared to the NHC ligands in **6-Ge** and **7-Ge**, where at room temperature no such decoordination phenomenon is observed in solution.

Dieses Werk ist copyrightgeschützt und darf in keiner Form vervielfältigt werden noch an Dritte weitergegeben werden.
Es gilt nur für den persönlichen Gebrauch.

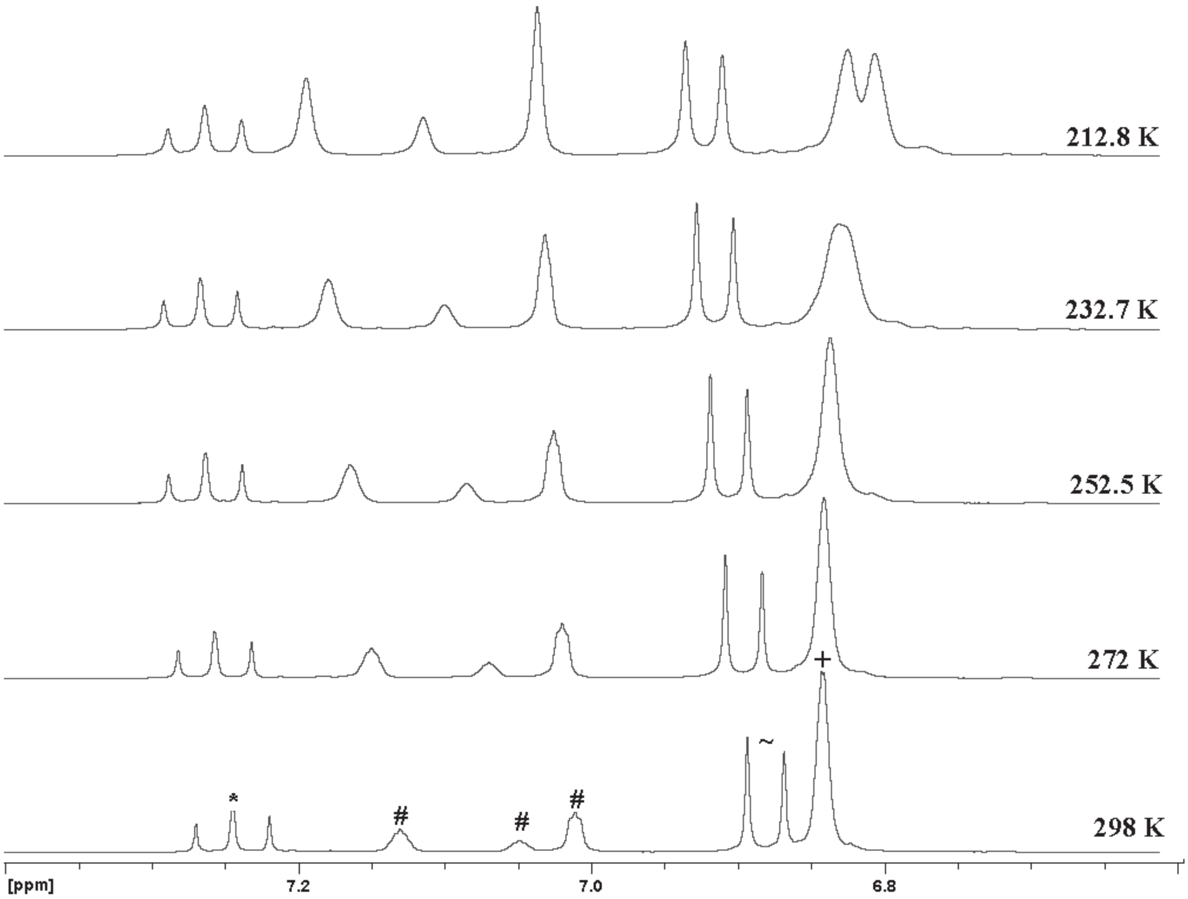

Figure 2.5.1: Stacked variable temperature ^{1}H NMR spectra of **8-Ge** in aromatic region (original scaling retained). # = residual solvent peaks (toluene); * = C^4-H (C_6H_3); ~ = $C^{3,5}$-H (C_6H_3); + = 2 × $C^{3,5}$-H (Mes): separates into two resonance signals between 212.8 K and 232.7 K.

Dieses Werk ist copyrightgeschützt und darf in keiner Form vervielfältigt werden noch an Dritte weitergegeben werden.
Es gilt nur für den persönlichen Gebrauch.

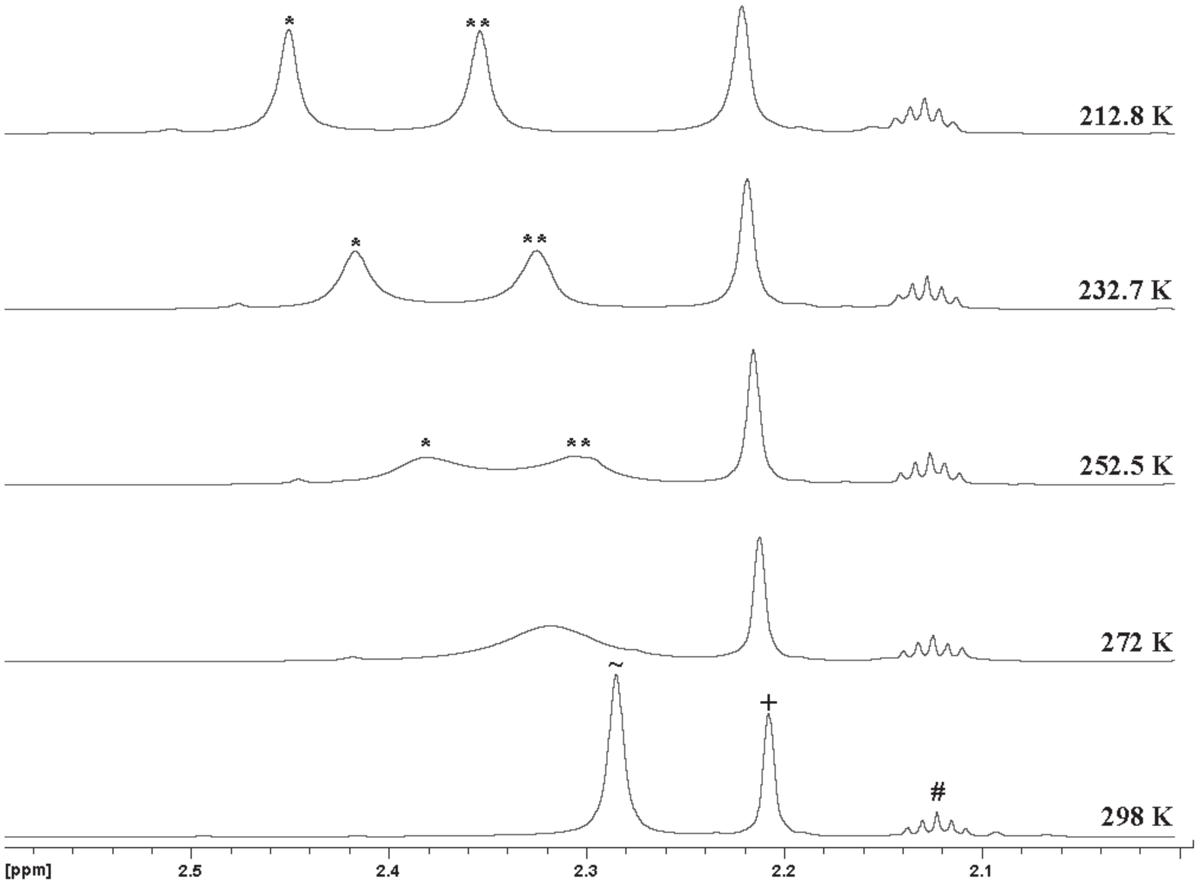

Figure 2.5.2: Stacked variable temperature ^{1}H NMR spectra of **8-Ge** in chemical shift range $\delta = 2.0 – 2.6$ ppm (original scaling retained). # = residual solvent peaks (toluene); + = 2 × C^{4}-CH_3, Mes: ~ = 2 × $C^{2,6}$-CH_3, Mes: signal separates at 252.5 K into two resonance signals * = 2 × C^{6}-CH_3 ** = 2 × C^{2}-CH_3

Variable temperature $^{31}P\{^{1}H\}$ NMR spectroscopy of compound **8-Ge** points to a similar phenomenon as in the corresponding ^{1}H NMR spectra: A broad resonance signal is observed at ambient temperature, and on cooling a migration of the signal to lower field is observed with simultaneous sharpening of the signal ($\Delta\nu_{½}$ reduction). The migration of the resonance signal to lower fields is a consequence of the coordination of the PMe_3 to the Ge centre, compared to the broad signal at higher fields at room temperature, being the time averaged resonance of free PMe_3 and **8-Ge**.

Dieses Werk ist copyrightgeschützt und darf in keiner Form vervielfältigt werden noch an Dritte weitergegeben werden.
Es gilt nur für den persönlichen Gebrauch.

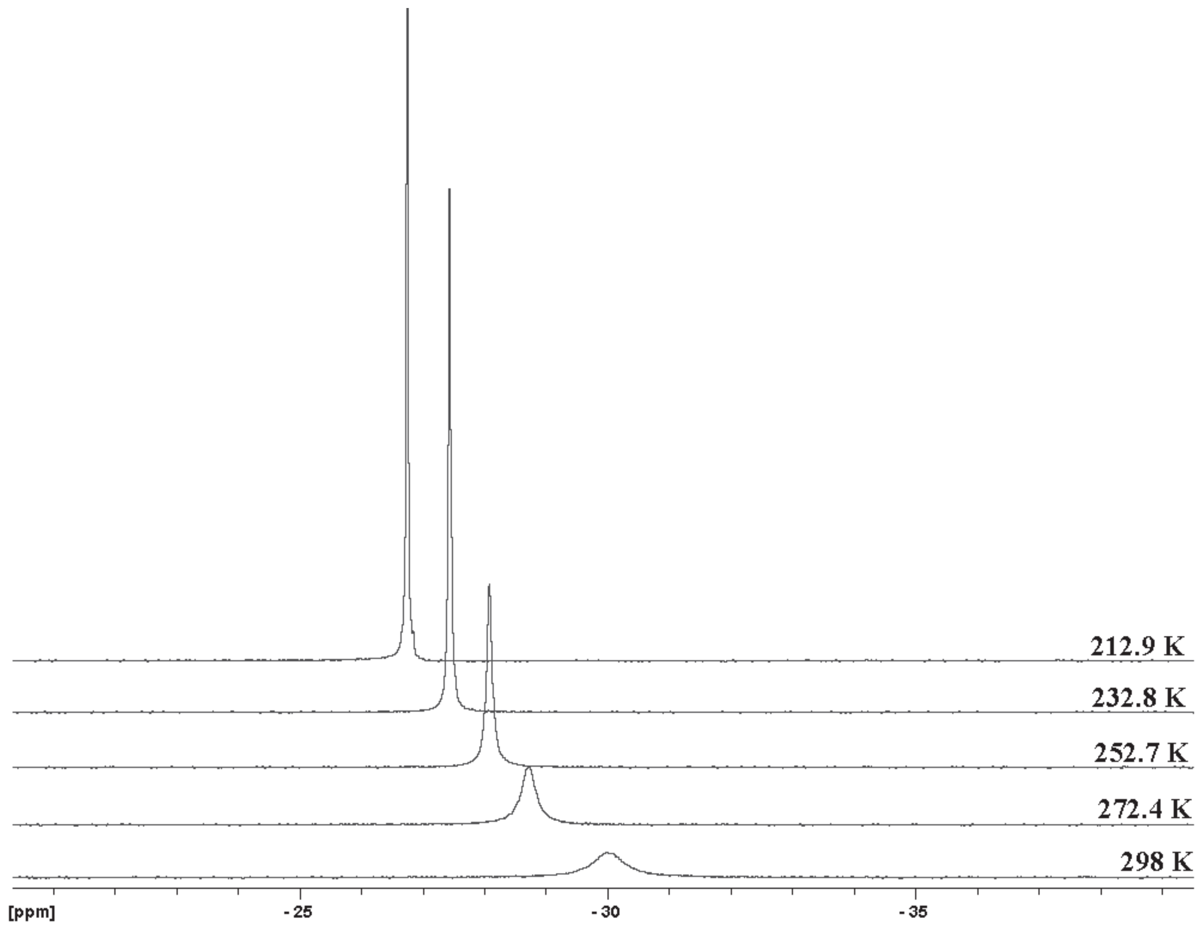

Figure 2.5.3: Stacked variable temperature $^{31}P\{^{1}H\}$ NMR spectra of compound **8-Ge** in toluene-d_8 (original scaling retained). Migration to lower fields, and progressive signal sharpening are visible, indicative of the PMe_3 complexed form of **8-Ge** at lower temperatures.

Crystals of compound **7-Ge** suitable for X-ray diffraction analysis were grown from a C_6D_6 solution of the compound at room temperature with slow evaporation of the solvent in the glove box. The molecular structure features an included C_6D_6 molecule, which is disordered. Figure 2.5.4 shows the molecular structure of **7-Ge** with the included solvent molecule omitted for clarity.

Dieses Werk ist copyrightgeschützt und darf in keiner Form vervielfältigt werden noch an Dritte weitergegeben werden.
Es gilt nur für den persönlichen Gebrauch.

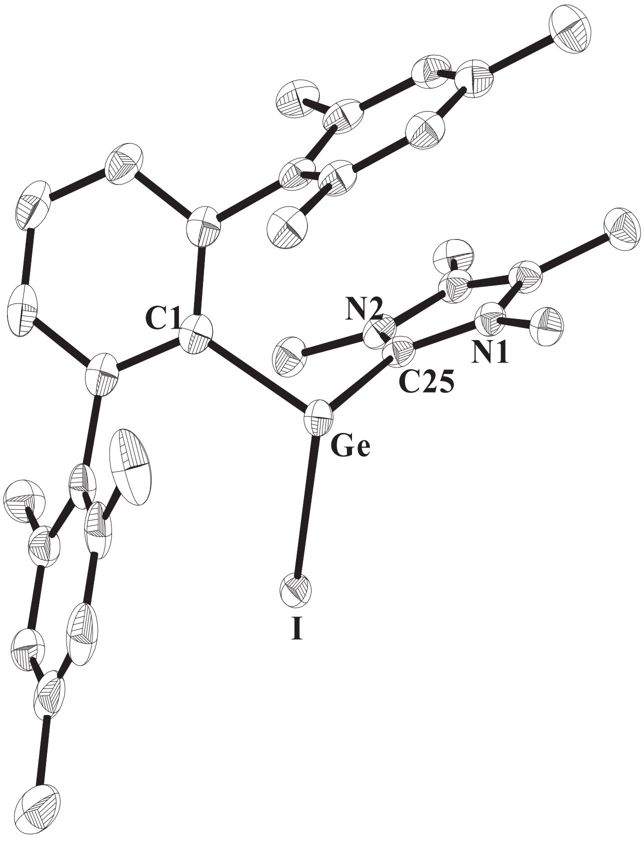

Figure 2.5.4: DIAMOND plot of **7-Ge·C_6D_6** in the solid state. Thermal ellipsoids set at 50 % probability, H atoms omitted for clarity. Selected bond lengths [Å]: Ge–C1 2.065(4), Ge–C25 2.074(3), Ge–I 2.7359(4), C25–N1 1.259(4), C25–N2 1.346(4). Selected bond angles [°]: C1-Ge-I 105.47(10), C1-Ge-C25 97.0(1), C25-Ge-I 90.38(9).

No examples of structurally characterised Ge(II) compounds, mutually bearing an aryl substituent and iodide ligand exist, and this is the first example in this class. The Ge centre in **7-Ge** is pyramidalised, as shown by the sum of the angles around Ge (292.85°), indicative of the presence of a stereochemically active lone pair residing on Ge. The Ge to carbene C (Ge–C25) bond length is comparable to the analogous bond length in $GeI_2(IMe_2{}^iPr_2)$ (2.087(3) Å),[250] while the Ge–I bond length is slightly elongated in comparison to the average of the Ge–I bond lengths in $GeI_2(IMe_2{}^iPr_2)$ (2.6721(9) Å), reflecting the effect of the bulky *m*-terphenyl substituent. The carbene ligand is orientated in a parallel planar arrangement to the Mes substituent, reflecting a possible weak π-π interaction. The distance between the centres of gravity of the Mes substituent and the carbene nucleus are 3.701 Å, which is within the range of weak π-π interaction distances.[251]

Crystals, suitable for X-ray diffraction analysis of **8-Ge** were grown from toluene at –30 °C. The molecular structure of **8-Fe** in the solid state is shown in figure 2.5.5 below.

Dieses Werk ist copyrightgeschützt und darf in keiner Form vervielfältigt werden noch an Dritte weitergegeben werden.
Es gilt nur für den persönlichen Gebrauch.

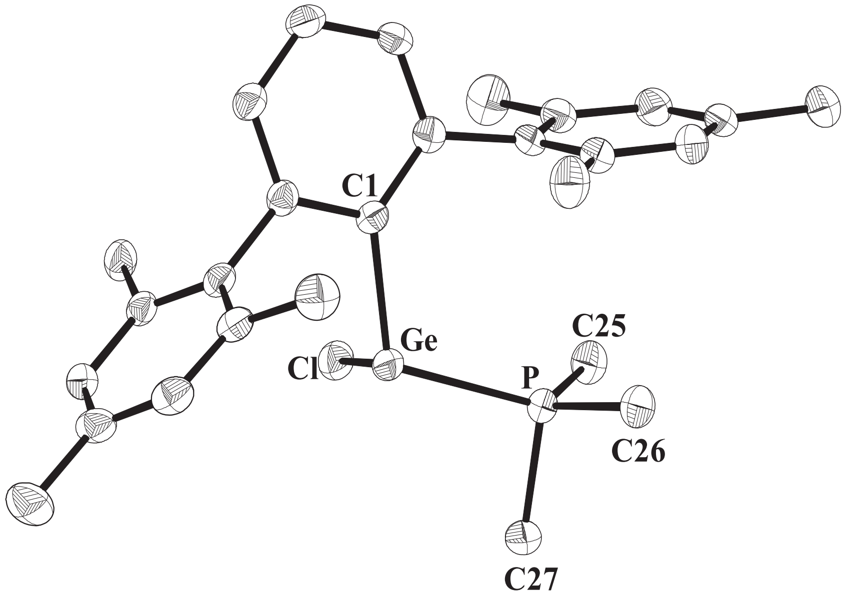

Figure 2.5.5: DIAMOND plot of compound **8-Ge** in the solid state. Thermal ellipsoids set at 50 % probability. H atoms omitted for clarity. Selected bond lengths [Å]: Ge–Cl 2.3477(6), Ge–P 2.4624(6), Ge–C(1) 2.023(2), P–C25 1.807(2), P–C26 1.801(3), P–C27 1.819(2). Selected bond angles [°]: C(1)-Ge-Cl 94.62(6), Cl-Ge-P 86.43(2), C(1)-Ge-P 112.09(6).

Only one other structurally characterised example of a germanium(II) compound bearing PMe_3 as a ligand exists, where it is a dimer: Ar'$(H)_2$GeGeAr'·PMe_3; Ar' = 2,6-$Dipp_2$-C_6H_3.[252] This makes compound **8-Ge** the first structurally characterised mononuclear germanium compound with PMe_3 as ligand. The Ge centre in **8-Ge** is pyrimidalised, as in **7-Ge** as shown by the sum of angles around the Ge atom of 293.14° (slightly larger in magnitude than those calculated for GeH_3^-: 279-283°)[253] indicating the presence of a stereochemically active lone pair of electrons at the Ge(II) centre. Two sets of angles around the Ge atom lie close in magnitude to 90° (C(1)-Ge-Cl (94.62(6)° and Cl-Ge-P 86.43(2)°), while the third angle C(1)-Ge-P is notably larger at 112.09(6)°. The enlargement of the last mentioned angle is due to steric repulsion between the PMe_3 ligand and the mesityl ring. These metric parameters reflect a reduced tendency of the Ge atom to undergo hybridisation, and suggest the lone pair to reside in an orbital of high s-character, and the remaining orbitals to be of high p-character and is supported by calculations of the related compound GeCl(2,6-$Trip_2$-C_6H_3)(IMe_2Me_2).

The Ge–C(1) and Ge–Cl bond lengths of 2.023(2) Å and 2.3477(6) Å respectively are both slightly elongated in comparison to the analogous bond lengths found in the germylene, **2-Ge** (which forms dimers with a Ge-Ge bond) (2.000(6) Å and 2.120(2) Å), but comparable to

Dieses Werk ist copyrightgeschützt und darf in keiner Form vervielfältigt werden noch an Dritte weitergegeben werden.
Es gilt nur für den persönlichen Gebrauch.

that of GeCl(2,6-Trip$_2$-C$_6$H$_3$)(IMe$_2$Me$_2$) (2.035(3) Å and 2.338(1) Å). This suggests the introduction of a σ-donating ligand at the Ge centre has an elongation effect on these two bonds in particular, and effectively makes them slightly weaker. The Ge–P bond length of 2.4624(6) Å is slightly longer than that of Ar'(H)$_2$GeGeAr'·PMe$_3$ and slightly shorter than the mean Ge-P bond length of GeCl$_2$(PPh$_3$) and GeI$_2$(PPh$_3$) (2.51 Å), previously reported.[254,255]

2.5.2 UV/Vis spectroscopic investigations

The compounds **5-Ge**, **6-Ge** and **8-Ge** were also the subject of a UV/Vis investigation (Figure 2.5.6, 2.5.7, 2.5.8). In all cases a weak shoulder absorption band is observed in the range 277 nm – 330 ± 5 nm. UV/Vis data on the germylene **1-Ge** has been reported and exhibits an absorption band at λ_{max} = 393 nm in hexane, attributed to an n→p transition, where the p orbital is vacant on the Ge centre. [45b] The related base stabilised germylene, **1-Ge**·pyridine, on the other hand, exhibits a slightly blue shifted absorption band at λ_{max} = 380 nm.[256] A similar blue shift trend is observable in **6-Ge** and **8-Ge**, compared to **1-Ge**[††††] albeit to a much larger extent. Since, in the case of base stabilised germylenes the once vacant p-orbital is occupied, the transition is rather an n→σ* transition, where the σ* orbital is germanium centred.[257] This provides an explanation for the observed blue shifts in the absorption bands, compared to the free germylenes, since more energy is required to effect the transition from the lone pair orbital to the more distantly located σ* orbital

---

[††††] The UV/Vis spectrum of the germylene **2-Ge** has not been reported, however, it can reasonably be assumed to exhibit a similar absorption value as **1-Ge**, given that the only difference is the replacement of Me groups with ^{i}Pr groups on the *m*-terphenyl substituent.

Dieses Werk ist copyrightgeschützt und darf in keiner Form vervielfältigt werden noch an Dritte weitergegeben werden.
Es gilt nur für den persönlichen Gebrauch.

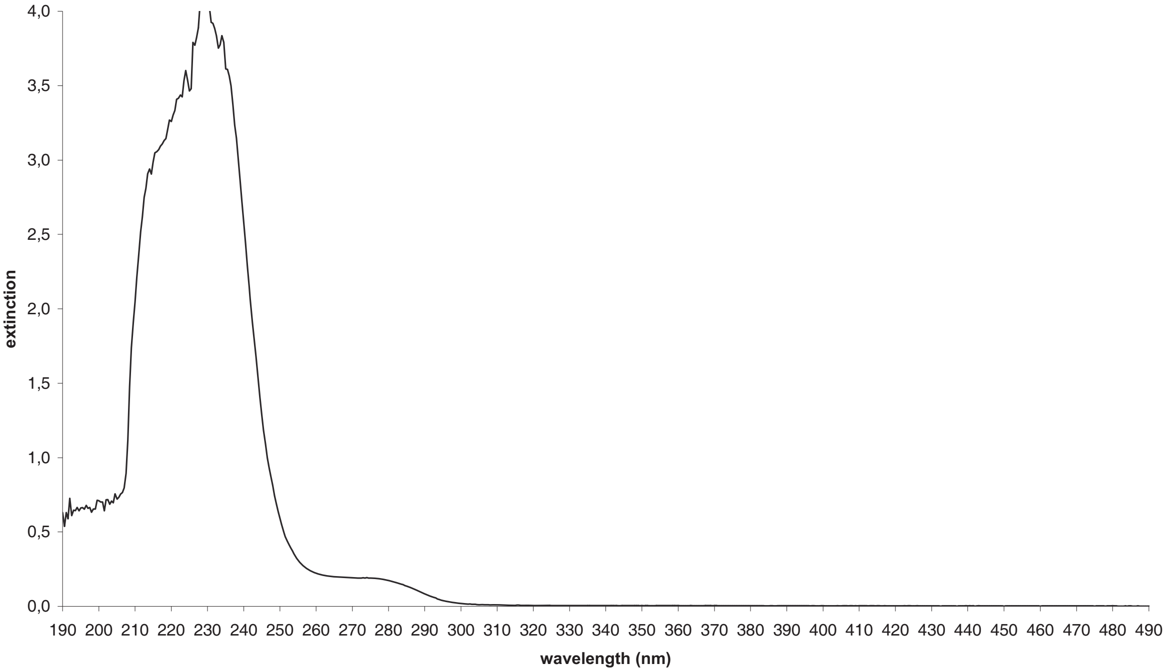

Figure 2.5.6: UV/Vis spectrum of **5-Ge** in THF. λ_{max} = 277 nm

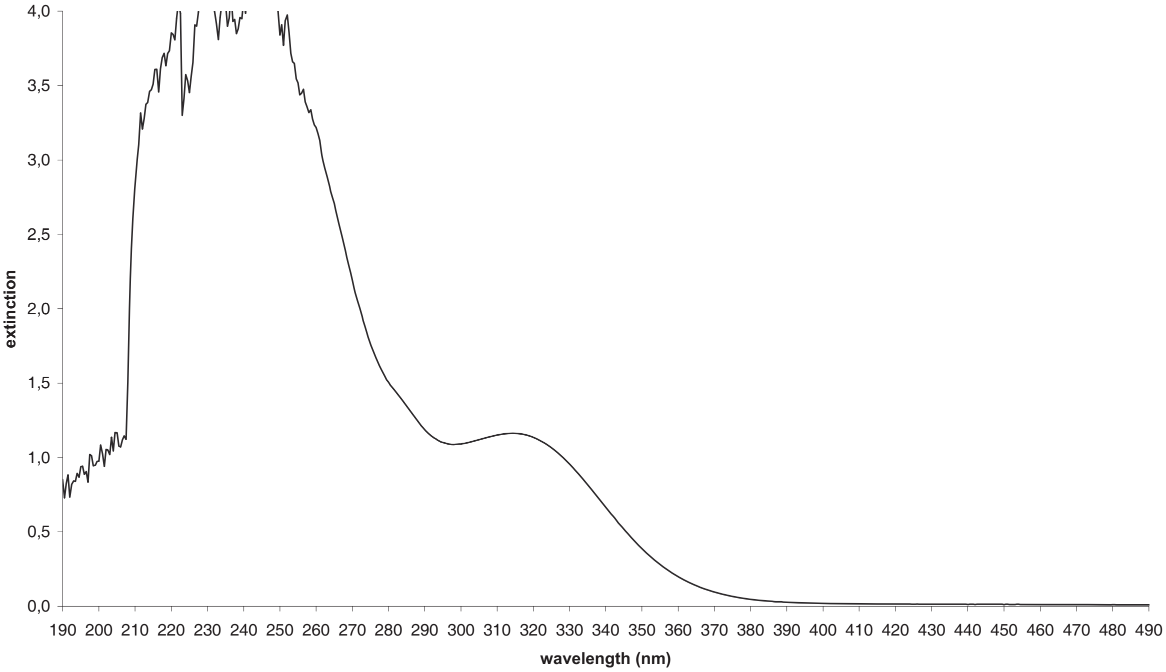

Figure 2.5.7: UV/Vis spectrum of **6-Ge** in THF. λ_{max} = 315 nm

Dieses Werk ist copyrightgeschützt und darf in keiner Form vervielfältigt werden noch an Dritte weitergegeben werden.
Es gilt nur für den persönlichen Gebrauch.

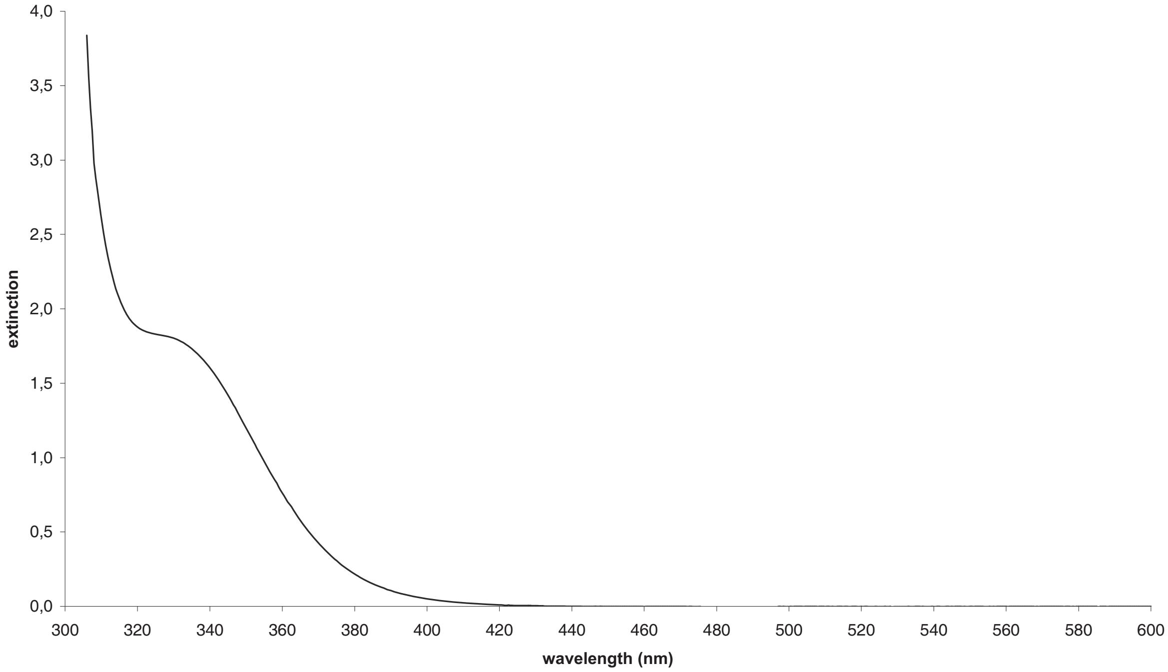

Figure 2.5.8: UV/Vis spectrum of **8-Ge** in toluene. $\lambda_{max} = 330 \pm 5$ nm.

Dieses Werk ist copyrightgeschützt und darf in keiner Form vervielfältigt werden noch an Dritte weitergegeben werden.
Es gilt nur für den persönlichen Gebrauch.

3. Summary, conclusion and outlook

3.1 Summary

The current work principally focused on exploring the reactivity of ylenes of the type EClR E = Ge, R = 2,6-Trip$_2$-C$_6$H$_3$ (**1-Ge**); E = Ge, R = 2,6-Mes$_2$-C$_6$H$_3$ (**2-Ge**) or E = Sn, R = 2,6-Mes$_2$-C$_6$H$_3$ (**1-Sn**) towards an array of late transition metal complexes in groups 8 (Fe and Ru), 9 (Rh) and 10 (Pd), with an overall goal of preparing late transition metal complexes featuring triple bonding to Ge and Sn, hitherto unprecedented.

The reactivity of the stannylene **1-Sn** and germylene **1-Ge** towards Pd(II) square planar complexes of the type [Pd(L–L)Cl$_2$], bearing chelating ligands (L-L = 1,5-cyclooctadiene (cod) (**1-Pd**) or dppe (**2-Pd**)) was first investigated (section 2.1). In this context it was found that the ylenes insert into the Pd–Cl bond, in a general sense, resulting in complexes of the type [PdCl(L–L){ECl$_2$R}] (See Scheme 3.1) all of which where fully spectroscopically and structurally characterised. In addition, related insertion reactions of SnCl$_2$ and GeCl$_2$ with [PdCl$_2$(cod)] was also discussed, yielding [PdCl(L–L){ECl$_3$}] E = Sn (**6-Pd**) and Ge (**7-Pd**) respectively, where **7-Pd** is the first structurally characterised trihalogermyl complex of Pd (**7-Ge**). All of these insertion products (**3-Pd**, **4-Pd**, **5-Pd**, **6-Pd**, **7-Pd**) featured an elongated Pd-L bond distance trans to the germyl or stannyl ligand, showing they exert a greater *trans* influence in comparison to the chloride ligand.

This insertion behaviour was shown however not to occur in the case of the stannylene [SnCp*Cl] (**2-Sn**), which rather results in a novel Cp* transfer reaction to Pd, resulting in the complex [Pd(Cp*)(cod)][SnCl$_3$] (**8-Pd**).

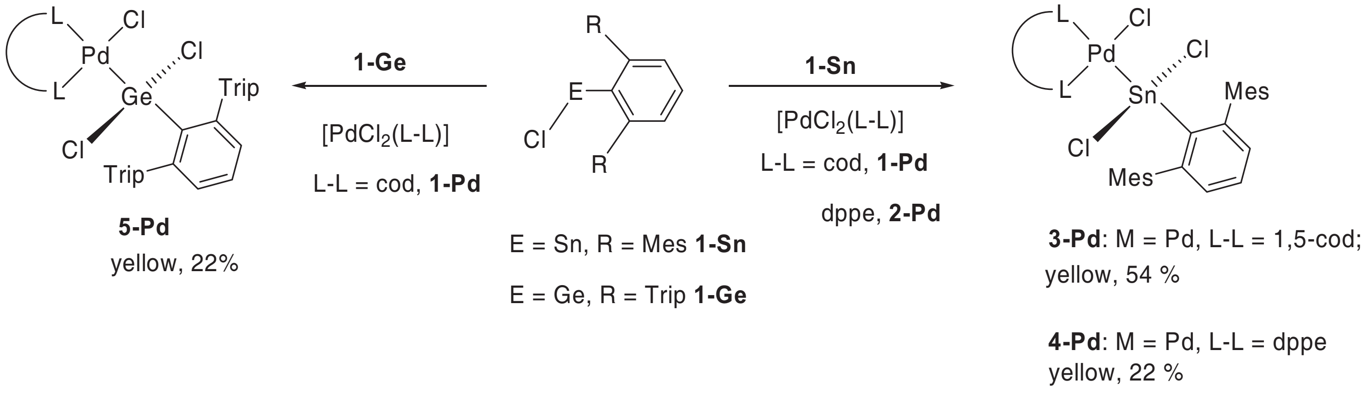

Dieses Werk ist copyrightgeschützt und darf in keiner Form vervielfältigt werden noch an Dritte weitergegeben werden.
Es gilt nur für den persönlichen Gebrauch.

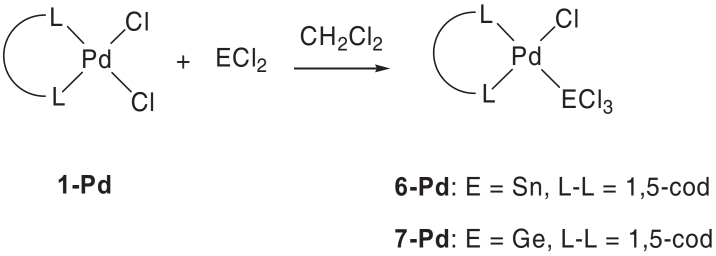

Scheme 3.1: Pd(II) 16 VE complexes facilitate insertion of germylenes and stannylenes (**2-Ge**) and (**1-Sn**). Additionally, $SnCl_2$ and $GeCl_2$(1,4-dioxane) inserts into Pd-Cl bonds.

The reactivities of **1-Sn** and **1-Ge** towards a Rh(I) d^8 configured complex, $[RhCl(\eta^2\text{-}C_2H_4)_2]_2$ (**1-Rh**) was next investigated (section 2.2). In this case the ability of the ylenes to insert into the Rh–Cl bond, in addition to the coordination of one of the peripheral Mes or Trip substituents to the Rh centre, with concomitant C_2H_4 elimination, was showcased resulting in the novel arene stabilised chelate complexes: $[\{SnCl_2(2\text{-Mes-}C_6H_3)(\eta^6\text{-Mes})\}Rh(\eta^2\text{-}C_2H_4)]$ (**2-Rh**) and $[\{GeCl_2(2\text{-Trip-}C_6H_3)(\eta^6\text{-Trip})\}Rh(\eta^2\text{-}C_2H_4)]$ (**3-Rh**), where **3-Rh** was found to exhibit the shortest Ge-Rh bond length to date (Scheme 3.2).

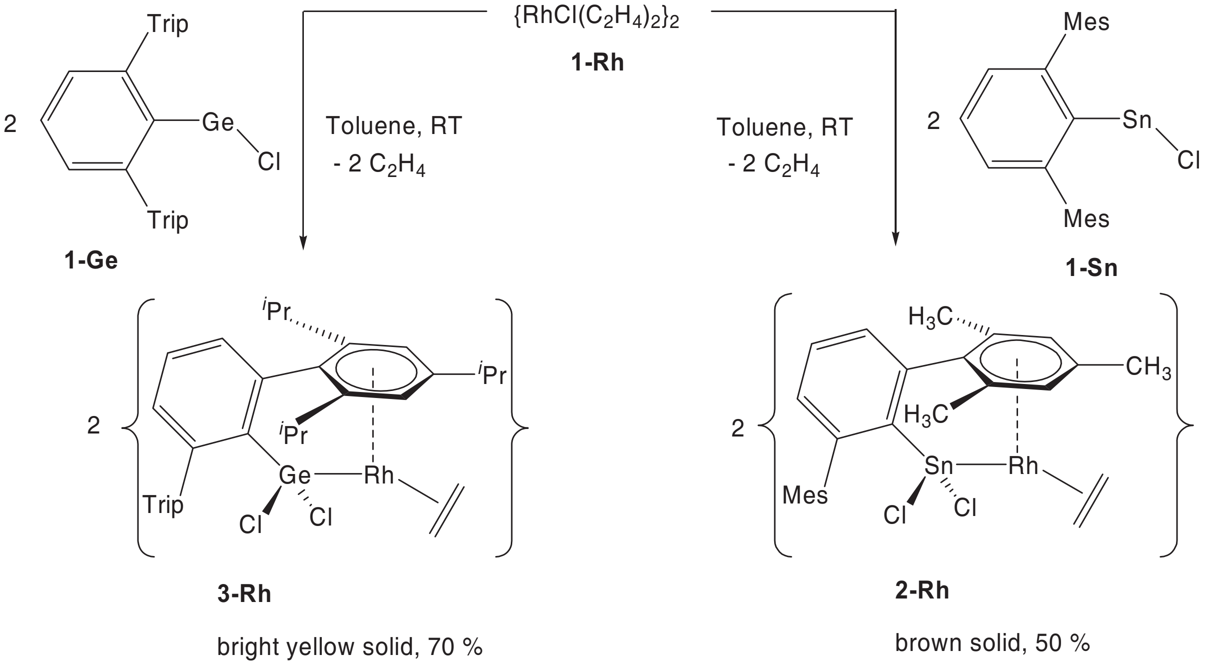

Scheme 3.2: Reactivity of germylene **1-Ge** and stannylene **1-Sn** with $\{RhCl(C_2H_4)_2\}_2$.

Dieses Werk ist copyrightgeschützt und darf in keiner Form vervielfältigt werden noch an Dritte weitergegeben werden.
Es gilt nur für den persönlichen Gebrauch.

Section **2.3** comprised the bulk of the work. In section **2.3.1.1** The reactivity of **1-Sn** towards a reactive d^8 configured Fe(0) complex, $[Fe(depe)_2(N_2)]$ (**1-Fe**) was discussed. Here, dinitrogen elimination at the Fe centre resulted in the first example of an iron halostannylidene complex $[(depe)_2Fe{=}SnCl(2,6\text{-}Mes_2\text{-}C_6H_3)]$ (**3-Fe**), which is also the first structurally characterised halostannylidene complex of any transition metal to date.

Section **2.3.1.2** looked at strategies to effect halogen abstraction of **3-Fe** resulting in the first examples of stannylidyne complexes to iron and outside group 6, which happen to be ionic in nature: $[Fe(depe)_2{\equiv}Sn(2,6\text{-}Mes_2\text{-}C_6H_3)][SnCl_2(2,6\text{-}Mes_2\text{-}C_6H_3)$ (**4-Fe**), $Fe(depe)_2{\equiv}Sn(2,6\text{-}Mes_2\text{-}C_6H_3)][BCl(C_6F_5)_3]$ (**5-Fe**) and $[Fe(depe)_2{\equiv}Sn(2,6\text{-}Mes_2\text{-}C_6H_3)][B\{C_6H_3\text{-}3,5\text{-}(CF_3)_2\}_4]$ (**6-Fe**). The analogous chemistry with Ge was also presented in section **2.3.1.3** resulting in the first germylidyne complexes outside group 6: $[Fe(depe)_2{\equiv}Ge(2,6\text{-}Trip_2\text{-}C_6H_3)][GeCl_2(2,6\text{-}Trip_2\text{-}C_6H_3)]$ (**8-Fe**) and $[Fe(depe)_2{\equiv}Ge(2,6\text{-}Mes_2\text{-}C_6H_3)][GeCl_2(2,6\text{-}Mes_2\text{-}C_6H_3)]$ (**9-Fe**) (Scheme 3.3).

Section **2.3.3** details the reactivity of **1-Sn** towards the dimer $[\{Fe(dmpe)_2\}_2(\mu\text{-}dmpe)]$ (**15-Fe**) and the monomer $[Fe(dmpe)_2(PMe_3)]$ (**17-Fe**) respectively, both of which by phosphane elimination result in the chlorostannylidene complex, $[(dmpe)_2Fe{=}SnCl(2,6\text{-}Mes_2\text{-}C_6H_3)]$ (**16-Fe**). The spectroscopic and solid state structural differences in changing the steric bulk at Fe from the more sterically demanding depe to dmpe are discussed. The first example of a chlorogermylidene complex of iron was prepared in an analogous way, resulting in $[(dmpe)_2Fe{=}GeCl(2,6\text{-}Mes_2\text{-}C_6H_3)]$ (**16-Fe-2**), which could be converted to the germylidyne complex $[(dmpe)_2Fe{\equiv}Ge\ (2,6\text{-}Mes_2\text{-}C_6H_3)][BCl(C_6F_5)_3]$ (**16-Fe-3**) by chloride abstraction (Scheme 3.4).

Dieses Werk ist copyrightgeschützt und darf in keiner Form vervielfältigt werden noch an Dritte weitergegeben werden.
Es gilt nur für den persönlichen Gebrauch.

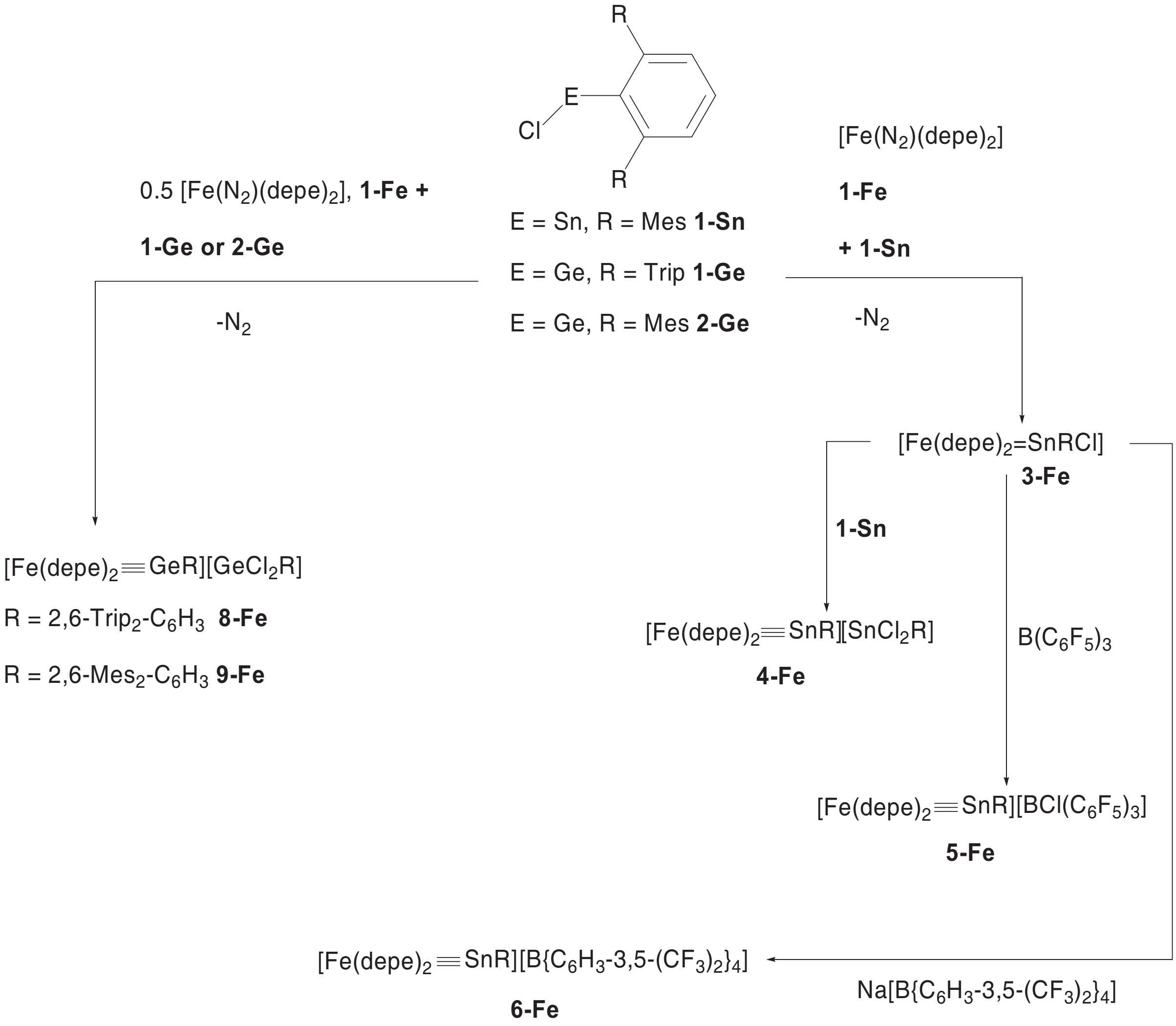

Scheme 3.3: Facile access to several new compound classes by N_2 elimination from $[Fe(N_2)(depe)_2]$ **1-Fe**: the iron stannylidene complex (**3-Fe**), iron stannylidyne complexes (**4-Fe, 5-Fe, 6-Fe**) and iron germylidyne complexes (**8-Fe**, **9-Fe**).

Dieses Werk ist copyrightgeschützt und darf in keiner Form vervielfältigt werden noch an Dritte weitergegeben werden.
Es gilt nur für den persönlichen Gebrauch.

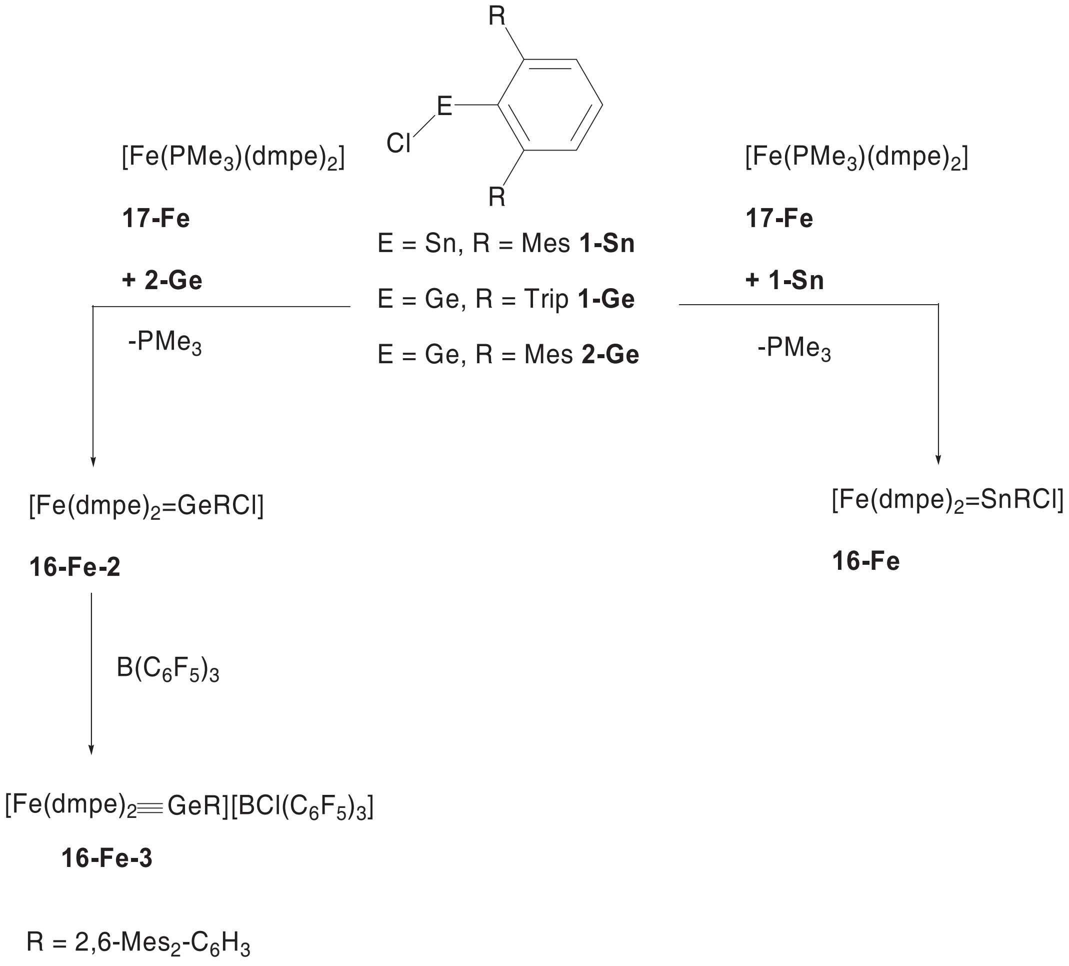

Scheme 3.4: Facile access to iron tetrylidene and tetrylidyne complexes by PMe_3 elimination from $[Fe(PMe_3)(dmpe)_2]$ **17-Fe**: iron stannylidene (**16-Fe**), and germylidene (**16-Fe-2**) and germylidyne (**16-Fe-3**) upon reaction with the stannylene (**1-Sn**) and germylene (**2-Ge**).

The first systematic ^{57}Fe Mößbauer spectroscopic investigation on a selection of the new classes of Fe complexes prepared was discussed in section **2.3.6**. First the Fe(0) germylidyne, stannylidyne and chlorostannylidene complexes were discussed (**2.3.6.1**) and their isomer shifts and quadruple splitting values rationalised, all consistent with low valent Fe centres, as expected. A new phenomenon was uncovered, which was the spectroscopic observation of both trigonal bipyramidal and square pyramidal stereoisomers in the ^{57}Fe Mößbauer spectra of some of the ylidyne complexes. It was shown that the relative distribution of these stereoisomers in largely driven by the reaction conditions, and is a solvent effect.

Dieses Werk ist copyrightgeschützt und darf in keiner Form vervielfältigt werden noch an Dritte weitergegeben werden.
Es gilt nur für den persönlichen Gebrauch.

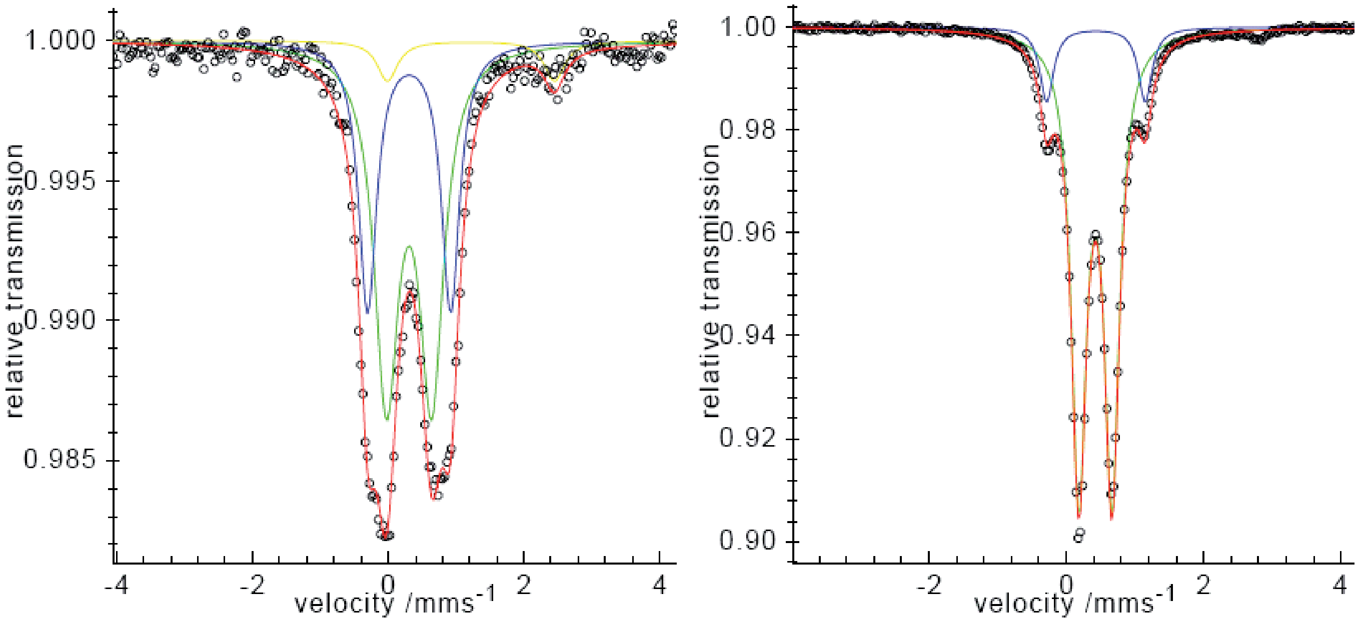

4-Fe

6-Fe

Figure 3.1: The co-existence of trigonal bipyramidal (outer doublet) and square pyramidal (inner doublet) stereoisomers for the stannylidyne complexes **4-Fe** and **6-Fe** observed by ^{57}Fe Mößbauer spectroscopy.

Section **2.3.7** discussed the UV–Vis spectra of the iron stannylidene complex **3-Fe**, and was compared to that of the ionic stannylidyne complexes **4-Fe** and **6-Fe**. The UV–Vis spectrum of the germylidyne complex, **8-Fe** was also discussed. The results confirmed the expected trends in decreasing π-bond strengths on descent from Ge to Sn, based on the wavelength of absorption, which is a reflection of the π–π^* transitional energy.

Section **2.3.5** discussed some reactivity studies of complex **3-Fe** towards HCl, $Na[HBEt_3]$ and MeLi. Reaction of **3-Fe** with an excess of HCl results in a mixture of the complexes *trans*-$[FeCl(SnCl_3)(depe)_2]$ (**29-Fe**) and *trans*-$[FeH(SnCl_3)(depe)_2]$ (**28-Fe**), both of which were selectively synthesised and fully characterised, along with their Ge analogues. Reaction of **3-Fe** with an excess of Na[HBEt] resulted in the formation of the hydridostannylidene complex $[(depe)_2Fe{=}SnH(2,6\text{-}Mes_2\text{-}C_6H_3)]$ (**27-Fe**), while reaction with MeLi resulted in $[(depe)_2Fe{=}Sn(CH_3)(2,6\text{-}Mes_2\text{-}C_6H_3)]$ (**26-Fe**).

Dieses Werk ist copyrightgeschützt und darf in keiner Form vervielfältigt werden noch an Dritte weitergegeben werden.
Es gilt nur für den persönlichen Gebrauch.

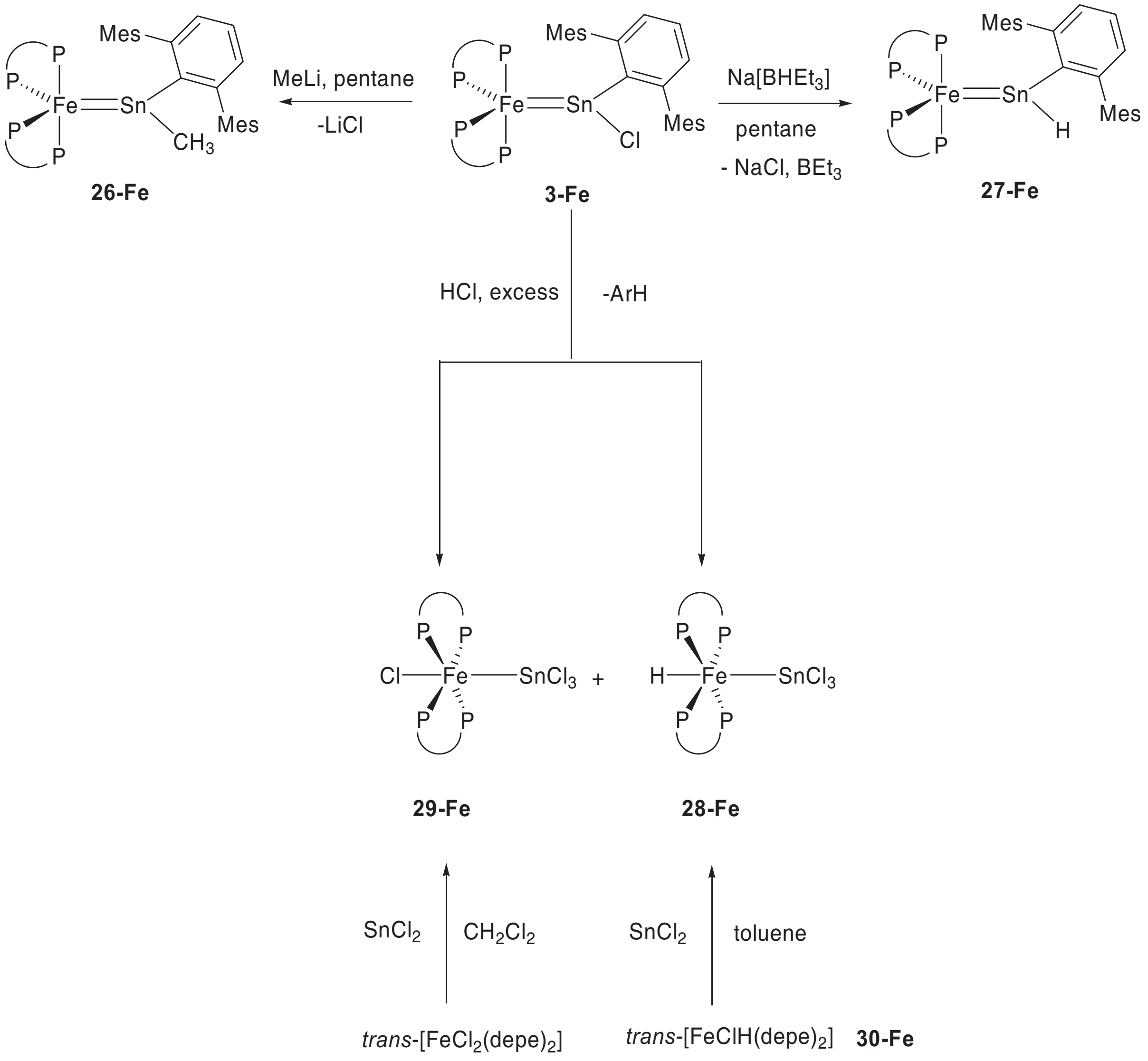

depe = 1,2-bis(diethylphosphino)ethane

Scheme 3.5: Probing the reactivity of iron stannylidene complex **3-Fe**.

The comparative reactivity of the plumbylene [PbBr(2,6-Trip$_2$-C$_6$H$_3$)] (**1-Pb**) towards **1-Fe** was also discussed (section **2.3.2**) resulting in Fe(I) species, rather than the expected plumbylidene/dyne complexes, which prompted an excursion into Fe(I) chemistry: (discussed in section **2.3.2.1**) Particularly, the first Fe(I) alkyl complex, [Fe(depe)$_2$(CH$_3$)] (**12-Fe**) was prepared and spectroscopically and structurally investigated. The first structurally characterised Fe(I) chloride complex, [Fe(depe)$_2$Cl] (**10-Fe**) was also discussed in this section.

Dieses Werk ist copyrightgeschützt und darf in keiner Form vervielfältigt werden noch an Dritte weitergegeben werden.
Es gilt nur für den persönlichen Gebrauch.

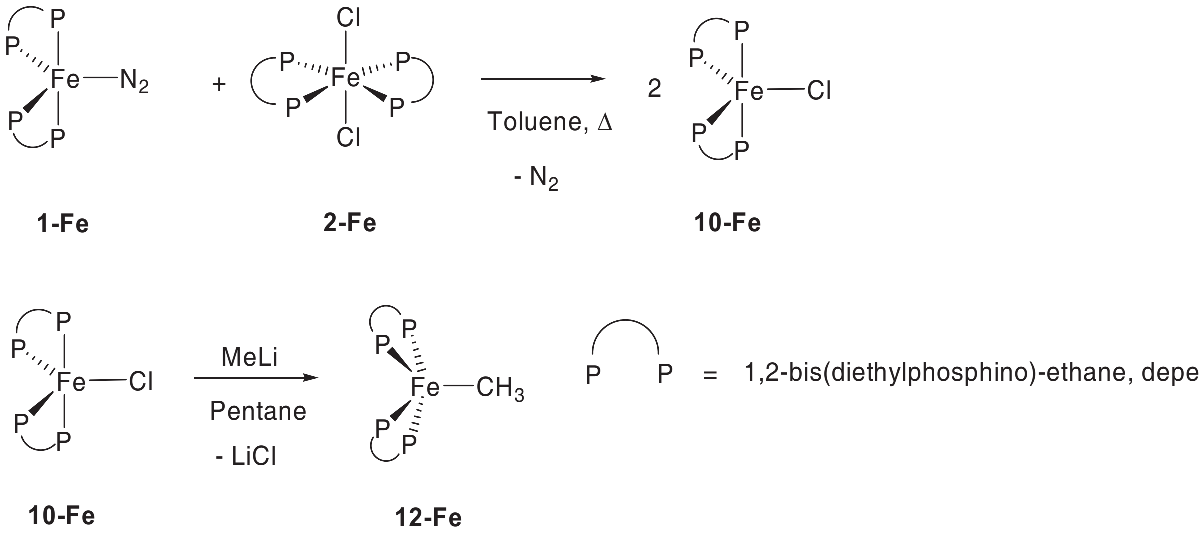

Scheme 3.6: Facile access to the first structurally characterised Fe(I) chloride complex, **10-Fe** and the first Fe(I) alkyl complex **12-Fe**.

Section **2.3.4** dealt with the reactivity of **1-Sn** towards C-H activated Fe complexes and were contrasted to that of similar work carried out for C-H activated complexes of W. For example, the complex $[FeH(PMe_3)_3\{\eta^2\text{-}Me_2PCH_2\}]$ (**18-Fe**) reacts with **1-Sn** selectively to yield the insertion product $[FeH(PMe_3)_3\{\eta^2\text{-}Me_2PCH_2\}]$ (**20-Fe**) in high yields as a mixture of stereo-isomers, in contrast to similar reactions of **1-Ge** with $[WH(PMe_3)_3\{\eta^2\text{-}Me_2PCH_2\}]$, yielding the germylidyne complexes. In addition the reactivity of other C-H activated complexes towards **1-Sn** was also discussed.

Preliminary results obtained from photolytic experiments of **1-Ge** and **1-Sn** with cis/trans-$[Ru(depe)_2H_2]$ were reported in section **2.4**. The goal here was the extension of triple bonding to Sn and Ge with Rh, by photochemical means. Although this was not successful, the first structurally characterised stannyl complex of Ru featuring a *trans* positioned hydride resulting from this reaction is discussed: *trans*-$[RuH\{SnCl_2(2,6\text{-}Mes_2\text{-}C_6H_3\}(depe)_2]$ (**5-Ru**).

Section **2.5** detailed an excursion into base stabilised germylenes of the type $[GeCl(2,6\text{-}Mes_2\text{-}C_6H_3)L]$, where L = PMe_3 or the *N*-heterocyclic carbene IMe_2Me_2 (IMe_2Me_2 = 1,3,4,5-tetramethylimidazol-2-ylidene).

Dieses Werk ist copyrightgeschützt und darf in keiner Form vervielfältigt werden noch an Dritte weitergegeben werden.
Es gilt nur für den persönlichen Gebrauch.

3.2 Conclusion

In conclusion, a systematic study of the various reactivity patterns of ylenes of the type EXR (E = Ge or Sn, X = Cl, R = 2,6-Trip$_2$-C$_6$H$_3$ or 2,6-Mes$_2$-C$_6$H$_3$) towards Fe, Ru, Rh and Pd complexes was studied in this work. This resulted, for Fe, in the first know examples of triple bonding between a late transition metal element (or any transition metal element outside group 6) and *any* main group element atom ($n \geq 3$), constituting a significant academic advance at the interface of main group and transition metal chemistry.

3.3 Outlook

3.2.1 Ylidyne complexes of other late transition metal elements

This work has demonstrated, for the first time, the possibility of preparing complexes featuring triple bonds between the elements Ge and Sn with transition metal element atoms outside group 6. It is hence conceivable that this concept could be logically extended to other transition metal complexes, by employing a similar strategy. Some possible future areas of pursuit could be:

The preparation of Ru ylidyne complexes

This work, and earlier work for W and Mo has shown that metals in a low oxidation state (typically 0), bearing an electron rich polyphosphane ligand sphere in addition to one or more N$_2$ ligands, capable of elimination represents ideal precursors for the preparation of ylidyne complexes on reaction with ylenes, generally. In this context, the recently published five coordinate complex: [Ru(N$_2$)(P^{i}P$_3$)] where P^{i}P$_3$ = P(CH$_2$CH$_2$P^{i}Pr$_2$) by Field and co-workers[258] represents an ideal precursor for the synthesis of Ru ylidyne complexes. It is likely, based on the chemistry performed in this work with **1-Fe**, that this complex upon reaction with 1 eq. **1-Sn** should result in the complex: [(P^{i}P$_3$)Ru=SnCl(2,6-Mes$_2$-C$_6$H$_3$)], where halogen abstraction can subsequently be performed as in this work, resulting in ionic stannylidyne complexes. The same could conceivably be carried out with Ge, in analogy to this work.

Dieses Werk ist copyrightgeschützt und darf in keiner Form vervielfältigt werden noch an Dritte weitergegeben werden.
Es gilt nur für den persönlichen Gebrauch.

Recently, in our group, extension of this chemistry to Ru by using $[Ru(depe)_2(PMe_3)]$ as a precursor was carried out. Reaction thereof with 1 eq ArSnCl yields the chloro-stannylidene complex $[Ru(depe)_2{=}SnCl(2,6\text{-}Mes_2\text{-}C_6H_3)]$, the Ru analogue of **3-Fe**.[259] Furthermore, it was also possible to prepare $[Ru(depe)_2{=}GeCl(2,6\text{-}Mes_2\text{-}C_6H_3)]$ in an analogous way, and following chloride abstraction using $B(C_6F_5)_3$, obtain the cationic germylidyne complex: $[Ru(depe)_2{\equiv}Ge(2,6\text{-}Mes_2\text{-}C_6H_3)][BCl(C_6F_5)_3]$. These results indicate a proof of principle, that it is possible to extend the work highlighted in this dissertation, to other late transition metal elements, and thereby highlight the importance, applicability and possible generality thereof.

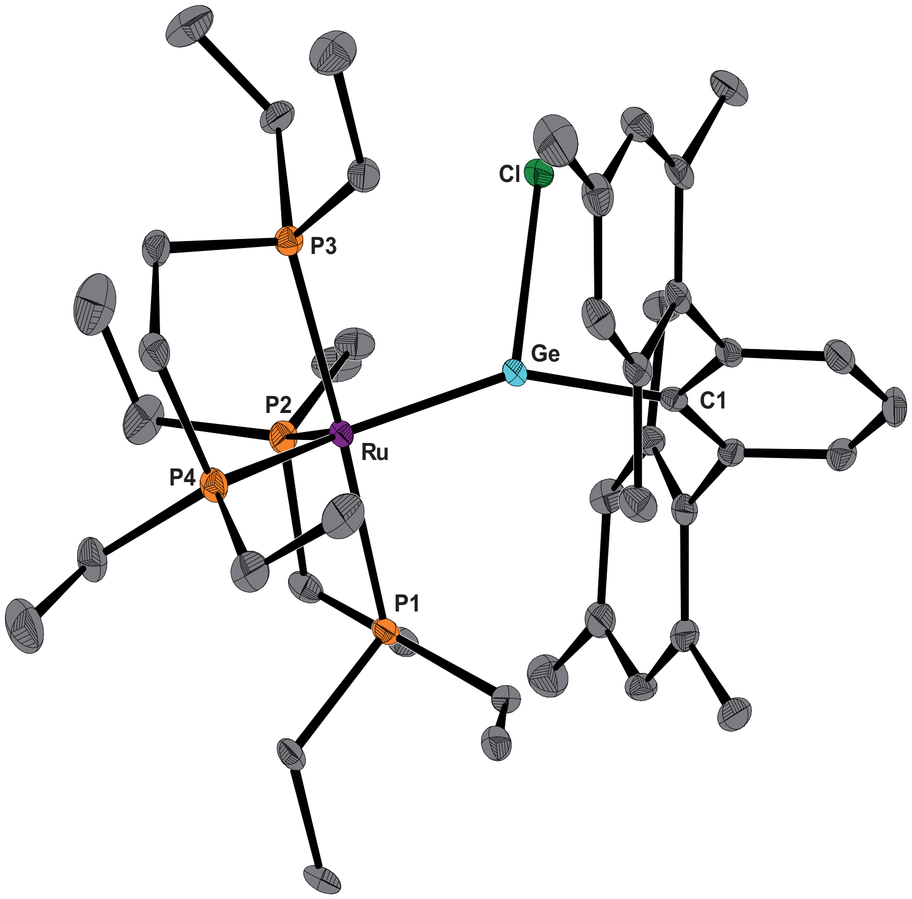

Figure 3.3.1: DIAMOND plot of the molecular structure of a ruthenium germylidene complex in the solid state. Thermal ellipsoids are set at the 50% probability level, H atoms are omitted for clarity. Selected bond lengths [Å] and bond angles [°]: Ru-Ge 2.3176(4), Ru-P1 2.2149(8), Ru-P2 2.2938(9), Ru-P3 2.3433(8), Ru-P4 2.3059(9), Ge-C1 2.053(3), Ge-Cl 2.3343(8), Ge-Ru-P1 92.61(2), Ge-Ru-P2 106.65(2), Ge-Ru-P3 90.30(2), Ge-Ru-P4 139.98(3), P1-Ru-P2 83.39, P1-Ru-P3 175.40(3), P1-Ru-P4 93.44(3), P2-Ru-P3 99.22(3), P2-Ru-P4 113.34(3), P3-Ru-P4 82.05(3), C1-Ge-Cl 90.04(8), Ru-Ge-C1 154.31(8), Ru-Ge-Cl 114.67(2). (Taken from ref 259)

Dieses Werk ist copyrightgeschützt und darf in keiner Form vervielfältigt werden noch an Dritte weitergegeben werden.
Es gilt nur für den persönlichen Gebrauch.

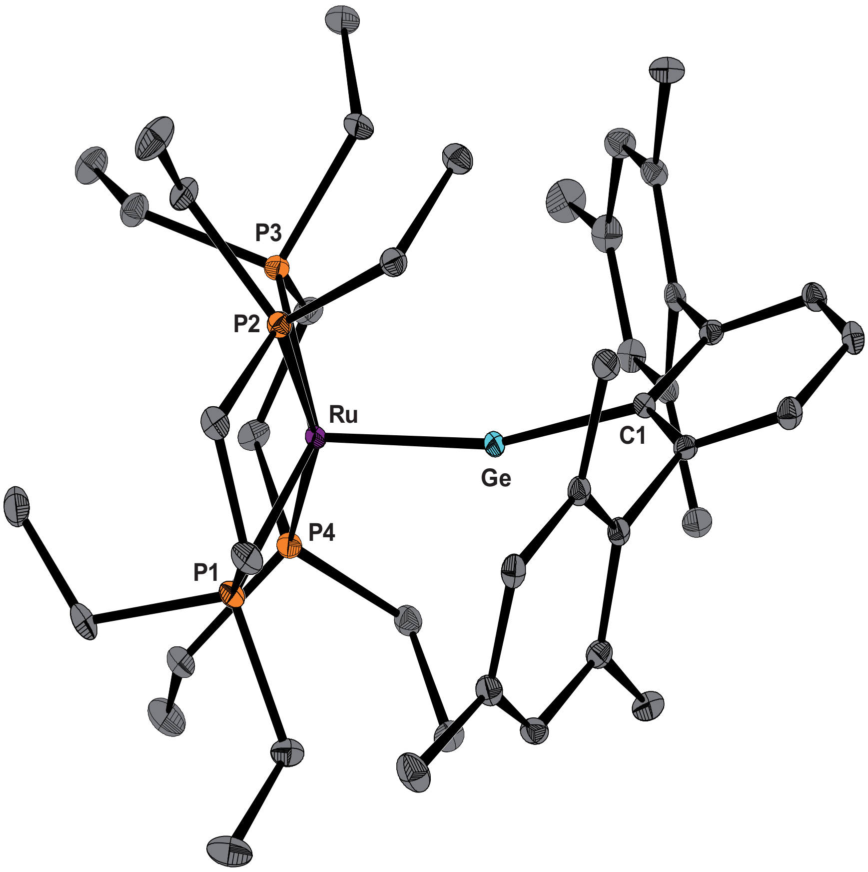

Figure 3.3.2: DIAMOND plot of the molecular structure of the square pyramidal complex cation in the solid state. Thermal ellipsoids are set at the 50% probability level, H atoms are omitted for clarity. Selected bond lengths [Å] and bond angles [°]: Ru-Ge 2.2218(3), Ru-P1 2.3415(6), Ru-P2 2.3407(7), Ru-P3 2.3413(6), Ru-P4 2.3836(7), Ge-C1 1.995(2), Ge-Ru-P1 110.23(2), Ge-Ru-P2 95.89(2), Ge-Ru-P3 107.70(2), Ge-Ru-P4 103.17(2), P1-Ru-P2 81.55(2), P1-Ru-P3 144.99(2), P1-Ru-P4 92.26(2), P2-Ru-P3 92.29(2), P2-Ru-P4 160.93(2), P3-Ru-P4 81.37(2), Ru-Ge-C1 161.88(7). (From ref 259).

Dieses Werk ist copyrightgeschützt und darf in keiner Form vervielfältigt werden noch an Dritte weitergegeben werden.
Es gilt nur für den persönlichen Gebrauch.

4. Experimental Section

4.1 General section

All experiments were carried out under an atmosphere of argon (99.998 %), with exception the preparation of dinitrogen complexes which were carried out under an atmosphere of dinitrogen (99.999 %), using standard Schlenk or glove box techniques, unless otherwise stated.[260] The glove-box (MBraun) was maintained under an argon atmosphere (typically +1.5 mbar), and it was purified by passage through a column of activated charcoal, a copper catalyst and molecular sieves (4 Å) to insure removal of solvent vapours, oxygen and water respectively. Regeneration of the internal glove-box catalyst at regular intervals was also carried out (typically every six - twelve months) using 5 % H_2 doped Ar regeneration gas and the automatic regeneration routine of the glove-box.

Solvents were initially pre-dried over suitable drying agents, then distilled under argon at normal pressure over other suitable drying agents into vessels containing activated molsieves (of varying size) where they were stored (Table 4.1). In the case of benzene, Et_2O, and THF benzophenone was used as indicator, and distillation only carried out if the colour of the solvent at ambient temperature, before commencement of distillation, was purple.

Solvent	Pre-drying	Distillation	Molesieve size
Pentane	-	Na	3 Å
Hexane	-	Na/K	3 Å
Benzene	$CaCl_2$	Na / Benzophenone	4 Å
Toluene	$CaCl_2$	Na	4 Å
Et_2O	KOH	Na/Benzophenone	4 Å
THF	KOH	Na/Benzophenone	4 Å
CH_2Cl_2	$CaCl_2$	Sicapent®	4 Å
C_6H_5F	-	CaH_2	-

Table 4.1: Summary of solvent pre-drying procedures, and distillation.

In the case of moisture or oxygen sensitive reactions, the solvents were subsequently further dried by an additional step: C_6H_5F and CH_2Cl_2 were additionally dried by stirring over CaH_2 at ambient temperatures, while Pentane, hexane, benzene, toluene, Et_2O and THF by stirring over grey $LiAlH_4$ powder at room temperature in Schlenk tubes. The latter mentioned

Dieses Werk ist copyrightgeschützt und darf in keiner Form vervielfältigt werden noch an Dritte weitergegeben werden.
Es gilt nur für den persönlichen Gebrauch.

solvents were alternatively stored over potassium mirrors in vacuum tight Young vessels. These mirrors were prepared by adding small quantities of potassium metal (*ca.* 5 mm × 5 mm × 5 mm) to the Young vessels in the glove-box, and subsequently heating them under active vacuum to 650 °C. Prior to use, the solvents were vacuum transferred using glass recondensation bridges (in the case of transfer from solvents over $LiAlH_4$ or CaH_2, these contained a glass sinter frit) under static vacuum into receptacle Schlenk tubes, and the recondensed solvent degassed by two or three freeze-pump-thaw cycles. These solvents were either used directly, or stored in the glove-box under Argon over appropriate molesieves for later use.

For transfer of solvents or solutions stainless steel cannulas were used, which were stored in the oven at 110 °C. The transfer was enabled by the vessel of origin being left under a positive pressure of protective gas, and the receptacle vessel closed with a pressure release valve (typically a hypodermic needle inserted into the septum). In the case of filtrations, stainless steel cannula containing a filter-head at one end were utilised. Whatman® (GF/B 25) filters were affixed to the filter end of the cannula with Teflon tape, and stored for two or three minutes in the over at 110 °C prior to use. After use, cannulae were cleaned by thorough rinsing with dilute HCl, followed by distilled water, and acetone.

All glassware was cleaned by storage in a KOH/isopropanol bath (typically overnight), thoroughly washed with distilled water, then placed in a dilute HCl bath (again overnight), washed additionally with distilled water, then acetone and finally stored in the oven. The glassware was dried in the oven at approximately 110 °C (for at least 2 h), assembled hot, and baked *in vacuo* prior to use at 650 °C and allowed to cool to ambient temperatures under active vacuum before use. All glass joints were greased with Glisseal® HV laboratory grease, or in the case of higher temperature reactions, involving refluxing solvents, Teflon grease was employed.

In the case of low temperature reactions, Dewar vessels were filled with Acetone and dry-ice was added, until reaching the desired temperature. Isopropanol / liquid nitrogen was also employed as a suitable alternative in this respect.

Dieses Werk ist copyrightgeschützt und darf in keiner Form vervielfältigt werden noch an Dritte weitergegeben werden.
Es gilt nur für den persönlichen Gebrauch.

4.2 Analytical methods

4.2.1 Nuclear Magnetic Resonance (NMR) spectroscopy

NMR samples of non-sensitive samples were prepared in solvents as received from commercial suppliers in normal 5 mm sample tubes and stoppered. Samples of air and/or moisture sensitive compounds were all prepared in the glove-box either in stoppered 5 mm sample tubes (which were then stored in Schlenk tubes under argon and immediately measured) or Young type NMR tubes with rotaflo gas-tight Teflon stoppers, the latter being the preferred method. The deuterated solvents were dried by stirring over Na sand (benzene-d_8, toluene-d_8, THF-d_8) or CaH_2 (dichloromethane-d_2) for approximately 24 h, degassed at least twice, vacuum transferred and stored in the glove-box in Young vessels over suitable molesieves for use. Samples were typically made up as 0.5 mL solutions in the appropriate solvent and transferred by syringe into the NMR tubes for measurement.

The spectra were recorded on one of the following spectrometers from the *Bruker* company: DMX300, DPX300, DPX400, DRX500 or DMX500). The ^{1}H and ^{13}C{^{1}H} NMR spectra were calibrated against the residual proton and natural abundance ^{13}C resonances of the deuterated solvent relative to tetramethylsilane (benzene-d_6, δ_H 7.15 ppm and δ_C 128.0 ppm; dichloromethane-d_2, δ_H 5.32 ppm and δ_C 53.8 ppm, chloroform-d_1 δ_H 7.24 ppm and δ_C 77.0 ppm, THF-d_8, δ_H 1.73 ppm and δ_C 25.3 ppm, toluene-d_8 δ_H 2.09 ppm and δ_C 20.4 ppm). Heteronuclear spectra were calibrated as follows: ^{19}F{^{1}H}: external $CFCl_3$; ^{31}P{^{1}H}: external 85 % H_3PO_4; ^{119}Sn{^{1}H}: external $SnMe_4$; whereby in each case a 1 mm glass capilliary tube containing the standard substance was placed in the appropriate solvent in a 5 mm NMR tube and the spectrum recorded.

1-D spectra were processed on 1D-WinNMR 6.0 and 2-D spectra on TopSpin 2.05, from *Bruker*. The abbreviations used to denote the multiplicity of the signals are as follows: s = singlet, d = doublet, t = triplet, q = quartet, quint = quintet, sext = sextet, sept = septet, m = multiplet, ps d = pseudo doublet, ps t = pseudo triplet, br = broad. A combination of H,H-COSY, H,C-COSY (HMQC, HSQC)-HMBC and DEPT experiments were carried out to unambiguously assign the signals in the ^{1}H and ^{13}C spectra of new compounds. Diasteriotopic groups (of the depe, dmpe ligand systems, or that of the methyl groups of the isopropyl substituents in Trip compounds) were labelled with superscript letters A or B; X or

Dieses Werk ist copyrightgeschützt und darf in keiner Form vervielfältigt werden noch an Dritte weitergegeben werden.
Es gilt nur für den persönlichen Gebrauch.

Y; 1 or 2. The designation used for the assignment of resonance signals in the *m*-terphenyl substituents are either *ortho/meta/para* or $C^{2,6}$/ $C^{3,5}$/C^4 respectively for the central phenyl ring aas well as the Mes ot Trip substituents.

4.2.2 Infra-red spectroscopy

Far IR spectra (500 – 100 cm^{-1}) were recorded on a Bruker Equinox IR spectrometer, against polyethylene as background, where samples of the compound under investigation were mixed with polyethylene powder and compressed under *ca.* 10 ton pressure into pellets of *ca.* 1 mm thickness. The quoted wavenumber in reciprocal centimetres (cm^{-1}) is that of the maxima of the absorption band. IR spectra (4000 – 400 cm^{-1}) were recorded on a Bruker Vector 22 or IFS-55 spectrometer, the chamber of which was maintained under an atmosphere of dry air, at room temperature. The quoted wavenumber in reciprocal centimetres (cm^{-1}) is that of the maxima of the absorption band. Samples of solids were measured in paraffin oil (Nujol) between NaCl or KBr windows, and measured against the background (air). Air or moisture sensitive samples were prepared in the glove-box, and measure immediately, while air stable samples were prepared outside. The windows were immediately washed after use (with pentane or Et_2O) and placed in the ante-chamber of the glove-box under active vacuum for *ca.* 10–15 minutes. Solution IR spectra were recorded in airtight, stainless steel curvets sealed with Teflon stoppers with CaF_2, NaCl or KBr windows. The spectra were processed using the program OPUS (version 5.5 or 6.5) from Bruker, and the abbreviations associated with the absorptions quoted are: vs = very strong; s = strong, m = medium; w = weak, vw = very weak, br = broad, the intensities of which were assigned on the basis of visual inspection.

4.2.3 UV-Vis Spectrometry

UV-Vis spectrophotometric investigations were carried out on an Evolution 300 spectrophotometer from the Thermo electron corporation. Pure samples of the investigated substance were dissolved in dry and degassed solvents, the preparation of which was carried out in the glove-box. In the case of **3-Fe**, **4-Fe**, **6-Fe** and **8-Fe** spectra of varying and exact concentrations were recorded, and the extinction coefficient (ε) determined by plotting absorbance to concentration of the appropriate absorbance band, and determining the gradient of the linear regressed line through the data points using Microsoft Excel. In the

Dieses Werk ist copyrightgeschützt und darf in keiner Form vervielfältigt werden noch an Dritte weitergegeben werden.
Es gilt nur für den persönlichen Gebrauch.

case of **8-Fe** this line did not pass through the origin, although it was linear, whereas in all the other cases a reasonable R^2 value was attained. For the base stabilised germylenes, **5-Ge**, **6-Ge** and **8-Ge** the extinction coefficient was not determined, and the spectra were only recorded at one concentration so as only to determine the λ_{max} value which in these compounds occurred as shoulder absorption bands.

In the case of **10-Fe**, a solid state single crystal UV-Vis-NIR spectrum was recorded in the research group of Prof. R. Glaum at the University of Bonn Institute of Inorganic Chemistry. A single crystal of **10-Fe** was carefully placed in a glass capillary tube in the glove-box and the spectrum recorded. The band position(s) were estimated by visual inspection.

4.2.4 Mößbauer Spectroscopy

Samples for Mößbauer spectroscopy were prepared by placing *ca.* 50 mg of the pure sample between two Teflon discs (diameter = 1 cm, *ca.* 2 mm thickness), wrapped in aluminium foil, and stored under argon, or submerged in liquid nitrogen prior to the actual measurements. All spectra were recorded at the Max-Planck-Institute for Bioinorganic Chemistry in Mulheim an der Ruhr, on a spectrometer with alternating constant acceleration. The sample temperature was maintained in an Oxford Instruments Variox cryostat. The γ-source was approximately 0.6 GBq ^{57}Co/Rh. The quoted isomer shifts are relative to Fe metal at 300 K. The zero-field splitting spectra were simulated by using Lorenzian doublets.

4.2.5 Melting Point determinations

Samples for melting point determinations were prepared in glass capillary tubes (typically 1 mm × 80 mm) under a normal pressure of argon, in the glove-box and sealed off. The melting points were determined on a Buchi SMP 500 apparatus (Dr. Tottoli, Pat. 320338) whereby the first sample was used to determine the crude melting point or range/decomposition temperature point or range, and the second sample with a slow heating rate of between 1 and 2 K/minute was used to find the accurate melting point or range / decomposition temperature point or range. The melting points / decomposition temperatures determined in this way were corrected according to the calibration curve: $T_{corrected} = 1.03966(T_{measured}) - 2,6811$. The calibration curve was determined by using the standard substances: vanillin, phenancillin and caffeine and plotting their observed melting

Dieses Werk ist copyrightgeschützt und darf in keiner Form vervielfältigt werden noch an Dritte weitergegeben werden.
Es gilt nur für den persönlichen Gebrauch.

points to the actual literature values. Melting points were alternatively determined in duplicate using the automated Buchi-Melting point B-545 device.

4.2.6 Elemental analysis

Air or moisture sensitive samples were prepared in “tin-boats” in the glove box which were sealed off as tightly as possible so as to minimize any contact with the atmosphere. The C, H, N analyses of all compounds were carried out three times on a Elementar Vario Micro elemental analyser or a Leco CHNS-932 analyser. The individual C, H, N values did not generally differ by more than ± 0.3. The mean C, H, N values are quoted for each compound. Cl analyses were conducted by combusting a sample of the compound in a Nickel-micro cylinder (combustion chamber) with sodium peroxide, adding water to the resulting mass and re-heating the sample to destroy excess peroxide, after which a suitable acid was added. A precipitation titration with $AgNO_3$ was subsequently carried out and the equivalence point determined potentiometrically using a Metrohm DMP-Titrino 785 device. This procedure was also carried out in triplicate and the mean values are reported in each case. All other elements (Sn, Ge, P etc.) were determined using ICP (inductively coupled plasma) analysis on a Thermo IRIS Advantage Duo device.

4.2.7 Electron paramagnetic resonance spectroscopy (EPR)

Very dilute pentane solutions of **10-Fe** and **12-Fe** were prepared in the glove-box, rapidly transferred to suitable EPR glass sample tubes and degassed by two freeze-pump-thaw cycles, after which the tubes were sealed off under vacuum and stored in liquid nitrogen prior to measurement. The spectra were recorded at the University of Bonn, Institut für Physikalische und Theoretische Chemie, at T = 30 K on a Bruker Elexsys E580 spectrometer equipped with an ER4102ST rectangular resonator. The microwave frequency was 9.44 GHz and the microwave power 63 mW. The modulation amplitude amounted to 0.5 mT.

4.2.8 Mass Spectrometry

Mass spectra were recorded at the University of Bonn (Institut für Anorganische chemie) mass spectrometry department. Mass spectra were recorded on a MAT 90 or MAT 95 XL Thermo Finnigan for EI (electron impact) spectra. ESI mass spectra were recorded on a

Dieses Werk ist copyrightgeschützt und darf in keiner Form vervielfältigt werden noch an Dritte weitergegeben werden.
Es gilt nur für den persönlichen Gebrauch.

Brucker MicrOTOF-Q spectrometer. DCTB = 2-[(2E)-3-(4-tert-butylphenyl)-2-methylprop-2-enylidene]malononitrile was used in Maldi-ToF experiments as matrix.

4.2.9 X-ray diffraction analysis

Harvested crystals, suitable for X-ray crystallographic analysis were stored under argon, covered in Fumbolin® and rapidly transferred to a microscope slide, where a selection of a suitable crystal was made for each compound for the measurement. Data were collected on a STOE IPDS IIT, equipped with a low-temperature device (Oxford Cryostream 700er series, Oxford Cryosystems) or a Bruker X8-KappaApexII diffractometer equipped with a low-temperature device (KRYOFELX, Bruker-AXS) or a Nonius Kappa CCD equiped with a Oxford Cryostream 600er series, low temperature device all using graphite monochromated Mo-K_α radiation (λ = 0.71073 Å). Intensities were measured by using the rotation method and upon complete data collection were corrected for background, polarization and Lorentz effects. The absorption correction (numerical or seimi-empirical from equivalents), structure solution (direct or Patterson methods), and structure refinement, using full-matrix least squares on F^2, were carried out using the SHELX-97 programs.[‡‡‡‡] All atoms with the exception of hydrogen were anisotropically refined, unless otherwise stated. The hydrogen atoms were included isotropically using the riding model on the bound carbon atoms. Metal hydride hydrogen atoms were located by the difference in the Fourier synthesis map and isotropically refined. In all cases, the graphical representation of the molecular structures was carried out using DIAMOND version 2.1c. The details for the individual structure solutions included in this dissertation are available in the appendix.

(‡‡‡‡) G. M. Sheldrick, SHELXS97 and SHELXL97, University of Göttingen, Germany, 1997.

Dieses Werk ist copyrightgeschützt und darf in keiner Form vervielfältigt werden noch an Dritte weitergegeben werden.
Es gilt nur für den persönlichen Gebrauch.

4.3 Starting materials prepared according to literature procedures

Compound	Reference(s)	Experimentor
C_6H_3I-2,6-Trip$_2$	[44]	Weidemann
C_6H_3I-2,6-Mes$_2$	[44]	Hofer
GeCl(2,6-Mes$_2$-C_6H_3)	[261]	Liu
C_6H_3(2,6-Mes$_2$-C_6H_3)Li	[48]	Blom/Beile
C_6H_3(2,6-Trip$_2$-C_6H_3)Li(OEt$_2$)	[177]	Blom/Beile
GeCl(2,6-Trip$_2$-C_6H_3)	[177]	Blom/Beile
$GeCl_2$·(1,4-dioxane)	[262]	Blom/Beile
[PdCl$_2$(cod)]	[263]	Blom
[PdCl$_2$(dppe)]	[264]	Blom
[SnCl(η^5-C_5Me_5)]	[118]	Portius
$FeCl_2$	[265]	Blom/Belie
$B(C_6F_5)_3$	[266]	Weidemann
Na[B{C_6H_3-3,5-$(CF_3)_2$}$_4$]	[267]	Weidemann
depe	[268,269,270]	Blom/Wezisla/Kühnel-Lysek/Kühlmorgen
[PbCl(Ctms$_3$)]	[271]	Philippopoulos
[PbBr(2,6-Trip$_2$-C_6H_3)]	[49]	Arp
Na sand	[272]	Weidemann
dmpe	[273]	Kühnel-Lysek
PMe_3	[274]	Arp/Hofer
KC_8	[275]	Chernov/Puffler
HCl/Et_2O	–	Blom/Wezisla/Chakraborty
IMe$_2$Me$_2$	[276]	Chernov
Na/Hg	[277]	Arp
Ru(DMSO)$_4$	[237]	Beile
(*cis/trans*) RuH_2(depe)$_2$	[235]	Beile
(*cis/trans*) $RuCl_2$(depe)$_2$	[238]	Blom/Beile

Dieses Werk ist copyrightgeschützt und darf in keiner Form vervielfältigt werden noch an Dritte weitergegeben werden.
Es gilt nur für den persönlichen Gebrauch.

4.4 Commercially available starting materials

Reagent	Supplier	Pre-purification
$PdCl_2$		–
1,5-cod	Aldrich	–
dppe (>97 %)	Alfa Aesar	–
anhydrous $SnCl_2$	Fluka	–
$TlPF_6$	Strem	–
$RhCl_3 \cdot 3H_2O$	Merck-Schuchardt	–
$[Rh(C_2H_4)_2Cl]_2$ **1-Rh** (99 %)	Alfa Aesar	Extracted with CH_2Cl_2 evaporated to dryness
C_2H_4 (3.5)	Praxair	–
Fe powder	Fluka	–
MeLi/1.6 M in Et_2O	Aldrich	–
H_2 (3.0)	Praxair	–
HCl (gas)	Praxair	–
C_2H_2 (tech.)	Praxair	Purified by passage through activated molesieves (4Å) and activated charcoal
n-BuLi / Hexane 1.6 M	Aldrich	
n-BuLi /Hexane 2.5 M	Aldrich	
1,5-dioxane (>99 %)	Grüssing	Stored over KOH, distilled over Na, degassed.
$GeCl_4$	Aldrich	–
$LiAlH_4$	Aldrich	–
$Na[BHEt_3]$/ Toluene 1.0 M	Aldrich	–
DMSO (> 99.9 %)	Aldrich	Degassed
K metal	Aldrich	Washed with pentane prior to use
LiI (> 98%)	Fluka	–
MeOH	Aldrich	–
EtOH	Riedel-de Haën	–
Mg turnings	Aldrich	–

Dieses Werk ist copyrightgeschützt und darf in keiner Form vervielfältigt werden noch an Dritte weitergegeben werden.
Es gilt nur für den persönlichen Gebrauch.

4.5 Synthesis and full characterisation of new compounds

4.5.1 [PdCl{SnCl$_2$(2,6-Mes$_2$-C$_6$H$_3$)}(cod)] (3-Pd)

A Schlenk tube was charged with **1-Sn** (0.233 g, 0.498 mmol) and **1-Pd** (0.143 g, 0.50 mmol) and placed in an acetone-dry ice bath. Toluene (20 mL) was pre-cooled to –78 °C and added to the mixture of the starting materials. The cooling bath was removed and the orange suspension was allowed to warm to room temperature and stirred for 2 h. During this time the suspension turned into a dark red solution. The reaction was stored at –30 °C overnight and filtered at –30 °C to remove a green insoluble precipitate. The clear orange filtrate was concentrated *in vacuo* till incipient crystallisation and cooled to –78 °C. A yellow precipitate was formed, isolated by filtration from the supernatant orange solution at –78 °C and dried *in vacuo* for 2 h at room temperature to afford compound **3-Pd** as a yellow solid. Yield: 0.204 g (0.271 mmol, 54%). Crystals suitable for X-ray crystallographic analysis were grown from toluene at room temperature, with slow evaporation in the glove-box.

Properties: Very soluble in CH_2Cl_2, soluble in benzene. Moderately air stable.

Melting Point: 162 – 166 °C (dec.).

Elemental analysis: calcd (%) for $C_{32}H_{37}Cl_3PdSn$ (753.06 g.mol^{-1}): C 51.03, H 4.95; found: C 50.90, H 5.11%.

Spectroscopic Data:

FIR (polyethylene, cm^{-1}): ν = 339 (m, br), 328 (m), 287 (w), 265 (w).

^{1}H NMR: (300.1 MHz, C_6D_6, 303 K, ppm): δ = 1.45 – 1.78 (several multiplets, 8H, 4 × CH_2, cod), 2.16 (s, 6H, 2 × *p*-CH_3, Mes), 2.41 (s, 6H, 4 × *o*-CH_3, Mes), 4.88 (m, 2H, C^5H=C^6H, cod), 5.51 (m, 2H, C^1H=C^2H, cod), 6.87 (s, 4H, 4 × *m-H*, Mes), 6.88 (d, ^3J(H,H) = 7.5 Hz, 2 × *m-H*, C_6H_3), 7.18 (t, ^3J(H,H) = 7.5 Hz, 1H, *p-H*, C_6H_3).

Dieses Werk ist copyrightgeschützt und darf in keiner Form vervielfältigt werden noch an Dritte weitergegeben werden.
Es gilt nur für den persönlichen Gebrauch.

$^{13}\mathrm{C}\{^{1}\mathrm{H}\}$ NMR: (75.47 MHz, C_6D_6, 303 K, ppm): δ = 21.3 (s, 2 × *p*-CH$_3$, Mes), 22.2 (s, 4 × *o*-CH$_3$, Mes), 27.0 (s, 2C, $C^{3,8}H_2$, cod), 31.1 (s, 2C, $C^{4,7}H_2$, cod), 102.2 (s, $C^{5}H{=}C^{6}H$, cod), 126.4 (s, $C^{1}H{=}C^{2}H$, cod), 128.9 (s, 4 × *m*-CH, Mes), 129.4 (s, 2 × *m*-CH, C_6H_3), 131.3 (s, *p*-CH, C_6H_3), 137.4 (s, 2 × *p*-C, Mes), 138.1 (s, 4 × *o*-C, Mes), 139.0 (s, 2 × *ipso*-C, Mes), 143.9 (s, *ipso*-C, C_6H_3), 148.4 (2 × *o*-C, C_6H_3).

$^{119}\mathrm{Sn}\{^{1}\mathrm{H}\}$ NMR: (111.9 MHz, C_6D_6, 303 K, ppm): δ = –211.5 (s).

4.5.2 [PdCl{SnCl$_2$(2,6-Mes$_2$-C$_6$H$_3$)}(dppe)] (4-Pd)

1-Sn (0.233 g, 0.498 mmol) and [PdCl$_2$(dppe)] (0.288 g, 0.500 mmol) were weighted in a Schlenk tube. Toluene (20 mL) was pre-cooled (–78 °C) and added to the mixture at –78 °C with stirring. The suspension was stirred for 5 min at –78 °C and then allowed to warm to room temperature. Stirring was continued for 2 h at ambient temperature, and the resulting yellow suspension was concentrated to approximately half the volume and cooled for 2 h at –40 °C. The supernatant solution was removed by cannula filtration, and the bright yellow precipitate dried *in vacuo* overnight at ambient temperature. The obtained solid was stirred in 20 mL of pentane for 15 min, the pentane washing was discarded and the bright yellow solid dried *in vacuo* to afford compound **4-Pd**. Yield: 0.130 g (0.125 mmol, 25%) Crystals suitable for X-ray crystallographic analysis were grown at 6 °C from a concentrated C_6D_6 solution of **4-Pd** and crystallised with included C_6D_6 molecules.

Properties: Very soluble in CH_2Cl_2, only sparingly in benzene. Moderately air stable.

Melting Point: 191 – 195 °C (dec.)

Elemental analysis: calcd (%) for $C_{50}H_{49}Cl_3P_2PdSn$ (1043.27 g.mol^{-1}): C 57.56, H 4.73; found: C 57.16, H 4.78%.

Dieses Werk ist copyrightgeschützt und darf in keiner Form vervielfältigt werden noch an Dritte weitergegeben werden.
Es gilt nur für den persönlichen Gebrauch.

Spectroscopic Data:

^{1}H NMR: (300.1 MHz, CD_2Cl_2, 303 K, ppm): δ = 2.02 (s, 12H, 4 × *o–*$\mathit{CH_3}$, Mes), 2.16 (s, 12H, 2 × *p–*C$\mathit{H_3}$, Mes), 2.37 (m, 2H, C$\mathit{H_2}$, dppe), 2.47 (m, 2H, C$\mathit{H_2}$, dppe), 6.54 (s, 4H, 4 × *m–H*, Mes), 6.89 (d, ^{3}J(H,H) = 7.6 Hz, 2H, 2 × *m–H*, C_6H_3), 7.37 (t, ^{3}J(H,H) = 7.6 Hz, 1H, *p–H*, C_6H_3), 7.42 – 7.79 (several multiplets, 20H, 4 × $C_6\mathit{H_5}$, dppe).

^{13}C{^{1}H} NMR: (75.47 MHz, CD_2Cl_2, 303 K, ppm): δ = 21.3 (s, 2 × *p–C*H_3, Mes), 21.9 (s, 4 × *o–C*H_3, Mes), 24.1 (dd, ^{1}J(C,P) = 27.8 Hz, ^{2}J(C, P) = 10.1 Hz,1 × *C*H_2, dppe), 33.7 (dd, ^{1}J(C,P) = = 33.9 Hz, ^{2}J(C,P) = 23.9 Hz 1 × *C*H_2, dppe), 128.3 (s, 4 × *m–C*H, C_6H_3), 129.2 (d, ^{3}J(C,P) = 11.3 Hz, 4 × *m–C*H, Ph, dppe), 129.3 (s, 2 × *m–C*H or *p–C*H, C_6H_3), 129.5 (d, ^{3}J(C,P) = 10.3 Hz, 4 × *m-C*H, dppe), 129.67 (d, ^{n}J(C,P) = 20.2 Hz, 2 × *ipso–C* ,Ph, dppe), 129.70 (s, 2 × *m–C*H or *p–C*H, C_6H_3), 130.3 (d, ^{n}J(C,P) = 6.8 Hz, Sn–*C*, C_6H_3), 131.98 (d, ^{4}J(C,P) = 2.6 Hz, 2 × *p-C*, Ph, dppe), 132.14 (d, ^{4}J(C,P) = 2.6 Hz, 2 × *p-C*, Ph, dppe), 133.5 (d, ^{2}J(C,P) = 11.0 Hz, 4 × *o-C*, Ph, dppe), 134.1 (d, ^{2}J(C,P) = 12.3 Hz, 4 × *o-C*, Ph, dppe), 136.3 (s, 4 × *o-C*, Mes), 137.5 (s, 2 × *ipso-C* or 2 × *p-C*, Mes), 140.0 (s, 2 × *ipso-C* or 2 × *p-C*, Mes), 148.5 (s, 2 × *o-C*, C_6H_3) 150.1 (d, ^{n}J(C,P) = 33.6 Hz, 2 × *ipso-C*, Ph, dppe).

^{31}P{^{1}H} NMR: (121.5 MHz, CD_2Cl_2, 303 K, ppm): δ = 49.8 (d, ^{2}J(P,P) = 26.7 Hz, ^{2}J(P,^{119}Sn) = 3812 Hz, ^{2}J(P,^{117}Sn) = 3643 Hz), 55.3 (d, ^{2}J(P,P) = 26.7 Hz, ^{2}J(P,^{119}Sn) = 145 Hz, ^{2}J(P,^{117}Sn) = 139 Hz).

^{119}Sn{^{1}H} NMR: (111.9 MHz, CD_2Cl_2, 303 K, ppm): δ = –57.1 (dd, ^{2}J(^{119}Sn,^{31}P) = 3812 Hz, ^{2}J(^{119}Sn,^{31}P) = 145 Hz).

m/z: 1079 (M^+ + Cl), 1942 (M^+), 1007 (M^+- Cl), 972 (M^+- 2Cl), 904 (M^+- 3Cl), 752 (M^+- 3Cl – 2 Ph), 730, 649, 620 (M^+- 3 Cl – 4 Ph), 539 [Pd-Sn($C_6H_3Mes_2$)]$^+$, 504 [Pd(dppe)]$^+$, 433 [Sn($C_6H_3Mes_2$)]$^+$, 397 [dppe]$^+$, 314 [$C_6H_3Mes_2$]$^+$

Dieses Werk ist copyrightgeschützt und darf in keiner Form vervielfältigt werden noch an Dritte weitergegeben werden.
Es gilt nur für den persönlichen Gebrauch.

4.5.3 [PdCl(SnCl$_3$)(cod)] (6-Pd)

A mixture of **1-Pd** (0.200 g, 0.700 mmol) and SnCl$_2$ (0.132 g, 0.696 mmol) was suspended in 10 mL of toluene. After stirring for 10 min at ambient temperature, 5 mL of CH$_2$Cl$_2$ was added to the suspension. The reaction mixture was stirred overnight at room temperature. The resulting yellow suspension, with an orange supernatant solution was stored at –30 °C overnight. A yellow-green precipitate was separated from the orange supernatant solution by filtration and dried *in vacuo* at ambient temperature to afford compound **6-Pd**. Yield: 0.257 g (0.541 mmol, 78 %). Crystals suitable for X-ray crystallographic analysis were grown from CH$_2$Cl$_2$ at –30 °C.

Properties: Soluble in CH$_2$Cl$_2$, insoluble in benzene.

Melting Point.: 191 – 195 °C (dec.).

Elemental analysis: calcd (%) for $C_8H_{12}Cl_4PdSn$ (475.12 g.mol^{-1}): C 20.22, H 2.55; found: C 20.35, H 2.56%.

Spectroscopic Data:

FIR (polyethylene, cm^{-1}): ν = 432 (w), 379 (w), 355 (m, sh), 334 (s), 303 (m), 279 (w), 138 (w), 90 (m).

^{1}H NMR: (300.1 MHz, CD$_2$Cl$_2$, 303 K, ppm): δ = 2.69 (br s, 4H, 2 × CH_2, cod), 2.75 (br s, 4H, 2 × CH_2, cod), 5.94 (br s, 2H, C$^5\mathit{H}$=C$^6\mathit{H}$, cod), 6.38 (br s, 2H, C$^1\mathit{H}$=C$^2\mathit{H}$, cod).

^{13}C{^{1}H} NMR: (75.47 MHz, CD$_2$Cl$_2$, 303 K, ppm): δ = 28.4 (s, 2 × CH$_2$, cod), 32.5 (s, 2 × CH$_2$, cod), 107.8 (s, C^5H=C^6H, cod), 129.5 (s, C^1H=C^2H, cod).

^{119}Sn{^{1}H} NMR: (111.9 MHz, CD$_2$Cl$_2$, 303 K, ppm): δ = – 310.8 (s)

Dieses Werk ist copyrightgeschützt und darf in keiner Form vervielfältigt werden noch an Dritte weitergegeben werden.
Es gilt nur für den persönlichen Gebrauch.

4.5.4 [PdCl($GeCl_3$)(cod)] (7-Pd)

1-Pd (0.185 g; 0.648 mmol) and $GeCl_2$·(1,4-dioxane) were added to a Schlenk tube. CH_2Cl_2 (15 mL) was added to the mixture at –78 °C with rapid stirring. The resulting suspension (bright yellow) was stirred at –78 °C for 0.5 h, and then allowed to warm to room temperature and stirred overnight. The resulting translucent yellow solution was concentrated *in vacuo* to incipient crystallisation, and subsequently cooled for 6 h at –30 °C then at –60 °C overnight. A bright yellow, micro-crystalline precipitate was formed, isolated by filtration at –78 °C and dried *in vacuo* at room temperature for 1 h. A second crop of the product was obtained upon concentration of the mother liquor, and cooling to –60 °C, and isolating the resulting yellow solid again by cannula filtration and drying it *in vacuo* for 1 h at room temperature. Combined yield: 0.271 g (0.632 mmol, 98 %). Crystals suitable for X-ray crystallographic analysis were grown from CH_2Cl_2 at –30 °C.

Properties: Soluble in CH_2Cl_2, insoluble in benzene.

Melting Point.: 160 – 164 ° C.

Elemental analysis: calcd (%) for $C_8H_{12}Cl_4GePd$ (428.97 g.mol^{-1}): C 22.39, H 2.82;
found: C 22.40, H 2.99 %.

Spectroscopic Data:

FIR (polyethylene, cm^{-1}): $\nu = 435$ (w), 390 (m, sh), 375 (s), 345 (m), 311 (m), 279 (w), 252 (w), 214 (w), 178 (vw), 162 (m), 151 (m), 108 (w).

^{1}H NMR: (300.1 MHz, CD_2Cl_2, 303 K, ppm): $\delta = 2.63 - 2.72$ (m, 4H, 2 × CH_2, cod), 2.73 – 2.87 (m, 4H, 2 × CH_2, cod), 5.91 (m, $C^5H{=}C^6H$, cod), 6.37 (m, $C^1H{=}C^2H$, cod).

$^{13}C\{^1H\}$ NMR: (75.47 MHz, CD_2Cl_2, 303 K, ppm): $\delta = 28.5$ (s, 2 × CH_2, cod), 32.4 (s, 2 × CH_2, cod), 111.1 (s, $C^5H{=}C^6H$, cod), 129.0 (s, $C^1H{=}C^2H$, cod).

Dieses Werk ist copyrightgeschützt und darf in keiner Form vervielfältigt werden noch an Dritte weitergegeben werden.
Es gilt nur für den persönlichen Gebrauch.

4.5.6 [(depe)$_2$Fe=SnCl(2,6-Mes$_2$-C$_6$H$_3$)] (3-Fe)

A Schlenk tube was charged with **1-Sn** (0.312 g, 0.667 mmol) and **1-Fe** (0.332 g, 0.669 mmol) in the glove-box. Pre-cooled pentane (50 mL, –78 °C) was added *via* cannula to this solid mixture with rapid stirring, as the vessel was submerged in a –78 °C bath. The reaction was stirred at –78 °C for 5 minutes, after which it was taken out of the cold bath and stirred at room temperature for 4 h. an immediate colour change to brown is noticed on addition of the solvent to the reaction mixture. (The reaction was followed by *in-situ* ^{31}P{^{1}H} NMR spectroscopy which showed consumption of **1-Fe** after 2h, and the formation of a new singlet resonance signal at δ = 77 ppm). At this point the reaction solution took on a dark brown colour. The reaction solution was filtered *via* cannula and the residue was extracted with pentane (2 × 10 mL), and the filtrates combined. The resulting dark brown solution was concentrated to *ca*. 5 mL, and cooled to –30 °C for 1 h, then –60 °C overnight, resulting in a dark brown solid as precipitate. This precipitate was collected by filtering off the mother liquor (at –60 °C) *via* cannula, discarding it, and drying the remaining dark brown solid *in vacuo* for 2 h at ambient temperature, yielding **3-Fe** as a product. Yield: 0.490 g (0.524 mmol, 78 %). Crystals suitable for X-ray crystallographic analysis were grown from Et$_2$O at –30 °C in the glove-box.

Properties: Soluble in Et$_2$O, pentane, benzene and THF. Very air sensitive: turns colourless on contact with air, and susceptible to hydrolysis.

Melting Point: 148 – 152°C (dec.).

Elemental analysis: calcd (%) for $C_{44}H_{73}ClFeP_4Sn$ (935.95 g.mol^{-1}): C 56.45, H 7.86; found: C 55.39, H 7.65 %.

Spectroscopic data:

IR (NaCl plates, nujol, cm^{-1}): ν = 2938 (br s), 2907(s), 2899(s), 2827 (br s), 1612 (br vw), 1579 (br w), 1310 (br vw), 1239 (br vw), 1174 (br vw), 1019 (br w), 867 (br vw), 866 (w), 798 (w), 734 (m), 693 (vw), 657 (br vw), 609 (br vw).

Dieses Werk ist copyrightgeschützt und darf in keiner Form vervielfältigt werden noch an Dritte weitergegeben werden.
Es gilt nur für den persönlichen Gebrauch.

$^{1}H\{^{31}P\}$ NMR: (300.1 MHz, C_6D_6, 298 K, ppm): $\delta = 0.85$ (dd, ^{3}J(H,H) = 7.6 Hz, ^{3}J(H,H) = 7.5 Hz 12H, 4 × CH_3^{X}), 0.96 (dd, ^{3}J(H,H) = 7.5 Hz, ^{3}J(H,H) = 7.6 Hz, 12H, 4 × CH_3^{Y}), 1.03 – 1.12 (m, 8H, 2 × P-$CH^{1}H^{2}CH^{1}H^{2}$), 1.24 (dq, ^{2}J(H,H) = 14.4 Hz, ^{3}J(H,H) = 7.6 Hz, 4H, 4 × $CH^{1}H^{2}CH_3^{Y}$), 1.27 (dq, ^{2}J(H,H) = 14.6 Hz, ^{3}J(H,H) = 7.6 Hz 4H, 4 × $CH^{1}H^{2}CH_3^{X}$), 1.68 (dq, ^{2}J(H,H) = 14.6 Hz, ^{3}J(H,H) = 7.5 Hz, 4H, 4 × $CH^{1}H^{2}CH_3^{X}$), 1.79 (dq, ^{2}J(H,H) = 14.4 Hz, ^{3}J(H,H) = 7.5 Hz, 4H, 4 × $CH^{1}H^{2}CH_3^{Y}$),[*] 2.20 (s, 6H, 2 × C^{2}-CH_3, Mes), 2.23 (s, 6H, 2 × C^{4}-CH_3, Mes), 2.76 (s, 6H, 2 × C^{6}-CH_3, Mes), 6.77 (s, 2H, 2 × C^{3}-H, Mes), 6.86 (s, 2H, 2 × C^{5}-H, Mes), 7.05 (d, ^{3}J (H,H) = 7.5 Hz, 2H, $C^{3,5}$-H, C_6H_3), 7.27 (t, ^{3}J (H,H) = 7.5 Hz, 1H, C^{4}-H, C_6H_3).

^{1}H NMR: (300.1 MHz, THF-d_8, 298 K, ppm): $\delta = 0.95$ (br $\Delta\nu_{½}$ = 28.6 Hz, 24H, 4 × CH_3^{X} + 4 × CH_3^{Y}), 1.05 – 1.32 (br m, 12H, 2 × P-$CH^{1}H^{2}CH^{1}H^{2}$ + 4 × $CH^{1}H^{2}CH_3^{Y}$), 1.32 – 1.50 (br m, 4H, 4 × $CH^{1}H^{2}CH_3^{X}$), 1.61 – 1.89 (br m underneath solvent signal, 8H, 4 × $CH^{1}H^{2}CH_3^{Y}$ + 4 × $CH^{1}H^{2}CH_3^{X}$), 2.03 (s $\Delta\nu_{½}$ = 9.8 Hz, 6H, 2 × C^{2}-CH_3, Mes), 2.23 (s $\Delta\nu_{½}$ = 8.1 Hz, 6H, 2 × C^{4}-CH_3, Mes), 2.34 (s $\Delta\nu_{½}$ = 8.8 Hz, 6H, 2 × C^{6}-CH_3, Mes), 6.73 (s $\Delta\nu_{½}$ = 9.9 Hz, 2 × C^{3}-H, Mes), 6.81 (s $\Delta\nu_{½}$ = 11.0 Hz, 2 × C^{5}-H, Mes), 6.87 (d, ^{3}J(H,H) = 6.9 Hz, 2H, $C^{3,5}$-H, C_6H_3), 7.24 (ps t, 1H, C^{4}-H, C_6H_3).

$^{31}P\{^{1}H\}$ NMR: (121.5 MHz, C_6D_6, 298 K, ppm): $\delta = 76.75$ (s, $^{2}J(^{119/117}Sn, P)$ = 100 Hz) $\Delta\nu_{½}$ = 3.1 Hz.

$^{31}P\{^{1}H\}$ NMR: (121.5 MHz, THF-d_8, 298 K, ppm): $\delta = 77.05$ (s, $^{2}J(^{119/117}Sn, P)$ = 103 Hz) $\Delta\nu_{½}$ = 4.1 Hz.

$^{13}C\{^{1}H\}$ NMR: (75.47 MHz, C_6D_6, 298 K, ppm): $\delta = 9.7$ (s, 4 × CH_3^{X}), 9.9 (s, 4 × CH_3^{Y}), 21.3 (s, 2 × C^{4}-CH_3, Mes), 22.5 (s, 2 × $C^{2-}CH_3$, Mes), 23.3 (s, 2 × C^{6}-CH_3), 23.9 (m, 4 × P-CH_2), 26.7 (m, 4 × $CH_3^{X}CH_2$), 31.8 (m, 4 ×

---

[*] Coupling constants retrieved by simulation.

Dieses Werk ist copyrightgeschützt und darf in keiner Form vervielfältigt werden noch an Dritte weitergegeben werden.
Es gilt nur für den persönlichen Gebrauch.

$CH_3{}^Y\mathit{C}H_2$), 127.6 (s, 1 × C^4, C_6H_3), 128.1 (signal obscured by resonance signal of the solvent, 2 × C^3-H, Mes), 129.25 (s, 2 × C^5-H, Mes), 129.3 (s, $C^{3,5}$-H, C_6H_3), 135.7 (s, 2 × C^4, Mes), 136.3 (s, 2 × C^2, Mes), 138.8 (s, 2 × C^6, Mes), 141.9 (s, 2 × C^1, Mes), 146.1 (s, $C^{2,6}$, C_6H_3), 175.1 (s, C^1, C_6H_3).

$^{13}C\{^1H\}$ NMR: (75.47 MHz, THF-d_8, 298 K, ppm): δ = 9.8 (s, 4 × $CH_3{}^X$), 10.1 (s, 4 × $CH_3{}^Y$), 21.4 (s, 2 × C^4-CH_3, Mes), 22.7 (s, 2 × C^2-CH_3, Mes), 23.2 (s, 2 × C^6-CH_3, Mes), 24.3 (quint, $^1J(^{13}C, P)$ = 12.2 Hz, 4 × P-CH_2), 27.2 (br, 4 x $CH_3{}^X\mathit{C}H_2$), 32.0 (quint, $^1J(^{13}C, P)$ = 6.0 Hz, 4 x $CH_3{}^Y\mathit{C}H_2$), 127.5 (s, C^4-H, C_6H_3), 128.6 (s, 2 × C^3-H, Mes), 129.4 (s, 2 × C^5-H, Mes + $C^{3,5}$-H, C_6H_3), 136.3 (s, 2 × C^4, Mes), 136.8 (s, 2 × C^2, Mes), 138.7 (s, 2 × C^6, Mes), 142.2 (s, 2 × C^1, Mes), 146.5 (s, $C^{2,6}$, C_6H_3), 175.5 (s, C^1, C_6H_3).

$^{119}Sn\{^1H\}$ NMR: (111.92 MHz, C_6D_6, 298 K, ppm): δ = 471.5 (quint, $^2J(^{119}Sn,^{31}P)$ = 100 Hz).

$^{119}Sn\{^1H\}$ NMR: (111.92 MHz, THF-d_8, 298 K, ppm): δ = 461.5 (quint, $^2J(^{119}Sn,^{31}P)$ = 106 Hz).

^{57}Fe Mößbauer (80 K, mms^{-1}): $\delta = 0.31$, $\Delta E_Q = 1.00$

UV-Vis (THF): λ_{max} = 431 nm, ε = 4142.1 l·mol^{-1}·cm^{-1}

4.5.7 [(depe)$_2$Fe≡Sn(2,6-Mes$_2$-C$_6$H$_3$)][SnCl$_2$(2,6-Mes$_2$-C$_6$H$_3$)] (4-Fe)

Method 1 : Direct synthesis from **1-Fe**

A Schlenk tube was charged with **1-Fe** (0.200g, 0.403 mmol) and **1-Sn** (0.376 g, 0.804 mmol) and placed in a –78 °C bath. Pre-cooled (–78 °C) pentane (60 mL) was added *via* cannula to this mixture with rapid stirring under exclusion of light. The mixture was stirred for 5 minutes at –78 °C and then at room temperature. On stirring at room temperature a orange-brown suspension was observed, with a red supernatant. The intensity of this red

Dieses Werk ist copyrightgeschützt und darf in keiner Form vervielfältigt werden noch an Dritte weitergegeben werden.
Es gilt nur für den persönlichen Gebrauch.

colour decreased with time, and at 2 h reaction time it was concentrated *in vacuo* to 5 mL and the supernatant filtered off at room temperature, with a dark brown solid remaining. (The filtrate was evaporated to dryness and the remaining residue (10 mg) discarded). The brown solid was dissolved in a minimum amount of toluene and pentane added till incipience (1 : 2) and stored at –30 °C for 2 days. The mother liquor was filtered off at –40 °C, discarded, and the remaining brown solid washed with pentane (3 × 10 mL) and dried *in vacuo* for 3 h at room temperature. Yield: 0.408 g (0.291 mmol, 72 %). Crystals, suitable for X-ray diffraction analysis were grown from a concentrated toluene solution, to which pentane was added drop wise until it went cloudy, and then cooled to 6 °C.

Method 2 : Synthesis from [(depe)Fe=SnCl(2,6-Mes_2-C_6H_3)]:

A Schlenk tube was charged with **3-Fe** (0.280 g, 0.299 mmol) and **1-Sn** (0.140 g, 0.299 mmol) and thoroughly mixed. Pentane (20 mL) was added to this solid mixture *via* cannula at room temperature under rapid stirring. The reaction was allowed to stir at room temperature for 2 h during which the formation of a pentane insoluble brown precipitate was noticed, with a brown supernatant liquid. The filtrate was separated from the brown solid by cannula filtration, the filtrate discarded, and the remaining brown residue washed with pentane (3 × 10 mL), the washings were also discarded. The brown residue was dried *in vacuo* at room temperature for 1 h. Yield: 0.306 g (0.218 mmol, 73 %).

Properties: insoluble in pentane, soluble benzene and very soluble in THF. Very air sensitive: turns colourless on contact with air.

Melting Point: 229 – 232 °C (dec.).

Elemental analysis: calcd (%) for $C_{68}H_{98}Cl_2FeP_4Sn_2$ (1403.57 g.mol^{-1}): C 58.19, H 7.04; found C 57.88, H 7.03 %.

Spectroscopic data:

IR (nujol, cm^{-1}): (KBr) ν = 2940(s), 2914(s), 2727(s), 2359(vw), 1610 (m) [ν(C=C), *m*-terphenyl)], 1569 (m) [ν(C=C), *m*-terphenyl)], 1419 (w), 1301 (vw), 1247 (w), 1169 (w), 1130 (vw), 1093 (vw), 1077 (w), 1076 (w), 1021 (m), 1001 (m), 985 (m), 871 (w), 849 (m), 849.5 (m), 800 (m), 758

Dieses Werk ist copyrightgeschützt und darf in keiner Form vervielfältigt werden noch an Dritte weitergegeben werden.
Es gilt nur für den persönlichen Gebrauch.

(m), 752 (m), 732 (m), 696 (w), 692 (w), 683 (w), 668 (w), 659 (w), 613 (w), 589 (w), 573 (vw), 547 (vw), 505 (vw), 459 (vw), 447 (w), 413 (m).

^{1}H NMR: (300.1 MHz, C_6D_6, 298 K, ppm): δ = 0.77 (br, 24H, 8 × $\mathrm{C}H_3^{X+Y}$), 0.94 (br, 8H, 4 × $\mathrm{C}H_2$), 1.14 (br, 8H, 4 × $\mathrm{C}H_2$), 1.41 (br, 8H, 4 × $\mathrm{C}H_2$), 2.00 (s br, 12H, 4 × *o*–$\mathrm{C}H_3$, Mes^{B}), 2.20 (s br, 6H, 2 × *p*-$\mathrm{C}H_3$, Mes^{B}), 2.32 (s br, 6H, 2 × *p*-$\mathrm{C}H_3$, Mes^{A}), 2.60 (s br, 12 H, 4 × *o*-$\mathrm{C}H_3$, Mes^{A}), 6.74 (m br, 4H, 4 × *m-H*, Mes^{B}) + (1H, 1 × *p-H*, $C_6H_3^{B}$) + (2H, 2 × *m-H*, $C_6H_3^{B}$), 7.00 (s, 4H, 4 × *m-H*, Mes^{A}), 7.15 (signal obscured by the resonance signal of the solvent, 2H, 2 × *m-H*, $C_6H_3^{A}$), 7.36 (ps t, 1H, 1 × *p-H*, $C_6H_3^{A}$).

^{31}P{^{1}H} NMR: (121.5 MHz, C_6D_6, 298 K, ppm): δ = 77.0 (s).

^{13}C{^{1}H} NMR: (75.47 MHz, C_6D_6, 298 K, ppm): δ = 9.4 (s, 4C, 4 × $\mathrm{CH_2}C\mathrm{H}_3^{X}$), 9.6 (s, 4C, 4 × $\mathrm{CH_2}C\mathrm{H}_3^{Y}$), 20.9 (s, 4C, 4 × *o*–$CH_3$, Mes^{B}), 21.1 (s, 2C, 2 × *p*-$C\mathrm{H}_3$, Mes^{B}), 21.6 (s, 2C, 2 × *p*-$C\mathrm{H}_3$, Mes^{A}), 22.6 (s, 4C, 4 × *o*-$C\mathrm{H}_3$, Mes^{A}), 24.8 (m br, 8C, 8 × $C\mathrm{H}_2$), 33.7 (m br, 4C, 4 × $C\mathrm{H}_2$), 127.5 (s, 1C, 1 × *p-C*, $C_6H_3^{A}$), 128.2 (s, 2C, 2 × *m-C*, $C_6H_3^{A}$), 128.3 (s, 4C, 4 × *m-C*, Mes^{A}), 128.4 (s, 1C, 1 × *p-C*, $C_6H_3^{B}$), 129.3 (s, 4C, 4 × *m-C*, Mes^{B}), 135.1, 135.7, 136.2, 136.5, 137.4 (s, 2C, 2 × *p-C*, Mes^{A}), 139.4 (m br), 142.0 (s, 2C, 2 × C^{1}, Mes^{A}), 146.0, 149.4 (s, 2C, 2 × *o-C*, $C_6H_3^{A}$), 173.1 (s br, ipso-*C*, $C_6H_3^{A+B}$).

^{119}Sn{^{1}H} NMR: (111.92 MHz, C_6D_6, 298 K, ppm): δ= 208.8 ppm ($\Delta\nu_{½}$ = 1162 Hz, line broadening value = 15 Hz), no other signals detectible.

^{57}Fe Mößbauer Spectroscopy (mms^{-1}): δ = 0.31, ΔE_Q = 0.67 (59.60 %) (Square pyramidal isomer); δ = 0.31, ΔE_Q = 1.22 (34.57 %) (Trigonal bipyramidal isomer).

UV-Vis (THF): λ = 429 nm, ε = 6055.7 l·mol^{-1}·cm^{-1} (similar λ value as with **3-Fe**)

Dieses Werk ist copyrightgeschützt und darf in keiner Form vervielfältigt werden noch an Dritte weitergegeben werden.
Es gilt nur für den persönlichen Gebrauch.

4.5.8 $[(\mathrm{depe})_2\mathrm{Fe{\equiv}Sn}(2,6\text{-}\mathrm{Mes}_2\text{-}\mathrm{C}_6\mathrm{H}_3)][\mathrm{BCl}(\mathrm{C}_6\mathrm{F}_5)_3]$ (5-Fe)

To a pentane (8 mL) solution of **1-Fe** (0.250 g, 0.504 mmol), was added a toluene (10 mL) solution of **1-Sn** (0.239 g, 0.511 mmol) drop wise at room temperature with rapid stirring. A colour change to dark brown was noticed, indicating the *in situ* formation of **3-Fe**. This reaction was stirred at room temperature for 2 h. The brown solution was filtered *via* cannula in the glove box, into another Schlenk tube, and a toluene solution (2 mL) of $B(C_6F_5)_3$ (0.262 g, 0.511 mmol) was added to it drop wise at room temperature. The intensity of the brown colour darkens on addition of the $B(C_6F_5)_3$ to the solution. The reaction was stirred for a further 3.5 h at room temperature, and the solvent removed *in vacuo*. The remaining brown solid was suspended in 5 ml pentane, stirred for 1 minute, and the pentane removed *in vacuo*. The brown solid was washed with pentane (3 × 8 mL), the pentane washings discarded, and the brown solid subsequently frozen in a liquid nitrogen bath and scratched into a fine powder, and dried *in vacuo*. This powder was subsequently dissolved in a minimum amount of toluene and pentane added until incipience, and cooled to –30 °C overnight. The recrystallised brown solid was isolated by cannula filtration at –30 °C, the brown filtrate discarded, and the remaining brown powder dried *in vacuo* at room temperature for 1 h. Yield: 0.430 g (0.297 mmol, 59 %). Crystals suitable for X-ray crystallography were grown from a 1:1 toluene : pentane solution of the substance at – 30°C.

Elemental analysis: calcd (%) for $C_{62}H_{73}FeClBF_{15}SnP_4$ (1447.93 g.mol^{-1}): C 51.43, H 5.08; found : C 50.15, H 4.51.

Spectroscopic Data:

^{1}H NMR: (300.13 MHz, C_6D_6, 298 K, ppm): $\delta = 0.69$ (br s, 12H, 4 x CH_3^{A}), 0.80 (br s, 12H, 4 x CH_3^{B}), 0.95 (br m, CH_2), 1.38 (br m, CH_2), 1.94 (s, 12H, *o*-CH_3, Mes), 2.22 (s, 6H, *p*-CH_3, Mes), 6.70 (left line of signal overlapping with singlet signal at 6.73 ppm) (ps d, 2H, $C^{3,5}$-*H*, C_6H_3), 6.73 (s, 4H, $C^{3,5}$-*H*, Mes), 7.22 (t, ^{3}J(H,H) = 7.5 Hz, 1H, C^{4}-*H*, C_6H_3)

^{31}P{^{1}H} NMR: (121.49 MHz, C_6D_6, 298 K, ppm): $\delta = 77.2$ (s) ppm.

Dieses Werk ist copyrightgeschützt und darf in keiner Form vervielfältigt werden noch an Dritte weitergegeben werden.
Es gilt nur für den persönlichen Gebrauch.

$^{11}B\{^{1}H\}$ NMR: (96.29 MHz, C_6D_6, 298 K, ppm): $\delta = -7.4$ (br s).

$^{19}F\{^{1}H\}$ NMR: (470.59 MHz, C_6D_6, 298 K, ppm): $\delta = -166.7$ (td, ^{3}J(F,F) = 22.0 Hz, ^{3}J(F,F) = 5.6 Hz, 6F, *m*-F, BAr_f), –162.3 (t, ^{3}J(F,F) = 20.1 Hz, 3F, *p*-F, BAr_f), –131.3 (ps q, 6F, *o*-F, BAr_f).

4.5.9 [(depe)$_2$Fe≡Sn(2,6-Mes$_2$-C$_6$H$_3$)][B(3,5-(CF$_3$)$_2$-C$_6$H$_3$)$_4$] (6-Fe)

To a solution of **3-Fe** (0.550, 0.588 mmol) in 20 mL of toluene, was added, with rapid stirring at room temperature, $Na[B\{C_6H_3\text{-}3,5\text{-}(CF_3)_2\}_4]$ (0.520 g, 0.588 mmol) in small portions, as a solid to the reaction. On complete addition of the $Na[B\{C_6H_3\text{-}3,5\text{-}(CF_3)_2\}_4]$, the Schlenk tube was rinsed down with an additional 10 mL toluene, to ensure all the solid $Na[B\{C_6H_3\text{-}3,5\text{-}(CF_3)_2\}_4]$ entered the reaction mixture. The reaction was stirred overnight in the glove box, and then 5 mL of pentane was added to the mixture, and it was filtered. The filtrate was discarded, and the remaining brown residue was rinsed with an additional portion of Toluene : pentane (10:1) (11 mL) and the filtrate removed again by filtration at room temperature, and again discarded. At this point a combination of ^{1}H and $^{31}P\{^{1}H\}$ NMR spectroscopy showed the brown residue to be almost entirely pure. To remove the NaCl formed during the reaction, the remaining brown residue was extracted with fluorobenzene : pentane (5 : 1) (24 mL), the brown filtrate evaporated to dryness, and dried *in vacuo* for 2 h at room temperature, yielding a brown solid as product. Yield: 0.616 g (0.349 mmol, 59 %).

Properties: insoluble in pentane and benzene / toluene and very soluble in THF, and fluorobenzene. Very air sensitive: turns colourless on contact with air.

Melting Point: 138 – 139 °C (dec).

Elemental analysis: calcd (%) for $C_{76}H_{85}FeBF_{24}SnP_4$ (1763.7 g.mol^{-1}): C 51.76, H 4.86; found: C 51.34, H 4.75.

Spectroscopic data:

Dieses Werk ist copyrightgeschützt und darf in keiner Form vervielfältigt werden noch an Dritte weitergegeben werden.
Es gilt nur für den persönlichen Gebrauch.

^{1}H NMR: (500.13 MHz, THF-d_8, 298 K, ppm): δ = 0.93 (br m, 12H, 4 × CH_3^{A}), 1.10 (br m, 12H, 4 × CH_3^{B}), 1.24 (br, 4H, 2 × P-CH^{X}H^{Y}CH^{X}H^{Y}-P), 1.33 (m, 4H, 4 × CH$_3^{A}$CH^{X}H^{Y}) + (m, 4H, 2 × CH$_3^{B}$CH^{X}H^{Y}), 1.72 (br m, 4H, 4 × CH$_3^{B}$CH^{X}H^{Y}) + (m, 4H, 4 × CH$_3^{A}$CH^{X}H^{Y}), 1.83 (br m, 4H, 2 × P-CH^{X}H^{Y}CH^{X}H^{Y}-P), 2.08 (s, 12H, 4 × o-CH_3, Mes), 2.35 (s, 2 × p-CH_3, Mes), 6.99 (s, 4H, C^{3,5}-H, Mes), 7.03 (d, ^{3}J(H,H) = 7.6 Hz, C$^{3.5}$-H, C$_6$H$_3$), 7.59 (br s, 4H, C^{4}-H, BAr$_f$), 7.60 (t, ^{3}J(H,H) = 7.6 Hz, 1H, C^{4}-H, C$_6$H$_3$), 7.80 (t, ^{4}J(H,H) = 2.3 Hz, 8H, C^{2,6}-H, BAr$_f$).

^{11}B{^{1}H} NMR: (96.29 MHz, THF-d_8, 298 K, ppm): δ = –6.5 ppm.

^{19}F{^{1}H} NMR: (470.59 MHz, THF-d_8, 298 K, ppm): δ = –63.3 (s, 8 × CF_3, BAr$_f$) ppm.

^{31}P{^{1}H} NMR: (202.45 MHz, THF-d_8, 298 K, ppm): δ = 77.5 (s) ppm.

^{119}Sn{^{1}H} NMR: (186.5 MHz, THF-d_8, 298 K, ppm): δ = 983 (br s) ppm.

^{13}C{^{1}H} NMR: (125.76 MHz, THF-d_8, 298 K): δ = 9.2 (s, 4 × CH$_3^{A}$), 9.8 (s, 4 × CH$_3^{B}$), 21.3 (s, 2 × p-CH$_3$, Mes), 21.4 (s, 4 × o-CH$_3$, Mes), 25.0 – 25.6 (m (unresolved), CH$_2$), 35.4 (CH$_2$), 118.2 (s, 4 × C^{4}-H, BAr$_f$), 125.5 (q, ^{1}J(^{13}C,^{19}F) = 272 Hz, 4 × C^{3,5}-CF$_3$, BAr$_f$), 129.6 (s, $C^{3,5}$-H, C$_6$H$_3$), 130.0 (qq, ^{3}J(^{13}C,^{11}B) = 3.0 Hz; ^{2}J(^{13}C,^{19}F) = 32 Hz, 4 × $C^{3,5}$-CF$_3$, BAr$_f$), 130.1 (s, $C^{3,5}$-H, Mes), 131.3 (s, C^{4}-H, C$_6$H$_3$) 135.6 (s, 4 × $C^{2,6}$, BAr$_f$), 137.0 (s, 2 × $C^{2,6}$-CH$_3$, Mes) 138.7 (s, 2 x C^{4}, Mes), 139.8 (s, 2 × C^{1}, Mes), 146.8 (s, C^{2,6}, C$_6$H$_3$), 162.8 (q, ^{1}J(^{11}B,^{13}C) = 49 Hz, B-C, BAr$_f$), 174.4 (s, Sn-C).

^{57}Fe Mößbauer Spectroscopy (80 K, mms^{-1}): δ = 0.42, ΔE_Q = 0.48 (87.06 %) (Square pyramidal isomer); δ = 0.43, ΔE_Q = 1.44 (12.94 %) (Trigonal bipyramidal isomer).

UV-Vis (THF): λ_{max} = 388.5 nm, ε = 21640.1 l·mol^{-1}·cm^{-1}

Dieses Werk ist copyrightgeschützt und darf in keiner Form vervielfältigt werden noch an Dritte weitergegeben werden.
Es gilt nur für den persönlichen Gebrauch.

4.5.10[(depe)$_2$Fe≡Ge(2,6-Trip$_2$-C$_6$H$_3$)][GeCl$_2$(2,6-Trip$_2$-C$_6$H$_3$)] (8-Fe)

A Schlenk tube was charged with a 1 : 2 solid mixture of [Fe(depe)$_2$(N$_2$)] (0.100g, 0.20 mmol) and **1-Ge** (0.237 g, 0.40 mmol) in the glove box. Pre-cooled pentane (25cm^3), -78°C was added to this mixture *via* cannula with rapid stirring as it was submerged in a dry-ice/acetone bath. It was stirred at this – 78°C for 5 minutes, then at room temperature for 2.5 h. On taking the reaction mixture out of the bath it was an dark-orange-brown suspension, and on warming to room temperature, an orange solid is noted precipitating out of the pentane solvent. The supernatant solution was filtered, washed with pentane (3 x 5 cm^3), and the orange precipitate was dried in vacuo at room temperature for 2 hours. Yield : 0.196 g, 60 %.

Properties: insoluble in pentane, soluble in and benzene / toluene and very soluble in THF. Very air sensitive: turns colourless on contact with air.

Melting Point: 148-151 °C (dec)

Elemental analysis: calcd (%) for $C_{92}H_{146}Cl_2FeGe_2P_4$ (1648.07): C 67.05, H 8.93; found : C 64.18 H 8.80

Spectroscopic data:

IR (nujol, cm^{-1}): KBr windows: ν = 1604 (m, br) 1565 (m, br) 1362 (vs) 1315 (w) 1260 (br,w) 1168 (vw) 1152 (w) 1130 (w) 1100 (m) 1038 (m) 1024 (m) 940 (w) 872 (m) 803 (m) 766 (m) 746 (w) 686 (vw).

^{1}H NMR: (300 MHz, C$_6$D$_6$, 298 K, ppm): $\delta = 0.69$ (br m, 12 H, 4 × CH$_3^{A}$), 0.86 – 0.93 (br, 4 H, 2 × PCH^XH^{Y}CH^XH^{Y}P) + (br m, 12 H, 4 × CH$_3^{B,}$), 0.89 (d, ^{3}*J*(H,H) = 6.9 Hz, 12 H, 4 x *o*-CH$_3$CHCH_3^{A}, Trip^A), 1.05 (br m, 8 H, CH_2), 1.21(d, ^{3}*J*(H,H) = 6.9 Hz 12 H, 4 × *o*-CH$_3$CHCH_3^{B}, Trip^A), 1.31(d, ^{3}*J*(H,H) = 6.9 Hz, 12 H, 2 × *p*-CH_3CHCH_3, Trip^A), 1.31 (d, ^{3}*J*(H,H) = 6.9 Hz, 12 H, 4 × *o*-CH$_3$CHCH_3^{A}, Trip^B), 1.41 (d, ^{3}*J*(H,H) = 6.9 Hz 12 H, 2 × *p*-CH_3CHCH_3, Trip^B), 1.58 (br m, 8H, P-CH$_2$), 1.77 (d, ^{3}*J*(H,H) = 6.9 Hz, 4 × *o*-CH$_3$CHCH_3^{B}, Trip^B), 1.97 (br m, 4 H, 2 ×

Dieses Werk ist copyrightgeschützt und darf in keiner Form vervielfältigt werden noch an Dritte weitergegeben werden.
Es gilt nur für den persönlichen Gebrauch.

$\mathrm{PCH}^{X}H^{Y}\mathrm{CH}^{X}H^{Y}\mathrm{P}$), 2.71 (sept, ^{3}J(H,H) = 6.9 Hz, 4 H,4 x *o*-$\mathrm{CH_3C}H\mathrm{CH_3}$,Trip$^{\mathrm{A}}$), 2.87 (sept, ^{3}J(H,H) = 6.9 Hz, 2 H, 2 x *p*-$\mathrm{CH_3C}H\mathrm{CH_3}$, Trip$^{\mathrm{A}}$), 3.02 (sept, ^{3}J(H,H) = 6.9 Hz, 2 H, 2 x *p*-$\mathrm{CH_3C}H\mathrm{CH_3}$, Trip$^{\mathrm{B}}$), 3.68 (sept, ^{3}J(H,H) = 6.9 Hz ,4 H, 4 x *o*-$\mathrm{CH_3C}H\mathrm{CH_3}$, Trip$^{\mathrm{B}}$), 6.78 (d, ^{3}J(H,H) = 7.6 Hz, 2 H, $\mathrm{C}^{3,5}$-*H*, $\mathrm{C_6H_3}^{\mathrm{A}}$), 6.96 (t, ^{3}J(H,H) = 7.6 Hz, 1 H, C^{4}-*H*, $\mathrm{C_6H_3}^{\mathrm{A}}$), 7.07 (s, 4 H, $\mathrm{C}^{3,5}$-*H*, Trip$^{\mathrm{A}}$), 7.28 (doublet and triplet overlapping, 3 H, $\mathrm{C}^{3,4,5}$-*H*, $\mathrm{C_6H_3}^{\mathrm{B}}$), 7.32 (s, 4 H, $\mathrm{C}^{3,5}$-*H*, Trip$^{\mathrm{B}}$).

^{1}H NMR (300.13 MHz, THF-d_8, 298 K, ppm): $\delta = 0.83$ (br, 12 H, 4 × $\mathrm{C}H_3{}^{\mathrm{A}}$), 0.94 (d, 12 H, 4 × *o*-$\mathrm{CH_3CH}CH_3{}^{\mathrm{A}}$, Trip$^{\mathrm{A}}$), 0.96 (d, 12 H, 4 x *o*-$\mathrm{CH_3CH}CH_3{}^{\mathrm{A}}$, Trip$^{\mathrm{B}}$), 1.08 (br, 12 H, 4 × $\mathrm{C}H_3{}^{\mathrm{B}}$), 1.24 - 1.27 (d, ^{3}J(H,H) = 6.9 Hz,12 H, 4 x *o*-$\mathrm{CH_3CH}CH_3{}^{\mathrm{B}}$, Trip$^{\mathrm{B}}$) + (d, ^{3}J(H,H) = 6.8 Hz 12 H, 2 x *p*-$\mathrm{C}H_3\mathrm{CHC}H_3$, Trip$^{\mathrm{B}}$), 1.34 (d, ^{3}J(H,H) = 6.9 Hz, 12 H, 4 x *o*-$\mathrm{CH_3CH}CH_3{}^{\mathrm{B}}$, Trip$^{\mathrm{A}}$), (d, ^{3}J(H,H) = 6.9 Hz, 12 H, 2 x *p*-$\mathrm{C}H_3\mathrm{CHC}H_3$, Trip$^{\mathrm{A}}$), 1.84 (br, 4 H, $\mathrm{C}H_2$) 1.92 (br, 4 H, $\mathrm{C}H_2$), 2.14 (br, 4H, $\mathrm{C}H_2$), 2.77 (sept, ^{3}J(H,H) = 6.9 Hz, 4 H, 4 x *o*-$\mathrm{CH_3C}H\mathrm{CH_3}$, Trip$^{\mathrm{A}}$), 2.82 (sept, ^{3}J(H,H) = 6.8 Hz 2 H, 2 x *p*-$\mathrm{CH_3C}H\mathrm{CH_3}$, Trip$^{\mathrm{B}}$), 2.97 (sept, ^{3}J(H,H) = 6.9 Hz, 2 H, 2 x *p*-$\mathrm{CH_3C}H\mathrm{CH_3}$, Trip$^{\mathrm{A}}$), 3.06 (sept, ^{3}J(H,H) = 6.9 Hz, 4 H, 4 x *o*-$\mathrm{CH_3C}H\mathrm{CH_3}$, Trip$^{\mathrm{B}}$), 6.75 (d, 2 H, Ar*H*), 6.87 (s, 4 H, Ar*H*), 6.97 – 7.00 (m, triplet and doublet overlapping, 3 H, Ar*H*), 7.15 (s, 4 H, Ar*H*), 7.42 (t, 1 H, Ar*H*).

$^{31}\mathrm{P}\{^{1}\mathrm{H}\}$ NMR: (121.5 MHz, $\mathrm{C_6D_6}$, 298 K, ppm): $\delta = 78.4$ (s)

$^{31}\mathrm{P}\{^{1}\mathrm{H}\}$ NMR: (THF-d_8, 202.45 MHz, 298 K, ppm): $\delta = 79.1$, $\Delta\nu_{1/2} = 6.57$ Hz
$^{31}\mathrm{P}\{^{1}\mathrm{H}\}$ NMR: (THF-d_8, 202.45 MHz, 273 K, ppm): $\delta = 79.3$, $\Delta\nu_{1/2} = 8.97$ Hz
$^{31}\mathrm{P}\{^{1}\mathrm{H}\}$ NMR: (THF-d_8, 202.45 MHz, 233 K, ppm): 79.8, $\Delta\nu_{1/2} = 56$ Hz
$^{31}\mathrm{P}\{^{1}\mathrm{H}\}$ NMR: (THF-d_8, 202.45 MHz, 213 K, ppm): 80.1, $\Delta\nu_{1/2} = 175$ Hz
$^{31}\mathrm{P}\{^{1}\mathrm{H}\}$ NMR: (THF-d_8, 202.45 MHz, 203 K, ppm): $\delta = 80.6$ $\Delta\nu_{1/2} = 1246$ Hz
$^{31}\mathrm{P}\{^{1}\mathrm{H}\}$ NMR: (THF-d_8, 202.45 MHz, 193 K, ppm): $\delta = 75.1$ (v br) and 85.3 (v br) ($\Delta\nu = 1944$ Hz)

Dieses Werk ist copyrightgeschützt und darf in keiner Form vervielfältigt werden noch an Dritte weitergegeben werden.
Es gilt nur für den persönlichen Gebrauch.

^{31}P{^{1}H} NMR: (THF-d_8, 202.45 MHz, 183 K, ppm): $\delta = 74.7$, $\Delta\nu_{1/2} = 192$ Hz, 85.8 $\Delta\nu_{1/2} = 203$ Hz ($\Delta\nu = 2206$ Hz)

^{13}C{^{1}H} NMR: (125.76 MHz, C_6D_6, 298 K, ppm) $\delta = 10.1$ (s, 4 × $C\mathrm{H}_3^{\mathrm{A}}$), 11.1 (s, 4 × $C\mathrm{H}_3^{\mathrm{B}}$), 22.7 (s, 4 × *o*-$\mathrm{CH_3CH}C\mathrm{H}_3^{\mathrm{B}}$ Trip$^{\mathrm{A}}$), 22.9, 24.2 (s, 4 × *o*-$\mathrm{CH_3CH}C\mathrm{H_3}$, Trip$^{\mathrm{B}}$), 24.3, 24.3, 24.8 (s, 2 × *p*-$C\mathrm{H_3CH}C\mathrm{H_3}$, Trip$^{\mathrm{B}}$), 26.3 (s, 4 × *o*-$\mathrm{CH_3CH}C\mathrm{H_3}$, Trip$^{\mathrm{A}}$), 31.0 (s, 4 × *o*-$\mathrm{CH_3}C\mathrm{HCH_3}$, Trip$^{\mathrm{A}}$), 31.2 (s, 4 × *o*-$\mathrm{CH_3}C\mathrm{HCH_3}$, Trip$^{\mathrm{B}}$), 34.4, 34.4 (s, 2 × *p*-$\mathrm{CH_3}C\mathrm{HCH_3}$ Trip$^{\mathrm{A}}$), 34.9 (s, 2 ×, *p*-$\mathrm{CH_3}C\mathrm{HCH_3}$ Trip$^{\mathrm{B}}$), 37.7 (m, 2 × $\mathrm{P}C\mathrm{H_2}C\mathrm{H_2P}$), 120.0, 121.6 (s, 2 × $C^{3,5}$, Trip$^{\mathrm{A}}$), 125.2 (s, 1 × C^{4}, $\mathrm{C_6H_3}^{\mathrm{B}}$), 130.4 (s, $C^{3,5}$, $\mathrm{C_6H_3}^{\mathrm{B}}$), 132.0 (s, 2 × $C^{3,5}$, $\mathrm{C_6H_3}^{\mathrm{A}}$), 137.7 (s, 2 × C^{1}, Trip$^{\mathrm{A}}$), 140.4 (s, 2 ×, C^{1}, Trip$^{\mathrm{B}}$), 144.1 (s, 2 × $C^{2,6}$, $\mathrm{C_6H_3}^{\mathrm{A}}$), 146.2 (s, 2 × C^{4}, Trip$^{\mathrm{B}}$), 146.4 (s, 2 × $C^{2,6}$,Trip$^{\mathrm{A}}$), 146.6 (s, $C^{2,6}$, $\mathrm{C_6H_3}^{\mathrm{B}}$), 147.7 (s, 2 × $C^{2,6}$, Trip$^{\mathrm{B}}$), 149.1 (s, 2 × C^{4}, Trip$^{\mathrm{A}}$), 163.4 (s, C^{1}, $\mathrm{C_6H_3}^{\mathrm{B}}$), 163.7 (s, C^{1}, $\mathrm{C_6H_3}^{\mathrm{A}}$).

Mößbauer Spectroscopy (80 K, mms^{-1}): $\delta = 0.23$, $\Delta E_Q = 0.58$

4.5.11 [(depe)$_2$Fe≡Ge(2,6-Mes$_2$-C$_6$H$_3$)][GeCl$_2$(2,6-Mes$_2$-C$_6$H$_3$)] (9-Fe)

In the glove box, a pentane solution of **1-Fe** (3 mL) (0.046 g, 0.09 mmol) was stirred at room temperature. A suspension of **2-Ge** (0.078 g, 0.18 mmol) in 4 mL pentane was added to this solution at room temperature. The initial orange suspension turns brown within minutes, with the formation of a terracotta brown precipitate. The reaction mixture was stirred at room temperature for 2 h, and filtered *via* cannula and the filtrate was discarded. The brown solid that remained in the reaction vessel after the filtration was washed with pentane (3 × 10 mL), and dried *in vacuo* for 1 h at room temperature. Yield: 60 mg (0.045 mmol, 51 %). Crystal suitable for X-ray crystallographic analysis were grown from a concentrated C_6D_6 solution of **9-Fe** at room temperature with slow evaporation in the glove box.

Properties: insoluble in pentane, soluble in and benzene / toluene and very soluble in THF. Very air sensitive: turns colourless on contact with air.

Dieses Werk ist copyrightgeschützt und darf in keiner Form vervielfältigt werden noch an Dritte weitergegeben werden.
Es gilt nur für den persönlichen Gebrauch.

Melting Point: 65 – 67 °C (dec).

Elemental Analysis: calcd (%) for $C_{68}H_{98}Cl_2FeGe_2P_4$ (1311.4 g.mol^{-1}): C 62.28, H 7.53; found: C 61.83, H 7.42.

Spectroscopic Data:

IR (Nujol, cm^{-1}): (KBr) ν = 1610 (w), 1564 (m), 1304 (w), 1155 (w), 1099 (vw), 1078 (vw), 1057 (m), 1025 (m), 870 (w), 851 (m), 840 (w), 812 (w), 801 (w), 761 (m), 743 (m), 733 (s).

^{1}H NMR: (300 MHz, C_6D_6, 298 K, ppm): $\delta = 0.72$ (br s, 16H, 4 × CH_3^{A}, depe + 2 × $PCH^{X}H^{Y}CH^{X}H^{Y}P$), 0.90 (br s, 12H, 4 × CH_3^{B}, depe), 1.04 – 1.11 (br m: 8H, 4 × $CH_3^{A}CH^{X}H^{Y}$ + 4 × $CH_3^{B}CH^{X}H^{Y}$), 1.40 – 1.60 (br m, 8H, 4 × $CH_3^{A}CH^{X}H^{Y}$ + 2 × $PCH^{X}H^{Y}CH^{X}H^{Y}P$), 1.70 – 1.85 (br m, 4H, 4 × $CH_3^{B}CH^{X}H^{Y}$), 1.90 (s, 12H, 4 × *o*-CH_3, Mes^{A}), 2.22 (s, 6H, 2 × *p*-CH_3, Mes^{A}), 2.34 (s, 6H, 2 × *p*-CH_3, Mes^{B}), 2.67 (s, 12H, 4 × *o*-CH_3, Mes^{B}), 6.55 (d, 2H, ^3J(H,H) = 7.3 Hz, $C^{3,5}$-*H*, $C_6H_3^{A}$), 6.73 (s, 4H, 2 × $C^{3,5}$-*H*, Mes^{A}), 7.02 (s, 4H, 2 × $C^{3,5}$-*H*, Mes^{B}), 7.13 (signals overlapping with solvent: 2H, $C^{3,5}$-*H*, $C_6H_3^{B}$ + 1H, C^{4}-*H*, $C_6H_3^{A}$), 7.37 (t, 1H, ^3J(H,H) = 7.3 Hz, C^{4}-*H*, $C_6H_3^{B}$).

^{1}H NMR: (300.13 MHz, THF-d_8, 298 K, ppm): $\delta = 0.87$ (br s, 12H, 4 × CH_3^{A}), 1.14 (br, 4H, 2 × $PCH^{X}H^{Y}CH^{X}H^{Y}P$), 1.14 (br, 12H, 4 × CH_3^{B}), 1.31 (br m, 4 × $CH_3^{A}CH^{X}H^{Y}$ + 4 × $CH_3^{B}CH^{X}H^{Y}$), 1.79 (br, 4 × $CH_3^{A}CH^{X}H^{Y}$ + 2 × $PCH^{X}H^{Y}CH^{X}H^{Y}P$), 2.04 (s, 12H, 2 × $C^{2,6}$-CH_3, Mes^{A}), 2.09 (s, 12H, 2 × $C^{2,6}$-CH_3, Mes^{B}), 2.22 (s, 6H, 2 × C^{4}-CH_3, Mes^{B}), 2.36 (s, 6H, 2 × C^{4}-CH_3, Mes^{A}), 6.61 (d, ^3J(H,H) = 7.4 Hz, 2H, $C^{3,5}$-*H*, $C_6H_3^{B}$), 6.67 (s, 4H, $C^{3,5}$-*H*, Mes^{B}), 6.88 (d, ^3J(H,H) = 7.2 Hz, 2H, $C^{3,5}$-*H*, $C_6H_3^{A}$), 6.98 (s, 4H, $C^{3,5}$-*H*, Mes^{A}) 7.09 (t, ^3J(H,H) = 7.5 Hz, 1H, C^{4}-*H*, $C_6H_3^{B}$), 7.57 (t, ^3J(H,H) = 7.5 Hz, 1H, C^{4}-*H*, $C_6H_3^{A}$).

^{1}H NMR: (500.13 MHz, THF-d_8, 298 K, ppm): $\delta = 0.91$ (br s, 12H, 4 × CH_3^{A}), 1.08 (br, 4H, 2 × $PCH^{X}H^{Y}CH^{X}H^{Y}P$), 1.13 (br s, 12H, 4 × CH_3^{B}), 1.29

Dieses Werk ist copyrightgeschützt und darf in keiner Form vervielfältigt werden noch an Dritte weitergegeben werden.
Es gilt nur für den persönlichen Gebrauch.

(br m, 4 × $\mathrm{CH_3^AC}H^\mathrm{X}\mathrm{H^Y}$ + 4 × $\mathrm{CH_3^BC}H^\mathrm{X}H^\mathrm{Y}$), 1.77 (br, 4 × $\mathrm{CH_3^ACH^X}H^\mathrm{Y}$ + 2 × $\mathrm{PCH^X}H^\mathrm{Y}\mathrm{CH^X}H^\mathrm{Y}\mathrm{P}$), 2.06 (s, 12H, 2 × C^{2,6}-CH_3, Mes$^\mathrm{A}$) , 2.09 (s, 12H, 2 × C^{2,6}-CH_3, Mes$^\mathrm{B}$), 2.22 (s, 6H, 2 × C^4-CH_3, Mes$^\mathrm{B}$), 2.34 (s, 6H, 2 × C^4-CH_3, Mes$^\mathrm{A}$), 6.60 (d, ^3J(H,H) = 7.4 Hz, 2H, C^{3,5}-H, $\mathrm{C_6H_3^B}$), 6.66 (s, 4H, C^{3,5}-H, Mes$^\mathrm{B}$) 6.86 (d, ^3J(H,H) = 7.2 Hz, 2H, C^{3,5}-H, $\mathrm{C_6H_3^A}$), 6.95 (s, 4H, C^{3,5}-H, Mes$^\mathrm{A}$), 7.08 (t, ^3J(H,H) = 7.5 Hz, 1H, C^4-H, $\mathrm{C_6H_3^B}$), 7.52 (t, ^3J(H,H) = 7.5 Hz, 1H, C^4-H, $\mathrm{C_6H_3^A}$).

^{1}H NMR: (500.13 MHz, THF-d_8, 283 K, ppm): δ = 0.91 (br s, 12H, 4 × C$H_3{}^\mathrm{A}$), 1.09 (br, 4H, 2 × $\mathrm{PC}H^\mathrm{X}\mathrm{H^YC}H^\mathrm{X}\mathrm{H^YP}$), 1.14 (br s, 12H, 4 × C$H_3{}^\mathrm{B}$), 1.26 – 1.40 (br m, 4 × $\mathrm{CH_3^AC}H^\mathrm{X}\mathrm{H^Y}$ + 4 × $\mathrm{CH_3^BC}H^\mathrm{X}H^\mathrm{Y}$), 1.80 (br, 4 × $\mathrm{CH_3^ACH^X}H^\mathrm{Y}$ + 2 × $\mathrm{PCH^X}H^\mathrm{Y}\mathrm{CH^X}H^\mathrm{Y}\mathrm{P}$), 2.05 (s, 12H, 2 × C^{2,6}-CH_3, Mes$^\mathrm{A}$), 2.09 (s, 12H, 2 × C^{2,6}-CH_3, Mes$^\mathrm{B}$), 2.22 (s, 6H, 2 × C^4-CH_3, Mes$^\mathrm{B}$), 2.35 (s, 6H, 2 × C^4-CH_3, Mes$^\mathrm{A}$), 6.60 (d, ^3J(H,H) = 7.4 Hz, 2H, C^{3,5}-H, $\mathrm{C_6H_3^B}$), 6.67 (s, 4H, C^{3,5}-H, Mes$^\mathrm{B}$) 6.87 (d, ^3J(H,H) = 7.2 Hz, 2H, C^{3,5}-H, $\mathrm{C_6H_3^A}$), 6.96 (s, 4H, C^{3,5}-H, Mes$^\mathrm{A}$), 7.08 (ps t, ^3J(H,H) = 7.5 Hz, 1H, C^4-H, $\mathrm{C_6H_3^B}$), 7.53 (ps t, C^4-H, $\mathrm{C_6H_3^A}$).

^{1}H NMR: (500.13 MHz, THF-d_8, 243 K, ppm): δ = 0.90 (br s, 12H, 4 × C$H_3{}^\mathrm{A}$), 1.01 (br, 4H, 2 × $\mathrm{PC}H^\mathrm{X}\mathrm{H^YC}H^\mathrm{X}\mathrm{H^YP}$), 1.13 (br s, 12H, 4 × C$H_3{}^\mathrm{B}$), 1.22 – 1.46 (br m, 4 × $\mathrm{CH_3^AC}H^\mathrm{X}\mathrm{H^Y}$ + 4 × $\mathrm{CH_3^BC}H^\mathrm{X}H^\mathrm{Y}$), 1.80 (br, 4 × $\mathrm{CH_3^ACH^X}H^\mathrm{Y}$ + 2 × $\mathrm{PCH^X}H^\mathrm{Y}\mathrm{CH^X}H^\mathrm{Y}\mathrm{P}$), 2.06 (br s, 12H, 2 × C^{2,6}-CH_3, Mes$^\mathrm{A}$), 2.08 (br s, 12H, 2 × C^{2,6}-CH_3, Mes$^\mathrm{B}$), 2.23 (br s, 6H, 2 × C^4-CH_3, Mes$^\mathrm{B}$), 2.35 (br s, 6H, 2 × C^4-CH_3, Mes$^\mathrm{A}$), 6.60 (d, ^3J(H,H) = 7.4 Hz, 2H, C^{3,5}-H, $\mathrm{C_6H_3^B}$), 6.67 (s, 4H, C^{3,5}-H, Mes$^\mathrm{B}$) 6.89 (br, 2H, C^{3,5}-H, $\mathrm{C_6H_3^A}$), 6.96 (br s, 4H, C^{3,5}-H, Mes$^\mathrm{A}$), 7.11 (br t 1H, C^4-H, $\mathrm{C_6H_3^B}$), 7.57 (br, 1H, C^4-H, $\mathrm{C_6H_3^A}$).

^{31}P{^{1}H} NMR: (121.5 MHz, $\mathrm{C_6D_6}$, 298 K, ppm): δ = 78.3 (s).

^{31}P{^{1}H} NMR: (121.5 MHz, THF-d_8, 298 K, ppm): δ = 76.6 (s) $\Delta\nu_{1/2}$ = 15.7 Hz.
^{31}P{^{1}H} NMR: (121.5 MHz, THF-d_8, 287 K, ppm): δ = 76.7 (s) $\Delta\nu_{1/2}$ = 27.4 Hz.
^{31}P{^{1}H} NMR: (121.5 MHz, THF-d_8, 269 K, ppm): δ = 76.8 (s) $\Delta\nu_{1/2}$ = 69.7 Hz.
^{31}P{^{1}H} NMR: (121.5 MHz, THF-d_8, 233 K, ppm): δ = 77.1 (s) $\Delta\nu_{1/2}$ = 20.3 Hz.

Dieses Werk ist copyrightgeschützt und darf in keiner Form vervielfältigt werden noch an Dritte weitergegeben werden.
Es gilt nur für den persönlichen Gebrauch.

^{31}P{^{1}H} NMR: (121.5 MHz, THF-d_8, 217 K, ppm): $\delta = 77.2$ (s) $\Delta\nu_{½} = 10.1$ Hz.

^{31}P{^{1}H} NMR: (121.5 MHz, THF-d_8, 191 K, ppm): $\delta = 77.3$ (s) $\Delta\nu_{½} = 21.7$ Hz.

^{13}C{^{1}H} NMR: (125.76 MHz, C_6D_6, 298 K, ppm) $\delta = 9.8$ (s, 4 × CH_3^{A}), 10.5 (s, 4 × CH_3^{B}), 21.3 (s, 2 × *p*-CH_3, Mes^{A}), 21.5 (s, 4 × *o*-CH_3, Mes^{A}), 21.6 (s, 2 × *p*-CH_3, Mes^{B}), 22.8 (s, 4 × *o*-CH_3, Mes^{B}), 24.4 (m, CH_2), 24.7 (s, CH_2), 35.8 (quint, $^{1}J(^{13}\text{C,P}) = 6.5$ Hz, CH_2), 127.3 (s, 1 × C^4, $C_6H_3^{B}$), 127.5 (s, 2 × $C^{3,5}$-H, Mes^{B}), 128.5 (s, 1 × $C^{3,5}$, $C_6H_3^{B}$), 128.7 (s, $C^{3,5}$-H, $C_6H_3^{A}$), 129.2 (s, 2 × $C^{3,5}$-H, Mes^{A}), 131.0 (s, C^4, $C_6H_3^{A}$), 134.3 (s, 2 × C^4, Mes^{B}), 136.1 (s, 2 × $C^{2,6}$, Mes^{A}), 137.4 (s, 2 × $C^{2,6}$, Mes^{B}), 137.7 (s, 2 × C^4, Mes^{A}), 138.5 (s, 2 × C^1, Mes^{A}), 142.2 (s, 2 × C^1, Mes^{B}), 145.9 (s, 1 × $C^{2,6}$, $C_6H_3^{A}$), 148.2 (s, 1 × $C^{2,6}$, $C_6H_3^{B}$), 161.0 (s, 1 × C^1, $C_6H_3^{B}$), 161.7 (s, 1 × C^1, $C_6H_3^{A}$).

^{13}C{^{1}H} NMR: (75.5 MHz, THF-d_8, 298 K, ppm) $\delta = 10.0$ (s, 4 × CH_3^{A}), 10.9 (s, 4 × CH_3^{B}), 21.4 (s, 2 × C^4-CH_3, Mes^{A}), 21.6 (s, 2 × C^4-CH_3, Mes^{B}), 21.9 (s, 2 × $\text{C}^{2,6}$-CH_3, Mes^{A}), 22.5 (s, 2 × $\text{C}^{2,6}$-CH_3, Mes^{A}), 36.9 (ps quint, all CH_2), 127.1 (s, 1 × C^4, $C_6H_3^{B}$), 127.7 (s, 2 × $C^{3,5}$, Mes^{B}), 128.4 (s, 1 × $C^{3,5}$, $C_6H_3^{B}$), 129.6 (s, 1 × $C^{3,5}$, $C_6H_3^{A}$), 129.9 (s, 2 × $\text{C}^{3,5}$-H, Mes^{A}) 131.8 (s, 1 × C^4, $C_6H_3^{A}$), 134.4 (s, 2 × C^4, Mes^{B}), 136.9 (s, 2 × $C^{2,6}$, Mes^{A}), 137.3 (s, 2 × $C^{2,6}$, Mes^{B}), 138.5 (s, 2 × C^4, Mes^{A}), 139.2 (s, 2 × C^1, Mes^{A}), 142.4 (s, 2 × C^1, Mes^{B}), 146.7 (s, 1 × $C^{2,6}$, $C_6H_3^{A}$), 148.3 (s, 1 × $C^{2,6}$, $C_6H_3^{B}$), 161.9 (s, 1 × C^1, $C_6H_3^{B}$), 162.3 (s, 1 × C^1, $C_6H_3^{A}$).

Mößbauer Spectroscopy (80 K, mms^{-1}): $\delta = 0.25$, $\Delta E_Q = 1.11$.

4.5.12 [FeCl(depe)$_2$] (10-Fe)

A Schlenk tube was charged with **2-Fe** (0.221 g, 0.410 mmol) and **1-Fe** (0.203 g, 0.410 mmol). Toluene (10 mL) was added to this mixture with rapid stirring at room temperature. An immediate colour change to dark green is noticed. It was stirred at room temperature for 1.5 h, and an *in situ* ^{31}P{^{1}H} NMR spectrum revealed incomplete consumption of the starting materials. The reaction solution was subsequently heated at 60 °C for 2 h, and the solvent removed *in vacuo*. The green residue was extracted with pentane (10 mL), to remove some

Dieses Werk ist copyrightgeschützt und darf in keiner Form vervielfältigt werden noch an Dritte weitergegeben werden.
Es gilt nur für den persönlichen Gebrauch.

black decomposition, filtered, and the filtrate concentrated to incipience and stored at –30 °C for 14 h. A dichroic orange-green crystalline solid was separated from the mother liquor by cannula filtration at –78 °C and dried *in vacuo* for 1 h at room temperature, and the supernatant liquid discarded. Yield: 0.319 g (0.633 mmol, 77 %). Crystals suitable for X-ray crystallographic analysis were grown from pentane at –30 °C in the glove-box.

Properties: Soluble in pentane and benzene. Very air sensitive: turns brown on contact with air.

Elemental analysis: calcd (%) for $C_{20}H_{48}ClFeP_4$ (503.78 g·mol^{-1}): C 47.68, H 9.60; found: C 47.48, H 9.49 %.

Spectroscopic data:

IR (Nujol, cm^{-1}): (KBr): ν = 2727 (vw), 1417 (s), 1262 (vw), 1236 (m), 1182 (vw), 1159 (vw), 1113 (vw), 1066 (w), 1037 (s), 1024 (vs), 934 (m), 978 (m), 868 (m), 807 (m), 746 (vs), 731 (vs), 697 (s), 667 (m), 650 (m), 610 (m), 458 (w), 412 (m).

^{1}H NMR: (300.1 MHz, C_6D_6, 298 K, ppm): δ = -1.17 (br s, $\Delta\nu_{½}$ = 314.57 Hz), small percentage signals corresponding to $FeCl_2(depe)_2$; no other signals detected in the range +200 to -200 ppm.

VT ^{1}H NMR: (Toluene-d_8): no new signals observed in the range -200 to +200 ppm, only small changes in $\Delta\nu_{½}$ of signal at -1.17 ppm.

UV/Vis (Cyclohexane): λ = 614 nm; λ = 754 nm, ε = 358.13 l.mol^{-1}.cm^{-1}; λ = 954 nm.

UV/Vis (Solid state): λ = 780 nm, λ = 1250 nm, λ = 400 – 540 nm.

Mößbauer spectroscopy (80 K, mms^{-1}): δ = 0.29, ΔE_Q = 0.59

EPR Spectroscopy (30 K): *g* = 2.0023 (no hyperfine structure: structureless)

Dieses Werk ist copyrightgeschützt und darf in keiner Form vervielfältigt werden noch an Dritte weitergegeben werden.
Es gilt nur für den persönlichen Gebrauch.

4.5.13 [Fe(CH_3)(depe)$_2$] (12-Fe)

10-Fe (0.100 g, 0.195 mmol) was dissolved in 10 mL of pentane at stirred at room temperature. MeLi (0.15 mL, 1.6 M in Et_2O) was added drop wise to the green **10-Fe** solution at room temperature through a rubber septum. An immediate colour change to orange is noticed on commencement of the addition MeLi. On complete addition of the MeLi, the solution took on a milky orange appearance. The reaction mixture was stirred for 1 h at room temperature, filtered *via* cannula and the clear orange filtrate was concentrated to 0.5 mL *in vacuo* and stored at –60 °C for 3 days. A red-orange solid was separated from the mother liquor, which was discarded, using a syringe, and the resulting solid dried *in vacuo* for 1 h at room temperature. Yield: 0.065 g (0.13 mmol, 69 %). Crystals suitable for X-ray crystallographic analysis were grown from and Et_2O solution of **12-Fe** at –60 °C.

Properties: Soluble in pentane and benzene. Very air sensitive: turns brown on contact with air.

Melting Point: 51 – 52 °C

Elemental analysis: calcd (%) for $C_{21}H_{51}FeP_4$ (483.37 g·mol^{-1}): C 52.18, H 10.60;
found: C 52.24, H 10.22 %.

Spectroscopic data:

IR (Nujol, cm^{-1}): (KBr): ν = 2721 (vw), 1419 (m), 1262 (w), 1237 (m), 1182 (vw), 1152 (vw), 1113 (vw), 1064 (w), 1023 (vs), 981 (m), 863 (m), 803 (m), 756 (s), 728 (s), 711 (s), 673 (m), 653 (m), 648 (m), 606 (s), 470 (w).

^{1}H NMR: (300.1 MHz, C_6D_6, 298 K, ppm): $\delta = -1.49$ (v br, $\Delta\nu_{½} = 447.5$ Hz) and diamagnetic signals, corresponding to *cis* and *trans*-[Fe(CH_3)$_2$(depe)$_2$].

Mößbauer Spectroscopy (80 K, mms^{-1}): $\delta = 0.26$, $\Delta E_Q = 0.53$.

EPR Spectroscopy (30 K): $g_x = 2.14$ (1:2:2:1 hyperfine pattern), $g_y = 2.09$, $g_z = 2.01$ (1:2:3:3:2:1 hyperfine pattern).

Dieses Werk ist copyrightgeschützt und darf in keiner Form vervielfältigt werden noch an Dritte weitergegeben werden.
Es gilt nur für den persönlichen Gebrauch.

4.5.14 [(dmpe)$_2$Fe=SnCl(2,6-Mes$_2$-C$_6$H$_3$)] (16-Fe)

Method using 17-Fe

A Schlenk tube was charged with **17-Fe** (0.100 g, 0.231 mmol) and **1-Sn** (0.108 g, 0.231 mmol) and thoroughly stirred at room temperature. Et$_2$O (35 mL) was added *via* cannula to the stirring mixture at room temperature. An instantaneous colour change to dark brown is noticed on addition of the Et$_2$O. The reaction was stirred for 1 h at room temperature at which point ^{31}P{^{1}H} *in situ* NMR spectroscopy revealed a ratio of 89 : 11 **16-Fe** : **17-Fe** and selective conversion. The reaction was stirred for a further 15 min, and the brown reaction mixture was filtered *via* cannula at room temperature, to remove a small amount of a light brown precipitate, which was discarded (0.011 g). The dark brown filtrate was concentrated *in vacuo* to *ca.* 5 mL at which point a dark brown solid precipitated. Cooling to –30 °C for 3 h and then to –60 °C overnight followed, and then the brown supernatant solution was separated from the brown solid at –78 °C. The remaining dark brown solid was dried *in vacuo* for 1 h at room temperature. Yield : 0.091 g, (0.110 mmol, 48 %). Crystals suitable for X-ray crystallographic analysis were grown from a concentrated C$_6$D$_6$ solution with slow evaporation at room temperature in the glove box.

Properties: Highly soluble in benzene, pentane, Et$_2$O. Very air sensitive, decolourising on contact with air. It is stable in Et$_2$O as evidenced by *in situ* ^{31}P{^{1}H} NMR spectroscopy.

Spectroscopic data:

^{1}H NMR:	(300.1 MHz, C$_6$D$_6$, 298 K, ppm): δ = 0.99 (br s, $\Delta\nu_{½}$ = 7.0 Hz, 12H, 4 × CH_3^A), 1.16 – 1.29 (m, 4H, 2 × PCH^XH^{Y}CH^XH^{Y}P), 1.33 (br s, $\Delta\nu_{½}$ = 7.6 Hz, 12H, 4 × CH_3^B), 1.37 – 1.47 (m, 4H, 2 × PCH^XH^YCH^XH^YP), 2.19 (s, 6H, 2 × C^2-CH_3, Mes), 2.23 (s, 6H, 2 × C^4-CH_3, Mes), 2.70 (s, 6H, 2 × C^6-CH_3, Mes), 6.74 (s, 2H, 2 × C^3-*H*, Mes), 6.92 (s, 2H, 2 × C^5-*H*, Mes), 7.08 (ps d, ^3J(H,H) = 7.5 Hz, 2H, C^{3,5}-*H*, C$_6$H$_3$), 7.25 (ps t, ^3J (H,H) = 7.5 Hz, 1H, C^4-*H*, C$_6$H$_3$).

Dieses Werk ist copyrightgeschützt und darf in keiner Form vervielfältigt werden noch an Dritte weitergegeben werden.
Es gilt nur für den persönlichen Gebrauch.

$^{1}H\{^{31}P\}$ NMR: (300.1 MHz, C_6D_6, 298 K, ppm): $\delta = 0.99$ (s, $\Delta\nu_{½} = 2.0$ Hz, 12H, 4 × $CH_3{}^{A}$), 1.22 – 1.28 (m, 4H, 2 × $PCH^{X}H^{Y}CH^{X}H^{Y}P$), 1.33 (s, $\Delta\nu_{½} = 2.0$ Hz, 12H, 4 × $CH_3{}^{B}$), 1.38 – 1.45 (m, 4H, 2 × $PCH^{X}H^{Y}CH^{X}H^{Y}P$), 2.19 (s, 6H, 2 × $C^{2}\text{-}CH_3$, Mes), 2.23 (s, 6H, 2 × $C^{4}\text{-}CH_3$, Mes), 2.70 (s, 6H, 2 × $C^{6}\text{-}CH_3$, Mes), 6.74 (s, 2H, 2 × $C^{3}\text{-}H$, Mes), 6.92 (s, 2H, 2 × $C^{5}\text{-}H$, Mes), 7.08 (ps d, $^{3}J(H,H) =$ 7.5 Hz, 2H, $C^{3,5}\text{-}H$, C_6H_3), 7.25 (ps t, $^{3}J(H,H) =$ 7.5 Hz, 1H, $C^{4}\text{-}H$, C_6H_3).

$^{31}P\{^{1}H\}$ NMR: (121.5 MHz, C_6D_6, 298 K, ppm): $\delta = 60.2$ (s, $^{2}J(^{119/117}Sn, ^{31}P) = 49.6$ Hz, $\Delta\nu_{½} = 2.6$ Hz.)

$^{13}C\{^{1}H\}$ NMR: (75.47 MHz, C_6D_6, 298 K, ppm): $\delta = 21.2$ (s, 2 × $C^{4}\text{-}CH_3$, Mes), 22.6 (s, 2 × $C^{2\text{-}}CH_3$, Mes), 23.2 (s, 2 × $C^{6}\text{-}CH_3$), 24.0 (quint, $^{1}J(P,^{13}C) = 3.9$ Hz, 4 × $CH_3{}^{A}$), 30.0 (quint, $^{1}J(P,C) = 6.7$ Hz, 4 × $CH_3{}^{B}$), 34.3 (quint, $^{1}J(P,C) = 13.1$ Hz, 2 × PCH_2CH_2P), 127.6 (s, 1 × C^{4}, C_6H_3), 128.1 (signal obscured by resonance signal of the solvent, 2 × C^{3}-H, Mes), 129.2 (s, 2 × C^{5}-H, Mes), 129.3 (s, $C^{3,5}$-H, C_6H_3), 135.9 (s, 2 × C^{4}, Mes), 136.2 (s, 2 × C^{2}, Mes), 138.9 (s, 2 × C^{6}, Mes), 141.3 (s, 2 × C^{1}, Mes), 146.1 (s, $C^{2,6}$, C_6H_3), 175.5 (s, C^{1}, C_6H_3).

$^{119}Sn\{^{1}H\}$ NMR: (111.9 MHz, C_6D_6, 298 K, ppm): $\delta = 527.2$ (quint, $^{2}J(^{119}Sn,P) = 51.1$ Hz).

Method using **15-Fe**:

An NMR scale experiment was carried out: To an orange solution of $[\{Fe(dmpe)_2\}_2(\mu\text{-}dmpe)]$ (0.010 g, 0.012 mmol) in C_6D_6 (0.5 mL) was added a solution of $[SnCl(2,6\text{-}Mes_2\text{-}C_6H_3)]_2$ (0.011 g, 0.024 mmol) in C_6D_6 (0.5 mL) in a young type NMR tube. An instantaneous colour change to dark brown is noticed on addition of the two orange solutions. The brown solution was submitted for a combination of ^{1}H and $^{31}P\{^{1}H\}$ NMR spectroscopy after 5 h which showed complete conversion of the dimer to **16-Fe** with $[FeCl_2(dmpe)_2]$, resulting from redox chemistry in a ratio 15 : 1.

Dieses Werk ist copyrightgeschützt und darf in keiner Form vervielfältigt werden noch an Dritte weitergegeben werden.
Es gilt nur für den persönlichen Gebrauch.

4.5.15 [Fe(dmpe)$_2$(PMe$_3$)] (17-Fe)

A Schlenk tube was charged with [FeCl$_2$(dmpe)$_2$] (0.662 g, 1.55 mmol) and KC$_8$ (0.662 g, 4.90 mmol) and thoroughly mixed. PMe$_3$ (1.5 mL, 14.49 mmol) was added *via* syringe to THF (60 mL), and the solution cooled to 0 °C, and added rapidly *via* cannula under rapid stirring to the solid mixture of [FeCl$_2$(dmpe)$_2$] and KC$_8$ which was also cooled to 0 °C. An orange-green solution is noted with a black precipitate on addition of the solvent. The reaction was stirred for 3 h at 0 °C at which point *in situ* ^{31}P{^{1}H} NMR spectroscopy revealed a 1:2 ratio of **17-Fe** : [FeCl$_2$(dmpe)$_2$]. Stirring was continued for a further 1.5 h at 0 °C and then stirred at room temperature for a further 0.5 h at which point *in situ* ^{31}P{^{1}H} NMR spectroscopy revealed a 1 : 1 ratio **17-Fe** : [FeCl$_2$(dmpe)$_2$]. Stirring was continued for a further 2.5 h at room temperature and *in situ* ^{31}P{^{1}H} NMR spectroscopy then showed a 95 : 5 ratio of **17-Fe** : [FeCl$_2$(dmpe)$_2$]. Stirring for an additional hour at room temperature resulted in complete consumption of the starting material, and clean conversion to the desired product. The reaction mixture was concentrated *in vacuo* at room temperature to approximately 20 mL, and pentane (40 mL) was added *via* cannula to the dark red solution with a black precipitate. Filtration of the resulting solution at room temperature *via* cannula followed and the remaining residue was extracted twice with pentane (1 × 20 mL; 1 × 10 mL). The resulting dark red filtrate was concentrated *in vacuo* to dryness, resulting in an orange powder-like solid. Yield: 0.611 g (1.41 mmol, 91 %). Crystal suitable for X-ray crystallographic analysis were grown from toluene at room temperature by slow evaporation in the glove box.

Properties: Very soluble in benzene, THF, Et$_2$O, sparingly soluble in pentane. Highly air sensitive: turns dark brown on contact with air.

Elemental analysis: calcd (%) for C$_{15}$H$_{41}$FeP$_5$ (432.20 g·mol^{-1}): C 41.68, H 9.56; found: C 41.83, H 10.09 %.

Spectroscopic data:

^{1}H NMR: (300.1 MHz, C$_6$D$_6$, 298 K, ppm): δ = 1.01 (br s, $\Delta\nu_{½}$ = 11.0 Hz, 9H, 1 × P(CH_3)$_3$), 1.26 (br s, $\Delta\nu_{½}$ = 10.5 Hz, 12H, 4 × CH_3^A), 1.50 (br s,

Dieses Werk ist copyrightgeschützt und darf in keiner Form vervielfältigt werden noch an Dritte weitergegeben werden.
Es gilt nur für den persönlichen Gebrauch.

$\Delta\nu_{\frac{1}{2}}$ = 11.2 Hz, 16H, 4 × CH_3^B + 2 × $PC\mathit{H}^XH^Y\ C\mathit{H}^XH^YP$), 1.70 (br s, $\Delta\nu_{\frac{1}{2}}$ = 27.1 Hz, 4H, 2 × $PCH^X\mathit{H}^Y\ CH^X\mathit{H}^YP$).

(the signal are broad due to high concentration, at lower concentration, sharper signals are seen).

$^{31}P\{^1H\}$ NMR: (121.5 MHz, C_6D_6, 298 K, ppm): δ = –0.1 (quint, ^2J(P,P) = 11.4 Hz, 1P, 1 × *P*Me_3), 62.1 (d, ^2J(P,P) = 11.4 Hz, 4P, 2 × $Me_2\mathit{P}CH_2CH_2\mathit{P}Me_2$).

$^{13}C\{^1H\}$ NMR: (75.47 MHz, C_6D_6, 298 K, ppm): δ = 25.0 – 25.3 (m, 1 × $P(\mathit{C}H_3)_3$), 29.8 – 30.1 (m, 4 × $\mathit{C}H_3^A$), 30.4 – 31.0 (m, 4 × $\mathit{C}H_3^B$), 34.1 – 35.0 (ps quint, 2 × $P\mathit{C}H_2\mathit{C}H_2P$).

Mößbauer Spectroscopy (80 K, mms^{-1}): δ = 0.17, ΔE_Q = 2.03.

4.5.16 [$(PMe_3)_3FeH\{SnCl(2,6\text{-}Mes_2\text{-}C_6H_3)(CH_2PMe_2)\}$] (20-Fe)

$FeCl_2(PMe_3)_2$ **19-Fe** (0.890 g, 3.19 mmol) was dissolved in THF (30 mL), and cooled to 0 °C. PMe_3 (1.6 g, 2.2 ml) was added to the grey solution *via* syringe. The colour changed to green. Sodium amalgam (5 mL, w(Na) = 7.5 % by mass) was added to the green THF solution using a fortuna pipette at 0 °C, with rapid stirring. An immediate colour change to brown-green is noticed. The reaction solution was left to stir at 0 °C for 1 h, and the solvent removed at 0 °C (the resulting C,H activated complex is thermolabile) *in vacuo*. Pre-cooled (to 0 °C) pentane (50 mL) was transferred to the remaining yellow-brown residue, which was also in a 0 °C ice bath and stirred for some minutes. Filtration of the yellow supernatant *via* cannula followed and the filtrate was stored at –10 °C. The residue in the reaction vessel was discarded. The solvent of the filtrate was removed under reduced pressure to afford a yellow oily material, [$FeH\{CH_2PMe_2\}(PMe_3)_3$] which was used as is in the next step, without characterisation owing to its lability. Yield: (0.75 g, 62 %). A portion of [$FeH\{CH_2PMe_2\}(PMe_3)_3$] was transferred to another Schlenk tube by dissolving it is pentane and syringing over a portion of the yellow pentane solution into a pre-weighed vessel, and removing the solvent (0.480 g, 1.33 mmol). **1-Sn** (0.622 g, 1.33 mmol) was added to the yellow oil and pre-cooled (–40 °C) pentane (30 mL) added to the mixture under rapid stirring. The reaction was stirred at –40 °C for 1 h and then at room temperature for an

Dieses Werk ist copyrightgeschützt und darf in keiner Form vervielfältigt werden noch an Dritte weitergegeben werden.
Es gilt nur für den persönlichen Gebrauch.

additional 1 h. The reaction solution was subsequently filtered *via* cannula, to separate a brown solid from a reddish supernatant. The brown solid was subsequently extracted with 20 mL toluene, the toluene filtrates combined, concentrated to incipience, and cooled to –30 °C overnight. An orange solid was separated from the mother liquor by cannula filtration at –30 °C, and dried *in vacuo* at room temperature for 3 h, to afford **20-Fe** as a mixture of 3 stereoisomers. Yield: 0.710 g (0.86 mmol, 64 %).

Properties: sparingly soluble in pentane, soluble in and benzene / toluene and very soluble in THF. Moderately air sensitive.

Elemental analysis: calcd (%) for $C_{36}H_{61}P_4SnClFe$ (827.77 g·mol^{-1}): C 52.23, H 7.43; found: C 52.15, H 7.15;

Spectroscopic Data:

IR (Nujol, cm^{-1}): (KBr) ν = 3031 (m), 3018 (m), 2728 (vw), 1930 (br, vw) (Fe-H), 1867 (br, vw) (Fe-H), 1752 (vs), 1700 (w), 1684 (vw), 1653 (w), 1646 (vw), 1635 (m), 1607 (m), 1570 (w), 1558 (m), 1553 (m), 1521 (vw), 1506 (vw), 1447 (s), 1436 (s), 1421 (s), 1346 (w), 1299 (s), 1286 (m), 1277 (s), 1209 (w), 1175 (w), 1101 (w), 1078 (w), 1033 (br w), 993 (w), 963 (m), 957 (s), 936 (br s), 894 (s), 846 (s), 823 (w), 800 (m), 736 (m), 710 (m br), 667 (s, br), 641 (w br), 591 (w), 549 (w), 535 (s), 472 (w).

^{1}H NMR: (300.13 MHz, C_6D_6, 298 K, ppm): δ = –16.33 (m, ^{2}J(H, $^{117/119}$Sn) = 191 Hz, Fe-$H_{\text{trans isomer}}$), –11.99 (m, ^{2}J(H, $^{117/119}$Sn) = 260 Hz, Fe-$H_{\text{cis isomer a}}$), –9.43 (m, ^{2}J(H, $^{117/119}$Sn) = 260 Hz, Fe-$H_{\text{cis isomer b}}$). (other resonance signals omitted).

^{119}Sn{^{1}H} NMR: (111.92 MHz, C_6D_6, 298 K, ppm): δ = –33.9 (br), –84.5 (br) ppm.

m/z (ESI positive): 1204.12, 1111.24, 793.21[M-Cl]$^{+}$, 717.16 [M-Cl-PMe_3]$^{+}$, 677.03, 595.18, 524.00, 449.09, 389.24, 312.19.

^{57}Fe Mößbauer Spectroscopy (80 K, mms^{-1}): δ = 0.19, ΔE_Q = 1.12.

Dieses Werk ist copyrightgeschützt und darf in keiner Form vervielfältigt werden noch an Dritte weitergegeben werden.
Es gilt nur für den persönlichen Gebrauch.

4.5.17 [(depe)Fe=Sn(CH_3)(2,6-Mes_2-C_6H_3)] (26-Fe)

A Schlenk tube was charged with **3-Fe** (0.296 g, 0.320 mmol) and dissolved in 20 mL of pentane in the glove box as a brown solution. Under rapid stirring MeLi (0.25 mL, 1.6 M, 0.40 mmol) was added dropwise *via* syringe to the brown solution at room temperature. No obvious colour change was observed. The reaction was stirred for 1 h at room temperature, and filtered *via* cannula, and the brown filtrate reduced to 3 mL *in vacuo*. This was stored at –60 °C for 48 h, during which time a brown solid precipitated. This brown solid was separated from the supernatant solution at –78 °C by cannula filtration, the filtrate discarded and the brown residue dried *in vacuo* for 1.5 h at room temperature. Yield: 0.207 g (0.226 mmol, 71 %). Crystals suitable for X-ray analysis were grown from a pentane solution of the substance at –30 °C.

Properties: Very soluble in pentane and benzene / toluene. Air sensitive: turns colourless on contact with air.

Melting point: 64 °C (decomposition).

Elemental Analysis: calcd (%) for $C_{45}H_{76}FeP_4Sn$ (915.53 $g\cdot mol^{-1}$): C 59.03, H 8.37; found: C 57.42, H 8.00.

Spectroscopic Data:

IR (Nujol, cm^{-1}): (KBr) ν = 2854 (m), 2361 (vw), 2341 (vw), 1700 (vw), 1653 (vw), 1611 (vw), 1559 (vw), 1541 (vw), 1157 (vw), 1027 (vw), 849 (vw), 802 (vw), 721 (w), 668 (vw), 599 (vw), 460 (vw), 419 (vw).

^{1}H-NMR: (300.1 MHz, C_6D_6, 298 K, ppm): δ = 0.45 (s, 3H, Sn-CH_3), 0.95 (s, 32H, 8 × CH_3, 2 × CH_2CH_2), 1.30 (m, 8H, 4 × CH_2), 1.49 (m, 4H, 2 × CH_2), 1.69 (m, 4H, 2 × CH_2), 2.24 (s, 6H, 2 × *p*-CH_3, Mes), 2.33 (s, 6H, 2 × C^6-CH_3, Mes), 2.37 (s, 6H, 2 × C^2-CH_3, Mes), 6.81 (s, 2H, 2 × C^5-H, Mes), 6.84 (s, 2H, 2 × C^3-H, Mes), 7.04 (d, 2H, ^3J(H,H) = 7.6 Hz, $C^{3,5}$-H, C_6H_3), 7.29 (t, 1H, ^3J(H,H) = 7.6 Hz, C^4-H, C_6H_3).

Dieses Werk ist copyrightgeschützt und darf in keiner Form vervielfältigt werden noch an Dritte weitergegeben werden.
Es gilt nur für den persönlichen Gebrauch.

$^{13}C\{^1H\}$-NMR: (75.5 MHz, C_6D_6, 298 K, ppm): δ = 9.6 (s, 4 C, 4 × CH_2CH_3), 9.8 (s, 4 C, 4 × CH_2CH_3,), 21.3 (s, 2 × C^4-CH_3, Mes), 22.4 (s, 2 × C^2-CH_3, Mes), 23.0 (s, 2 × C^6-CH_3, Mes), 24.6 (m, 2 × CH_2CH_2), 27.5 (s, 4 C, 4 × CH_2CH_3), 28.3 (s, 1 × Sn-CH_3), 30.6 (m, 4 C, 4 × CH_2CH_3), 126.0 (s, C^4, C_6H_3), 128.6 (s, 2 × C^5, Mes), 128.6 (s, 2 × C^3, Mes), 129.1 (s, $C^{3,5}$, C_6H_3), 135.4 (s, 2 × C^4, Mes), 136.8 (s, 2 × C^6, Mes), 136.9 (s, 2 × C^2, Mes), 142.9 (s, 2 C, C^1, Mes), 146.8 (s, $C^{2,6}$, C_6H_3), 173.9 (s, C^1, C_6H_3).

$^{31}P\{^1H\}$-NMR: (121.5 MHz, C_6D_6, 298 K, ppm): δ = 76.9 (s, $^2J(^{119/117}Sn, P)$ = 180 Hz).

$^{119}Sn\{^1H\}$-NMR: (111.9 MHz, C_6D_6, 298 K, ppm): δ = No resonance signal found in the range δ = –650 to + 1400 ppm.

4.5.18 [(depe)$_2$Fe=SnH(2,6-Mes$_2$-C$_6$H$_3$)] (27-Fe)

A Schlenk tube was charged with **3-Fe** (0.300 g, 0.321 mmol) and dissolved in 10 mL of pentane. This was cooled to –45 °C, where upon it was a brown suspension. 1.6 mL of a 0.4 M solution of Na[BEt$_3$H] (2 eq) was added to this suspension dropwise *via* syringe. On completion of the addition, a dark brown precipitate with an almost colourless supernatant solution is observed. The reaction was stirred for 1 minute at –45 °C, after completion of the addition, then taken out of the bath and stirred at room temperature for 0.5 h. On warming to room temperature a brown suspension in a reddish supernatant solution is observed. The reaction mixture was filtered *via* cannula at room temperature and the brown-red filtrate separated from 60 mg of a brown material, which was discarded. The filtrate was dried *in vacuo* resulting in an oil which was dried *in vacuo* for a further 0.5 h at room temperature. The oil was frozen in a bath of liquid nitrogen under static vacuum, and scratched into a powder, and re-dried for 0.5 h at room temperature. Crude Yield: 0.234 g. This solid was dissolved in a minimum amount of pentane (2 mL), and cooled to –30 °C for 72 h, upon which a brown solid crystallised out. The brown solid was separated from the brown-red supernatant solution at –78 °C *via* cannula, the supernatant solution was discarded, and the brown solid dried *in vacuo* at room temperature for 1 h. Yield : 0.140 g, (0.155 mmol, 48 %)

Dieses Werk ist copyrightgeschützt und darf in keiner Form vervielfältigt werden noch an Dritte weitergegeben werden.
Es gilt nur für den persönlichen Gebrauch.

Properties: Soluble in pentane and benzene / toluene. Air sensitive: turns colourless on contact with air.

Spectroscopic Data:

^{1}H NMR: (300.13 MHz, C_6D_6, 298 K, ppm): δ = 0.89 (br m, 24H, 8 × $\mathrm{C}H_3^{\mathrm{A+B}}$), 1.05 – 1.17 (m, 12H, 4 × $\mathrm{PC}H^{\mathrm{X}}H^{\mathrm{Y}}$ + 4 × $\mathrm{CH_3^BC}H^{\mathrm{X}}\mathrm{H^Y}$), 1.28 – 1.43 (m, 8H, 4 × $\mathrm{CH_3^AC}H_2^{\mathrm{X+Y}}$), 1.88 – 1.97 (m, 4H, 4 × $\mathrm{CH_3^BCH^X}H^{Y}$), 2.25 (s, 6H, 2 × $\mathrm{C^4\text{-}C}H_3$, Mes), 2.40 (s, 12H, 2 × $\mathrm{C^{2,6}\text{-}C}H_3$, Mes), 6.84 (s, 4H, 2 × $\mathrm{C^{3,5}}$-*H*, Mes), 7.08 (d, ^3J(H,H) = 7.4 Hz, 2H, $\mathrm{C^{3,5}}$-*H*, C_6H_3), 7.30 (t, ^3J(H,H) = 7.4 Hz, 1H, $\mathrm{C^4}$-*H*, C_6H_3), 14.50 (quint, ^3J(H,P) = 7.37 Hz, ^1J(H, $^{119/117}$Sn) = 509 Hz), 1H, Sn-*H*).

^{13}C{^{1}H}-NMR: (75.5 MHz, C_6D_6, 298 K, ppm): δ = 9.6 (s, 4 × $C\mathrm{H_3^A}$), 9.7 (s, 4 × $C\mathrm{H_3^B}$), 21.3 (s, 2 × $\mathrm{C^4\text{-}}C\mathrm{H_3}$, Mes), 22.1 (s, 2 × $\mathrm{C^{2,6}\text{-}}C\mathrm{H_3}$, Mes), 24.6 (m, $\mathrm{P}C\mathrm{H^XH^Y}$ or $\mathrm{CH_3^B}C\mathrm{H^XH^Y}$), 26.9 (m, 4 × $\mathrm{CH_3^A}C\mathrm{H_2^{X+Y}}$), 28.9 (m, $\mathrm{P}C\mathrm{H^XH^Y}$ or $\mathrm{CH_3^B}C\mathrm{H^XH^Y}$), 126.4 (s, C^4, C_6H_3), 128.2 (s, $C^{3,5}$, C_6H_3), 128.7 (s, 2 × $C^{3,5}$, Mes), 135.1 (s, 2 × $\mathrm{C^4}$, Mes), 136.6 (br s, 2 × $C^{2,6}$, Mes), 142.8 (s, 2 × $\mathrm{C^1}$, Mes), 147.7 (s, $C^{2,6}$, C_6H_3), 167.8 (s, C^1, C_6H_3).

^{31}P{^{1}H}-NMR: (121.5 MHz, C_6D_6, 298 K, ppm): δ = 79.4 (^2J($^{119/117}$Sn, P) = 206 Hz).

^{119}Sn{^{1}H}-NMR: (111.9 MHz, C_6D_6, 298 K, ppm): δ = 578.7 (quint, ^2J(^{119}Sn, P) = 213 Hz).

4.5.19 *trans*-[FeH($SnCl_3$)(depe)$_2$] (28-Fe)

A Schlenk tube was charged with *trans*- [FeClH(depe)$_2$] (0.100 g, 0.198 mmol) and dissolved in 10 mL of toluene at room temperature as an orange solution. To this orange solution, under rapid stirring at room temperature was added $SnCl_2$ (0.037 g, 0.20 mmol). An additional 20 mL of toluene was added to ensure all the $SnCl_2$ was in the reaction mixture. Initially the reaction was an orange solution with a white suspension ($SnCl_2$). The reaction was stirred for 18 h at room temperature during which the formation of a yellow precipitate

Dieses Werk ist copyrightgeschützt und darf in keiner Form vervielfältigt werden noch an Dritte weitergegeben werden.
Es gilt nur für den persönlichen Gebrauch.

was noticed, in an orange supernatant solution. *In situ* ^{31}P{^{1}H} NMR spectroscopy at this point revealed the formation of *trans*-[FeH(SnCl$_3$)(depe)$_2$], with unreacted *trans*-[FeClH(depe)$_2$] in a ratio 1:2. The reaction was allowed to stir for a further 8 h at room temperature, during which the supernatant solution turned green, and a substantial amount of yellow precipitate was noticed. *In situ* ^{31}P{^{1}H} NMR spectroscopy revealed complete consumption of *trans*- [FeClH(depe)$_2$], with *trans*-[FeH(SnCl$_3$)(depe)$_2$] visible and also *trans*-[FeCl$_2$(depe)$_2$]. The reaction solution was filtered *via* cannula at room temperature, and the green supernatant solution separated from the yellow precipitate. The green supernatant solution was evaporated to dryness and revealed by ^{1}H and ^{31}P NMR spectroscopy to be a mixture of *trans*-[FeClH(depe)$_2$] and *trans*-[FeH(SnCl$_3$)(depe)$_2$] (0.057 g). The yellow residue was extracted with THF (10 mL) and filtered *via* cannula. The yellow filtrate evaporated to dryness and the remaining yellow solid was dried *in vacuo* for 1h at room temperature. Yield: 0.065 g (0.094 mmol, 47 %)

Elemental Analysis: calcd (%) for $C_{20}H_{49}FeP_4SnCl_3$ (694.4 g.mol^{-1}): C 34.59, H 7.11; found: C 34.44, H 6.97 %.

Spectroscopic Data:

IR (Nujol, cm^{-1}): (KBr) ν = 1902 (br, m) (Fe-H), 1561 (vw), 1259 (w), 1153 (vw), 1096 (w), 1072 (w), 1025 (m), 874 (m), 809 (w), 762 (s), 749 (s), 717 (s), 680 (m), 667 (m), 617 (m), 606 (m), 473 (m), 455 (m), 423 (m).

^{1}H NMR: (300.13 MHz, THF-d_8, 298 K, ppm): $\delta = -19.68$ (quint, ^{2}J(H,P) = 52.5 Hz, ^{2}J(H,$^{117/119}$Sn) = 300 Hz, 1H, Fe-*H*), 1.02 – 1.16 (m, 12H, 4 × CH_3^{A}), 1.16 – 1.34 (m, 12H, 4 × CH_3^{B}), 1.39 – 1.57 (m, 4H, 4 × CH$_3^{\mathrm{A}}$$H^{\mathrm{X}}H^{\mathrm{Y}}$), 1.75 – 2.10 (m, 16H, 2 × PCH^{X}H$^{\mathrm{Y}}$CH^{X}H$^{\mathrm{Y}}$ + 2 × PCH$^{\mathrm{X}}$$H^{\mathrm{Y}}CH^{\mathrm{X}}$$H^{\mathrm{Y}}$ + 4 × CH$_3^{\mathrm{A}}$CH$^{\mathrm{X}}$$H^{\mathrm{Y}}$ + 4 × CH$_3^{\mathrm{B}}$CH^{X}H$^{\mathrm{Y}}$), 2.45 – 2.62 (m, 4H, CH$_3^{\mathrm{B}}$CH^{X}H$^{\mathrm{Y}}$).

^{31}P{^{1}H} NMR: (121.49 MHz, THF-d_8, 298 K, ppm): $\delta = 85.2$ (d, ^{2}J(P, $^{117/119}$Sn) = 274.6 Hz).

Dieses Werk ist copyrightgeschützt und darf in keiner Form vervielfältigt werden noch an Dritte weitergegeben werden.
Es gilt nur für den persönlichen Gebrauch.

$^{13}C\{^1H\}$ NMR: (75.47 MHz, THF-d_8, 298 K, ppm): δ = 9.8 (s, 4 × CH_3^A), 10.0 (s, 4 × CH_3^B), 22.6 – 23.4 (m, 4 × $CH_3^BCH_2$), 26.9 – 27.4 (m, 4 × PCH_2), 28.5 – 29.0 (m, 4 × $CH_3^ACH_2$).

$^{119}Sn\{^1H\}$ NMR: (111.92 MHz, THF-d_8, 298 K, ppm): δ = 83.07 (ps quint).

4.5.20 *trans*-[FeCl(SnCl$_3$)(depe)$_2$] (29-Fe)

A Schlenk tube was charged with **2-Fe** (0.300 g, 0.556 mmol) and anhydrous $SnCl_2$ (0.105 g, 0.556 mmol). Dichloromethane (20 mL) was added *via* cannula at room temperature to this solid mixture under rapid stirring. An emerald green solution is noticed with a white suspension immediately after addition. The reaction was stirred for 18 h at room temperature at which time the reaction had a greenish-turquoise colour, and was clear. The reaction solution was concentrated *in vacuo* to 1.5 mL and cooled to –30 °C for 2 h. A dark turquoise solid was separated from a greenish filtrate at –60 °C by cannula filtration, the filtrate discarded, and the remaining solid dried *in vacuo* at room temperature for 1 h, affording a dark turquoise solid as product, the NMR spectra of which were tentatively assigned on the basis of the $GeCl_3$ analogue, **31-Fe**. Yield: 0.352 g (0.483 mmol, 87 %) Crystals suitable for X-ray crystallographic analysis were grown from toluene with cooling to –30 °C, but yielded a poor quality data set – the structural motif was, however, as expected.

Properties: insoluble in pentane, soluble in and benzene / toluene. Air sensitive: turns brown on contact with air.

Melting Point: 120.5 °C (turns light green), 121.7 (turns brown).

Elemental Analysis: calcd (%) for $C_{20}H_{48}Cl_4FeP_4Sn$ (728.86): C 32.96, H 6.64, Cl 19.46; found: C 33.29, H 6.70, Cl 19.1 %

Spectroscopic Data:

IR (Nujol, cm^{-1}): (KBr) ν = 1418 (m), 1031 (s), 981 (vw), 875 (w), 820 (w), 756 (m), 727 (m), 701 (m), 677 (m), 616 (w), 602 (w), 477 (w), 457 (w).

Dieses Werk ist copyrightgeschützt und darf in keiner Form vervielfältigt werden noch an Dritte weitergegeben werden.
Es gilt nur für den persönlichen Gebrauch.

^{1}H NMR: (300.13 MHz, C_6D_6, 298 K, ppm): $\delta = 0.90$ (br, $\Delta\nu_{1/2} = 71.3$ Hz, 24H), 1.44 – 2.43 (two br overlapping signals, 20H), 3.43 (br, 4H).

^{1}H NMR: (300.13 MHz, Toluene-d_8, 298 K, ppm): $\delta = 1.02$ (br, $\Delta\nu_{1/2} = 71.3$ Hz, 24H,), 1.42 – 2.39 (two br overlapping signals, 20H), 2.69 (br, 4H).

^{1}H NMR: (300.13 MHz, Toluene-d_8, 212.6 K, ppm): $\delta = 0.91$ (br, $\Delta\nu_{1/2} = 46.0$ Hz, 12H), 1.17 (br, $\Delta\nu_{1/2} = 42.5$ Hz, 20H), 1.43 – 1.80 (br, 8H), 1.82 – 2.57 (br, 4H), 2.75 (br, $\Delta\nu_{1/2} = 45.4$ Hz).

^{31}P{^{1}H} NMR: (121.5 MHz, C_6D_6, 298 K, ppm): $\delta = 62.6$ (br, $\Delta\nu_{1/2} = 121.3$ Hz), flanked with broad $^{119/117}$Sn satellites.

^{31}P{^{1}H} NMR: (121.5 MHz, Toluene-d_8, 298 K, ppm): $\delta = 62.9$ (br, $\Delta\nu_{1/2} = 105.3$ Hz), flanked with broad $^{119/117}$Sn satellites).

^{31}P{^{1}H} NMR: (121.5 MHz, Toluene-d_8, 212.7 K, ppm): $\delta = 63.7$ (^2J(P,$^{119/117}$Sn) = 472 Hz, $\Delta\nu_{1/2} = 12.3$ Hz), $\delta = 62.3$ (**2-Fe**).

4.5.21 *trans*-[FeCl(GeCl$_3$)(depe)$_2$] (31-Fe)

To a solid mixture of FeCl$_2$(depe)$_2$ (0.200 g, 0.371 mmol) and GeCl$_2$(1,4-dioxane) (0.086 g, 0.37 mmol) was added dichloromethane (30 mL) which was pre-cooled to -78 °C under rapid stirring. An immediate colour change to purple-blue is noticed, with a white precipitate. The reaction was stirred at room temperature for 18 h, during which time the reaction went clear, indicating that all the GeCl$_2$·(1,4-dioxane) had reacted. The solvent was removed *in vacuo* at room temperature, resulting in a purple oily solid, which was scratched into a powder after freezing it under static vacuum in a liquid nitrogen bath. This purple powder was dried *in vacuo* at room temperature for a further 0.5 h and subsequently washed with pentane (2 × 5 mL). The pentane washings were discarded, and the resulting powder dried *in vacuo* for an additional hour at room temperature. This afforded a lavender coloured solid as product. Yield: 0.212 g (0.310 mmol, 84 %). Crystal suitable for X-ray diffraction analysis were grown from a toluene solution of the compound at –30 °C.

Dieses Werk ist copyrightgeschützt und darf in keiner Form vervielfältigt werden noch an Dritte weitergegeben werden.
Es gilt nur für den persönlichen Gebrauch.

Properties: insoluble in pentane, soluble in and benzene / toluene. Air sensitive: turns brown on contact with air.

Melting Point: 134.4 °C (turns green), 149.9 °C (green-black)

Elemental Analysis: calcd (%) for $C_{20}H_{48}Cl_4FeP_4Ge$ (682.79 g·mol^{-1}): C 35.18, H 7.09, Cl 20.77; found: C 34.80, H 6.73, Cl 20.8.

Spectroscopic Data:

IR (Nujol, cm^{-1}): (KBr) ν = 1411 (m), 1031 (s), 983 (vw), 874 (w), 820 (w), 756 (m), 727 (m), 701 (m), 678 (m), 617 (w), 602 (w), 475 (w), 452 (w), 419 (w).

^{1}H NMR: (300.13 MHz, C_6D_6, 298 K, ppm): $\delta = 0.95$ (br, 12H, 4 × CH_3^A), 1.17 (br, 12H, 4 × CH_3^B), 1.57 – 1.83 (m, 4H, 4 × $CH_3^ACH^XH^Y$) + (m, 4H, 2 × $PCH^XH^YCH^XH^YP$), 1.83 – 2.11 (m, 4H, 4 × $CH_3^ACH^XH^Y$) + (m, 4H, 4 ×$CH_3^BCH^XH^Y$), 2.20 (m, 4H, 2 × $PCH^XH^YCH^XH^YP$), 2.84 – 3.04 (m, 4H, 4 ×$CH_3^BCH^XH^Y$).

^{13}C{^{1}H} NMR: (75.47 MHz, C_6D_6, 298 K, ppm): $\delta = 9.9$ (s, 4 × CH_3^B), 10.1 (s, 4 × CH_3^A), 20.7 – 21.0 (m, 4 × $CH_3^ACH_2$ + 2 × PCH_2CH_2P), 23.5 (ps quint, $^nJ(^{13}C,P) = 5.7$ Hz $CH_3^BCH_2$).

^{31}P{^{1}H} NMR: (121.49 MHz, C_6D_6, 298 K, ppm): $\delta = 65.1$ (s, $\Delta\nu_{1/2} = 3.18$ Hz).

4.5.22 *trans*-[FeH(GeCl$_3$)(depe)$_2$] (32-Fe)

trans-[FeHCl(depe)$_2$] (0.150 g, 0.297 mmol) was dissolved in toluene (3.5 mL) and stirred as a clear orange solution at room temperature. $GeCl_2$·(1,4-dioxane) (0.069 g, 0.30 mmol) was added to the orange toluene solution as a solid. The walls of the reaction vessel were washed down with additional toluene (2 mL) to ensure all the $GeCl_2$·(1,4-dioxane) was in the reaction solution. The orange supernatant solution turns green after 5 minutes of stirring at room temperature, and a bright yellow precipitate is observed. The reaction was allowed to stir for

Dieses Werk ist copyrightgeschützt und darf in keiner Form vervielfältigt werden noch an Dritte weitergegeben werden.
Es gilt nur für den persönlichen Gebrauch.

a further 20 minutes at room temperature, and a khaki-green supernatant solution separated from the bright yellow precipitate by cannula filtration at room temperature. The khaki-coloured supernatant solution was discarded, and the remaining yellow precipitate dried *in vacuo* for 1 h at room temperature to afford **32-Fe** as product. Yield: 0.100 g (0.154 mmol, 51 %). Crystals suitable for X-ray diffraction analysis were grown from a concentrated THF solution of **32-Fe** at –30 °C

Elemental Analysis: calcd (%) for $C_{20}H_{49}Cl_3FeP_4Ge$ (648.34 g·mol^{-1}): C 37.05, H 7.62; found: C 36.25, H 7.32%.

Spectroscopic Data:

IR (Nujol, cm^{-1}): (KBr) ν = 1890 (w), 1878 (w) (both Fe-H), 1412 (m), 1261(w), 1249 (w), 1099 (w), 1025 (s), 998 (s), 876 (w), 856 (w), 811 (w), 758 (vs), 748 (s), 626 (m), 606 (m), 475 (w), 453 (w), 425 (w), 408 (w).

^{1}H NMR: (300.13 MHz, THF-d_8, 298 K, ppm): $\delta = -18.79$ (quint, ^2J(H, P) = 52.0 Hz, 1H, Fe-*H*), 1.03 – 1.15 (m, 12H, $4 \times C\mathit{H}_3^{A}$), 1.15 – 1.27 (m, 12H, $4 \times C\mathit{H}_3^{B}$), 1.39 – 1.61 (m, 4H, $4 \times CH_3^{A}\mathit{H}^{X}H^{Y}$), 1.69 – 2.13 (m, 16H, $2 \times PC\mathit{H}^{X}H^{Y}C\mathit{H}^{X}H^{Y} + 2 \times PCH^{X}\mathit{H}^{Y}CH^{X}\mathit{H}^{Y} + 4 \times CH_3^{A}CH^{X}\mathit{H}^{Y} + 4 \times CH_3^{B}C\mathit{H}^{X}H^{Y}$), 2.68 – 2.88 (m, 4H, $CH_3^{B}C\mathit{H}^{X}H^{Y}$).

^{31}P{^{1}H} NMR: (121.49 MHz, THF-d_8, 298 K, ppm): $\delta = 85.8$ (s)

^{13}C{^{1}H} NMR: (75.47 MHz, THF-d_8, 298 K, ppm): $\delta =$ 9.92 (s, $4 \times \mathit{C}H_3^{A}$), 9.93 (s, $4 \times \mathit{C}H_3^{B}$), 21.7 – 22.4 (m, $4 \times CH_3^{B}\mathit{C}H_2$), 25.7 – 26.2 (m underneath solvent signal, $4 \times P\mathit{C}H_2$), 28.1 – 28.6 (m, $4 \times CH_3^{A}\mathit{C}H_2$).

4.5.23 [GeCl$_2$(IMe$_2$Me$_2$)] (5-Ge)

A Schlenk tube was charged with GeCl$_2$·(1,4-dioxane) (0.913 g, 3.942 mmol) and the germanium compound suspended in 2 mL of toluene. A solution of IMe$_2$Me$_2$ (0.490, 3.946 mmol) in 20 mL toluene was added rapidly *via* cannula to the first suspension at room temperature under rapid stirring. An immediate colour change to yellow was noticed with the

Dieses Werk ist copyrightgeschützt und darf in keiner Form vervielfältigt werden noch an Dritte weitergegeben werden.
Es gilt nur für den persönlichen Gebrauch.

solution containing an amorphous orange solid. The reaction was stirred for 2 h at room temperature, and the resulting clear, near colourless solution was filtered from a waxy orange insoluble material. The remaining orange residue was extracted with toluene (2 × 1 mL), and the filtrates were combined. The filtrate was concentrated *in vacuo* at 35 – 40 °C to ca 2.5 mL, upon which an off white solid precipitated. The green-yellow mother liquor was separated from the solid by filtration and was discarded. The off-white precipitate was washed with hexane (2 mL) at room temperature, then pentane (1 mL) at – 60 °C, and finally toluene (2 × 0.5 mL) at –25 °C, and again pentane (2 × 1 mL) at –60 °C. The remaining solid was dried *in vacuo* at room temperature for 1 h, to afford compound **5-Ge** as an off white, microcrystalline powder. Yield: 0.759 g (2.835 mmol, 72%).

Melting Point: 104 °C.

Elemental analysis: calcd (%) for $C_7H_{12}Cl_2GeN_2$ (267.68 g·mol^{-1}): C 31.41, H 4.52, N 10.47, Cl 26.49; found: C 31.62, H 4.47, N 10.31, Cl 26.2 %.

Spectroscopic Data:

^{1}H NMR: (300.1 MHz, C_6D_6, 298 K, ppm): $\delta = 1.07$ (s, 6H, 2 × C*H*$_3$), 3.19 (s, 6H, 2 × NC*H*$_3$). ^{1}H NMR (400.1 MHz, THF-d$_8$, 298 K, ppm): $\delta = 2.19$ (s, 6H, 2 × CC*H*$_3$), 3.93 (s, 6H, 2 × NC*H*$_3$). ^{13}C{^{1}H} NMR (75.5 MHz, C_6D_6, 298 K, ppm): $\delta = 7.5$ (s, 2 × C*C*H$_3$, IMe$_2$Me$_2$), 33.0 (s, 2 × N*C*H$_3$, IMe$_2$Me$_2$), 125.7 (s, 2 × *C*CH$_3$, IMe$_2$Me$_2$), 166.1 (s, 1 × Ge-*C*, IMe$_2$Me$_2$).

UV-Vis: (THF): $\lambda_{max} = 277$ nm.

4.5.24 [GeCl(2,6-Mes$_2$-C$_6$H$_3$)(IMe$_2$Me$_2$)] (6-Ge)

A suspension of GeCl$_2$(IMe$_2$Me$_2$) (0.370 g, 1.382 mmol) in 15 mL of toluene was cooled to –78 °C. A pre-cooled (–78 °C) solution of Li(C$_6$H$_3$-2,6-Mes$_2$) (0.443 g, 1.383 mmol) in 15 mL of toluene, was added rapidly *via* cannula to the first suspension with stirring. The reaction mixture was stirred for 1 h at – 78 °C, at which point an almost colourless solution with a white insoluble solid were present. The Schlenk tube was then transferred to a –20 °C

Dieses Werk ist copyrightgeschützt und darf in keiner Form vervielfältigt werden noch an Dritte weitergegeben werden.
Es gilt nur für den persönlichen Gebrauch.

cooling bath and stirring was continued for a further 1 h upon which the reaction solution turned light blue. The mixture was then warmed to 0 °C and stirred at this temperature for an additional 2 h, to afford a Prussian blue coloured solution with a white precipitate. Upon stirring of the reaction mixture at room temperature for 0.5 h the colour of the solution turned orange and a white precipitate was present. 15 mL pentane was added to the mixture, and the suspension was filtered *via* cannula at room temperature. The residue was extracted with a toluene/pentane mixture (2 : 1) (2 × 10 mL), and the filtrates were combined leaving 120 mg of a white residue (LiCl) in the reaction vessel. The clear orange filtrate was concentrated *in vacuo* at room temperature to ca. 2 mL. Pre-cooled (0 °C) pentane (5 mL) was added to the filtrate *via* cannula, precipitating a light yellow solid, which was filtered off, washed with pentane (2 mL), and dried *in vacuo* for 0.5 h at room temperature to afford the product as a light yellow powder. Yield: 0.667 g (1.222 mmol, 88%).

Melting Point: 185 °C (dec).

Elemental analysis: calcd (%) for $C_{31}H_{37}ClGeN_2$ (545.67 g·mol^{-1}): C 68.23, H 6.83, N 5.14, Cl 6.50; found: C 68.91, H 6.86, N 4.71, Cl 5.7 %.

Spectroscopic Data:

^{1}H NMR: (300.1 MHz, C_6D_6, 298 K, ppm): δ = 1.15 (s, 6H, 2 × C*H*$_3$, IMe$_2$Me$_2$), 2.09 (s, 6H, 2 × C^2-C*H*$_3$, Mes), 2.17 (s, 6H, 2 × C^4-C*H*$_3$, Mes), 2.51 (s, 6H, 2 × C^6-C*H*$_3$, Mes), 2.91 (s, 6H, 2 × NC*H*$_3$, IMe$_2$Me$_2$), 6.64 (s, 2H, 2 × C^3-*H*, Mes), 6.87 (s, 2H, 2 × C^5-*H*, Mes), 6.98 (d, ^3J(H,H) = 7.5 Hz, 2H, C^{3,5}-*H*, C_6H_3), 7.24 (t, ^3J(H,H) = 7.5 Hz, 1H, 1 × C^4-*H*, C_6H_3).

^{1}H NMR: (400.1 MHz, THF-*d*$_8$, 298 K, ppm): δ = 1.92 (s, 6H, 2 × C*H*$_3$, Mes), 2.02 (s, 6H, 2 × CC*H*$_3$, IMe$_2$Me$_2$), 2.18 (s, 6H, 2 × C*H*$_3$, Mes), 2.25 (s, 6H, 2 × C*H*$_3$, Mes), 3.30 (s, 6H, 2 × NC*H*$_3$, IMe$_2$Me$_2$), 6.64 (s, 2H, 2 × C-*H*, Mes), 6.74 (d, ^3J(H,H) = 7.5 Hz, 2H, C^{3,5}-*H*, C_6H_3), 6.77 (s, 2H, 2 × C-*H*, Mes), 7.16 (t, ^3J(H,H) = 7.5 Hz, 1H, 1 × C^4-*H*, C_6H_3).

Dieses Werk ist copyrightgeschützt und darf in keiner Form vervielfältigt werden noch an Dritte weitergegeben werden.
Es gilt nur für den persönlichen Gebrauch.

^{13}C{^{1}H} NMR: (75.5 MHz, C$_6$D$_6$, 298 K, ppm): δ = 7.8 (s, 2 × C*C*H$_3$, IMe$_2$Me$_2$), 21.1 (s, 2 × C^4-*C*H$_3$, Mes), 21.2 (s, 2 × C^2-*C*H$_3$, Mes), 21.9 (s, 2 × C^6-*C*H$_3$, Mes), 34.0 (s, 2 × N*C*H$_3$, IMe$_2$Me$_2$), 124.2 (s, 2 × *C*CH$_3$, IMe$_2$Me$_2$), 126.7 (s, 1 × C^4, C$_6$H$_3$), 128.1 (s, 2 × C^3-H, Mes), 128.7 (s, 2 × C^5-H, Mes), 129.1 (s, 1 × $C^{3,5}$, C$_6$H$_3$), 135.3 (s, 2 × C^4, Mes), 135.7 (s, 2 × C^2, Mes), 136.7 (s, 2 × C^6, Mes), 141.3 (s, 2 × C^1, Mes), 147.1 (s, 1 × $C^{2,6}$, C$_6$H$_3$), 156.0 (s, 1 × C^1, C$_6$H$_3$), 170.5 (s, 1 × Ge-*C*, IMe$_2$Me$_2$).

UV-Vis (THF): λ_{max} = 315 nm

4.5.25 [GeI(2,6-Mes$_2$-C$_6$H$_3$)(IMe$_2$Me$_2$)] (7-Ge)

0.154 g (0.282 mmol) of Ge(C$_6$H$_3$-2,6-Mes$_2$)Cl(Im-Me$_4$) was suspended in 15 mL of diethyl ether, and LiI (0.049 g, 0.37 mmol) was added to the stirred suspension at ambient temperature. The reaction mixture was stirred for 16 h, and the solvent subsequently removed *in vacuo*. The pale yellow residue was extracted with a 2:1 toluene-pentane mixture (2 × 10 mL), and the filtered extract evaporated to dryness. The residue was taken up in 1 mL of toluene, and 3 mL of pentane was added to the solution and cooled to –78 °C. A pale lemon-yellow solid was separated from the supernatant solution, isolated by filtration at –78 °C, and dried *in vacuo* at room temperature for 0.5 h. The solid was taken up in a toluene-pentane mixture (10 × 2 mL), and the mixture cooled to –78 °C, after which a small amount of a white solid (LiCl/LiI) had precipitated. The supernatant yellow solution was separated from the white precipitate by filtration at –78 °C, and evaporated to dryness at ambient temperature. The resulting residue was washed with 2 mL of pentane, and dried *in vacuo* at ambient temperature for 0.5 h to afford the pentane hemisolvate of **7-Ge** as a pale lemon-yellow solid. Yield: 0.080 g (0.119 mmol, 42%).

Elemental analysis: calcd (%) for C$_{33.5}$H$_{43}$GeIN$_2$ (673.22 g·mol^{-1}): C 59.77, H 6.44, N 4.16; found: C 59.35, H 6.34, N 4.21%.

Spectroscopic Data:

^{1}H NMR: (300.1 MHz, C$_6$D$_6$, 298 K, ppm): δ = 0.86 (t, ^3J(H,H) = 7.0 Hz, 3H, 2 × *Me*, 0.5 pentane), 1.16 (s, 6H, C^{4,5}-*Me*, Im-Me$_4$), 1.20 – 1.27 (m, 3H,

Dieses Werk ist copyrightgeschützt und darf in keiner Form vervielfältigt werden noch an Dritte weitergegeben werden.
Es gilt nur für den persönlichen Gebrauch.

$3 \times CH_2$, 0.5 pentane), 2.04 (s, 6H, $2 \times C^2$-*Me*, Mes), 2.17 (s, 6H, $2 \times C^4$-*Me*, Mes), 2.49 (s, 6H, $2 \times C^6$-*Me*, Mes), 2.92 (br s, 6H, 2 × N-*Me*, Im-Me_4), 6.63 (s, 2H, $2 \times C^3$-*H*, Mes), 6.88 (s, 2H, $2 \times C^5$-*H*, Mes), 6.96 (d, ^3J(H,H) = 7.5 Hz, 2H, $C^{3,5}$-*H*, C_6H_3), 7.21 (t, ^3J(H,H) = 7.5 Hz, 1H, C^4-*H*, C_6H_3).

$^{13}C\{^1H\}$ NMR: (75.47 MHz, C_6D_6, 298 K, ppm): $\delta = 7.9$ (s, $C^{4,5}$-*Me*, Im-Me_4), 14.2 (s, 2 × *Me*, 0.5 pentane), 21.0 (s, $2 \times C^2$-*Me*, Mes), 21.1 (s, $2 \times C^4$-*Me*, Mes), 21.8 (s, $2 \times C^6$-*Me*, Mes), 22.7 (s, $2 \times CH_2$, 0.5 pentane), 34.4 (s, $1 \times CH_2$, 0.5 pentane), 34.9 (br s, 2 × N-*Me*, Im-Me_4), 124.5 (s, $C^{4,5}$, Im-Me_4), 126.8 (s, C^4-H, C_6H_3), 128.1 (s, $2 \times C^3$-H, Mes), 129.08 (s, $2 \times C^5$-H, Mes), 129.11 (s, $C^{3,5}$-H, C_6H_3), 135.8 (s, $2 \times C^4$, Mes), 136.3 (s, $2 \times C^2$, Mes), 136.6 (s, $2 \times C^6$, Mes), 141.1 (s, $2 \times C^1$, Mes), 147.4 (s, $C^{2,6}$, C_6H_3), 150.7 (s, C^1, C_6H_3), 166.9 (s, Ge-C^2, Im-Me_4).

4.5.26 [GeCl(2,6-Mes_2-C_6H_3)(PMe_3)] (8-Ge)

[$GeCl_2(PMe_3)$] (0.300g, 1.366 mmol) was dissolved in 20 mL of toluene and cooled to –78 °C, as an opaque but colourless solution. To this under rapid stirring was added dropwise *via* cannula a yellow 30 mL solution of Li(2,6-Mes_2-C_6H_3) (0.437 g, 1.366 mmol) in Toluene. On completion of the addition the reaction mixture is opaque and light yellow. The reaction was stirred at –78 °C for 5 minutes, and then at room temperature for 2 h. During this time, no further colour changes were noticed. Benzene (25 mL) was added to the reaction mixture, along with pentane (15 mL), and the reaction mixture filtered at room temperature *via* cannula. The light yellow filtrate was concentrated to 3 mL and pentane was added (10 mL), and cooled to –30 °C overnight. A small amount of white precipitate remained behind in the original reaction vessel. No crystalline material was observed upon storing the compound overnight at –30 °C, so the solvent was removed completely *in vacuo* at room temperature, dried for 0.5 h at room temperature *in vacuo* at which point it was a yellow oil. The yellow oil was frozen under static vacuum in a liquid nitrogen bath, and scratched to a powder. This process was repeated twice, resulting in an amorphous yellow solid at room temperature. Pentane was added to the solid, which resulted in a fine yellow powder-like solid, which was stored at –78 °C for 15 minutes, and the supernatant liquid removed *via* cannula filtration at

Dieses Werk ist copyrightgeschützt und darf in keiner Form vervielfältigt werden noch an Dritte weitergegeben werden.
Es gilt nur für den persönlichen Gebrauch.

–78 °C. The remaining yellow solid showed by NMR to be impure, so it was carefully washed with pentane (2 × 5 mL), the pentane washings discarded, and the remaining yellow solid dried *in vacuo* at RT for 1 h. Yield: 0.477 g (0.958 mmol, 70 %)

Elemental Analysis: calcd (%) for $C_{27}H_{34}GeClP$ (497.63 g·mol^{-1}): C 65.17, H 6.89, Cl 7.12; found: C 64.52, H 6.73, Cl 7.0 %.

Spectroscopic Data:

^{1}H NMR: (300.1 MHz, C_6D_6, 298 K, ppm): δ = 0.51 (d, ^{2}J(H,P) = 8.4 Hz, 9H, P(C*H*$_3$)$_3$), 2.16 (s, 6H, *p*-C*H*$_3$, Mes), 2.30 (s, 12H, *o*-C*H*$_3$, Mes), 6.84 (s, 4H, *m-H*, Mes), 8.40 (d, ^{3}J(H,H) = 7.5 Hz, C^{3,5}-*H*, C_6H_3), 7.22 (t, ^{3}J(H,H) = 7.5 Hz, C^{4}-*H*, C_6H_3).

^{1}H NMR: (300.1 MHz, Toluene-*d*$_8$, 298 K, ppm): δ = 0.53 (d, ^{2}J(H,P) = 9.4 Hz, 9H, P(C*H*$_3$)$_3$), 2.18 (s, 6H, *p*-C*H*$_3$, Mes), 2.25 (s, 12H, *o*-C*H*$_3$, Mes), 6.81 (s $\Delta\nu_{½}$ = 6.8 Hz, 4H, *m-H*, Mes), 6.85 (d, ^{3}J(H,H) = 7.5 Hz, C^{3,5}-*H*, C_6H_3), 7.21 (t, ^{3}J(H,H) = 7.5 Hz, C^{4}-*H*, C_6H_3).

^{1}H NMR: (300.1 MHz, Toluene-*d*$_8$, 273 K, ppm): δ = 0.49 (d, ^{2}J(H,P) = 9.4 Hz, 9H, P(C*H*$_3$)$_3$), 2.18 (s, 6H, *p*-C*H*$_3$, Mes), 2.28 (br s $\Delta\nu_{½}$ = 16.2 Hz, 12H, *o*-C*H*$_3$, Mes), 6.81 (s $\Delta\nu_{½}$ = 3.0 Hz, 4H, *m-H*, Mes), 6.86 (d, ^{3}J(H,H) = 7.5 Hz, C^{3,5}-*H*, C_6H_3), 7.22 (t, ^{3}J(H,H) = 7.5 Hz, C^{4}-*H*, C_6H_3).

^{1}H NMR: (300.1 MHz, Toluene-*d*$_8$, 253 K, ppm): δ = 0.46 (d, ^{2}J(H,P) = 9.4 Hz, 9H, P(C*H*$_3$)$_3$), 2.18 (s, 6H, *p*-C*H*$_3$, Mes), 2.27 (br s, 6H, C^{2}-C*H*$_3$, Mes), 2.34 (br s, 6H, C^{6}-C*H*$_3$, Mes) 6.80 (s $\Delta\nu_{½}$ = 3.8 Hz, 4H, *m-H*, Mes), 6.87 (d, ^{3}J(H,H) = 7.5 Hz, C^{3,5}-*H*, C_6H_3), 7.23 (t, ^{3}J(H,H) = 7.5 Hz, C^{4}-*H*, C_6H_3).

^{1}H NMR: (300.1 MHz, Toluene-*d*$_8$, 233 K, ppm): δ = 0.462 (d, ^{2}J(H,P) = 9.7 Hz, 9H, P(C*H*$_3$)$_3$), 2.18 (s, 6H, *p*-C*H*$_3$, Mes), 2.29 (br s $\Delta\nu_{½}$ = 5.7 Hz, 6H, C^{2}-C*H*$_3$, Mes), 2.38 (br s $\Delta\nu_{½}$ = 5.4 Hz, 6H, C^{6}-C*H*$_3$, Mes) 6.80 (br s

Dieses Werk ist copyrightgeschützt und darf in keiner Form vervielfältigt werden noch an Dritte weitergegeben werden.
Es gilt nur für den persönlichen Gebrauch.

$\Delta\nu_{1/2}$ = 7.6 Hz , 4H, *m-H*, Mes), 6.87 (d, ^{3}J(H,H) = 7.5 Hz, $C^{3,5}$-*H*, C_6H_3), 7.23 (t, ^{3}J(H,H) = 6.9 Hz, C^4-*H*, C_6H_3).

$^{13}C\{^{1}H\}$ NMR: (75.47 MHz, C_6D_6, 298 K, ppm): δ = 10.4 (d, $^{1}J(^{13}C,P)$ = 15.3 Hz, P(CH_3)$_3$), 21.1 (s, 2 × *p*-CH_3, Mes), 22.0 (s, 4 × *o*-CH_3, Mes), 128.7 (s, 4 × *m-C*, Mes) + (2 × *m-C*, C_6H_3), 129.0 (s, 1 × *p-C*, C_6H_3), 136.6 (s, 2 × *p-C*, Mes), 137.1 (s, 4 × *o-C*, Mes), 141.6 (s, 2 × C^1, Mes), 147.4 (s, 2 × *o-C*, C_6H_3), 154.9 (s, *C*-Ge).

$^{31}P\{^{1}H\}$ NMR: (121.49 MHz, C_6D_6, 298 K, ppm): δ = –29.5 (br s, $\Delta\nu_{1/2}$ = 53.2 Hz).

$^{31}P\{^{1}H\}$ NMR: (121.49 MHz, Toluene-d_8, 273 K, ppm): δ = –29.6 (br s, $\Delta\nu_{1/2}$ = 33.9 Hz).

$^{31}P\{^{1}H\}$ NMR: (121.49 MHz, Toluene-d_8, 253 K, ppm): δ = –28.1 (br s, $\Delta\nu_{1/2}$ = 12.5 Hz).

$^{31}P\{^{1}H\}$ NMR: (121.49 MHz, Toluene-d_8, 233 K, ppm): δ = –27.4 (br s, $\Delta\nu_{1/2}$ = 5.4 Hz).

4.5.27 [Rh{$SnCl_2(C_6H_3$-2-Mes-6-η^6-Mes)}(η^2-C_2H_4)] (2-Rh)

To a stirred suspension of [RhCl(η^2-C_2H_4)$_2$]$_2$ (0.045 g, 0.12 mmol) in 3 mL of toluene was added *via* syringe at room temperature a solution of 0.109 g (0.12 mmol) of {SnCl(2,6-Mes_2-C_6H_3)}$_2$ (in 3 mL of toluene. Initially the reaction mixture had a red-brown appearance, and after several hours turned into a red-orange suspension. The reaction mixture was stirred for a total of 17 h at room temperature. Filtration *via* a cannula separated a red-brown filtrate from an olive-green, insoluble solid (0.074 g). The filtrate was evaporated to dryness and the residue washed with 4 mL of pentane and dried *in vacuo* at room temperature for 0.5 h to afford compound **1** as a brown powder. Yield: 0.074 g (0.12 mmol, 50%). Crystals suitable for X-ray analysis were grown from a concentrated toluene solution at –30 °C.

Elemental analysis calcd (%) for $C_{26}H_{29}Cl_2RhSn$ (634.03 g·mol^{-1}): C 49.25, H 4.61, Cl 11.18; found: C 49.09, H 4.68, Cl 11.23%.

Dieses Werk ist copyrightgeschützt und darf in keiner Form vervielfältigt werden noch an Dritte weitergegeben werden.
Es gilt nur für den persönlichen Gebrauch.

Spectroscopic Data:

^{1}H-NMR: (300.1 MHz, $\mathrm{C_6D_6}$, 298 K, ppm): δ = 1.11 (s, 3H, $\mathrm{C^{4}}$-$\mathrm{C}H_{3}$, η^{6}-Mes), 1.74 (s, 6H, $\mathrm{C^{2,6}}$-$\mathrm{C}H_{3}$, η^{6}-Mes), 2.20 (s, 3H, $\mathrm{C^{4}}$-$\mathrm{C}H_{3}$, Mes), 2.35 (s, 6H, $\mathrm{C^{2,6}}$-$\mathrm{C}H_{3}$, Mes), 2.80 (d, ^{2}J(H,Rh) = 2.5 Hz, 4H, $\mathrm{C_2}H_4$), 5.50 (s, 2H, $\mathrm{C^{3,5}}$-H, η^{6}-Mes), 6.99 (dd, ^{3}J(H,H) = 7.5 Hz, ^{4}J(H,H) = 1.2 Hz, 1H, $\mathrm{C^{5}}$-H, $\mathrm{C_6H_3}$), 7.05 (br s, 2H, $\mathrm{C^{3,5}}$-H, Mes), 7.09 (dd, ^{3}J(H,H) = 7.5 Hz, ^{4}J(H,H) = 1.2 Hz, 1H, $\mathrm{C^{3}}$-H, $\mathrm{C_6H_3}$), 7.22 (t, ^{3}J(H,H) = 7.5 Hz, 1H, $\mathrm{C^{4}}$-H, $\mathrm{C_6H_3}$).

^{13}C{^{1}H}-NMR: (75.47 MHz, $\mathrm{C_6D_6}$, 289 K, ppm): δ = 16.6 (s, $\mathrm{C^{4}}$-$C\mathrm{H_3}$, η^{6}-Mes), 19.8 (s, $\mathrm{C^{2,6}}$-$C\mathrm{H_3}$, η^{6}-Mes), 21.3 (s, $\mathrm{C^{4}}$-$C\mathrm{H_3}$, Mes), 21.8 (s, $\mathrm{C^{2,6}}$-$C\mathrm{H_3}$, Mes), 36.8 (d, ^{1}J(C,Rh) = 13.5 Hz, $C_2\mathrm{H_4}$), 103.0 (d, ^{1}J(C,Rh) = 1.9 Hz, C^{4}-$\mathrm{CH_3}$, η^{6}-Mes), 103.2 (d, ^{1}J(C,Rh) = 2.3 Hz, $C^{3,5}$-H, η^{6}-Mes), 113.3 (d, ^{1}J(C,Rh) = 2.9 Hz, $C^{2,6}$-$\mathrm{CH_3}$, η^{6}-Mes), 123.1 (d, ^{1}J(C,Rh) = 4.8 Hz, C^{1}, η^{6}-Mes), 125.0 (s, C^{5}-H, $\mathrm{C_6H_3}$), 128.7 (s, $C^{3,5}$-H, Mes), 129.9 (s, C^{3}-H, $\mathrm{C_6H_3}$), 130.6 (s, C^{4}-H, $\mathrm{C_6H_3}$), 136.3 (s, $C^{2,6}$-$\mathrm{CH_3}$, Mes), 137.3 (s, C^{4}-$\mathrm{CH_3}$, Mes), 138.6 (s, C^{1}, Mes), 138.8 (s, C^{6}, $\mathrm{C_6H_3}$), 150.2 (s, C^{2}, $\mathrm{C_6H_3}$), 166.2 (d, ^{2}J(C,Rh) = 8.1 Hz, Sn-C^{1}, $\mathrm{C_6H_3}$).

^{119}Sn-NMR: (111.9 MHz, $\mathrm{C_6D_6}$, 298 K, ppm): δ = 54.3 (d, ^{1}J(Sn,Rh) = 1095 Hz).

4.5.28 [Rh{GeCl$_2$(C$_6$H$_3$-2-Trip-6-η^6-Trip)}(η^2-C$_2$H$_4$)] (3-Rh)

A solution of GeCl($\mathrm{C_6H_3}$-2,6-$\mathrm{Trip_2}$) (0.606 g, 1.027 mmol) in 10 mL of toluene was added *via* syringe at room temperature to a stirred suspension of [RhCl(η^{2}-$\mathrm{C_2H_4}$)$_2$]$_2$ (0.200 g, 0.514 mmol) in 5 mL of toluene. The reaction mixture was stirred for 18 h at room temperature, during which it became a clear orange solution. The solution was filtered, the filtrate was evaporated to dryness, and the resulting residue dried *in vacuo* for 1 h at room temperature. The obtained solid was subsequently washed with pentane (2 × 5 mL), and dried *in vacuo* for 1 h at room temperature to afford compound **3-Rh** as a bright yellow powder. Yield: 0.530 g

Dieses Werk ist copyrightgeschützt und darf in keiner Form vervielfältigt werden noch an Dritte weitergegeben werden.
Es gilt nur für den persönlichen Gebrauch.

(0.701 mmol, 68%). Crystals suitable for X-ray analysis were grown from a concentrated toluene solution at –30 °C

Melting Point: 88 °C

Elemental analysis: calcd (%) for $C_{38}H_{53}Cl_2GeRh$ (756.24 g·mol^{-1}): C 60.35, H 7.06, Cl 9.38; found: C 59.90, H 7.07, Cl 9.20 %.

Spectroscopic Data:

IR (Nujol, cm^{-1}): ν = 3060 (m), 3045 (m), 3035 (m), 1606 (m), 1559 (m), 1542 (w), 1500 (vw), 1416 (m), 1354 (s), 1336 (w), 1312 (m), 1253 (vw), 1231 (vw), 1193 (m), 1169 (m), 1153 (w), 1100 (m), 1078 (m), 1048 (w), 1030 (vw), 955 (w), 938 (w), 871 (w), 822 (vw), 800 (m to s), 764 (w), 748 (w), 722 (vw), 709 (vw), 651 (vw).

^{1}H NMR: (300.1 MHz, C_6D_6, 298 K, ppm): δ = 0.73 (d, ^3J(H,H) = 6.9 Hz, 6H, C^4-CH(C$\mathit{H_3}$)$_2$, η^6-Trip), 0.93 (d, ^3J(H,H) = 6.9 Hz, 6H, $C^{2,6}$-CH(C$\mathit{H_3^A}$)(CH$_3^B$), η^6-Trip), 1.15 (d, ^3J(H,H) = 6.9 Hz, 6H, $C^{2,6}$-CH(C$\mathit{H_3^A}$)(CH$_3^B$), Trip), 1.29 (d, ^3J(H,H) = 6.9 Hz, 12H, $C^{2,6}$-CH(CH$_3^A$)(C$\mathit{H_3^B}$) (η^6-Trip) + , C^4-CH(C$\mathit{H_3}$)$_2$ (Trip)), 1.63 (d, ^3J(H,H) = 6.9 Hz, 6H, $C^{2,6}$-CH(CH$_3^A$)(C$\mathit{H_3^B}$), Trip), 1.88 (sept, ^3J(H,H) = 6.9 Hz, 1H, C^4-CH(CH$_3$)$_2$, η^6-Trip), 2.44 (sept, ^3J(H,H) = 6.9 Hz , 2H, $C^{2,6}$-CH(CH$_3^A$)(CH$_3^B$), η^6-Trip), 2.91 (sept, ^3J(H,H) = 6.9 Hz, 1H, C^4-CH(CH$_3$)$_2$, Trip), 3.01 (sept, ^3J(H,H) = 6.9 Hz, 2H, $C^{2,6}$-CH(CH$_3^A$)(CH$_3^B$), Trip), 3.07 (d, ^2J(H,Rh) = 2.4 Hz, 4H, $C_2\mathit{H_4}$), 6.25 (s, 2H, $C^{3,5}$-H, η^6-Trip), 7.19 (t, ^3J(H,H) = 7.3 Hz, 1H, C^4-H, C_6H_3), 7.32 (s, 2H, $C^{3,5}$-H, Trip), 7.35 – 7.40 (overlapping multiplets, 2H, C^3-H + C^5-H, C_6H_3).

^{13}C{^{1}H}-NMR: (75.47 MHz, C_6D_6, 298 K, ppm): δ = 22.8 (s, $C^{2,6}$-CH(CH$_3^A$)(CH$_3^B$), Trip), 22.9 (s, C^4-CH(CH$_3$)$_2$, η^6-Trip), 24.40 and 24.44 (s each, $C^{2,6}$-CH(CH$_3^A$)(CH$_3^B$) (η^6-Trip) + C^4-CH(CH$_3$)$_2$ (Trip)), 24.9 (s, $C^{2,6}$-CH(CH$_3^A$)(CH$_3^B$), η^6-Trip), 26.6 (s, $C^{2,6}$-CH(CH$_3^A$)(CH$_3^B$), Trip), 29.5

Dieses Werk ist copyrightgeschützt und darf in keiner Form vervielfältigt werden noch an Dritte weitergegeben werden.
Es gilt nur für den persönlichen Gebrauch.

(s, $\mathrm{C}^{2,6}$-CH($\mathrm{CH_3}^{\mathrm{A}}$)($\mathrm{CH_3}^{\mathrm{B}}$), η^6-Trip), 31.5 (s, $\mathrm{C}^{2,6}$-CH($\mathrm{CH_3}^{\mathrm{A}}$)($\mathrm{CH_3}^{\mathrm{B}}$), Trip), 32.6 (s, C^4-CH($\mathrm{CH_3}$)$_2$, η^6-Trip), 34.9 (s, C^4-CH($\mathrm{CH_3}$)$_2$, Trip), 41.9 (d, ^1J(C,Rh) = 13.6 Hz, $C_2\mathrm{H}_4$), 98.9 (d, ^1J(C,Rh) = 1.6 Hz, $C^{3,5}$-H, η^6-Trip) 118.2 (d, ^1J (C,Rh) = 1.0 Hz, C^4, η^6-Trip), 119.5 (d, ^1J(C,Rh) = 4.9 Hz, C^1, η^6-Trip), 120.5 (s, $C^{3,5}$-H, Trip), 124.0 (d, ^1J(C,Rh) = 3.5 Hz, $C^{2,6}$, η^6-Trip), 125.8 (s, C^3-H or C^5-H, $\mathrm{C_6H_3}$), 128.7 (s, C^4-H, $\mathrm{C_6H_3}$), 132.7 (s, C^3-H or C^5-H, $\mathrm{C_6H_3}$), 135.7 (s, C^1, Trip), 138.2 (s, C^6, $\mathrm{C_6H_3}$), 146.8 (C^2, $\mathrm{C_6H_3}$), 147.0 (s, $C^{2,6}$, Trip), 148.9 (s, C^4, Trip), 160.1 (d, ^2J(C,Rh) = 7.4 Hz, Ge-C^1, $\mathrm{C_6H_3}$).

Dieses Werk ist copyrightgeschützt und darf in keiner Form vervielfältigt werden noch an Dritte weitergegeben werden.
Es gilt nur für den persönlichen Gebrauch.

4.6 Starting materials, not commercially available prepared by modified literature procedures[§§§§]

4.6.1 [GeCl$_2$(PMe$_3$)] (4-Ge)

To a yellow suspension of GeCl$_2$(1,4-dioxane) (1.00g, 4.32 mmol) in 30 mL of toluene was added dropwise at RT 1.3 eq. PMe$_3$ (0.67 mL, 0.492 g, 6.48 mmol) *via* syringe through a rubber septum. No observable colour changes are noted and the reaction takes on the appearance of a yellow suspension. The reaction was stirred for 14 h at RT, upon which another 0.67 mL PMe$_3$ was added. Stirring was continued for another 1 h at RT and the reaction mixture filtered *via* cannula. The filtrate was a clear colourless solution, while a yellowish residue (25 mg) remained behind in the reaction vessel, which was discarded. Pentane (15 mL) was added to the colourless filtrate, upon which a white solid precipitated. This was cooled to –63 °C for 1 h to complete precipitation, and filtration at –78 °C *via* cannula resulted in the separation of a white solid from a colourless supernatant which was discarded. The white remaining solid was dried *in vacuo* for 1 h at RT. Yield: 0.780 g (3.552 mmol, 82 %)

Spectroscopic Data:

^{1}H-NMR: (300.1 MHz, C$_6$D$_6$, 298 K, ppm): δ = 0.64 (d, ^2J(H,P) = 11.0 Hz, 9H, P(CH_3)$_3$).

^{31}P{^{1}H} NMR: (121.5 MHz, C$_6$D$_6$, 298 K, ppm): δ = –20.1

4.6.2 [SnCl(2,6-Mes$_2$-C$_6$H$_3$)] (1-Sn)

With rapid stirring, a solution of **1-Li** (1.134 g, 3.54 mmol) in toluene (35 mL), cooled to –78 °C, was added slowly to a suspension of SnCl$_2$ (0.705 g, 3.71 mmol) in toluene (27 mL) which was also cooled to –78 °C, *via* cannula. Stirring for 0.5 h at –78 °C resulted in a light blue suspension, which upon warming to –30 °C, and stirring for 20 minutes, resulted in a reddish solution, which turned violet. The reaction was allowed to slowly reach room

---

[§§§§] New data is indicated in each case with *

Dieses Werk ist copyrightgeschützt und darf in keiner Form vervielfältigt werden noch an Dritte weitergegeben werden.
Es gilt nur für den persönlichen Gebrauch.

temperature where a colour change to orange was immediately followed by the work up procedure. This was done by adding pentane (25 mL) to the reaction mixture and filtering *via* cannula. The residue was extracted two additional times by each time adding toluene (10 mL), stirring the residue for 10 minutes, then adding pentane (5 mL) and filtering *via* cannula. The filtrates were combined and concentrated to *ca.* 5 ml volume, and pentane (30 mL) added to the concentrated solution. The mixture was stored at –30 °C overnight, and the yellow product isolated by cannula filtration, and dried *in vacuo* for 0.5 h at room temperature. Yield: 1.272 g (2.720 mmol, 77 %).

Spectroscopic Data:

The resonance signals in ^{1}H NMR in C_6D_6 are slightly concentration dependant:*

^{1}H NMR: (300.13 MHz, C_6D_6, 298 K, 10 mg.ml^{-1}, ppm): $\delta = 2.17$ br (s, 12H, $\mathrm{C}^{2,6}$-CH_3, Mes) + (s, 6H, C^4- CH_3, Mes), 6.81 (s, 4H, $\mathrm{C}^{3,5}$-H, Mes) 6.99 (d, ^3J(H,H) = 7.5 Hz, 2H, $\mathrm{C}^{3,5}$-H, C_6H_3), 7.22 (t, ^3J(H,H) = 7.5 Hz, 1H, C^4-H, C_6H_3).

^{1}H NMR: (300.13 MHz, C_6D_6, 298 K, 14 mg.ml^{-1}, ppm): $\delta = 2.17$ br (s, 12H, $\mathrm{C}^{2,6}$- CH_3, Mes) + (s, 6H, C^4- CH_3, Mes), 6.81 (s, 4H, $\mathrm{C}^{3,5}$-H, Mes) 6.99 (d, ^3J(H,H) = 7.5 Hz, 2H, $\mathrm{C}^{3,5}$-H, C_6H_3), 7.21 (t, ^3J(H,H) = 7.5 Hz, 1H, C^4-H, C_6H_3).

^{1}H NMR: (300.13 MHz, C_6D_6, 298 K, 20 mg.ml^{-1}): $\delta = 2.17$ (s, 12H, $\mathrm{C}^{2,6}$- CH_3, Mes); 2.18 (s, 6H, C^4- CH_3, Mes), 6.81 (s, 4H, $\mathrm{C}^{3,5}$-H, Mes) 6.98 (d, ^3J(H,H) = 7.5 Hz, 2H, $\mathrm{C}^{3,5}$-H, C_6H_3), 7.21 (t, ^3J(H,H) = 7.5 Hz, 1H, C^4-H, C_6H_3).

^{1}H NMR: (300.13 MHz, C_6D_6, 298 K, 30 mg.ml^{-1}, ppm): $\delta = 2.17$ (s, 12H, $\mathrm{C}^{2,6}$-CH_3, Mes); 2.19 (s, 6H, C^4- CH_3, Mes), 6.81 (s, 4H, $\mathrm{C}^{3,5}$-H, Mes) 6.98 (d, ^3J(H,H) = 7.5 Hz, 2H, $\mathrm{C}^{3,5}$-H, C_6H_3), 7.21 (t, ^3J(H,H) = 7.5 Hz, 1H, C^4-H, C_6H_3).

Dieses Werk ist copyrightgeschützt und darf in keiner Form vervielfältigt werden noch an Dritte weitergegeben werden.
Es gilt nur für den persönlichen Gebrauch.

^{1}H NMR: (300.13 MHz, C_6D_6, 298 K, 40 mg.ml^{-1}, ppm): δ = 2.16 (s, 12H, $C^{2,6}$-C*H*$_3$, Mes); 2.21 (s, 6H, C^4- C*H*$_3$, Mes), 6.81 (s, 4H, $C^{3,5}$-*H*, Mes) 6.97 (d, ^3J(H,H) = 7.5 Hz, 2H, $C^{3,5}$-*H*, C_6H_3), 7.20 (t, ^3J(H,H) = 7.5 Hz, 1H, C^4-*H*, C_6H_3).

^{1}H NMR: (300.13 MHz, C_6D_6, 298 K, 50 mg.ml^{-1}, ppm): δ = 2.16 (s, 12H, $C^{2,6}$-C*H*$_3$, Mes); 2.22 (s, 6H, C^4- C*H*$_3$, Mes), 6.81 (s, 4H, $C^{3,5}$-*H*, Mes) 6.97 (d, ^3J(H,H) = 7.5 Hz, 2H, $C^{3,5}$-*H*, C_6H_3), 7.20 (t, ^3J(H,H) = 7.5 Hz, 1H, C^4-*H*, C_6H_3).

^{1}H NMR: (300.13 MHz, C_6D_6, 298 K, 80 mg.ml^{-1}, ppm): δ = 2.15 (s, 12H, $C^{2,6}$-C*H*$_3$, Mes); 2.23 (s, 6H, C^4- C*H*$_3$, Mes), 6.81 (s, 4H, $C^{3,5}$-*H*, Mes) 6.97 (d, ^3J(H,H) = 7.5 Hz, 2H, $C^{3,5}$-*H*, C_6H_3), 7.20 (t, ^3J(H,H) = 7.5 Hz, 1H, C^4-*H*, C_6H_3).

4.6.3 $[Rh(C_2H_4)_2Cl]_2$ (1-Rh)

The original procedure: Cramer, R. *Inorg. Chem.* **1962**, *3*, 722. employs the bubbling of ethylene gas through a solution of $RhCl_3.3H_2O$, while we carried the reaction out in a glass autoclave, which results in approximately the same yield but in less time and with the added advantage of consuming less ethylene: A 100 mL glass autoclave was charged with $RhCl_3.3\,H_2O$ (1.00 g, 3.79 mmol), H_2O (1.5 mL) and MeOH (25 mL). The autoclave was closed, and purged 5 times by pressurising with ethylene gas at 6.5 bar and releasing the pressure each time. Finally, the autoclave was pressurised to 6.5 bar pressure, and left open to the ethylene cylinder to ensure the maintenance of this pressure, and stirred at room temperature. Initially the reaction solution had a dark red appearance, but after 0.5 h an orange precipitate started to develop. The reaction was continued under these conditions for a further 4 h, where the amount of the orange precipitate was notably more than in the beginning, and the intensity of colour in the supernatant solution decreased. The reactor was depressurised, and the orange precipitate isolated by filtration in air, followed by washing with MeOH (2 × 5 mL), and subsequently dried *in vacuo* for 1 h at room temperature to afford $[RhCl(\eta^2\text{-}C_2H_4)_2]_2$ as a bright orange powder. Yield: 0.420 g, (1. 08 mmol, 57 %).

Dieses Werk ist copyrightgeschützt und darf in keiner Form vervielfältigt werden noch an Dritte weitergegeben werden.
Es gilt nur für den persönlichen Gebrauch.

Spectroscopic Data:

^{1}H NMR: (400.1 MHz, $CDCl_3$, 298 K, ppm): δ = 3.15 (br s $\nu_{½}$= 54.9 Hz, 4 × CH_2=CH_2).

^{13}C{^{1}H}-NMR (300.1 MHz, $CDCl_3$, 298 K,ppm): δ = 61.3 (br s $\nu_{½}$= 57.9 Hz, 4 × CH_2=CH_2).

4.6.4 [Fe(depe)$_2$(N$_2$)] (1-Fe)

A solid mixture of **2-Fe** (1.042 g, 1.933 mmol) and Na sand (0.100 g, 2.33 eq) was stirred under an atmosphere of N_2 (1.2 bar) in nitrogen saturated THF (60 mL) at room temperature. The reaction was periodically placed for 5 minutes in the ultrasonic bath to ensure maximum surface area of Na sand. The mixture was stirred for 5 days until a red- brown reaction solution is noticed. The solvent was removed *in vacuo* and the brown tar like residue extracted with pentane (3 × 15 mL). The pentane filtrates were combined, concentrated to 5 mL, and cooled to –60 °C overnight. (This extraction procedure can be carried out under Ar). An orange solid was separated from the mother liquor (which was discarded) at –60 °C by cannula filtration and dried *in vacuo* for 1 h at room temperature. Yield: 0.849 g,(1.710 mmol, 89 %).

Elemental analysis: calcd (%) for $C_{20}H_{48}N_2FeP_4$ (496.35 g·mol^{-1}): C 48.40, H 9.75, N 5.64; found: C 48.69, H 9.67, N 5.08 %;

Spectroscopic Data:

IR (THF, cm^{-1}): ν = 1965 [ν(N$_2$)].

^{1}H NMR: (300.1 MHz, C_6D_6, 298 K, ppm): δ = 1.04 (br s, 24H, 8 × CH_3), 1.33 - 1.36 (br m, 8H, 4 × CH_2), 1.44 (br s, 8H, 4 × CH_2), 1.81 (br s, 8H, 4 × CH_2).

^{31}P{^{1}H} NMR (121.49 MHz, C_6D_6, 298 K, ppm): δ = 84.7 (s) $\Delta\nu_{½}$ = 2.97 Hz.

Dieses Werk ist copyrightgeschützt und darf in keiner Form vervielfältigt werden noch an Dritte weitergegeben werden.
Es gilt nur für den persönlichen Gebrauch.

$^{13}C\{^1H\}$ NMR* (75.46 MHz, C_6D_6, 298 K, ppm): δ = 9.1 (s, 8 × CH_3), 24.7 – 26.5 (m, CH_2), 26.6 – 27.3 (m, CH_2).

^{57}Fe Mößbauer Spectroscopy* (mms^{-1}): δ = 0.24, ΔE_Q = 2.14.

4.6.5 [$FeCl_2(depe)_2$] (2-Fe)

To a suspension of anhydrous $FeCl_2$ (0.641 g, 4.84 mmol) in toluene (30 ml) was added depe (2.00 g, 9.69 mmol) *via* syringe. An immediate colour change to green is noticed. The reaction was stirred for 3 h at room temperature, concentrated to incipient crystallisation, and cooled to –60 °C for 3h. It was subsequently filtered *via* cannula and a light green solid separated from the light green supernatant, which was discarded. The light green solid was dried *in vacuo* overnight. Yield: 2.403 g (4.456 mmol, 92 %).

Elemental analysis: calcd (%) for $C_{20}H_{48}Cl_2FeP_4$ (539.24 g·mol^{-1}): C 44.55, H 8.97; found: C 44.50, H 8.74 %

Spectroscopic Data:

^1H NMR: (400.1 MHz, C_6D_6, 298 K, ppm): δ = 1.16 (br t, ^3J(H,H) = 7.5 Hz, 24H, 8 × CH_3), 1.86 (br, 8H, 4 ×P–CH_2), 2.15 – 2.27 (br m, 16H, 8 ×CH_2).

$^{13}C\{^1H\}$NMR: (100.61 MHz, C_6D_6, 298 K, ppm): δ = 9.7 (s, 8 × CH_3), 17.9 (s, 8 × CH_3CH_2), 20.2 (s, 4 × PCH_2, bridge).

$^{31}P\{^1H\}$ NMR (161.97 MHz, C_6D_6, 298 K, ppm): δ = 75.13 (v br).

VT $^{31}P\{^1H\}$ NMR*: (121.49 MHz, $C_6D_5CD_3$):

T = 273 K, δ = 65.0, $\Delta\nu_{1/2}$ = 322.3 Hz;
T = 263 K, δ = 63.2 $\Delta\nu_{1/2}$ = 121.0 Hz;
T = 253 K, δ = 62.8 $\Delta\nu_{1/2}$ = 48.4 Hz;
T = 243 K, δ = 62.8 $\Delta\nu_{1/2}$ = 23.6 Hz;

Dieses Werk ist copyrightgeschützt und darf in keiner Form vervielfältigt werden noch an Dritte weitergegeben werden.
Es gilt nur für den persönlichen Gebrauch.

T = 233 K, δ = 62.9 $\Delta\nu_{½}$ = 11.4 Hz.

4.6.6 [FeCl$_2$(dmpe)$_2$] (14-Fe)

Anhydrous FeCl$_2$ (0.422 g, 3.33 mmol) was suspended in toluene (12 mL) and stirred rapidly at room temperature in the glove box. A solution of dmpe (1.00 g, 6.66 mmol) in toluene (12 mL) was added to this suspension rapidly *via* syringe. An immediate colour change to bright green is noticed. The reaction was stirred at room temperature for 2 h, after which time it was still a turbid green solution. More toluene (25 mL) was added, upon which all insoluble product dissolved. The reaction was filtered *via* cannula at room temperature, and the green supernatant concentrated *in vacuo* to 10 mL and cooled to –78 °C for 2 h. A precipitated green solid was collected by filtering off the light green supernatant solution at –78 °C which was discarded, and the solid was dried *in vacuo* at room temperature for 1h, resulting in a turquoise-green solid as product. Yield : 1.166 g (2.731 mmol, 82 %)

Elemental analysis: calcd (%): $C_{12}H_{32}Cl_2FeP_4$ (427.01 g·mol^{-1}): C 33.75, H 7.55; found: C 33.96, H 7.52.

Spectroscopic Data:

^{1}H NMR: (300.1 MHz, C_6D_6, 298 K, ppm): δ = 1.35 (ps quint, ^2J(H,P) = 2.0 Hz, 24H, 8 × CH_3), 1.96 (ps quint, 8H, 4 × CH_2).

^{31}P{^{1}H} NMR (121.5 MHz, C_6D_6, 298 K, ppm): δ = 59.6 (s).

^{13}C{^{1}H} NMR: (75.47 MHz, C_6D_6, 298 K, ppm): δ = 12.9 (ps quint, ^nJ(^{13}C, P) = 5.5 Hz, 8 × CH$_3$), 30.1 (ps quint, ^nJ(^{13}C, P) = 12.3 Hz, 4 × CH$_2$).

4.6.7 [{Fe(dmpe)$_2$}$_2$(μ-dmpe)] (15-Fe)

Method 1:

A Schlenk tube was charged with [FeCl$_2$(dmpe)$_2$] (0.200 g, 0.467 mmol) and Na sand (0.025 g, 1.09 mmol). THF (15 mL) was added to the solid mixture under rapid stirring *via* cannula

Dieses Werk ist copyrightgeschützt und darf in keiner Form vervielfältigt werden noch an Dritte weitergegeben werden.
Es gilt nur für den persönlichen Gebrauch.

at room temperature. Immediately following this, free dmpe (0.035 g, 0.233 mmol) was added to this solution *via* syringe at room temperature. A green solution is noted with no obvious colour changes. The reaction was then placed in the ultrasonic bath for 10 minutes, after which the solution took on a darker green appearance. The reaction was stirred for a further 0.5 h at room temperature, and then again placed in the ultrasonic bath for 10 minutes. After a further 1 h of stirring *in situ* $^{31}P\{^1H\}$ NMR spectroscopy was conducted on the reaction mixture. This showed a ratio of 25 : 5 [$FeCl_2(dmpe)_2$] : [$Fe(dmpe)_3$]. The reaction was stirred for a further 19 h, and at this point *in situ* $^{31}P\{^1H\}$ NMR spectroscopy revealed 24 : 6 : 3 [$FeCl_2(dmpe)_2$] : [$Fe(dmpe)_3$] : [$\{Fe(dmpe)_2\}_2(\mu\text{-}dmpe)$]. It was placed in the ultrasonic bath for a further 10 min, and then stirred for an additional 25 h, at which point repeated *in situ* $^{31}P\{^1H\}$ NMR spectroscopy revealed a ratio 15 : 7 : 17 [$FeCl_2(dmpe)_2$] : [$Fe(dmpe)_3$] : [$\{Fe(dmpe)_2\}_2(\mu\text{-}dmpe)$]. Stirring was continued for a further 24 h following this, and *in situ* $^{31}P\{^1H\}$ NMR spectroscopy revealed a ratio 1 : 2 [$FeCl_2(dmpe)_2$] : [$\{Fe(dmpe)_2\}_2(\mu\text{-}dmpe)$].The reaction was finally stirred for an additional 24 h, at which point it was assumed that the reaction was complete. Pentane (25 mL) added to the reaction mixture *via* cannula, and the reaction mixture filtered *via* cannula filtration at room temperature, yielding an orange filtrate. The solvent was removed *in vacuo* at room temperature, and the remaining orange residue dried *in vacuo* at room temperature for 1 h, yielding an orange solid as product. Yield: 0.159 g (0.184 mmol, 79 %). Crystals suitable for X-ray diffraction analysis* were grown at –30 °C from a THF : pentane solution of the complex.

Properties: Very soluble in C_6D_6 and THF. Sparingly soluble in Et_2O, and pentane. Very air sensitive: turns dark brown immediately on contact with air.

Spectroscopic Data:

^{1}H NMR: (300.1 MHz, C_6D_6, 298 K, ppm): $\delta = 1.01$ (d, $^2J(H,P) = 3.3$ Hz, 12H, 4 × CH_3, μ-dmpe), 1.26 (br s, $\Delta\nu_{½} = 6.6$ Hz, 24H, 8 × CH_3^A), 1.28 – 1.32 (m, 4H, PCH_2CH_2P, μ-dmpe), 1.47 – 1.53 (overlapping partially with signal at $\delta = 1.56$) (m, 8H, 4 × $PCH^XH^YCH^XH^YP$), 1.56 (br s, $\Delta\nu_{½}$ = 7.0 Hz, 24H, 8 × CH_3^B), 1.64 – 1.82 (m, 8H, 4 × $PCH^XH^YCH^XH^YP$).

Dieses Werk ist copyrightgeschützt und darf in keiner Form vervielfältigt werden noch an Dritte weitergegeben werden.
Es gilt nur für den persönlichen Gebrauch.

$^{31}P\{^1H\}$ NMR: (121.5 MHz, C_6D_6, 298 K, ppm): δ = 8.2 - 8.7 (m, 2P, 1 × μ-dmpe), 61.5 (d, ^2J(P,P) = 11.4 Hz, 8P, 4 × dmpe).

Method 2:

A Schlenk tube was charged with [$FeCl_2$(dmpe)$_2$] (0.140 g, 0.329 mmol) and KC_8 (0.140 g, 1.04 mmol) and thoroughly stirred. Free dmpe (0.024 g) was added to THF (20 mL), and the solution added slowly *via* syringe under stirring at room temperature to the solid mixture of KC_8 and [$FeCl_2$(dmpe)$_2$]. The reaction was stirred at room temperature for 2 h and *in situ* $^{31}P\{^1H\}$ NMR spectroscopy conducted which revealed complete consumption of [$FeCl_2$(dmpe)$_2$] and a ratio of 8 : 3 [Fe(dmpe)$_3$] : [{Fe(dmpe)$_2$}$_2$(μ-dmpe)].

4.6.8 [$FeCl_2(PMe_3)_2$] (19-Fe)

A Schlenk tube was charged with anhydrous $FeCl_2$ (1.00 g, 7.88 mmol) and suspended in Toluene (50 ml). PMe_3 (1.800 g, 2.5 ml, 3 eq.) was added to this suspension *via* syringe under rapid stirring. An immediate colour change to light green is noticed. The reaction is very rapid, an the $FeCl_2$ reacts into solution within minutes. After stirring the reaction for 1 h, the reaction solution was filtered *via* cannula, concentrated to incipience, and crystallised at –60 °C overnight. An off white, slightly green solid was separated from the mother liquor and dried *in vacuo* at 35 °C for 4h. The product is extremely air sensitive and decomposes immediately on contact with air. Yield: 1.89 g (6.776 mmol, 86 %).

Elemental analysis: calcd (%) for $C_6H_{18}Cl_2FeP_4$ (278.91 gmol^{-1}): C 25.84, H 6.51; found : C 24.01, H 5.96;

Spectroscopic Data:

IR (Nujol, cm^{-1}) 3050 (w), 2813 (w), 2362 (vw), 2253 (vw), 2019, 1952, 1424 (s), 1304 (vw), 1287 (s), 944 (br vs) (P-C), 734 (w) (P-C), 668 (m).

No lock signal could be found for ^{1}H, and the spectrum was ^{31}P silent in the normal range at room temperature in C_6D_6.

Dieses Werk ist copyrightgeschützt und darf in keiner Form vervielfältigt werden noch an Dritte weitergegeben werden.
Es gilt nur für den persönlichen Gebrauch.

4.6.9 Synthesis of [FeH(η^3-$Et_2PCH_2CH_2PEt\{CHCH_3\}$)(depe)} (22-Fe)

To a mixture of **2-Fe** (1.00g, 1.85 mmol) and Na sand (0.102g, 2.4 eq., 4.4 mmol) was added THF (50 mL). The green solution was placed in an ultrasonic bath for 10 mins. and stirred for 30 h at room temperature. At this time the reaction mixture was brown, and an *in situ* $^{31}P\{^1H\}$ NMR spectrum revealed consumption of the starting material. The THF was removed under reduced pressure and the brown residue extracted with pentane (3 × 20 mL). The orange filtrate was evaporated to dryness to yield an orange viscous oil as product. Yield: 0.705 g (1.505 mmol, 81 %).

Spectroscopic data:

^{1}H NMR:	(300 MHz, THF-d_8, 298 K, ppm): $\delta = -15.57$ (dddd, $^2J(H,P_A) = 87.4$ Hz, $^2J(H,P_B) = 40.6$ Hz, $^2J(H,P_C) = 38.3$ Hz, $^2J(H,P_D) = 25.2$ Hz, 1H, 1 × Fe-*H*), –0.84 (m, 2H, 1 × Fe-C*H*), 0.85 – 1.71 (unresolved m, CH_2 and CH_3).
$^{31}P\{^1H\}$ NMR:	(121.5 MHz, THF-d_8, 298 K, ppm): $\delta = 51.3 - 51.7$ (m, 1P), 82.1 – 82.3 (m, 1P), 87.8 – 88.3 (m, 1P), 91.7 – 92.2 (m, 1P)(these signals match signal resonances in ref 187)
$^{31}P\{^1H\}$ NMR	(121.5 MHz, C_6D_6, 298 K, ppm): signals match those reported in ref. 187: to be a mixture of **22-Fe**, and cis/trans FeDPh(depe)$_2$.

4.6.10 [FeH(dppe){η^3-$Ph_2PCH_2CH_2PPhC_6H_4$}] (24-Fe)

A Schlenk tube was charged with a mixture of $FeCl_2$(dppe) (0.500 g, 0.952 mmol) and free dppe (0.379 g, 0.052 mmol). Another Schlenk tube was charged with Mg(athracene)(thf)$_x$ (1.674 g, 4.2 eq). THF (60 ml) was vacuum transferred to the first Schlenk tube, and 20 ml to the second one containing the Mg(anthracene)(thf)$_x$. Both mixtures were cooled to 0°C in an ice bath, and the Mg(anthracene) suspension added slowly *via* cannula to the Schlenk tube containing a mixture of (dppe)$_2FeCl_2$ and free dppe. An immediate colour change to red brown is noticed on the addition. After complete addition of the Mg(anthracene), the reaction mixture was stirred at 0 °C for 0.5 h, then at room temperature for 0.5 h. The product was

Dieses Werk ist copyrightgeschützt und darf in keiner Form vervielfältigt werden noch an Dritte weitergegeben werden.
Es gilt nur für den persönlichen Gebrauch.

isolated by a sequence of fractional crystallisations: The reaction mixture was filtered *via* cannula, and the filtrate concentrated to incipience, and stored at –30 °C overnight. A black solid was separated from the filtrate, and discarded, and the filtrate was evaporated to dryness. Pentane (20 mL) was added to this orange residue and filtered, concentrated to incipience and re-cooled to –30 °C. An orange solid was re-separated from this crystallisation, and the filtrate evaporated to dryness, to yield $\{FeH[Ph_2PCH_2CH_2PPhC_6H_4](dppe)\}$ contaminated with THF and Mg(anthracene) (*ca.* 5 mol %) Yield (0.360 g, 44 %). Crystals suitable for X-ray crystallographic analysis* were grown from an Et_2O solution of the complex at 6 °C.

Spectroscopic Data:

IR (solid ZnSe ATR crystal, cm^{-1}): ν = 1820 (w), br ν(Fe-H), 1652 (w), 1584 (vw), 1569, 1551 (vw), 1481 (s), 1435 (vs), 1409 (s), 1328 (w), 1327 (w), 1260 (vs), 1223 (vw), 1186 (vw), 1181 (vw), 1160 (vw), 1153 (vw), 1097 (vs), 1088 (s), 1026 (vs), 1025 (s), 1012 (s), 998 (s), 878 (m), 868 (m), 858 (m), 816 (s), 799 (vs), 752 (m), 745 (vs), 692 (vs), 670 (vs), 660 (vs), 634 (m) , 616 (w).

^{1}H NMR: (300.1 MHz, C_6D_6, 298 K, ppm): δ = –14.31 (m, 1H, Fe-*H*, s in $^1H\{^{31}P\}$ NMR spectrum), 1.22 (m, C*H*$_2$), 1.62 (m, C*H*$_2$) 1.77 (m, C*H*$_2$ + THF), 1.99 (m), 2.10 (s), 2.23 (s), 2.38 – 2.60 (m), 3.57 (s, br, THF), 3.63 (s, THF) 6.18 – 8.65 (m, 40H, Ar*H*).

$^{31}P\{^1H\}$ NMR: (121.5 MHz, C_6D_6, 298 K, ppm): δ = 25.15 (ddd, $^2J(P_A,P_B)$ = 23 Hz, $^2J(P_A,P_C)$ = 6.5 Hz, $^2J(P_A,P_D)$ = 19 Hz, P_A), 95.5 – 96.0 (ddd, $^2J(P_B,P_A)$ = 23 Hz, $^2J(P_B,P_C)$ = 29 Hz, $^2J(P_B,P_D)$ = 18 Hz, P_B), 96.8 – 97.1 (ddd, $^2J(P_C,P_A)$ = 6.5 Hz, $^2J(P_C,P_B)$ = 29 Hz, $^2J(P_C,P_D)$ = 111

Dieses Werk ist copyrightgeschützt und darf in keiner Form vervielfältigt werden noch an Dritte weitergegeben werden.
Es gilt nur für den persönlichen Gebrauch.

Hz, P_C), 101.2 – 102.4 (ddd, $^2J(P_D,P_A)$ = 19 Hz, $^2J(P_D,P_B)$ = 18 Hz, $^2J(P_D,P_C)$ = 111 Hz, P_D). [*****]

4.6.11 *trans*-[FeClH(depe)$_2$] (30-Fe)

Procedure 1 in toluene:

The complex **2-Fe** (1 eq, 0.600 g , 1.113 mmol) was dissolved in toluene (25 mL), which formed a green solution. The solution was cooled to −78 °C for 10 min. To the green solution was added Na[Et_3BH] (1.1 eq, 1.2 mL, 1.2 mmol) dropwise. The solution was stirred for another 10 min at −78 °C. The colour of solution turned brown gradually.

The solution was allowed to warm to RT and was allowed to stir for another 3 h. The colour of solution turned orange after 30 min. To the orange solution, pentane (2.5 mL) was added. The solution then was filtered by cannula filtration at RT. The solvent was removed *in vacuo* and the orange powder was isolated. The orange powder was washed with pentane (3mL) at −78 °C and dried *in vacuo* at RT. Based on the ^{1}H NMR, the orange powder was characterized as the mixture of 75% **30-Fe** and 25% **2-Fe**.The orange powder (1 eq, 0.320 g, 0.634 mmol) was dissolved in toluene (15 mL). The resulting orange solution was cooled to −78 °C and stirred for 10 min. To the orange solution was added Na[Et_3BH] (0.25 eq, 0.158 mL, 0.158 mmol) dropwise. The solution was stirred for another 10 min at −78 °C. Precipitation of a black powder occurred immediately. The solution was heated to RT and was allowed to stir for another 3 hours. After 10 min, the black powder was dissolved in solution. To the orange solution, pentane (1.5 mL) was added. The solution was cooled to −60 °C for 64 h. The solution was filtered by cannula filtration at −78 °C. The solvent was removed *in vacuo* and the orange powder was isolated. The orange powder was washed with pentane (3 mL) at −78 °C and dried *in vacuo* at RT. Based on the ^{1}H and ^{31}P{^{1}H} NMR, the orange powder was characterized as pure *trans*-[FeHCl(depe)$_2$]. Yield: 0.214 g (0.424 mmol, 38 %).

[*****] Coupling constants are identical to those reported in S. D. Ittel, C. A. Tolman, P. J. Krusic, A. D. English, J. P. Jesson, *Inorg. Chem.* **1978**, *17*, 3432.

Dieses Werk ist copyrightgeschützt und darf in keiner Form vervielfältigt werden noch an Dritte weitergegeben werden.
Es gilt nur für den persönlichen Gebrauch.

Procedure 2: in THF:

The compound $\mathrm{FeCl_2(depe)_2}$ (1 eq, 0.250 g , 0.464 mmol) was dissolved in THF (15 mL), which formed a green solution. The green solution was cooled to −78 °C for 10 min. To the green solution was added $\mathrm{Na[Et_3BH]}$ (1.1 eq, 0.51 mL, 5.1 mmol) dropwise. The solution was stirred for another 10 min at −78 °C. The colour of solution was unchanged at −78 °C. The solution was allowed to warm to RT and was allowed to stir for another 18 hours. The colour of the solution turned brown after 10 min. *In situ* ^{1}H and ^{31}P{^{1}H} NMR were performed after 1 h, which indicated the starting material, **2-Fe**, was consumed. To the brown solution, pentane (1.5 mL) was added. The solution was filtered by cannula filtration at RT. The solvent was removed *in vacuo* and the brown powder was isolated. The brown powder was extracted with 11 mL toluene:pentane = 10:1. The extract was a clear orange solution while the remaining precipitate resembled a black-green oil. The solvent of the orange solution was removed *in vacuo* and the orange powder was isolated. The orange powder was washed with pentane (2 × 3mL) at −78 °C and dried *in vacuo* at RT for 30 min. Based on the ^{1}H and ^{31}P{^{1}H} NMR, the orange powder was characterized as pure *trans*-[FeHCl(depe)$_2$]. Yield: (0.130g, 56 %).

Elemental analysis: calcd (%) for $\mathrm{C_{20}H_{49}ClFeP_4}$ (504.8 g·mol^{-1}): C 47.59, H 9.78; found: C 48.03, H 9.77 %

-

Spectroscopic data:

IR (Nujol, cm^{-1}): ν = 1851 (Fe-*H*) (other stretching vibrations omitted)

^{1}H NMR: (300.13 MHz, $\mathrm{C_6D_6}$, 298 K, ppm): δ = –31.91 (quint, ^{2}J(H, P) = 48.0 Hz, 1H, Fe-*H*), 0.84 (br $\Delta\nu_{1/2}$ = 18.8 Hz, 12H, 4 × $\mathrm{C}H_3^{\mathrm{A}}$), 1.02 – 1.26 (m, 16H, 4 × $\mathrm{C}H_3^{\mathrm{B}}$ + 4 × $\mathrm{CH_3^{A}C}H^{\mathrm{X}}\mathrm{H^{Y}}$), 1.39 (br $\Delta\nu_{1/2}$ = 25.4 Hz, 4H, 2 × $\mathrm{PC}H^{\mathrm{X}}\mathrm{H^{Y}C}H^{\mathrm{X}}\mathrm{H^{Y}P}$), 1.60 – 1.88 (m, 12H, 4 × $\mathrm{CH_3^{A}CH^{X}}H^{\mathrm{Y}}$ + 4 × $\mathrm{CH_3^{B}CH^{X}}H^{\mathrm{Y}}$ + 2 × $\mathrm{PCH^{X}}H^{\mathrm{Y}}\mathrm{CH^{X}}H^{\mathrm{Y}}\mathrm{P}$), 2.54 – 2.74 (m, 4H, 4 × $\mathrm{CH_3^{A}C}H^{\mathrm{X}}\mathrm{H^{Y}}$).

^{31}P{^{1}H} NMR: (121.49 MHz, $\mathrm{C_6D_6}$, 298 K, ppm): δ = 88.1 (s).

Dieses Werk ist copyrightgeschützt und darf in keiner Form vervielfältigt werden noch an Dritte weitergegeben werden.
Es gilt nur für den persönlichen Gebrauch.

$^{13}C\{^{1}H\}$ NMR: (100.61 MHz, C_6D_6, 298 K, ppm): δ = 9.0 (s, 4 × CH_3^A), 9.2 (s, 4 × CH_3^B), 20.3 – 20.4 (m, 4 × $CH_3^BCH_2$), 22.9 (ps quint, ^nJ(P, ^{13}C) = 12.3 Hz, 4 × PCH_2), 23.5 – 24.1 (m, 4 × $CH_3^ACH_2$).

4.6.12 [$FeCl_2$(dppe)] (25-Fe)

A Schlenk tube was charged with $FeCl_2$ (0.39 g, 3.1 mmol) and dppe (2.64 g, 6.6 mmol). Toluene, (60 mL) was added to this mixture *via* syringe, and the mixture heated at 90 °C for 3 h. At this time the reaction mixture had the appearance of a white suspension, with a yellow supernatant. The reaction mixture was filtered *via* cannula, the filtrate evaporated to dryness, and found to be unreacted dppe by melting point determination. The remaining white residue in the reaction vessel was dried *in vacuo* at room temperature for several hours, and analysed as $FeCl_2$(dppe) by elemental analysis. Yield: 1.60 g (3.04 mmol, 98 %).

Elemental analysis: calcd (%) for $C_{26}H_{24}FeCl_2P_4$ (525.17 g·mol^{-1}): C 59.46, H 4.61; found: C 59.66, H 4.76 %.

Dieses Werk ist copyrightgeschützt und darf in keiner Form vervielfältigt werden noch an Dritte weitergegeben werden.
Es gilt nur für den persönlichen Gebrauch.

4.7 New partially characterised compounds [†††††]

4.7.1 [Pd(η^5-C_5Me_5)(cod)][$SnCl_3$] (8-Pd) and its derivative (8-Pd-b)

[SnCl(η^5-C_5Me_5)] (0.579 g, 2.00 mmol) and $PdCl_2$(cod) (0.571 g, 2.00 mmol) were weighed into a Schlenk tube in the glove box, and placed in a - 78 °C bath. Toluene, also pre-cooled to –78 °C (50 mL) was added *via* cannula to the solid mixture under rapid stirring. A colour change to red-brown is noticed on completion of the addition. The reaction was left to stir in the ice bath overnight, with slow warming to room temperature. A brown suspension resulted, with a brown supernatant solution. The solvent was removed *in vacuo* yielding a brown solid. Attempts at recrystallising this solid from CH_2Cl_2 : pentane (5 : 1) at – 60 °C were unsuccessful, so more pentane was added to the mixture, until incipience. A red-brown solid was separated from the supernatant solution by cannula filtration, the filtrate discarded, and the remaining solid dried *in vacuo* at room temperature. The solid was then washed with toluene until washings were colourless, and re-dried *in vacuo*, resulting in a red-brown solid as product. Yield : (0.758 g, 66 %). Reaction of this product with $TlPF_6$ in CH_2Cl_2 resulted in **8-Pd-b**, of which single crystals were grown from CH_2Cl_2 at –30 °C, and the structure of the cation positively identified by X-ray diffraction analysis.

Spectroscopic Data (8-Pd):

IR (Polyethylene, cm^{-1}):	ν = 451 (vw), 370 – 250 (br vs), 227 (vw), 202 (vw), 139 (vw), 120 (m).
^{1}H NMR:	(300.1 MHz, CD_2Cl_2, 303 K, ppm): δ = 1.90 (s, 15 H, 5 × CH_3), 1.99 (s, 4 H, unknown impurity), 2.34 (s, 1 H, unknown impurity), 2.63 (m, 8 H, 4 × CH_2), 4.93 (m, 4 H, 2 × CH_2=CH_2). (^{1}H NMR spectrum of **8-Pd-b** identical, except impurity signals no longer visible).
^{119}Sn{^{1}H} NMR:	(111.9 MHz, CD_2Cl_2, 303 K, ppm): δ = -50.6 ppm
Mass Spectrometry:	(Maldi ToF +, DCTB Matrix): 349.1 [M^+].

[†††††] This section contains procedures that resulted in incompletely characterised compounds, or mixtures which could not be purified, but identified on the basis of spectroscopy or crystallographic analysis

Dieses Werk ist copyrightgeschützt und darf in keiner Form vervielfältigt werden noch an Dritte weitergegeben werden.
Es gilt nur für den persönlichen Gebrauch.

4.7.2 16 $[(PMe_3)_3FeH\{=Sn(2,6\text{-}Mes_2\text{-}C_6H_3)(CH_2PMe_2)\}][ClB(C_6F_5)_3]$ (21-Fe)

In the glove box, a Schlenk tube was charged with $[(PMe_3)_3Fe\{PMe_2CH_2Sn(C_6H_3\text{-}2,6\text{-}Mes_2)Cl\}H]$ (which was shown to be a mixture of stereo-isomers) (0.200 g, 0.24 mmol), and dissolved in THF (7 ml). In another Schlenk tube $B(C_6F_5)_3$ (0.123 g, 0.24 mmol) and dissolved in THF (5 ml). The $B(C_6F_5)_3$ solution was added rapidly to the solution containing the $[(PMe_3)_3Fe\{PMe_2CH_2Sn(Ar)Cl\}H]$ *via* syringe at room temperature. An immediate colour change to purple-black is noticed on completing the addition. The reaction mixture was stirred for 5 h at room temperature, then concentrated to 2 ml, and 3 ml hexane was added, and the mixture cooled first to -30 °C for 1 h, then -60 °C overnight. A blue-purple solid was isolated by filtration at -60 °C *via* cannula, and the brown supernatant liquid separated from the blue-purple compound. The solid was dried in *vacuo* for 1 h at room temperature. Yield: (0.160 g, 50 %). The structural motif was confrimed attitionally by X-ray crystallographic analysis.

Elemental analysis: calcd (%) for $C54H_{61}BF_{15}P_4SnClFe$ (1339.7 gmol^{-1}): C 48.41, H 4.59; found : C 47.38, H 4.15;

Spectroscopic Data:

^{1}H NMR: (300.13 MHz, THF-d_8, 298 K, ppm): δ = –16.34 (br, Fe-$H_{\text{isomer 1}}$), -13.10 (br, Fe-$H_{\text{isomer 2}}$), -9.64 (br, Fe-$H_{\text{isomer 3}}$), 1.18 (br), 1.27 (br), 2.07 (br, 12H, 4 × *o*-C*H*$_3$, Mes), 2.28 (br, 6H, 2 × *p*-C*H*$_3$, Mes), 6.72 – 7.06 (br m, 6H, Ar-*H*)), 7.46 (br, 2H, Ar-*H*);

^{31}P{^{1}H} NMR: (121.49 MHz, THF-d_8, 298 K, ppm): –4.9 (br m), 2.4 (br m), 9.6 (br m), 15.5 (br, ps q or dd), 17.2 (br m), 23.7 (br m), 33.5 (br m); The compound seems to decompose in THF over a long period from blue to orange, possibly indication the re-formation of the starting material).

Dieses Werk ist copyrightgeschützt und darf in keiner Form vervielfältigt werden noch an Dritte weitergegeben werden.
Es gilt nur für den persönlichen Gebrauch.

4.7.3 Reaction of SnCl(2,6-Mes$_2$-C$_6$H$_3$) with [FeH(dppe){η^3-Ph$_2$PCH$_2$CH$_2$PPhC$_6$H$_4$}] resulting in [FeCl(dppe)] 25-Fe

A Schlenk tube was charged with {SnCl(2,6-Mes$_2$-C$_6$H$_3$)}$_2$ (0.107 g, 0.115 mmol) and FeH(dppe){η^3-Ph$_2$PCH$_2$CH$_2$PPhC$_6$H$_4$}] (0.159 g, 0.23 mmol) in the glove box. Toluene, pre-cooled to –50 °C (15 mL) was added to this mixture which was placed in a –50 °C cooling bath with rapid stirring. The mixture was stirred at –50 °C for 10 minutes and then shock heated at 50 °C for 20 minutes. *In situ* ^{31}P{^{1}H} NMR spectroscopy at this point revealed a new signal at 81.3 ppm in a ratio 13:87 (new product : starting material). At a total reaction time of 1.5 h with heating at 50 °C the starting material was completely consumed and only a singlet peak at 84 ppm was visible in ^{31}P{^{1}H} NMR spectrum. The reaction mixture was filtered *via* cannula at room temperature, and concentrated to incipience, and stored at –30 °C overnight. A brown-orange solid which crystallised was separated from the mother liquor by cannula filtration and the filtrate discarded. This was dried *in vacuo* for 3 h at room temperature to afford [FeCl(dppe)] (**25-Fe**), confirmed only on the basis of X-ray diffraction analysis.

4.7.4 Reaction of [FeH(η^3-Et$_2$PCH$_2$CH$_2$PEt{CHCH$_3$})(depe)} (22-Fe) with 1-Sn to yield a mixture of 3-Fe and [FeH(η^3-Et$_2$PCH$_2$CH$_2$PEt{CHCH$_3$SnCl(2,6-Mes$_2$-C$_6$H$_3$)})(depe)} (23-Fe)

[FeH(η^3-Et$_2$PCH$_2$CH$_2$PEt{CHCH$_3$})(depe)} (0.664 g, 1.417 mmol) and SnCl(2,6-Mes$_2$-C$_6$H$_3$) **1-Sn** (0.663 g, 1.417 mmol) was added into a Schlenk tube in the glove box. Pentane (70 mL) was added to this mixture with rapid stirring at room temperature and an immediate colour change to brown is noticed. The reaction was stirred for 2 h at room temperature, and an *in situ* ^{31}P NMR spectrum revealed near consumption of the starting material, with peaks at 77 ppm, corresponding to **3-Fe** and several multiplets corresponding to the insertion product, in a ratio of 40 : 60 **3-Fe**: insertion compound). At 3 h total reaction time, the mixture was filtered at room temperature, and concentrated to incipience and cooled to –60 °C overnight. A brown solid was separated from the mother liquor by cannula filtration and dried *in vacuo* for 1h, and the recrystallisation procedure repeated again, to yield a brown product; shown by NMR to be a 60 : 40 mixture of (depe)$_2$Fe=Sn(Cl)Ar (**3-Fe**) : insertion compound (**23-Fe**). Yield: 0.670 g (mixture).

Dieses Werk ist copyrightgeschützt und darf in keiner Form vervielfältigt werden noch an Dritte weitergegeben werden.
Es gilt nur für den persönlichen Gebrauch.

Spectroscopic data:

^{1}H NMR: (300.1 MHz, C_6D_6, 298 K): δ = –13.15 (m, Fe-*H*), –11.25 (m, Fe-*H*).

^{31}P{^{1}H} NMR: (121.5 MHz, C_6D_6, 298 K, ppm): δ = 75.3 (ddd, $^{2}J(P_A,P_B)$ = 13.1 Hz, $^{2}J(P_A,P_C)$ = 28.9 Hz, $^{2}J(P_A,P_D)$ = 29.8 Hz, insertion product, P_A), 76.80 (s, $^{2}J(P,^{119/117}Sn)$ = 100 Hz, stannylidene), 82.4 (ddd, $^{2}J(P_B,P_A)$ = 13.1 Hz, $^{2}J(P_B,P_C)$ = 49.3 Hz, $^{2}J(P_B,P_D)$ = 69.7 Hz, insertion product, P_B), 86.0 (ddd, $^{2}J(P_C,P_A)$ = 28.9 Hz, $^{2}J(P_C,P_B)$ = 49.3 Hz, $^{2}J(P_C,P_D)$ = 34.2 Hz, P_C), 98.3 (ddd, $^{2}J(P_D,P_A)$ = 29.8 Hz, $^{2}J(P_D,P_B)$ = 69.7 Hz, $^{2}J(P_D,P_C)$ = 34.2 Hz, insertion product, P_D)

^{119}Sn{^{1}H} NMR: (111.92 MHz, C_6D_6, 298 K, ppm): δ = 22.7 ppm (br, insertion product), 470.8 (quint (see elsewhere for isolated complex), **3-Fe**).

4.7.5 Reaction of $Fe(N_2)(depe)_2$ with $[Pb(Ctms_3)Cl]$

To a solution of $[Fe(N_2)(depe)_2]$ (0.047 g, 0.095 mmol) in pentane (4 mL) at –78 °C was slowly added a solution of $\{Pb(Ctms_3)Cl\}$ (0.046 g, 0.096 mmol) in pentane (3 mL) *via* cannula. The reaction was stirred under exclusion of light. The reaction was stirred at –78 °C for 2 h, and no reaction had occurred as evidenced by *in situ* ^{31}P{^{1}H} NMR spectroscopy. The reaction was subsequently stirred at room temperature for 3h, after which it was filtered *via* cannula and separated from a small amount of an insoluble black precipitate (10 mg). The filtrate was concentrated to incipience, and cooled to –30 °C overnight. A brown solid was separated from the mother liquor by filtration, and dried *in vacuo*. At this point NMR spectroscopy revealed a mixture of at least two products, so fractional crystallisation from pentane at –30 °C enabled isolation of a small amount of compound, positively identified as $[(depe)_2FeCl]$, **10-Fe** by comparison to an authentic sample in ^{1}H NMR spectroscopy, and by X-ray crystallographic analysis.

4.7.6 $[(dmpe)_2Fe{=}GeCl(2,6\text{-}Mes_2\text{-}C_6H_3)]$ (16-Fe-2)

$[Fe(dmpe)_2(PMe_3)]$ (0.100g, 231 µmol) and **2-Ge** (0.098g, 231 µmol) were added to a Schlenk tube and cooled to –78 °C. Pentane (15 mL) (also pre-cooled to –78 °C) was added

Dieses Werk ist copyrightgeschützt und darf in keiner Form vervielfältigt werden noch an Dritte weitergegeben werden.
Es gilt nur für den persönlichen Gebrauch.

under rapid stirring to this mixture. An orange solution with a light precipitate is noticed upon addition of the solvent. The reaction was allowed to stir at –78 °C for 2 minutes, then removed from the bath and stirred at RT. On warming to RT a brown solution is observed. After 1 h stirring at room temperature, *in situ* $^{31}P\{^{1}H\}$ spectroscopy revealed complete consumption of the starting material and the development of a singlet resonance signal at δ = 60 ppm. The reaction mixture was filtered (to remove a small amount (10 mg) of a greyish residue), and the brown supernatant solution concentrated to 1 mL and cooled to –60 °C. The green-brown precipitated solid was isolated by cannula filtration at –60 °C, washed with cold (–60 °C) pentane (2 × 1 mL), the washings and filtrate combined and discarded, and the remaining solid dried *in vacuo* at room temperature for 45 minutes. Yield: (0.137 g, 77 %). Crystals suitable for X-ray crystallographic analysis were obtained from the *in situ* NMR sample by cooling to –30 °C in the glove box.

Spectroscopic data:

^{1}H NMR: (300.1 MHz, C_6D_6, 298 K, ppm): δ = 1.01 (br s, $\Delta\nu_{1/2}$ = 7.2 Hz, 12H, 4 × CH_3^{A}), 1.05 – 1.27 (m, 8H, 2 × $PCH^{X}H^{Y}CH^{X}H^{Y}P$), 1.35 (br s, $\Delta\nu_{1/2}$ = 7.7 Hz, 12H, 4 × CH_3^{B}), 2.24 (s, 6H, 2 × C^{4}-CH_3, Mes), 2.46 (br s, $\Delta\nu_{1/2}$ = 48.6 Hz, 12H, 2 × C^{2}-CH_3 + 2 × C^{6}-CH_3, Mes), 6.83 (br s, $\Delta\nu_{1/2}$ = 8.3 Hz, 4H, 2 × C^{3}-*H* + 2 × C^{5}-*H*, Mes), 6.99 (ps d, ^{3}J(H,H) = 7.4 Hz, 2H, $C^{3,5}$-*H*, C_6H_3), 7.18 (ps t, ^{3}J (H,H) = 7.5 Hz, 1H, C^{4}-*H*, C_6H_3).

$^{1}H\{^{31}P\}$ NMR: (300.1 MHz, C_6D_6, 298 K, ppm): δ = 1.01 (s, $\Delta\nu_{1/2}$ = 2.0 Hz, 12H, 4 × CH_3^{A}), 1.04 – 1.27 (m, 8H, 2 × $PCH^{X}H^{Y}CH^{X}H^{Y}P$), 1.36 (s, $\Delta\nu_{1/2}$ = 1.9 Hz, 12H, 4 × CH_3^{B}), 2.24 (s, 6H, 2 × C^{4}-CH_3, Mes), 2.46 (br s, $\Delta\nu_{1/2}$ = 45.8Hz, 12H, 2 × C^{2}-CH_3 + 2 × C^{6}-CH_3, Mes), 6.83 (br s, $\Delta\nu_{1/2}$ = 8.1 Hz, 4H, 2 × C^{3}-*H* + 2 × C^{5}-*H*, Mes), 6.99 (ps d, ^{3}J(H,H) = 7.4 Hz, 2H, $C^{3,5}$-*H*, C_6H_3), 7.19 (ps t, ^{3}J(H,H) = 7.5 Hz, 1H, C^{4}-*H*, C_6H_3).

$^{31}P\{^{1}H\}$ NMR: (121.5 MHz, C_6D_6, 298 K, ppm): δ = 60.0 (s).

$^{13}C\{^{1}H\}$ NMR: (75.47 MHz, C_6D_6, 298 K, ppm): δ = 21.2 (s, 2 × C^{4}-CH_3, Mes), 23.2 – 23.5 (m, 4 × CH_3^{A} + 2 × $C^{2-}CH_3$ + 2 × C^{6}-CH_3), 27.4 (ps quint, 4 × CH_3^{B}), 33.9 (ps quint, 2 × PCH_2CH_2P), 127.2 (s, 1 × C^{4}, C_6H_3), 128.1

Dieses Werk ist copyrightgeschützt und darf in keiner Form vervielfältigt werden noch an Dritte weitergegeben werden.
Es gilt nur für den persönlichen Gebrauch.

(signal obscured by resonance signal of the solvent, 2 × $C^{3,5}$-H, Mes), 129.8 (s, $C^{3,5}$-H, C_6H_3), 136.1 (s, 2 × $C^{2,6}$, Mes), 141.0 (s, 2 × C^1, Mes), 144.1 (s, $C^{2,6}$, C_6H_3), 164.5 (s, C^1, C_6H_3).

4.7.7 [$(dmpe)_2Fe{\equiv}Ge(2,6\text{-}Mes_2\text{-}C_6H_3)$][$ClB(C_6F_5)_3$] (16-Fe-3)

A Schlenk tube was charged with [$(dmpe)_2Fe{=}(2,6\text{-}Mes_2\text{-}C_6H_3)Cl$] (0.195 g, 251 µmol) and dissolved in 2 mL toluene and stirred at room temperature. To this solution, a 1.5 mL toluene solution of $B(C_6F_5)_3$ (0.128 g, 251 µmol) was added dropwise via syringe in the glove box A red brown solution is noticed after the completion of the addition of the borane. The reaction was stirred at RT overnight resulting in an olive-green coloured solution. The toluene was removed under reduced pressure resulting in a brown solid. The brown solid was washed with pentane (2 × 2.5 mL) at room temperature, the pentane washings discarded, and the remaining solid dried *in vacuo* at room temperature resulting in a golden solid as product **16-Fe-3** contanimated with trace amounts of [$FeCl_2(dmpe)_2$] (0.242 g, 226 µmol) 82 % .

Spectroscopic data:

^{1}H NMR: (300.1 MHz, THF-d_8, 298 K, ppm): δ = 1.17 (br s, 12H, 4 × CH_3^A), 1.23 – 1.28 (m, 4H, 2 × $PCH^XH^YCH^XH^YP$), 1.58 (br s, 12H, 4 × CH_3^B),1.80 – 2.00 (m, 4H, 2 × $PCH^XH^YCH^XH^YP$), 2.07 (s, 12H, 2 × C^2-CH_3 + 2 × C^6-CH_3, Mes), 2.36 (s, 6H, 2 × C^4-CH_3, Mes), 6.97(d, ^3J(H,H) = 7.6 Hz, 2H, $C^{3,5}$-H, C_6H_3), 6.99 (s, 4H, 2 × $C^{3,5}$-H, Mes) 7.18 (t, ^3J (H,H) = 7.6 Hz, 1H, C^4-H, C_6H_3).

^{1}H{^{31}P} NMR: (300.1 MHz, THF-d_8, 298 K, ppm): δ = 1.17 (br s, 12H, 4 × CH_3^A), 1.33 (ps quint, 4H, 2 × $PCH^XH^YCH^XH^YP$), 1.58 (br s, 12H, 4 × CH_3^B), 1.90 (ps quint, 4H, 2 × $PCH^XH^YCH^XH^YP$), 2.07 (s, 12H, 2 × C^2-CH_3 + 2 × C^6-CH_3, Mes), 2.36 (s, 6H, 2 × C^4-CH_3, Mes), 6.97(d, ^3J(H,H) = 7.6 Hz, 2H, $C^{3,5}$-H, C_6H_3), 6.99 (s, 4H, 2 × $C^{3,5}$-H, Mes) 7.18 (t, ^3J (H,H) = 7.6 Hz, 1H, C^4-H, C_6H_3).

Dieses Werk ist copyrightgeschützt und darf in keiner Form vervielfältigt werden noch an Dritte weitergegeben werden.
Es gilt nur für den persönlichen Gebrauch.

$^{31}P\{^1H\}$ NMR: (121.5 MHz, THF-d_8, 298 K, ppm): δ = 62.5 (s).

$^{13}C\{^1H\}$ NMR: (75.47 MHz, THF-d_8, 298 K, ppm): δ = 21.3 (s, 2 × C^4-*C*H_3, Mes), 21.7 (s, C^{2-}*C*H_3 + 2 × C^6-*C*H_3), 22.2 (ps quint, 4 × *C*H_3^A), 30.8 (ps quint, 4 × *C*H_3^B), 34.8 (ps quint, 2 × P*C*H_2*C*H_2P), 129.4 (s, 2 × C^4, Mes), 130.0 (s, 1 × C^4, C_6H_3), 132.5 (signal obscured by resonance signal of the solvent, 2 × $C^{3,5}$-H, Mes), 136.8 (s, $C^{3,5}$-H, C_6H_3), 138.86 (s, 2 × $C^{2,6}$, Mes), 138.9 (s, 2 × C^1, Mes), 146.3 (s, $C^{2,6}$, C_6H_3), 162.2 (s, C^1, C_6H_3). (signals of cation could not be found)

$^{11}B\{^1H\}$ NMR: (96.29 MHz, THF-d_8, 298 K, ppm): δ = –7.5 (br s).

4.7.8 *trans*-[RuH($SnCl_2$(2,6-Mes_2-C_6H_3)(depe)$_2$] (5-Ru)

A quartz NMR tube was charged with **1-Sn** (0.090 g, 0.19 mmol) and *cis/trans*-[RuH_2(depe)$_2$] (0.050 g, 0.096 mmol) and dissolved in 5 mL C_6D_6. The NMR tube was placed in a dewar with a Hg lamp, λ : 254 nm and irradiated for 1h. During this time the colour of the C_6D_6 solution turned dark red. *In situ* $^{31}P\{^1H\}$ NMR spectroscopy at this time revealed complete consumption of the *cis/trans* [RuH_2(depe)] and the development of two new resonance signals at δ = 64.5 and δ = 62.4 ppm (42:58). The signal at δ = 64.5 ppm exhibited Sn satellites ^2J(Sn,P) = 160.3 Hz. The reaction solution was quantitatively transferred to another vessel, Et_2O added (1 mL) and the solution cooled to –30 °C. A green insoluble solid was separated from a red supernatant solution and discarded, while the red liquid was cooled to 6 °C for a period of 3 days during which colourless crystals were obtained, which on the basis on X-ray crystallographic analysis were shown to be **5-Ru**.

Dieses Werk ist copyrightgeschützt und darf in keiner Form vervielfältigt werden noch an Dritte weitergegeben werden.
Es gilt nur für den persönlichen Gebrauch.

5. Appendices

5.1 Appendix A: Crystallographic Data

3-Pd

Empirical formula	$C_{32}H_{37}Cl_3PdSn$
Formula weight	753.06
Temperature	123(2) K
Wavelength	0.71073 A
Crystal system, space group	Orthorhombic, P b c a
Unit cell dimensions	a = 12.28470(10) Å $\alpha = 90°$
	b = 14.8959(2) Å $\beta = 90°$
	c = 33.5690(4) Å $\gamma = 90°$
Volume	6142.85(12) Å^3
Z, Calculated density	8, 1.629 Mg/m^3
Absorption coefficient	1.679 mm^{-1}
F(000)	3008
Crystal size	0.32 × 0.16 × 0.08 mm
θ range for data collection	2.73 to 30.02 deg.
Limiting indices	$-17 \le h \le 17$, $-16 \le k \le 20$, $-47 \le l \le 46$
Reflections collected / unique	42826 / 8928 [R(int) = 0.0602]
Completeness to θ = 30.02	99.5 %
Absorption correction	Semi-empirical from equivalents
Max. and min. transmission	0.83217 and 0.70988
Refinement method	Full-matrix least-squares on F^2
Data / restraints / parameters	8928 / 0 / 340
Goodness-of-fit on F^2	0.915
Final R indices [I>2sigma(I)]	R1 = 0.0301, wR2 = 0.0513
R indices (all data)	R1 = 0.0593, wR2 = 0.0551
Largest diff. peak and hole	0.603 and -0.762 e.Å^{-3}

Dieses Werk ist copyrightgeschützt und darf in keiner Form vervielfältigt werden noch an Dritte weitergegeben werden.
Es gilt nur für den persönlichen Gebrauch.

4-Pd·$\frac{13}{6}$ C_6D_6

Empirical formula	6(C_{50} H_{49} Cl_3 P_2 Pd Sn), 13(C_6 H_6)
Formula weight	7275.04
Temperature	123(2) K
Wavelength	0.71073 Å
Crystal system, space group	Trigonal, R -3
Unit cell dimensions	a = 46.9628(7) Å α = 90°
	b = 46.9628(7) Å β = 90°
	c = 13.21030(10) Å γ = 120°
Volume	25232.0(6) $Å^3$
Z, Calculated density	3, 1.436 Mg/m^3
Absorption coefficient	1.005 mm^{-1}
F(000)	11106
Crystal size	0.24 × 0.16 × 0.16 mm
θ range for data collection	2.94 to 30.02°
Limiting indices	$-65 \le h \le 66$, $-57 \le k \le 66$, $-18 \le l \le 18$
Reflections collected / unique	104895 / 16385 [R(int) = 0.0938]
Completeness to θ = 30.02	99.8 %
Absorption correction	Semi-empirical from equivalents
Max. and min. transmission	0.90461 and 0.71717
Refinement method	Full-matrix least-squares on F^2
Data / restraints / parameters	16385 / 0 / 638
Goodness-of-fit on F^2	0.918
Final R indices [I>2sigma(I)]	R1 = 0.0376, wR2 = 0.0618
R indices (all data)	R1 = 0.0848, wR2 = 0.0695
Extinction coefficient	0.000015(4)
Largest diff. peak and hole	1.786 and -0.714 e.$Å^{-3}$

Dieses Werk ist copyrightgeschützt und darf in keiner Form vervielfältigt werden noch an Dritte weitergegeben werden.
Es gilt nur für den persönlichen Gebrauch.

6-Pd

Empirical formula	$C_8 H_{12} Cl_4 Pd Sn$
Formula weight	475.07
Temperature	123(2) K
Wavelength	0.71073 Å
Crystal system, space group	Monoclinic, P 21/c
Unit cell dimensions	a = 9.2913(4) Å α = 90° b = 11.0103(5) Å β = 107.381(2)° c = 13.5238(4) Å γ = 90°
Volume	1320.31(9) $Å^3$
Z, Calculated density	4, 2.390 Mg/m^3
Absorption coefficient	4.024 mm^{-1}
F(000)	896
Crystal size	0.24 × 0.24 × 0.24 mm
θ range for data collection	2.95 to 30.00°
Limiting indices	$-13 \leq h \leq 7$, $-15 \leq k \leq 13$, $-19 \leq l \leq 18$
Reflections collected / unique	10656 / 3832 [R(int) = 0.0404]
Completeness to θ = 30.00	99.5 %
Absorption correction	Semi-empirical from equivalents
Max. and min. transmission	0.51476 and 0.48287
Refinement method	Full-matrix least-squares on F^2
Data / restraints / parameters	3832 / 0 / 128
Goodness-of-fit on F^2	0.909
Final R indices [I>2sigma(I)]	R1 = 0.0210, wR2 = 0.0408
R indices (all data)	R1 = 0.0297, wR2 = 0.0427
Extinction coefficient	0.00306(11)
Largest diff. peak and hole	0.692 and -0.680 $e.Å^{-3}$

Dieses Werk ist copyrightgeschützt und darf in keiner Form vervielfältigt werden noch an Dritte weitergegeben werden.
Es gilt nur für den persönlichen Gebrauch.

7-Pd

Empirical formula	$C_8 H_{12} Cl_4$ Ge Pd	
Formula weight	428.97	
Temperature	123(2) K	
Wavelength	0.71073 Å	
Crystal system, space group	Monoclinic, P 21/c	
Unit cell dimensions	a = 9.0679(4) Å	α = 90°
	b = 11.0257(7) Å	β = 109.022(3)°
	c = 13.6193(8) Å	γ = 90°
Volume	1287.30(12) $Å^3$	
Z, Calculated density	4, 2.213 Mg/m^3	
Absorption coefficient	4.522 mm^{-1}	
F(000)	824	
Crystal size	0.52 × 0.12 × 0.06 mm	
θ range for data collection	3.01 to 27.99°	
Limiting indices	$-11 \leq h \leq 10, -14 \leq k \leq 14, -14 \leq l \leq 17$	
Reflections collected / unique	10117 / 3096 [R(int) = 0.0458]	
Completeness to θ = 27.99	99.9 %	
Absorption correction	Semi-empirical from equivalents	
Max. and min. transmission	0.49437 and 0.43053	
Refinement method	Full-matrix least-squares on F^2	
Data / restraints / parameters	3096 / 0 / 127	
Goodness-of-fit on F^2	0.943	
Final R indices [I>2sigma(I)]	R1 = 0.0244, wR2 = 0.0453	
R indices (all data)	R1 = 0.0379, wR2 = 0.0477	
Largest diff. peak and hole	0.915 and -0.678 e.$Å^{-3}$	

Dieses Werk ist copyrightgeschützt und darf in keiner Form vervielfältigt werden noch an Dritte weitergegeben werden.
Es gilt nur für den persönlichen Gebrauch.

8-Pd-b·CH_2Cl_2

Solution (a)

Empirical formula	C_{19} H_{29} Cl_5 F_5 P Pd Sn
Formula weight	785.73
Temperature	123(2) K
Wavelength	0.71073 Å
Crystal system, space group	Monoclinic, P 21/n
Unit cell dimensions	a = 14.9958(12) Å alpha = 90°
	b = 10.0284(8) Å beta = 110.341(4)°
	c = 19.2797(11) Å gamma = 90°
Volume	2718.6(3) $Å^3$
Z, Calculated density	4, 1.920 Mg/m^3
Absorption coefficient	2.172 mm^{-1}
F(000)	1536
Crystal size	0.20 × 0.16 × 0.04 mm
θ range for data collection	2.25 to 27.50°
Limiting indices	$-19 \le h \le 19$, $-12 \le k \le 13$, $-25 \le l \le 25$
Reflections collected / unique	31041 / 6232 [R(int) = 0.1412]
Completeness to θ = 27.50	99.9 %
Absorption correction	Semi-empirical from equivalents
Max. and min. transmission	0.93684 and 0.66047
Refinement method	Full-matrix least-squares on F^2
Data / restraints / parameters	6232 / 0 / 294
Goodness-of-fit on F^2	1.036
Final R indices [I>2sigma(I)]	R1 = 0.0607, wR2 = 0.1286
R indices (all data)	R1 = 0.1397, wR2 = 0.1545
Largest diff. peak and hole	0.895 and -1.020 e.$Å^{-3}$

Dieses Werk ist copyrightgeschützt und darf in keiner Form vervielfältigt werden noch an Dritte weitergegeben werden.
Es gilt nur für den persönlichen Gebrauch.

Solution (b)

8-Pd-b·CH_2Cl_2

Empirical formula	$C_{19} H_{29} Cl_5 F_3 O_2$ P Pd Sn
Formula weight	779.73
Temperature	123(2) K
Wavelength	0.71073 Å
Crystal system, space group	Monoclinic, P 21/n
Unit cell dimensions	a = 14.9958(12) Å α = 90°
	b = 10.0284(8) Å β = 110.341(4)°
	c = 19.2797(11) Å γ = 90°
Volume	2718.6(3) $Å^3$
Z, Calculated density	4, 1.905 Mg/m^3
Absorption coefficient	2.167 mm^{-1}
F(000)	1528
Crystal size	0.20 × 0.16 × 0.04 mm
θ range for data collection	2.25 to 27.50°
Limiting indices	$-19 \le h \le 19, -12 \le k \le 13, -25 \le l \le 25$
Reflections collected / unique	31041 / 6232 [R(int) = 0.1412]
Completeness to θ = 27.50	99.9 %
Absorption correction	Semi-empirical from equivalents
Max. and min. transmission	0.93684 and 0.66047
Refinement method	Full-matrix least-squares on F^2
Data / restraints / parameters	6232 / 0 / 294
Goodness-of-fit on F^2	1.038
Final R indices [I>2sigma(I)]	R1 = 0.0600, wR2 = 0.1234
R indices (all data)	R1 = 0.1390, wR2 = 0.1478
Largest diff. peak and hole	0.928 and -1.024 e.$Å^{-3}$

Dieses Werk ist copyrightgeschützt und darf in keiner Form vervielfältigt werden noch an Dritte weitergegeben werden.
Es gilt nur für den persönlichen Gebrauch.

2-Rh

Device Type	X8-KappaApexII
Empirical formula	$C_{26}\ H_{29}\ Cl_{2}\ Rh\ Sn$
Formula weight	633.99
Temperature	100(2) K
Wavelength	0.71073 Å
Crystal system, space group	Monoclinic, C 2/c
Unit cell dimensions	a = 37.643(2) Å α = 90°
	b = 8.6265(5) Å β = 96.258(2)°
	c = 15.8271(9) Å γ = 90°
Volume	5108.9(5) Å^{3}
Z, Calculated density	8, 1.649 Mg/m^{3}
Absorption coefficient	1.844 mm^{-1}
F(000)	2512
Crystal size	0.39 × 0.37 × 0.16 mm
θ range for data collection	3.08 to 28.00°
Limiting indices	$-49 \le h \le 49$, $-11 \le k \le 10$, $-20 \le l \le 20$
Reflections collected / unique	64753 / 6158 [R(int) = 0.0251]
Completeness to θ = 28.00	99.7 %
Absorption correction	Integration
Max. and min. transmission	0.79773 and 0.53338
Refinement method	Full-matrix least-squares on F^{2}
Data / restraints / parameters	6158 / 0 / 293
Goodness-of-fit on F^{2}	1.073
Final R indices [I>2sigma(I)]	R1 = 0.0227, wR2 = 0.0587
R indices (all data)	R1 = 0.0247, wR2 = 0.0605
Largest diff. peak and hole	2.470 and -0.360 e.Å^{-3}

Dieses Werk ist copyrightgeschützt und darf in keiner Form vervielfältigt werden noch an Dritte weitergegeben werden.
Es gilt nur für den persönlichen Gebrauch.

3-Rh·C_7H_{13}

Device Type	STOE IPDS 2T
Empirical formula	C_{45} H_{61} Cl_2 Ge Rh
Formula weight	848.34
Temperature	123(2) K
Wavelength	0.71073 Å
Crystal system, space group	Triclinic, P -1
Unit cell dimensions	a = 9.262(7) Å α = 89.08(4)°
	b = 13.619(6) Å β = 78.75(5)°
	c = 17.388(8) Å γ = 74.18(5)°
Volume	2068.2(19) A^3
Z, Calculated density	2, 1.362 Mg/m^3
Absorption coefficient	1.284 mm^{-1}
F(000)	884
Crystal size	0.60 × 0.50 × 0.20 mm
θ range for data collection	2.82 to 29.17°
Limiting indices	$-12 \leq h \leq 12$, $-18 \leq k \leq 16$, $-23 \leq l \leq 23$
Reflections collected / unique	37003 / 11088 [R(int) = 0.0746]
Completeness to θ = 29.17	99.2 %
Absorption correction	Numerical
Max. and min. transmission	0.8263 and 0.6031
Refinement method	Full-matrix least-squares on F^2
Data / restraints / parameters	11088 / 0 / 471
Goodness-of-fit on F^2	0.985
Final R indices [I>2sigma(I)]	R1 = 0.0321, wR2 = 0.0760
R indices (all data)	R1 = 0.0441, wR2 = 0.0783
Largest diff. peak and hole	0.677 and -1.174 e.$Å^{-3}$

Dieses Werk ist copyrightgeschützt und darf in keiner Form vervielfältigt werden noch an Dritte weitergegeben werden.
Es gilt nur für den persönlichen Gebrauch.

3-Fe

Device Type	STOE IPDS 2T
Empirical formula	$C_{44}H_{73}$ Cl Fe P4 Sn
Formula weight	935.89
Temperature	150(2) K
Wavelength	0.71073 Å
Crystal system, space group	Monoclinic, P 21/n
Unit cell dimensions	a = 10.7471(6) Å α = 90°
	b = 23.2249(11) Å β = 92.863(5)°
	c = 18.4344(10) Å γ = 90°
Volume	4595.5(4) $Å^3$
Z, Calculated density	4, 1.353 Mg/m^3
Absorption coefficient	1.085 mm^{-1}
F(000)	1960
Crystal size	0.20 × 0.15 × 0.12 mm
θ range for data collection	2.24 to 26.00°
Limiting indices	$-13 \leq h \leq 8$, $-19 \leq k \leq 28$, $-22 \leq l \leq 19$
Reflections collected / unique	19188 / 8915 [R(int) = 0.1436]
Completeness to θ = 26.00	98.7 %
Absorption correction	Integration
Max. and min. transmission	0.8861 and 0.7089
Refinement method	Full-matrix least-squares on F^2
Data / restraints / parameters	8915 / 0 / 474
Goodness-of-fit on F^2	0.697
Final R indices [I>2sigma(I)]	R1 = 0.0673, wR2 = 0.0911
R indices (all data)	R1 = 0.1966, wR2 = 0.1189
Largest diff. peak and hole	0.790 and -0.581 e.$Å^{-3}$

Dieses Werk ist copyrightgeschützt und darf in keiner Form vervielfältigt werden noch an Dritte weitergegeben werden.
Es gilt nur für den persönlichen Gebrauch.

4-Fe

Device Type	STOE IPDS 2T
Empirical formula	$C_{68}\ H_{98}\ Cl_2\ Fe\ P_4\ Sn_2$
Formula weight	1403.47
Temperature	123(2) K
Wavelength	0.71073 Å
Crystal system, space group	Triclinic, P -1
Unit cell dimensions	a = 18.3800(4) Å α = 103.039(2)°
	b = 19.5452(4) Å β = 95.723(2)°
	c = 19.8058(5) Å γ = 100.162(2)°
Volume	6750.3(3) Å^{3}
Z, Calculated density	4, 1.381 Mg/m^{3}
Absorption coefficient	1.158 mm^{-1}
F(000)	2904
Crystal size	0.22 × 0.18 × 0.09 mm
θ range for data collection	2.13 to 27.50°
Limiting indices	$-23 \le h \le 23$, $-25 \le k \le 25$, $-25 \le l \le 25$
Reflections collected / unique	105176 / 30889 [R(int) = 0.0754]
Completeness to θ = 27.50	99.6 %
Absorption correction	Integration
Max. and min. transmission	0.9354 and 0.7864
Refinement method	Full-matrix least-squares on F^2
Data / restraints / parameters	30889 / 33 / 1455
Goodness-of-fit on F^2	0.819
Final R indices [I>2sigma(I)]	R1 = 0.0595, wR2 = 0.1341
R indices (all data)	R1 = 0.1244, wR2 = 0.1500
Largest diff. peak and hole	3.283 and -1.770 e.Å^{-3}

Dieses Werk ist copyrightgeschützt und darf in keiner Form vervielfältigt werden noch an Dritte weitergegeben werden.
Es gilt nur für den persönlichen Gebrauch.

5-Fe

Device Type	STOE IPDS 2T
Empirical formula	$C_{62} H_{73} B Cl F_{15} Fe P_4 Sn$
Formula weight	1447.88
Temperature	123(2) K
Wavelength	0.71073 Å
Crystal system, space group	Monoclinic, P 21/n
Unit cell dimensions	a = 23.2366(12) Å $\alpha = 90°$
	b = 14.4134(7) Å $\beta = 91.691(4)°$
	c = 37.9290(18) Å $\gamma = 90°$
Volume	12697.6(11) Å^3
Z, Calculated density	8, 1.515 Mg/m^3
Absorption coefficient	0.848 mm^{-1}
F(000)	5904
Crystal size	0.05 × 0.05 × 0.01 mm
θ range for data collection	1.97 to 25.25°
Limiting indices	$-27 \leq h \leq 27, -15 \leq k \leq 17, -36 \leq l \leq 45$
Reflections collected / unique	48339 / 22224 [R(int) = 0.3262]
Completeness to θ = 25.25	96.7 %
Absorption correction	Integration
Max. and min. transmission	0.9146 and 0.8156
Refinement method	Full-matrix least-squares on F^2
Data / restraints / parameters	22224 / 204 / 1531
Goodness-of-fit on F^2	0.576
Final R indices [I>2sigma(I)]	R1 = 0.0671, wR2 = 0.1048
R indices (all data)	R1 = 0.3197, wR2 = 0.2080
Largest diff. peak and hole	0.546 and -0.521 e.Å^{-3}

Dieses Werk ist copyrightgeschützt und darf in keiner Form vervielfältigt werden noch an Dritte weitergegeben werden.
Es gilt nur für den persönlichen Gebrauch.

8-Fe.C_6D_6

Device Type	STOE IPDS 2T
Empirical formula	C_{98} H_{146} D_6 Cl_2 Fe Ge_2 P_4
Formula weight	1726.01
Temperature	150(2) K
Wavelength	0.71073 Å
Crystal system, space group	Monoclinic, P 21/n
Unit cell dimensions	a = 13.7649(3) Å $\alpha = 90°$
	b = 35.7410(6) Å $\beta = 105.422(2)°$
	c = 20.4130(5) Å $\gamma = 90°$
Volume	9681.0(4) Å^3
Z, Calculated density	4, 1.184 Mg/m^3
Absorption coefficient	0.928 mm^{-1}
F(000)	3696
Crystal size	0.5 × 0.4 × 0.2 mm
θ range for data collection	1.91 to 28.00°
Limiting indices	$-15 \leq h \leq 18$, $-45 \leq k \leq 45$, $-23 \leq l \leq 26$
Reflections collected / unique	81514 / 23132 [R(int) = 0.0715]
Completeness to θ = 28.00	99.0 %
Absorption correction	Integration
Max. and min. transmission	0.9337 and 0.7382
Refinement method	Full-matrix least-squares on F^2
Data / restraints / parameters	23132 / 0 / 996
Goodness-of-fit on F^2	0.896
Final R indices [I>2sigma(I)]	R1 = 0.0424, wR2 = 0.0953
R indices (all data)	R1 = 0.0666, wR2 = 0.1011
Largest diff. peak and hole	1.545 and -0.994 e.Å^{-3}

Dieses Werk ist copyrightgeschützt und darf in keiner Form vervielfältigt werden noch an Dritte weitergegeben werden.
Es gilt nur für den persönlichen Gebrauch.

9-Fe

Device Type	Nonius KappaCCD
Empirical formula	$C_{68}H_{98}Cl_2FeGe_2P_4$
Formula weight	1311.27
Temperature	123(2) K
Wavelength	0.71073 Å
Crystal system, space group	Triclinic, P -1
Unit cell dimensions	a = 18.3174(4) Å α = 103.8661(11)°
	b = 19.4795(3) Å β = 96.8888(9)°
	c = 19.6668(4) Å γ = 100.2307(12)°
Volume	6606.9(2) $Å^3$
Z, Calculated density	4, 1.318 Mg/m^3
Absorption coefficient	1.337 mm^{-1}
F(000)	2760
Crystal size	0.31 × 0.18 × 0.08 mm
Theta range for data collection	2.36 to 28.00°
Limiting indices	$-24 \leq h \leq 23, -25 \leq k \leq 25, -25 \leq l \leq 25$
Reflections collected / unique	79827 / 31550 [R(int) = 0.0649]
Completeness to θ = 28.00	99.0 %
Absorption correction	Semi-empirical from equivalents
Max. and min. transmission	0.88204 and 0.73825
Refinement method	Full-matrix least-squares on F^2
Data / restraints / parameters	31550 / 0 / 1455
Goodness-of-fit on F^2	0.911
Final R indices [I>2sigma(I)]	R1 = 0.0407, wR2 = 0.0781
R indices (all data)	R1 = 0.0852, wR2 = 0.0877
Largest diff. peak and hole	1.069 and -0.835 e.$Å^{-3}$

Dieses Werk ist copyrightgeschützt und darf in keiner Form vervielfältigt werden noch an Dritte weitergegeben werden.
Es gilt nur für den persönlichen Gebrauch.

10-Fe

Device Type	Nonius KappaCCD
Empirical formula	$C_{20}H_{48}ClFeP_4$
Formula weight	503.76
Temperature	123(2) K
Wavelength	0.71073 Å
Crystal system, space group	Orthorhombic, P b n 21
Unit cell dimensions	a = 10.2987(2) Å α = 90°
	b = 14.2290(4) Å β = 90°
	c = 17.8246(5) Å γ = 90°
Volume	2612.02(12) $Å^3$
Z, Calculated density	4, 1.281 Mg/m^3
Absorption coefficient	0.929 mm^{-1}
F(000)	1084
Crystal size	0.5 × 0.16 × 0.16 mm
θ range for data collection	3.34 to 28.00°
Limiting indices	$-13 \leq h \leq 10$, $-18 \leq k \leq 18$, $-22 \leq l \leq 23$
Reflections collected / unique	19466 / 6032 [R(int) = 0.0495]
Completeness to θ = 28.00	99.8 %
Absorption correction	Semi-empirical from equivalents
Max. and min. transmission	0.79771 and 0.70236
Refinement method	Full-matrix least-squares on F^2
Data / restraints / parameters	6032 / 1 / 244
Goodness-of-fit on F^2	0.961
Final R indices [I>2sigma(I)]	R1 = 0.0296, wR2 = 0.0518
R indices (all data)	R1 = 0.0418, wR2 = 0.0540
Absolute structure parameter	0.237(10)
Largest diff. peak and hole	0.320 and -0.286 e. $Å^{-3}$

Dieses Werk ist copyrightgeschützt und darf in keiner Form vervielfältigt werden noch an Dritte weitergegeben werden.
Es gilt nur für den persönlichen Gebrauch.

12-Fe

Device Type	STOE IPDS 2T
Empirical formula	$C_{21} H_{51} Fe P_4$
Formula weight	483.35
Temperature	123(2) K
Wavelength	0.71073 Å
Crystal system, space group	Monoclinic, P 21/c
Unit cell dimensions	a = 9.4549(7) Å α = 90°
	b = 20.4366(9) Å β = 103.624(6)°
	c = 14.2383(9) Å γ = 90°
Volume	2673.8(3) $Å^3$
Z, Calculated density	4, 1.201 Mg/m^3
Absorption coefficient	0.81 mm^{-1}
F(000)	1052
Crystal size	0.32 × 0.16 × 0.04 mm
θ range for data collection	1.99 to 26.00°
Limiting indices	$-11 \leq h \leq 10$, $-25 \leq k \leq 25$, $-17 \leq l \leq 17$
Reflections collected / unique	18633 / 5261 [R(int) = 0.1354]
Completeness to θ = 26.00	100.0 %
Absorption correction	Integration
Max. and min. transmission	0.9414 and 0.7749
Refinement method	Full-matrix least-squares on F^2
Data / restraints / parameters	5261 / 0 / 244
Goodness-of-fit on F^2	0.920
Final R indices [I>2sigma(I)]	R1 = 0.0673, wR2 = 0.1535
R indices (all data)	R1 = 0.1132, wR2 = 0.1717
Largest diff. peak and hole	1.275 and -0.688 e. $Å^{-3}$

Dieses Werk ist copyrightgeschützt und darf in keiner Form vervielfältigt werden noch an Dritte weitergegeben werden.
Es gilt nur für den persönlichen Gebrauch.

15-Fe

Device Type	X8-KappaApexII
Empirical formula	$C_{30} H_{80} Fe_{2} P_{10}$
Formula weight	862.34
Temperature	100(2) K
Wavelength	0.71073 Å
Crystal system, space group	Monoclinic, P 21/n
Unit cell dimensions	a = 16.3362(7) Å α = 90°
	b = 13.8484(6) Å β = 90.1630(10)°
	c = 19.7389(8) Å γ = 90°
Volume	4465.5(3) $Å^{3}$
Z, Calculated density	4, 1.283 Mg/m^{3}
Absorption coefficient	1.028 mm^{-1}
F(000)	1848
Crystal size	0.32 × 0.10 × 0.02 mm
θ range for data collection	1.62 to 25.25°
Limiting indices	$-19 \leq h \leq 19$, $-16 \leq k \leq 16$, $-22 \leq l \leq 23$
Reflections collected / unique	27100 / 8078 [R(int) = 0.0576]
Completeness to θ = 25.25	99.8 %
Absorption correction	Semi-empirical from equivalents
Max. and min. transmission	0.9797 and 0.7345
Refinement method	Full-matrix least-squares on F^{2}
Data / restraints / parameters	8078 / 114 / 417
Goodness-of-fit on F^{2}	1.041
Final R indices [I>2sigma(I)]	R1 = 0.0959, wR2 = 0.2184
R indices (all data)	R1 = 0.1279, wR2 = 0.2364
Largest diff. peak and hole	2.422 and -0.869 e. $Å^{-3}$

Dieses Werk ist copyrightgeschützt und darf in keiner Form vervielfältigt werden noch an Dritte weitergegeben werden.
Es gilt nur für den persönlichen Gebrauch.

16-Fe

Device Type	X8 KappaApexII
Empirical formula	C_{36} H_{57} Cl Fe P_4 Sn
Formula weight	823.69
Temperature	100(2) K
Wavelength	0.71073 Å
Crystal system, space group	Monoclinic, P 21/c
Unit cell dimensions	a = 16.2529(4) Å $\alpha = 90°$
	b = 11.9620(3) Å $\beta = 90.1510(10)°$
	c = 20.0209(6) Å $\gamma = 90°$
Volume	3892.39(18) Å^3
Z, Calculated density	4, 1.406 Mg/m^3
Absorption coefficient	1.271 mm^{-1}
F(000)	1704
Crystal size	0.22 × 0.18 × 0.06 mm
θ range for data collection	1.98 to 28.00°
Limiting indices	$-20 \leq h \leq 21$, $-12 \leq k \leq 15$, $-26 \leq l \leq 26$
Reflections collected / unique	26552 / 9359 [R(int) = 0.0363]
Completeness to $\theta = 28.00$	99.6 %
Absorption correction	Semi-empirical from equivalents
Max. and min. transmission	0.9276 and 0.7674
Refinement method	Full-matrix least-squares on F^2
Data / restraints / parameters	9359 / 0 / 402
Goodness-of-fit on F^2	1.041
Final R indices [I>2sigma(I)]	R1 = 0.0401, wR2 = 0.1002
R indices (all data)	R1 = 0.0517, wR2 = 0.1080
Largest diff. peak and hole	3.549 and -1.056 e.A^{-3}

Dieses Werk ist copyrightgeschützt und darf in keiner Form vervielfältigt werden noch an Dritte weitergegeben werden.
Es gilt nur für den persönlichen Gebrauch.

17-Fe

Device Type	Bruker X8-KappaApexII
Empirical formula	$C_{15} H_{41} Fe P_5$
Formula weight	432.18
Temperature	100(2) K
Wavelength	0.71073 Å
Crystal system, space group	Orthorhombic, P b c a
Unit cell dimensions	a = 10.3382(5) Å α = 90°
	b = 15.4616(9) Å β = 90°
	c = 28.2260(15) Å γ = 90°
Volume	4511.8(4) $Å^3$
Z, Calculated density	8, 1.272 Mg/m^3
Absorption coefficient	1.017 mm^{-1}
F(000)	1856
Crystal size	0.24 × 0.12 × 0.04 mm
θ range for data collection	1.44 to 28.00°
Limiting indices	$-13 \leq h \leq 10$, $-20 \leq k \leq 11$, $-37 \leq l \leq 32$
Reflections collected / unique	20414 / 5445 [R(int) = 0.0672]
Completeness to θ = 28.00	99.9 %
Absorption correction	Semi-empirical from equivalents
Max. and min. transmission	0.9604 and 0.7923
Refinement method	Full-matrix least-squares on F^2
Data / restraints / parameters	5445 / 0 / 202
Goodness-of-fit on F^2	0.991
Final R indices [I>2sigma(I)]	R1 = 0.0393, wR2 = 0.0709
R indices (all data)	R1 = 0.0836, wR2 = 0.0837
Largest diff. peak and hole	0.416 and -0.394 $e.Å^{-3}$

Dieses Werk ist copyrightgeschützt und darf in keiner Form vervielfältigt werden noch an Dritte weitergegeben werden.
Es gilt nur für den persönlichen Gebrauch.

20-Fe

Device Type	STOE IPDS 2T
Empirical formula	C_{36} H_{60} Cl Fe P_4 Sn
Formula weight	826.71
Temperature	123(2) K
Wavelength	0.71073 Å
Crystal system, space group	Monoclinic, P 21/c
Unit cell dimensions	a = 12.0462(4) Å α = 90°
	b = 11.8413(5) Å β = 99.612(3)°
	c = 28.1077(10) Å γ = 90°
Volume	3953.1(3) $Å^3$
Z, Calculated density	4, 1.389 Mg/m^3
Absorption coefficient	1.252 mm^{-1}
F(000)	1716
Crystal size	0.33 × 0.22 × 0.09 mm
θ range for data collection	2.26 to 26.00°
Limiting indices	$-14 \leq h \leq 14$, $-13 \leq k \leq 14$, $-29 \leq l \leq 34$
Reflections collected / unique	16099 / 7608 [R(int) = 0.0508]
Completeness to θ = 26.00	97.8 %
Absorption correction	Integration
Max. and min. transmission	0.8858 and 0.7313
Refinement method	Full-matrix least-squares on F^2
Data / restraints / parameters	7608 / 0 / 409
Goodness-of-fit on F^2	0.942
Final R indices [I>2sigma(I)]	R1 = 0.0576, wR2 = 0.1448
R indices (all data)	R1 = 0.0843, wR2 = 0.1548
Largest diff. peak and hole	2.199 and -1.134 e.$Å^{-3}$

Dieses Werk ist copyrightgeschützt und darf in keiner Form vervielfältigt werden noch an Dritte weitergegeben werden.
Es gilt nur für den persönlichen Gebrauch.

21-Fe

Device Type	STOE IPDS 2T
Empirical formula	$C_{54} H_{61} B Cl F_{15} Fe P_4 Sn$
Formula weight	1339.71
Temperature	123(2) K
Wavelength	0.71073 Å
Crystal system, space group	Monoclinic, P 21/c
Unit cell dimensions	a = 18.3781(7) Å $\alpha = 90°$
	b = 14.0531(4) Å $\beta = 99.334(3)°$
	c = 22.2951(8) Å $\gamma = 90°$
Volume	5681.9(3) $Å^3$
Z, Calculated density	4, 1.566 Mg/m^3
Absorption coefficient	0.940 mm^{-1}
F(000)	2712
Crystal size	0.13 × 0.10 × 0.02 mm
θ range for data collection	1.97 to 27.00°
Limiting indices	$-23 \leq h \leq 23$, $-17 \leq k \leq 17$, $-27 \leq l \leq 28$
Reflections collected / unique	35909 / 12381 [R(int) = 0.1176]
Completeness to $\theta = 27.00$	99.8 %
Absorption correction	Semi-empirical from equivalents
Max. and min. transmission	0.9958 and 0.9335
Refinement method	Full-matrix least-squares on F^2
Data / restraints / parameters	12381 / 8 / 760
Goodness-of-fit on F^2	0.866
Final R indices [I>2sigma(I)]	R1 = 0.0607, wR2 = 0.1015
R indices (all data)	R1 = 0.1427, wR2 = 0.1228
Largest diff. peak and hole	1.617 and -1.051 e.$Å^{-3}$

Dieses Werk ist copyrightgeschützt und darf in keiner Form vervielfältigt werden noch an Dritte weitergegeben werden.
Es gilt nur für den persönlichen Gebrauch.

24-Fe·1¼ Et_2O

Device Type	STOE IPDS 2T
Empirical formula	$C_{228} H_{242} Fe_4 O_5 P_{16}$
Formula weight	3781.14
Temperature	123(2) K
Wavelength	0.71073 Å
Crystal system, space group	Triclinic, P -1
Unit cell dimensions	a = 11.1152(4) Å α = 88.674(3)°
	b = 19.9556(8) Å β = 87.067(3)°
	c = 22.3028(9) Å γ = 87.134(3)°
Volume	4933.3(3) $Å^3$
Z, Calculated density	1, 1.273 Mg/m^3
Absorption coefficient	0.475 mm^{-1}
F(000)	1994
Crystal size	0.20 × 0.08 × 0.06 mm
θ range for data collection	2.01 to 27.50°
Limiting indices	$-14 \leq h \leq 14$, $-23 \leq k \leq 25$, $-28 \leq l \leq 28$
Reflections collected / unique	65531 / 22630 [R(int) = 0.1200]
Completeness to θ = 27.50	99.9 %
Absorption correction	Integration
Max. and min. transmission	0.9769 and 0.8461
Refinement method	Full-matrix least-squares on F^2
Data / restraints / parameters	22630 / 17 / 1139
Goodness-of-fit on F^2	0.643
Final R indices [I>2sigma(I)]	R1 = 0.0509, wR2 = 0.0897
R indices (all data)	R1 = 0.1463, wR2 = 0.1050
Largest diff. peak and hole	1.562 and -1.028 e.$Å^{-3}$

Dieses Werk ist copyrightgeschützt und darf in keiner Form vervielfältigt werden noch an Dritte weitergegeben werden.
Es gilt nur für den persönlichen Gebrauch.

25-Fe·C_6D_6

Device Type	STOE IPDS 2T
Empirical formula	C_{58} H_{48} D_6 Cl Fe P_4
Formula weight	966.19
Temperature	123(2) K
Wavelength	0.71073 Å
Crystal system, space group	Triclinic, P -1
Unit cell dimensions	a = 12.7592(4) Å α = 83.153(3)°
	b = 13.6590(4) Å β = 79.824(3)°
	c = 14.1580(4) Å γ = 79.702(3)°
Volume	2379.69(12) $Å^3$
Z, Calculated density	2, 1.348 Mg/m^3
Absorption coefficient	0.547 mm^{-1}
F(000)	1010
Crystal size	0.50 × 0.35 × 0.30 mm
θ range for data collection	2.02 to 28.00°
Limiting indices	$-16 \leq h \leq 16$, $-18 \leq k \leq 18$, $-18 \leq l \leq 18$
Reflections collected / unique	32043 / 11485 [R(int) = 0.0539]
Completeness to θ = 28.00	99.9 %
Absorption correction	Integration
Max. and min. transmission	0.8774 and 0.7861
Refinement method	Full-matrix least-squares on F^2
Data / restraints / parameters	11485 / 0 / 577
Goodness-of-fit on F^2	0.894
Final R indices [I>2sigma(I)]	R1 = 0.0363, wR2 = 0.0844
R indices (all data)	R1 = 0.0500, wR2 = 0.0870
Largest diff. peak and hole	0.381 and -0.850 e.$Å^{-3}$

Dieses Werk ist copyrightgeschützt und darf in keiner Form vervielfältigt werden noch an Dritte weitergegeben werden.
Es gilt nur für den persönlichen Gebrauch.

26-Fe

Device Type	X8-KappaApexII
Empirical formula	C_{45} H_{76} Fe P_4 Sn
Formula weight	915.48
Temperature	100(2) K
Wavelength	0.71073 Å
Crystal system, space group	Monoclinic, P 21/c
Unit cell dimensions	a = 19.6275(12) Å α = 90°
	b = 23.1517(13) Å β = 92.204(4)°
	c = 40.617(3) Å γ = 90°
Volume	18443.3(19) Å^3
Z, Calculated density	16, 1.319 Mg/m^3
Absorption coefficient	1.024 mm^{-1}
F(000)	7712
Crystal size	0.36 × 0.32 × 0.08 mm
θ range for data collection	1.01 to 27.95°
Limiting indices	$-24 \le h \le 25$, $-29 \le k \le 30$, $-53 \le l \le 53$
Reflections collected / unique	91291 / 40850 [R(int) = 0.0831]
Completeness to θ = 27.95	92.2 %
Absorption correction	Semi-empirical from equivalents
Refinement method	Full-matrix-block least-squares on F^2
Data / restraints / parameters	40850 / 318 / 2168
Goodness-of-fit on F^2	1.072
Final R indices [I>2sigma(I)]	R1 = 0.0720, wR2 = 0.1741
R indices (all data)	R1 = 0.1570, wR2 = 0.2169
Largest diff. peak and hole	1.550 and -1.014 e. Å^{-3}

Dieses Werk ist copyrightgeschützt und darf in keiner Form vervielfältigt werden noch an Dritte weitergegeben werden.
Es gilt nur für den persönlichen Gebrauch.

31-Fe

Device Type	STOE IPDS 2T
Empirical formula	$C_{20}\ H_{48}\ Cl_4\ Fe\ Ge\ P_4$
Formula weight	682.70
Temperature	123(2) K
Wavelength	0.71073 Å
Crystal system, space group	Monoclinic, P 21/c
Unit cell dimensions	a = 16.2800(4) Å α = 90°
	b = 19.5397(3) Å β = 90.023(2)°
	c = 37.1802(8) Å γ = 90°
Volume	11827.3(4) $Å^3$
Z, Calculated density	16, 1.534 Mg/m^3
Absorption coefficient	2.094 mm^{-1}
F(000)	5664
Crystal size	0.283 × 0.226 × 0.082 mm
θ range for data collection	3.65 to 28.00°
Limiting indices	$-21 \leq h \leq 14$, $-25 \leq k \leq 25$, $-49 \leq l \leq 35$
Reflections collected / unique	62218 / 27922 [R(int) = 0.1092]
Completeness to θ = 28.00	97.7 %
Absorption correction	Integration
Max. and min. transmission	0.8237 and 0.5981
Refinement method	Full-matrix least-squares on F^2
Data / restraints / parameters	27922 / 0 / 1114
Goodness-of-fit on F^2	0.852
Final R indices [I>2sigma(I)]	R1 = 0.0482, wR2 = 0.1001
R indices (all data)	R1 = 0.0753, wR2 = 0.1080
Largest diff. peak and hole	1.035 and -1.219 e.$Å^{-3}$

Dieses Werk ist copyrightgeschützt und darf in keiner Form vervielfältigt werden noch an Dritte weitergegeben werden.
Es gilt nur für den persönlichen Gebrauch.

32-Fe

Empirical formula	$C_{20}H_{49}Cl_3FeGeP_4$
Formula weight	648.26
Temperature	100(2) K
Wavelength	0.71073 Å
Crystal system, space group	Monoclinic, P 21/c
Unit cell dimensions	a = 19.2541(5) Å α = 90°
	b = 17.3525(5) Å β = 116.0220(10)°
	c = 19.4143(6) Å γ = 90°
Volume	5828.9(3) $Å^3$
Z, Calculated density	8, 1.477 Mg/m^3
Absorption coefficient	2.032 mm^{-1}
F(000)	2704
Crystal size	0.40 × 0.40 × 0.32 mm
Theta range for data collection	3.08 to 28.00°
Limiting indices	$-21 \leq h \leq 25$, $-20 \leq k \leq 22$, $-25 \leq l \leq 22$
Reflections collected / unique	34060 / 14037 [R(int) = 0.0268]
Completeness to theta = 28.00	99.7 %
Absorption correction	Semi-empirical from equivalents
Max. and min. transmission	0.5625 and 0.4970
Refinement method	Full-matrix least-squares on F^2
Data / restraints / parameters	14037 / 0 / 547
Goodness-of-fit on F^2	1.023
Final R indices [I>2sigma(I)]	R1 = 0.0268, wR2 = 0.0599
R indices (all data)	R1 = 0.0385, wR2 = 0.0639
Largest diff. peak and hole	0.742 and -0.699 e. $Å^{-3}$

Dieses Werk ist copyrightgeschützt und darf in keiner Form vervielfältigt werden noch an Dritte weitergegeben werden.
Es gilt nur für den persönlichen Gebrauch.

4-Ru

Device Type	Nonius KappaCCD
Empirical formula	C_{20} H_{49} Cl P_4 Ru
Formula weight	549.99
Temperature	123(2) K
Wavelength	0.71073 Å
Crystal system, space group	Monoclinic, P 21/c
Unit cell dimensions	a = 18.2669(8) Å α = 90°
	b = 10.7345(6) Å β = 97.525(3)°
	c = 27.4322(14) Å γ = 90°
Volume	5332.7(5) $Å^3$
Z, Calculated density	8, 1.370 Mg/m^3
Absorption coefficient	0.933 mm^{-1}
F(000)	2320
Crystal size	0.52 × 0.52 × 0.48 mm
θ range for data collection	2.04 to 28.00°
Limiting indices	$-24 \leq h \leq 23$, $-14 \leq k \leq 13$, $-36 \leq l \leq 35$
Reflections collected / unique	64884 / 12648 [R(int) = 0.2543]
Completeness to θ = 28.00	98.3 %
Absorption correction	Semi-empirical from equivalents
Max. and min. transmission	0.6630 and 0.6426
Refinement method	Full-matrix least-squares on F^2
Data / restraints / parameters	12648 / 26 / 493
Goodness-of-fit on F^2	1.030
Final R indices [I>2sigma(I)]	R1 = 0.0709, wR2 = 0.1618
R indices (all data)	R1 = 0.1897, wR2 = 0.2036
Largest diff. peak and hole	1.273 and -1.044 e.$Å^{-3}$

Dieses Werk ist copyrightgeschützt und darf in keiner Form vervielfältigt werden noch an Dritte weitergegeben werden.
Es gilt nur für den persönlichen Gebrauch.

5-Ru

Empirical formula	$C_{44} H_{74} Cl_2 P_4$ Ru Sn
Formula weight	1017.57
Temperature	123(2) K
Wavelength	0.71073 Å
Crystal system, space group	Monoclinic, P 21
Unit cell dimensions	a = 10.2469(2) Å α = 90°
	b = 20.5695(6) Å β = 105.706(2)°
	c = 11.4399(3) Å γ = 90°
Volume	2321.20(10) $Å^3$
Z, Calculated density	2, 1.456 Mg/m^3
Absorption coefficient	1.146 mm^{-1}
F(000)	1052
Crystal size	0.33 × 0.20 × 0.10 mm
Theta range for data collection	2.06 to 28.00°
Limiting indices	$-13 \leq h \leq 13$, $-27 \leq k \leq 27$, $-15 \leq l \leq 15$
Reflections collected / unique	20041 / 11194 [R(int) = 0.0338]
Completeness to theta = 28.00	99.9 %
Absorption correction	Semi-empirical from equivalents
Max. and min. transmission	0.86206 and 0.80698
Refinement method	Full-matrix least-squares on F^2
Data / restraints / parameters	11194 / 2 / 486
Goodness-of-fit on F^2	0.979
Final R indices [I>2sigma(I)]	R1 = 0.0388, wR2 = 0.0904
R indices (all data)	R1 = 0.0444, wR2 = 0.0921
Absolute structure parameter	-0.022(18)
Largest diff. peak and hole	1.610 and -1.191 $e.Å^{-3}$

Dieses Werk ist copyrightgeschützt und darf in keiner Form vervielfältigt werden noch an Dritte weitergegeben werden.
Es gilt nur für den persönlichen Gebrauch.

8-Ge

Device Type	Nonius KappaCCD
Empirical formula	C_{27} H_{34} Cl Ge P
Formula weight	497.55
Temperature	123(2) K
Wavelength	0.71073 Å
Crystal system, space group	Monoclinic, C 2/c
Unit cell dimensions	a = 29.0813(13) Å α = 90°
	b = 11.6006(6) Å β = 117.154(2)°
	c = 17.0601(8) Å γ = 90°
Volume	5121.1(4) Å^3
Z, Calculated density	8, 1.291 Mg/m^3
Absorption coefficient	1.375 mm^{-1}
F(000)	2080
Crystal size	0.60 × 0.60 × 0.40 mm
θ range for data collection	2.75 to 29.00°
Limiting indices	$-37 \le h \le 39$, $-14 \le k \le 15$, $-23 \le l \le 23$
Reflections collected / unique	21223 / 6658 [R(int) = 0.0649]
Completeness to θ = 29.00	97.8 %
Absorption correction	Semi-empirical from equivalents
Max. and min. transmission	0.68 and 0.51
Refinement method	Full-matrix least-squares on F^2
Data / restraints / parameters	6658 / 0 / 280
Goodness-of-fit on F^2	0.937
Final R indices [I>2sigma(I)]	R1 = 0.0376, wR2 = 0.0837
R indices (all data)	R1 = 0.0683, wR2 = 0.0910
Largest diff. peak and hole	0.700 and -0.652 e.Å^{-3}

Dieses Werk ist copyrightgeschützt und darf in keiner Form vervielfältigt werden noch an Dritte weitergegeben werden.
Es gilt nur für den persönlichen Gebrauch.

5.2 Appendix B: Commonly Used Abbreviations

2D	two dimensional
ATR	attenuated total reflection
br	broad
^{n}Bu	n-butyl substituent
^{t}Bu	tert-butyl substituent
ca.	circa
calcd.	calculated
Cp	cyclopentadienyl ligand (C_5H_5)
Cp*	pentamethylcyclopentadienyl ligand (C_5Me_5)
C_g	centre of gravity
cod	1,5-cyclooctadiene
COSY	correlation spectroscopy
$\Delta\nu_{½}$	half height width
d	doublet
dec.	decomposition
DEPT	distortionless enhancement by polarisation transfer
depe	1,2-bis(diethylphosphino)ethane
DFT	density functional theory
Dipp	2,6-diisopropylphenyl substituent (C_6H_3-2,6-Dip$_2$)
dmpe	1,2-bis(dimethylphosphino)ethane
μ-dmpe	bridging dmpe ligand
DMSO	dimethylsulphoxide
dppe	1,2-bis(diphenylphosphino)ethane
E	element in group 14 (C, Si, Ge, Sn or Pb)
EA	elemental analysis
EI	electron impact
EPR	electron paramagnetic resonance spectroscopy
eq.	equivalents
ESI	electrospray ionisation
Et	ethyl substituent
Et_2O	diethyl ether
et al.	and others

Dieses Werk ist copyrightgeschützt und darf in keiner Form vervielfältigt werden noch an Dritte weitergegeben werden.
Es gilt nur für den persönlichen Gebrauch.

FT	Fourier transform
Fig.	figure
h	hour
HMBC	heteronuclear multiple bond correlation
HMQC	heteronuclear multiple quantum coherence
HSQC	heteronuclear single quantum coherence
in situ	latin: place
IMe$_2$Me$_2$	1,3,4,5-tetramethylimidazol-2-ylidene
^{i}Pr	isopropyl substituent
IR	infra red
L	ligand (any)
L-L	bidentate ligand (any)
LB	line broadening
m	multiplet
m/z	mass to charge ratio
M	metal
M$^+$	positively charged metal cation
Me	methyl substituent
Mes	2,4,6-trimethylphenyl substituent (C_6H_3-2,4,6-Me$_3$)
min	minute
mp	melting point
MS	mass spectrometry
NMR	nuclear magnetic resonance
P	monodentate phosphane ligand
P-P	bidentate phosphane ligand
Ph	phenyl substituent
PMe$_3$	trimethylphosphane
ppm	parts per million
ps	pseudo (typically used in conjunction with multiplicities)
q	quartet
quint	quintet
RT	room temperature
s	singlet (or strong)
sept	septet

Dieses Werk ist copyrightgeschützt und darf in keiner Form vervielfältigt werden noch an Dritte weitergegeben werden.
Es gilt nur für den persönlichen Gebrauch.

sext	sextet
t	triplet
THF	tetrahydrofuran
tms	trimethylsilyl substituent
Trip	2,4,6-triisopropylphenyl (C_6H_2-2,4,6-$^iPr_3$)
UV	ultraviolet
vbr	very broad
vw	very weak
vs	very strong
ν	wavenumber
VE	valence electron
Vis	visible
WBI	Wilberg bond index
X	halogen
X-Ray	X-ray diffraction analysis

Dieses Werk ist copyrightgeschützt und darf in keiner Form vervielfältigt werden noch an Dritte weitergegeben werden.
Es gilt nur für den persönlichen Gebrauch.

5.3 Scientific Contributions

5.3.1 Scientific Publications from this work

A. C. Filippou, O. Chernov, B. Blom, K. W. Stumpf, G. Schnakenburg, *Chem. Eur. J.* **2010**, *26*, 2866.

5.3.2 Conference Contributions

(a) A. C. Filippou, B.Blom, H. Cui, P. Portius and G. Schnakenburg (Poster)

Reactivity studies of [Sn(Ar)Cl] (Ar = 2,6-dimesityl phenyl): Insertion into M-Cl bonds (M = Pd, Pt) and N_2 substitution in [Fe(depe)$_2$(N_2)]: International Conference on Coordination Chemistry (ICCC), Jerusalem, July 2008.

(b) B.Blom, G. Schnakenburg , L. Zimmer, A. C. Filippou (Poster)
Iron-Germanium and Iron-Tin Triple Bonds: Unprecedented Triple Bonding to Late Transition Metal Element Atoms: EuChems Conference, Nürnberg, Germany, September 2010.

(c) B. Blom, M. van Gastel, G. Schnakenburg, A. C. Filippou, (Poster)
Facile Entry to Fe(I) Chlorido and Alkyl Complexes: SFB 813 Chemistry at Spin Centres Symposium, Bad Honnef, September, 2010.

5.3.3 Scientific Lectures

(a) Inorganic Chemistry Colloquium Series, University of Bonn: Insertion and substitution reactions of [Sn(Ar)Cl]$_2$: (Ar = 2,6-dimesityl-phenyl). June, 2008.

(b) GDCh Colloquium: Junge Forscher der Bonner Chemie stellen sich vor: Iron ylidyne complexes, a new class of compounds. July, 2010.

(c) Royal Society of Chemistry Young Chemists Seminar Series, University of Cape Town, South Africa: Unprecedented heavy main group to late transition metal triple bonds- March 2011.

Dieses Werk ist copyrightgeschützt und darf in keiner Form vervielfältigt werden noch an Dritte weitergegeben werden.
Es gilt nur für den persönlichen Gebrauch.

5.4 Curriculum Vitae

Personal Details :

Name: Burgert
Surname: Blom
Citizenship: South African
Birth date: 14 October 1980
Address: 85 Prinz-Albert Straße
53113-Bonn (Germany)
Languages: English and Afrikaans: Native fluency, German: Conversational fluency
Email address: blomb@uni-bonn.de
Home phone: +49 (228) 44676458 (after hours).

Educational History/ Academic Degrees

* Studied for the degree: **Dr.rer.nat**
Universität Bonn, Institut für Anorganische Chemie, (March 2007 – March 2011):
Topic: Reactivity of Ylenes at Late Transition Metal Centers.

* **Masters degree**
University of Cape Town, (Jan 2003 – Dec 2004).
Thesis topic: Superbulky cyclopentadienyl group VI(a) complexes as ethene trimerisation catalysts.

* **BSc (HONS)** Chemistry, University of Cape Town, 2002, First class.

* **BSc** (Majors: Chemistry and Mathematics), University of Pretoria (1999-2001).

Dieses Werk ist copyrightgeschützt und darf in keiner Form vervielfältigt werden noch an Dritte weitergegeben werden.
Es gilt nur für den persönlichen Gebrauch.

Representative Academic Achievements

* Awarded Travel grant by the GDCh (Gesellschaft Deutscher Chemiker) for attendance at the Euchems **2010** Conference, Nürnberg.

* Awarded Travel grant by the Wilhelm und Else Heraeus Stiftung, for attendance at the GDNÄ (Gesellschaft Deutscher Naturforscher und Ärzte) conference in Dresden, **2010**.

* Awarded University of Cape Town entrance merit scholarship for MSc studies, **2003**.

* Awarded RSC (Royal Society of Chemistry) Bursary for attendance to Dalton Discussion 6 Conference, York University, York, UK, **2003**.

* Selected to go on SIDA / NRF (Swedish International development agency, National research foundation) student exchange program as visiting scientist, Lund University and Chalmers institute of technology, Sweden, **2003**.

* Awarded second place at International science and engineering fair, Chemistry category, **1999**, Philadelphia Pennsylvania, USA.

* Awarded third place by ACS (American Chemical Society), Prize for Chemistry, Intel ISEF, **1999**, Philadelphia Pennsylvania, USA.

* Awarded Dr. S. Meiring Naude Award, National science fair, **1998**.

Research and Academic Work Experience

* PhD Student: Institut für Anorganische Chemie, Rheinische Friedrich-Wilhelms Universität Bonn, Bonn, Germany (March 2007 – present).

* Lecturer, Inorganic Chemistry Second Year Course (CHE 211), University of South Africa (July 2006 – Feb 2007).

Dieses Werk ist copyrightgeschützt und darf in keiner Form vervielfältigt werden noch an Dritte weitergegeben werden.
Es gilt nur für den persönlichen Gebrauch.

* Research Chemist, Sastech R & D, Sasolburg Jan-Apr 2005.

Published Peer Reviewed Scientific Articles in International Journals:

(1) A. C. Filippou, O. Chernov, B. Blom, K. W. Stumpf, G. Schnakenburg, *Chem. Eur. J.,* **2010**, *16*, 2866.

(2) N. Brennan, B. Blom, D. Liles, S. Lotz and P. H. van Rooyen, *Inorg. Chim. Acta.* **2008**, *361*, 3042.

(3) B. Blom, G. Klatt, J. R. Moss, *Inorg. Chim. Acta.* **2007**, *360*, 2890.

(4) B. Blom, H. Clayton, M. Kilkenny, J. R. Moss, *Adv. Organomet. Chem.* **2006,** ***54,*** 149.

(5) B. Blom, R. Meijboom, M. J. Overett, J. R. Moss, *Inorg. Chim. Acta.* **2005**, *358*, 3491.

(6) Numerous International Conference Proceedings (eg. Dalton Discussion 6, York, 2003 and ICCC, Jerusalem, 2008).

Involvements / Participation in Scientific Societies

* Elected to membership of SAAWK (Suid Afrikaanse Akademie vir Wetenskap en kuns), 2007.

* RSC (Royal society of chemistry) committee member, Southern section, South Africa, 2003/2004.

Other interests

Acting/Theatre – Member of “the Bonn Players” – Participation in several productions. In cast of FEATS (Festival of English Anglophone Theatrical Societies) 2008 production – 1st Prize – best overall production, Stockholm, Sweden.

Dieses Werk ist copyrightgeschützt und darf in keiner Form vervielfältigt werden noch an Dritte weitergegeben werden.
Es gilt nur für den persönlichen Gebrauch.

References

Prof. A. C. Filippou, Institute of Inorganic Chemistry, University of Bonn
Email address: filippou@uni-bonn.de

Assoc. Prof. T. J. Egan, University of Cape Town, Department of Chemistry.
Email address : tegan@science.uct.ac.za

Assoc. Prof. A. T. Hutton, University of Cape Town
Email address: athutton@science.uct.ac.za

Prof. J. R. Moss, Jameson Professor of Inorganic Chemistry, University of Cape Town (deceased)

Dieses Werk ist copyrightgeschützt und darf in keiner Form vervielfältigt werden noch an Dritte weitergegeben werden.
Es gilt nur für den persönlichen Gebrauch.

6. References

[1] An early proponent of this theory was Pauling see: L. Pauling, *J. Am. Chem. Soc.* **1931**, *53*, 1367.

[2] F. S. Kipping, *Proc. Chem. Soc.* **1911**, *27*, 143.

[3] F. S. Kipping, J. E. Sands, *J. Chem. Soc. (Trans.)* **1921**, *119*, 830.

[4] F. S. Kipping, J. E. Sands, *J. Chem. Soc. (Trans.)* **1921**, *119*, 848.

[5] F. S. Kipping, *Proc. R. Soc. Ser. A* **1937**, *159*, 139.

[6] A. H. Cowley, *Polyhedron* **1984**, *3*, 389.

[7] K. S. Pitzer, *J. Am. Chem. Soc.* **1948**, *70*, 2140;

[8] R. S. Mulliken, *J. Am. Chem. Soc.* **1955**, *77*, 884.

[9] See as an example highlighting this fact this quote: "Silicon, germanium, tin and lead do not form from multiple bonds using pπ orbitals. Consequently numerous types of carbon compounds, such as alkenes, alkynes, ketones and nitriles, have no analogues" Taken from: *Advanced Inorganic Chemistry*, Cotton and Wilkinson, 4th edition, John Wiley and Sons, **1980**. page 377.

[10] P. Jutzi, *Angew. Chem. Int. Ed. Engl.* **1975**, *14*, 232.

[11] Strictly speaking, Lappert's 1976 report of a distannene was the first well defined example, including a structure, violating the double bond rule. For a perspective on this see: R. West, *Science* **2004**, *305*, 1724.

[12] A. G. Brook, F. Abdesaken, B. Gutekunst, G. Gutekunst, K. Kallury, *J. Chem. Soc., Chem. Commun.* **1981**, 191.

[13] A. G. Brook, S. C. Nyburg, F. Abdesaken, B. Gutekunst, G. Gutekunst, R. Krishna, M. R. Kallury, Y. C. Poon, Y.-M. Chang, W. Wong-Hg, *J. Am. Chem. Soc.* **1982**, *104*, 5667.

[14] R. West, M. J. Fink, J. Michl, *Science* **1981**, *214*, 1343.

[15] Announced in 1981, published in 1982: M. Yoshifuji, I. Shima, N. Inamoto, K. Hirotsu, T. Higuchi, *J. Am. Chem. Soc.* **1982**, *103*, 4587.

[16] H. Meyer, G. Baum, W. Massa, A. Berndt, *Angew. Chem., Int. Ed. Engl.* **1987**, *26*, 546.

[17] A. Berndt, H. Meyer, G. Baum, W. Massa, S. Berger, *Pure Appl. Chem.* **1987**, *59*, 1011.

[18] C. Couret, J. Escudié, J. Satagé, M. Lazraq, *J. Am. Chem. Soc.* **1987**, *109*, 4411.

[19] H. Meyer, G. Baum, W. Massa, S. Berger, A. Berndt, *Angew. Chem., Int. Ed. Engl.* **1987**, *26*, 546.

Dieses Werk ist copyrightgeschützt und darf in keiner Form vervielfältigt werden noch an Dritte weitergegeben werden.
Es gilt nur für den persönlichen Gebrauch.

[20] For a recent example of a Si=Si compound, stabilised by NHC carbene ligands alone, see: Y. Wang, Y. Xie, P. Wei, B. King, H. F. Schaefer III, P. v. R. Schleyer, G. H. Robinson, *Science* **2008**, *321*, 1069.

[21] S. Masamune, Y. Hanzawa, *J. Am. Chem. Soc.* **1982**, *104*, 6136.

[22] J. T. Snow, S. Murakami, S. Masamune, D. J. Williams, *Tett. Lett.* **1984**, *25*, 4191.

[23] D. E. Goldberg, D. H. Harris, M. F. Lappert, K. H. Thomas, *J. Chem. Soc. Chem. Commun.* **1976**, *7*, 261.

[24] K. W. Klinkhammer, T. F. Fässler, H. Grützmacher, *Angew. Chem.* **1998**, *110*, 114.

[25] P. P. Power, *Chem. Rev.* **1999**, *99*, 3463, and references therein.

[26] C. Liang, L. C. Allen, *J. Am. Chem. Soc.* **1990**, *112*, 1039.

[27] M. Karni, Y. Apeloig, *J. Am. Chem. Soc.* **1990**, *112*, 8589.

[28] Y. Apeloig, T. Müller, *J. Am. Chem. Soc.* **1995**, *117*, 5363.

[29] P. P. Power, *Chem. Commun.* **2003**, 2091.

[30] G. Trinquier, J-P. Malrieu, P. Rivière, *J. Am. Chem. Soc.* **1982**, *104*, 4529.

[31] J-P. Malrieu, G. Trinquier, *J. Am. Chem. Soc.* **1989**, *111*, 5916.

[32] H. Jacobsen, T. Ziegler, *J. Am. Chem. Soc.* **1994**, *116*, 3667.

[33] W. Petz, *Chem. Rev.* **1986**, *86*, 1019.

[34] R. West, J. D. Cavalieri, J. J. Buffy, C. Fry, K. W. Zilm, J. C. Duchamp, M. Kira, T. Iwamoto, T. Müller, Y. Apeloig, *J. Am. Chem. Soc.* **1997**, *119*, 4972.

[35] P. Jutzi, A. Becker, H. G. Stammler, B. Neumann, *Organometallics* **1991**, *10*, 1647.

[36] T. Fjeldberg, A. Haarland, B. E. R. Schilling, M. F. Lappert, A. J. Thorne, *J. Chem. Soc. Dalton. Trans.* **1986**, 1551.

[37] M. Kira, R. Yauchibara, R. Hirano, C. Kabuto, H. Sakurai, *J. Am. Chem. Soc.* **1991**, *113*, 7785.

[38] G.-H. Lee, R. West, T. Müller, *J. Am. Chem. Soc.* **2003**, *125*, 8114.

[39] D. H. Harris, M. F. Lappert, *J. Chem. Soc. Chem. Commun.* **1974**, 895.

[40] M. P. Bigwood, P. J. Corvan, J. J. Zuckerman, *J. Am. Chem. Soc.* **1981**, *103*, 7643.

[41] S. Brooker, J.-K. Buijink, F. T. Edelmann, *Organometallics* **1991**, *10*, 25.

[42] S. Brooker, J.-K. Buijink, F. T. Edelmann, *Organometallics* **1991**, *10*, 25.

[43] J. E. Bender, M. M. Banaszak Holl, J. W. Kampf, *Organometallics* **1997**, *16*, 2743.

[44] C.-J. F. Du, H. Hart, K.-K. D. Ng, *J. Org. Chem.* **1986**, *51*, 3162.

[45] For the Mes system: (a) R. S. Simons, L. Pu, M. M. Olmstead, P. P. Power, *Organometallics* **1997**, *16*, 1920; For the Trip system: (b) L. Pu, M. M. Olmstead, P. P. Power, B. Schiemenz, *Organometallics* **1998**, *17*, 5602.

Dieses Werk ist copyrightgeschützt und darf in keiner Form vervielfältigt werden noch an Dritte weitergegeben werden.
Es gilt nur für den persönlichen Gebrauch.

[46] G. H. Spikes, Y. Peng, J. C. Fettinger, P. P. Power, *Z. Anorg. Allg. Chem.* **2006**, *632*, 1005.

[47] P. Jutzi, C. Leue, *Organometallics* **1994**, *13*, 2898.

[48] K. Ruhlandt-Senge, J. J. Ellison, R. J. Wehmschulte, F. Pauer, P. P. Power, *J. Am. Chem. Soc.* **1993**, *115*, 11353.

[49] L. Pu, B. Twamley, P. P. Power, *Organometallics* **2000**, *19*, 2874.

[50] L. Pu, B. Twamley, P. P. Power, *J. Am. Chem. Soc.* **2000**, *122*, 3524.

[51] M. Lein, A. Krapp, G. Frenking, *J. Am. Chem. Soc.* **2005**, *127*, 6290.

[52] H. Preut, F. Huber, *Z. Anorg. Allg. Chem.* **1976**, *419*, 92.

[53] M. Kaupp, P. v. R. Schleyer, *J. Am. Chem. Soc.* **1993**, *115*, 1061.

[54] M. S. Stender, A. D. Phillips, R. J. Wright, P. P. Power, *Angew. Chem.* **2002**, *114*, 1863.

[55] A. F. Wells, *Structural Inorganic Chemistry*, 5th ed., Oxford, **1984**, 1279.

[56] T. L. Allen, W. H. Fink, P. P. Power, *J. Chem. Soc.*, *Dalton Trans.* **2000**, 407.

[57] A. D. Phillips, R. J. Wright, M. M. Olmstead, P. P. Power, *J. Am. Chem. Soc.* **2002**, *124*, 5930.

[58] N. Takagi, S. Nagase, *Organometallics* **2001**, *20*, 5498.

[59] R. C. Fischer, L. Pu, J. C. Fettinger, M. A. Brynda, P. P. Power, *J. Am. Chem. Soc.* **2006**, *128*, 11366.

[60] A. Sekiguchi, R. Kinjo, M. Ichinohe, *Science* **2004**, *305*, 1755.

[61] M. Weidenbruch, *The Chemistry of Organic Silicon Compounds,* Z. Rappoport, Y. Apeloig, Eds. Wiley, Chichester, UK, **2001**, vol 3, chap. 5.

[62] G. Frenking, A. Krapp, S. Nagase, N. Takagi, A. Sekiguchi, *Chem. Phys. Chem.* **2006**, *7*, 799.

[63] C. A. Pignedoli, A. Curioni, W. Andreoni, *Chem. Phys. Chem.* **2005**, *6*, 1795.

[64] C. A. Pignedoli, A. Curioni, W. Andreoni, *Chem. Phys. Chem.* **2006**, *7*, 801.

[65] J. Su, X-W. Li, R. C. Crittendon, G. H. Robinson, *J. Am. Chem. Soc.* **1997**, *119*, 5471.

[66] F. A. Cotton, A. H. Cowley, X. Feng, *J. Am. Chem. Soc.* **1998**, *120*, 1795.

[67] Y. Peng, M. Brynga, B. D. Ellis, J. C. Fettinger, E. Rivard, P. P. Power, *Chem. Commun.* **2008**, 6042.

[68] G. H. Spikes, J. C. Fettinger, P. P. Power, *J. Am. Chem. Soc.* **2005**, *127*, 12232.

[69] Y. Peng, B. D. Ellis, X. Wang, J. C. Fettinger, P. P. Power, *Science* **2009**, *325*, 1668.

[70] G. H. Spikes, Y. Peng, J. C. Fettinger, J. Steiner, P. P. Power, *Chem. Commun.* **2005**, 6041.

Dieses Werk ist copyrightgeschützt und darf in keiner Form vervielfältigt werden noch an Dritte weitergegeben werden.
Es gilt nur für den persönlichen Gebrauch.

[71] C. Cui, M. M. Olmstead, J. C. Fettinger, G. H. Spikes, P. P. Power, *J. Am. Chem. Soc.* **2005**, *127*, 17530.

[72] L. Pu, A. D. Phillips, A. F. Richards, M. Stender, R. S. Simons, M. M. Olmstead, P. P. Power, *J. Am. Chem. Soc.* **2003**, *125*, 11626.

[73] C. Bibal, S. Mazières, H. Gornizka, C. Couret, *Angew. Chem.* **2001**, *113*, 978.

[74] W. Setaka, K. Hirai, H. Tomioka, K. Sakamoto, M. Kira, *J. Am. Chem. Soc.* **2004**, *126*, 2696.

[75] Survey of the CCDC carried out May 2010.

[76] E. O. Fischer, A. Maasböl, *Angew. Chem.* **1964**, *76*, 645.

[77] O. S. Mills, A. D. Redhouse, *Angew. Chem.* **1965**, *77*, 1142.

[78] O. S. Mills, A. D. Redhouse, *J. Chem. Soc. A: Inorg. Phys. Theor.* **1968**, 642.

[79] R. R. Schrock, *J. Am. Chem. Soc.* **1974**, *96*, 6796.

[80] At that time there was only one example of a carbene complex with the carbon atom of the carbene bearing a hydrogen atom: B. Cetinkaya, M. F. Lappert, K. Turner, *J. Chem. Soc. Chem . Commun.* **1972**, 851.

[81] M. J. S. Dewar, *Bull. Soc. Chim. Fr.* **1951**, C71.

[82] J. Chatt, L. A. Duncanson, *J. Am. Chem. Soc.* **1953**, 2939.

[83] P. Jutzi, W. Steiner, *Angew. Chem.* **1976**, *88*, 21.

[84] M. F. Lappert, S. J. Miles, P. P. Power, A. J. Carty, N. J. Taylor, *J. Chem. Soc. Chem. Commun.* **1977**, *13*, 458.

[85] W. A. Hermann, H.-J. Kneuper, E. Herdtweck, *Angew. Chem.* **1985**, *97*, 1060.

[86] S. D. Grumbine, T. D. Tilley, F. P. Arnold, A. L. Rheingold, *J. Am. Chem. Soc.* **1993**, *115*, 7884.

[87] M. F. Lappert, R. S. Rowe, *Coord. Chem. Rev.* **1990**, *100*, 267.

[88]P. Jutzi, B. Hampel, K. Stroppel, C. Krüger, K. Angermund, P. Hofman, *Chem. Ber.* **1985**, *118*, 2789.

[89] A. L. Bach, D. E. Oram, *Organometallics* **1988**, *7*, 155.

[90] I. Saur, S. G. Alonso, J. Barrau, *Appl. Organomet. Chem.* **2005**, *19*, 414.

[91] J. D. Korp, I. Bernal, R. Horlein, R. Serrano, W. A. Herrmann, *Chem. Ber.* **1985**, *118*, 340.

[92] W. Gade, E. Weiss, **1981**, *213*, 451.

[93] E. O. Fischer, G. Kreis, C. G. Kreiter, J. Müller, G. Huttner, H. Lorenz, *Angew. Chem.* **1973**, *85*, 618.

Dieses Werk ist copyrightgeschützt und darf in keiner Form vervielfältigt werden noch an Dritte weitergegeben werden.
Es gilt nur für den persönlichen Gebrauch.

[94] S. J. McLain, C. D. Wood, L. W. Messerle, R. R. Schrock, *J. Am. Chem. Soc.* **1978**, *100*, 5962.

[95] R. S. Simons, P. P. Power, *J. Am. Chem. Soc.* **1996**, *118*, 11966.

[96] L. Pu, B. Twamley, S. T. Haubrich, M. M. Olmstead, B. V. Mork, R. S. Simons, P. P. Power, *J. Am. Chem. Soc.* **2000**, *122*, 650.

[97] A. C. Filippou, A. I. Philippopoulos, P. Portius, D. U. Neumann, *Angew. Chem.* **2000**, *112*, 2881.

[98] A. C. Filippou, P. Portius, A. I. Philippopoulos, H. Rohde, *Angew. Chem.* **2003**, *115*, 461.

[99] A. C. Filippou, A. I. Philippopoulos, G. Schnakenberg, *Organometallics* **2003**, *22*, 3339.

[100] A. C. Filippou, H. Rohde, G: Schnakenberg, *Angew. Chem.* **2004**, *116*, 2293.

[101] A. C. Filippou, N. Weidemann, G. Schnakenberg, H. Rohde, A. I. Philippopoulos, *Angew. Chem.* **2004**, *116*, 6674.

[102] G. Schnakenberg, Doctoral dissertation, University of Bonn, **2009**.

[103] B. V. Mork, T. D. Tilley, *Angew. Chem.* **2003**, *115*, 371.

[104] A. C. Filippou, O. Chernov, K. W. Stumpf, G. Schnakenburg, *Angew. Chem.* **2010**, *122*, 3368.

[105] M. van den Akker, F. Jellinek, *J. Organomet. Chem*. **1967**, *10*, P37.

[106] R. Mason, P. O. Whimp, *J. Chem. Soc. (A): Inorg. Phys. Theor*. **1969**, *18*, 2709.

[107] See as examples: (a) J. Kjellgren, H. Sunden, K. J. Szabo, *J. Am. Chem. Soc.* **2005**, *127*, 1787; (b) J. Kjellgren, H. Sunden, K. J. Szabo, *J. Am. Chem. Soc.* **2004**, *126*, 474; (c) E. Shirakawa, Y. Nakao, Y. Murota, T. Hiyama, *J. Organomet. Chem.* **2003**, *670*, 132; (d) C. Lee, J. Lee, S. W. Lee, S. O. Kang, J. Ko, *Inorg. Chem.* **2002**, *41*, 3084; (e) T. N. Mitchell, A. Amamria, H. Killing, D. Rutschow, *J. Organomet. Chem.* **1983**, *241*, C45.

[108] See as examples: (a) G. M. de Lima, C. A. L. Filgueiras, M. T. S. Giotto, Y. P. Mascarenhas, *Trans. Met. Chem.* **1995**, *20*, 380. (b) M. Grassi, S. V. Meille, Musco, P. R. Alfredo, A. Sironi, *J. Chem. Soc.* **1989**, *4*, 615; (c) A. Musco, R. Pontellini, M. Grassi, A. Sironi, S. V. Meille, H. Ruegger, C. Ammann, P. S. Pregosin, *Organometallics* **1988**, *7*, 2130; (d) V. V. Bashilov, V. I. Sokolov ,Yu L. Slovokhotov, Yu T. Struchkov, E. G. Mednikov, N. K. Eremenko, *J. Organomet. Chem.* **1987**, *327*, 285.

[109] See for example: (a) T. A. K. Al. Alaf, *J. Organomet. Chem.* **2002**, *654*, 21 (and references therein), (b) M. C. Janzen, M. C. Jennings, R. J. Puddephatt, *Organometallics*

Dieses Werk ist copyrightgeschützt und darf in keiner Form vervielfältigt werden noch an Dritte weitergegeben werden.
Es gilt nur für den persönlichen Gebrauch.

2001, *20*, 4100 (and references therein); (b) T. A. K. Al. Allaf, *J. Organomet. Chem.* **1999**, *590*, 25 (and references therein).

[110] See as examples: (a) G. Cavinato, G. De Munno, M. Lami, M. Marchionna, L. Toniolo, D. Viterbo, *J. Organomet. Chem.* **1994**, *466*, 277; (b) H. C. Clark, G. Ferguson, M. J. Hampden-Smith, H. Ruegger, B. L. Ruhl, *Can. J. Chem.* **1988**, *66*, 3120.

[111] This complex was prepared, crystallised and characterised by Dr. Peter Portius, in Bonn in 2007. It is included here for the sake of comparison. Procedure: A Schlenk tube was charged with a mixture of equimolar amounts of **1-Pd** (36 mg, 0.13 mmol) and **1-Ge** (75 mg, 0.13 mmol). A yellow solution was formed upon addition of ca. 20 ml of toluene (from K mirror) at −78 °C. The mixture was allowed to warm to RT and stirred. After 3 h an orange-brown solution had formed, wherefrom all volatile material was evaporated *in vacuo*. The remaining oil was extracted with n-pentane (from K mirror) (ca. 20 ml). The olive extraction residue (< 10 mg) was discarded, and the orange extract concentrated to 5 mL and cooled to –30 °C. This procedure afforded a yellow precipitate which was filtered off and dried (83 mg). Re-crystallisation of a saturated solution in n-hexane afforded yellow needles of **5-Pd**$\cdot\mathbf{C_6H_{14}}$ (27 mg, yield 22 %). 91-94 °C (dec). Elemental Analysis, calcd. C, 62.46; H, 7.86%, found C, 62.05; H, 7.59%. ^{1}H NMR / COSY (500 MHz, Tol-d_8, 223 °C): δ = 0.94 (t, 6H, ^3J(H,H) = 7.2 Hz, $\mathrm{C}H_3$ n-hexane), 1.16 (d, 6H, ^3J(H,H) = 6.6 Hz, $\mathrm{CH^B}(\mathrm{C}H_3)(\mathrm{CH'_3})$), 1.22 (d, 6H, ^3J(H,H) = 7.1 Hz, $\mathrm{CH^C}(\mathrm{C}H_3)(\mathrm{CH'_3})$, 1.28 (m, 8H, $\mathrm{C}H_3$ n-hexane), 1.31 (d, 12H, ^3J(H,H) = 6.9 Hz, $\mathrm{CH^A}(\mathrm{C}H_3)_2$), 1.32 (m, 4H, $\mathrm{C}H_2^{\mathrm{A}}$ cod), 1.60 (m, 4H, $\mathrm{C}H_2^{\mathrm{B}}$ cod), 1.73 (d, 6H, ^3J(H,H) = 6.4 Hz, $\mathrm{CH^B}(\mathrm{CH_3})(\mathrm{C}H_3')$), 1.76 (6H, ^3J(H,H) = 6.4 Hz, $\mathrm{CH^C}(\mathrm{CH_3})(\mathrm{C}H'_3)$), 2.85 (sept, 2H, ^3J(H,H) = 6.8 Hz, $\mathrm{C}H^{\mathrm{A}}(\mathrm{CH_3})_2$), 3.22 (sept, 2H, ^3J(H,H) = 6.6 Hz, $\mathrm{C}H^{\mathrm{B}}(\mathrm{CH_3})_2$), 3.58 (sept, 2H, ^3J(H,H) = 6.5 Hz, $\mathrm{C}H^{\mathrm{C}}(\mathrm{CH_3})_2$), 4.78 (bs, 2H, $\mathrm{C}H^{\mathrm{A}}$ cod), 5.68 (bs, 2H, $\mathrm{C}H^{\mathrm{B}}$ cod), 7.12 (pt, 1H, ^3J(H,H) = 7.2, 8.0 Hz, H-4), 7.22 (bd, 2H, ^3J(H,H) = 7.5 Hz, H-3 & H-4), 7.29 (s, 4H, 2 × H-3' & 2 × H-5'). ^{1}H NMR (500 MHz, Tol-d_8, 243 °C): δ = 0.93 (t, 6H, ^3J(H,H) = 7.1 Hz, $\mathrm{C}H_3$ n-hexane), 1.13 (d, 6H, ^3J(H,H) = 6.7 Hz, $\mathrm{CH^B}(\mathrm{C}H_3)(\mathrm{CH'_3})$), 1.23 (d, 6H, ^3J(H,H) = 6.7 Hz, $\mathrm{CH^C}(\mathrm{C}H_3)(\mathrm{CH'_3})$, 1.28 (m, 8H, $\mathrm{C}H_3$ n-hexane), 1.31 (d, 12H, ^3J(H,H) = 7.0 Hz, $\mathrm{CH^A}(\mathrm{C}H_3)_2$), 1.41 (m, 4H, $\mathrm{C}H_2^{\mathrm{A}}$ cod), 1.66 (m, 4H, $\mathrm{C}H_2^{\mathrm{B}}$ cod), 1.69 (d, 6H, ^3J(H,H) = 6.6 Hz, $\mathrm{CH^B}(\mathrm{CH_3})(\mathrm{C}H_3')$), 1.73 (6H, ^3J(H,H) = 6.6 Hz, $\mathrm{CH^C}(\mathrm{CH_3})(\mathrm{C}H'_3)$), 2.86 (sept, 2H, ^3J(H,H) = 6.9 Hz, $\mathrm{C}H^{\mathrm{A}}(\mathrm{CH_3})_2$), 3.18 (sept, 2H, ^3J(H,H) = 6.7 Hz, $\mathrm{C}H^{\mathrm{B}}(\mathrm{CH_3})_2$), 3.56 (sept, 2H, ^3J(H,H) = 6.6 Hz, $\mathrm{C}H^{\mathrm{C}}(\mathrm{CH_3})_2$), 4.79 (bs, 2H, $\mathrm{C}H^{\mathrm{A}}$ cod), 5.67 (bs, 2H, $\mathrm{C}H^{\mathrm{B}}$ cod), 7.14 (pt, 1H, overlapped with solvent, H-4),

Dieses Werk ist copyrightgeschützt und darf in keiner Form vervielfältigt werden noch an Dritte weitergegeben werden.
Es gilt nur für den persönlichen Gebrauch.

7.21 (bd, 2H, ^3J(H,H) = 7.4 Hz, H-3 and H-4), 7.27 (s, 2H, 2 × H-3'), 7.28 (s, 2H, 2 × H-5'). Samples in benzene and toluene always show signals of free cod, which indicates its weak coordination to the complex.

[112] C. Stader, B. Wrackmeyer, *J. Organomet. Chem.* **1985**, *295*, C11.

[113] R. Trebbe, F. Schager, R. Goddard, K.-R. Pörschke, *Organometallics* **2000**, *19*, 521.

[114] K. H. A. O. Starzewski, P. S. Pregosin, H. Rüegger, *Helv. Chim. Acta* **1982**, *65*, 785.

[115] M. Noskowska, E. Sliwinska, W. Duczmal, *Trans. Met. Chem.* **2003**, *28*, 756.

[116] A search for complexes featuring a Pd–$GeCl_3$ moeity yielded only five citations: (a) B. Crociani, T. Boschi, M. Nicolini, *Inorg. Chim. Acta* **1970**, *4*, 577; (b) T. Boschi, B. Crociani, *Inorg. Chim. Acta* **1971**, *5*, 477; (c) J.-C. Guo, S.-D. Li, *Thermochem* **2007**, *816*, 59; (d) P. G. Antanov, T. T. Zamsueva, I. A. Agapov, L. V. Konovalov, *Zh. Prikl. Khim.* **1993**, *66*, 2695; (e) P. G. Antonov, D. S. Manasevich, *Zh. Prikl. Khim.* **2000**, *73*, 1774.

[117] As a representative consise paper refering to this matter see R. A. Jackson, *J. Organomet. Chem.* **1979**, *166*, 17.

[118] S. P. Constantine, G. M. De Lima, P. B. Hitchcock, J. M. Keates, G. A. Lawless, I. Marziano, *Organometallics* **1997**, *16*, 793.

[119] O. V. Gusev, L. N. Morozova, M. G. Peterleitner, S. M. Peregudova, P. V. Petrovskii, N. A. Ustynyuk, P. M. Maitlis, *J. Organomet. Chem.* **1996**, *509*, 95.

[120] I. Objartel, H. Ott, D. Stalke, *Z. Anorg. Allg. Chem.* **2008**, *634*, 2373.

[121] M. J. Fernandez-Trujillo, M. Jimenez-Tenorio, M. C. Puerta, *I. Organomet. Chem.* **1989**, *377*, 241.

[122] Only three examples exist: (a) H.-J. Kraus, H. Werner, C. Kruger, *Z. Naturforsch. B: Chem. Sci.* **1983**, *38*, 733; (b) N. M. Boag, D. Boucher, J. A. Davies, R. W. Miller, A. A. Pinkerton, R. Syed, *Organometallics* **1988**, *7*, 791: (c) M. Suginome, Y. Kato, N. Takeda, H. Oike, Y. Ito, *Organometallics* **1998**, *17*, 495.

[123] L. Benchekroun, P. Herpin, *J. Organomet. Chem.* **1977**, *128*, 275.

[124] R. Cramer, *Inorg. Chem.* **1962**, *1*, 722.

[125] As representative examples of neutral Rh arene complexes see: (a) M. J. Nolte, G. Gafner, *Acta. Crystallogr., Sect. B: Struct. Crystallogr. Cryst. Chem.* **1974**, *30*, 738; (b) S. G. Shore, W.-L. Hsu, M. R. Churchill, C. Bueno, *J. Am. Chem. Soc.* **1983**, *105*, 655; (c) M. R. Churchill, C. Bueno, *J. Organomet. Chem.* **1983**, *256*, 357; (d) W. E. Marsh, D. A. Clemente, *Inorg. Chim. Acta.* **2007**, *360*, 4017; (e) M.-J. Fernandez, M. A.

Dieses Werk ist copyrightgeschützt und darf in keiner Form vervielfältigt werden noch an Dritte weitergegeben werden.
Es gilt nur für den persönlichen Gebrauch.

Esteruelas, L. A. Oro, J. Ruiz, A. J. Smith, P. M. Maitlis, *J. Organomet. Chem.* **1987**, *330*, 179.

[126] A plethora of cationic Rh arene complexes exists. See as representative examples: (a) B. J. Holliday, P. A. Ulmann, C. A. Mirkin, C. L. Stern, L. N. Zakharov, A. L. Rheingold, *Organometallics* **2004**, *23*, 1671; (b) L. A. Oro, C. Foces-Foces, F. H. Cano, S. Garcia-Blanco, *J. Organomet. Chem.* **1982**, *236*, 385; (c) J. S. Siegel, K. K. Baldridge, A. Linden, R. Dorta, *J. Am. Chem. Soc.* **2006**, *128*, 10644; (d) J. R. Bleeke, A. J. Donaldson, *Organometallics* **1988**, *7*, 1588; (e) M. S. Lim, J.Y. Baeg, S. W. Lee, *J. Organomet. Chem*. **2006**, *691*, 4100; (f) T. M. Douglas, S. K. Brayshaw, R. Dallanegra, G. Kociok-Kohn, S. A. MacGregor, G. L. Moxham, A. S. Weller, T. Wondimagegn, P. Vadivelu, *Chem. –Eur. J.* **2008**, *14*, 1004; (g) M. R. Thompson, C. S. Day, V. W. Day, R. I. Mink, E. L. Muetterties, *J. Am. Chem. Soc.* **1980**, *102*, 2979; (h) J. R. Farrell, A. H. Eisenberg, C. A. Mirkin, I. A. Guzei, L. M. Liable-Sands, C. D. Incarvito, A. L. Rheingold, C. L. Stern, *Organometallics* **1999**, *18*, 4856.

[127] (a) S. M. Hawkins, P. B. Hitchcock, M. F. Lappert, *J. Chem. Soc., Chem. Commum.* **1985**, 1592; (b) M. Kilian, H. Wadepohl, L. H. Gade, *Organometallics* **2008**, *27*, 524; (c) M. Kilian, H. Wadepohl, L. H. Gade, *Dalton Trans.* **2008**, 582.

[128] J. M. Dysard, T. D. Tilley, *Organometallics* **2000**, *19*, 2671.

[129] (a) R. D. Adams, J. L. Smith, *Inorg. Chem.* **2005**, *44*, 4276; (b) M. Veith, A. Muller, L. Stahl, M. Notzel, M. Jarczyk, V. Hich, *Inorg. Chem.* **1996**, *35*, 3848.

[130] A dilute ^{1}H NMR spectrum of this compound was recorded in $CDCl_3$, but the signals could not be assigned.

[131] (a) H. Werner, G. Canepa, K. Ilg, J. Wolf, *Organometallics* **2000**, *19*, 4756. (b) G. Canepa, C. D. Brandt, K. Ilg, J. Wolf, H. Werner, *Chem. –Eur. J.* **2003**, *9*, 2502.

[132] See as a recent example: C. W. Landorf, M. M. Haley, *Angew. Chem., Int. Ed.* **2006**, *45*, 3914.

[133] Holt, M.S.; Wilson, W. L.; Nelson, J. H. *Chem. Rev.* **1989**, *89*, 11 (and references therein).

[134] S. C. Bart, E. Lobkovsky, P. J. Chirik, *J. Am. Chem. Soc.* **2004**, *126*, 13797.

[135] T. A. Betley, J. C. Peters, *J. Am. Chem. Soc.* **2003**, *125*, 10782.

[136] J. M. Lopez-Alcala, M. C. Puerta, F. Gonzalez-Vilchez, *Polyhedron*, **1984**, *3*, 623.

[137] T. A. George, D. J. Rose, Y. Chang, Q. Chen, J. Zubieta, *Inorg. Chem.* **1995**, *34*, 1295.

[138] On this subject, the complex of Chirik was later shown to contain a redox active ligand which rather exists as a two electron reduced chelate see: S. C. Bart, K. Chlopek, E. Bill,

Dieses Werk ist copyrightgeschützt und darf in keiner Form vervielfältigt werden noch an Dritte weitergegeben werden.
Es gilt nur für den persönlichen Gebrauch.

M. W. Bouwkamp, E. Lobkovsky, F. Neese, K. Wieghardt, P. J. Chirik, *J. Am. Chem. Soc.* **2006**, *128*, 13901.

[139] S. Komiya, M. Akita, A. Yoza, N. Kasuga, A. Fukuoka ,Y. Kai, *J. Chem. Soc., Chem. Commun.* **1993**, 787.

[140] M. Hirano, M. Akita, T. Morikita, H. Kubo, A. Fukuoka, S. Komiya, *Dalton Trans.* **1997**, 3453.

[141] J. Chatt, R. G. Hayter, *J. Chem. Soc.* **1961**, 5507.

[142] G. Winter, *Inorg. Synth.* **1973**, 101.

[143] R. S. Berry, *J. Chem. Phys.* **1960**, *32*, 933.

[144] C. Perthuisot, W. D. Jones, *Can. J. Chem.* **1994**, *18*, 621.

[145] This index (τ) describes numerically, in five coordinate systems, the degree to which they are trigonal bipyramidal or square pyramidal, and can be considered a continuum. It is calculated by the formula $\tau = (\alpha - \beta)/60$, where α and β are the two largest angles around the central atom. A perfect TBP geometry hence yields a τ value of unity, while a perfect SQPY geometry a value of $\tau = 0$, and distortions from either parent geometry result in values inbetween these two extremes. See: A. W. Anderson, T. N. Rao, J. Reedijk, J. v. Rijn, G. C. Verschoor, *J. Chem. Soc. Dalton Trans.* **1984**, 1349.

[146] This value is the median obtained from CCDC survey (May, 2010) of all complexes containing the moiety „Fe-SnR_3", where R is a non metal substituent. LQ/HQ = 2.499 Å /2.579 Å, n = 73. (LQ =lower quartile, HQ = higher quartile)

[147] To our knowledge, there is only one structurally characterised example of an iron stannylidene complex, [$(CO)_4Fe=SnRR'$], (R = 2,4,6-$^tBu_3$-C_6H_3, R' = $CH_2C(CH_3)_2$-3,5-$^tBu_2$-C_6H_3) where the tin atom is three coordinate: M. Weidenbruch, A. Stilter, K. Peters and H. G. von Schnering, *Chem. Ber.* **1996**, *129*, 1565.

[148] L. Zimmer, Inorganic Chemistry Colloquium lecture, Dec 2009, University of Bonn.

[149] Even for the element carbon: An input of "Fe≡C" into the Cambridge crystallographic database resulted in no hits. Additionally, a similar search for compounds containing the "Fe=C" moiety resulted in exclusively 3 coordinate C atoms (alkylidenes), or complexes of the containing the moiety: "Fe=C=C" or "Fe=C=N".

[150] To our knowledge $[(PPh_3)(CO)_3Fe{\equiv}C{-}N(^iPr)_2]^+$ is the only published example of an iron "carbyne" complex, structurally characterised to date: E. O. Fischer, J. Schneider, D. Neugebauer, *Angew. Chem.* **1984**, *96*, 814. However, This according to our calculations (Performed by G. Schnakenburg) have shown the NRT-BO in

Dieses Werk ist copyrightgeschützt und darf in keiner Form vervielfältigt werden noch an Dritte weitergegeben werden.
Es gilt nur für den persönlichen Gebrauch.

$[(PPh_3)(CO)_3Fe{\equiv}C{-}N(^iPr)_2]^+$ to be 1.59 (B3LYP/IIa) showing it rather comprises cumulated double bonds caused by π-donation from the lone pair at the N atom, and hence it would be more correct to classify this complex as a carbene complex.

[151] H. Grützmacher, T. F. Fässler, *Chem. Eur. J.* **2000**, *6*, 2317 and references therein.

[152] J. Zhou, S. J. Lancaster, D. A. Walker, S. Beck, M. Thornton-Pett, M. Bochmann, *J. Am. Chem. Soc.* **2001**, *123*, 223.

[153] P.-G. Lassahn, V. Lozan, B. Wu, A. S. Weller, C. Janiak, *Dalton Trans.* **2003**, 4437.

[154] See as a recent example: C. Bibal, C. C. Santini, Y. Chauvin, C. Vallée, H. Oliver-Bourbigou, *Dalton Trans.* **2008**, 2866.

[155] M. S. Holt, W. L. Wilson, J. H. Nelson, *Chem. Rev.* **1989**, *89*, 11.

[156]The electron localisation function of shows the typical toroidal distribution of localised electron density as found for the triple bond in acetylene. The remarkably high isosurface value of ELF=0.88 shows a high localisation of the triple bond.

[157] Several examples of compounds with $[GeCl_3]^-$ anions exist for example : a) L. Apostolico, M. F. Mahon, K. C. Molloy, R. Binions, C. S. Blackman, C. J. Carmalt, I. P. Parkin, *Dalton Trans.* **2004**, 470; b) R. West, D. F. Moser, I. A. Guzei, C.-H. Lee, A. Naka, W. Li, A. Zabula, S. Bukalov, L. Leites, *Organometallics,* **2006**, *25*, 2709; c) G. Kociok-Köhn, J. G. Winter, A. C. Filippou, *Acta. Cryst.* **1999**, *C55*, 351.

[158] Hollemann Wiberg, Lehbuch der anorganische chemie, pp 133, Walter de Gruyter, **1985**, 91.-100. auflage.

[159] H. Friebolin, „Ein-und zweidimensionale NMR-Spektroskopie“ (Eine Einführung) 3rd edition, Wiley-VCH, Weinheim **1999**, 307; this equation results from the Eyring equation: $\Delta G^{\#} = RT(23.76 - \ln(k/T))$ and the correlation equation : $k_c=2.22\Delta\nu$, where k_c is the rate constant at the coalescence temperature.

[160] Performed by G. Schnakenburg, University of Bonn, **2008**, Unpublished results.

[161] *Atoms in Molecules: A quantum Theory*, R. F. W. Bader, Oxford University Press**, 1994.**

[162] C. Ni, B. D. Ellis, J. C. Fettinger, G. J. Long, P. P Power, *Chem. Commun.* **2008**, 1014.

[163] (a) H. Kandler, C. Gauss, W. Bidell, S. Rosenberger, T. Bürgi, I. L. Eremenko, D. Veghini, O. Orama, P. Burgert, H. Berke, *Chem. Eur. J.* **1995**, *1*, 541. (b) A. G. Orpen, N. G. Connelly, M. W. Whiteley, P. Woodward, *J. Chem. Soc., Dalton Trans.* **1989**, 1751.

Dieses Werk ist copyrightgeschützt und darf in keiner Form vervielfältigt werden noch an Dritte weitergegeben werden.
Es gilt nur für den persönlichen Gebrauch.

[164] C. Bianchini, F. Laschi, D. Masi, F. M. Ottavini, A. Pastor, M. Peruzzini, P. Zanelle, F. Zanobini, F. *J. Am. Chem. Soc.* **1993**, *115*, 2723.

[165] As some examples: (a) J.-R. Hamon, D. Astruc, P. Michaud, *J. Am. Chem. Soc.* **1981**, *103*, 758. (b) R. L. Harlow, R. J. McKinney, S. D. Ittel, *J. Am. Chem. Soc.* **1979**, *101*, 7496. (c) J. H. MacNeil, A. C. Chiverton, S. Fortier, M. C. Baird, R. C. Hynes, A. J. Williams, K. F. Preston, T. Ziegler, *J. Am. Chem. Soc.* **1991**, *113*, 9834. (d) J. M. Smith, A. R. Sadique, T. R. Cundari, K. R. Rodgers, G. Lukat-Rodgers, R. J. Lachicotte, C. J. Flaschenriem, J. Vela, P. L. Holland, *J. Am. Chem. Soc.* **2006**, *128*, 756. (e) A. R. Sadique, E. A. Gregory, W. W. Brennessel, P. L. Holland, *J. Am. Chem. Soc.* **2007**, *129*, 8112. (f) D. Astruc, D. Mandon, A. Madonik, P. Michaud, N. Ardoin, F. Varret, *Organometallics* **1990**, *9*, 2155.

[166]R. Wesendrup, C. A. Schalley, D. Schröder, H. Schwarz, *Organometallics* **1996**, *15*, 1435.

[167] C. C. Lu, C. T. Saouma, M. W. Day, J. C. Peters, *J. Am. Chem. Soc.* **2007**, *129*, 4.

[168](a) S. W. Ragsdale, M. Kumar, *Chem. Rev.* **1996**, *96*, 2515. (b) D. J. Evans, *Coord. Chem. Rev.* **2005**, *249*, 1582.

[169] D. Lexa, J.-M. Savéant, D. L. Wang, *Organometallics* **1986**, *5*, 1428.

[170](a) P. J. Krusic, D. J. Jones, D. C. Roe, *Organometallics* **1986**, *5*, 456. (b) P. J. Krusic, W. J. Cote, *J. Am. Chem. Soc.* **1984**, *106*, 4642.

[171]M. W. Bouwkamp, S. C. Bart, E. J. Hawrelak, R. J. Trovitch, E. Lobkovsky, P. J. Chirik, *Chem. Commun.* **2005**, 3406.

[172]S. C. Bart, K. Chłopek, E. Bill, M. W. Bouwkamp, E. Lobkovsky, F. Neese, K. Wieghardt, P. J. Chirik, *J. Am. Chem. Soc.* **2006**, *128*, 13901.

[173]The samples were confirmed pure by both elemental analysis, and by Mößbauer spectroscopy. Owing to the observation of minor Fe(II) impurities in the NMR spectra, Mößbauer spectra where simulated to determine the *maximum* relative percentage Fe(II) impurity that would be required to be visible in the Mößbauer spectra. The results showed convincingly, that no more than approximately 5 % of the Fe(II) could be present, which represents an upper limit of the contamination of the Fe(I) complexes.

[174] G. J. Leigh, M. Jimenez-Tenorio, *J. Am. Chem. Soc.* **1991**, *113*, 5862.

[175] L. D. Field, H. L. Li, A. M. Magill, *Inorg. Chem.* **2009**, *48*, 5.

[176] C. A. Tolman, S. D. Ittel, A. D. English, J. P. Jesson, *J. Am. Chem. Soc.* **1978**, *100*, 4080.

[177] N. Weidemann, *Dissertation,* Humboldt University of Berlin, **2009**.

Dieses Werk ist copyrightgeschützt und darf in keiner Form vervielfältigt werden noch an Dritte weitergegeben werden.
Es gilt nur für den persönlichen Gebrauch.

[178] D. L. Hughes, G. J. Leigh, C. N. McMahon, *J. Chem. Soc., Dalton Trans.* **1999**, 909.

[179] C. Elschenbroich, M. Nowotny, A. Behrendt, K. Harms, S. Wocadlo, J. Pebler, *J. Am. Chem. Soc.* **1994**, *116*, 6217.

[180] R. B. King, M. Chang, M. G. Newton, *J. Organomet. Chem.* **1985**, *296*, 15.

[181] W. K. Wong, K. W. Chiu, G. Wilkinson, A. J. Howes, M. Motevalli, M. B. Hursthouse, *Polyhedron*, **1985**, *4*, 603.

[182] These differences are determined from the $^{31}P\{^{1}H\}$ NMR spectrum of authentic samples of depe and dmpe measured in C_6D_6 at room temperature, and comparing the chemical shifts to **3-Fe** and **16-Fe** also measured in C_6D_6 respectively.

[183] N. Weidemann, *Disseration,* Humboldt University of Berlin, **2009**. P 43 and 56.

[184] J. W. Rathke, E. L. Muetterties, *J. Am. Chem. Soc.* **1975**, *97*, 3272.

[185] T. V. Harris, J. W. Rathke, E. L. Muetterties, *J. Am. Chem. Soc.* **1978**, *100*, 6966.

[186] Survey of CCDC, January 2009.

[187] M. V. Baker and L. D. Field, *Organometallics* **1986**, *5*, 821.

[188] M. V. Baker and L. D. Field, *J. Am. Chem. Soc.* **1986**, *108*, 7437.

[189] M. Aresta, G. M. Rossi, A. Sacco, *Inorg. Chim. Acta.,* **1971**, *5*, 115.

[190] G. Hata, H. Kondo, A. Miyake, *J. Am. Chem. Soc.,* **1968**, *90*, 2278.

[191] S. D. Ittel, C. A. Tolman, P. J. Krusic, A. D. English, J. P. Jesson, *Inorg. Chem.* **1978**, *17*, 3432.

[192] N. A. Alcock, *Adv. Inorg. Chem. Radiochem.* **1972**, *15*, 1.

[193] (a) A. Maldotti, S. Sostero, O. Traverso, *Inorg. Chim. Acta* **1981**, *54*, L271; (b) H. Azizian, R. H. Morris, *Inorg. Chem.* **1983**, *22*, 6; (c) S. D. Ittel, M. A. Cushing, *Inorg. Synth.* **1982**, *21*, 90.

[194]See for example: (a) R. D. Adams, A. Davison, J. P. Selegue, *J. Am. Chem. Soc.* **1979**, *101*, 7232; (b) T. O'Connor, A. J. Carty, M. Mathew, G. J. Palenik, *J. Organomet. Chem.* **1972**, *38*, C15.

[195] P. G. Hayes, C. Beddie, M. B. Hall, R. Waterman, T. D. Tilley, *J. Am. Chem. Soc.* **2006**, *128*, 428.

[196] P. G. Hayes, C. W. Gribble, R. Waterman, T. D. Tilley, *J. Am. Chem. Soc.* **2009**, *131*, 4606.

[197] In hydride complexes, for example, the Fe-*H* chemical shift in ^{1}H NMR spectra occur consistently upfield from the corresponding Ru-*H* or Os-*H* resonance signals. See in this context for example: E. Rocchini, P. Rigo, A. Mezzetti, T. Stephan, R. H. Morris, A. J. Lough, C. E. Forde, T. P. Fong, S. D. Drouin, *Dalton Trans.* **2000**, 3591.

Dieses Werk ist copyrightgeschützt und darf in keiner Form vervielfältigt werden noch an Dritte weitergegeben werden.
Es gilt nur für den persönlichen Gebrauch.

[198] A. Jana, H. W. Roesky, C. Schulzke, A. Döring, *Angew. Chem.* **2009**, *121*, 1126.

[199] H. A. Bent, *Chem. Rev.* **1960**, 275.

[200] See as an example: V. S. Petrosyan, A. B. Permin, O. A. Reutov, *J. Mag. Res.* **1980**, *40*, 511.

[201] Prepared before in a similar fashion by reflux of **2-Fe** with $SnCl_2$ in benzene: G. M. Bancroft, M. J. Mays, B. E. Prater, *J. Chem. Soc. (A): Inorg. Phys. Theor.* **1970**, *6*, 956.

[202] *The organometallic Chemistry of the transition metals*, R. H. Crabtree, P.14.

[203] J. H. Nelson, W. L. Wilson, L. W. Cary, N. W. Alcock, H. J. Clase, G. S. Jas, L. Ramsey-Tassin, J. W. Kenney III, *Inorg. Chem.* **1996**, *35*, 883.

[204] D. M. Bancroft, G. Cerantola, *Can. J. Chem.* **1976**, *54*, 1285.

[205] J. Chatt, R. G. Hayter, *J. Chem. Soc.* **1961**, 5507.

[206] M. J. Mays, B. E. Prayter, *Inorg. Synth.* **1974**, *15*, 21.

[207] M. V. Baker, L. D. Field, D. J. Young, *Appl. Organomet. Chem.* **1990**, *4*, 551.

[208] $GeCl_2$.(1,4-dioxane) exists as a coordination polymer See: M. K. Denk, M. Khan, A: J. Lough, K. Shuchi, *Acta Cryst.* **1998**, *C54*, 1830.

[209] U. M. Tripathi, G. L. Wegner, A. Schier, A. Jockisch, H. Schmidbaur, *Z. Naturforsch., B: Chem. Sci.* **1998**, *53*, 939.

[210] (a) T. Szymańska-Buzar, T. Głowiak, *J. Organomet. Chem.* **1998**, *564*, 143; (b) A. Malinowska, M. Górski, A. Kochel, T. Szymańska-Buzar, *Inorg. Chem. Commun.* **2007**, *10*, 1233; (c) A. C. Filippou, P. Portius, J. G. Winter, G. Kociok-Köhn, *J. Organomet. Chem.* **2001**, *628*, 11.

[211](a) M. Górski, A. Kochel, T. Szymańska-Buzar, *Inorg. Chem. Commun.* **2005**, *8*, 500; (b) M. Górski, A. Kochel, T. Szymańska-Buzar, *J. Organomet. Chem.***2001**, *691*, 3708.

[212] (a) T. Szymańska-Buzar, T. Głowiak, I. Czeluśniak, M. Górski, *Inorg. Chem. Commun.* **2002**, *5*, 682; (b) J. Handzlik, M. Stosur, A. Kochel, T. Szymańska-Buzar, *Inorg. Chim. Acta.* **2008**, *361*, 502.

[213] H. Tobita, K. Ishiyama, Y. Kawano, S. Inomata, H. Ogino, *Organometallics* **1998**, *17*, 789.

[214] Commented on in above reference. See ref 2 of above reference.

[215] *Infrared Spectroscopy: Fundamentals and Applications,* B. H. Stuart, Wiley, **2004**, page 12.

[216] R. V. Parish, P. J. Rowbotham, *J. Chem. Soc., Dalton Trans.* **1973**, 37.

[217] R. N. Haszeldine, R. V. Parish, J. H. Setchfield, *J. Organomet. Chem.* **1973**, *57*, 279.

[218] D. J. Cardin, S. A. Keppie, M. F. Lappert, *J. Chem. Soc. (A)* **1970**, 2594.

Dieses Werk ist copyrightgeschützt und darf in keiner Form vervielfältigt werden noch an Dritte weitergegeben werden.
Es gilt nur für den persönlichen Gebrauch.

[219] (a) R. L. Mössbauer, *Z. Phys.* **1958**, *151*, 124; (b) R. L. Mössbauer, *Z. Naturforsch. A* **1959**, *14a*, 211; (c) R. L. Mössbauer, *Naturwissenschaften* **1958**, *45*, 538.

[220] As a good reference highlighting the use of Mößbauer spectroscopy in heterogeneous catalysis see: J.-M. M. Millet, *Adv. Catal.* **2007**, *51*, 309 and references therein.

[221] W. E. Lamb, *Phys. Rev.* **1939**, *55*, 190.

[222] G. M. Bancroft, M. J. Mays, B. E. Prater, *J. Chem. Soc. A* **1970**, 956.

[223] G. M. Bancroft, M. J. Mays, B. E. Prater, F. P. Stefanini, *J. Chem. Soc. A* **1970**, 2146.

[224] G. M. Bancroft, E. T. Libbey, *J. Chem. Soc. Dalton Trans.* **1973**, 2103.

[225] J. M. Bellerby, M. J. Mays, P. L. Sears, *J. Chem. Soc. Dalton Trans.* **1976**, 1232.

[226] D. J. Evans, M. J. Jimenez-Tenorio, G. J. Leigh, *J. Chem. Soc. Dalton Trans.* **1991**, 1785.

[227] R. L. Collins, R. Pettit, *J. Chem. Phys.* **1963**, *39*, 3433.

[228] W. E. Carroll, F. A. Deeney, J. A. Delaney, F. J. Lalor, *J. Chem. Soc. Dalton Trans.* **1973**, 718.

[229] B. A. Sosinsky, N. Norem, R. G. Shong, *Inorg. Chem.* **1982**, *21*, 4229.

[230] B. A. Sosinsky, J. Shelly, R. Shong, *Inorg. Chem.* **1981**, *20*, 1370.

[231] See as an example: *Inorganic electronic structure and spectroscopy Volume 1: Methodology*, p 181, Ed: E. I. Solomon, A.B.P Lever, John Wiley & Sons, 1999

[232] T. R. Dugan, P. L. Holland, *J. Organomet. Chem.* **2009**, *694*, 2825.

[233] O. Frankie, B. E. Wiesler, N. Lehnert, G. Peters, P. Burger, F. Tuczek, *Z. Anorg. Allg. Chem.* **2006**, *632*, 1247.

[234] L. Zimmer, Private communication.

[235] M. T. Bautista, E. P. Cappellani, S. D. Drouin, R. H. Morris, C. T. Schweitzer, A. Sella, J. Zubkowski, *J. Am. Chem. Soc.* **1991**, *113*, 4876.

[236] L. Cronin, M. C. Nicasio, R. N. Perutz, R. G. Peters, D. M. Roddick, M. K. Whittlesey, *J. Am. Chem. Soc.* **1995**, *117*, 10047.

[237] a) P. Evans, G. Wilkinson, *J. Chem. Soc. Dalton.* **1973**, 204; b) A. Mercer, J. Trotter, *J. Chem. Soc. Dalton.* **1975**, 2480; c) E. Alessio, G. Mestroni, G. Nardin, W. M. Attia, M. Calligaris, G. Sava, S. Zorzet, *Inorg. Chem.* **1988**, *27*, 4099.

[238] a) R. F. Winter, B. M. Brunner, T. Scheiring, *Inorg. Chim. Acta.* **2000**, *310*, 21; b) J. Chatt, R. G. Hayter, *J. Chem. Soc.* **1961,** 896.

[239] The hydride chemical shift was reported in $CHCl_3$ and quoted in τ: Conversion to the modern δ scale follows using the equation $\delta = 10 - \tau$ see: E. R. Birnbaum, *Inorg. Nucl. Chem. Lett.* **1971**, *7*, 233.

Dieses Werk ist copyrightgeschützt und darf in keiner Form vervielfältigt werden noch an Dritte weitergegeben werden.
Es gilt nur für den persönlichen Gebrauch.

[240] Ru complexes featuring a mutually *trans* arrangement of stannyl and H ligands are rare. In one example, the complex *trans*-[(dmpe)$_2$RhH(SnPh$_3$)] is reported to have a ^{2}J(P,Sn) = 174.6 Hz, in close range to **5-Ru** see: A. W. Kaplan, R. G. Bergman, *Organometallics* **1998**, *17*, 5072.

[241] M. Akita, R. Hua, S. Nakanishi, M. Tanaka, Y. Moro-oka, *Orgtanometallics* **1997**, *16*, 5572.

[242] (a) R. D. Adams, B. Captain, L. Zhu, *Inorg. Chem.* **2005**, *44*, 6623; (b) R. D. Adams, B. Captain, W. Fu, M. D. Smith, *Inorg. Chem.* **2002**, *41*, 5593; (c) R. D. Adams, B. Captain, M. D. Smith, *Inorg. Chem.* **2002**, *41*, 2302; (d) J. A. Cabeza, S. García-Granda, A. Llamazares, V. Riera, J. F. V. d. Maelen, *Organometallics* **1993**, *12*, 157: (e) R. D. Adams, D. A. Katahira, *Organometallics* **1982**, *1*, 53; (f) C. Bois, J. A. Cabeza, R. J. Franco, V. Riera, E. Saborit, *J. Organomet. Chem.* **1998**, *564*, 201.

[243] R. D. Adams, B. Captain, E. Trufan, L. Zhu, *J. Am. Chem. Soc.* **2007**, *129*, 7545.

[244] (a) R. S. Ghadwal, H. W. Roesky, S. Merkel, J. Hemm, D. Stalke, *Angew. Chem.* **2009**, *121*, 5793; (b) A. C. Filippou, O. Chernov, G. Schnakenburg, *Angew. Chem.* **2009**, *121*, 5797.

[245] A. C. Filippou, O. Chernov, B. Blom, K. W. Stumpf, G. Schnakenburg, *Chem. Eur. J.* **2010**, *26*, 2866.

[246] All The Silicon work which is refered to in this section was carried out by O. Chernov, AK Filippou, Institute of Inorganic Chemistry, University of Bonn, Bonn 2009.

[247] K. W. Stumpf, *Diplomarbeit*, University of Bonn 2009; unpublished work.

[248] P. A. Rupar, M. C. Jennings, K. M. Baines, *Organometallics* **2008**, *27*, 5043.

[249] K. L. Hurni, P. A. Rupar, N. C. Payne, K. M. Baines, *Organometallics* **2007**, *26*, 5569.

[250] P. A. Rupar, V. N. Staroverov, P. J. Ragogna, K. M. Baines, *J. AM. Chem. Soc.* **2007**, *129*, 15138.

[251] C. Janiak, *Dalton Trans.* **2000**, 3885.

[252] A. F. Richards, A. D. Phillips, M. M. Olmstead, P. P. Power, *J. Am. Chem. Soc.* **2003**, *125*, 3204.

[253] Q.-S. Li, R.-H. Lü, Y. Xie, H. F. Schaefer III, *J. Comput. Chem.* **2002**, *23*, 1642 and references therein.

[254] N. G. Bokii, Yu. T. Struchkov, S. P. Kolesnikov, I. S. Rogazhin, O. M. Neterov, *Izv. Akad. Nauk SSSR, Ser. Khim.* **1975**, 872.

[255] Y. Inoguchi, K. Mochida, A. Itai, *Bull. Chem. Soc. Jpn.* **1985**, *58*, 974.

[256] M. Stender, L. Pu, P. P. Power, *Organometallics* **2001**, *20*, 1820.

Dieses Werk ist copyrightgeschützt und darf in keiner Form vervielfältigt werden noch an Dritte weitergegeben werden.
Es gilt nur für den persönlichen Gebrauch.

[257] This is the case with NHC stabilised Ge centres: L. Zimmer, Private communication, March 2010.

[258] L. D: Field, R. W. Guest, K. Q. Vuong, S. J. Dalgarno, P. Jensen, *Inorg. Chem.* **2009**, *48*, 2246.

[259] D. Geiß, Dimplomarbeit, University of Bonn, 2010; b) D. Geiß, B. Blom, A. C. Filippou, manuscript in preparation. (This project was carried out under the mutual supervision of B. Blom and A. C. Filippou, after the completion of the work mentioned in this dissertation, as an extension to Ru).

[260] *The Manipulation of Air Sensitive Compounds,* D. F. Shriver, M. A. Drezdzon, Wiley, Chichester, **1986**.

[261] C. Lindlahr, Private communication.

[262] J. Kouvetakis, A. Haarland, D. J. Shorokhov, H. V. Volden, G. V. Girichev, V. I. Sokolov, P. Matsunaga, *J. Am. Chem. Soc.* **1998**, *120*, 6738.

[263] D. Drew, J. R. Doyle, *Inorg. Synth.* **1990**, 346.

[264] G. T. L. Broadwood-Strong, P. A. Chaloner, P. B. Hitchcock, *Polyhedron*, **1993**, *12* 721.

[265] G. Winter, *Inorg. Synth.* **1973**, *14*, 101.

[266] A. G. Massey, A. J. Park, *J. Organomet. Chem.* **1964**, *2*, 245.

[267] J. B. Lambert, S. Zhang, S. M. Ciro, *Organometallics* **1994**, *13*, 2430.

[268] J. Chatt, F. A. Hart, *J. Chem. Soc.* **1960**, 1378.

[269] K. Issleib, W. Seidel, *Chem. Ber.* **1959**, *92*, 2681.

[270] Also synthesised by an inhouse developed route, different to that described in the above two references. To be published.

[271] C. Eaborn, P. B. Hitchcock, J. D. Smith, S. E. Sözerli, *Organometallics* **1997**, *16*, 5653.

[272] T. P. Whaley, C. C. Chappelow, *Inorg. Synth.* **1957**, *5*, 6.

[273] Synthesised by an inhouse developed route, yet to be published.

[274] M. L. Luetkens, A. P. Sattelberger, H. H. Murray, J. D. Basil, J. P. Fackler, *Inorg. Synth*. **1989**, *26*, 7.

[275] A. Fürstner, H. Weidmann, *J. Organomet. Chem.* **1988**, *354*, 15.

[276] N. Kuhn, T. Kratz, *Synthesis,* **1993**, 561.

[277] S. H. Babcock, *Inorg. Synth.* **1939**, *1*, 10.

Dieses Werk ist copyrightgeschützt und darf in keiner Form vervielfältigt werden noch an Dritte weitergegeben werden.
Es gilt nur für den persönlichen Gebrauch.

7. Oath of compliance with academic integrity

I hereby affirm that this dissertation was prepared independently at the Institute of Inorganic Chemistry at the Rheinische Friedrich-Wilhelms University of Bonn under the guidance of Prof. Dr. A. C. Filippou, where all references and additional aid sources have been appropriately cited.

Burgert Blom

Bonn, April 2011.

Dieses Werk ist copyrightgeschützt und darf in keiner Form vervielfältigt werden noch an Dritte weitergegeben werden.
Es gilt nur für den persönlichen Gebrauch.

Dieses Werk ist copyrightgeschützt und darf in keiner Form vervielfältigt werden noch an Dritte weitergegeben werden.
Es gilt nur für den persönlichen Gebrauch.

Dieses Werk ist copyrightgeschützt und darf in keiner Form vervielfältigt werden noch an Dritte weitergegeben werden.
Es gilt nur für den persönlichen Gebrauch.

Dieses Werk ist copyrightgeschützt und darf in keiner Form vervielfältigt werden noch an Dritte weitergegeben werden.
Es gilt nur für den persönlichen Gebrauch.